Cranfield University

Aaron Altman

A Conceptual Design Methodology for Low Speed High Altitude Long Endurance Unmanned Aerial Vehicles

College of Aeronautics

Ph.D. Thesis

Cranfield University

College of Aeronautics

Department of Air Vehicle Technology

Ph.D. Thesis

May 2000

Aaron Altman

A Conceptual Design Methodology for Low Speed High Altitude Long Endurance Unmanned Aerial Vehicles

Supervisor : R.I.Jones

Presented 3 May 2000

This thesis is submitted in partial fulfillment of the requirements for the degree of Doctor of Philosophy

Abstract

A Conceptual Design Methodology for Low Speed High Altitude Long Endurance Unmanned Aerial Vehicles

A conceptual design methodology was produced and subsequently coded into a Visual C++ (GUI) environment to facilitate the rapid comparison of several possible configurations to satisfy High Altitude Long Endurance (HALE) unmanned aircraft (UAV) missions in the Low Speed (propeller driven aircraft) regime.

Several comparative studies were performed to verify the applicability of traditional design methods. The traditional computational design methodologies fail in several areas such as high aspect ratio wing weight estimation and design, low Reynolds number wing design, high altitude engine performance, low Reynolds number drag estimation, unmanned aircraft design, and the conceptual design of unconventional configurations. The methodology developed for this thesis was robust enough to allow not only for consideration of these areas of inadequacy in traditional methods, but also to allow for the inclusion of advancements in the relevant technologies as they become more widely available.

The following configurations were evaluated for suitability to the Low Speed HALE UAV application: conventional, canard, twin boom, multiple fuselage (conventional or canard), tandem wing, multiple fuselage tandem wing or flying wing configuration. The configurations were compared on the basis of aircraft endurance for takeoff weights ranging from 2,000 to 20,000 pounds and wing loadings ranging from 5 to 25 lbs/ft^2.

Initial drag estimates were made using traditional parabolic drag estimation techniques. A more refined drag buildup was performed using a vortex lattice drag estimation for the lift induced drag (for all lifting components) and calculated skin friction coefficients for the parasite drag. Statistically based methods were used for other components of drag having much smaller contributions. In addition, a statistical approach was taken to the weight estimation of the major aircraft components. However, this approach made comparison of alternative configurations more difficult. Thus wing bending moments trends were evaluated and utilized in the development of weight saving values for multiple fuselage wing weight estimation.

The comparative performance of each configuration is justified with direct reference to the terms in the Breguet Endurance equation. Validation was performed where possible on all modules and segments associated with the methodology, as well as for the macroscopic results. In addition, parametric studies on endurance were performed for the conventional configuration for geometric characteristics and operating conditions directly and indirectly effecting the calculated endurance and generalized results presented. Finally, a case study was performed to demonstrate this capability.

A new relation was developed for aircraft empty weight prediction, a low speed airfoil figure of merit was proposed, and new constants were offered for UAV fuselage length prediction. In addition, horizontal and vertical tail volume coefficients were proposed for all of the Low Speed HALE UAV configurations considered. It was determined that the multiple fuselage configurations showed comparatively superior endurance performance across a range of takeoff weights, with several other configurations demonstrating marginal endurance improvements. Finally, a highly flexible and robust computer based conceptual design methodology was developed and validated enabling the quick comparison of a greater number of possible configurations to satisfy a given mission for Low Speed HALE UAV's and providing detailed drag and weight breakdown data.

Acknowledgements

I would like to thank the following people :

My father, who gave me a love of the scientific process at a very young age, and has fostered its growth in me throughout the years. Who has provided unlimited support in every way throughout my entire seemingly eternal education.

My mother, who has been there in every way in perfect complement to my father. For asking the question, "What's wrong with that teacher?", not "What's wrong with my son?".

To my sisters, who have all had to defeat their own demons and lived through the experience to show me that I, too, can do it.

To H.C. Wilcox and all the guys at the shop, who taught me what an honest day's work was really all about, and who had so little, but gave so much.

To Mr. Chuck Innes, for destroying my faith in mathematics, and telling me I would never do anything in mathematics or engineering.

To Laurence Hood, for restoring my faith in myself, and mathematics.

To Bernd Chudoba, for standing by his convictions and always keeping me on my toes academically.

To ultimate frisbee, and everyone at 9 West Rd. and 3 the Drive for keeping me sane.

To the Vice Chancellor, Dr. Frank Hartley, for adamantly supporting students issues.

To Lynn, Ian, Sue, Gareth, and Grace at the CSA, for helping me to turn things around.

To Dr. Robert Jones, for his patience and skillful handling of a very difficult student and occasional(?) administrative nightmare.

And finally, to the person who restored my faith in love. The most wonderful person in the world. The person who gave me the best incentive to finish when I needed it the most,

Servane.

Table of Contents

List of Figures vi
List of Symbols x
1. Introduction : General Background 1
2. Review of the Literature 6

2.A The Conceptual Design Stage *6*
2.A.1 Conceptual Design Definition 6
2.A.2 Existing Methodologies 8
2.A.3 Problem with Existing Methodologies 9
2.A.4 Existing Computational Methodologies 10

2.B Difficulties with Discretizing the Conceptual Design Process *11*

2.C Explicit Shortcomings of Existing Methodologies *15*
2.C.1 Wing Design 16
2.C.1.a Low Reynolds Number Wing Profile Data 16
2.C.1.b Computational Airfoil Profile Drag Solutions 18
2.C.1.c Wing Planform Design 19
2.C.1.d Computational Lift Induced Drag Prediction 22
2.C.1.e Aerodynamic Efficiency 23
2.C.1.f Trim Drag 26
2.C.1.g Spanwise Variations in Profile Drag at Low Re 30
2.C.1.h Spanwise Camber 31
2.C.1.i Winglets 33
2.C.1.j Differences in Sailplane Aerodynamic Design 34
2.C.1.k Wing-Fuselage Interactions 35
2.C.1.l Component Drag Breakdown 36
2.C.2 Weight Estimation/Structure 37
2.C.3 Power Plant Selection and Performance Estimation 43
2.C.4 Tail Sizing/Stability 49
2.C.4.a Tail Sizing 49
2.C.4.b Downwash 51
2.C.5 Design of Alternative Configurations 52
2.C.5.a General 53
2.C.5.b Twin Boom / Twin Fuselage 55
2.C.5.c Canard 57
2.C.5.d Tandem Wing 63
2.C.5.e Flying Wing 64
2.C.5.f Telescoping Wings 66
2.C.6 Cooling Drag Estimation 66
3. Overview of the Methodology 69

3.A Parallel Currents *69*

3.B The Methodology *70*

3.C The Procedure *72*
4. Preliminary Sizing 75

4.A Specification of the Critical Constants *75*

4.B Creation of the Constraint Diagram *76*
4.B.1 Maximum Load/Turn 77
4.B.2 Endurance 78

4.B.3 Cruise 78
4.B.4 Rate of Climb (RofC)/Ceiling 78
4.B.5 Takeoff Distance 79
4.B.6 Stall Condition 79
4.C Evaluation of the Realism of the Constraints *79*
4.D Selection of the Design Point *81*
4.E Sensitivity on Takeoff Weight and Cruise Velocity *81*
4.F Selection of the Payload Weight or Wing Area *84*
4.G Selection of the Preliminary Weight Fractions *85*
4.H Selection of the # of Engines, Fuel Consumption, and Excess Power Available for Climb *87*
4.I Calculation of the Initial Endurance and Time to Climb *88*
4.J Selection of the Configuration *89*
5. Aircraft Layout and Geometry 91
5.A Moment Arm Length Definitions *92*
5.A.1 Conventional Configuration 92
5.A.2 Canard Configuration 93
5.A.3 Twin Boom & Multiple Fuselage Conventional Configurations 95
5.A.4 Multiple Fuselage Canard 96
5.A.5 Tandem Wing 97
5.A.5.a Single Fuselage 97
5.A.5.b Multiple Fuselage 97
5.B Fuselage Dimension and Location Specification *98*
5.B.1 Default Fuselage Case 98
5.B.1.a Fuselage Length Calculation 99
5.B.1.b Multiple Fuselage/Boom Length Calculation for the Default Configuration Case 100
5.B.1.c Default Fuselage Height and Width 102
5.B.1.d Wing Position on Fuselage, Moment Arm Length Estimation 102
5.B.2 Designer Modified Fuselage Case 105
5.B.2.a Specification of the Fuselage Geometric Parameters 105
5.B.2.b Fuselage Length Calculation for The Remaining Configurations 106
5.B.2.c Wing Position on Fuselage, or Moment Arm Length Estimation 106
5.C Specification of the Wing Planform Geometry *108*
5.C.1 The Default Case 109
5.C.2 The Designer Modified Wing Planform Geometry 111
5.D Wing/Canard/Tandem/Tail Profile Specification *111*
5.D.1 Provision of Wing Profile Characteristics 112
5.D.2 Provision of Tail/Canard/Tandem Profile Characteristics 113
5.E Tail Sizing Characteristics Specification *114*
5.E.1 Default Tail Sizing 114
5.E.1.a Specification of Default Tail Geometric Characteristics 114
5.E.1.b Default Tail Volume Coefficient Specification 116
5.E.2 Difficulties with the Vertical Tail Volume Coefficient Definition 117
5.E.3 Tail Volume Coefficients for All Configurations 117
5.F Location and Performance of the Engine(s) *119*
5.F.1 Location of the Engine(s) 119
5.F.1.a Propeller Specification 120
5.F.1.b Propeller/Engine Configuration 122
5.F.2 Engine Geometry and Performance Specification 124
6. Aircraft Drag Estimation 127

6.A Determination of Major Aerodynamic Variables *128*

6.B Determination of the Lift Curve Slope *129*

6.C The Vortex Lattice Method *130*
6.C.1 Wing Profile Drag and the Vortex Lattice Method 130
6.C.2 Potential Flow Theory and Lifting Surface Interaction 131
6.C.3 Validation of the Vortex Lattice Method Implementation 135
6.C.3.a The Rectangular Wing Analogy 135
6.C.3.b Sine and Cosine Spacing of Spanwise and Chordwise Points 139
6.C.3.c Wing-Tail and Wing-Fuselage Interactions 141
6.C.3.d Canard-Wing Interference Effects 143
6.C.3.e Tandem Wing-Wing Interference Effects 144

6.D Wing Drag *146*

6.E Tail Drag *148*
6.E.1 Tail Parasite and Lift Induced Drag 148
6.E.2 Configuration Dependent Tail Drag 149

6.F Fuselage Drag *150*

6.G Engine Nacelle Drag *152*

6.H Cooling Drag *154*

6.I Wing-Fuselage Interference *155*

6.J Total Drag *156*

7. Detailed Weight Estimation 157

7.A Wing Weight Estimation *157*

7.B Spanwise Wing Bending Moment Study *162*
7.B.1 Single Engine Study 163
7.B.2 Twin Engine Study 166

7.C Fuselage Weight Estimation *169*

7.D Horizontal Tail/Canard Weight Estimation *172*

7.E Vertical Tail Weight Estimation *175*

7.F Engine Weight Estimation *176*

7.G Engine Nacelle Weight Estimation *179*

7.H Fuel System Weight Estimation *181*

7.I Electronics/Avionics/Instruments Weight Estimation *182*

7.J Surface Controls Weight Estimation *183*

8. Center of Gravity, Static Margin, and Trim 186

8.A Aircraft Center of Gravity Calculation *186*

8.B Static Margin Calculation *190*

8.C Trim Condition *194*

9. Implementation of the Methodology 197

9.A Event Driven Programming *198*

9.B Structure of the Overall Program *200*

9.C Preliminary Sizing *202*

9.D Creation of the Default Aircraft *206*

9.E Modification of the Existing Geometry *210*

9.F Analysis of the Aircraft *217*
10. Results and Discussion 219

10.A Validation *220*
10.A.1 Boeing Condor 221
10.A.2 Aurora Flight Sciences Perseus B 222
10.A.3 Aurora Flight Sciences Theseus 223
10.A.4 Scaled Composites Raptor 225
10.A.5 General Atomics Altus 226
10.A.6 General Atomics Predator (RQ-1A) 227
10.A.7 Israeli Aircraft Industries Heron 227
10.A.8 Scaled Composites Proteus 228
10.A.9 Teledyne Ryan Global Hawk (RQ-4A) 229
10.A.10 Summary of the Results of the Validation 231

10.B The Conventional Configuration *232*
10.B.1 Breguet Endurance Equation Revisited 232
10.B.2 General Results from the Variation of W/S, W_{to}, and W_{PL} / W_{to} 234
10.B.2.a Endurance Results 235
10.B.2.b Results for the Fuel Fraction and Endurance Terms 237
10.B.2.c Summary of the General Endurance Results 241
10.B.2.d Other Interesting Results 242
10.B.3 Study of Wing Geometry Effects 244
10.B.3.a Aspect Ratio Study 244
10.B.3.b Taper Ratio Study 249
10.B.3.c Airfoil Study 251
10.B.4 Study of the Effects of Operating Conditions 253
10.B.4.a Altitude Study 253
10.B.4.b Lift Coefficient Study 257
10.B.5 Study of the Effects of Engine Configuration 258
10.B.5.a Single Engine Pusher Propeller Configuration Study 258
10.B.5.b Twin Engine Study 259
10.B.6 Proposed Empty Weight Fraction Relation 264

10.C Alternative Configurations *266*
10.C.1 Canard 266
10.C.1.a Single Engine Canard Tractor 267
10.C.1.b Single Engine Canard Pusher 268
10.C.2 Twin Boom 270
10.C.2.a Single Engine Tractor Twin Boom 270
10.C.2.b Single Engine Pusher Twin Boom 272
10.C.3 Multiple Fuselage Conventional and Canard 273
10.C.3.a 2,000 pound Takeoff Weight 273
10.C.3.b 10,000 pound Takeoff Weight Case 278
10.C.3.c 20,000 pound Takeoff Weight 283
10.C.4 Single Fuselage Tandem Wing 284
10.C.4.a 2000 pound Takeoff Weight 285
10.C.4.b 10,000 pound Takeoff Weight 287
10.C.4.c 20,000 pound Takeoff Weight 289
10.C.5 Multiple Fuselage Tandem Wing 290
10.C.5.a 2000 pound Takeoff Weight 291
10.C.5.b 10,000 pound Takeoff Weight 294
10.C.5.c 20,000 pound Takeoff Weight 296
10.C.5.d Tandem Wing Aircraft Summary 297
10.C.6 Flying Wing 298

10.D Case Study *301*
10.D.1 Conventional Configuration 302
10.D.2 Two Fuselage Conventional Single Engine 304

11. Conclusions and Recommendations 307

11.A Conclusions *307*

11.B Recommendations *309*

11.B.1 Further Utilization of the Methodology 309

11.B.1.a Twin Engine Alternative Configurations 309

11.B.1.b Tandem Wing Study 310

11.B.1.c Detailed Drag Breakdown, Weight Breakdown, or Trim Penalty Studies 310

11.B.1.d Optimal Engine 311

11.B.1.e Link Program to an Optimizer 311

11.B.2 General Recommendations for Further Study 311

11.B.2.a Lightweight High Aspect Ratio Wing Weight Estimation 311

11.B.2.b Simplified Viscous Drag Model 312

11.B.2.c High Altitude Engine Model 312

11.B.2.d Low Speed High Aspect Ratio Wing Wind Tunnel Data 312

11.C Concluding Remarks *313*

References 314

List of Figures

Figure 2.1 *shows the historical trend in the aspect ratio of sailplanes.* **20**
Figure 2.2 *the historical trends in maximum lift to drag ratio (Hermanspann[25]).* **24**
Figure 2.3 *the maximum possible aerodynamic efficiency and how several aircraft compare.* **25**
Figure 2.4 *shows the tail lift vector perpendicular to the local flow direction.* **29**
Figure 2.5 *shows spanwise variations in drag coefficient at low Reynolds number.* **30**
Figure 2.6 *shows the variation in aerodynamic efficiency term (k) (Lowson[55]).* **32**
Figure 2.7 *is the component drag breakdown of the canard sailplane Solitaire.* **37**
Figure 2.8 *shows the comparative structural weight fractions of some aircraft.* **39**
Figure 2.9 *the boundaries for high performance sailplanes with Light and Medium structures.* **42**
Figure 2.10 *is a detailed diagram of the engine implementation for the Condor and Strato 2C.* **47**
Figure 2.11 *the limits in altitude and fuel consumption for various types of HALE UAV's* **48**
Figure 2.12 *the effects of changing tail area on aerodynamic efficiency* **50**
Figure 2.13 *the difference in wing bending moment between a single and multiple fuselage* **56**
Figure 2.14 *the canard induced drag sensitivity with changes in static margin and canard area.* **62**
Figure 2.15 *shows the average chord and trailing edge kink dimension for a flying wing* **65**
Figure 3.1 *is the structure of the Conceptual Design Methodology used throughout the thesis.* **71**
Figure 4.1 *is the Critical Constants or Basic Aircraft Constants dialog box.* **76**
Figure 4.2 *a demonstration of the comparative abilities of the methodology..* **80**
Figure 4.3 *is one of the sensitivity diagrams.* **82**
Figure 4.4 *a sensitivity diagram on takeoff weight as a function of wing loading and wing area..* **83**
Figure 4.5 *is the Weight Fraction Selection dialog box.* **86**
Figure 4.6 *is the main configuration selection window* **90**
Figure 5.1 *the definition of the tail moment arm length for the conventional configuration.* **92**
Figure 5.2 *shows the definition of the tail moment arm length for the canard configuration.* **93**
Figure 5.3 *shows the definition of tail moment arm for the twin boom (left) and multiple fuselage conventional (right) configurations.* **95**
Figure 5.4 *shows the definition of tail moment arm for the multi fuselage canard configuration.* **96**
Figure 5.5 *shows the definition of the single fuselage tandem wing moment arm length.* **97**
Figure 5.6 *is the definition of tail moment arm length for the tandem wing multiple fuselage.* **98**
Figure 5.7 *shows the relationship between fuselage length and aircraft takeoff weight* **99**
Figure 5.8 *is the Wing Profile and Drag Specification dialog box.* **113**
Figure 5.9 *is the Power Plant Details dialog box.* **120**
Figure 5.10 *is the Engine Selection dialog box.* **123**
Figure 5.11 *highlights the differences in the engine length estimation methods* **125**
Figure 6.1 *defines the terms relating to the panel normal vector.* **132**
Figure 6.2 *defines the terms used in the implementation of the Vortex Lattice Method equations.* **133**
Figure 6.3 *the lift dependent drag results of the VLM for different grid densities.* **136**
Figure 6.4 *the variation of the accuracy of the results depending on the grid selected.* **136**
Figure 6.5 *shows the variation in* C_L *with* α *for the vortex lattice method.* **137**
Figure 6.6 *compares the curve fit correction for the lift curve slope with 2d theory.* **138**
Figure 6.7 *compares the normalized spanwise lift force distribution resulting from using different spanwise grid spacing techniques in the vortex lattice method.* **139**
Figure 6.8 *compares the normalized spanwise lift coefficient results from using different chordwise grid spacing techniques using the vortex lattice method.* **140**
Figure 6.9 *normalized lift force results for different combined wing and tail situations* **142**
Figure 6.10 *shows the normalized spanwise lift force results for wing-fuselage and wing-fuselage-tail effects using the vortex lattice method.* **143**
Figure 6.11 *canard on wing aerodynamic effects must be considered if the canard is placed within two chord lengths of the wing.* **144**
Figure 6.12 *is a snapshot of the coded methodology, representing the effects of the fore wing trailing vortex sheet on the aft wing lift distribution.* **145**
Figure 6.13 *shows the absolute spanwise location of the impinging trailing vortices of the forward wing on the aft wing.* **146**

Figure 6.14 *is the Drag Summary dialog box.* **155**
Figure 7.1 *the type of analysis done to determine the best wing weight estimation technique(s).* **158**
Figure 7.2 *is the summary of the wing weight (per unit wing planform area, lbs/ft^2) estimations performed for aircraft in the HALE UAV or similar class.* **159**
Figure 7.3 *the spanwise bending moment of the single engine non-tandem configurations.* **163**
Figure 7.4 *a comparison of the single engine tandem aircraft spanwise bending moment.* **165**
Figure 7.5 *the large negative bending moments at the aircraft longitudinal centerline for multiple fuselage/boom configurations for the twin engine non-tandem aircraft.* **167**
Figure 7.6 *compares the twin engine tandem aircraft spanwise bending moment distributions.* **168**
Figure 7.7 *compares the fuselage weight estimation methods evaluated.* **169**
Figure 7.8 *is a comparison of different horizontal tail weight estimation methods* **172**
Figure 7.9 *is a comparison of different vertical tail weight estimation methods.* **175**
Figure 7.10 *is a comparison of different engine weight estimation methods.* **177**
Figure 7.11 *compares Raymer's engine weight estimation method with some known aircraft engine only (uninstalled) weights as a function of horsepower output.* **178**
Figure 7.12 *is a comparison of different nacelle weight estimation methods.* **180**
Figure 7.13 *is a comparison of different fuel system weight estimation methods* **181**
Figure 7.14 *compares different electronics, avionics, and instrument weight estimation methods* **183**
Figure 7.15 *compares several different classes of surface controls, their associated weights, and the results of these methods* **184**
Figure 8.1 *is the Center of Gravity and Static Margin Summary dialog box..* **189**
Figure 8.2 *is the Trim Effects dialog box..* **195**
Figure 9.1 *shows the structure and largest groupings of modules for the overall code.* **201**
Figure 9.2 *shows a more detailed breakdown of the structure of the preliminary sizing segment.* **202**
Figure 9.3 *is a graphical representation of the Preliminary Sizing Segment* **203**
Figure 9.4 *the structure of the Default Configuration Creation segment.* **206**
Figure 9.5 *details the inputs and outputs of the more important modules that are invoked by the class MainConf in the process of drawing the Default Configuration.* **207**
Figure 9.6 *shows the choices presented to and the interaction between the designer and the class MainConf in the process of re-drawing the designer specified aircraft.* **211**
Figure 9.7 *is the module responsible for the Modification of the Aircraft Geometry* **212**
Figure 9.8 *shows the Wing/Tail Profile and Drag Data container class.* **214**
Figure 10.1 *shows the overall aircraft endurance as a function of wing loading.* **235**
Figure 10.2 *shows overall aircraft endurance as a function of takeoff weight.* **236**
Figure 10.3 *the fuel fraction component of the aircraft endurance as a function of wing loading.* **237**
Figure 10.4 *the fuel fraction component of the endurance as a function of the takeoff weight.* **238**
Figure 10.5 *shows the payload effects on the fuel fraction component of the overall aircraft endurance as a function of wing loading for three different takeoff weights.* **239**
Figure 10.6 *the endurance term/aerodynamic efficiency component of the aircraft endurance.* **241**
Figure 10.7 *shows the predicted empty weight fraction as a function of wing loading.* **242**
Figure 10.8 *the increase in predicted cruise power required for increasing takeoff weights.* **244**
Figure 10.9 *the change in aircraft endurance for aircraft with different aspect ratios.* **245**
Figure 10.10 *shows a 20% decrease in the endurance term for aircraft with lower aspect ratios.* **246**
Figure 10.11 *the increase in fuel fraction endurance term for aircraft with lower aspect ratios.* **247**
Figure 10.12 *the increase in required cruise power resulting from an increase in aspect ratio.* **248**
Figure 10.13 *shows a less severe effect of changing the taper ratio compared to the effects of aspect ratio changes on the overall aircraft endurance* **249**
Figure 10.14 *shows that the effects of taper ratio changes are less dramatic than the effects of aspect ratio changes on the structural efficiency of the aircraft.* **250**
Figure 10.15 *the effect of exchanging two low Re high lift airfoils on the aircraft endurance.* **251**
Figure 10.16 *the effect of a change in airfoil on the 3d aircraft aerodynamic efficiency term.* **252**
Figure 10.17 *the effects on structural efficiency of a slight change in thickness to chord ratio.* **253**
Figure 10.18 *shows the dramatic effect of increased altitude on overall aircraft endurance.* **254**
Figure 10.19 *shows a curious decrease in aerodynamic efficiency with an increase in altitude.* **255**
Figure 10.20 *shows a very slight decrease in structural efficiency due to an increased cruise velocity corresponding to the increased altitude.* **256**
Figure 10.21 *shows the very large increase in power required to cruise resulting from an increase in cruise altitude of 15,000 feet.* **256**

Figure 10.22 *shows a nominal effect of a large increase in lift coefficient on overall aircraft endurance for the aircraft using the NLF(1)-1015.* **257**
Figure 10.23 *shows the increase in aerodynamic efficiency resulting from an increase in lift coefficient for the NLF(1)-1015 airfoil.* **258**
Figure 10.24 *a decrease in aircraft endurance due to a change in propeller configuration from a tractor to a pusher for the conventional configuration.* **259**
Figure 10.25 *shows an unfair performance comparison between the single and twin engine.* **260**
Figure 10.26 *compares the endurance terms of the single and twin engine configurations.* **260**
Figure 10.27 *the decrease in structural efficiency of the twin engine configuration.* **261**
Figure 10.28 *shows the increase in cruise power required for the twin engine configuration.* **261**
Figure 10.29 *a very minute advantage in endurance for the pusher configured twin engine.* **262**
Figure 10.30 *shows a deviation in endurance term from the conventional twin configuration only for the 2000 pound takeoff weight case.* **263**
Figure 10.31 *shows a significant improvement in endurance of the twin engine push-pull configuration 2000 pound case over the conventional twin engine tractor.* **263**
Figure 10.32 *the increase in aerodynamic efficiency resulting from the removal of much of the nacelle wetted area by placing the engines in a push-pull configuration.* **264**
Figure 10.33 *compares the endurance of the conventional single engine tractor to the canard single engine tractor configuration.* **267**
Figure 10.34 *displays increased slope for the aerodynamic efficiency curve of the canard tractor aircraft at low wing loadings when compared to the conventional tractor.* **267**
Figure 10.35 *compares the endurance of the single engine canard pusher aircraft to the single engine conventional tractor aircraft.* **268**
Figure 10.36 *shows greater aerodynamic efficiency for the canard pusher aircraft at a lower takeoff weight when compared to the conventional tractor configuration.* **269**
Figure 10.37 *the endurance performance of the tractor propeller configured twin boom.* **270**
Figure 10.38 *the endurance terms for the twin boom and conventional tractor configurations.* **271**
Figure 10.39 *an explanation for the source of the increasing endurance of the twin boom.* **271**
Figure 10.40 *the endurance of the twin boom aircraft in the pusher configuration compared to the endurance of the conventional aircraft in the tractor configuration.* **272**
Figure 10.41 *is a comparison of the different 2 fuselage configurations.* **274**
Figure 10.42 *the performance of the different 3 fuselage configurations.* **275**
Figure 10.43 *the fuel fraction term for similar 2 and 3 fuselage pusher configurations.* **275**
Figure 10.44 *shows oscillations in the tractor configured two fuselage aircraft.* **277**
Figure 10.45 *reveals the large deviation in endurance between the two conventionally configured 3 fuselage aircraft.* **278**
Figure 10.46 *compares the overall endurance for the 10,000 pound two fuselage conventional and canard configured aircraft.* **279**
Figure 10.47 *the endurance of the three fuselage conventional and canard configurations.* **280**
Figure 10.48 *shows the large increase in fuel fraction term of the two fuselage configuration.* **280**
Figure 10.49 *the flat behavior of the canard two fuselage aircraft endurance term compared to the two fuselage conventionally configured aircraft.* **281**
Figure 10.50 *a decrease in the difference in endurance term between the three fuselage canard and conventionally configured aircraft.* **282**
Figure 10.51 *shows the comparative endurance for the 20,000 pound two fuselage aircraft.* **283**
Figure 10.52 *shows the 20,000 pound three fuselage aircraft endurance results.* **284**
Figure 10.53 *shows the overall endurance results for the 2000 pound single fuselage tandem* **285**
Figure 10.54 *shows the surprising result of greater aerodynamic efficiency for the 75/25 area split tandem wing, in both pusher and tractor configurations.* **286**
Figure 10.55 *hints towards the superior structural efficiency of the tandem wing aircraft.* **287**
Figure 10.56 *the improvement of the tandem when compared to the conventional configuration.* **288**
Figure 10.57 *shows a relative decrease in performance by the tandems.* **288**
Figure 10.58 *shows a significant advantage in structural efficiency for the tandem aircraft* **289**
Figure 10.59 *shows a significant improvement in overall endurance of the tandem wing aircraft at lower wing loadings when compared to the conventional configuration.* **290**
Figure 10.60 *compares the 2000 pound multiple fuselage tandem wing aircraft to the single fuselage tandem wing aircraft as a baseline.* **291**
Figure 10.61 *a greater slope in the aerodynamic efficiency of the two fuselage tandem aircraft.* **292**

Figure 10.62 *shows that the fuel fraction term is the primary reason for the poor overall endurance performance of the three fuselage tandem pusher* **293**
Figure 10.63 *shows a slight leftward shift (of wing loading) in optimum endurance for the multiple fuselage tandem wing aircraft in addition to a higher maximum endurance for the 10,000 pound takeoff weight cases.* **294**
Figure 10.64 *shows much better agreement in the endurance term for the multi fuselage tandem aircraft for the 10,000 pound takeoff weight case.* **295**
Figure 10.65 *compares the fuel fraction terms for the multiple fuselage tandem aircraft* **295**
Figure 10.66 *shows endurance behavior extremely similar to the 10,000 pound takeoff weight tandem endurance figure above wing loadings of 10 lbs/ft^2* **296**
Figure 10.67 *the endurance of the untrimmed flying wing compared to the conventional configuration.* **298**
Figure 10.68 *shows the coincidence of the endurance term curves for the flying wing case.* **299**
Figure 10.69 *shows the improvement in structural efficiency for the flying wing configuration* **300**
Figure 10.70 *shows the two fuselage single engine conventional configuration.* **305**

List of Symbols

3-d	Three Dimensional
a	Constant used in Raymer's Fuselage Length Calculations
ACT	Air Charge Temperature
ADAS	A Conceptual/Preliminary Design and Optimization Program Developed at Delft University of Technology
AR	Aspect Ratio
ASW 17	Sailplane
ASW 19	Sailplane
ASW 24	Sailplane
A_{wet}	Wetted Area
b	Span
C	Constant used in Raymer's Fuselage Length Calculations
c	Chord
C_D	Drag Coefficient
C_{Do}	Zero Lift Drag Coefficient
C_{DI}	Induced Drag Coefficient
$C_{DinducedVLMwing}$	Wing Lift induced Drag Output from VLM
$C_{DparasiteWing}$	Wing Parasite Drag Coefficient
$C_{dProfileWing}$	Wing Profile Drag Coefficient
C_{Dtot}	Total Aircraft Drag Coefficient
C_E	Constant used in Glider Mass Estimation
C_f	Skin Friction Coefficient
CFD	Computational Fluid Dynamics
$C_{fLaminar}$	Laminar Skin Friction Coefficient
$C_{fTurbulent}$	Turbulent Skin Friction Coefficient
cg	Center of Gravity
$CG_{average}$	Average of the Fore and Aft Center of Gravity Limits
c_{HT}	Horizontal Tail Volume Coefficient
$\bar{c}_{Htail}$	Horizontal Tail Average Chord
C_L	Lift Coefficient
$C_{L,0}$	Lift Coefficient at Zero Angle of Attack
$C_{l\alpha}$	$= \frac{dC_l}{d\alpha} \equiv$ Wing Profile Lift Curve (C_l-α) Slope
$C_{LAftWing}$	Aft Wing Lift Coefficient for Tandem Wing Aircraft
$C_{l\alpha_{HT}}$	$= \frac{dC_{lHT}}{d\alpha} \equiv$ Horizontal Tail Lift Curve (C_l-α) Slope
$C_{l\alpha_{HTcan}}$	$= \frac{dC_{lHTcan}}{d\alpha} \equiv$ Horizontal Tail or Canard Lift Curve (C_l-α) Slope
$(C_{L\alpha})_{w/b}$	$= \left(\frac{dC_l}{d\alpha}\right)_{w/b} \equiv$ Wing-Body Combined Lift Curve (C_l-α) Slope
$C_{l\alpha_{wing3D}}$	Lift Coefficient Correction for Three Dimensional Effects
$C_{L\alpha_{wing/body}}$	Lift Coefficient Correction for Three Dimensional Effects

$C_{l\beta}$	$= \frac{dC_l}{d\beta} \equiv$ Vertical Tail Profile Lift Curve (C_l-β) Slope
$C_{Laircraft}$	Total Aircraft lift coefficient
$C_{Lcruise}$	Cruise Lift Coefficient
$C_{LForeWing}$	Forward Wing Lift Coefficient for Tandem Wing Aircraft
C_{Lmax}	Maximum Lift Coefficient
$C_{L\,max\,L/D}$	Maximum Lift over Drag ratio Lift Coefficient
C_{LminPR}	Lift Coefficient for Minimum Power Required
C_{Ltrim}	Trimmed Aircraft Lift Coefficient
C_{mo}	Zero Lift Moment Coefficient
$C_{m,ac}$	Moment Coefficient About the Aircraft Aerodynamic Center
$C_{m,ac\ w/b}$	Moment Coefficient About the Wing-Body Aerodynamic Center
$C_{m,profile}$	Profile Moment Coefficient
$C_{m,w/b}$	Wing-Body Moment Coefficient
$c_{rootWing}$	Wing Root Chord
c_{Rwing}	Wing Root Chord
c_{Twing}	Wing Tip Chord
c_{VT}	Vertical Tail Volume Coefficient
$\bar{c}_{wing}$	Wing Average Chord
D	Flying Wing Trailing Edge Kink Dimension
D	Drag
DAR	Design Analysis and Research
D_{fuse}	Fuselage Diameter
D_{prop}	Propeller Diameter
ERAST	Environmental Research Aircraft and Sensor Technology Program, NASA
ESDU	Engineering Sciences Data Unit PLC
f	Fineness Ratio
FORTRAN	FORmula TRANslator, High Level Programming Language
H	Height Dimension
H	Altitude of Climb Iteration
HALE	High Altitude Long Endurance
H_{fuse}	Fuselage Height
HOLIST	Hypersonic Aircraft Design Synthesis Program Written by Boeing
HP	Horsepower
$\frac{HP}{W}$	Thrust or Power Loading
IAI	Israeli Aircraft Industries
IPPD	Integrated Product and Process Development
ISES	Airfoil Drag Prediction Software Written by Mark Drela at MIT
K	$= \frac{1}{\pi AR\varepsilon} \equiv$ Three-dimensional Lift Distribution Correction Factor
K_a	$= \frac{1}{AR} - \left(\frac{1}{1+AR^{1.7}}\right) \equiv$ Constant used in Wing Downwash Estimation
K_b	Cantilever Factor used in Wing Mass Estimation
K_{dwf}	=1.0 Delta Wing Factor used in Wing Downwash Estimation
K_e	=0.95 for Twin Engine, else 1.0, used in Wing Mass Estimation

K_h	$\left(1-\frac{z_{HT}}{b}\right)\left(\frac{2L_t}{b}\right)^{1/3}$ ≡Constant used in Wing Downwash Estimation
K_{HT}	=1.0 for Fixed Horizontal Tail +1.1 for an all Moving Tail used in Horizontal Tail Weight Estimation
K_λ	$=(1+\lambda)^{0.4}$ used in Wing Weight Estimation
K_{no}	$=1+\sqrt{\frac{b_{ref}\cos\Lambda_{1/2}}{b}}$ b_{ref}=6.25ft used in Wing Weight Estimation
K_{st}	=1.0 for Low Subsonic Aircraft used in Wing Weight Estimation
K_{uc}	=0.95 if Under Carriage is Attached to Wing, else 1.0, used in Wing Weight Estimation
L	Lift
L'	Constant used with Roskam Wing Profile Drag Coefficient Estimation Method
$L_{AftWing}$	Aft Wing Lift Force used with Tandem Wing Configurations
LAURA	Low Altitude/Airspeed Unmanned Research Aircraft US Navy Research Program
L_{boom}	Boom Length for Multiple Boom Aircraft
L_c	Canard Lift
$(L/D)_{max}$	Maximum Lift over Drag Ratio
L_{engine}	Engine Length
$L_{ForeWing}$	Forward Wing Lift Force used with Tandem Wing Configurations
L_{fuse}	Fuselage Length
LS 3	Sailplane
L_t	Tail Moment Arm Lenght
L_W	Wing Lift
m	Mass
M	Mach number
MAC	Mean Aerodynamic Chord
NACA	National Advisory Council on Aeronautics, US
NASA	National Aeronautics and Space Administration, US
N_{blades}	Number of Blades per Propeller
$N_{engines}$	Number of Engines
N_{props}	Number of Propellers
N_{tanks}	Number of Fuel Tanks
n_{ult}	Ultimate Load Factor in g's
P_{avail}	Available Power from Engines in Climb
P_{cruise}	Cruise Power
P_{excess}	Excess Power in Climb
PIK 20	Sailplane
$P_{reqd,New}$	New Power Required
Q	$=1/2\rho V^2$
Re	Reynolds Number
Re_{fuse}	Fuselage Reynolds Number
RFP	Request For Proposal
R_{ls}	Constant used in the Determination of Roskam Wing Profile Drag Coefficient

RoC	Rate of Climb
RPV	Remotely Piloted Vehicle
R_{wf}	Constant used in the determination of Roskam Wing Profile Drag Coefficient
S	Wing Area
$S_{AftWing}$	Aft Wing Tandem Wing Area
SB 11	Sailplane
S_c	Canard Planform Area
SFC	Specific Fuel Consumption
$S_{ForeWing}$	Forward Wing Tandem Wing Area
S_{HT}	Horizontal Tail Planform Area
$(S_{HT,can})_{slipstream}$	Area of the Horizontal Tail or Canard in the Propeller Slipstream
$SM(W_{empty})$	Static Margin at the Aircraft Empty Weight
$SM(W_{to})$	Static Margin at the Aircraft Take Off Weight
$S_{netWing}$	Area of Wing Minus Area where Wing Passes Through Fuselage
$S_{planformWing}$	Wing Planform Area
SR-71	Lockheed Strategic Reconnaissance 71
S_{ref}	Reference Area used in Drag Calculations
S_{VT}	Vertical Tail Planform Area
S_W	Wing Planform Area
$S_{wetWing}$	Wing Wetted Area
$\frac{t}{c}$	Thickness to Chord Ratio
T	Temperature
TtoClimb	Time to Climb
UAV	Unmanned Aerial Vehicle
UNIX	Operating System
V_{climb}	Climb Velocity
V_{cruise}	Cruise Velocity
V_{des}	Design Dive Speed
V_{fuel}	Fuel Volume
$V_{fuel/fuselage}$	Volume of Fuel in Fuselage
$V_{fuel/integral}$	Volume of Fuel in Integral Fuel Tanks
$V_{fuel/wing}$	Volume of Fuel in Wings
VLM	Vortex Lattice Method
V_{so}	Stall Speed
w	Width
W	Weight
$\frac{W}{S}$	Wing Loading
$W_{controls}$	Weight of Surface Control Systems
W_{des}	Design Aircraft Empty Weight
W_E	Aircraft Empty Weight
$W_{electronics}$	Weight of Electronics, Avionics, and Instruments
W_{empty}	Empty Weight
W_{fuel}	Weight of Fuel
$W_{fuelsys}$	Weight of the Fuel System
w_{fuse}	Fuselage Width
$w_{fuselage}$	Fuselage Width

$W_{fsComponents}$	Weight of Fuel System Components
$W_{maxfuel}$	Maximum Fuel Weight
W_{maxPL}	Maximum Payload Weight
W_{to}	Aircraft Take-off Weight
x	Chordwise Location
X_{ac}	Aerodynamic Center Position
$X_{ac,can}$	Aerodynamic Center Position of the Canard
$X_{ac,HT}$	Aerodynamic Center Position of the Horizontal Tail
$X_{ac,w/b}$	Aerodynamic Center Position of the Wing/Body
$X_{CG,Aircraft}$	Aircraft Center of Gravity Position
X Foil	Low Reynolds Number Airfoil Drag Prediction Software by Mark Drela at MIT
$z_{1/4}$	Average ¼ Chord
$z_{1/4tail}$	Average Tail ¼ Chord
$z_{1/4wing}$	Average Wing ¼ Chord
Z_{HT}	Vertical Height of the Horizontal Tail Relative to the Wing

Subscripts

3D	Three Dimensional
ac	Aerodynamic Center
avg	Average
basic	Basic Drag Component
can	Canard
D	Drag
eff	Effective
engine	Engine
frontal	Frontal area only
fuel	Fuel
HT	Horizontal Tail
L	Lift
m	Moment
Nacelle	Engine Nacelle
ref	Reference
slipstream	Propeller Slipstream Effect
suppl	Supplemental Drag Component
to	Take-off
VT	Vertical Tail
w/b	Wing/Body
Wing	Wing
WingFuse	Wing-Fuselage Junction
WingGuess	Guess for the Wing Weight

Greek Symbols

α	Angle of Attack
β	$=(1-M^2)^{1/2} \equiv$ Aerodynamic Compressibility Factor

δ	Fraction of Total Wing Area Comprised by the Aft Wing
Δ_{fuse}	Change in a Quantity Relating to the Fuselage
ε	Oswald Efficiency Factor
η_p	Propeller Efficiency in Cruise
η_{slip}	Propeller Slipstream Effects
$\eta_{slip,\ can}$	Fraction of the Canard Planform Area in the Propeller Slipstream
$\eta_{slip,\ HT}$	Fraction of the Horizontal Tail Planform Area in the Propeller Slipstream
λ	Taper Ratio
$\Lambda_{1/4}$	¼ Chord Sweep Angle
μ_{cruise}	Kinematic Viscosity for the Cruise Condition
π	Pi=3.14159265 Constant
ρ_{cruise}	Air Density in Cruise
ρ_{SL}	Air Density at Sea Level

Vortex-Lattice Symbols

A_{ij}	Panel Influence Coefficient Represents Flow Induced on Panel i Resulting from the Vortex on Panel j
β_i	Angle of Panel i Relative to Mean Camber Line
D_i	Drag of Panel i
dS	See Figure 5.2
Φ	Angle of Panel j Relative to Panel i
Γ_j	Circulation Velocity of Panel j
h	See Figure 5.2
K	See Figure 5.2
L_i	Lift of Panel i
Q	$= \sin(\alpha - \beta_i) \cong (\alpha - \beta_i) \cong \alpha - \left(\frac{dZ}{dx}\right)_i$
R_r	See Figure 5.2
S	See Figure 5.2
V_n	Velocity Normal to the Surface
V_∞	Mean Stream Velocity
w_i	Downwash Velocity of Panel i
x	See Figure 5.2
X	See Figure 5.2
y	See Figure 5.2
Y	See Figure 5.2

Chapter I

Through the picture, I see reality.

Through the word, I understand it.

--- Sven Lidman

Ad Inexplorate (Into the Unknown)

1. Introduction : General Background

It has taken a century for unmanned aircraft to find a niche in modern aviation. For many years the possibility of unmanned flight has been discussed, and to some small degree achieved, but it is only in the past several years that technology has advanced to the point where unmanned aircraft can be trusted to reliably achieve their goals.

One of the early uses for UAV's was the conversion of older aircraft to target drones. Other aircraft that could be interpreted as unmanned are cruise missiles, which have been around in crude form since World War II and in much more deadly, accurate, and reliable form today. In these applications, the aircraft were really only designed to complete one mission.

These aircraft were either not true aircraft in the sense that they were expendable like bombs or missiles, or they were not originally designed as unmanned. It wasn't until the 1960's that unmanned reconnaissance aircraft (*Firebee, and Firefly, or Compass Arrow*) were designed, built and deployed (in Vietnam). The first modern unmanned air vehicle designed to remove the pilot in a traditional role (high altitude long endurance reconnaissance) was the Teledyne Ryan *Compass Cope* in 1972.

Then there was a lull of approximately 15 years until the Boeing *Condor* was designed. Then several smaller drones were built for the next 9 years or so. These drones were used for shorter distance and short duration military reconnaissance. Finally, in the early 1990's larger unmanned aircraft projects slowly began to obtain funding for various military and government applications (*Global Hawk, Darkstar*). The late 1990's saw the first public commercially contracted aircraft designed for the possibility of unmanned

flight, with the Scaled Composites *Proteus* high altitude long endurance communications relay and reconnaissance aircraft.

Now, High Altitude Long Endurance (HALE) Unmanned Aerial Vehicles (UAV's) are increasingly being considered to perform a wide range of tasks. Recent years have seen greater use of UAV's by the West in the military reconnaissance arena, first in the Persian Gulf war, with the use of small UAV's, and more recently over Bosnia and Kosovo with medium sized UAV's. The Israeli military have used small to medium UAV's for over 15 years for battlefield and border reconnaissance.

The NASA ERAST program uses HALE UAV's for environmental sensing and atmospheric monitoring. The military establishment in the United States and the United Kingdom has investigated using HALE UAV's for Theater Ballistic Missile defense, as well as general battlefield reconnaissance. Proposals have been made to use HALE UAV's for communications relay, long term surveillance (with a degree of flexibility not available from satellites), border surveillance, power line monitoring, forest fire detection, drug interdiction, automobile traffic monitoring, disaster relief, and many others. Finally, there has been discussion on producing a HALE UAV to fly in the Martian atmosphere, since atmospheric conditions there are similar to those found on earth at extremely high altitudes[1].

By removing the pilot, UAV's reduce risk, not only to the potential pilot, but also to politically sensitive situations. Removal of the pilot provides an overall simplification of the aircraft (with possible exception to flight control systems). It also provides for a greater variability of possible configurations by removing the need for a pilot to see out and sit up, removal of complex environmental controls, the need to accommodate other activities necessary for human subsistence (this requires little imagination for a 48 hour mission).

The justification for using Low Speed HALE UAV's is that the low speed regime is more advantageous for environmental sampling. Low Speed HALE UAV's are less likely to disturb the composition of the air around them. For example, imagine if the Mach 3+ SR-71 were used for atmospheric sampling in cruise. Low Speed HALE UAV's have lower first cost as demonstrated by the comparative program costs of the entire NASA ERAST programs (*Perseus, Theseus, Raptor, Pathfinder, Centurion/Helios*) when compared to the program costs of *Global Hawk* and *Darkstar*. In addition, they have lower fuel consumption. Unlike turbofans, the engines don't have to be oversized by a factor of 10 to

fly at high design altitudes as do turbofans. Internal combustion reciprocating engines normally necessitate more complex systems for cooling and air charge, as well as propeller gearboxes. However as demonstrated by the engine choices for the NASA ERAST aircraft, *Condor*, and *Strato 2C* the fuel consumption is still much lower than those for turbofans. In addition, engine, propeller gearboxes, and cooling component sizes/weights are still much smaller than a factor of 10 larger than that necessary at Sea Level.

High altitude flight is generally considered above 55,000 feet and is normally above jetstream activity. High altitude flight is desirable for providing a wider field of view for environmental sensing and military reconnaissance. It is also the lower end of the regime of interest for ozone layer composition/chemistry tests. The air is more stable which supplies a more stable sensor platform. It is also the altitude of lower wind speed, and is above commercial airways (for the time being).

Long endurance is desired so that full solar day sensing can be carried out. When used in the disaster relief or cellular telephone relay role, the airplane is required to be on station for a maximum number of hours. In addition, in the military reconnaissance role it is desirable to watch developing problem areas for a long period of time. Of course in the anti-ballistic missile role, it would be advantageous to stay on station awaiting the launch of enemy missiles indefinitely.

Having introduced a range of possible missions for a Low Speed HALE UAV, it is now possible to make intelligent assumptions regarding some of the more basic performance parameters, thereby enabling the conceptual sizing of the aircraft to begin.

Once this process has been begun, several difficulties immediately become obvious. For a well-established mode or regime of flight, any number of common conceptual and preliminary design methodologies could be followed in order to proceed with the initial sizing and comparison of multiple possible configurations. The problem arises with the application of these common methodologies to the very demanding mission requirements of the Low Speed HALE UAV.

It is quickly discovered that there is no parametric data available to these methods with which to begin the sizing. Immediately the literature must be referred to for information on weight fractions. There are no existing aircraft types that have nearly as large a fuel fraction, or as small a structure fraction as that expected from a Low Speed HALE UAV. As the investigation proceeds, it is found that the weight estimation techniques do not apply to aircraft with extremely high aspect ratios and in fact, rarely

apply for aspect ratios higher than 12. Once a gross estimate of the aircraft weight has been obtained, an attempt at a refined drag analysis is normally undertaken. Then it is noticed that there is no information on aerodynamic drag estimation for extremely high aspect ratio wings at low Reynolds numbers. Intuitively, the lift distribution should be close to elliptical in shape, but how close is not known, and there is no method for finding this out available in the common methodologies. It is also intuitively known that a very large proportion of the drag of this aircraft will be due to the wing, but how much? When an attempt at a drag breakdown of the aircraft is made, none of the aircraft types in these methodologies seem to be appropriate for comparison. Surely an aircraft with such a large wing will have a smaller fraction of component drag, but how much smaller for each component?

If the stability of the candidate aircraft is desired, wing downwash angle information at the tailplane (for a conventional configuration) is required, however, there is no information available on the wake of such a high aspect ratio wing. If consideration of any slightly unconventional configurations is desired, limited information on canard configured aircraft is available. Most likely, no information on the class of area ratios required by a HALE UAV and little or no information on the effect of downwash on the main wing by the canard will be found. Similar problems arise if, say, a flying wing or spanloading aircraft configuration is considered. Powerplant performance and cooling at altitude experience a similar absence of necessary literature. After mentioning a limited number of the problems discovered, a nascent understanding of the specific shortcomings of common design methodologies as they apply to Low Speed HALE UAV's should now exist. This understanding provides a footing from which begin an explanation of the aims of this thesis.

The primary aim of this thesis is to provide a flexible, robust methodology for the early conceptual design of Low Speed HALE UAV's. It will be demonstrated that at present, this capability does not exist due to a variety of failings with existing methods. In the process of creating this methodology, a code will be developed in order to enact it and thus facilitate the communication of information to the designer in a clear, coherent, and intuitive manner. This partial automation of the sizing, layout, and analysis of the Low Speed HALE UAV methodology will greatly speed up the conceptual design process and allow for the production of a wealth of comparative Low Speed Sizing data. The underlying theory will be presented where relevant and validated where possible, however

it is noted that the parametric database for this type of aircraft is quite small making a thorough validation of every component of the methodology impossible. Consequently, much of the validation will be performed on the macroscopic results and based on the few known performance and sizing data for these aircraft.

This thesis will begin by providing a sound background on the state of the art in the design of low speed high altitude long endurance aircraft and all of the areas necessary to enable the comparison of multiple potential configurations. It will also highlight the areas in which common methodologies fail and include suggestions from the literature on how to overcome these problems. The next chapter will outline the methodology used. The following chapter describes the preliminary sizing and the theory behind its implementation. The next chapter will involve a detailed description of the specification of the aircraft layout and geometry. The next series of chapters involve the analysis of the designer specified geometry. The subsequent chapter will describe the theory behind the drag estimation, another chapter will describe the theory behind the weight estimation, and another will describe theory behind the calculation and determination of the center of gravity, static margin, and calculation of trim. Then there is a chapter dedicated to the computational implementation of the methodology. Subsequently, a comprehensive discussion regarding the results of applying this data and the resulting performance of the various designs will be included. Finally, there will be a chapter on the conclusions drawn from this work, and any future work that might be undertaken as a consequence of these conclusions or as a consequence of utilizing this methodology.

Before this progression can be begun, a definition of the problem, and an assertion of the state of the art must first be presented.

Chapter II

For once you have tasted flight,

You will walk the earth with your eyes turned skyward;

For there you have been,

And there you long to return

--- Leonardo Da Vinci

No him, no me -- Dizzy Gillespie of Louis Armstrong

2. Review of the Literature

The primary purpose of the introduction was to provide justification for *why* this research was undertaken. To describe what the possible uses for this class of aircraft are, and why the Low Speed High Altitude Long Endurance Unmanned approach is necessary.

The first purpose of this chapter is to define the problem, or *what* this thesis intends to achieve. The main purpose behind this chapter is to demonstrate that sufficient background research was undertaken to ensure that the work in this thesis is original. In addition, that good use was made of the most recent literature available to undertake the formulation of the design methodology. This chapter will outline the present state of the art for Low Speed High Altitude Long Endurance aircraft design, and in the process will highlight the failings of common design methodologies already in wide use for other classes of aircraft. Most importantly, this chapter will provide the foundation from which a Low Speed HALE UAV design methodology can be created.

2.A The Conceptual Design Stage

2.A.1 Conceptual Design Definition

The definition of the problem must be clearly delineated before a solution is attempted. It is first necessary to define Conceptual design as there is often much overlap between the definitions of Conceptual and Preliminary design. Since several differing

definitions exist for exactly what Conceptual design is, the definition that will be followed in this dissertation must be clarified. From Raj[2] , the definition for conceptual design,

> "In this stage, the task is to conceive solution concepts, typically represented by sketches that can functionally meet the design requirements, such as range, payload, takeoff and landing distances, etc., as dictated by the intended mission. A good sketch includes the approximate wing and tail geometry, fuselage shape, engine location, etc. This information can be used to estimate performance and weight fractions by comparison to previous designs..A sizing process uses these estimates to determine the required total weight and fuel weight to perform the mission. The first order sizing provides the necessary information to develop an initial layout with more details such as landing gear, inlet ducts, cockpit, major avionics, etc. to ensure that everything fits.
>
> The initial layout is analyzed to refine the first set of estimates of aerodynamics, weights, and installed propulsion characteristics. Performance capabilities are calculated compared with design requirements. Optimization techniques may be used to determine the lightest or lowest cost aircraft to meet the mission. The results of these trade-off studies are used to revise the initial layout.
>
> The process is repeated many times, and for several competing concepts depending upon the available resources, in attempts to devise an optimal solution. Functional specialists periodically review the design to ensure its soundness from their perspective. The resulting layout is then ready for preliminary design."

Raj then continues with broad definitions for synthesis and analysis. He states that Synthesis covers defining, refining, and altering concepts and configurations. Analysis encompasses methods, tools, and expertise to produce data and the use of this data in evaluating competing concepts and configurations.

Regarding the differences between Raj's definition of Conceptual design and the definition used in this thesis, this methodology will not perform a detailed *first order* sizing. Optimization techniques will not be used, although it would not be difficult for someone skilled in optimization to utilize the methodology for optimization due to the consistent modularity of the implementation of the methodology. The number of iterations possible for any given concept will also be limited by the time available and obvious limitations in manpower ! Finally, due to the fact that functional specialists were not available for consultation due to the nature of the thesis and degree, that aspect of the Conceptual design process will be included to the extent covered by the research.

Thus, it is by these definitions that a Conceptual Design Synthesis and Analysis methodology and corresponding computer code were created. This code will be used as a tool in providing results for the comparison of several possible configurations to satisfy the Low Speed High Altitude Long Endurance Unmanned Aircraft role. Exactly *how* this

is achieved will be covered in detail in a subsequent chapter. First it is necessary to describe the background research that forms the foundation for the methodology.

2.A.2 Existing Methodologies

It is fundamental to this thesis that existing methodologies are wholly inadequate for the design of Low Speed HALE UAV's. Several common conceptual design methodologies exist already[3, 4, 5, 6, 7]. All of these methodologies fail in the high altitude regime, in the low speed (low Reynolds number) regime, and for the unmanned aircraft type.

There have been a few papers published on related areas in Conceptual design. Smrcek[8] described a potential methodology for use in the Conceptual/Aerodynamic design of motorgliders. The majority of this paper was concerned with the aerodynamic design, and with the process of teaching design for University level course-work. It did include a drawing of the detailed methodology, however no detail was provided as to how any of the shortcomings of common methodologies were overcome, with the exception of the aerodynamics, which took a simplified approach compared to the one used in this thesis.

There is an excellent book by Thomas[9] on the design of gliders and sailplanes. Unfortunately, gliders are designed to a completely different set of specifications. Despite the outward similarities in their appearance, glider design is driven by a mostly unrelated set of performance requirements. Despite these differences, the glider is the closest relative of the Low Speed HALE aircraft with any detailed information available. These differences will be discussed in detail in a subsequent section.

Jaxa-Malachowski[10] outlines the iterative process used in the conceptual and preliminary design of UAV's in general. The difference between this class of aircraft (general, UAV design) and Low Speed HALE UAV's is quite clear, and the paper doesn't outline any of the design characteristics specific to UAV's. There is no mention of structural or fractional weights due to the absence of an onboard pilot, or of the weights of control systems and actuators. In fact, there is precious little detail, and the paper is written strictly to outline the methodology similar to that of Smrcek.

A few published attempts have been made to create design methodologies specifically for HALE aircraft. These attempts have been computational in nature and discussion on

their merits will be included in a subsequent section. The remaining possible approaches are limited primarily to existing methodologies to design a Low Speed HALE UAV. This approach, however, is replete with difficulties.

2.A.3 Problem with Existing Methodologies

In general, design methods found in the literature are based on data from existing aircraft types[16]. Inherently, these methods pertain to aircraft technology which is at least 10 years old and more often 20 years old and older. The robustness of any of these methodologies is built in with regards to the means by which newer information or methods can be integrated or substituted at any point in the process manually. Computational methodologies in general, in the past were not afforded this luxury. It is therefore safe to say that most of the information in current computational methodologies is older than 10 years.

With the cost and complexity of present generation designs increasing exponentially over previous generations, a new approach is necessary if there is to be a sustainable aerospace industry in the future. Advances in aircraft design have been achieved using traditional design practices, however, the deficiencies of these practices makes them unsuitable for meeting tomorrow's challenges. Traditional design practices are not conducive to reducing time and risk while improving quality, and utility. One of the major deficiencies of the traditional design approach is long cycle time due to its ***sequential*** nature. For modern airplanes, completing a design cycle using the sequential process can take a very long time. As a result the number of cycles that can be completed to explore a wide spectrum of alternatives within schedule and cost is quite confined.

As manufacturers move towards the Concurrent Engineering concept, and begin to implement the Integrated Product and Process Development (IPPD) approach, certain elements are necessary for the success of this design paradigm. The following 3 attributes are excerpted from Raj[2] in his discussion of effective implementation of an IPPD design environment:

- Integrated design and analysis tools using digital product model to capture and refine product and process design data.
- Integrated design automation tools to streamline the design process and assure understanding of design intent.

- Extensive use of Physics-based analysis methods and simulation tools for improved product performance with fewer design/build/test iterations.

Each of these statements supports the need for a more efficient and complete way to compare the relative merits of different designs, in addition to utilizing more efficient/effective methods to improve on initial design concepts. This leads us to a brief survey of the existing computational conceptual design methodologies, and the discussion on the specific shortcomings of present methodologies will be presented in another section.

2.A.4 Existing Computational Methodologies

Many computational conceptual/preliminary design methodologies exist[11, 12], but these are all strongly based on the common conceptual design methodology textbooks which fail in the aforementioned areas which will be detailed later. An excellent example can be found in Roskam[12] from a comment made regarding his Design, Analysis and Research (DAR) program in wide use : "*Currently time does not permit the evaluation of innovative configurational design approaches*". His code was written and specifically funded for application to general aviation aircraft, though the code he has marketed is capable of a wider range of aircraft types, it is still not capable of handling the majority of configurations addressed in the methodology presented in this thesis.

A couple of HALE UAV computational design methodologies have been produced. These have either been proprietary and not available for general use outside of the companies they were developed by[13], or they were written in the FORTRAN programming language for use at higher flight speeds (turbojet)[14] and encompassed more preliminary design considerations with the choice of configuration severely limited.

In addition, all design programs written in FORTRAN restrict the user in many ways. Firstly, the user is quite limited in how the design process is iterated (linearly/sequentially), which results in the designer being further removed from the design process. Secondly, in order to receive graphical feedback on results of the various stages of execution of the program, the user must exit the FORTRAN program, and use another code to visualize the resulting output. This takes time, and when numerous different configurations must be compared, it is rudimentary and unnecessary by today's computing standards.

A few papers have been written on the topic of computational aircraft design methodologies in general and their characteristics and the difficulties in writing and maintaining them. An aircraft design synthesis program developed by Boeing for Hypersonic Aircraft design. "HOLIST[15]" was written using FORTRAN and C and was based on a UNIX platform. This project was immense and involved the linking of several extremely complex modules coupling flight controls and aerodynamics. Neither of these modules would be appropriate for Low Speed HALE aircraft, however the difficulties mentioned paralleled those experienced in this thesis.

Bil[16] describes ADAS, a system that was being developed by Delft University of Technology. The ADAS program includes optimization and other attributes that would classify it as a preliminary design tool by the definitions used in this thesis.

Kroo[17] discusses in detail the problems of maintaining data integrity in systems with thousands of variables. He also outlines a few possible classifications for methods of approaching the problem of aircraft design within the computational framework. Kroo also uses optimization in his solution, but describes a non-procedural architecture (nonlinear, non-sequential, object oriented approach) and the necessity for such an approach for modeling the conceptual design process. None of these programs have the ability to design Low Speed HALE UAV's since they both need to be developed and integrated with existing design methodologies, which, as will be shown, do not have the capacity to deal with the design problems inherent in Low Speed HALE UAV designs.

2.B Difficulties with Discretizing the Conceptual Design Process

Conceptual and preliminary design is a creative and heuristic process, which is not easily adaptable to the formalized structure required by the computer. One of the more difficult tasks to achieve is modeling the paths taken by the human mind and the number of infinite possible directions it can take when given a complex problem to solve. While the tools available to solve the problem are quite often identical, or at the very least, quite similar, the final solution to the same problem is often quite different. An excellent example of this would be the different evolution of rocket propulsion technology between the United States and the former Soviet space programs.

In the past, traditional design synthesis codes could not balance the amount of human interaction and input into the design process with the degree of automation and automated analysis. Quite often, designers would find many of the more relevant decisions being made for them, and in a hidden manner. This removes the designer from a very important part of the design process, as they are unaware of the path taken to the solution. This path is often more important than the solution itself.

One of the biggest reasons for the solution method being hidden, however inadvertently, was FORTRAN, the most common programming language used by the engineer. FORTRAN is a powerful and fast mathematical language, and is able to emulate all of the basic computational constructs. Nonetheless, to use compulsory modern non-sequential/object oriented programming practices, as well as more complex data structures that allow for the implementation of data validation, the engineer ***MUST*** utilize another programming language. Without these programming practices, software such as CATIA and data visualization of fluid dynamics and structures codes (such as Fluent and NASTRAN) would be impossible.

In FORTRAN, visual feedback of relevant design parameters and how they relate can only be achieved by outputting the data from the FORTRAN program. This data must be subsequently input into a data visualization program (such as Microsoft Excel) or data post-processor specifically designed for a given software package (Fluent, NASTRAN, where the post-processor is always written in another language). Additionally, the physical layout of a specific aircraft and how it might compare to that of another potential design are all left to the user's imagination, due to FORTRAN's inability to provide graphical feedback. An important part of the design process has been removed, that is, does a design "look" right. Apart from executing a code on several different computers, FORTRAN has no facility for comparing several different designs and viewing their relevant performance and geometrical parameters side by side in real time. If FORTRAN is used, this must be done when all solutions have been compiled manually, or printed out, all methods that cost time.

Each of these factors taken alone may not seem terribly inconvenient. Yet, when 200 design concepts are being compared, each with a rather subtle difference, the ability to visualize and immediately compare concepts on their relative merits is not only convenient, but in light of the present day competitive environment, indispensable.

Once another programming language is selected that allows for more flexibility and process control, several new problems arise. Kroo[17] encountered these problems and others associated with creating computational design synthesis programs. He states that aircraft synthesis programs are well known for their complexity and corresponding difficulty with documentation and maintenance. Large computer codes with data shared among hundreds of subroutines are not only difficult to understand, but are not easily modified or extended. Such capabilities are especially important in the multidisciplinary evaluation of new technology or new design concepts.

A logical extension from the need for a more structured programming language and a more structured approach to the computational modeling of the aircraft design process, has led to the development of "loosely coupled" systems of analysis routines, managed by executive routines. Several examples of such systems have been described in the literature. The present method employed by Kroo, consists of a large number of procedural routines, executed, when required, by an executive system. The structure of the Conceptual design synthesis code written for this thesis is quite similar.

The primary difference here, between FORTRAN and the programming method used, is that with FORTRAN, all of the decision paths are hardwired at compile time. It is not possible to follow a path that has not been pre-defined. This greatly reduces run-time flexibility, however greatly reduces the workload on the programmer in terms of verifying and validating potential program paths. With modern object-oriented languages, the paths taken are not necessarily all pre-determined at compile time, and can in fact be changed and manipulated in run-time.

Kroo continues by outlining the approach to solving the design problem by describing the method of approach. He calls the first critical concept the Quasi-Procedural Concept. The Quasi-Procedural Concept is the basic architecture used and is a form of non-procedural programming. Unlike conventional (FORTRAN) codes in which computation proceeds from given inputs to outputs with a rigid structure, non-procedural systems are free to organize computations so as to produce the required results in an efficient way. However, programmers can often generate more efficient, short procedural routines and many are widely used. It is the complex interconnections among these routines that are difficult to manage. Unlike non-procedural programs that deal with relationships among data on a line-by-line basis, the present approach deals with compiled, procedural subroutines as the smallest program unit.

The second critical concept he denotes as Nonlinear Analysis Structures. A Nonlinear Analysis Structure is where computations requiring iteration include sets of analysis modules for which the output of a routine is required as the input for another routine and output from the second routine is needed as an input to the first routine. Such situations arise frequently in aircraft synthesis problems and lead to difficulties in the generation of computational paths. The one solution to this problem is to recognize such situations and automatically perform the iteration. This of course results in complex logical constructs and decision trees.

An alternative method is to recognize iteration loops, but to not iterate on them. Instead a new design variable is introduced that represents the input guess for the iterated variable. Consequently, every time a program variable is input, the program inputs and outputs must be examined carefully to ensure that no further calculation or iteration must be done somewhere upstream of where the program variable was input. The simple task of examining the program inputs and outputs is a difficult one when the parameters number in the thousands.

One approach uses an object-oriented description of the problem. A strict, hierarchical description appears to work very well in the description of aircraft geometry, but this constitutes a small fraction of the parameters used in the synthesis process. The connections between parameters can be very convoluted (e.g. payload location effects cg , which effects tail moment arm, which effects trim drag and tail sizing, which ultimately effects endurance).

Finally, once the technique for discretizing the Conceptual Design process is selected, you must decide how much control you are going to allow the user to enjoy. Bil[16] outlines 3 possible approaches to drive the optimization process and control the search strategy. They are:

- *Traditional Design Approach:* The designer selects and modifies design parameters primarily on the basis of intuition and experience. In principle, only little use is made of computer codes.

- *Parametric Survey or Explicit Optimization:* A range of design configurations are systematically analyzed. An optimum design point can be selected from a graphical representation of the results. This approach is particularly useful for sensitivity analysis and trade-off studies.

- *Multivariate or Implicit Optimization:* The search strategy is controlled by an optimization algorithm. With this technique, many design parameters can be optimized, but only one design point obtained.

In the extreme, the first approach makes little use of the computer, and draws almost exclusively on the experience of the aircraft designer, providing little help beyond automating monotonous calculations. The last approach essentially removes any intuition the aircraft designer might have, and greatly restricts the amount of robustness and flexibility the method could have. It essentially removes the designer from the execution of the program.

Again, the programmer is faced with a difficult decision in how to implement the methodology. For the purposes of this thesis, the *Parametric Survey or Explicit Optimization* approach will be used. Based on the arguments for the need for expedience and graphical feedback in the modern aircraft design process, the *Traditional Design Approach* has been discarded. This approach was nevertheless used for the validation of the resulting methodology when possible.

Based on a personal belief that the designer should always be kept in the loop as much as possible, and the experience of the designer should always be included if available, the *Multivariate or Implicit Optimization* approach was not considered. In addition, this approach removes the designer from the problem to the extent that the fundamental understanding of the variation of the driving parameters of the design with changes in the relevant design variables can be compromised. This approach is quite useful once the problem is well understood, and an existing design is being refined. Though, in the early stages of comparison of the relative merits of multiple potential configurations this approach is considered inadequate. With the general background discussion of computational and traditional methodologies complete, the detailed problems with existing methodologies can now be addressed.

2.C Explicit Shortcomings of Existing Methodologies

Assuming certain basic configuration and performance related constants are available, have been specified in the mission requirements, or can be approximated for the

design of the aircraft based on the selected mission, an initial sizing of the aircraft can begin.

One of the first encounters with the failure of common design methodologies is in the specification of the wing design. In the scope of the design of this type of aircraft, this is a major failure since up to 70% of the total air vehicle drag is generated by the wing *lift* alone[18,19,20]. This will be the first discrepancy found in all of the common methodologies considered, but many others will be discussed as well. These include the weight estimation and structure, powerplant selection and performance, tail sizing and stability, design of alternative configurations, and cooling drag estimation.

2.C.1 Wing Design

This is the first major area in which the common methodologies fail, there are many areas within the wing design in which the common methodologies fail.

- Low Reynolds number drag estimation techniques are absent
- Wing profile design and specification can't be performed within one of these methodologies
- No possibility for direct inclusion of the above information
- Three-dimensional lift and drag data are nonexistent for aircraft with Aspect Ratios greater than approximately 22 and rare for aircraft with Aspect Ratios above 12
- Aerodynamic center for wings and wing-body combinations are also unavailable[21]
- Wing downwash angle and downwash angle rate variation with angle of attack are also unavailable.

These are just the major shortcomings, but many others exist. The first section begins with an evaluation of available information on low Reynolds number airfoils.

2.C.1.a Low Reynolds Number Wing Profile Data

In recent years a substantial amount of research has been done on low Reynolds number airfoil design. Typical cruise Reynolds numbers for this class of aircraft are in the region of half a million and below. This is well above the Micro UAV class of vehicle, but well below common General Aviation cruise Reynolds numbers and does not fit well with glider or sailplane operations.

The challenge in low Reynolds number airfoil design is to prevent laminar separation (to maintain low airfoil drag) without restricting the maximum lift coefficients attainable for the airfoil, in order to obtain high section lift to drag ratios. For a front loaded airfoil, the gentle adverse pressure gradient requirement puts a restriction on the allowable minimum pressure peak, which in turn limits the maximum lift coefficients attainable.

Evangelista and Pfenninger[22] proposed a 10% thick airfoil designed to have high lift to drag ratios at lift coefficients close to 1.0 in low Reynolds number flow (100,000 < Re < 300,000). Their design approach maintains low airfoil drag without severely restricting the lifting potential of the airfoil.

One of the best low Reynolds number airfoil sources is the book created by Donovan and Selig[23]. They essentially compiled a textbook from airfoil shapes by Eppler, Wortmann, Miley, NACA, and shapes that were sent to them by model airplane builders across the world, and then proceeded to test them (62 airfoil sections) in the Low Speed Wind Tunnel at Princeton University. Since many of the shapes were from model airplanes, the design Reynolds numbers were in the region of interest for Low Speed HALE UAV's in cruise. In the process of compiling the book many interesting observations were made with respect to low Reynolds number airfoil design. These observations were too many to mention and relate directly to airfoil design, however if any detailed low Reynolds airfoil design improvements are to be made, this book or their web site at the University of Illinois is an excellent starting point.

In 1987, Maughmer and Somers[24] presented an airfoil design for a High Altitude Long Endurance Remotely Piloted Vehicle. They mention that the preliminary design and sizing of a HALE RPV is complicated by the fact that data regarding suitable airfoils are limited. This is due to the fact that such vehicles, unlike those for which the majority of airfoils have been developed in the past, operate at fairly high lift coefficients and at relatively low Reynolds numbers.

In discussing the aerodynamic efficiency of gliding vehicles in 1994, Hermanspann[25] states that today's airfoils can provide laminar flow over 80% (lower wing surfaces) at Reynolds numbers of one million. McGhee and Walker[26] provide good experimentally obtained pressure distribution, lift, and drag data for low Reynolds number airfoils. Boermans and Timmer[27] present the results of experimental investigations on two low Reynolds number airfoils under a variety of modifications such as turbulators, strips, zig-

zag tape and bumps. If detailed design were going to be undertaken, this approach might prove useful in lowering drag.

In addition to strictly aerodynamic considerations for low Reynolds number airfoils, there are several less obvious constraints on a wing profile design. Given the long endurance constraint, an extremely high aspect ratio wing is expected and a huge amount of fuel would also be expected. Vitali and Tsach[28] in designing the Israeli Aircraft Industry's medium altitude long endurance UAV, Heron, found that a high wing thickness ratio was the best combination for structural rigidity and increased volume for internal fuel.

The papers and books discussed above only begin to detail the recent work done on low Reynolds number wing profile aerodynamics. Several international conferences were also held and their proceedings may be easily obtained, however the Reynolds number tends to be too high for Low Speed HALE UAV's. Of all of the areas stated in which modern design methodologies fail, this would be the easiest to remedy. There is a wealth of information available in several aspects of low Reynolds number airfoil design. Any modern HALE UAV methodology would have to be robust enough to not only allow for the inclusion of this data, but to allow for the inclusion of future work. Finally, there has been much work done in the advancement of computational techniques for low Reynolds number airfoil design. A few of these methods will be mentioned in the next section.

2.C.1.b Computational Airfoil Profile Drag Solutions

Mark Drela[29] from The Massachusetts Institute of Technology wrote a low Reynolds number airfoil program called XFOIL. In his paper he discusses the underlying theory behind the computational method. There is some allotment in the code to solve for laminar separation bubbles. For validation, his method compared quite favorably to experimental results obtained for the Eppler 387 at low Reynolds numbers.

Referring back to the previously mentioned Donovan and Selig[23] paper, they compared their experimental results to two different computational codes. The Eppler and Somers code formulates the design problem in such a way that allows quick and easy manipulation of the airfoil shape. With a minimum number of parameters, almost any desired velocity distribution can be obtained. However, they found that this code did not accurately predict the performance of airfoils in the Reynolds number range considered in their work,

which consequently is the Reynolds number regime of interest for Low Speed HALE UAV's.

They did discover in their investigation, however, that the Drela - ISES code predicted airfoil performance more accurately over the Reynolds number range of interest.

Liebeck[30] also used the ISES code to create various low Reynolds number airfoils with varying thickness ratios and degrees of aft loading. Verification of the computational procedure was performed on some existing low Reynolds number airfoils and some other airfoils created at Douglas aircraft and the results compared favorably to experimental data where available.

Richard Eppler[31] was renowned for his low speed airfoil design. He published many papers subsequent to his book of low speed profiles. In 1994 he published the results of three different airfoils with only one using flaps and were compared on their relative lift to drag ratio properties with the E688 triumphing. Drag polars were computed by means of the Eppler-Somers Low Reynolds number profile drag code.

Similar to Selig and Donovan but not as comprehensive, Evangelista and McGhee[32] compared the two computational airfoil analysis methods, the Eppler-Somers code and ISES, the Drela-Giles code. Calculations were performed for Reynolds numbers between 60,000 and 460,000. Experimental results were also included. The basic conclusions from this analysis were the same as those of Selig and Donovan. When a laminar separation bubble is present the Eppler-Somers code breaks down, and the Drela-Giles code correctly predicts the drag.

2.C.1.c Wing Planform Design

In the design of the wing planform geometry, there are a limited number of design variables to choose from. The primary design variables of interest are aspect ratio, taper, and sweep. A historical survey of Aspect Ratio in sailplanes is presented in Figure 2.1. The data for this diagram was taken from Hermanspann[25].

This diagram makes several interesting points about trends in the aspect ratio of sailplanes. It would appear that for the Standard/15 meter class sailplane, that an ideal aspect ratio for the span has been reached. You can see from the unlimited class, though, that there is a definite nearly linear trend towards the highest aspect ratio attainable. This

has direct implications on the expected planform of a Low Speed HALE UAV. With the exception of hang gliders, none of the wings were swept.

In the Low Speed HALE UAV application, there is little aerodynamic justification for using anything but very moderate sweep, as compressibility effects are expected to be quite small even at altitude with a cruise velocity in the range of 0.3 to 0.4 Mach. Therefore, if sweep is to be considered, it will be exclusively to satisfy difficulties with a given configuration.

Theory states that the wing planform with the elliptical shape will have the minimum lift induced drag. In practice it is quite costly to build an elliptical planform. The next option is to approximate the elliptical shape using taper.

With regards to taper, much of the aerodynamic theory was developed rather early in the history of modern aeronautics. Glauert[33,34,35] published much of this original theory in the early 1920's. These papers dealt with the theory behind lift and drag coefficients, and also developed the theory for calculating lift induced drag on a rectangular wing. This was later extended to include theoretical prediction of lift induced drag for straight tapered wings with the assumption of an elliptical lift distribution.

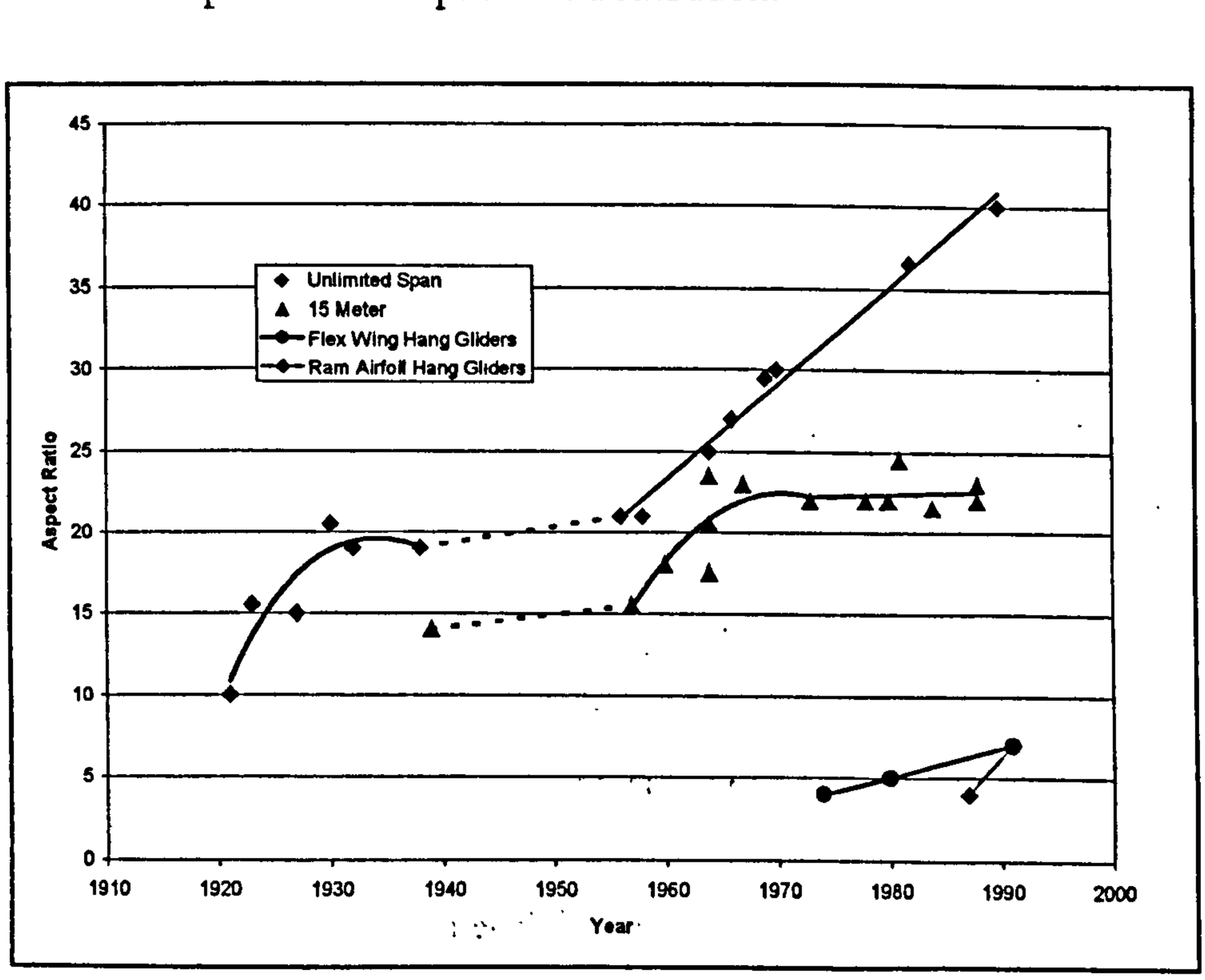

Figure 2.1 ***This figure shows the historical trend in the aspect ratio of sailplanes.***

More recently, Traub[36] derived a method for the analytical prediction of vortex induced drag for tapered high aspect ratio wings. Again, this method is limited in its application as it assumes an elliptical lift distribution. This is the extent to which the theory can be applied to the solution of induced drag prediction without invoking the use of a computer. Unfortunately, there haven't been any published data regarding experimental validation of the shape of lift distributions on extremely high aspect ratio wings. In the absence of experimental data there is no way to verify the assumption of an elliptical lift distribution apart from the implementation of numerical methods. Intuition would lead to the same assumption as the Prandtl "infinite wing" case, but strangely enough, this has never been experimentally verified in the literature. It should be noted that there is a wealth of data for much lower aspect ratio wings. However, any extrapolation of this data would be impossible due to incompatible sweep, Mach number, or aspect ratios so much lower than those considered in this thesis the extrapolation would be suspect.

Boermans, Waibel[37] performed a planform optimization procedure applied to the design of standard class gliders. Their analysis was based on Lifting Line theory assuming linear section lift data with a spanwise distribution of circulation expressed in terms of Fourier series. They found that at equal tip taper, the difference in induced drag between double and triple taper wings was negligible.

In addition, they discovered that the most effective way to improve wing performance at higher lift coefficients is to increase the aspect ratio. Also from the aerodynamic study of sailplanes, Marsden[38] found that the relative importance of induced drag is not reduced by very high aspect ratio. This means that regardless of the mission segment, the total percentage of induced drag will remain at approximately 70% of total aircraft drag. Again, this has direct implications on the design of a Low Speed HALE UAV planform.

Eppler[31] observed that the mean aerodynamic chord of the wings of modern sailplanes varies little on average with span. This means that regardless of the taper and different classes of sailplane, the average chord remains the same. Furthermore, he verified that the performance improvement due to increasing span was higher at low spans than at high spans.

It should be noted, once again, that even sailplane aspect ratios are lower on average than those considered for HALE UAV's. The general trends of the above sailplane results should, however, be applicable to HALE UAV's.

2.C.1.d Computational Lift Induced Drag Prediction

Given the lack of appropriate high aspect ratio wing data, another solution method had to be found for the low speed low Reynolds number cruise environment of the HALE UAV. There is a large body of data available on suitable computational methods.

As mentioned in the previous section, the theory for such methods was developed long before the modern computer. As the modern computer was evolving, several extensions to the original theory were developed to handle some of the more difficult aspects of fluid flow to predict such as unsteady flow and turbulent separation. Neither of these complications is necessary for the Low Speed HALE UAV in cruise, thus simplifying its application. In addition, for the early Conceptual design phase in which multiple configurations are compared, complex and time consuming Computational Fluid Dynamic (CFD) solutions are not practical or even reasonable.

This leaves various Vortex methods. For a comprehensive textbook on the subject, Katz and Plotkin[39] cover all of the background theory in detail. A brief discussion of the theory and its implementation used for this thesis are included in Chapter VI, Section 3.

For the aerodynamic design of a motor-glider, Smrcek[8] investigated several methods for lift induced drag estimation. The methods studied were generally in the form of either a stand alone equation giving lift coefficients as a function of aspect ratio, used graphical parameters variously derived from Prandtl's Lifting Line theory, or were empirical.

More specifically, he evaluated Lowry and Polham's method which gives the wing lift curve slope. Roskam provides a source of semi-empirical expressions supplemented with graphical relations for calculation of a range of aerodynamic derivatives, including lift curve slope and variation of drag coefficient with angle of attack. He also evaluated Schrenk's approximation which gives the distribution of additional lift coefficient over the semi-span. And finally, he evaluated Prandtl's Classical Lifting Line Theory which develops lift and drag characteristics from a purely theoretical fluid dynamical model of the finite wing.

Smrcek decided to assess the wing characteristics from first principles using Prandtl's lifting line model since the theory provides a comprehensive source of wing aerodynamic data pertinent to the aircraft design process with comparable accuracy to most semi-empirical methods available. The values for the lift curve slope, obtained using a computer program based on the Prandtl Lifting Line Theory and the method of Lowry and Polhams

were found to be within 1% of each other. He concluded that the method of Schrenk, Lowry and Polhams, and the Prandtl lifting line theory with three ordinates were equally satisfactory for estimation of the lift curve slope and lift distribution at the preliminary design stage.

Guglieri and Quagliotti[40] performed the evaluation of wing characteristics as a function of design parameters by means of the Weissinger[41] method. The Weissinger method is an extension of lifting line theory which is able to evaluate the effects of sweep in incompressible flow with acceptable precision, when a comparison is made with other methodologies. They concur that there are other computational methods that are obviously much more advanced, but they are generally quite time consuming.

The vortex method used for this thesis is slightly more advanced than the Weissinger extension to the Prandtl Lifting Line theory. It utilizes discrete vortex rings, which make up single panels. These panels are then combined to model the shape of the lifting surface being used. It is generally considered to be more accurate than either the Weissinger or Lifting Line methods and does not rely on the small sweep angle approximation inherent in the aforementioned methods.

Finally, in a paper by Owens[42], he warns that including nonlinear aerodynamics during the conceptual design phase for complex shapes using a Vortex based method is not a reasonable approach. It should be stated that the Vortex method used in this thesis makes no attempt at lift induced drag prediction in any phase of flight outside of cruise or climb. The shapes of the planforms considered were (for the purposes of induced drag prediction) simple straight tapered wing planforms.

2.C.1.e Aerodynamic Efficiency

One of the more commonly used measures of aerodynamic efficiency is the ratio of lift to drag (L/D). L/D ratios are frequently quoted in discussing the performance of gliders. In two dimensional space, a fixed velocity, wing area, and air density, this ratio is the same as the ratio of lift coefficient (C_L) to drag coefficient (C_D). A related ratio, $\frac{C_L^{3/2}}{C_D}$ is *extremely* important with respect to HALE UAV's. Its importance to the endurance of the aircraft can be seen in the Breguet equation for the endurance of propeller driven aircraft below :

$$\text{Endurance (hours)} = \frac{550\eta_p}{SFC}\frac{C_L^{3/2}}{C_D}\sqrt{\frac{2\rho_{SL}S_{ref}}{W_{to}}}\sqrt{\frac{\rho_{cruise}}{\rho_{SL}}}\left(\sqrt{\frac{W_{to}}{W_{to}-W_{fuel}}}-1\right) \qquad \textbf{(2.1)}$$

The $\frac{C_L^{3/2}}{C_D}$ term is in direct proportion with the endurance of the aircraft (the other terms and their importance will be discussed in a later chapter). Thus, for any improvement in aerodynamic efficiency, the endurance benefits directly.

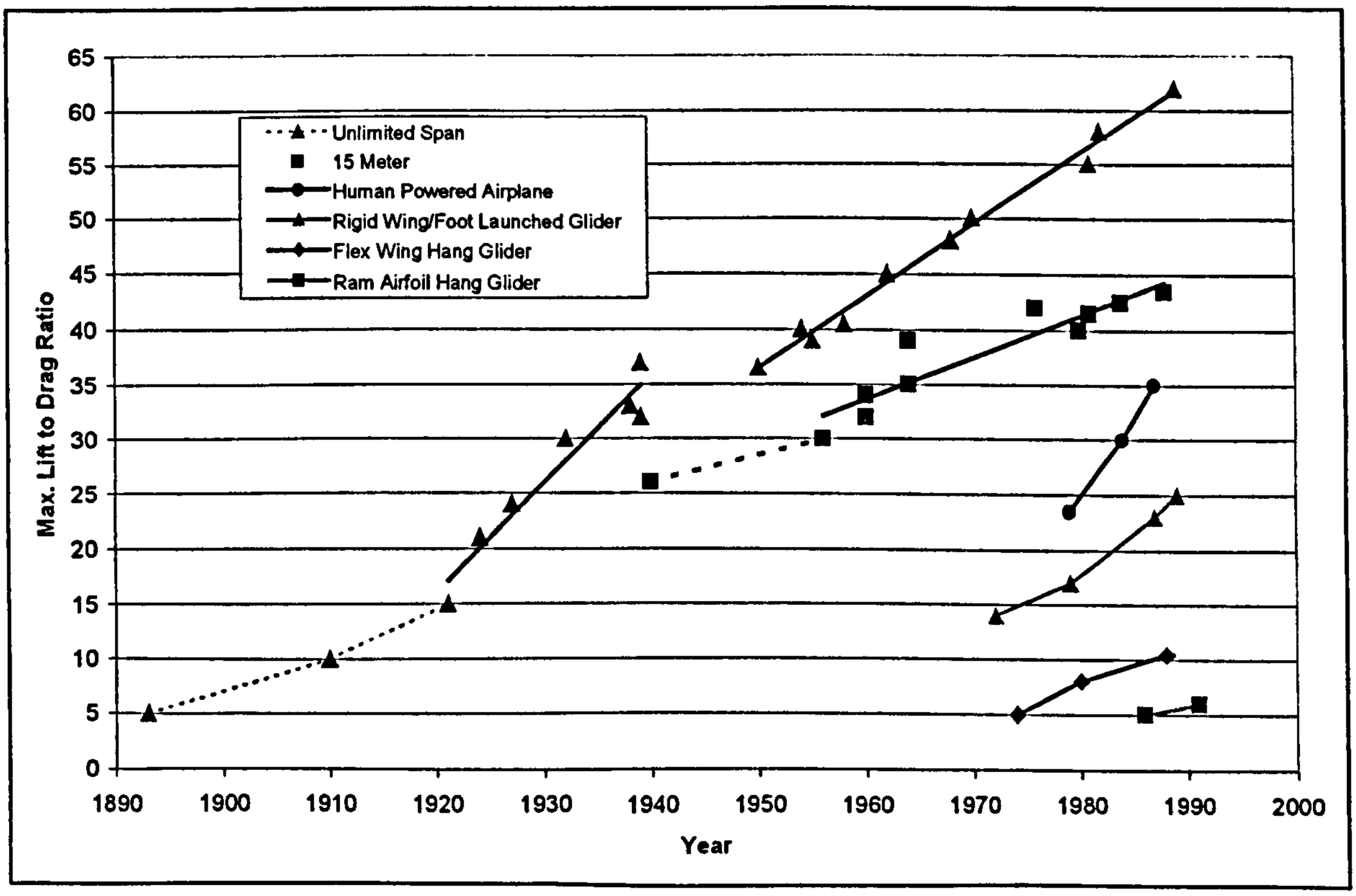

Figure 2.2 ***shows the historical trends in maximum lift to drag ratio (Hermanspann[25]).***

Mueller and Heuermann[43] discuss the recent history of L/D ratios in high performance gliders. In 1972 the SB10, 2 seater with 26m/29m span and aspect ratio (AR) of 36 had an L/D = 53. In 1981, with a 24.5m span, AR of almost 40, L/D's of 57 were obtained. Fred Thomas[44] (aerodynamic designer of the Grob *Strato 2C* HALE wing) states that L/D ratios of over 60 have recently been achieved.

Strojnik[45] agrees with the statement that a best glide ratio L/D approximately equal to 35 is poor for a 15m sailplane by today's standards. Hermanspann[25] includes several figures of interest. In his paper, he outlines a procedure for determining the Maximum L/D potential based upon three key performance parameters: Aspect Ratio, wetted area

ratio, A_{wet} / S_{ref}, where A_{wet} is the total aircraft wetted area, S_{ref} is the reference wing planform area., and extent of laminar flow $\left(x\sqrt{c}\right)$ where x is the chordwise location and c is the length of the chord. The wetted area ratio, the ratio of the exposed surface to wing area, would ideally only represent upper and lower wing surface. Conventional configurations requiring tail surfaces and a body (with wetted area ratios of 2.5 to 3) determine current $\left(\frac{L}{D}\right)_{max}$ potential. To provide an idea of the aerodynamic efficiency of some HALE aircraft, and compare them to some better known aircraft, Figure 2.2 shows the development/evolution of the maximum lift to drag ratio. It is easy to identify several linear trends in the 15 meter and unlimited categories. Figure 2.3 shows the evolution of aerodynamic efficiency for a number of different types of aircraft. The HALE aircraft included seem to be less efficient than most modern sailplanes.

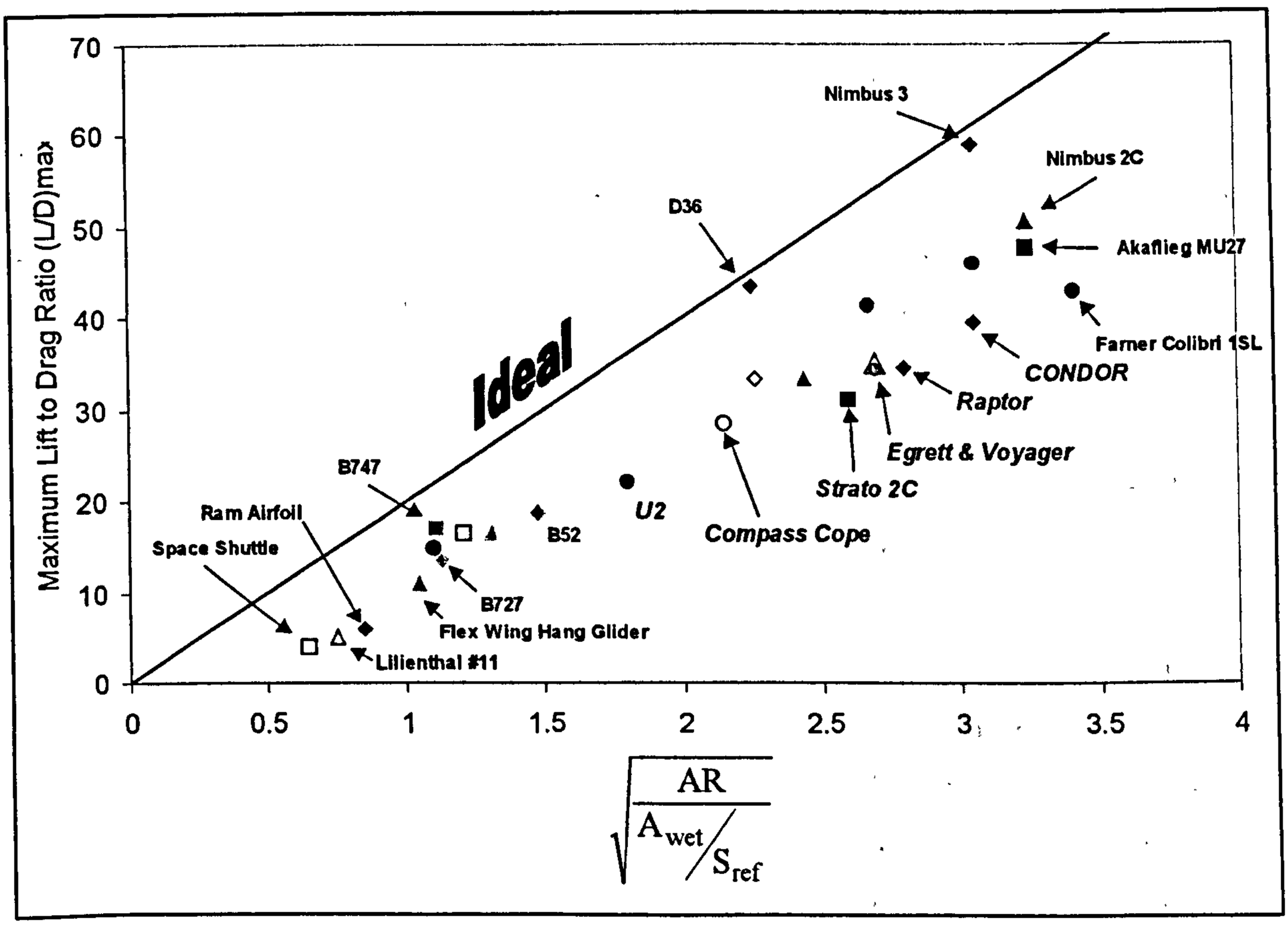

Figure 2.3 ***shows the maximum possible aerodynamic efficiency and how several aircraft compare (From Hermanspann[25] with modifications).***

These results and figures all provide a good concept of the state of the art in low speed aerodynamic design. None of the existing methodologies are able to incorporate the

advancements in aerodynamic efficiency of modern sailplane design. Another area in which drag savings can be achieved, but has received little attention in common methodologies is trim drag.

2.C.1.f Trim Drag

A great deal of work has been done in the area of trim drag, most of which has been ignored by the commonly used methodologies. Even though the total aircraft drag is largely due to the main wing, a substantial drag *saving* can be realized by implementing a few trim drag reduction design concepts arising from some recent observations. Furthermore, since a HALE UAV will require actuators and an automated flight control system, the idea of a longitudinally statically unstable platform does not increase the complexity of the aircraft substantially.

It is important, in order to minimize the trim drag for the Low Speed HALE UAV to take into consideration the airfoil moment coefficient when selecting a Low Speed airfoil. It is exceptionally important due to the fact that most Low Speed airfoils have very high zero lift moment coefficients. This will have bearing on the trim drag if this moment is not balanced by other means within the aircraft.

From Lutze[50] typically, a reduction in wing-body or tail profile drag directly reduces the trimmed drag, and considerable efforts are made in this direction in aircraft design. Additional reductions, although small (1-5%) can be made by paying careful attention to the lift distribution between the wing-body and the tail surfaces (maintaining zero pitching moment) so as to obtain proper tradeoffs in induced drag which minimize overall drag. Along these lines, Sachs[51] showed that the minimum trimmed drag is reduced when tail span is increased.

Laitone[46] showed that aircraft can have their maximum weight to drag ratio (W/D) occur when the tail load is slightly positive (upward tail lift). This would correspond to the minimum trimmed drag for modern conventional aircraft with an aft tail, except for the unfortunate fact that they do not have sufficient tail volume to permit the rearward center of gravity (cg) location. This rearward cg location would produce an upload on the tail and still maintain static longitudinal stability. Prior to World War II most aircraft were designed to cruise with either zero or slightly positive tail loads, but since then the design trend has been toward tail downloads at nearly all flight speeds.

An even greater tail upload is required for minimum aircraft drag when the usual aerodynamic interference between the fuselage, wing and tail are included. The physical explanation for why a tail upload produces less induced drag than a zero tail load is due to the reduced induced drag on the wing. In addition, the wing's lift vector is rotated forward due to the circulation vortex system produced by an upload on the tail that is not in the plane of the wing. These two effects are sufficient to overcome the additional induced drag on the tail, and rearward rotation of the tail lift vector.

Kroo[47] made several interesting observations in a paper concerned with trim drag, tail sizing and soaring performance. He found that large tail arms, small center of gravity ranges, and low speed operation make a sailplane's drag penalty due to trim lower than almost any other aircraft type. It should be noted that a similarly designed Low Speed HALE UAV is certainly possible.

He ultimately found that the tail's profile drag produces the greatest influence on total drag. With 10% of the area of the wing, a horizontal tail typically contributes 7% of a high performance sailplane's total flat plate drag area. The penalty due to the trim requirement increases with speed, primarily because of the increasing importance of parasite drag at high speeds. He notes that the difference in the sink rate polars is barely noticeable when comparing varying the cg from 20% to 40% of the wing's mean aerodynamic chord (0.14 < Static Margin < 0.34). This indicated that no significant saving in trim drag is possible by simply reducing the static stability. Tail area, tail span, and wing area are the primary variables affecting the trimmed drag of 15 meter sailplanes. Finally, he comments that sailplanes with larger tails require smaller wing areas.

Mayland[48], however, observes that low tail area and relatively low tail aspect ratio can provide some advantages. Applying these observations, he found that the minimum induced drag is decreasing with increasing tail span, but the higher profile drag due to increasing tail area is predominant. With increasing profile drag the Reynolds number effect becomes predominant. Only low total lift coefficients ($C_L = 0.2$) require high tail downloads resulting in greater differences. For the glider tested, the lowest possible drag is obtained with low ratios of tail area to total area. The tail plane designs have shown that the reduction of induced drag due to a higher tail span is less important than the influence of profile drag.

Vernon[49] provides a simple method for determining the trim drag coefficient. The method was used to derive trim drag coefficients for low and t-tail locations for a range of

parameters including cg position. For the t-tail it is necessary to know the location of the wing vortex sheet at the tailplane position, and a simple rule of thumb for determining this was derived.

He assumed that the effects of rolling up of the vortex sheet were negligible and that the spanwise load distributions on both surfaces were elliptical. With regards to an ordinary planform effect, the elliptical assumption is entirely justified. The increases in induced drag resulting from non-ellipticity of loading are unlikely to exceed 3% according to him.

He found that for the wing, interference effects must cause some disturbance to the lift distributions. For the wing, only a small fraction of the span is affected, and the effects are normally counted as part of the fuselage drag. For the tailplane, if mounted on the fuselage, except at low incidence, the vertical velocity component is upward, and close to the fuselage the magnification is sufficient to overcome the wing downwash completely and cause local upwash.

For T-tails the fuselage influence is almost absent and the interference of the tail lift on the wing is virtually unaffected by it since the tail span is so small compared to that of the wing. V-tails can be treated in the same way as low tails by using an equivalent flat-tail span. Also regarding tails, for cruise, low main wing camber gives the lowest trim drag; cg position is unimportant. Bearing in mind other considerations such as maximum lift coefficient and good handling characteristics, the optimum is probably typical medium camber with cg mid or a little aft which agrees well with the results of others.

Lutze[50] developed analytical expressions that clearly show the dependence of the optimal cg position on the various geometric and aerodynamic parameters. In particular, he showed that large changes in the position of the optimal cg can occur for small changes in tail downwash angle. This highlights the problem of finding an optimally designed and configured HALE UAV without accurate downwash data.

In a paper in which the results go against intuition, Sachs[51] states that the minimum induced drag is less for the combination of wing-plus-tail than for the wing alone. He shows that this is true even for the case where the optimum tail load is a download rather than an upload. The airflow direction at the tail location is tilted by the downwash angle due to wing circulation. This can be visualized in Figure 2.4. Therefore, the tail lift vector perpendicular to the local flow direction has a component in the main flow direction in which overall drag is measured.

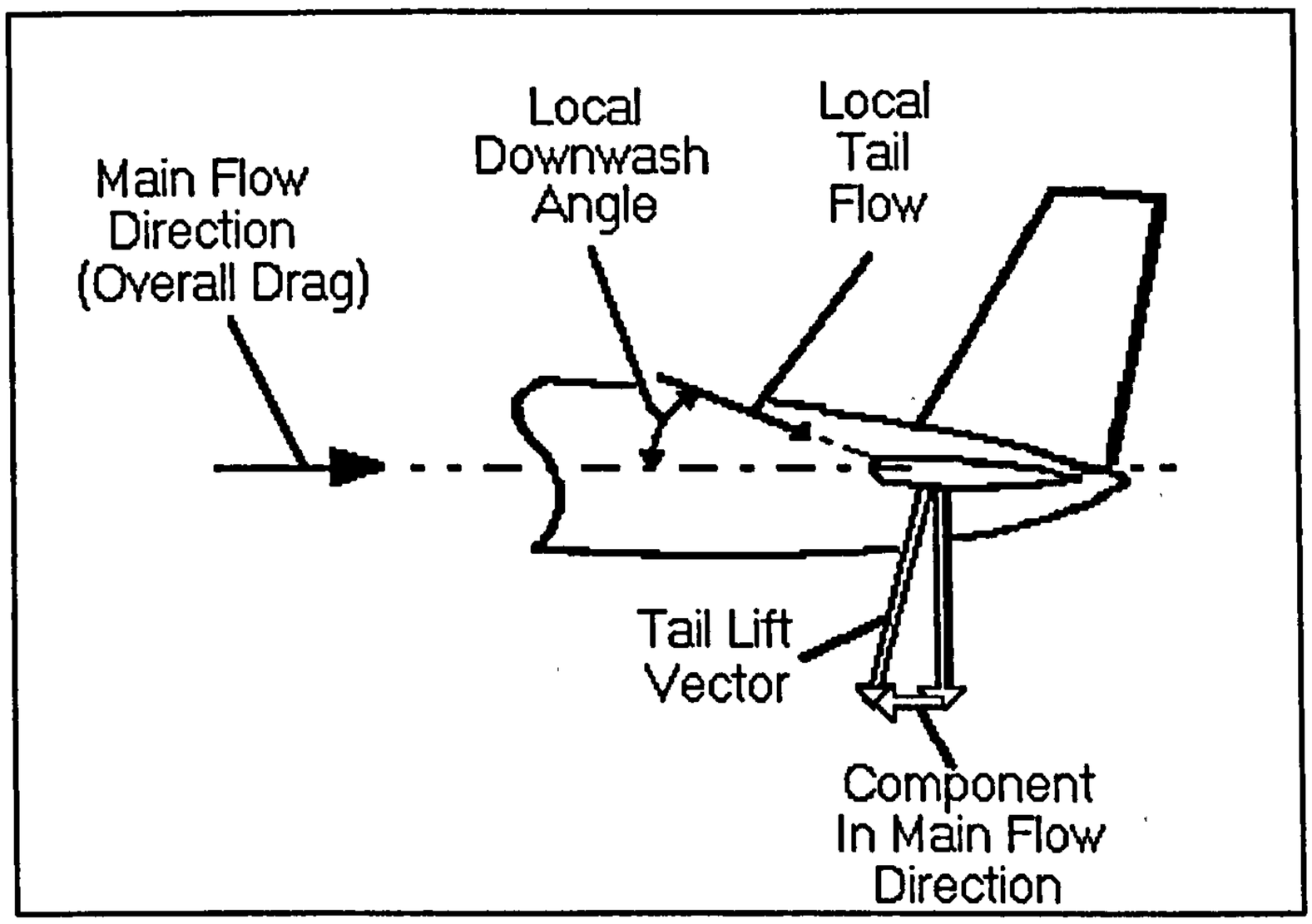

Figure 2.4 ***shows the tail lift vector perpendicular to the local flow direction, and the component of that vector in the flow direction acting opposite to drag.***

Laitone[52] extended and partially refuted the results of Sachs by stating that the reduction in total induced drag by a tail download was overestimated by using the total downwash for the wing on the tail, while neglecting downwash produced on the wing by the tail. However, the circulation vortex system of the tail upload produces an upwash on the wing that results in a "wing thrust" component that cancels the increased drag on the tail so that the total induced drag is a minimum with a positive tail load. Laitone proved, contrary to Sachs, that regardless of the relative dimensions of the tail with respect to the wing, the effect of the tail upon the wing cannot be neglected. If the upwash produced on the wing by a tail upload is considered, then the total induced drag of the wing-tail combination is a minimum with a tail upload. For this thesis, the effects of the tail on the wing were always considered.

Moreover, Laitone found that whenever the tail is above or below the wing, a tail download should be avoided because the induced drag can be increased more than 8% over that for a zero tail load. The location of the cg for a zero tail load would require a sufficiently large tail volume in order to attain the necessary aft cg and still maintain static longitudinal stability if a fully automated control system were not going to be employed. This is less of a concern for a UAV as a fully automated control system is normally in place.

Goldstein and Combs[53] devised an analytical method for estimating total trimmed drag polar for airplanes with two lifting surfaces. Drag due to lift was developed as a function of the load carried by each surface, its aerodynamic characteristics, and the inclination of the aft surface due to downwash.

They discovered that a clear advantage was shown for canard configurations with main wing-tip mounted vertical surfaces. Additionally, since trim drag is a function of the total lift generated and the relative load carried by the wing and tail, trim drag is of primary importance at high altitude. They noted that trim drag is reduced and the flight efficiency is improved with an increase in tail arm for both aft tail and canard configurations. Lifting aft tail configurations have the potential for handling larger cg ranges than do comparable canard configurations. The shape of the downwash field on the tail is directly related to trim drag calculations. This wake region is then directly effected by the variation in drag and lift across a loaded span. This aspect of the design for a HALE UAV is covered in this thesis/methodology by the lift induced drag calculation via a Vortex Lattice Method capable of resolving multiple lifting surface interactions.

2.C.1.g Spanwise Variations in Profile Drag at Low Re

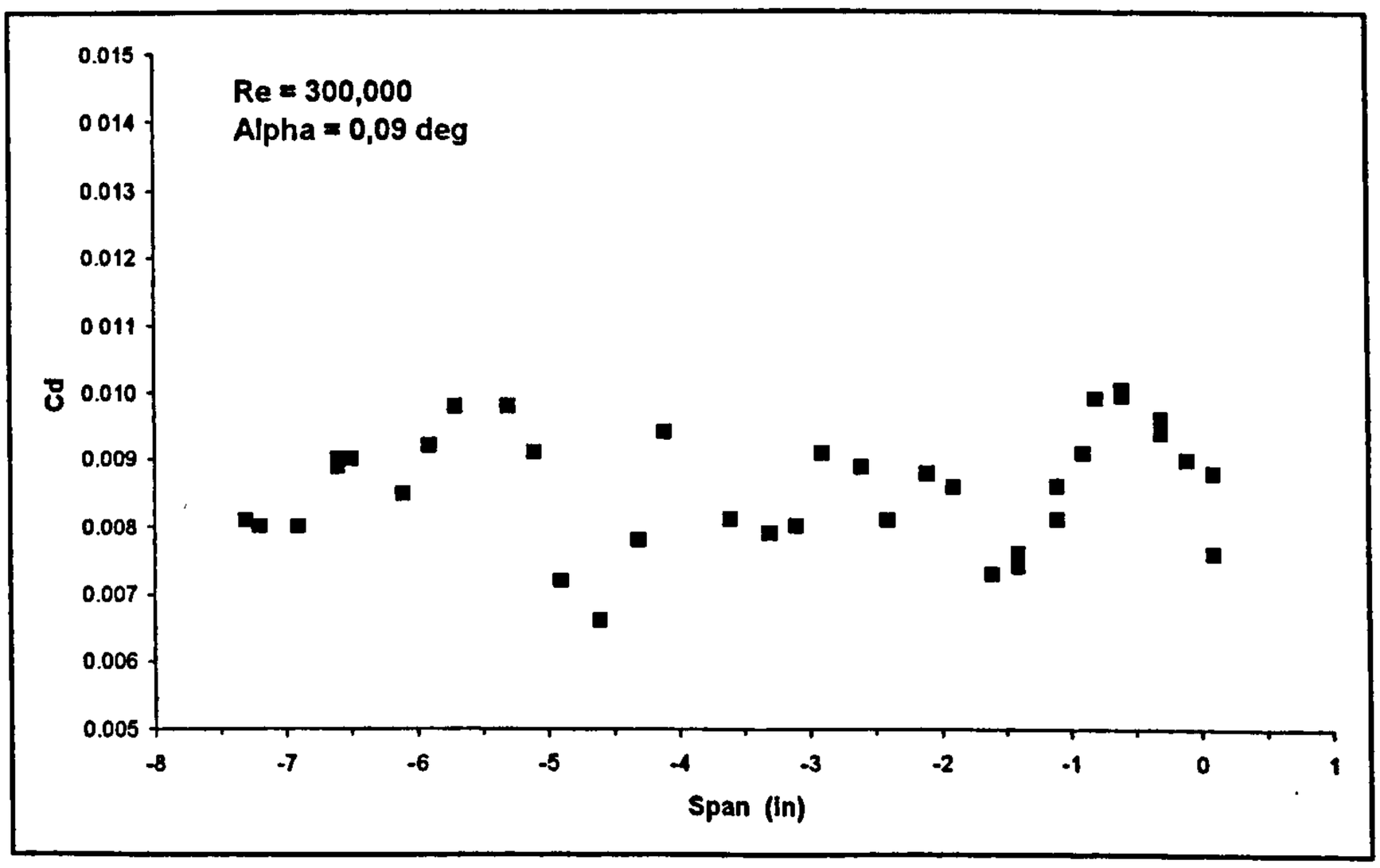

Figure 2.5 ***shows spanwise variations in drag coefficient at low Reynolds number.***

In another area in which very little investigation has been performed, Guglielmo and Selig[54] experimented with determining the effects of spanwise variations in profile drag

at low Reynolds numbers. They presented wind tunnel test data for the E374 and SD6060 airfoils at Reynolds numbers from 200,000 to 500,000. An example curve is included in Figure 2.5 for interest. It can clearly be seen that there is great deal of variation along the span in C_D depending on where the measurement is taken. They also showed that this variation continues into the wake for some distance. Their results showed a strong Reynolds number dependence on the magnitude of the oscillations at and below a Reynolds number of 300,000. Another area of interest that has received little attention but can provide a reduction in wing drag is spanwise camber.

2.C.1.h Spanwise Camber

The photographs of the Rutan *Voyager* aircraft shortly after maximum gross weight takeoff no doubt sets the mind wondering about the effects of spanwise camber on aerodynamic efficiency.

Since the original work of Munk, it has been known that spanwise camber can have significant effects in drag reduction. Munk's work suggests that study of spanwise camber can also give indications of potentially favorable planform shapes for reduced induced drag.

Munk's results have consequences that do not appear to be well known. In particular, it was shown that under optimum conditions the ratio of lift to induced drag is constant at all sections along the wing. There are several known analytic solutions to the spanwise camber problem, for example the circular arc wing and the wing with end plates.

In a curious paper by Lowson[55], linear theory was used to develop optimum circulation distributions and their associated minimum induced drag for wakes from lifting surfaces with various spanwise camber. New results were computed for polynomial and superelliptic camber lines. An empirical correlation was demonstrated between the induced drag factor and the inverse arc length for a variety of optimum cases.

The induced drag factor k is defined following the European practice, by : $C_{DI} = \frac{kC_L^2}{\pi AR}$. Thus, values of $k < 1$ imply reductions of induced drag. It was observed that the super-elliptic results gave low values of k and are therefore of some practical interest. There is a strong effect of spanwise camber distribution on induced drag. A comparison of

the results for various shapes demonstrates that it is the shape of the tip, and in particular, its vertical orientation that is the principal factor governing the benefits.

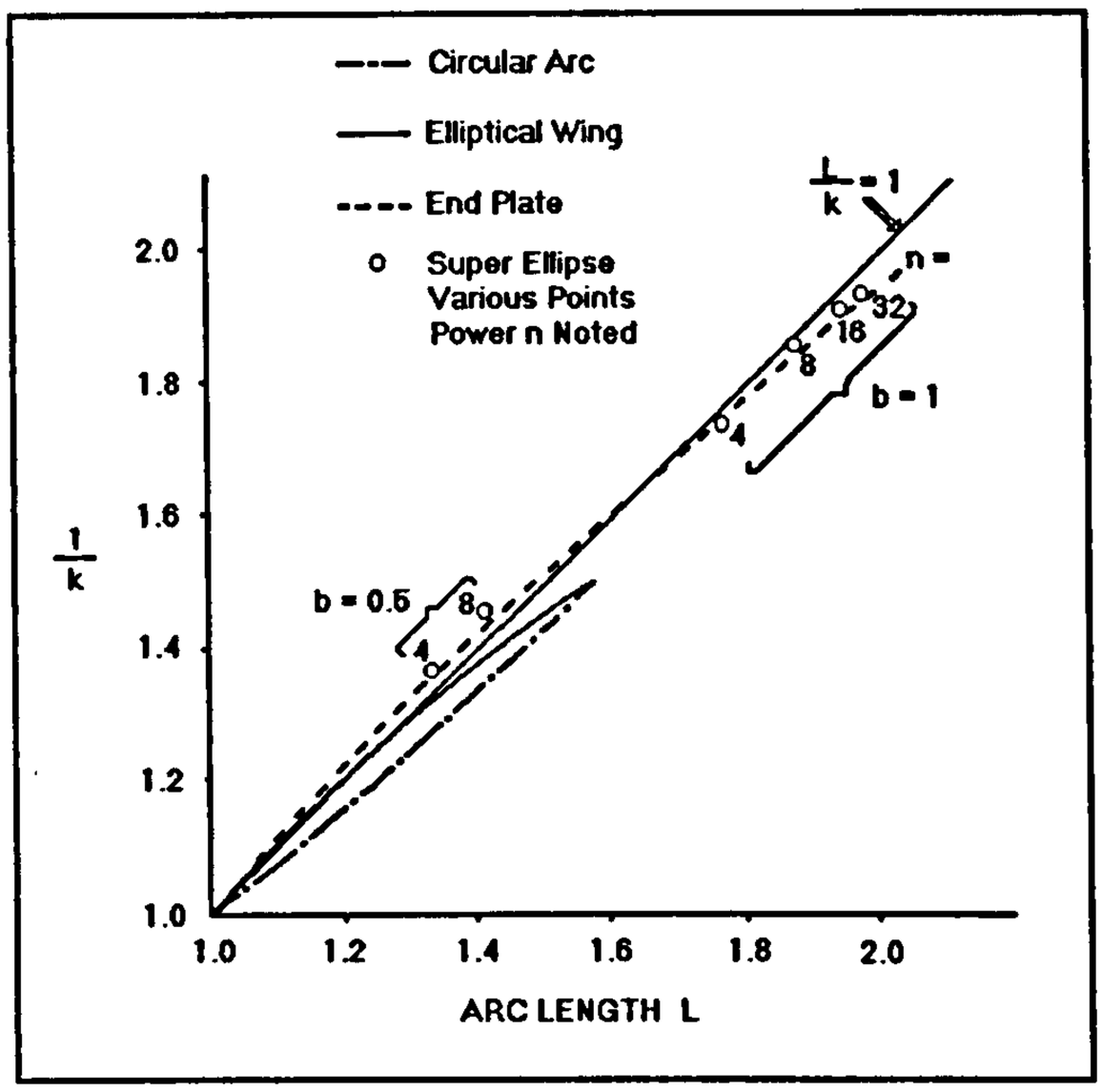

Figure 2.6 ***shows the variation in aerodynamic efficiency term (k) with arc length for several different wing shapes (Lowson[55]).***

The results also showed that total arc length of a cambered wing was a strong empirical predictor of induced drag. Figure 2.6 gives a plot of k^{-1} against total arc length for various wing shapes. The arc length and inverse drag factor are closely related for the more effective wing forms such as endplates, super-ellipse, etc. The most effective form for a fixed arc length is a broadly elliptic shape of modest overall camber. However, the induced drag is proportional to the inverse square of the span so that the best use of the arc length is generally to increase the span rather than to use camber.

The results gave a prescribed downwash and bound vorticity distribution for minimum induced drag under the assumptions of linearized theory. Computation of optimum lift distributions for cambered lifting lines showed the benefits largely due to camber near the tips. The most effective form of camber for a maximum given displacement was the end plate, but elliptic and super-elliptic shapes are slightly more effective in terms of minimum length of the wing for a given displacement.

One implication of these results for HALE UAV's is that if wing span becomes a limiting factor in terms of physical runway width or transportability, spanwise camber might become a reasonable option if manufacturing costs were found to be reasonable.

As a follow on from the above discussion of endplate effect, the next section will discuss winglets.

2.C.1.i Winglets

With aspect ratios occasionally exceeding 40, it would seem unlikely that winglets would have much effect on the reduction of lift induced drag for a Low Speed HALE UAV. However, winglets usually increase lift with a smaller increase in wing root bending moment when compared to the same lift increase due to a span extension. Once again, sailplanes have very similar aspect ratios and therefore a comparison with this particular feature proves useful.

Dressler[56] observed that the greatest improvements for sailplanes from winglets are to be expected at high lift coefficients, for example during thermaling and at low cruising speeds. At lower lift coefficients, the additional skin friction drag gains importance, and below a certain lift coefficient outweighs the favorable effect of the winglets on induced drag. It follows that if winglets were going to be considered for HALE UAV design that cruise lift coefficients would have to be high enough to outweigh the adverse effects of the additional skin friction drag of the winglets. Minimum power required lift coefficient (C_{LminPR}) tends to drive the cruise lift coefficients of Low Speed HALE UAV's reasonably high, which follows from the extremely high aspect ratios and low values of zero lift drag coefficients (C_{Do})

Of the parameters examined, Dressler found that the height of the winglets, exhibited the most important influence on the lift distribution of the wing. The optimum winglet height decreases with rising speed. Given the winglet chord length, the circulation can be adjusted by the winglet angle of incidence.

Marsden[57] comments on Dressler's findings, saying that Dressler found that the one meter high wing tip extensions did increase the maximum L/D ratio from 39 to 41, but realized that the gain would have been greater if the span had simply been extended in the plane of the wing. This of course provides further justification for even larger span HALE UAV's.

Flight tests on a *Nimbus 3* (glider) with winglets showed it to have the same performance as it had with the tip extensions to 24.5m span. This is equivalent to a 13% increase in effective aspect ratio due to the winglets. In addition, the winglets greatly

improved the roll rate. This statement supports the idea that the only reason to use winglets on a HALE UAV is in the event that runway width becomes limited, transportability becomes an issue, and span is restricted to a value lower than the performance would otherwise require.

A winglet changes the spanwise load distribution on a wing, resulting in more load carried by the wing tips. There is typically a 5% increase in wing root bending moment. Adding more structural material to compensate for this additional load would add about 1% to the empty weight of the aircraft [sailplane]. However, it was unclear from this paper whether this was an increase over that of an aircraft with the span increased to correspond to the effective aspect ratio increase due to the winglets. For a conventional configuration, this would be an obvious disadvantage, but for a span-loader, multiple fuselage, or flying wing, the effects of this problem are much smaller, and can even be advantageous.

There is a good deal of reliable experimental evidence that winglets can increase sailplane performance with measured improvements of 2 to 5 points in glide ratio. Adding winglets to an existing sailplane will increase skin friction drag which is most important at high speed. However, with properly designed winglets, the speed at which skin friction drag of the winglets cancels out the induced drag reduction is well above the normal cruising speed, and even at higher speeds the drag increment is almost too small to measure. These results should be taken with the consideration that many competition gliders are limited in span, depending on the class. Thus, the use of winglets would be justified more by the imposed restriction of any increase in span.

This highlights one particular difficulty with the extension of results intended for glider design being applied to the HALE UAV problem. This is discussed in detail in the next section.

2.C.1.j Differences in Sailplane Aerodynamic Design

Although many of the solutions available to fill the aerodynamic gaps existing in present methodologies come from recent glider and sailplane research, it should be noted that there are practical limitations to the use of this data. In the aerodynamic design of sailplanes, there are two competing factors. To optimize one is to sacrifice performance in the other.

McMasters[58] states that high speed performance is largely dependent on profile/parasite (viscous dependent) drag. Whereas weight and/or wing loading increase helps high speed performance, it seriously erodes minimum sink performance. Overall, then, for a racing sailplane the trend should be towards large span (to regain low speed performance) and high wing loading and extreme aerodynamic "cleanliness" to maximize high speed performance. In competition sailplanes (except for unlimited class), the span has an upper limit specified by international rules, thus there is a discrete span limit within which the glider aerodynamicist can work.

Many aerodynamic solutions that would improve minimum sink performance would degrade high-speed performance. For example, a racing sailplane optimized for minimum sink rate in a turn and a high forward speed in the region around 6.5-10 ft/s rate of sink should have a somewhat lower than customary aspect ratio. This means a larger area for a fixed class (span) of sailplane. Thus, absolute rectilinear L/D suffers somewhat, but the average cross-country speed (in the MacCready sense) increases. Ultimately, minimum sink rate is the fundamental performance objective, but there is always some degree of sacrifice in minimum sink rate performance for high-speed and turn performance.

Additionally, sailplanes are certified to rather stringent standards structurally, in order to withstand large gusts and high g loads in turns. A Low Speed HALE UAV would not encounter these conditions under normal climb or cruise (normal meaning not through the center of a thunderstorm). These structural limitations result in aerodynamic limitations in the form of forcing lower aspect ratios for gliders than would otherwise be possible in another application.

2.C.1.k Wing-Fuselage Interactions

An attempt was made to search the literature for wing-body lift and wing fuselage interactions for aircraft with extremely high aspect ratio. The correction factor for the drag created by wing-fuselage interactions in a Low Speed HALE UAV will have much less significance for an aircraft in which 70% of the total aircraft drag is due to the main wing. Information on how much less significance is not available, however.

In another situation where such information was not available, once again for gliders and sailplanes, Boermans and Terleth[59] performed wind tunnel tests of eight sailplane wing-fuselage combinations. In the case of a circular cylindrical fuselage the angle of attack

at the wing roots is doubled. Hence the spanwise lift distribution shows peaks at the wing roots, and the wing roots show suction peaks at the leading edge. For the most rearward wing location on one wing fuselage combination and for the intermediate wing location on another, this loss of lift starts at an even lower angle of attack. These combinations also show the highest drag increase with angle of attack. This implies that the placement of the wing on the fuselage should err on the fore side of the fuselage.

Finally, they suggested that in designing wing-fuselage combinations and fairings, basic potential flow information, obtained from a three dimensional (3-d) panel method, is indispensable. The reason for this is no doubt due to the lack of available information on the drag characteristics of well-faired wing-fuselage interactions for aircraft with large span, high aspect ratio wings.

The verification of this approach was carried out by Boermans and Waibel[37]. Their wind tunnel results also showed the importance of streamline shaping, i.e. fitting the fore-body to the streamlines of the wing to minimize cross-flow effects. This cross-flow effectively increases the angle of attack at the wing root area (up to approximately one fuselage diameter from the junction for a mid wing configuration).

2.C.1.1 Component Drag Breakdown

In addition to there being little known about the drag of wing-fuselage interactions in high aspect ratio large span wings, the breakdown of the drag of the individual components of this type of aircraft is also unknown. Again, in the common methodologies, there are tables with existing aircraft and aircraft types listed, with the drag of the components of interest and the parameters involved in their determination. Similar classes of aircraft are consulted for a minimal amount of information on the subject.

Enevoldsen and Bohn-Meyer[60] give the breakdown of the component drag for each part of a canard sailplane in the form of a C_D vs C_L^2 plot for each component in Figure 2.7. It can be seen that the wing/canard drag constitutes approximately 77 % of the total aircraft drag throughout the normal lift coefficient range.

In an evaluation of the cost of performance for gliders, Eppler[31] states the horizontal tail profile drag was assumed to be $C_d = 0.0045$. The vertical tail was assumed to have the same area as the horizontal tail, with $C_d = 0.0055$ because its sections are mostly thicker than those of the horizontal tail. More component drag data is available for sailplanes

from the common methodologies and additional methods of calculating component drags are available from Hoerner[61].

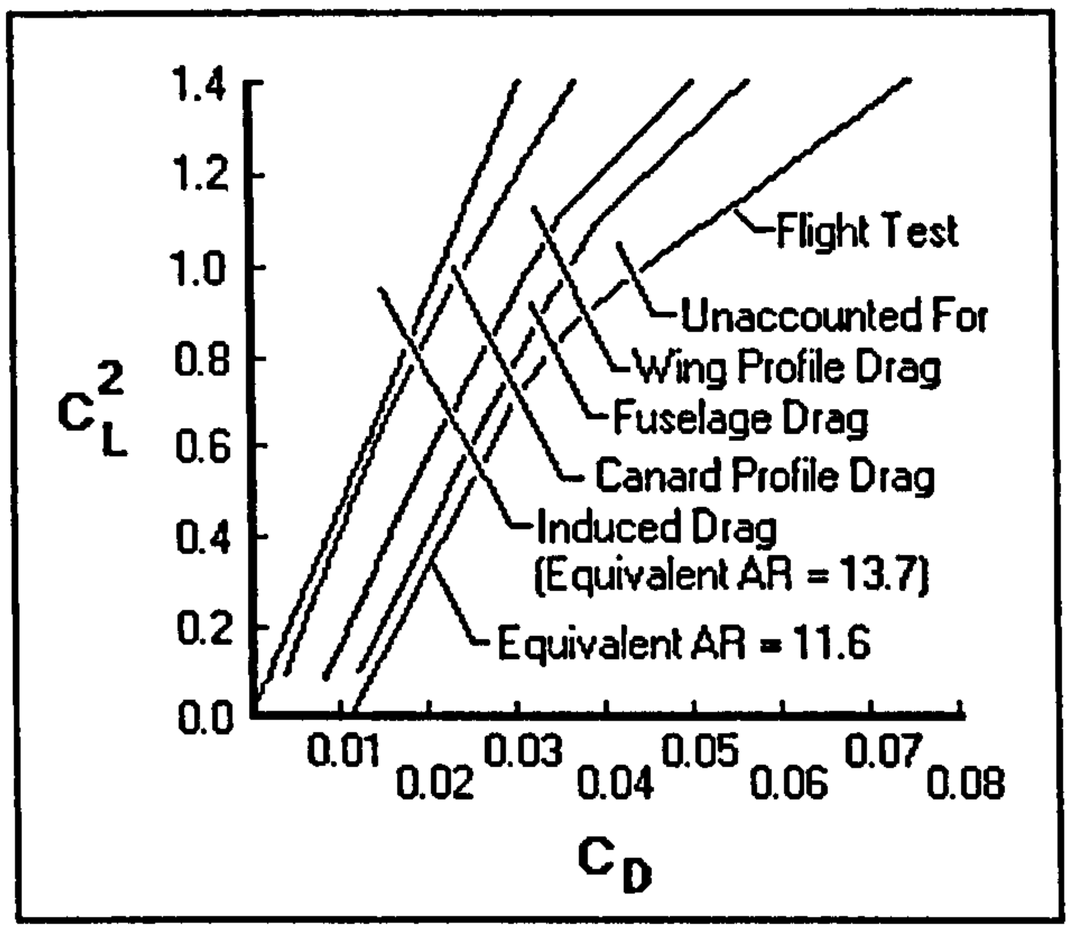

Figure 2.7 ***is the component drag breakdown of the canard sailplane Solitaire as a function of the square of the lift coefficient (Enevoldsen and Bohn-Meyer[60]).***

As an affirmation of what was probably already known, Hermanspann[25] states that for clean, streamlined shapes such as those used on sailplanes, skin friction over the exposed surfaces is the only constant (i.e. lift independent) drag contribution. Finally, due to the lack of availability of component drags for this class of aircraft, it is obvious that parametric data will not provide the answers necessary even for the validation of the method that will be used in this thesis. It follows that the validation of this work will most likely originate from a comparison of the macroscopic performance of the various configurations, as compared to the known achieved (not claimed) performance of existing aircraft.

Fortunately, there is slightly more information available on the weight breakdown of this class of aircraft. The next section will discuss this in detail.

2.C.2 Weight Estimation/Structure

When weight estimation calculations were performed for a Low Speed HALE UAV wing using conventional conceptual design methodology weight estimation techniques, some answers were wrong by a factor of 10 from the weights of the few known cases for such wings. Thus, the degree of confidence in these conventional techniques is weak. In

addition, in using those same methodologies to perform weight estimation for fuselages and fractional (based on takeoff gross weight) weights of payloads, fuel, structure, powerplant, systems, etc, further comparison has shown them to be unreliable for this class of aircraft. There is, however, a large body of information from which to draw some reasonable conclusions about how to approach the estimation of these quantities systematically for this class of aircraft.

In the extreme case, Juan Cruz[62] wrote a paper about his experiences and work in the weight analysis of the *Daedalus* human powered aircraft. He provides a detailed weight breakdown for the Human Powered Vehicle. He also developed equations for weight prediction for human powered aircraft. These equations would provide valuable information for an aircraft that will only perform a few flights, and those would all be at low altitude and much lower speed than the Low Speed HALE. This limits the forces to well below any that would be experienced by a HALE UAV.

In the slightly less extreme case, we look at the Rutan *Voyager*. Rutan's[63] goal for this aircraft was that the structure would weigh only 9% of the takeoff weight of the airplane. Although he did not succeed, he was reasonably close. This aircraft was designed to be durable enough to make it around the earth once without refueling. It lost a winglet on takeoff and needed to subsequently shake the other one off in flight. Although not the model of maximum toughness and durability, it does provide a valuable lower limit of what could be achieved with composite material technology for a multi-boom canard aircraft in 1993.

In a paper on the development of a HALE RPV concept in 1989 at Boeing corresponding to the *Condor* project, Baullinger and Page[19] discuss some fractional weights. They mention that in general, fuel fractions of 50% or more will be required for this class of aircraft. Based on total wetted area, the structural weight per unit weighted (exposed) area should be approximately 1 lb/ft^2 times the wetted area (S_{wet}). Estimated weight fractions for some aircraft can be seen in Figure 2.8. As can be seen from the figure, the *Voyager* marks the lowest end possible with the technology of 10 years prior to the writing of this thesis. Data on the Weight Fractions of Low Speed HALE aircraft will be provided later. A limit load factor of 2.0 times gravity (g's) (reduced from 2.5g for weight reduction) and an ultimate load factor of 2.5g (reduced from 3.0g for weight reduction) are considered reasonable.

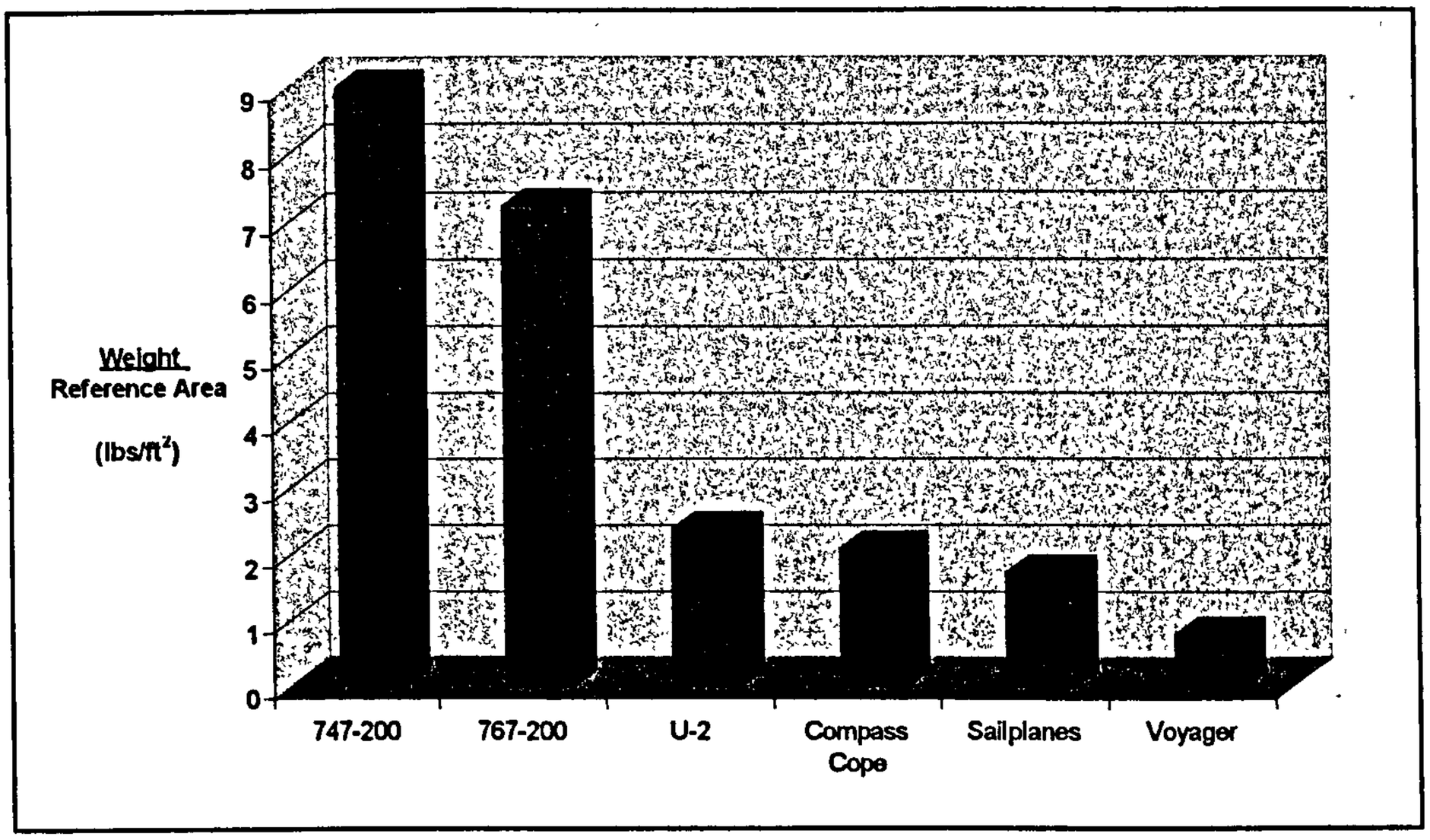

Figure 2.8 ***shows the comparative structural weight fractions of some aircraft.***

In another paper on the performance of the Boeing *Condor*, Breck Henderson[64] adds support for these numbers by stating that 60% of the takeoff gross weight was fuel, and 9% of the takeoff gross weight was due to the flight control system and the payload. He also states that the wing weight was only 2 lb/ft^2. It should be noted that in this application, the wing was used for fuel storage thereby creating a greater degree of uniform span loading for bending moment relief.

In another application, Israeli Aircraft Industries[65] (IAI) reported that for the design of the *Heron* aircraft (Medium Altitude Long Endurance, high aspect ratio, twin boom) they achieved wing weights of 2 lb/ft^2, with the center section of the wing holding fuel. They stated that one key to long endurance is that the ratio of fuel weight to takeoff weight should be as high as possible, and that the IAI design goals were 0.50 to 0.65. Nevertheless, in the same paper they propose a twin engine piston aircraft with a 32-hour endurance and 9140 pound takeoff weight. This proposed aircraft has a structure fraction of 0.606, a fuel fraction of 0.328, and a payload fraction of 0.066.

As an interesting comparison, Strojnik[45] , in a paper on motor-gliders reported that the wing weight for his aircraft worked out to 2 lb/ft^2. This wing weight was for an aircraft with an aspect ratio of 25 and one that would satisfy the stringent structural requirements placed on sailplanes and motor-gliders ***without*** the bending moment relief of fuel distributed across the span. The paper included a figure for Wing Weight versus Aspect

Ratio for 15 meter sailplanes showing a loosely defined inverse linear relationship. In terms of weight fractions, the wing weight fraction is 0.2, the total structure and systems weight for this aircraft was 0.5.

In another paper on sailplanes, Boermans and Waibel[37] discuss the weight breakdown of the *ASW 24*. The total structure and systems weight fraction is 0.44, of which 0.228 is composed of the wing weight fraction for a wing with an aspect ratio of 22.5. This places the *ASW 24* well below the inverse linear relationship mentioned by Strojnik.

In a paper on the design and testing of a canard sailplane/motorglider, Enevoldsen and Bohn-Meyer[60] show wing areas, as well as the weight breakdown of each of the major weight groups. This leads to a structure fraction of 0.52, and engine fraction of 0.08, and the pilot and parachute (payload) fraction was 0.36. This aircraft has a wing aspect ratio of 21, a combined wing/canard aspect ratio of 17, and was designed for +7 and –4 g's. This reflects durability and strength well above anything expected for a Low Speed HALE UAV.

When comparing materials, Johnstone and Arntz[18] state that a review of the materials showed a dramatic 2:1 weight reduction when high modulus graphite composites replace aluminum. They comment that the wing for the Boeing *Condor* weighed less than 2 lb/ft^2, and accommodated loads (in turns) as high as 2g. Furthermore, they commented that adding takeoff gear that would support the fully loaded wing imposed a very significant penalty on the takeoff gross weight and air vehicle empty weight (on the order of 15% and 20% respectively). This provides a reasonably compelling argument for the designed exclusion of landing gear in a Low-Speed HALE UAV.

Table 2.1 ***demonstrates the weight saving in the fuselages of some modern gliders resulting from the use of different composite materials.***

Muser[66]	Glass FRP Weight (lbs)	Carbon FRP Weight (lbs)	Weight Saving (%)
ASW 17	280	258	8
Mini-Nimbus	211	186	11.7
ASW 19, SB 11	229	203	11.2
LS 3	209	177	15

In discussing and comparing various materials for use in sailplane structures, Muser[66] states that weight savings (for carbon and aramid fibers) are in the range of 8% to 18% in comparison with glass fiber structures. All of the planes used in the comparison use a spar with carbon-fiber-reinforced epoxy and the weight savings are in the range of about 11%

to 14%. When carbon fabric is also used instead of some glass fiber fabric layers, weight savings increase up to 17.4% compared with the fully equipped wing or up to 24.3% compared with the wing structure itself.

Table 2.2 ***compares the wing weight of several modern gliders for different composite materials are used.***

Muser[66]	Glass FRP Weight (lbs)	Carbon FRP Weight (lbs)	Weight Saving (%)
Slingsby T59	220	193	12.2
ASW 17	309	275	10.9
Nimbus 2 Complete Wing	258	213	17.4
Nimbus 2 Structure	184	139	24.3
Mini-Nimbus	146	121	16.9
PIK 20 D	157	135	14.3

In the matter of fuselages (Table 2.1), he found that weight savings rates are lower, because there is higher weight percent of controls and of the landing gear. This would be expected to be different for HALE UAV's. When carbon is only used in fuselage stringers, weight savings are about 8%. If some of the glass layers are replaced by aramid or carbon fabric, the range will increase to about 15%. It is assumed that cost would be the determining factor in this material selection and use. Furthermore, this paper was written in 1979, and if nothing else, the cost of using these types of materials, as well as the expertise in how to implement them have only improved. Table 2.2 shows the results of the masses of sailplane wings when there is material substitution. As seen in the tables, much greater savings are had on average with material substitutions in the wings, however a 10 percent saving in weight in the fuselage is still substantial. To date, no post-1960's implementation of a HALE UAV has used anything but a composite wing construction.

Irving[67] provided a more specific analysis on the empty weight (W_E) of a sailplane. The empty weight of the sailplane is given by :

$$W_E = C_E K_E^{3/8} \tag{2.2}$$

where $K_E = nSb^3$ (here, S is wing area, and b is span). From Stender, the lower boundary of the diagram for single seaters corresponds to C_E=1.3, and the upper boundary to C_E=2.15. These values have been taken for the "light" and "heavy" structures for Irving's paper, while the "medium" structure corresponded to the mean of these values (1.725).

$$m = W_{pilot+instruments} + K_E \left(b^5 / A\right)^{3/8}, \tag{2.3}$$

where in accordance with JAR 22, n=8, and A is aspect ratio.

Irving presented results only up to aspect ratios of 22. His paper provided enough detail, after some derivation, to reproduce his results up to an aspect ratio of 40 while still respecting the original assumptions. Figure 2.9 shows the boundaries for sailplanes with light and medium structures (to the right of the stall curves).

Many general observations can be made that might help in the structural design of these aircraft. Irving[67] remarks that the combination of a light structure and a high maximum lift coefficient, $C_{L\max}$, provides the best combination. He says that achieving a high $C_{L\max}$ is more important than minimizing structure weight. Thus, achieving a good $C_{L\max}$ is much more important than attaining the lightest structure as shown in Figure 2.9.

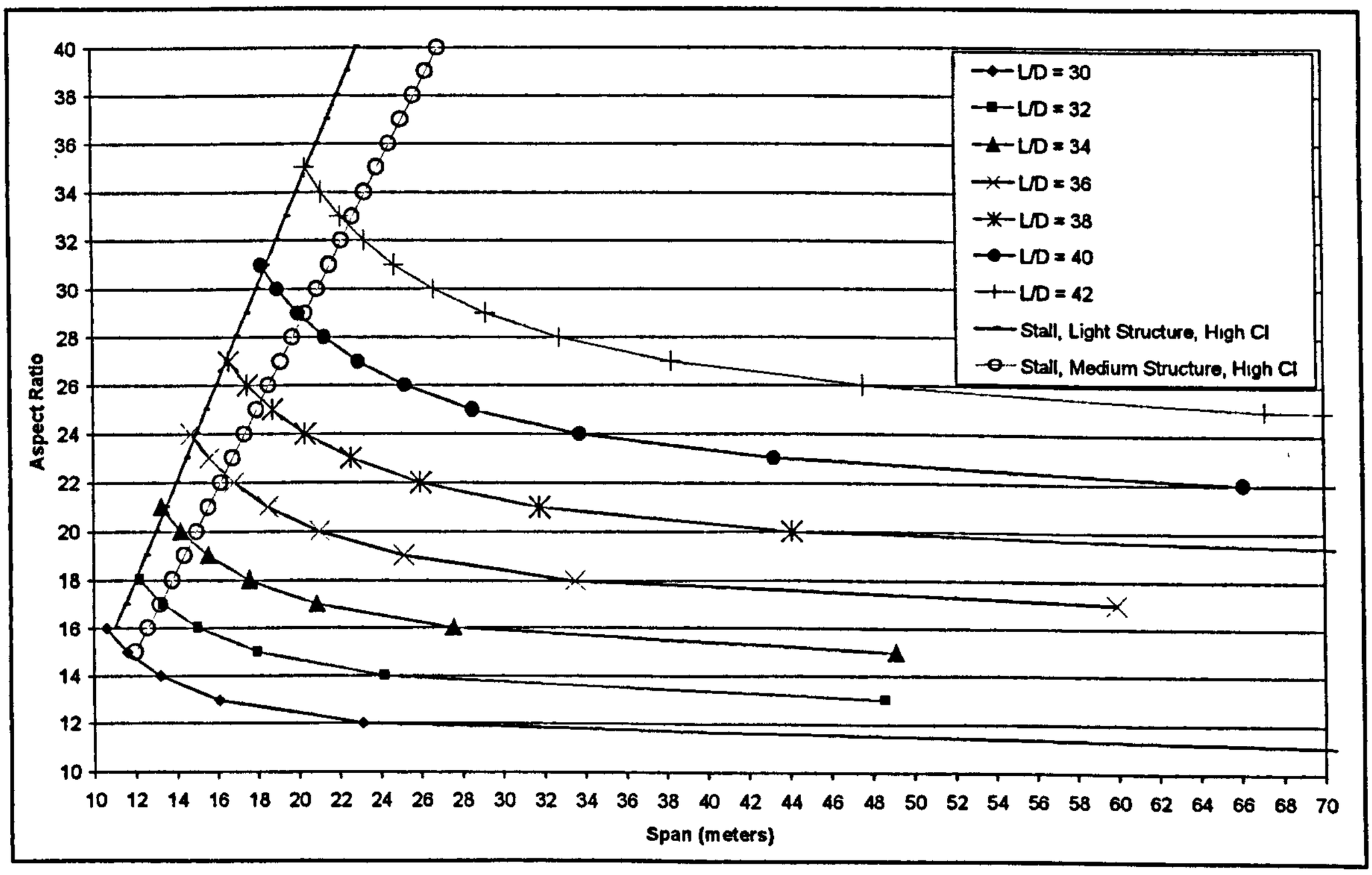

Figure 2.9 ***exhibits the boundaries for high performance sailplanes with "Light" and "Medium" structures for various lift to drag ratios.***

Hermanspann[25] comments that a high aspect ratio has always been the most visible indication of aerodynamic quality of a sailplane. It is limited by structural efficiency, meaning providing adequate strength at acceptable weight, and by constraints stemming from flutter, etc. Realized aspect ratios with wooden designs reached up to 20, while modern composite sailplanes nearly double that value.

Aerodynamic flutter is probably one of the greatest structural concerns with an aircraft with such an extremely high aspect ratio and span. There have been two papers written on this exact topic. Pendariès and Boiffier[68] et. al. wrote a paper specifically dealing with the simplified calculation of aerodynamic flutter for Low-Speed HALE UAV's. In a subsequent and clever paper, Pendariès[69] wrote about the possibility of using flexible wings and controlled flutter as an aid to propulsion by taking advantage of a flapping motion. In discussion with Mrs. Pendariès, it was decided that even the simplest flutter model she used, would be too computationally intensive and time consuming to include in this methodology.

It should be noted, though, that as computing power becomes more readily available such an analysis will become more feasible in a short enough computational time to make it applicable for early comparison of configurations. For this thesis, it is accepted that any design will have to undergo flutter analysis in the early preliminary design phase. Given that flutter is dependent upon mass distribution and structure stiffness, if the mass estimation is robust and the database of aircraft on which it is based do not suffer flutter, it is likely that a flutter-free aircraft can be designed at the estimated mass. The limits of present technology will be observed in this manner.

Finally, Eppler[31] observes that increasing the span causes more weight increase for high span than for low span. Very high spans are achieved only by means of materials stiffer than glass. This influences weights and prices. As an aside, he also states that it is justified to assume 5% less weight for gliders without flaps.

One of the major elements in the weight estimation of a Low-Speed HALE UAV is the powerplant. The next section includes discussion on some of the more important powerplant topics as they apply to the Low-Speed HALE UAV.

2.C.3 Power Plant Selection and Performance Estimation

For the purposes of this thesis, the turbojet was not explicitly considered due to the existence of a computational FORTRAN methodology specifically for sizing these aircraft[14]. This does not exclude the methodology from being capable of considering such configurations, however no special effort was expended in accommodating this class of aircraft. The only explicit changes that would have to be made would be the inclusion of

the compressibility factor in the parasite drag prediction and the change of the propeller endurance equation, though.

Aside from turbojet considerations, there are many problems associated with Low Speed HALE engine selection. Most important, however is the ability to operate at extremely high altitudes. There is precious little detailed data available from which to draw any parametric conclusions, but there are a couple of cases that provide crucial information.

One advantage to considering internal combustion reciprocating engines is that according to Arntz and Johnstone[18] from Boeing, with proper turbo and supercharging, the power output can be considered as reasonably constant all the way to cruise altitude. The challenge comes in predicting the fuel consumption, and engine performance at high altitudes with greatly diminished ability to shed unused heat.

Cyrus and Franz[70] summarized the advantages and disadvantages of using one propulsion form or another for a HALE mission. Fuel cells/electric drives, turboprops, diesel, spark ignition, and rotary engines were all considered. No selection was mentioned by the paper, as it was determined to be terribly mission specific as to which propulsion system was better..

In a thesis by D.L.G. Bizzarri[71], he compared the relative merits of piston engines to wankel and turboprop engines. Specific fuel consumption and specific power were used in the evaluation of the more appropriate propulsion system. He selected the piston engine despite lower specific power. He claimed that the engine had better efficiency than turboprops for the mission considered. He dismissed the other engine types as technologically unproven for the given application and thus the piston engine was deemed the most appropriate based on those criteria.

Henderson, McQuillen, and Lehman[72] present an interesting table comparing the benefits of four different types of propulsion systems to satisfy their need for a 400 horsepower (HP) motor. This table is duplicated as Table 2.3 below.

From the table it would appear that the rotary engine has many clear advantages. The greatest problem with this engine is that there simply is no data available on it or its operation, no matter how good it may appear. The turboprop efficiency is too poor in partial power settings, the diesel engines, like the rotaries, are simply not available for aircraft applications as yet. Their recommendations based on the results of this table were as follows (the paper was published in 1986):

Table 2.3 ***compares the various potential powerplants based on their benefits and drawbacks.***

Henderson, McQuillen, and Lehman[72]	Recip.Spark Ignition	Turboprop	Diesel	Rotary
Turbocharging	Yes (30:1)	No	Yes (64:1)	Yes (45:1)
Stratified Charge	Yes	No	Yes	Yes
Min. BSFC (lbs./hr/BHP)	0.35	0.33-0.36	0.3	0.32
Specific Weight (lbf/BHP)	2.7	1.2	2.7	2.1
Fuel Tolerance	Poor (req's Avgas)	Poor	MultiFuel	MultiFuel (best)
Major Advantages	Technology w/i Reasonable reach Wide Range of Engines Available	Min. Cooling Requirements Lowest Specific Weight	Best BSFC Accepts High Temp. Inlet Air	Good BSFC & Spec. Weight Compact MultiFuel Good Turbo Compatibility Few Parts
Major Disadvantages	Req's Intercooling for turbos Engine Cooling is high	BSFC too high At partial power Lean flammability Problems	Reduced Avail Turbo Energy Large Turbo Required High P_{inlet} Req'd Poor availability	High P_{inlet} Required

Near Term (1-5 years):

- Spark ignition reciprocating engine
- Two stage turbocharging system
- Turbine driven pumps and fans for cooling
- Bottoming Rankine cycle (turbo) for eng. heat rejection and avionics power generation
- Wing radiators for turbo intercooling and radar system cooling

Far Term (5-10 years) :

- Rotary engine (turbo compounded)
- Three stage turbocharging system
- Electrically driven pumps and fans for cooling
- Bottoming Rankine cycle for engine heat rejection and power generation
- Turbo intercooling and radar cooled with refrigeration cycle back to back with bottoming Rankine cycle.

Schirmer[73] presents a comparison of different engine types but the evaluation does not indicate a clear advantage for one of the investigated engine types, especially between the two stroke and rotary engine. The 2 stroke, 4 stroke, and rotary engines are compared using the engine concept evaluation matrix in Table 2.4. It should be noted that the usefulness of this matrix is limited when taken in the context of a HALE aircraft with present technology since neither the rotary nor the 2 stroke engine would be capable of having multiple turbocharging enhancements to their performance without significant technological investment.

Table 2.4 ***also compares a number of engine types but on a slightly different basis.***

Schirmer[73]	Two Stroke	Four Stroke	Rotary
Power/Weight Ratio	++	--	+
Power Density	++	--	+
Fuel Consumption	--	+	--
IR Emission	+	-	-
Noise Emission	-	+	+
Vibration	-	+	++
Reliability	-	+	-
Maintenance	+	-	++
Cost	++	-	-
TOTAL	+3	-3	+2

There have been several successful propulsion systems for Low Speed HALE aircraft. The Aurora Flight Sciences[74] *Perseus B* is powered by a conventional four-cylinder 80 HP Rotax 912 piston engine driving a rear mounted pusher prop. Additional airflow is provided to the engine via a three-stage, four turbine turbocharger capable of providing sea-level air pressure to the engine at altitude.

The propulsion system attempted for the *Perseus A* was a self contained internal combustion reciprocating system that provided oxygen for combustion at altitude. It experienced a great amount of difficulty in development, and was never reliable enough for a mission of even moderate endurance at altitude. The endurance and reliability of this propulsion configuration suffered as a result of the requirement to carry oxygen for high altitude flight and to recycle the exhaust as intake.

Tonskotter[75] wrote a paper describing the propulsion system for the Grob *Strato 2C* manned HALE science aircraft. The two engines used in this application were Teledyne Continental Motors TSIOL-555 direct drive liquid cooled opposed, each with a displacement of 550 cu. in. and a compression ratio of 7.5:1. This implementation used a compound propulsion system based on a highly supercharged liquid cooled piston engine with charge air intercooling and extensive use of available components. This system was designed for an 8-hour cruise at 80,000 ft and a 48-hour cruise at 60,000 ft altitude. The compression of intake air at altitude was accomplished through the use of a Pratt and Whitney Canada PW127 gas generator. The low-pressure charger provided charged air at a pressure that allows the engine to maintain full rated power at altitude. This Continental engine was the same used by Boeing for the *Condor*. Figure 2.10 shows a diagram of the two implementations of that engine.

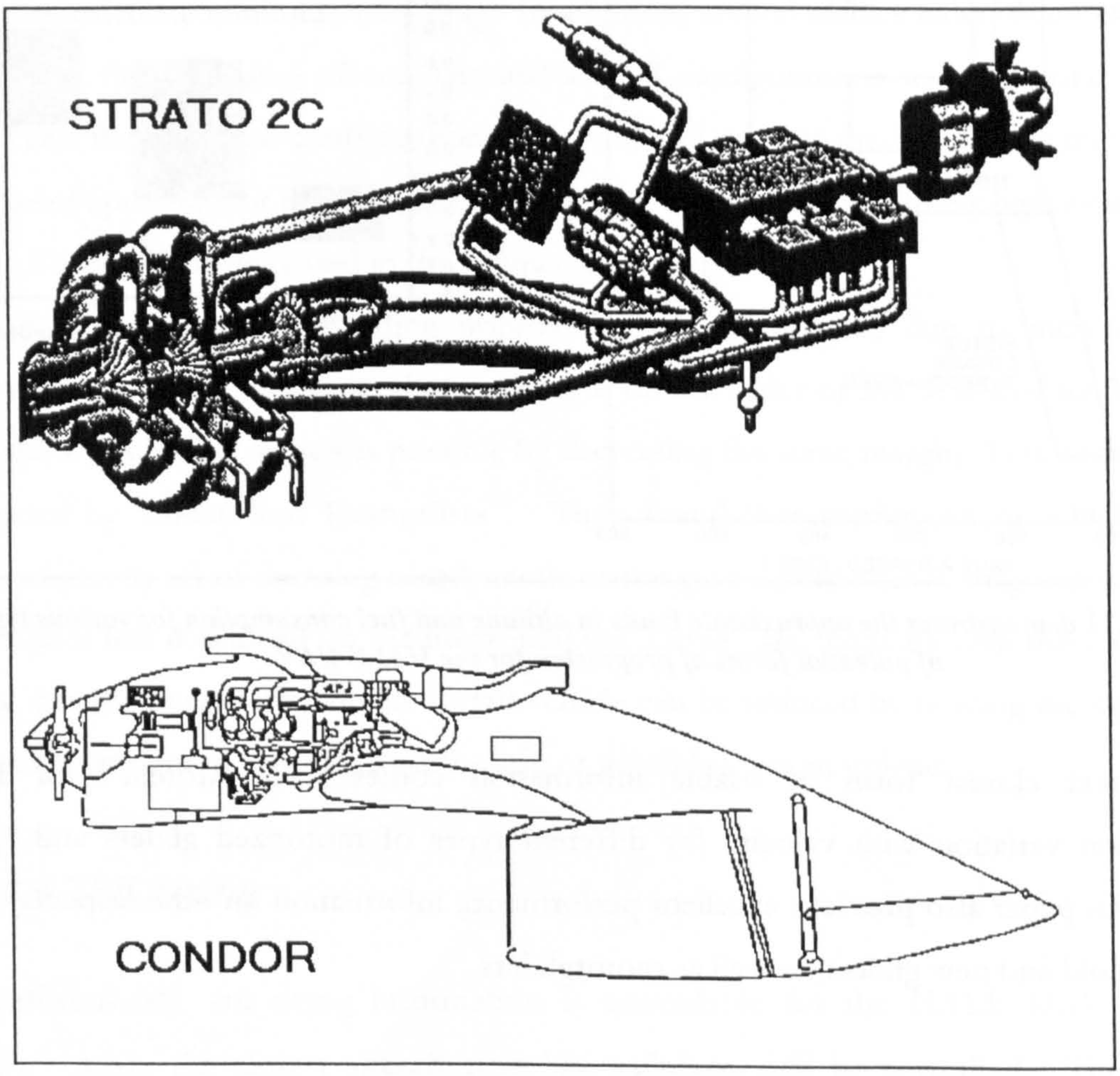

Figure 2.10 ***is a detailed diagram of the engine implementation for the Condor and Strato 2C, which used the same basic engine core.***

Tsach, Yaniv and Avni[65] confirm that piston engines with two stages of turbocharger can reach altitudes of 70,000 feet. With three stages, altitudes of 90,000 to 100,000 feet at a speed of 0.4 Mach could theoretically be reached. In Figure 2.11 the graph on the right roughly shows the thrust specific fuel consumption for various propulsion systems. The figure on the left shows the theoretical possibilities for the various propulsion systems based on the limitations of Mach number and altitude. These two figures essentially combine to visually represent the limitations on the regimes to be considered for each of the propulsion systems.

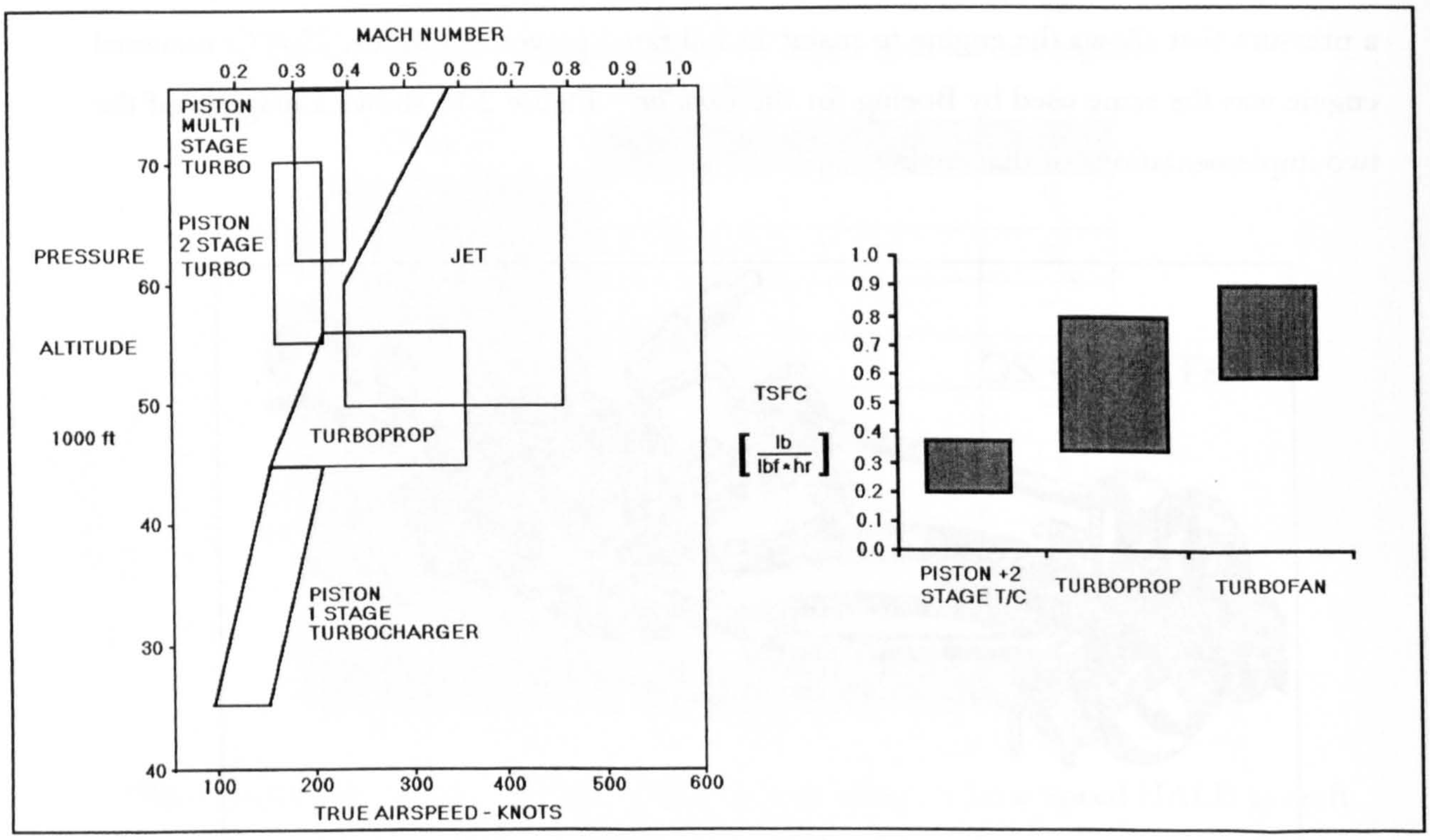

Figure 2.11 ***demonstrates the approximate limits in altitude and fuel consumption for various types of potential forms of propulsion for the HALE UAV***

The next closest form of usable information comes from Morelli[76] for fuel consumption variation with velocity for different types of motorized gliders and light aircraft. This paper also provides excellent performance information on other aspects of a number of old and new gliders, as well as motorgliders.

2.C.4 Tail Sizing/Stability

There are two areas within tail sizing and stability that require information beyond that available in conventional methodologies and literature. There is no information available on the sizing of the tail for this class of aircraft. This immediately causes concern in the area of stability of the aircraft, and additional information will have to be uncovered, or discovered in order to overcome this difficulty. Downwash angle information downstream of extremely high aspect ratio wings is nonexistent, and therefore another source of this information needs to be found as well. In attempting to find an alternative method of tail sizing, tail sizing information, or stability calculations, several observations were made.

Some experimentation has been performed in the relaxation of longitudinal static stability in order to gain improvements in trim drag. In order to calculate longitudinal static stability, it is necessary to know the downwash. Many methods have also been devised to calculate minimum trim drag. In addition, several studies have been performed to compare the total drag of conventional aft tail configurations with the total drag of canard and three surface configurations. None of the present methodologies incorporate this type of approach, or the information necessary to deal with extremely high aspect ratio wings. These will be discussed in the following sections.

Ende[77] found that aft loading improved cruise endurance, due to increased lift. Depending on the static margin, the trim drag is on the order of 3% to 6% of total aircraft drag, and a significant savings is possible by decreasing the static margin. This concept was confirmed by Siddiqi and Evangelista[78]. They found that configurations which had a center of gravity aft of the wing aerodynamic center gave a better lift to drag ratio, because they require less download on the horizontal tail. Lutze[50] also concurs with these findings, stating that the overall drag on an aft-tail vehicle can be reduced by moving the cg further aft, causing a reduced download on the tail, or possibly even an upload.

2.C.4.a Tail Sizing

Unfortunately, tail sizing information is unavailable for the HALE UAV class of aircraft. Again the closest aircraft type, the sailplane, will be consulted. The biggest problem with using data from sailplane design is that the tail is sized independent of any powerplant or powerplant problems. So for a multi-engine configuration where the

engines are not aligned along the same axis, tail volume coefficients must be approximated using multi-engine data from another class of aircraft. The only other alternative is to approximate mean aerodynamic chord for the main wing and tail of existing Low-Speed HALE UAV's from photographs and drawings, and derive approximate tail volume coefficients by hand.

In a paper on trim drag, tail sizing and soaring performance, Kroo[47] made several interesting observations. Figure 2.12 indicates that although the lower aspect ratio tails may produce lower profile drag due to higher Reynolds numbers, the improved low speed, circling performance of the higher aspect ratio tails compensates for this. This results in the optimal horizontal tail having an area of about 10% of the wing area with approximately 20% of the span (AR = 9). This result is valid for sailplanes, but obviously, the turn/low speed circling performance requirement is not necessary for HALE UAV's. Thus it would be expected that a slightly lower aspect ratio tail would be better.

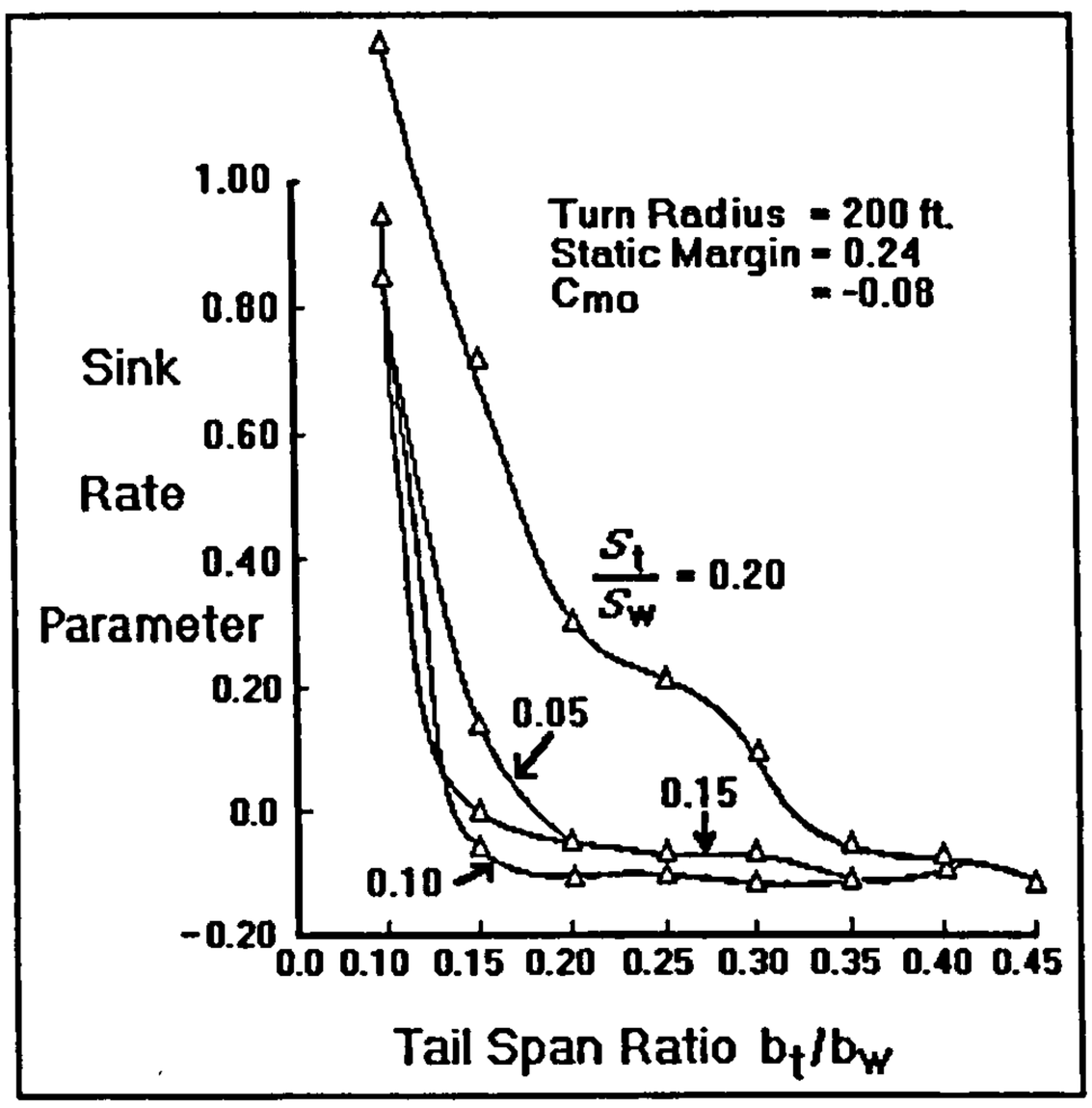

Figure 2.12 ***shows the effects of changing tail area (normalized by wing area) on aerodynamic efficiency as a function of the ratio of tail span to wingspan (Kroo[47]).***

As a confirmation of this, Kroo states that the results from the optimization procedure using minimum straight flight sink rate rather than fixed turn radius, lead to optimal tails with AR's of about 4 to 7 and do not yield as large a penalty for smaller tail areas.

Kroo made some other observations. In particular, that reducing the static margin leads to smaller tails and improved high-speed performance. Trim drag penalty due to the requirement for longitudinal stability and trim constitutes a small, but noticeable part of a conventional sailplane's drag. This result would be the same for a HALE UAV. Tails sized for optimal performance in combined circling flight and high speed cruise have larger spans (and AR's) than those based on straight flight calculations. This final observation allows us to use sailplane data, with a greater awareness of which quantities in tail sizing have been explicitly compromised due to sailplane specific performance drivers that are not shared by HALE UAV's.

Siddiqi and Kwa[79] were involved in the design, flight testing and comparison of various different configurations to satisfy a long endurance low altitude RPV mission. They determined that a horizontal tail volume factor of 0.34 (with S_{HT} /S = 0.15) and a vertical tail volume factor of 0.016 (with a vertical tail area ratio, S_{VT} / S = 0.15) taken from historical data would be adequate (where S_{HT} is horizontal tail area, and S_{VT} is vertical tail area).

In a paper on a comparison between canards and conventional configurations, Blackburn[80] suggests that in addition to his work, other studies have shown that for a conventional aircraft, a wing to horizontal tail ratio of between 7 and 10 gives best overall performance. In a paper about the performance of sailplanes Eppler[31] states that a tail volume coefficient was assumed to be 0.585 for all of the configurations considered in his paper. Finally, in the book by Fred Thomas[9], a comprehensive summary of historical vertical and horizontal tail volume coefficients for sailplanes and gliders is provided.

Another quantity that affects tail sizing will be discussed in the next section.

2.C.4.b Downwash

In the early days of aerodynamics, it was common to approximate the downwash in the wake through the use of Glauert's[81] original theory. This theory is useful if the lift distribution is known and easily integrable, or if it is rectangular (uniform) or elliptical. Outside of these situations, either it cannot be applied, or the lift distribution can be approximated as elliptical or uniform.

A number of years later, Diehl[82] presented a paper that reviewed the downwash theory to date, however, it didn't include any method of generalized downwash prediction. By this

time, an experimental database for downwash and wake characteristics was beginning to evolve. Silverstein and Katzoff[83] produced design charts for predicting downwash and wake characteristics behind plain and flapped wings. This paper was closely followed by Katzoff, Silverstein, and Bullivant[84] and their paper on downwash and wake behind plain and flapped wings. These two papers were rather comprehensive, however, the experiments were performed at a time when the Reynolds and Mach numbers of interest were climbing fast. It follows that the high aspect ratio low speed regime was not considered. Nor could their results be extrapolated with any degree of accuracy given that the maximum aspect ratio considered was 12.

There was one paper written by Whitcomb[85] on the investigation of the downwash angle behind a high aspect ratio wing with various amounts of sweep in the NASA Langley 8 foot High Speed Tunnel. Once again, the problem with using these results was that the aspect ratio was too low, and the paper focused more on the effects of sweep. In addition, in keeping with the area of study at the time, the Mach number was also too high.

Finally, the ESDU data sheets were considered for the determination of downwash. Still, they were based strongly on the aforementioned experimental data, and the maximum aspect ratios were so much lower and the Mach number so much higher, that they could not be extrapolated with any degree of confidence in the results.

Now that the non configuration specific difficulties have been discussed, the discussion on the problems associated with considering alternative configurations can begin.

2.C.5 Design of Alternative Configurations

One of the areas that common design methodologies fail in, even for more conventional missions is the area of alternative configurations. Since the nature of conceptual aircraft design is to make the best use of data on existing designs, by far the largest body of information exists for conventionally configured aircraft. In today's risk averse society, this is the most prudent approach to aircraft design. What this approach brings in low risk, it loses in creativity, originality, and overall innovative approach to problem solving. It is safe to say that a program like the NASA Apollo program of the 1960's and early 1970's would not have been possible in today's risk averse environment. It must be stated that such a risk averse approach is contrary to the advancement of the

human race, as few of the greatest accomplishments of mankind would ever have been achieved under such a shortsighted approach. Based on this belief alternative configurations comprise a sizable portion of the work in this thesis.

2.C.5.a General

Several papers have been written comparing the relative merits of different configurations and their ability to fulfill many different missions. The paper that is the closest in design considerations was by Baullinger and Page[19] of Boeing Advanced Systems. This paper essentially provides a background on the feasibility of the *Condor* at the time. Therefore, the conclusions reached parallel the decisions implemented in that aircraft. In the process of reaching those decisions, however, they considered four different aircraft concepts in this paper: a twin fuselage, joined wing, twin boom, and a blended wing. The primary difference between the resulting design selection in this paper and the one used for *Condor* was the absence of a canard on *Condor*.

After the Baullinger and Page paper, the three studies that most closely model what will be attempted for this thesis are Foch and Aillinger[20], Toot[86], and Siddiqi and Kwa[79]. They were part of the U.S. Navy's LAURA project. The acronym LAURA represents Low Altitude/Airspeed Unmanned Research Aircraft.

They performed some experimental comparisons for multiple configurations, small-scale low altitude, lower speed (25 – 50 Knots) long endurance aircraft with 10 ft. – 20 ft. spans. They considered joined wing, variable span wing, tandem wing, and three surface configurations. Although the scales of the aircraft were quite different, some general trends in the different configurations and how they compare for the long endurance low speed unmanned mission are similar to those of a high altitude mission. Overall, they claimed that because the drag of the airplane's non-lifting components is of secondary importance, overall flight performance is not very strongly a function of airplane configuration. This much is surprising due to the difference in the scale of the aircraft, where interference drag for an alternative configuration could easily overwhelm any of the benefits on such a small-scale model.

A paper by Goraj, Feydrychiewicz, and Winiecki[87] would on the surface seem to hold a great deal of useful information for the work undertaken in this thesis. Unfortunately, the authors down-selected the designs almost inexplicably very early in the analysis to a

biplane, a biplane with lifting tail, and a forward swept flying wing. Few of the configuration related decisions and assumptions made were justified in any way before the down-selection. The only real justification was that the decisions were based on the personal preference of the authors. In any event, apart from the flying wing, the configurations were significantly different from those addressed in this thesis. Details of the analysis undertaken were not made available in the paper, nor were any of the methods developed to overcome the aforementioned shortcomings in the aircraft design methodologies.

In another study conducted at the Naval Air Development Center by the U.S. Navy, Henderson, McQuillen, and Lehman[88] considered conventional, canard, and flying wing configurations and compared them on their merits as they applied to the requirements. They failed, however, to select one particular configuration over another for any given mission. On the other hand, they clearly stated the well-documented relative benefits and drawbacks associated with the selection of each configuration, but did not base these decisions on any analysis of the comparative performance, rather the arguments were all based on well established arguments seen in any design textbook.

California State Polytechnic University[89] produced a paper describing the work done by California State Polytechnic University in Pomona to satisfy the NASA/USRA project request for proposal (RFP) for a High Altitude Reconnaissance Aircraft. A flying wing, monoplane, canard, joined wing, biplane, and tandem wing were all considered to perform the High Altitude Long Endurance mission, with the biplane and two tandem wing configurations being down-selected for further study. The reasoning behind the elimination of one configuration in favor of another is given. In addition, the details of the 3 designs selected for further work are also given. Once again, though, no clear favorite was singled out for the Low Speed HALE UAV application, and the degree of the detail in aerodynamic estimation, weight estimation and propulsion was quite superficial leading to doubt as to the origins of some of the decisions.

The next section will begin the discussion regarding literature available on alternative configurations, starting with the twin boom/twin fuselage.

2.C.5.b Twin Boom / Twin Fuselage

There is a large body of anecdotal literature as to the relative merits of twin boom or twin fuselage configurations as compared to others. Unfortunately, there has been very little published on the detailed evaluation of these configurations. Problems such as placement of fuselages and booms for maximum structural benefit, fuselage lengths and tail volume coefficients with the twin tail arrangement for this class of aircraft are not addressed by present methods. The majority of papers on the subject simply compare one configuration against another based on pure performance, with no mention of the details of important design, layout and configuration related decisions.

In the Low Speed HALE UAV application, Venkayya and Tischler[90] describe a number of performance and economic advantages for the twin fuselage vehicle over the conventional single fuselage concept. Sharply reduced aircraft/payload interference, reduction in wing weight due to the load (bending moment) alleviation between fuselage segments, and reduction in landing gear weight are the most readily apparent. The rotating propellers in particular reflect signals to the antenna and cause interference. The antennae on the outboard side of the two fuselages could significantly reduce the interference problem due to reflection from the props as well as from the wing.

They do observe, however, that one of the major drawbacks of the twin fuselage plane with a connection only at the wing (no connection at the tail) is that the demand on the flight control system would be severe in order to maintain the fuselage alignment with control twist only. It is much easier to control the wing angle of attack variation along the span in a twin fuselage configuration. By appropriate selection of the spacing of the two fuselages the severity of the wing bending can be reduced by as much as 50 %. Another advantage to the twin fuselage configuration is the increased volume available for the radar/payload and fuel.

In another paper on Low Speed HALE UAV's, Patterson[91] makes the same justifications as Venkayya and Tischler for the selection of the twin fuselage configuration. He claims a sharply reduced aircraft/payload interference (particularly propeller interference), and sharply reduced wing weight, primarily by the load alleviation due to the multiple fuselages and their contents. The twin-fuselage configuration is more resistant to flutter (structural analysis indicates that the wing weight reduction is larger than the fuselage weight increase). Finally, he agreed that it sharply reduces the landing gear weight.

He concluded that substantial overall cost and weight benefits for twin-fuselage configurations, relative to single-fuselage configurations have already been shown in the literature for this type of application. An example of the extent of bending relief possible from a twin fuselage configuration can be found in Figure 2.13.

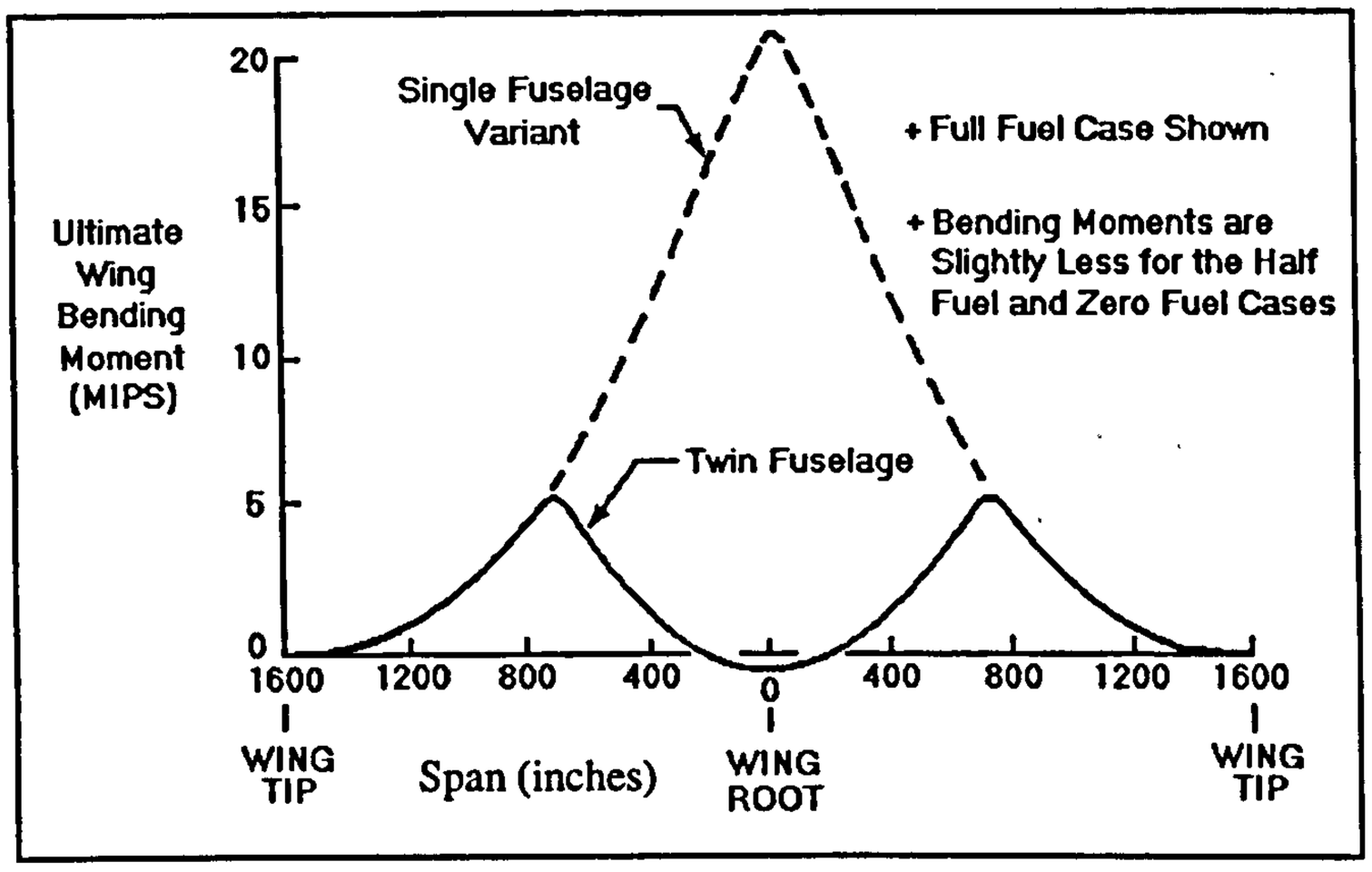

Figure 2.13 ***demonstrates the difference in peak wing bending moment between a single fuselage and a multiple fuselage configuration (Patterson[91])***

Vitali and Tsach[28] from Israeli Aircraft Industries selected the twin boom, rear engine (pusher) configuration for the *Heron* aircraft because it offered high mission flexibility in terms of payload installation (center of gravity and clean field of view for the sensors), and future potential growth.

At California State Polytechnic University[89] they worked under the assumption that one of the driving parameters of the design was limiting the wingspan. On this basis, they stated that a twin boom monoplane would have greater loads than a tandem wing twin boom, and therefore removed the twin boom monoplane from consideration since the greatest advantage of using two booms was load alleviation. They claim that the tandem wing configuration provided lower induced drag. They also stated that interference effects can be reduced significantly by employing negative stagger, which places the rear wing away from the downwash of the front wing.

Baullinger and Page[19] from Boeing arrived at an interesting result. In their paper, they discounted the twin fuselage concept because it would be too difficult to get propeller clearance on landing without fixed landing gear. For some reason, their down-selected twin fuselage concept had the engines fixed in the tail of each fuselage (presumably since

one of their design requirements was maximum radar field of view). It is an interesting result since the final *Condor* design didn't have fixed landing gear. They did, however echo the advantages of twin fuselages mentioned by the other papers. They did mention that this particular configuration only allowed for 240 degrees of radar coverage.

Their justification for the twin boom (***not*** twin fuselage) concept was that it was low risk. They discounted the concept on the basis of not being able to conserve laminar flow due to the tractor propulsion setup. They touted the advantages of distributing the load across the entire wing, and the good natural stability of the configuration, but were worried about high cg problems in taking off and landing.

Many of the twin fuselage configurations considered were also canard configured. The next section looks at the canard configuration type in greater detail.

2.C.5.c Canard

In contrast to the twin boom and twin fuselage concepts, there is a much larger body of data available on canard aircraft. Some of this data is just now beginning to be included in the more common methodologies, but they still lag far behind the data available in the common literature.

There are a large number of variables and design rules that need to be considered when designing aircraft with a canard (attention to spacing, stagger, gap, sum of lift distributions, vortex impingement on wing, etc.) which will be explained in this section. It would seem that very few canard aircraft have followed these rules to the extent necessary to be successful examples of how to design one. Like all aircraft designs, these aircraft have almost always had many conflicting mission requirements that force a sacrifice of the attributes that could make the canard the better choice. Since the majority of HALE UAV missions are mostly limited in their requirement for endurance and altitude, these mission requirements seem better suited to the use of a canard than other classes of aircraft. These characteristics will be discussed in the following section, however, it should be noted that these design rules for canards ***must*** be followed as closely as is possible, for any benefits to be realized.

Without any doubt the basis for any discussion on canard aircraft has to include the original work by Glauert[35]. He performed experimental tests for the vortex theory of airfoils and observed the effect of varying aspect ratio on C_L and other aerodynamic

constants. He also did some preliminary investigations into the biplane effects of stagger and gap. The investigations were extended later by Munk and Prandtl. This work formed the basis for all later work on this subject.

Many of the accepted characteristics of canards that come from high speed flow are not valid for Low Reynolds number flow. For example, Siddiqi and Evangelista[78] discuss some of the Low Reynolds number characteristics. They consider the wake rollup computations, which show that a low canard position will ensure that its vortex wake passes below the wing for high alpha. This may contradict high Reynolds number experience, where the interaction of the vortex wake and the wing upper surface is considered to be favorable. For the low Reynolds number case, the literature suggests that boundary layer separation may be induced on the wing upper surface by the close passage of the vortex wake.

Michelson, and Mueller[92] performed further work on the subject of wake impingement on the downstream airfoil. Their measurements showed that a maximum influence occurred when the wake center impinged near the leading edge of the downstream airfoil. All aerodynamic coefficients were reduced due to the velocity deficit in the wake. However, outside the wake, the lift was reduced by the upstream airfoil's downwash, and the drag was increased by the higher flow velocity induced by the wake blockage.

In order to make the aerodynamic problem theoretically tractable, many investigations of canard configured aircraft make the assumption of an elliptical lift distribution over each lifting surface to satisfy the Prandtl biplane equation. According to Kroo[93], when operating in the downwash field of a highly loaded canard, the wing's lift distribution tends to be shifted outboard due to the downwash directly behind, and upwash outboard, of the canard. He comments further that the assumption of an elliptical load distribution is reasonable when the vertical gap is large or when the surfaces have equal spans. Similarly, he claims that the lift distribution on a tail of significantly smaller span than the wing is not far from elliptical.

Laitone[94] found that when the larger span, either fore or aft, had a *uniform* lift distribution then the total mutually induced drag was less than that produced when the larger span had the ideal elliptical lift distribution. This decrease in the mutually induced drag when the larger span carried a uniform load was offset by the increase in the self-induced drag produced by the uniform load itself.

He showed that mutually induced drag of a canard or tandem aircraft could be decreased by having the larger span rear surface carry a load distribution similar to that produced by a constant chord wing. Although the total induced drag was increased, this modification of the larger span's elliptical load distribution allowed the smaller span front surface to carry a larger fraction of the aircraft weight at minimum induced drag condition.

Contrary to that conclusion, Laitone observed that any canard or tandem aircraft should have a finite gap sufficiently large so that the smaller span can carry its share of the aircraft's weight at the minimum drag condition. When the gap is one fifth the larger span, then either an elliptic or a uniform spanwise load distribution on the larger span requires approximately the same lift load on the smaller span in order to attain the minimum induced drag condition.

Michael and Selberg[95] performed a study of canard aircraft for General Aviation applications. Care must be taken when using their results since the class of aircraft is so different, however, some of the general trends of the results can still be helpful in the design of HALE UAV's.

They found that vertical distance between the lifting surfaces was found to be the main contributor to interference effects of their three-dimensional analysis. For designing a general aviation canard aircraft, results pointed toward large horizontal and vertical distances between the canard and wing, a large wing-to-canard area ratio, and the canard at a low-incidence angle relative to the wing. They noted strong two-dimensional coupling with a gap less than one and stagger less than three with moderate coupling for staggers between three and ten. These data represented all decalage angles considered. The three-dimensional induced drag results pointed toward a saving when the canard configuration had a large gap and a decalage angle equal to –2 degrees. Stagger varied the induced drag only slightly.

They then varied the canard and wing aspect ratio values individually between 6 and 12. They found that the highest aspect ratio for both lifting surfaces was the most efficient for all wing (S_w) to canard (S_c) area ratios. An approximate 16% decrease in drag for an increase in area ratio from $S_w/S_c = 50/50$ to 90/10 at $C_L = 0.55$. They also noted that as S_w/S_c increases, the canard configurations become less sensitive to stagger.

Static margins for this typical case varied from –0.1 for the aft center of gravity to –1.6 for the forward location of the center of gravity. As the decalage angle increased the canard loading increased, hence increasing the wing loading. Here the highest wing to

canard area ratios required the largest trim decalage angle and hence resulted in a higher trim drag penalty.

Finally, gap was the main contributing characteristic to the interference effects of induced drag, but some interference was encountered with different decalage angles, and very little for varying stagger values. As much as a 30% decrease in induced drag could be obtained if the two surfaces were out of plane and had nominal gaps. This agrees with the findings of Laitone mentioned previously.

Blackburn[80] wrote a paper in an attempt to dispel the myths about canard configured sailplanes. This paper, however, in its attempt to dispel myths about canards for sailplanes, supported many points that would make a canard a good choice for a Low Speed HALE UAV mission.

Several of the problems with canard sailplanes would also be problems for the HALE UAV mission and will therefore be discussed here. If the canard should stall in the flare, there is nothing to prevent the downward rotation of the nose into the runway. The solution is to approach well above the canard stall, but this has serious performance implications as well. Following from this, for models (conventional and canard) with essentially the same power and wing loading, canard configured aircraft require at least 50% more runway. Obviously in the HALE UAV application this is less of a problem as takeoff length is not generally a constraining factor.

Another of the problems with the canard that would effect a HALE UAV is with the center of gravity. One approach to solving the center of gravity problem is to add strakes as a highly swept forward extension of the inboard wing section to serve as fuel tanks. This solves the balance problem, but it creates some others. With fuel concentrated so close to the center of the fuselage, airborne wing bending moments will be greater than with fuel more evenly distributed along span. The result will be increased structural weight. Also there is more wetted area with the strakes, hence more parasite drag.

One way around this problem is with an implementation similar to the Rutan *Voyager*. With the *Voyager*, the fuel booms and large fuselage tanks forward of the cockpit made cg control relatively easy. There was even fuel in the canard. The fuel booms also acted as end plates which, when combined with the forward sweep of the canard made for a virtually constant downwash angle impinging on the inboard wing sections during a flight that was flown at nearly constant angle of attack. This statement serves to demonstrate

that if a canard configuration is implemented for the proper mission in an appropriate fashion, that the performance can exceed that of a conventional configuration.

In a paper on sailplanes, trim drag and tail sizing by Kroo[46], the design had a large fraction of lift carried by the canard ($L_c/L_w = 0.5$, where L_c is the lift of the canard and L_w is the lift of the wing). The performance of this design was therefore more sensitive to static margin changes than the conventional configuration. If carefully executed, a canard configuration might make an acceptable, although probably not an exceptional high performance sailplane. This acceptable performance is due to the need to balance performance in turns and cruise. This would not be a problem in a HALE UAV implementation.

Kroo also pointed out another interesting design difficulty. Unlike an aft tail, the canard airfoil must operate over a large range of lift coefficients. This leads to challenges in low Re airfoil design and inevitable penalties in profile drag.

A canard with 40% of the wing span, carrying 35% of the wing's lift, achieves a span efficiency (ε) of only 0.74. By employing a more optimal distribution of wing lift, this penalty may be reduced somewhat. However, the lift distribution required to achieve minimum induced drag is highly non-uniform. This leads to variations in section lift coefficient over the wing so that airfoil section tailoring is a necessity for such designs. This comment serves to repeat what was stated earlier, that in order for a canard configured aircraft to compete with a conventionally configured aircraft, certain aspects of the design are more critical, and therefore require greater attention in the preliminary design.

An aerodynamic tradeoff study of conventional and canard configured aircraft was performed by Selberg and Rokhsaz[96]. The primary objective of the study was to analyze the behavior of the ratio of trim lift coefficient (C_{Ltrim}) to lift induced drag (C_{Di}) over a range of static margins and area ratios.

For all of the parameters considered, at the lower stabilator aspect ratios C_{Ltrim}/C_D of the conventional aircraft was the highest, whereas for the highest stabilator aspect ratio considered the canard configuration had the highest C_{Ltrim}/C_D. They commented that many authors use variations of the Munk analysis for induced drag calculations. None of these methods accounts for either airfoil thickness or the deformation of the spanwise lift distribution as the result of three-dimensional coupling.

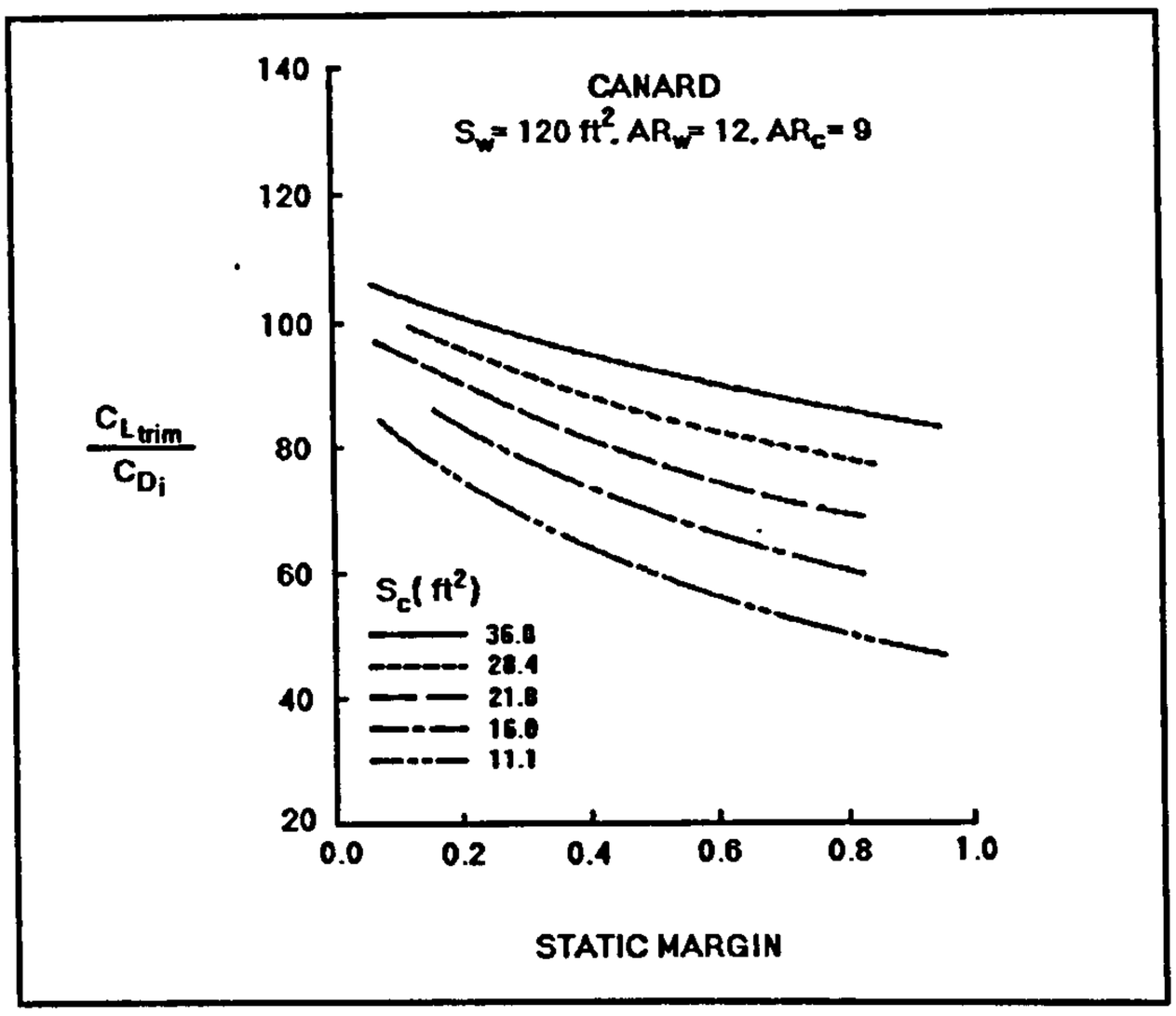

Figure 2.14 ***shows the canard configuration induced drag sensitivity with changes in static margin and canard area (Selberg and Rokhsaz[96]).***

C_L / C_{Di} for the canard configuration is shown in Figure 2.14 as a function of static margin and canard area. The changes in C_L / C_{Di} for a large range of static margin change are much less than those for the conventional or three surface configurations. Similarly, the largest area canard has the least induced drag and hence the highest C_L / C_{Di}. In addition, for larger static margins, it is the canard configuration that has the highest C_L / C_{Di}.

Induced drag and viscous drag results for canard aspect ratio to wing aspect ratio of 2.0 were compared for a static margin of 0.2. For these conditions, the canard configuration is superior from both induced and viscous drag considerations. When pressure drag and viscous drag are added to the induced drag , the C_{Ltrim}/C_D of the canard is the highest, followed by the conventional and then the tri-surface.

At the higher stabilator aspect ratios, the canard configuration has the least induced drag as well as the highest C_{Ltrim}/C_D ratio. However in all cases, the overall C_{Ltrim}/C_D is close enough that configuration selection will most probably be based on other considerations, i.e., stability and control, safety, structures, manufacturing costs, etc. It should be noted that one of the problems with this study is that it compared like control surfaces/areas for the different configurations. This is not practical or likely given that a

good design for a particular configuration would probably have a different area. This makes the basis for direct comparison questionable.

Feisteal used a Prandtl-Munk analysis to study various parameters such as span, gap, aspect ratio, etc. His results indicated that a ratio of canard aspect ratio (AR_c) to wing aspect ratio (AR_w) of 1.5 – 2.0 was necessary to achieve peak span efficiencies. Finally, Levy[97] produced a paper on downwash prediction for canard configurations. He developed a generalized formulation and design charts that could be used in a form similar to those produced by Katzoff and Silverstein, but that could be applied to canard configured aircraft. Unfortunately, the maximum aspect ratio considered was 12, thus making extrapolation a bit impractical.

The next section focuses on a specific kind of canard aircraft, the tandem wing.

2.C.5.d Tandem Wing

Many of the aerodynamic analyses on canards were applied in one of the extreme cases to the tandem wing. There is very little available in the form of useful data regarding the tandem wing configuration since there have been so few flying examples. Stinton[6] performed an aerodynamic analysis typical of the common methodologies. This analysis, however, didn't result in any real methodology through which to design an aircraft of this type. It is possible, though, to make some generalizations.

In their study for the HALE reconnaissance role, California Polytechnic Institute[89] used total wingspan as one of their constraints. This partially resulted in their preference for the tandem wing design. In addition, they claimed the wing bending and structural weight are better than the monoplane configuration. The tandem wing configuration also provided a lower induced drag. They stated that interference effects can be drastically reduced by employing a negative stagger. This places the rear wing away from the downwash of the front wing. In addition, if the upper wing is used for mounting the engines, ground clearance for the propellers is less of a problem.

On the subject of tandem wing sailplanes, Kroo[47] states that tails of very large span (tandems) are not advantageous for most aircraft since structural weight penalties outweigh the advantage in structural efficiency due to reduced span. For sailplanes it is not structural weight, but Reynolds number effects which eliminate tandem designs from contention. To determine when this Reynolds number penalty overcomes the increase in

span efficiency, the soaring performance of sailplanes with optimal wing area was computed for various tail geometry. The same problem is not likely given the even higher operating cruise lift coefficients (and thus relative domination of lift induced drag) of Low Speed HALE UAV's.

Cross and Donnelly[98] further support these comments in their paper on Low Reynolds number aerodynamics of multiple wing systems for RPV's. They state that for a given stalling speed and gross weight, a biplane or multiple wing vehicle can usually be made lighter and more stow-able than a monoplane of similar chord and wing area. An increased minimum drag coefficient is possible of only 5% to 15% above monoplane values. Their study consisted of an experimental investigation of a tandem wing configuration aircraft with many variations of wing location along the fuselage.

There remains one major classification of configuration that could be considered useful in the Low Speed HALE UAV role.

2.C.5.e Flying Wing

The most obvious application of the flying wing configuration to the Low Speed HALE UAV role is as a simple span loaded aircraft. This configuration was used in the Aerovironment *Pathfinder*, and will be used in the Aerovironment *Centurion* and *Helios* aircraft as well. This particular configuration is well suited to Low Speed flight, as it doesn't sacrifice any of the low speed flying qualities by sweeping the wing. It does, however, present a challenge in stabilizing the aircraft in yaw. In addition, special airfoil sections must be used in order to counter wing pitching moment. This field still has a great deal of evolution to endure before aerodynamic efficiency is not sacrificed too much.

As an example, Kroo[47] makes the statement for tailless sailplanes and airfoils with flaps, a static margin of 0.2 at a C_L of 1.0 (with zero lift moment coefficient, $C_{m0} = 0.2$) would entail completely unacceptable drag penalties. He observes that as in the canard case, some performance advantages are predicted but they are small, especially in light of the assumptions required in the analysis. These conclusions were the result of studying tailless gliders with small sweep.

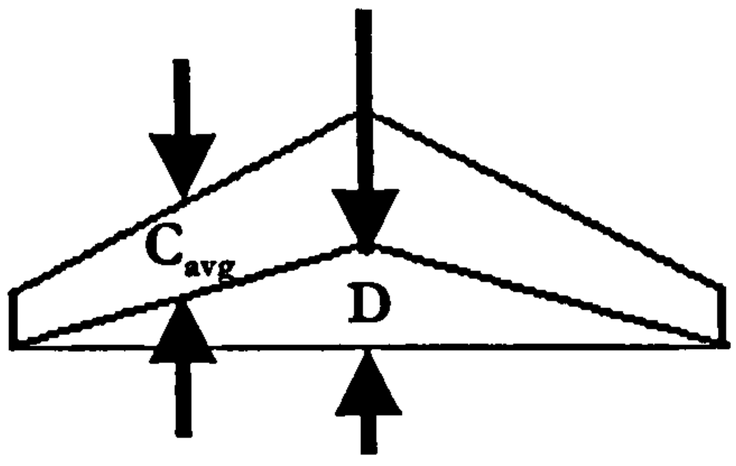

Figure 2.15 ***shows the average chord and trailing edge kink dimension for a flying wing configured aircraft***

Culver[99] provides a simple design criteria to use in order to avoid the problem of tumbling. The reason tumbling is a problem is that the machine gets trapped in its own lift circulation or vortex. The tumbling study suggested that a simple criteria for the borderline between tumbling and not tumbling, for the case of the cg in the wing chord plane vertically, and at 25% of the MAC, was D/C = 2. Here C is the average chord and D is the trailing edge kink dimension (Figure 2.15). High sweep angles alleviate the problem of the tendency towards Pilot Induced Oscillation in a machine with low pitch or yaw damping, but it is unlikely that this will be a consideration for anyone but the flight control system software manager. If plane tumbling were induced, the effect of a vertical offset of the cg for cg's of 1 average chord above or below the chord, the tumbling would not continue. Swept back wings have excessive roll due to yaw $+C_{l\beta}$ so Culver suggested using bent down tips for fins and rudders. These could be cranked as much as 45°. Bent tips at 45° are so powerful in producing $-C_{l\beta}$ that the wing can have some dihedral to give ground clearance as indicated both by theory and paper model tests.

Guglieri and Quagliotti[40] provide a flying wing, wing weight estimation as a linear function of wing surface area S. The difficulty with this formula is that it was written for solar cells covering 80 % of the area of the wing. This affects the structural rigidity as well as the weight.

The next section includes brief discussion about a configuration that has been considered mostly in sailplanes, but curiously could be used to overcome one of the limitations of Low Speed HALE UAV's.

2.C.5.f Telescoping Wings

Telescoping wings have been proposed previously in an attempt to change the wing loading in flight. The primary reason that the telescoping wing is a curious possibility for Low Speed HALE UAV's would only be clear if a time to climb requirement were imposed. In traditional sailplanes, this is attained using water ballast to alter the low speed and high-speed characteristics in flight.

In a study by Mueller and Heuermann[43], they discovered that the adaptation to the high speed and slow speed flight only with the aid of changes of wing areas and wing span didn't reach the performances achieved by changes in curvature and wing area for wing-flap wings. Their results from the design of the *SB 11* sailplane led to the knowledge that neglecting the flight properties in favor of the flight performance can lead to theoretically possible advantages not being obtained in flight. When commenting on the failure of the telescoping wing to improve the performance more than ballast for the cost, they stated that small performance related inferiority in individual items in favor of distinct superiority in other items could lead to substantial overall disadvantages.

2.C.6 Cooling Drag Estimation

One area that receives almost no attention in common methodologies is cooling drag. Most of the attempted Low Speed HALE UAV applications have used an internal combustion reciprocating engine. Depending on what load these engines are operating under, they can generate a great deal of waste heat. In normal circumstances, it would not be a large drag penalty to devise a cooling system for an aircraft with an extra heat load. The problem is that for a Low Speed HALE aircraft in cruise, the ability to transfer heat to the atmosphere is greatly diminished due to the extremely low air density resulting in very poor convection rates. This problem has received some attention in the literature.

In general, 3 different concepts for heat rejection in Low Speed HALE UAV's are discussed. Fuel tank heat sinks, flow through radiators, and surface heat exchangers. The fuel tank heat sinks were used in combination with surface heat exchangers for the Boeing *Condor*. The difficulty with employing this type of cooling method is estimating the weight of the plumbing necessary to implement it, and predicting the ability of the fuel to dissipate the heat in cruise as it is diminished in supply. In addition, there were no data

available on the topic of boundary layer transition being influenced by heat transfer on laminar flow airfoils. It is a well known result, however, that if enough heat is transferred through the surface of the wing that transition would occur earlier than if there were no heat transfer.

Petkus and Gallington[100] described some concepts for minimizing heat loads and rejecting waste heat effectively. Heat rejection concepts such as surface heat exchangers, fuel tank heat sinks, and conventional radiators, were discussed relative to their respective merits and weaknesses. They mention that forced heat convection at altitudes greater than 60,000 feet is similar to free convection at sea level. Also, that the heat rejected from a reciprocating engine is mainly a function of the horsepower being extracted and is not explicitly influenced by the altitude at which it is operating. Finally, they devised several mathematical relations for use as power losses, or corrections due to cooling drag. The derivation of these terms included some highly configuration dependent assumptions.

Since all of the internal combustion reciprocating engines use some form of combination of turbo and supercharging, there is some information available on the results of this approach. Nagurny[101] describes how a reverse Rankine cycle waste heat recovery system has the potential to increase the endurance of a HALE by up to 7% (over that obtainable with a baseline heat rejection system). The cycle operated with a thermodynamic efficiency of about 15%, assuming that the working fluid was adequately superheated. Using this system introduces additional weight and ram drag penalties; however, the net power gain claimed is well above the imposed losses.

Tonskotter[75] describes the system used in the Grob *Strato 2C*. The nacelle flow is heated when passing the heat exchangers and the internal drag of the nacelle is very low. A total heat rejection of about 225 HP at an altitude of about 80,000 feet requires very large heat exchangers with a total frontal area of 38 ft^2.

Russ and Drela[102] comment on the system devised for the *Perseus B* aircraft. For a given powerplant performance and cooling requirement, the tradeoffs for an optimum heat exchanger design were between cooling drag and installation weight. Preliminary sizing of the *Perseus* ram air heat exchangers showed that optimum designs would have frontal areas of approximately 7.5 ft^2 for the high temperature exhaust gas heat exchanger and approximately 6.5 ft^2 for the liquid coolant heat exchanger. Total heat transfer area for both heat exchangers is almost 3 times the wing area.

The aerodynamic layout and the exact location of the cooling duct was done such that the effect simulated the presence of an additional lifting surface. The effect on the longitudinal stability of the *Perseus* aircraft would balance out the shift in aft direction of the cg. Since the air charge temperature (ACT) of the engine was only allowed to be in a relatively narrow range, the exhaust gas heat exchanger exit temperature had to be actively controlled. An ACT above a certain limit would lead the engine into knocking and an ACT under 273 K would freeze the water in the exhaust gas created as a byproduct of combustion.

In another paper by Mark Drela[103] he discusses the integration of the heat exchanger into the wing, as was done on the *Theseus* aircraft. In the case of a wing leading edge inlet, an ineffective inlet geometry can have very adverse effects on the wing airfoil, as demonstrated in previous experimental studies. This makes a radiator installation that is separate from the wing less risky and more attractive. On the other hand, effective integration of the radiator with the wing airfoil also offers possibilities for favorable interactions and greater compactness, with possibly lower overall drag and lower system weight than with an equivalent isolated installation.

Drela derives a set of relations describing the drag of a radiator core arrangement based on the heat transfer through it. He mentions that a net thrust is obtained from the ramjet term over much of the range of operating altitudes. That if properly implemented, the radiator core drag is virtually nil even at the rather high pressure drop coefficient ($P = 10$), most of the frictional drag being canceled by the ramjet effect. Most of the problems inherent in the aft mounted radiator can be largely overcome with the front mounted installation, which does not subject any thick boundary layer to the cowl/radiator's pressure field and allows much smaller velocity ratios to be used. That along with the experimental and numerical results of this investigation, result in the conclusion that the front mounted configurations appear to be inherently superior.

Most of the items discussed in the literature review were introduced with the intention of justifying decisions taken later in the methodology and thesis. Although it may not have been readily apparent at the first reading, it is hoped it will start to become clearer with the topic of the next chapter, an introduction to the methodology.

Chapter III

If you want to truly understand something,

Try to change it

--- Kurt Lewis

3. Overview of the Methodology

In the Introduction an attempt was made to delineate the problem for which this thesis was written to address. Where the problem or need originates from was described, and how this thesis intends to address the problem in general terms of the design of Low Speed HALE UAV's was also described. The purpose of the Literature Review was to try to explain the scope of the problem and how aspects of the problem have already been addressed in the literature.

This chapter will begin the discussion of the ***methods*** used to approach the solution of the problems mentioned in the previous chapter and the Introduction. It will present the structure for the methodology that the entire thesis is based upon. This chapter will introduce the concept of the difficulty and challenge of programming this particular methodology as an object-oriented computer based application. In addition, the procedure used throughout this thesis to describe the structure of the methodology and its implementation will be highlighted.

3.A Parallel Currents

The writing of this thesis is even more of a challenge than the ordinary scientific dissertation. The difficulty arises in the description of the approach to the solution of the problem. There is a significant theoretical component in addition to a significant component resulting from the actual coding of this theory in the object-oriented environment. This has already been alluded to somewhat in the Literature Review.

On the surface, it would seem all that needs to be done is to code the equations and the methodology has been implemented. In reality, as described in the Literature Review, and as will be explained in more detail, this is rather far from the actual case. It is for this reason that the thesis has been broken down by a description of the theory used, and a description of the implementation of that theory for specific cases.

It will be extremely difficult in some cases to divorce the implementation from the theory since one often drives the other, however, some attempt will be made to leave discussion on the implementation for the chapter specifically designated to address it.

These are in effect *Parallel Currents*. The ideal way to explain the existing complementary nature between the theory and the application would be for the human mind to have two parallel input channels to enable the visualization of both simultaneously. Since that is likely to be invented farther in the future than this thesis will evaluated, a sequential format will be used, with the discussion of the theory preceding the discussion of the implementation.

The question might arise as to why there is any emphasis in this thesis on the implementation at all, as it may not at first appear to constitute a significant part of the original contribution in this work. It will be shown in the chapter on the implementation that it is in fact a considerable element in the process of the computational design of any aircraft.

3.B The Methodology

It would be untenable to claim that the methodology was entirely new or groundbreaking. Instead, the methodology used is described as an application of an existing analytical technique to the solution of a problem. Whereas the procedure for the analysis is similar to existing procedures, the analytical techniques utilized at each stage in the procedure are different from or are a conglomeration of existing techniques based on validation against a few existing design points. In addition, the ability to navigate freely about the procedure is also rather unique in a computational methodology.

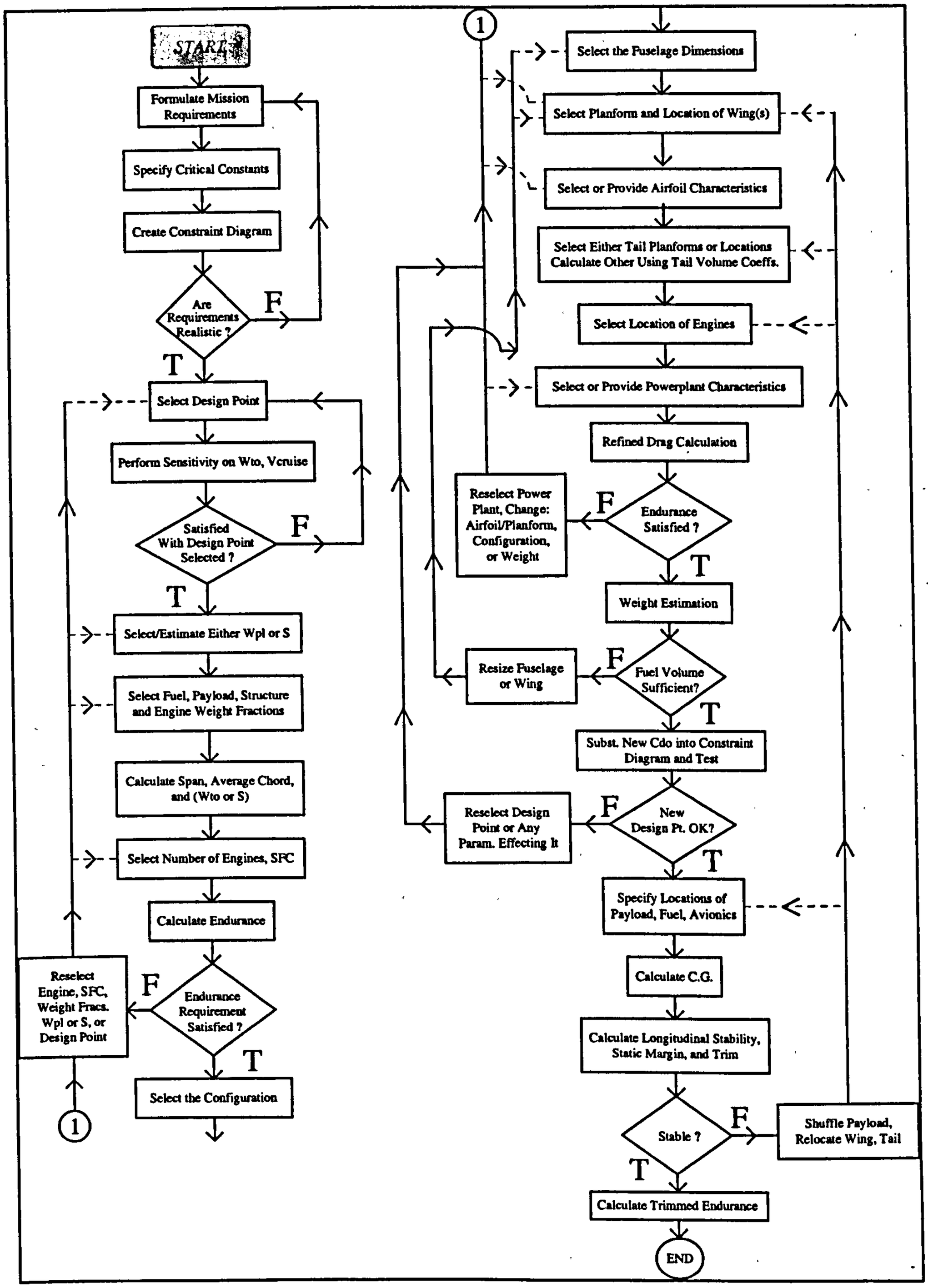

Figure 3.1 *is the structure of the Conceptual Design Methodology used throughout the thesis.*

The human machine performs many of these tasks giving little thought to the decisions that it is making. There are no existing equations or decision trees for this truly unique aspect of the methodology, however it will be discussed in greater detail in the implementation chapter.

In the past, the application of the computational design methodology has been rather sequential in nature. There are ***NO*** non-proprietary methodologies that allow you to freely construct multiple fuselage, multiple lifting surface aircraft, or to freely change the geometry of several different configurations and to visualize those changes side by side. It has not been possible before to quickly evaluate the effects of these changes on weight and drag in real time for the purposes of conceptual design and sizing. The implementation of this methodology allows that.

As noticed from the diagram of the methodology there are numerous feedback loops that simply cannot exist in other computational implementations of the general conceptual design procedure (this of course excludes MVO methods). The implementation of this methodology not only allows for that freedom, but the results obtained due to that freedom to navigate the procedure allows for a considerably greater understanding of the driving parameters in each of the design concepts considered (this includes MVO methods). The designer can, at any time in the design process, return to change any of the relevant design parameters without having to restart and re-execute the program. The procedure followed in the methodology will be mirrored in the development of the thesis. Therefore, detailed discussion of the methodology is left for the respective chapters outlined in the next section.

3.C The Procedure

The discussion of the various aspects of the procedure and the underlying theory will be as follows:

Chapter IV :

- Formulation of the Mission Requirements
- Specification of the Critical Constants
- Creation of the Constraint Diagram
- Evaluation of the Realism of the Constraints

- Selection of the Design Point
- Sensitivity on Takeoff Weight and Cruise Velocity
- Selection of the Payload Weight or Wing Area
- Selection of the Preliminary Weight Fractions (only used for the 1st estimate/Preliminary Sizing)
- Selection of the Number of Engines and Fuel Consumption and Excess Power Available for Climb
- Calculation of the Initial Endurance and Time to Climb
- Selection of the Configuration

Once the configuration has been selected, the next chapter will cover the details of the sizing of the default configuration and the re-sizing of existing configurations. In the execution of the program, this re-sizing happens in no particular order. Each procedure is invoked by the selection of the relevant button on the desktop or by clicking the mouse over the relevant part of the aircraft.

Chapter V :

- Fuselage Dimension and Location Specification
- Wing Planform Parameter Definition
- Airfoil Characteristics Specification
- Tail/Canard/Tandem Wing Planform/Sizing Characteristics Specification
- Location and Performance of Engine(s)

Chapter VI :

Chapter VI is reserved solely for discussion on the calculation of the drag of the aircraft and its components.

Chapter VII :

Chapter VII is reserved solely for discussion regarding the calculation of the aircraft and aircraft component weights.

Chapter VIII :

- Specification of the Location of the Payload in the fuselage
- Specification of the Center of Gravity of the Aircraft with and without Fuel

- Calculation of the Aerodynamic Center of the Aircraft
- Determination of the Aircraft Static Margin
- Calculation of the Effects of Trim Drag on the Endurance
- Recalculation of the Endurance based on Revised Drag and Weight estimations

As mentioned earlier, Chapter IX will discuss the problems specifically associated with attempting to program the above procedures in the object-oriented environment and the difficulties associated with knowing which decisions to leave in the hands of the designer, and how many decisions to automate.

Chapter IV

Perseverance is not a long race,

It is many short races one after another

--- Walter Elliot

4. Preliminary Sizing

This chapter will describe the methodology and theory used in the early preliminary sizing stage up to the specification of the configuration. Discussion of the Mission Specifications will be limited to the referral of the reader to the Introduction where most of the potential missions for the Low Speed HALE UAV were described. In general, selection of any of these missions specifies the critical constants to be discussed next. The particular missions to be used in generation of the results of this thesis will be described in the Results Chapter. It is, however, assumed that the methodology has been written in a way that insures that it can be applied to *any* of the potential missions described in the Introduction. For a detailed description of the actual design process followed in this chapter, the reader is referred to Figure 3.1.

It is again noted that the methodology was created as a tool for the identification of any relevant trends resulting from the variation of certain configurational, operational, or geometric characteristics. Thus, the organization of the methodology reflects this orientation. The methodology was not intended to allow the designer to specify an exact mission endurance, and to iterate or optimize based upon this information to find a unique solution.

4.A Specification of the Critical Constants

Any of the variables necessary to create a constraint diagram are considered to be constants critical to the early initial sizing of the aircraft. After setting up the equations relevant specifically to the Low Speed HALE UAV constraint diagram, the resulting

critical constants can be see in Figure 4.1. Figure 4.1 is a snapshot of the Critical Constants Dialog box. Once again, it is pointed out that reasonable values for all of these constants can either be derived using common sense, or obtained from the common literature.

The exact implementation for each of the constants will be explained in the next section. It is noted that the constants for Oswald efficiency and zero lift drag are used exclusively for the calculation of the constraints and time to climb. Once the configuration has been specified, the drag breakdown will be calculated explicitly.

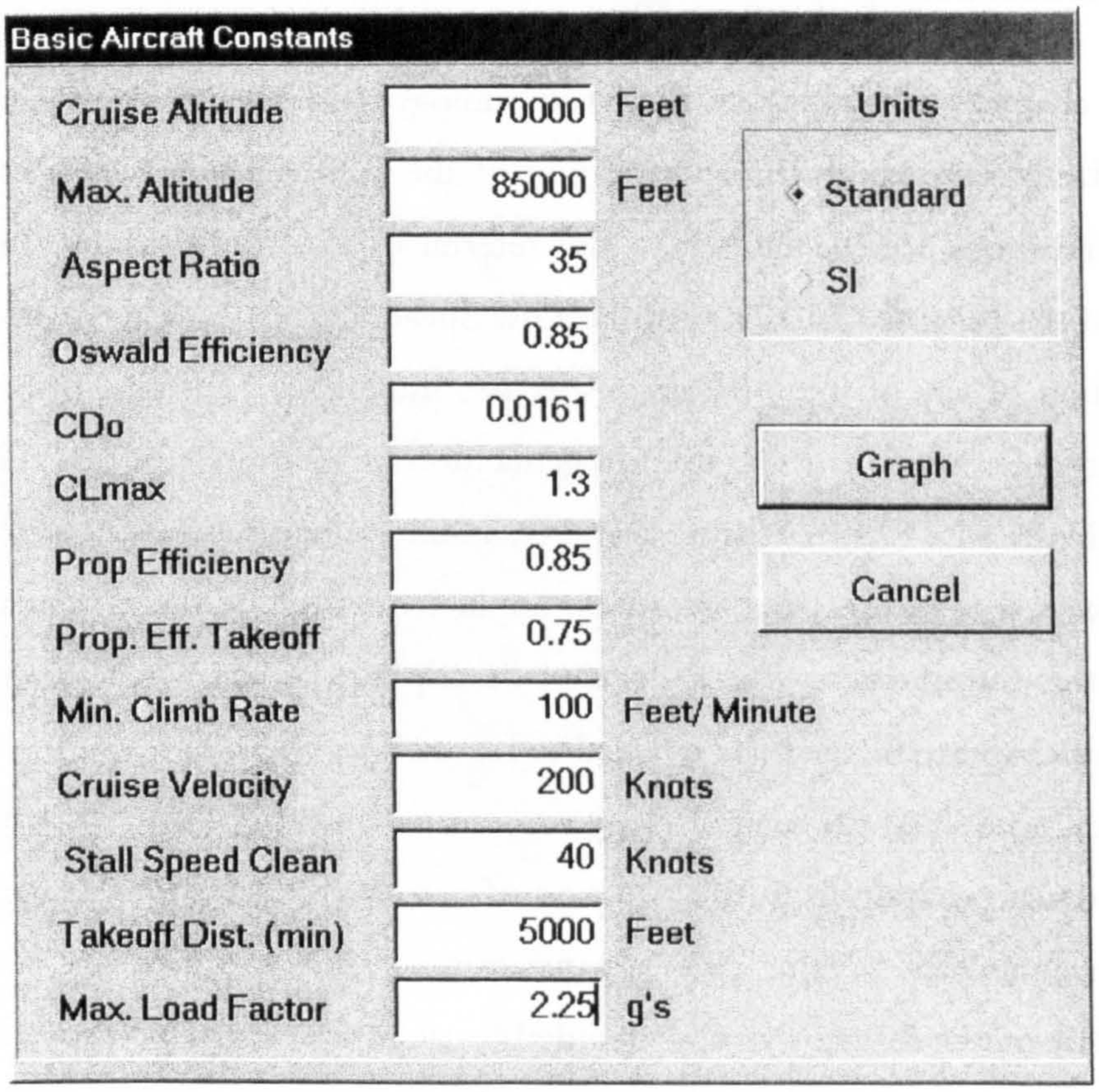

Figure 4.1 *is the Critical Constants or Basic Aircraft Constants dialog box which is used for the input of data necessary for the creation of the Constraint Diagram.*

4.B Creation of the Constraint Diagram

The Constraint Diagram is familiar to all in the aircraft design field. The design space for the aircraft must be defined in the early stages in order to size the aircraft properly without violating any of the basic laws of physics. The most general form for this diagram is Wing Loading (W/S) versus Thrust or Power Loading (HP/W).

This diagram has an inherent utility that is indispensable. The Constraint Diagram provides multiple possibilities from which to launch the non-unique iterative conceptual design process. Using the diagram, a general idea of the size of the aircraft is easily known. Using the present methodology, a comparison of two or more Constraint Diagrams side by side is possible. This quickly identifies how variation in any of the critical constants effects the constraints set out by a given mission.

In this way, the critical constants can be manipulated and the effects of each change can be plainly seen. This emphasizes which of the driving constraints that will have the most bearing on the design. It also identifies where a change in a given constraint will impact the performance of the aircraft the most. In the following section, the equations used for the creation of the constraint diagram are included. Their derivation is straightforward and can be found in most aircraft design textbooks.

All of the equations that follow are in terms of the horsepower to weight ratio as a function of the wing loading. In general, the equations are in terms of the lift coefficient. The conversion factor of 1/550 is present in all equations to convert from units of ft lbf/s to horsepower.

4.B.1 Maximum Load/Turn

A quick derivation based on the assumption of a parabolic drag polar yields the equation:

$$\frac{HP}{W} = \frac{1}{550\eta_p}\left[QC_{D_o}\left(\frac{S}{W}\right) + K\frac{n^2}{Q}\left(\frac{W}{S}\right)\right] \qquad \textbf{(4.1)}$$

This equation is written in terms of $(C_{Do}, Q, K, \text{and } n)$ where $Q = \frac{1}{2}\rho V^2$, and $K = \frac{1}{\pi AR\varepsilon}$ and assumes a constant velocity turn. In this equation, the density selected (ρ) was at cruise altitude . Propeller efficiency (η_p) is considered a constant value. Load factor (n) is provided depending on how robust a structure is necessary or desired, and what g loading the aircraft is to be designed for in a turn. The zero lift drag coefficient $\left(C_{D_o}\right)$ has already been specified by the designer.

As can be seen from this equation, for a given design (fixed η_p, C_{D_o}, K), maximum load will be most sensitive to changes in Altitude (ρ), maximum load factor (n), and velocity.

4.B.2 Endurance

$$\frac{HP}{W} = \frac{4}{550\eta_p} C_{D_o}^{1/4} \left(\frac{K}{3}\right)^{3/4} \left(\frac{2}{\rho}\frac{W}{S}\right)^{1/2} \tag{4.2}$$

In the endurance equation, again for a fixed design , the design is sensitive to the zero lift drag coefficient (C_{Do}), the aspect ratio (through K), and the altitude (ρ).

4.B.3 Cruise

$$\frac{HP}{W} = \frac{2}{550\eta_p} C_{D_o}^{1/4} K^{3/4} \left(\frac{2}{\rho}\frac{W}{S}\right)^{1/2} \tag{4.3}$$

In this equation, only aspect ratio (through K), C_{Do} and altitude have any effect on the sensitivity of the design to variation of the cruise parameters. For the creation of the constraint diagram, even though wing loading was varied, it was necessary to maintain C_{Do} as a constant, as specified. Although this would not be the case in reality, for the purposes in the early sizing phase of the methodology, it was thought appropriate.

4.B.4 Rate of Climb (RofC)/Ceiling

$$\frac{HP}{W} = \frac{1}{550\eta_p}\left[\mathrm{RoC} + \left(\frac{C_{D_o}}{C_{L_{\max}}^{3/2}} + KC_{L_{\max}}^{1/2}\right)\left(\frac{2}{\rho}\frac{W}{S}\right)^{1/2}\right] \tag{4.4}$$

In this equation, the parameters that affect sensitivity to a specific design are the altitude, aspect ratio, and the maximum lift coefficient ($C_{L\max}$). The maximum lift coefficient is used instead of the maximum lift to drag ratio or minimum power required lift coefficients. This is due to the fact that the true limiting factor in terms of lift coefficient at such a high altitude will most likely be stall speed for a given wing loading/power loading. Therefore, for the constraint diagram, the most limiting factor for the design is used.

To use this equation to calculate the absolute ceiling of the aircraft, the Rate of Climb (RofC) is simply set to zero.

4.B.5 Takeoff Distance

$$\frac{HP}{W} = \frac{2.44}{550\eta_p}\frac{1}{gd_{to}}\left(\frac{1}{\rho_{SL}C_{L_{\max}}}\frac{W}{S}\right)^{3/2} \tag{4.5}$$

For the takeoff distance constraint equation the greatest degree of sensitivity is found in the takeoff distance (d_{to}) specified and the maximum lift coefficient. The density is assumed to be that at sea level. The takeoff propeller efficiency should be that appropriate for takeoff with a cruise-maximized propeller unless a variable pitch propeller is assumed. The takeoff velocity is assumed to be 1.2 multiplied by the stall speed.

4.B.6 Stall Condition

$$\frac{W}{S} = \frac{\rho}{2}C_{L_{\max}}V_{So}^2 \tag{4.6}$$

This equation is sensitive to the assumed values of maximum lift coefficient and stall speed (V_{So}). The density is assumed to be at sea level for the constraint diagram since no other reasonable assumption could be made. Thus, this constraint is in effect a maximum allowable stall speed. This is chosen as a constraint for a UAV as it is often found that a Low Speed HALE UAV will be built without assuming the drag and weight penalties of a permanent undercarriage. With this in mind, the minimum possible speed at which the aircraft can touch down is desired, more so than for an aircraft with traditional landing gear.

4.C Evaluation of the Realism of the Constraints

Now that the Constraint Diagram has been created it is necessary to evaluate whether or not the Constraints resulting from the Critical Constants are realistic. For example if a cruise altitude of 120,000 feet was selected and a desired HP/W ratio of 0.04 was also desired this is quite obviously not possible based solely on the physics involved.

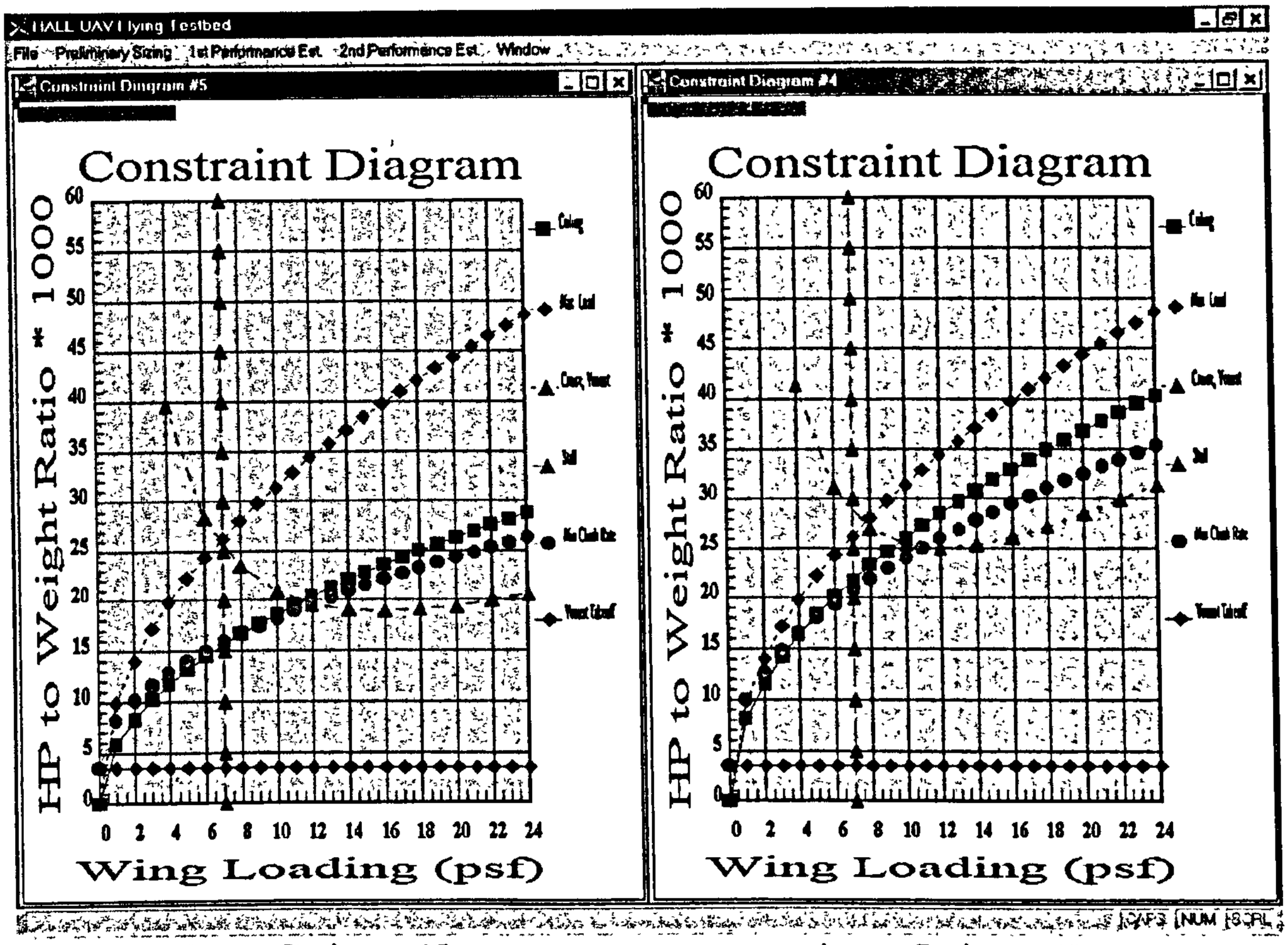

Aspect Ratio = 35 Aspect Ratio = 20

Figure 4.2 ***is a demonstration of the comparative abilities of the implementation of the methodology. In this case two constraint diagrams with differing aspect ratios, but otherwise identical constants are compared side by side.***

For each Critical Constant specified for any given mission, this type of analysis must be performed. The Constraint Diagram allows this process to occur quickly. Early tradeoffs in size and performance can be made even before a specific configuration has been selected. In addition, using the ability of the program to represent results of the variation of different parameters side by side, this process has been sped up considerably. An example of the Constraint Diagram variation due to a change in Aspect Ratio is provided in Figure 4.2. It can be observed from this diagram how much of a variation can occur in any given constraint based entirely on the variation of a single Critical Constant. This example roughly corresponds to the difference in Aspect Ratio of the Boeing *Condor* and the Aurora Flight Sciences *Perseus B*. It can also be observed from this diagram that at least for this particular set of Critical Constants, Takeoff Distance is the least constraining of the curves. The design space is bounded on the left by the Constant

Velocity Cruise Constraint, on the right by the Stall Constraint, and on the lower end by the Maximum Load in Turn Constraint.

4.D Selection of the Design Point

At this point, it is safe to assume that a reasonable Constraint Diagram has been created. A certain degree of trial and error may have been necessary to achieve this, and a better understanding of the critical constraints should now exist. The design space should now be acceptable enough in range to create a robust design with room for slight variation in any given Critical Constant without generating a conflict with any of the constraints. Now the design point can be selected.

It should be noted that even after the design point has been selected, it will always be possible during the program/methodology to return to the selection of the design point (or the selection of the critical constants). This can be done to create another configuration based on any desired variation (slight or major). This change can be for the purpose of comparison or for a better understanding of any parameter driving the design. It is also very important to note that the design point is a normalized quantity and as such represents a range of possible design solutions depending on the selection of takeoff weight, wing area, or HP.

4.E Sensitivity on Takeoff Weight and Cruise Velocity

In order to enhance the ability of the designer to make an educated choice even further, two separate sensitivity curves were created. The first compares the variation in Lift Coefficient as a function of and Wing Loading and Cruise Velocity. This was thought to be useful given the sensitivity of the left side bound on the design space. As can be seen in Figure 4.3, the Maximum Lift Coefficient is drawn as well as the Design Point if it has already been selected. The reason the Design Point is represented by a line on these figures was to provide the designer with the ability to visualize the effects of selecting one takeoff weight or one cruise velocity based upon the Wing Loading already selected. The most important aerodynamic characteristic on the plot is the minimum power required lift coefficient (C_{LminPR}). This term has direct significance in the endurance equation and

should ideally be the cruise lift coefficient. For aircraft with very large aspect ratios, practical limitations in maximum lift coefficient usually make this difficult to achieve. This results from the fact that C_{LminPR} scales almost directly with the square root of the aspect ratio for a given zero lift drag coefficient (see Equation 4.9). Thus, also included for interest is $C_{LmaxL/D}$.

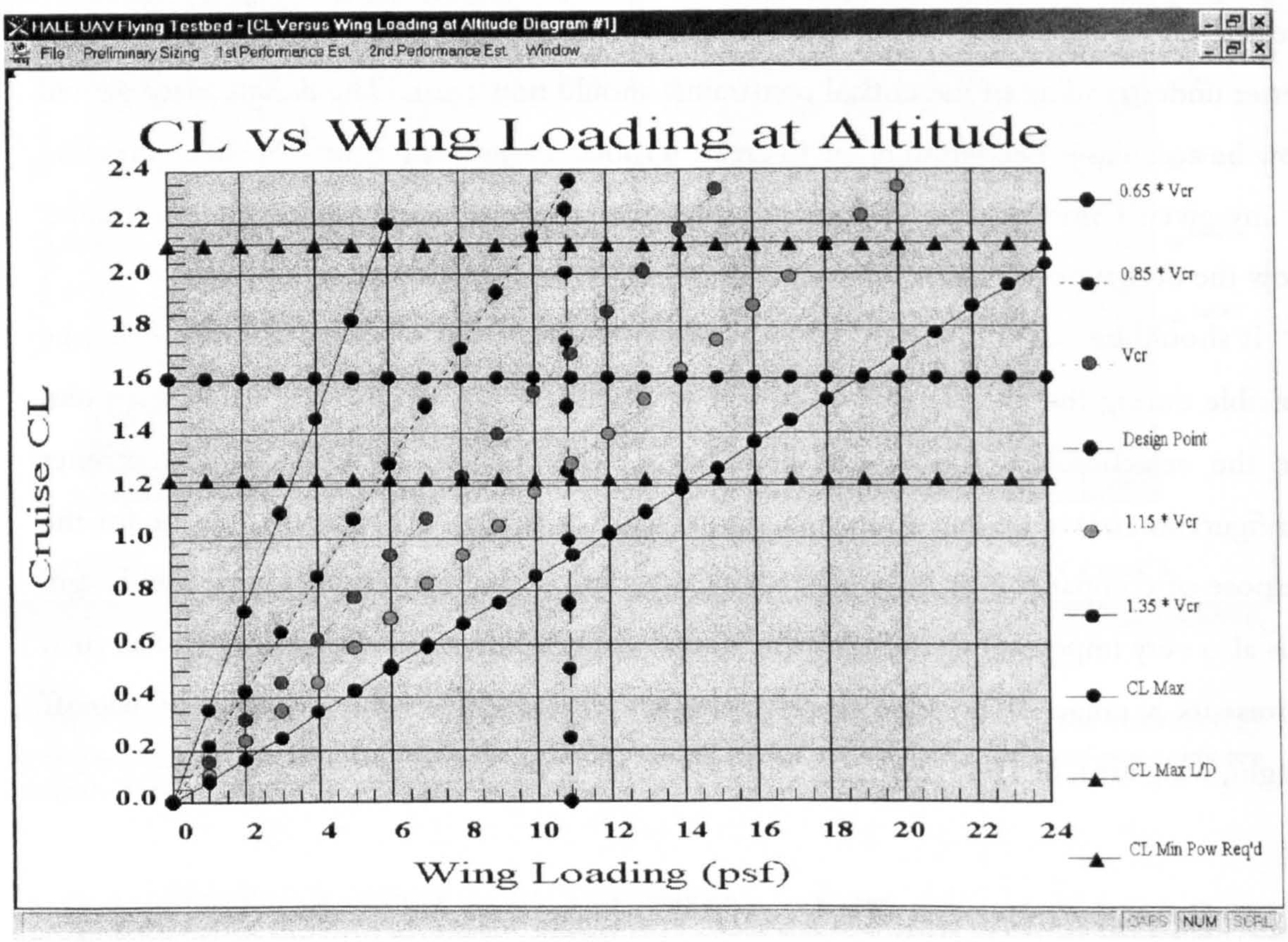

Figure 4.3 ***is one of the sensitivity diagrams. It shows the maximum lift to drag ratio and minimum power required lift coefficients, and a sensitivity on cruise velocity as a function of wing loading and lift coefficient.***

Another reason for including this curve is that approximately 70 percent of the aircraft drag is due to the wing. Thus the cruise lift coefficient would be of interest to the aerodynamicist for yet another reason. It can be observed from the figure that a 15% increase in cruise velocity results in an almost 25% change in possible wing loading at maximum lift coefficient for this particular set of critical constants. It can also be seen in the figure that for this particular set of critical constants, the C_{LminPR} is about 2.1. This is obviously not practical for an unflapped wing.

The second curve made available by the program is a sensitivity diagram for the variation in Wing Area as a function of Aircraft Takeoff Weight and Wing Loading. An

example of this curve can be seen in Figure 4.4. There are several excellent reasons for including this diagram.

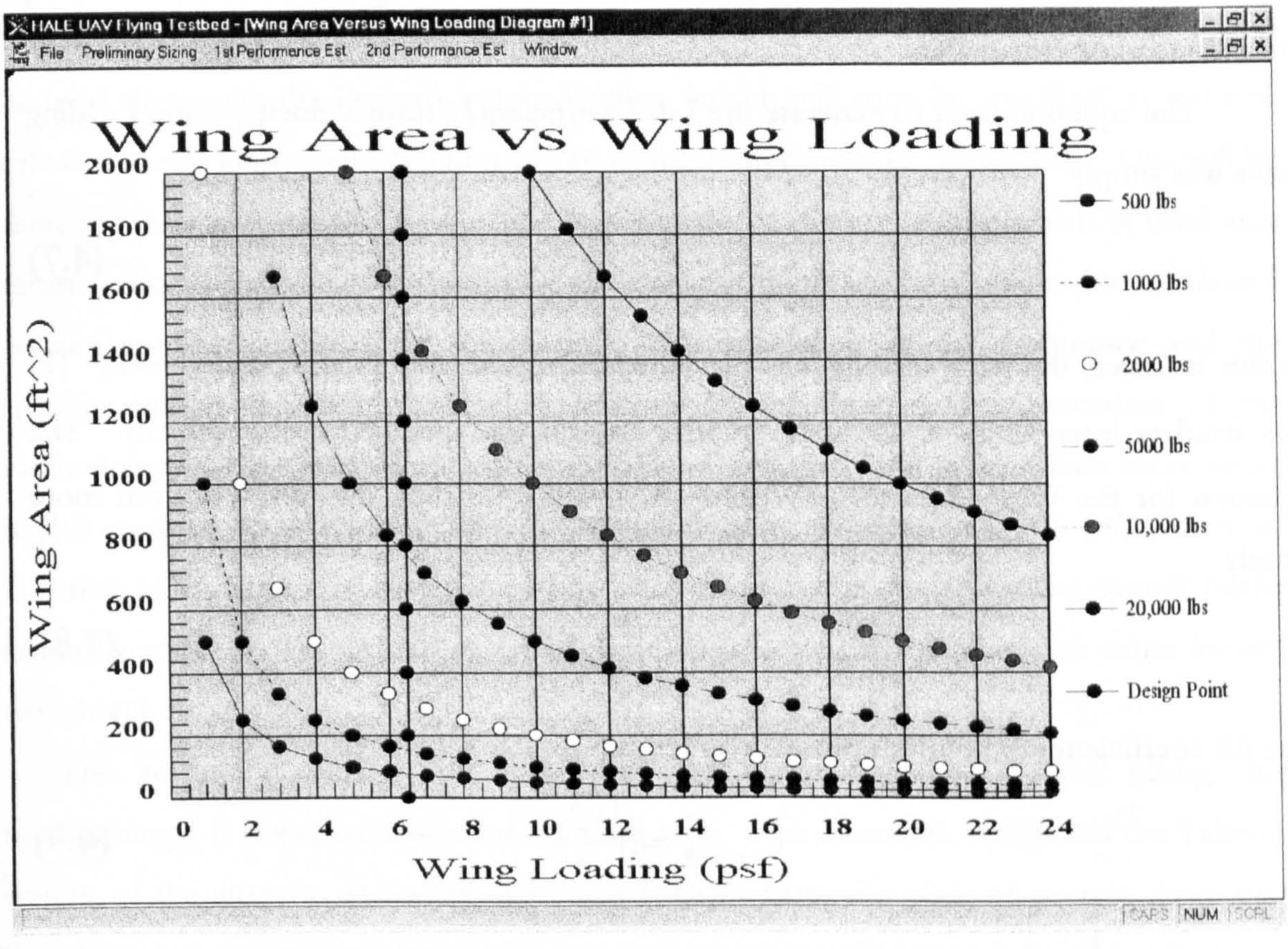

Figure 4.4 ***is a sensitivity diagram for takeoff weight as a function of wing loading and wing area. The selected design point is also drawn on the curve for interest. This is one of the two sensitivity diagrams available immediately following the selection of the design point.***

In general, the wing of the aircraft is going to be responsible for a very large portion of the drag. As mentioned before, approximately 70% of the drag of this type of aircraft is due to the wing. Interestingly, there is a balance between parasite and induced drag. At high values of cruise lift coefficient, lift induced drag dominates and at lower lift coefficients it is the parasite drag that dominates. Thus, for a Low Speed HALE UAV in cruise, the induced drag will be the dominating factor. If the lift coefficient is low, it represents a potential conflict in constraint. A low wing loading is desired in order to combat the effects of vortex drag, and a low wing area is desired to combat wetted area effects on drag. With some knowledge of the size of the payload desired, and the fractional weight of the payload relative to the entire aircraft, the takeoff weight of the aircraft can already be determined. This sensitivity diagram enables the designer to compare these quantities and visually interpret the tradeoffs.

It is obvious from this figure that there is a point at which the weight increases sharply for a given Wing Area. This diagram can be used to insure that the selected design point is within the flat range of the weight curve while minimizing wetted area and keeping the wing loading reasonable.

The equation used to generate the Lift Coefficient/Cruise Velocity/Wing Loading curve was simply:

$$C_L = \frac{1}{\frac{1}{2}\rho V^2}\frac{W}{S}. \tag{4.7}$$

In this instance, the wing loading was the independent variable (x-axis), the velocity (V) was fixed at intervals of ± 15% and ± 35% around the specified cruise velocity. The equation for the Wing Area (S_{ref})/Weight (W_{to})/Wing Loading diagram was even more simply:

$$S_{ref} = \frac{W_{to}}{\frac{W}{S}} \tag{4.8}.$$

The lift coefficient at minimum power required is :

$$C_{L\min PR} = \sqrt{\frac{3C_{do}}{K}} \tag{4.9}$$

where K is $\frac{1}{\pi AR\varepsilon}$. ε is the Oswald Efficiency factor specified by the designer. The maximum lift to drag ratio lift coefficient was calculated similarly without the factor of three in the square root used for calculation of minimum power required.

After having reviewed the relevant design space, the aforementioned sensitivity curves, and after reviewing the constraint diagram again, it is once more suggested to specify or re-specify the design point based upon the new information at hand.

4.F Selection of the Payload Weight or Wing Area

It is necessary in the early preliminary stages of the conceptual design methodology to start the iterative design process somewhere. Some methodologies claim to be original in terms of how they go about addressing this. In fact, there are few differences in how this process can ultimately be performed at present.

It is therefore with little justification that the iterative process for this methodology will be started with the selection of either the Payload Weight or the Wing Area. At first glance the Payload weight might seem a strange choice of entry points to the iterative process. Taking two steps down the procedure it can be seen that the Payload weight will be used along with the Payload weight fraction (which will soon be specified) in order to calculate the overall weight fraction of the major components of the aircraft. This will be done in order to provide an approximate estimate of the endurance which is used as a means to verify that the overall sizing of the aircraft can perform the mission desired based on the specified payload (in this case). The calculation of the endurance and the specification of the weight fractions occur a further along in the procedure of the methodology. The justification for using payload weight should make a little more sense in this context. It is noted the above discussion made no mention of the more obvious fact that often times the designer of this class of aircraft is designing the aircraft based around a very specific payload or set of payloads, the weights of which are often known (roughly) beforehand.

The second possibility for entry into the iterative design process (using this methodology) is the specification of the wing area. This essentially designates the Takeoff weight of the aircraft. It was thought that for this particular class of aircraft, these two quantities were more useful than the straightforward specification of the Takeoff weight itself. The wing area will drive the wing loading and the drag of this aircraft. These two quantities were also thought to have greater bearing on the final sizing of the Low Speed HALE UAV aircraft than the Takeoff weight alone.

4.G Selection of the Preliminary Weight Fractions

It should be noted that these weight fractions $\left(\frac{W}{W_{to}}\right)$ are merely used in the very early stages of this methodology until the default aircraft has been provided and a more detailed weight estimation can be performed. The quantities that are requested can be seen in Figure 4.5. Weight fractions are required for payload, engines, structure, and fuel. Although not many HALE UAV's have been built, there is enough information available to make sensible estimates for these values as seen in Table 4.1, with the exception of the powerplant weight fractions.

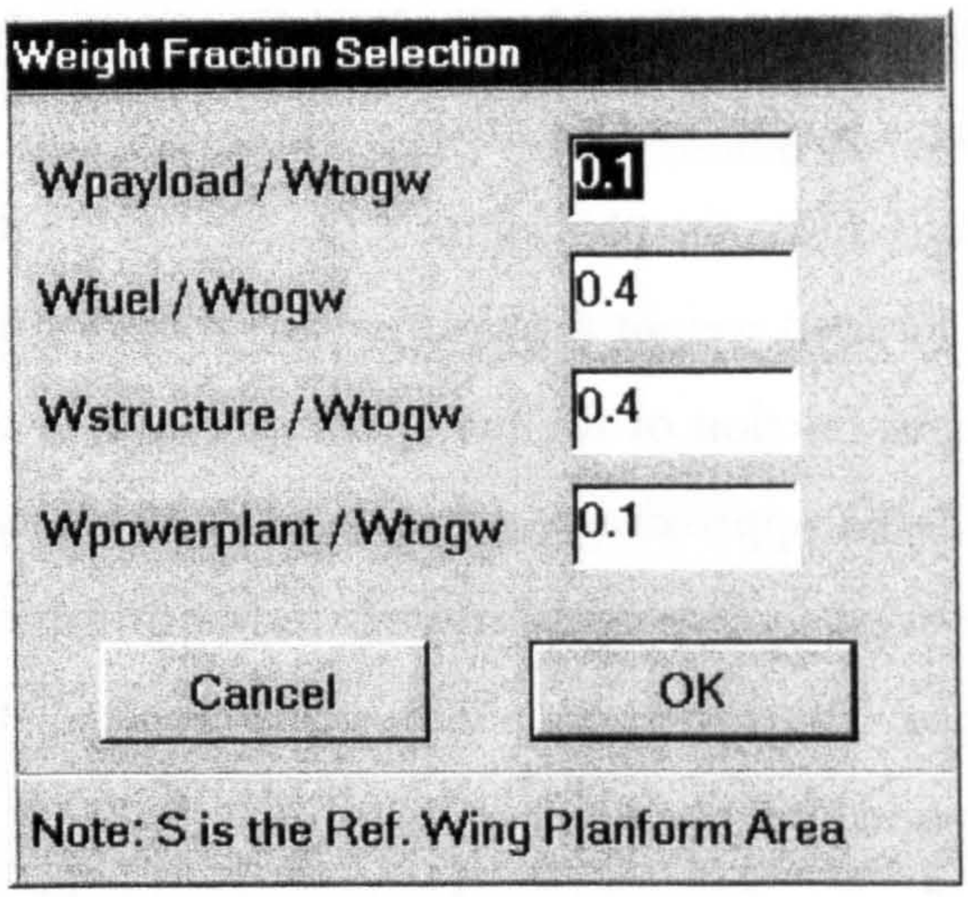

Figure 4.5 ***is the Weight Fraction Selection dialog box which enables the designer to enter early preliminary weight fraction data available from the literature.***

Of the aircraft shown in the table, the long endurance aircraft generally have lower than 40 percent structural weight, have less than 10 percent payload fractional weight, and fractional fuel weights of at least 40 percent.

Table 4.1 ***is a compilation of known weight fractions for aircraft similar to the Low Speed HALE UAV obtained from the literature.***

	W_{empty}/W_{to}	W_{maxPL}/W_{to}	$W_{maxfuel}/W_{to}$
Heron	0.544	0.093	0.363
Hermes 450	0.445	0.133	0.422
Aura (USN)	0.5	0.25	0.195
HiLine	0.543	0.041	0.416
Perseus A	0.765	0.104	0.131
Perseus B	0.454	0.120	0.426
Theseus	0.670	0.097	0.233
Altus	0.567	0.153	0.279
Predator	0.343	0.2	0.289
Raptor	0.431	0.040	0.447
Voyager	0.219	0.052	0.73
Condor	0.31	0.09	0.6

Specification of these quantities allows for the initial estimate of Time to Climb and Endurance. Despite a general dislike for the use of such gross fractional weights and their implementation in the early sizing process of conceptual design, it was thought useful to have an estimate of the total aircraft endurance before the more detailed and time consuming specification of the configuration has taken place. This enables the designer to

decide at an earlier stage whether or not the overall size of the aircraft is going to satisfy the mission requirements. If the mission requirements are not satisfied, it is simpler to return to re-select the design point at this stage rather than later.

4.H Selection of the # of Engines, Fuel Consumption, and Excess Power Available for Climb

The next step in the methodology is to select the number of engines, fuel consumption and excess power for climb. The number of engines desired will depend upon a very large number of factors, most of which will not be available at the time of overall sizing. Based upon the necessary Power Loading of the aircraft obtained from the Constraint Diagram and Design Point, the actual engine horsepower required for cruise is now available.

The decision of how many engines to use will be made based upon the available engines, which for this class of aircraft are quite limited at this time. In fact, only a few internal combustion reciprocating engines have ever performed at this altitude. Some data are available, however, as to the efficiency of the propellers and the fuel consumption in cruise for this class of aircraft, and for this stage of sizing, this information is thought to be sufficient. Later in the methodology, a more robust approach will be made available.

Very few engines operate efficiently across a wide range of available power. For this reason, it was necessary to allow for the definition of a climb available power, separate from that available for cruise. This climb power (for this class of aircraft) should have an associated increase in fuel consumption and this must be taken into account in the climb calculation. If the aircraft were assumed to climb using the same power setting as that used in cruise the aircraft would take an absurd amount of time to reach altitude. This was discovered in the original version of the methodology, which made no allotment for an increase in available power for the climb phase.

4.I Calculation of the Initial Endurance and Time to Climb

The calculation of the preliminary endurance depends first on a calculation of the time to climb. The calculation of the time to climb is the first calculation requiring more than a single equation and some algebraic manipulation. It was found that in order to get an accurate estimation of the time to climb (even for the early preliminary stage), that an integration needed to be performed. Given the excess power available for climb, an excess energy approach was taken to the climb. At least one quantity had to be assumed constant for the climb. After much experimentation, it was decided that C_L was the quantity to be kept constant. The only other option was velocity, however if velocity was kept constant from Sea Level to Altitude, the resulting power required to fly at Sea Level was absurdly high.

Thus, initially, C_L was calculated conventionally as:

$$C_{Lcruise} = \frac{1}{\frac{1}{2}\rho_{cruise}V_{cruise}^2}\left(\frac{W}{S}\right)_{cruise} \tag{4.10}$$

This lift coefficient was used to calculate the velocity of the climb inside of a loop that iterated on altitude in 500 foot increments. This assumes a continuous function and approximates the function by a series summation.

The velocity in the climb was given by :

$$V_{\text{climb}}(H) = \left[\frac{1}{\frac{1}{2}\rho(H)C_{Lcruise}}\left(\frac{W}{S}\right)\right]^{1/2} \tag{4.11}$$

Where H is the altitude of the specific iteration, V_{climb} is the climb velocity, and where the wing loading is adjusted by subtraction of the fuel burned. The drag of the aircraft was then calculated assuming a parabolic drag curve (for the preliminary sizing only) as:

$$C_D = C_{do} + KC_{Lcruise}^2 \tag{4.12}$$

based on the zero lift drag coefficient (C_{do}) specified in the Critical Constants dialog box and a constant C_L calculated based upon the Wing Loading, density and velocity at cruise. This gave a Cruise power of :

$$P_{cruise}(H) = \frac{\frac{1}{2}\rho(H)[V_{\text{climb}}(H)]^3 S_{ref}C_D}{\eta_p} \tag{4.13}$$

using the propeller climb efficiency specified in the Critical Constants dialog box and the density at the altitude of the given iteration.

Excess Power is then:

$$P_{excess}(H) = P_{avail} - P_{cruise}(H) \tag{4.14}$$

This gives a Rate of Climb of :

$$RoC(H) = \frac{P_{excess}(H)}{W_{to}(H)} \tag{4.15}$$

where the takeoff weight is adjusted on each iteration by the subtraction of the weight of the fuel burned.

The time to climb is therefore given by :

$$\text{TtoClimb} = \sum_{H=SeaLevel}^{CruiseAltitude} \frac{\Delta H}{RoC(H)} \tag{4.16}$$

At this point, the average aircraft weight in cruise is recalculated based upon the subtraction of the fuel burned in the climb. In addition, the aircraft cruise C_L is recalculated based upon this new wing loading. The Endurance is then calculated after the drag is recalculated applying the new cruise C_L. Using the Brequet Endurance equation (Equation 2.1) shown in the Aerodynamic Efficiency section of the Literature Review (Section 2.C.1.e) the first estimate for endurance is calculated. It is noted that all of the quantities required for the calculation of this quantity have either already been supplied to the program, or have been calculated by this point.

Once a rough knowledge of the possible (however optimistic) endurance and time to climb are available, the decision can be made to either return and re-designate any of the quantities effecting the endurance specified thus far, or if satisfied, to move on to the specification of the configuration.

4.J Selection of the Configuration

Prior to this stage in the methodology, the procedure followed has been reasonably sequential and generic in nature. It is at this point in the methodology that the procedure begins to branch out into parallel paths. Several general configurations are made available for selection. The selection of any configuration has a large number of calculations and

assumptions associated with it in order to present the designer with a default aircraft configuration from which to work.

Each of those assumptions and the more relevant calculations will be mentioned in the subsequent chapter. For the moment, it is beneficial to briefly mention the configurations considered to perform the Low Speed HALE UAV missions in this thesis. The major classification of configurations can be seen in Figure 4.6. They are :

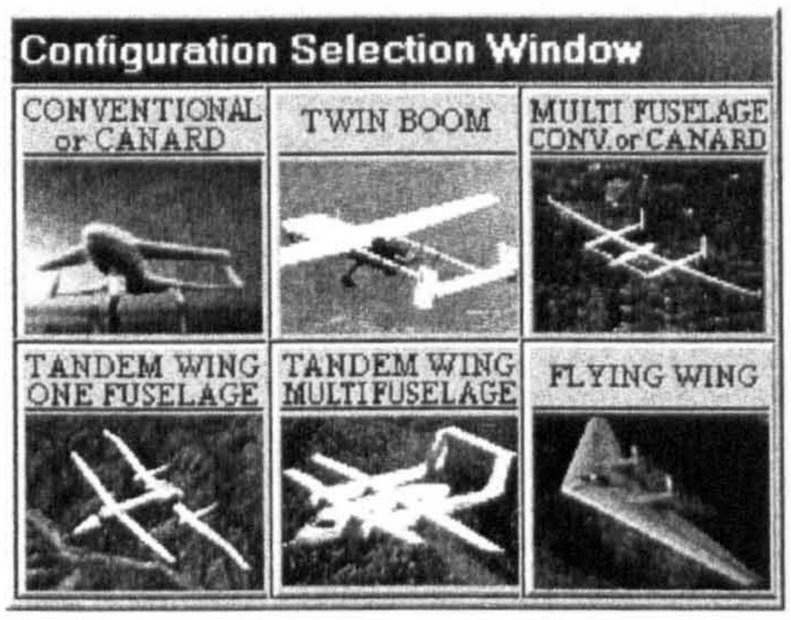

- Conventional or Canard
- Twin Boom
- Multiple Fuselage Conventional or Canard
- Single Fuselage Tandem Wing
- Multiple Fuselage Tandem Wing
- Flying Wing

Figure 4.6 ***is the main configuration selection window from which the default configuration to be created is selected***

The selection of these configurations was based mostly on the idea that since the aircraft is unmanned, that the actual layout of the aircraft is based more on the requirements of the payload. These requirements for this class of aircraft can vary widely depending on the mission, however in general a wide forward or side field of view for the payload is desirable. The decision to consider several of the configurations was based on the fact that similar aircraft have already been built. These existing aircraft should provide an adequate basis for validation of the methodology, even if data on these aircraft are scarce.

Each individual configuration was made available in Single Engine Tractor and Pusher configurations, Twin Engine Tractor, Twin Engine Pusher, and Twin Engine Push-Pull configurations. The Multiple Fuselage aircraft were all available in 2 and 3 fuselage configurations. Overall, this resulted in the possibility for 55 different configurations once the number of fuselages and possible engine configurations are considered. This is the first hint of the potential power of the resulting methodology. Once the individual modules have been explained in detail, the range and limitation of applicability of the methodology will be better understood and appreciated. The first steps in this object- oriented approach will be described in the next chapter.

Chapter V

It takes no more effort to design something beautiful

Than it does to design something that is not

--- Stelio Frati
(Designer of the SIAI Marchetti *SF260*)

5. Aircraft Layout and Geometry

Once the general configuration has been specified from one of the 55 possibilities, it is a requirement of the methodology and code that a default configuration be created from which to work. This eliminates the arduous task of setting up a general aircraft for every configuration to be considered. It removes the necessity for the designer to specify every geometric characteristic for the default configuration. Time was taken in order to insure that the default aircraft would have appropriate geometric properties to perform a generic Low Speed HALE UAV mission. The Fuselage, Tail/Canard/Tandem Wing, Main Wing, and locations for all of these quantities were specified in advance of the creation of the Main Configuration Window using the Critical Constants already specified. This required many assumptions.

Once inside the Main Configuration Window it is possible to change any of these quantities by either simply pressing the relevant button or clicking the mouse on the relevant component of the aircraft. The details of the sizing procedure for both the default and designer modified cases will be explained in detail in this chapter.

It should be noted that the discussion will proceed in the order of the original creation/calculation of the relevant quantities for the default configuration case. Once the default configuration has been created, the calculation for the individual components is limited to the effected components. For example, a change in Fuselage Length will often result in a change in Tail Moment Arm Length. In this instance, even though only the Fuselage Length was modified, the Tail Area and related characteristics will be recalculated. This type of interaction is one of the characteristics that makes coding the

design process considerably more challenging than just entering equations into a computer.

The discussion begins with the definition of the moment arm length for the various possible configurations.

5.A Moment Arm Length Definitions

At this stage of the methodology for the default configuration, the procedure becomes more complex. For each of the configurations considered (for the default case), a moment arm length for the sizing of the tail must be specified beforehand in order to continue with the construction of the default aircraft geometry. Thus, it is beneficial to begin the discussion with the various definitions for tail moment arm used for the different configurations. Afterwards, the placement of the wing on the fuselage and then the tail volume coefficients for all of the possible configurations will be presented and discussed.

5.A.1 Conventional Configuration

As can be seen from the Figure 5.1, the conventional configuration is the most straightforward. It is shown here for completeness. The moment arm length is defined as the distance from the tail (horizontal or vertical) quarter chord to the main wing quarter chord. In this application there is no difficulty with sharing the value of tail quarter chord between the horizontal and vertical tail as the difference is small. In this application, the horizontal tail quarter chord is selected, and the only error that is caused can be absorbed by an adjustment in the vertical tail volume coefficient.

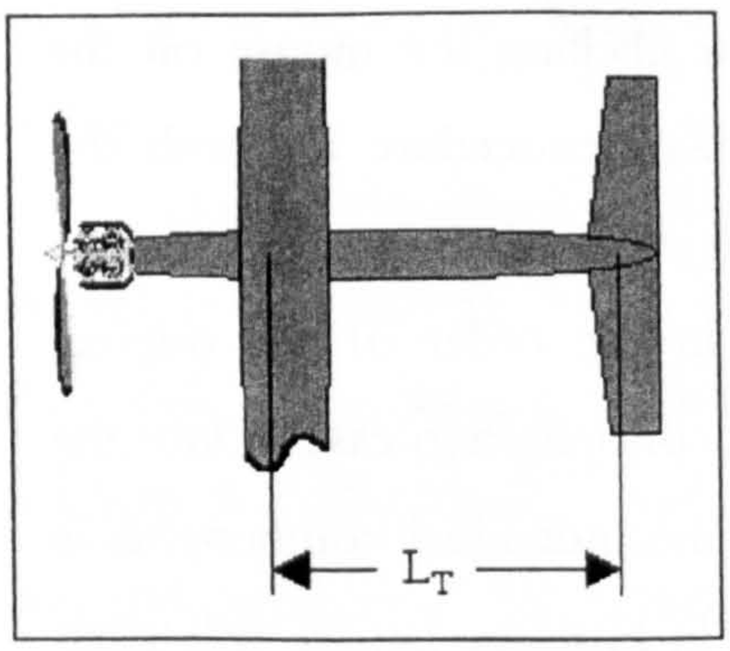

Figure 5.1 ***shows the definition of the tail moment arm length for the conventional configuration.***

In addition, since the aerodynamic center of the aircraft for this particular configuration is known to coincide with a location somewhere along the wing chord, the moment arm length selected will be reasonably close to the actual value.

5.A.2 Canard Configuration

For the canard configuration, the length used for the horizontal tail moment arm is shown. The difference in the way this is calculated from the conventional configuration is that for the conventional configuration, the main wing ¾ chord is added to the horizontal tail ¼ chord. For the canard, the canard ¾ chord is added to the main wing ¼ chord. It should be noted that Raymer[4] suggests using an area split for the sizing of canards instead of trying to use tail volume coefficients. Since the canard in this configuration is considered mostly for control, this option was not acceptable, and the canard had to be sized relative to changes in moment arm length, as would a normal horizontal tail and as suggested by Nicolai[3].

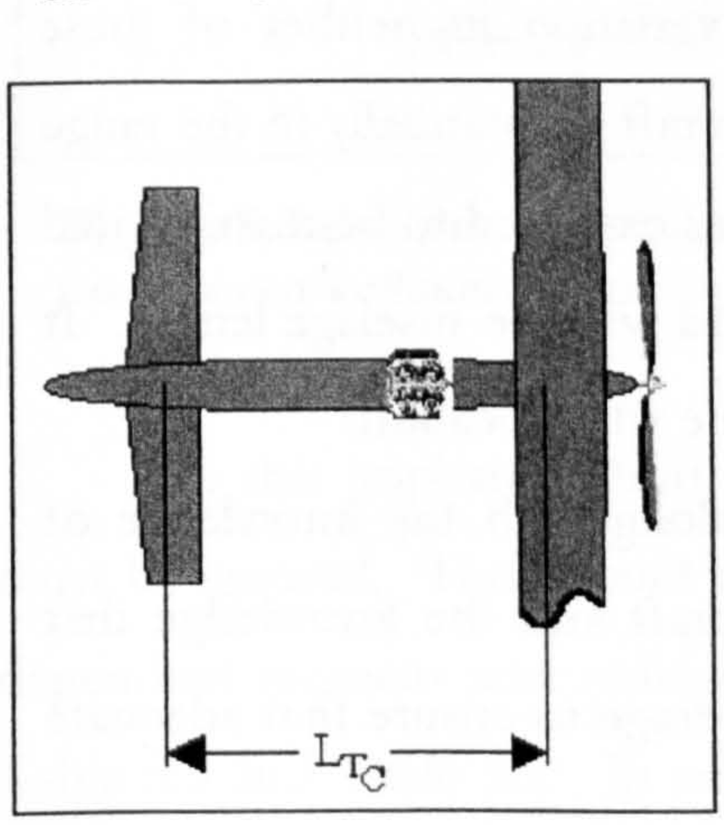

Figure 5.2 ***shows the definition of the tail moment arm length for the canard configuration.***

Given the decision to treat the canard more like a horizontal tail, an agreement must be made as to what length to use for the moment arm length. This is the origin of the *Modified* tail volume coefficient. The reason it is called modified is that the moment arm length used is not a true moment arm length in the traditional definition of the term discussed above.

For configurations like the canard, the longitudinal static stability is a strong function of the length of the moment arm. There is no way of knowing where the aircraft centers of gravity and lift will be for the canard configuration before performing the more detailed calculations of aerodynamics, weight and center of gravity. These values are not available when setting up the default configurations, nor are they known in the early sizing stages when the overall shape of the aircraft is being manipulated. Therefore, the length used to predict the moment arm distance must be fixed at some value, and kept consistent.

At a later time, these values, along with the values for tail volume coefficient should be validated against stability calculations. This process was carried out by iteration using the present methodology, and the final values for moment arm length are those cited and discussed in detail in Table 5.3 and Table 5.5 in Sections ***5.B.1.d*** and ***5.B.2.c*** respectively.

The decision for the Vertical tail moment arm length for the canard configuration was more difficult to validate since the methodology does not calculate yaw stability. Instead, once again, a moment arm length was selected and kept consistent throughout the method. This length was a fixed fraction of the fuselage length. This allowed for the resulting tail size changes due to any change in fuselage length. The remaining changes in vertical tail size due to changes in longitudinal engine location (meaning changes in cg relative to the aircraft neutral point, and thus changes in static margin) were absorbed by variations in the vertical tail volume coefficients.

The underlying assumption for this choice was the belief that the distance from the nose of the aircraft to the canard would change very little in the sizing process. Furthermore, the distance of the main wing from the vertical tail was assumed to change very little during the preliminary sizing. In addition, a variation in neither of these quantities was expected to change the yaw stability of the aircraft substantially in the range of longitudinal locations to be used. The one quantity that was expected to be manipulated at least as much as the locations of the main wing and canard was the fuselage length. It has an equal effect on yaw stability due to being coupled to the wing location.

This fraction of overall fuselage length was used along with the knowledge of existing vertical tail sizes for Low Speed HALE UAV aircraft and the knowledge that canard aircraft have slightly larger vertical tail surfaces on average to ensure that adequate tail surface area was provided.

It is beneficial to note that the utility of the vertical tail size to this methodology was limited to the weight and parasite drag estimations. It was decided that yaw stability was not crucial to the conceptual design methodology in the preliminary sizing phase. Where there were vertical tail size differences expected due to differences in configuration, these differences were applied to the methodology as above.

5.A.3 Twin Boom & Multiple Fuselage Conventional Configurations

As can be seen in Figure 5.3, the implementation for horizontal and vertical tail moment arm is essentially the same for these configurations as it is for the conventional configuration. The major difference in this instance is in the implementation. For the conventional configuration it was a simple matter to use the measured distance from between the ¼ chords of the wing and tail.

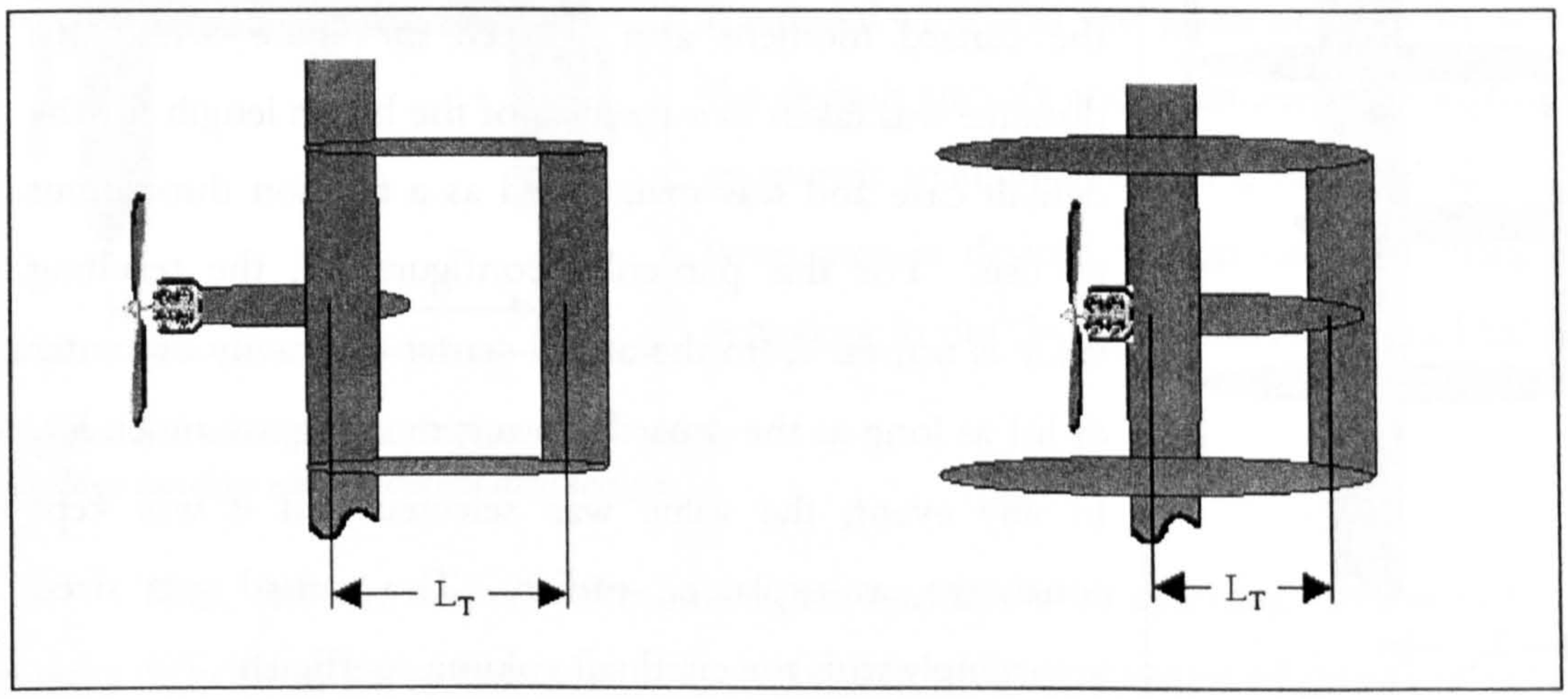

Figure 5.3 ***shows the definition of tail moment arm for the twin boom (left) and multiple fuselage conventional (right) configurations.***

In this implementation, the boom length must be used and the fuselage length must be ignored. This should elucidate the reasoning behind the different configuration dependent moment arm multiplying factors of either L_{boom} or L_{fuse} that will be seen in Table 5.3 and Table 5.5. In addition it should highlight one of the minor difficulties in programming the equations and identifying the different possible permutations. Each configuration must be dealt with separately, using common modules to perform the mathematics. This will be discussed further in the implementation chapter.

The vertical tail moment arm is treated the same as for the conventional configuration, except that the distance used is boom length and not fuselage length. The same assumptions are made about the proximity of the horizontal tail ¼ chord to the vertical tail ¼ chord. In this case, though, that entails slightly greater error due to the fact that the vertical tail surfaces are split in two (50/50 area split for all multiple fuselage/boom aircraft) as a result of the multiple fuselage format. This will reduce

average chord, which will increase the distance between the horizontal tail and vertical tail ¼ chords. Again, as long as the distances selected are kept constant, this error will be invisible, while allowing for reasonable guesses for the vertical tail size.

5.A.4 Multiple Fuselage Canard

For the Multiple Fuselage Canard configuration, the distance from the ¼ chord of the main wing to the ¼ chord of the canard was used for the canard moment arm as seen in Figure 5.4. This distance was taken as a fraction of the boom length for the default case and was maintained as a fraction throughout its use. For this particular configuration, the resulting value is not far from the actual center of gravity or center of lift as long as the canard is not generating too much lift. In any event, the value was selected and it was kept consistent, as explained earlier. The canard was sized accordingly with the cited tail volume coefficient.

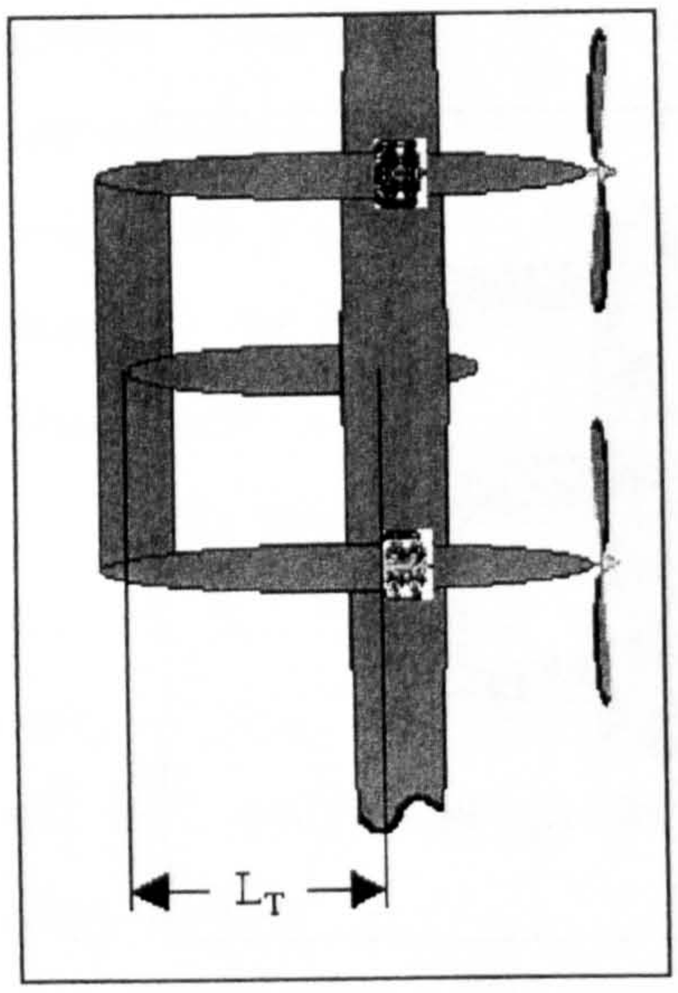

Figure 5.4 ***shows the definition of tail moment arm for the multi fuselage canard configuration.***

For the vertical tail moment arm, the same distance was used. While this has no basis in reality, it was numerically simpler than using a separate moment arm for the tail. Additionally, there was little possible justification for using any other distance with the information available at this stage in the methodology. If the distance to the main wing ¼ chord were used there is the danger of an extremely small to zero distance (zero moment arm length) from the vertical tail ¼ chord. In a computational application this was deemed unacceptable.

In this instance, the moment arm only changes as a function of canard distance from the main wing. It is realized that the vertical tail should also be sized relative to the span-wise distance of the engines for the twin engine case, however, without the possibility of verification through yaw stability and engine out analysis these surfaces could easily be oversized. It was thought better to try and maintain the surfaces within traditional values

found for this class of aircraft in the twin engine configuration (*Condor, Theseus, Strato 2C*). Again, two vertical tail surfaces of equal area were assumed, attached to the booms.

5.A.5 Tandem Wing

5.A.5.a Single Fuselage

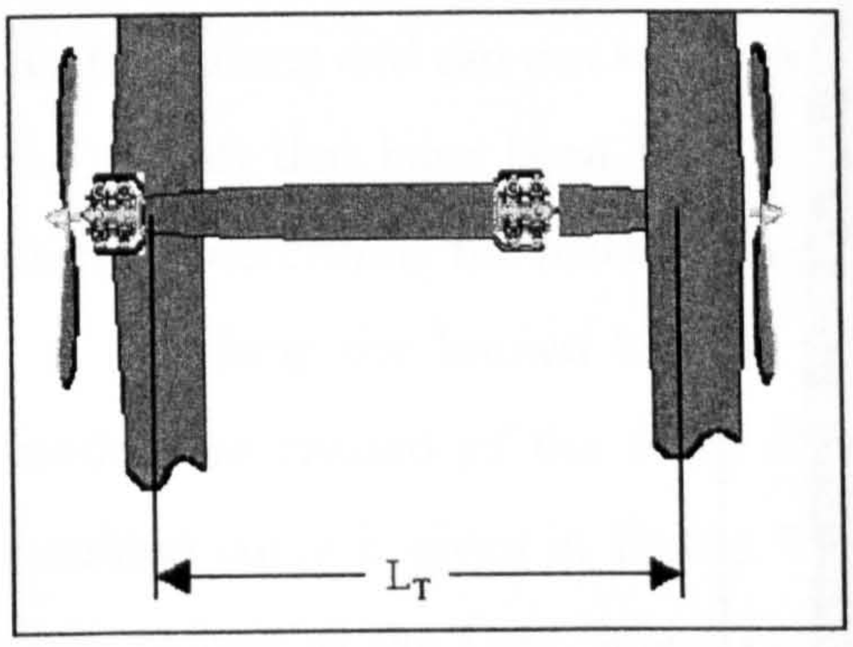

Figure 5.5 ***shows the definition of the single fuselage tandem wing moment arm length.***

For the single fuselage tandem wing, the forward wing was not sized as a canard or tail. The fractional wing area was given prior to the setup of the default aircraft and maintained throughout the geometric manipulation. If a different division of wing area is desired, it can only be changed by returning to the Configuration Selection Dialog.

Thus, only the vertical tail moment arm remains to be specified. In this instance, it is quite difficult to know beforehand even roughly where the center of gravity or center of lift will be. The variation in wing area and fuel placement for this configuration makes this prediction impossible without an explicit calculation of those quantities. Once again, a distance was selected that has no basis in reality (Figure 5.5), but provides a reference from which to calculate a vertical tail surface sufficient to control the aircraft based on what was considered a conservative moment arm length. The distance from the forward wing ¼ chord to the aft wing ¼ chord was used. As the forward wing is moved further forward, the tail volume required to control the aircraft in yaw will increase. The spacing between the two wings for the default aircraft was determined by trial and error as the best distance to balance the aircraft, without allowing for too great a proximity.

5.A.5.b Multiple Fuselage

Again, there is no horizontal tail moment arm for the case of the tandem wing, since the area is kept fixed throughout the process past the configuration selection window. For the vertical tail moment arm length for the Multiple Fuselage Tandem Wing configuration, the same distance is used as for the single fuselage case. The primary difference is that the distance is given as a fraction of boom length instead of fuselage

length. Thus, the difference is in the application of the same information. This is another occurrence of the difficulty of a structured computer code in duplicating a decision that would otherwise be made rather easily by a designer independent of the code or methodology. More examples of this type of situation will be given in the Implementation Chapter.

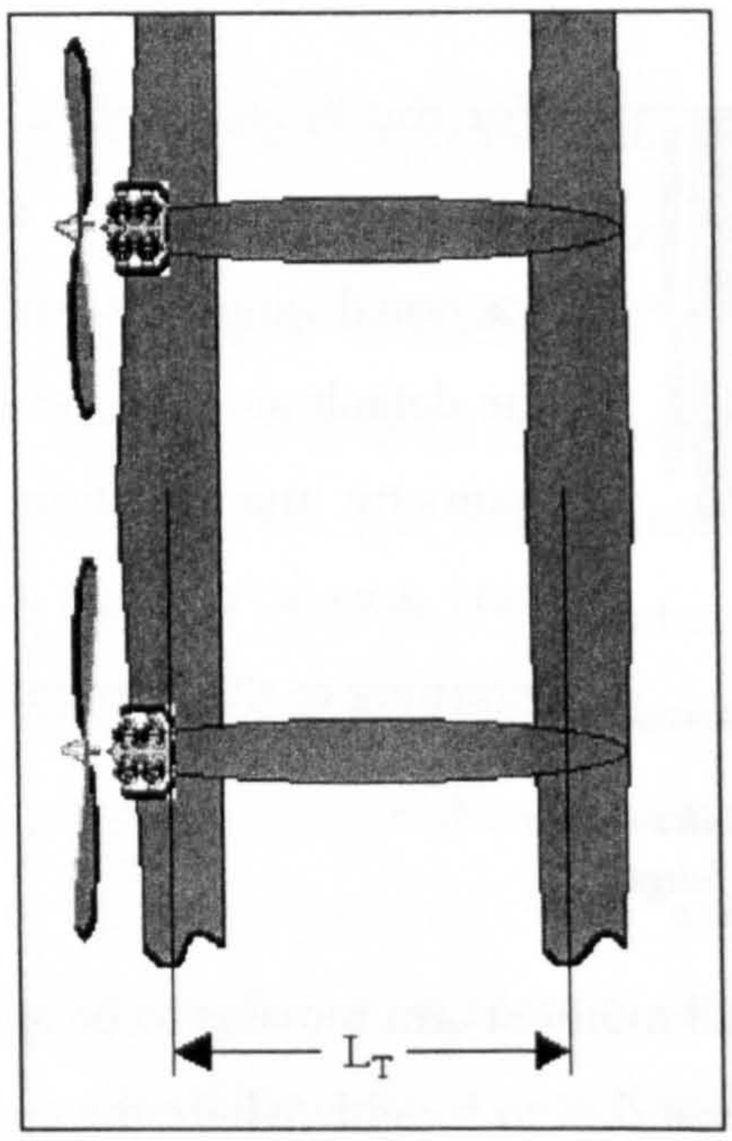

Figure 5.6 ***is the definition of tail moment arm length for the tandem wing multiple fuselage.***

5.B Fuselage Dimension and Location Specification

Several of the calculations performed for the default case are also performed for the designer edited case. There are, however, a number of calculations and assumptions required specific to the default case, so a separate section will address these issues.

5.B.1 Default Fuselage Case

For the most part, the generation of the default fuselage was a simplification of the more complicated designer specified case, with the addition of several values obtained through the execution of the methodology and the remainder of the values resulting from assumptions. The origin of the values obtained through the use of the program and the assumptions made to obtain the remaining values will be clearly explained in the following sections.

5.B.1.a Fuselage Length Calculation

Raymer[4] suggests the fuselage length (L_{fuse}) calculation take the form :

$$L_{fuse} = a(W_{to})^C \tag{5.1}$$

Where a and C are constants with values given depending on the aircraft configuration. Unfortunately, the only constants he supplies are for much more conventional configurations and can not be applied to Low Speed HALE UAV's when validated against the aircraft that have been built. Nevertheless, the form of the equation he provides is useful in describing the fuselage length for HALE UAV's.

Using the known lengths of several Low Speed HALE UAV aircraft, a revised model was created of the form above with a = 0.656 and C = 0.466. A plot of the resulting curve is given in Figure 5.7. The classes of aircraft available from Raymer that were closest to the Low Speed HALE UAV curve were included in this figure with the classes of aircraft having greater error being eliminated from the figure for simplicity.

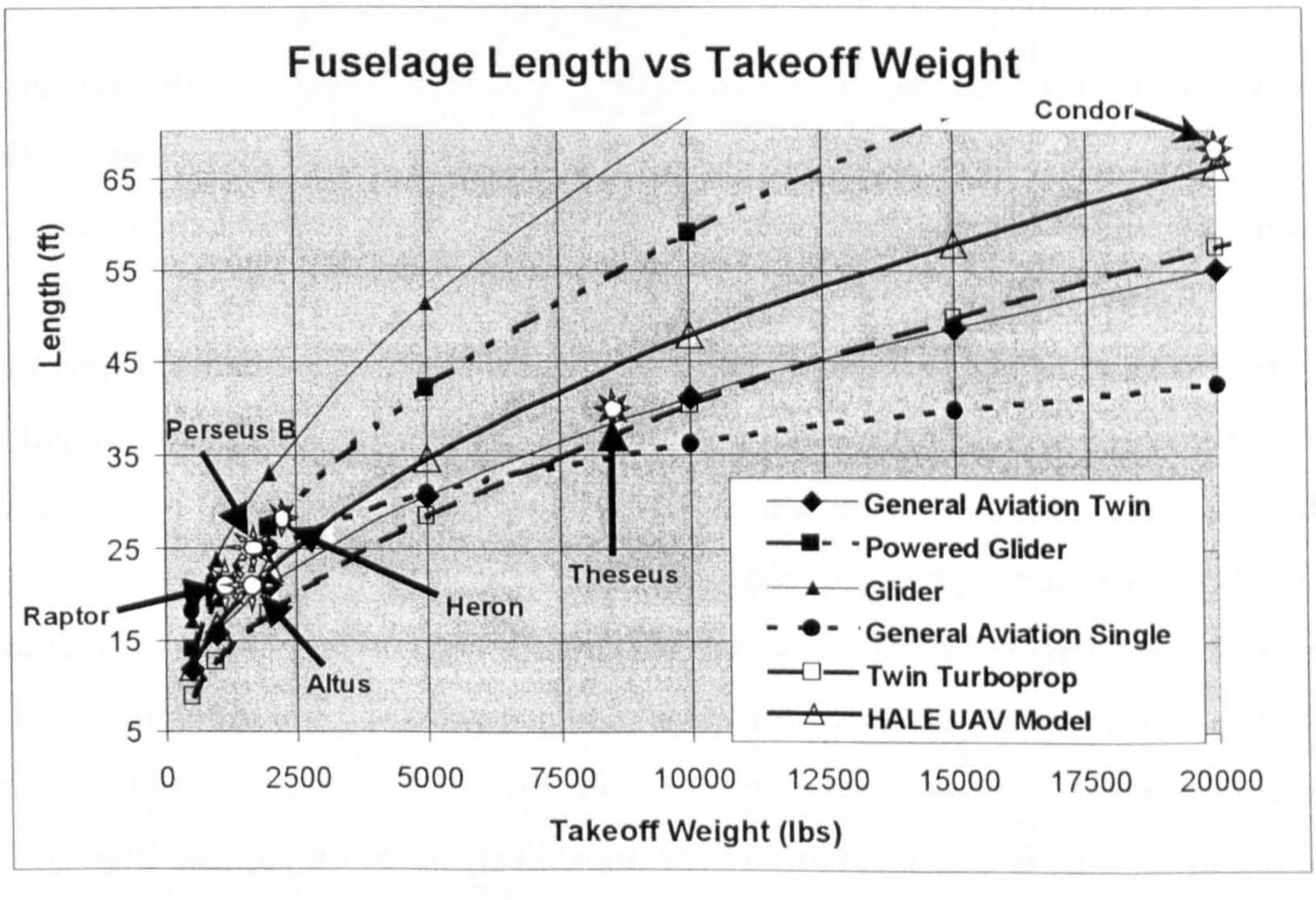

Figure 5.7 ***shows the relationship between fuselage length and aircraft takeoff weight for several different aircraft classes, including the new HALE UAV fuselage length model.***

The aircraft considered in the creation of the new UAV model can be seen in Table 5.1 and were the General Atomics *Altus*, the Scaled Composites *Raptor*, the Aurora Flight Sciences *Perseus A*, *Perseus B*, and *Theseus*, the Boeing *Condor*, and the Israel

Aircraft Industries *Heron*. It is pointed out that the Heron is not in fact a High Altitude UAV. The overall percentage error of this model when compared to the known lengths of these aircraft is actually less than 7 %. Looking at the evolved version of the *Perseus A*, it can be seen that the aircraft was 400 pounds heavier, but the fuselage was actually shorter. The average error of the new UAV method without the *Perseus A* is only 5.3%.

Table 5.1 ***compares known HALE UAV fuselage lengths to the length predicted by the new method, along with the error involved with using the new method for each aircraft.***

	Takeoff Weight (lbs)	Est.Length New UAV Method (ft)	Actual Length (ft)	% Error
Condor	20000	66.25	68	2.57
Heron	2425	24.78	28	11.48
Perseus A	1830	21.74	26	16.39
Perseus B	2205	23.71	25	5.16
Theseus	7716	42.50	40	6.26
Altus	2150	23.43	22	6.51
Raptor	1880	22.01	22	0.06
			Avg. Error	6.92

A systematic approach was taken in selection of these constants and the least error solution was selected. It can be noted from the figure that the nearest previously existing models were for the Powered Glider and the General Aviation Twin Engine aircraft. Although the General Aviation Single Engine aircraft looks quite good for lower Takeoff Weights, its accuracy fails miserably at higher Takeoff Weights. When the graph is expanded to the range of the Boeing *Condor* at a Length of 68 feet and Takeoff weight of 20,000 lbs, it is clear that none of the existing models even comes close to providing an accurate prediction of the length of this class of UAV.

Special consideration must be given to aircraft with twin booms or multiple fuselages. The determination of length for these configurations is quite different than for the more conventional configurations considered in Table 5.1 above. In addition, the length for the flying wing is calculated differently (most likely based on payload length).

5.B.1.b Multiple Fuselage/Boom Length Calculation for the Default Configuration Case

The most straightforward way to present the numbers used in each of the different situations is to list them as in Table 5.2. Where there was data available, the numbers were

taken directly from the source. Where the data was not available, a trial and error method was used in order to determine the most suitable relative length for each boom or fuselage. These decisions were based on the results of the stability calculations as well as a determination of whether or not there was suitable room for payload given the various possible engine locations. For the default configuration, the Single Engine Pusher, Twin Engine Pusher and Push-Pull configurations were neglected in the fuselage length algorithm.

Table 5.2 ***lists the different fractional conventional fuselage lengths used by the various alternative configurations in setting up the default aircraft.***

	Single Engine Tractor	Twin Engine Tractor
Twin Boom		
Center Fuselage	0.55	0.55
Booms	0.65	0.65
Multi Fuselage		
2 Fuse Conventional	0.9	0.9
2 Fuse Canard	0.9	0.9
3 Fuse Conventional		
Center Fuselage	0.594	0.45
Booms	0.9	0.9
3 Fuse Canard		
Center Fuselage	0.5	0.65
Booms	0.9	0.9
Tandem		
2 Fuse	0.705	0.705
3 Fuse		
Center Fuselage	0.705	0.7
Booms	0.705	0.705

All values are multiplied by the original Fuselage Length calculated using the modified UAV constants

The table will be re-presented in the section discussing the full range of potential fuselage/engine configurations available to the designer and most of the numbers cited here will change slightly. The reason for this is that for the default configuration, the average wing and tail chords must be approximated in the calculation of the moment arm length since the wing and tail geometry have yet to be specified. Once revised values are available from the geometry definitions of the wing and tail, they are included in the calculation of the fuselage and boom lengths. This will be discussed in greater detail in the next section. In the table, Fractional Conventional Fuselage Length represents a fraction

multiplied by the length of fuselage predicted for an equivalent conventional aircraft. The term 3 Fuselage Conventional is used to distinguish between conventional tail aft and canard 3 Fuselage aircraft.

5.B.1.c Default Fuselage Height and Width

For the aircraft in which these dimensions are actually known there is little variation for unmanned aircraft in this class. They have all been between 2 and 3 feet in each dimension. It was a fairly simple matter then to assume that the default height and width would be equal to 2 feet with a circular cross-section. In fact, most of the aircraft surveyed have square or rectangular cross sections. The option to specify a square or elliptical cross section will be made available to the designer once the default configuration has been calculated and drawn. The only exception to this geometrical specification of a default diameter of 2 feet is made for the Single Fuselage Tandem Wing configuration. The fuselage of this aircraft will experience higher torsional loads. Photographs of the Rutan *Proteus* would appear to confirm that a larger fuselage diameter is necessary for this type of aircraft.

Normally other factors such as engine size, payload requirements, and even stealthiness would have some influence on the selection of these dimensions, however in the early stages of outer fuselage definition it was thought excessive to include any direct influence of these quantities on the default configuration. As mentioned already, they can be changed at any time once the default configuration has been displayed.

5.B.1.d Wing Position on Fuselage, Moment Arm Length Estimation

At this early a stage in the conceptual design process, moment arm lengths for sizing the tail are normally given as some fraction of fuselage length. This can be made to work for the conventional configurations, but for unconventional configurations the process is more complicated. For each particular aircraft configuration, the argument had to be posed as to how to estimate the moment arm length and what reference datum to use. The problem is much more far-reaching than just the specification of the default configuration. This was described in detail in Section 5.A.

For the default conventional configuration, the tail moment arm will be defined in the traditional manner, in terms of some fraction of the fuselage length. In the non-

default case, it was shown that the distance from the quarter chord of the wing ($\bar{c}_{1/4wing}$) to the quarter chord of the tail (horizontal or vertical, $\bar{c}_{1/4tail}$) is used for the moment arm length, even though this distance may be inappropriate for several of the configurations considered. For the default cases, the moment arm factor (for the Horizontal Tail/Canard/ Tandem Wing) basically decides the location of the wing on the fuselage.

Since the moment arm length will be based on the distance between $\bar{c}_{1/4wing}$ to $\bar{c}_{1/4tail}$, some estimation needs to be made for these values before they have been explicitly calculated given the order assumed in this methodology (fuselage, wing, then tail). The assumption was as follows:

$$\bar{c}_{wing} = 0.1245 * L_{fuse} \quad \text{and} \quad \bar{c}_{HTail} = 0.1 * L_{fuse}. \qquad \textbf{(5.2,3)}$$

In practice, this assumption worked out quite well, with the difference between the default configuration and the second iteration being essentially invisible to the designer. It should be pointed out that these values are replaced as soon as the first calculation of the wing and tail geometry is made. It was unavoidable to provide a default configuration without making *some* assumptions. In this instance, the assumptions made were unknown to the designer since as soon as the full aircraft was generated, the calculated quantities replaced these assumed values. Thus, these values had no impact on the final sizing of the aircraft except to provide a point from which to launch the iterative process.

As already mentioned, for this stage in the methodology, the moment arm length was assumed as some fractional quantity of the overall fuselage (or boom) length. These values were determined in the same manner as the fuselage length values tabulated earlier.

The moment arm length fractions are listed in Table 5.3 for the default configurations. Once again, these values will be changed slightly from their default values for the non-default calculations. In addition, the moment arm lengths for the remaining possible configurations will be specified in the Tail Sizing section.

Where data was available from existing aircraft, they were incorporated into the model. Values for horizontal and vertical tail moment arms were estimated from drawings for the Boeing *Condor*, Aurora Flight Sciences *Perseus* and *Theseus* aircraft, and for the Israel Aircraft Industries *Heron*. The *Altus* has an inverted V-tail and it was impossible to derive tail sizing information from photographs of this aircraft. For the less conventional configurations, the moment arm length values resulted from a trial and error evaluation of

sufficient static margin (an attempt was made to keep static margin within ± 10%) in addition to a certain degree of intuition.

This was implemented and iterated via the existing computational methodology. Since there is no mechanism for iterating to an optimum solution for a given configuration, intuition was developed from the use of the methodology on the most judicious rearrangement of components on and in the aircraft to create a more favorable static margin. In many ways, these values constitute results of the methodology. These results, however, were deemed more appropriate for presentation in these sections of the discussion of the methodology.

Table 5.3 ***lists the fractional fuselage or boom lengths used for the wing-tail/canard/tandem moment arm length estimation for the set-up of the default aircraft.***

	Multiplied By	Single Engine Tractor	Twin Engine Tractor
Conventional	L_{fuse}	0.6	0.5
Canard	L_{fuse}	0.4	0.4
Twin Boom	L_{boom}	1	1
Multi Fuselage			
2 Fuse Conventional	L_{boom}	0.55	0.55
2 Fuse Canard	L_{boom}	0.9	0.9
3 Fuse Conventional	L_{boom}	0.45	0.55
3 Fuse Canard	L_{boom}	0.45	0.35
Tandem Single Fuse	L_{fuse}	0.5	0.5
Tandem			
2 Fuse	L_{boom}	0.705	0.705
3 Fuse	L_{boom}	0.7	0.7
Flying Wing	L_{fuse}	0.4	0.45

In the case of the Flying Wing configuration, the values were not used to size a tail, but were in fact used to place the fuselage on the wing. For the case of the Canard configured aircraft, these distances were used for the vertical tail as well. This assumes the distance to some fictional aerodynamic center, estimated to be some distance between the canard and the vertical tail. This distance can be specified by the designer later in the methodology but cannot be specified for the default case. All other values were fractions of either the boom or fuselage length as indicated. These distances were added or subtracted to the appropriate fractions of $\overline{c}_{1/4wing}$ and $\overline{c}_{1/4tail}$ depending on the configuration

being considered. This kept the moment arm distances reasonably constant despite not having the calculated quarter chord values available initially.

There is little to remark about the values themselves. All of the Canard configured aircraft values are significantly smaller, as would be expected based on the reduced distances associated with using an average distance to a fictional aerodynamic center, instead of the conventional moment arm length assumption of distances between the quarter chords of the wing and tail. The final comment related to these values is that in some instances the values would be expected to vary from a single engine configuration to a twin engine configuration. The reason for some of the values remaining the same is that the modified tail volume coefficients used for the stability calculations adopted any additional expected change in tail area resulting from a difference in configuration.

5.B.2 Designer Modified Fuselage Case

As already mentioned, the tables presenting various Fuselage/Boom lengths and moment arm lengths used in the construction of the default configurations were essentially simplified versions of what is necessary for the designer modified cases. The discussion in this section will begin with the quantities that are the easiest to process once supplied by the designer.

5.B.2.a Specification of the Fuselage Geometric Parameters

The methodology allows for the direct specification of a number of fuselage geometric parameters regardless of the configuration being considered. These include the :

- Fuselage Cross Sectional Shape (Circular, Square/Rectangular, Elliptical)
- Fuselage Width Dimension
- Fuselage Height Dimension
- Fuselage Length Dimension
- Fuselage Placement on the Main Wing, or Moment Arm Length.

In addition, for Canard or Tandem Wing configured aircraft the absolute location of the wing on the fuselage can be specified as well as the distance of the wing quarter chord to the canard/tandem quarter chord. For multiple fuselage or boom aircraft, the lateral distance of the fuselages or booms from the aircraft longitudinal centerline can also be specified.

Any change in fuselage length or wing placement on the fuselage relative to the tail or canard requires a corresponding recalculation of the tail or canard sizing. The structure of these modules and how they interact will be presented in the computational implementation chapter.

5.B.2.b Fuselage Length Calculation for The Remaining Configurations

Thus far, fuselage and boom lengths have only been specified for the Single and Twin-Engine Tractor engine configurations. The values for fuselage and boom length fractions for the remaining configurations that require a change in fuselage length based on a change in engine configuration are given in Table 5.4.

Table 5.4 ***lists the configurations that require a change in fuselage length based on a change in engine configuration, and how much of a change is needed due to the engine configuration.***

	Multiplied By	Single Engine Tractor	Single Engine Pusher	Twin Engine Tractor	Twin Engine Pusher	Twin Engine Push-Pull
Multi Fuselage						
3 Fuse Conventional	L_{boom}	0.66	0.75	0.45	0.45	0.45
3 Fuse Canard	L_{boom}	XX	0.7142	0.65	0.7	0.45

Due to the event driven nature of Visual C++, it was necessary to set these values for fuselage and boom lengths in the Power-plant Location dialog box. The reason for this will be explained in the implementation chapter. Nonetheless, any time the engine location is changed, the value given for fuselage length is modified unless a value has already been specified by the designer. Most of the values for these lengths go unchanged as a result of a change in engine configuration. This is not the case for the moment arm lengths or modified tail volume coefficients. The moment arm lengths will be provided in the next section. The modified tail volume coefficients will be discussed in a later section.

5.B.2.c Wing Position on Fuselage, or Moment Arm Length Estimation

Similar to the previous section, moment arm lengths have only been specified for the Single and Twin-Engine Tractor engine configurations. The values that require a change in moment arm length based on a change in engine configuration are given in

Table 5.5. Again, the moment arm length is specified based on the fuselage and boom length fractions for all of the remaining configurations. The values listed were determined using the same procedure mentioned in Sections ***5.B.1.b*** and ***5.B.1.d.***

Table 5.5 ***lists the change in moment arm length necessary due to changes in engine configuration for the alternative configurations.***

	Multiplied By	Single Engine Tractor	Single Engine Pusher	Twin Engine Tractor	Twin Engine Pusher	Twin Engine Push-Pull
Conventional	L_{fuse}	0.6	0.35	0.55	0.5	0.5
Canard	L_{fuse}	0.45	0.55	0.6	0.65	0.45
Twin Boom	L_{boom}	0.6	0.35	0.55	0.5	0.5
Multi Fuselage						
2 Fuse Conventional	L_{boom}	0.55	0.45	0.55	0.45	0.4
2 Fuse Canard	L_{boom}	0.45	0.5	0.35	0.45	0.4
3 Fuse Conventional	L_{boom}	0.45	0.45	0.55	0.45	0.4
3 Fuse Canard	L_{boom}	0.45	0.35	0.35	0.4	0.4
Tandem Single Fuse	L_{fuse}	0.5	0.5	0.5	0.5	0.5
Tandem						
2 Fuse	L_{boom}	0.7	0.7	0.7	0.7	0.7
3 Fuse	L_{boom}	0.7	0.7	0.7	0.7	0.7
Flying Wing	L_{fuse}	0.4	0.45	0.45	0.45	0.45

There are a few published results with which to compare a few of the values in this table. Raymer states his values should only be used as rough estimates, which is essentially the same assertion made in this thesis. For the Single Engine conventional (tractor) configuration, he suggests a value of $0.6*L_{fuse}$ (Raymer[4] p.110). This value was found to compare well to the existing conventional UAV Tail Moment Arms, and also produced satisfactory results when implemented in the present methodology.

For the Single Engine Conventional pusher configuration, he suggests a range from 0.45 to 0.5 times L_{fuse}. In application to the present methodology these values were found to be too large. It was discovered that with the immense fuel load in the main wing, the additional moment due to the aft engine could not be balanced at the values offered by Raymer if the payload was not given enough length ahead of the wing/fuel center of gravity for this configuration.

For the Single Engine Canard configuration, Raymer suggests $0.5* L_{fuse}$. This value was found to be close to the necessary value to create a stable aircraft, but still required some reduction due to the fact that Raymer had assumed a 25%-75% area split between

the canard and main wing. This area split was not even distantly obtained for the Low Speed HALE UAV due to the nature of the relative size of the HALE UAV wing.

Other estimated values of moment arm lengths for some relevant aircraft will be mentioned. The *Perseus* Single Engine Pusher had a moment arm length based on the fraction of fuselage length of 0.4734. This value is not close to the value used for this methodology due to the fact that a very long propeller shaft was used in order to locate the engine further forward in the aircraft. It should be noted that the tail volume coefficients used for this aircraft were far below even those found in gliders which generally have the lowest values for tail volume coefficients of any aircraft.

For the *Condor* Twin-Engine aircraft, a value of 0.54 was obtained. This value was found to produce reasonable results with little modification. For the *Theseus* Twin-Engine pusher aircraft, a value of 0.57 was obtained. Again, this value is quite close to that obtained from the iterative process utilizing the present methodology.

The *Heron* Single Engine Pusher Twin Boom aircraft had a value of 0.64. It is once again mentioned that this aircraft was designed for medium altitude and not high altitude flight. With that in mind, this value of moment arm length was found to be considerably too large. Incidentally, the Tail Volume Coefficient for this aircraft was also found to be quite large, however that will be discussed further in the Tail Sizing section.

Overall, there were not many aircraft to compare to, and many of the existing aircraft were configured differently to the default configurations supplied. Taking these points into consideration, for the configurations that were comparable, the values for moment arm length agreed quite well. Unfortunately, this type of data are not available at all for the less conventional configurations, however calculation of static margin based on detailed aerodynamic and weight estimations was thought to be adequate validation for an early Conceptual Design and Sizing methodology.

Once the fuselage parameters have been specified, the geometry and location of the wing can be specified for the default configuration.

5.C Specification of the Wing Planform Geometry

The most complicated aspect of setting up the wing has been performed by the fuselage calculation function; that is the location of the wing on the fuselage(s) and booms.

The actual implementation of the geometry of the wing is comparatively straightforward. First the default case will be discussed.

5.C.1 The Default Case

For the majority of the configurations, the specification of the wing planform geometry for the default case is fairly basic. The Critical Constants dialog box specified the Aspect Ratio. By the time the configuration is selected, the Takeoff Weight or Wing Area of the aircraft is known. This makes calculation of the wing geometrical parameters simple. Despite this simplicity, some assumptions still need to be made for the default case.

A single tapered wing planform was considered sufficient for the purposes of early conceptual sizing and configurational comparison. While it is realized that for an aircraft in this flight regime, a double tapered wing planform would likely be more efficient, a single tapered wing was considered for overall simplicity and ease of application of the methodology at this stage. Obviously addition of double taper would add another design variable, more accurate absolute values for endurance, and a wider range of possible solutions. This, however, would add little to the configurational comparison but would add greatly to the complexity and time required to obtain a single solution.

An assumption was made that for all of the default configurations the Taper Ratio (λ) would be set to 0.4. This value was selected due to the fact that without allowing for an elliptical planform shape, this is the Taper Ratio that generates the least vortex-induced drag. It should be noted that some of the assumptions in this methodology have greater impact on the overall outcome of the methodology.

For example, the assumption of Taper Ratio effects *all* of the configurations since the assumption is applied without regard for configuration. This would effect the final value for Endurance if it were flawed, but is unlikely to influence the advantages of one configuration when compared to another. Assumptions that are made that effect only one or a couple of configurations are considered more critical since the primary goal of the methodology is the ***comparison*** of the ability of any given configuration to perform better when applied to the specified Low Speed HALE UAV mission.

Returning to the specification of the wing planform, once the assumption has been made for a value of Taper Ratio, the remaining wing planform geometrical characteristics are calculated traditionally as follows:

$$b = \sqrt{AR \cdot S}\,,\quad \bar{c} = \frac{b}{AR},\ c_{Twing} = \frac{2\bar{c}\lambda}{1+\lambda},\ c_{Rwing} = \frac{c_{Twing}}{\lambda} \qquad (5.4,5,6,7).$$

Where $\bar{c}$ is average chord, c_{Twing} is the wing tip chord, and c_{Rwing} is the wing root chord. The configurations that resulted in slight modifications to the above equations were the Flying Wing and the Tandem Wing aircraft. For all aircraft except the Flying Wing, the default wing sweep angle was assumed to be zero.

The Literature Review covered the arguments *for* sweeping the wings of Low Speed HALE UAV's. None of these arguments were strong enough to consider sweeping the wings of any of the default configurations. The Flying Wing configuration has to be swept in order to provide an adequate moment arm to stabilize the aircraft.

The Tandem Wing configured aircraft required a slightly different approach. Previously, for the Canard configured aircraft, the canard was considered strictly for control and trim, and not as a primary lifting surface. For the Tandem Wing aircraft, the second wing was considered to generate a substantial percentage of the total aircraft lift. This required a slightly different approach to the sizing of the Main Wing planform, and for the sizing of the Tandem Wing as well.

Upon selection of the Tandem Wing configurations, the designer is prompted to specify the percentage of total wing area that the main [aft] wing comprises. The default value supplied (arbitrarily) for this is 60%. The areas of the wings are subsequently split between the Main [aft] Wing and Tandem [fore] Wing accordingly. This change required some modified decisional structures in the Drag and Weight estimation algorithms. The governing equations are more appropriate to those sections and will be discussed later in the thesis. For now, the division of total aircraft wing area between the main wing and the tandem wing is defined by the designer. This factor is multiplied by the total wing area sent to the Wing Geometry module. Thus, the above calculations take place for a main wing based on the reduced area. The construction of the tandem wing will be performed in the Tail calculation module. The greatest difference between the default and the designer specified cases is the consideration and calculation of changes in Taper Ratio and Sweep.

5.C.2 The Designer Modified Wing Planform Geometry

The Aspect Ratio provided in the Critical Constants dialog box is fixed as a constant. If the designer wants to change this value it is necessary to return to the Critical Constants dialog. The reason for fixing this value is that it was considered fundamental to the aerodynamic performance of the aircraft, and even though changes in Taper and Sweep may be desired, it was thought that the Aspect Ratio was more a fixed characteristic of a given design.

With this in mind, the designer has the option to modify any two of Taper Ratio, Leading Edge Sweep, Quarter Chord Sweep, or Trailing Edge Sweep angles. In addition, the ability to specify either High, Mid, or Low wing location for the wing on the fuselage is provided. The effect of this change is taken into account in the drag estimation. Although it may be thought to have a very minor effect on this type of aircraft, it was believed that when multiple fuselage configurations were being considered, one of the major differences in drag would be due to the type of interaction each wing-fuselage junction would experience. This will be discussed further in the Drag Estimation chapter.

For a given modification in Taper Ratio, the equations used in the previous section were applied. The effects of the sweep angle were actually only taken into account in the layout of the wing, which is later used for the drag and weight estimations, however none of the other wing planform geometrical parameters ($b, \bar{c}, c_{Twing}, c_{Rwing}, AR$) were changed as a result at this stage of the methodology. In fact, for the modification of the main wing planform geometry, the most difficult situation arises from the logic involved in dealing with the different possible combinations of input by the designer and deciding which variables to make available for variation. This will be discussed in detail in the Computational Implementation chapter.

5.D Wing/Canard/Tandem/Tail Profile Specification

The title of this section makes the section appear more complex than it is. In order to perform a reasonably accurate calculation of the drag for this class of aircraft, it was believed crucial to the quality of the results that accurate airfoil profile data be incorporated into the estimation of the drag. This stage is one of the more robust

characteristics of the methodology allowing for the inclusion of advancements in a given technology, while providing sufficient defaults in the absence of this information.

C_L vs α and C_D vs C_L curves obtained from experimental or advanced computational methods (discussed in the Literature Review) can be read in as a file for use in predicting the profile drag of the wing and canard/tandem/tail. The methodology, like the designer (independent of this program), is not limited in the scope of the drag data available. This of course raises a difficult problem when the final results will be presented, and that is ***which*** airfoil(s) to use. Appendix A is dedicated to the selection of appropriate airfoils, but for now, a description of the available input options will be presented.

5.D.1 Provision of Wing Profile Characteristics

In the event that no profile data are supplied, the assumption of a two-dimensional C_L vs α lift curve slope of 2π is made for all surfaces that are expected to generate lift. Therefore, if no value or curve has been provided, the wing angle of attack is predicted using this lift curve slope.

If no values are supplied for the profile drag variation with lift coefficient, a profile drag coefficient is calculated in a manner specified in the Drag Estimation Chapter. For the wing profile, a default moment coefficient of –0.156 was assumed. This value corresponds to that of an efficient Low Speed Eppler airfoil at a high value for lift coefficient. The default airfoil thickness to chord ratio for the wing $\left(\frac{t}{c}\right)_{wing}$ was assumed to be a conservative value of 0.14.

It is not likely that a Low Speed HALE UAV will use a much thinner profile. The value is considered conservative since some applications have used much thicker airfoils. Once again, this is only the default case, and if an airfoil has been selected, the associated $\left(\frac{t}{c}\right)_{wing}$ should be specified by the designer. An example of the Wing Profile dialog box is given in Figure 5.8. The available options can be seen, as well as the provision of the Chord Reynolds number from which to base the selection of drag and moment characteristics.

No allotment was made (in either the default or designer specified cases) to take into consideration changes of moment coefficient with angle of attack. While it is recognized that there is a variation in moment coefficient with angle of attack, this change tends to be relatively small. It is noted that if the designer desires, the wing lift coefficient is known and output to the designer thus making possible the modification of this number manually with changes in configuration and lift coefficient if so desired. The process will not be automatic, however, as it is for the angle of attack, lift coefficient, drag coefficient curves when specified.

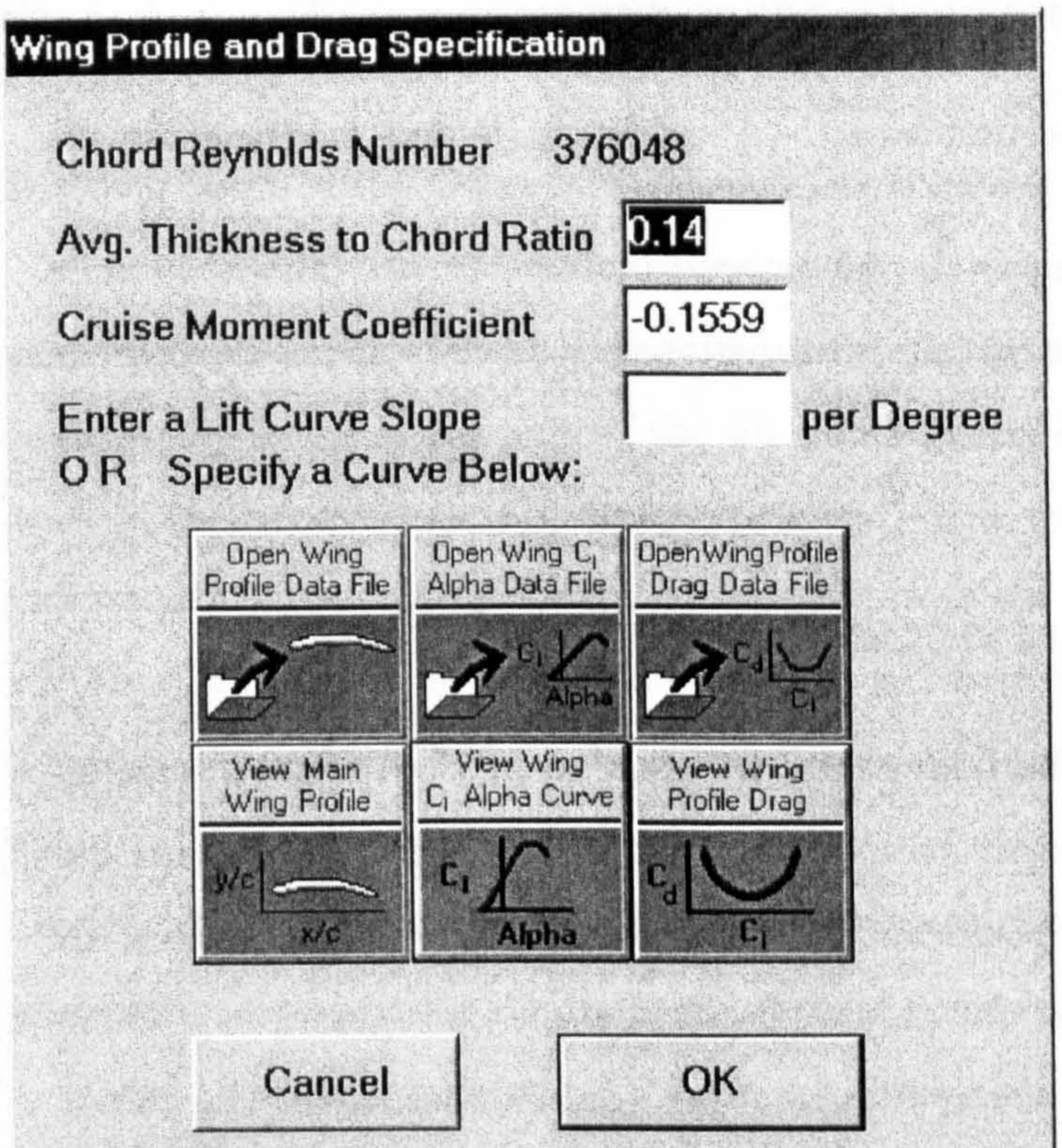

Figure 5.8 ***is the Wing Profile and Drag Specification dialog box from which all of the wing profile drag characteristics can be specified. Identical dialog boxes exist for the Horizontal Tail, Canard, or Tandem wing configurations.***

5.D.2 Provision of Tail/Canard/Tandem Profile Characteristics

An almost identical dialog box is provided for the specification of the Tail/Canard/Tandem profile characteristics. The primary difference is that the default values used in the instance of no designer specified data are more appropriate to values for a horizontal tail. The characteristics of a NACA 0009 were assumed for both the horizontal and vertical tails. It is noted that a rather large majority of gliders and sailplanes used the Wortmann FX71-L-150/30 or 150/25 profiles. Unfortunately, due to the lack of availability of the *Stuttgarter Profilkatalog* second volume (1982) by Althaus and Wortmann, the characteristics of this profile were not available in time to be included in this thesis. It is also noted that the profiles used for the tail on a glider are more important

due to the amount of time spent in reasonably small radius turns. It was thought that the NACA 0009 would suffice for application to the Low Speed HALE UAV missions in which the only turns would have a much larger radius on average.

For the Vertical tail, only the provision for a $\left(\frac{t}{c}\right)_{VT}$ and a single drag coefficient at the given Reynolds number are made. It was thought since yaw stability was not going to be considered in this methodology the given information would be sufficient for the calculation of drag and weight of the Vertical Tail.

5.E Tail Sizing Characteristics Specification

The next major steps in the methodology and the creation of the default aircraft in addition to the maintenance of the proper geometrical form of the overall aircraft are the Tail Calculation and Tail Variable Specification functions. A very large number of constants were created in order to size the tails of these possible configurations. These constants are based on the traditional sizing criteria of tail volume coefficient with minor modifications for the configurations for which the traditional approach is difficult to apply.

5.E.1 Default Tail Sizing

The specification of tail moment arms has already been detailed in previous sections. Thus far, none of the tail geometric characteristic parameters have been specified. For the majority of the tail geometric characteristics, historical data is available from which to base the default values. The same cannot be done for the tail volume coefficients. The reason for this will be described following the mention of the default values for the tail geometric characteristics.

5.E.1.a Specification of Default Tail Geometric Characteristics

The majority of the assumptions made for values of tail aspect ratios, sweep angle and taper ratios for the default case and conventional configurations were extracted from Roskam[5] (Pt.II, p.207) and from glider data from Thomas[9]. The horizontal tail taper ratio

was 0.7 for the Conventional and Canard Configurations, 1.0 for the Twin Boom and all Multiple Fuselage configurations except for the Tandem Wing. The reason for this was that if these surfaces were tapered, that would produce a large stress concentration at the junctions of the surface to the multiple fuselages/booms. Additionally, historically, very few twin boom aircraft have had anything but constant chord horizontal tails.

In some instances, it would be desirable to sweep the canard in a multiple fuselage case (the default single fuselage canard is swept). This was done with the Rutan *Voyager* in order to try to tailor the sum of the lift distributions of the canard and main wing in an attempt to maximize aerodynamic efficiency. This would obviously not be done in the early stages of conceptual design and was therefore also not included as an option.

The Tandem Wing configurations had a Taper Ratio of 0.4 for the default. The default value for all tail constants for the Flying Wing was 0.0 as it was assumed to have no tail.

Only the horizontal tail for the Conventional and Canard configurations had a nonzero sweep angle (15 degrees). All of these values were selected from historical data. It is realized that the sweeping of these tail surfaces increases mass, reduces aerodynamic efficiency and decreases the moment arm. Despite these facts, practically all of the Low Speed HALE UAV's have had swept tail surfaces. It was therefore deemed prudent to include the deleterious effects of including sweep for these surfaces.

The assumed values for the horizontal tail aspect ratios were 6 for the Single Engine case and 7 for the Twin-Engine case. This applied to all of the configurations except the Tandem Wing, which was given a default aspect ratio of 22, the same aspect ratio as the *Perseus* aircraft. The reason the single and twin engine aircraft horizontal tail surfaces had different aspect ratios was thought to be due to propeller slipstream effects, however these data were again taken from historical values.

For all of the vertical tails with the exception of aircraft with 2 or more fuselages, the aspect ratio was given a default value of 2, a quarter chord sweep angle of 15 degrees, and a taper ratio of 0.5 for Single Engine aircraft or 0.6 for Twin-Engine aircraft.

For aircraft with 2 or more fuselages or booms, the tail area was split (always in two, regardless of the number of booms/fuselages) and the tail geometric characteristics were sized based on that area split (50/50). Although the listing of information in paragraph format is generally arduous to read through, a tabulated format for the assumed values above would not have been more clear due to the number and nature of the exceptions.

5.E.1.b Default Tail Volume Coefficient Specification

Tabulated values are given in Table 5.6 for the Modified tail volume coefficients. The "XX" for the Tandem Wing Horizontal Tail values denotes the fact that the Tandem Wing was sized as previously described, without the use of volume coefficients. The values of horizontal tail volume coefficient for the Conventional and Canard configurations were selected from Raymer[4] in the range for Sailplanes. It was discovered during the initial iterations through the methodology that any other available values simply oversized the horizontal tail. The evaluation of what constituted "oversized" was determined from information extracted from existing Low Speed HALE UAV's. The drag penalties (usually parasite/profile) from oversizing the tail can be large and are unacceptable for Low Speed HALE UAV's.

It is difficult to explain the nature of these modified tail volume coefficient values at this point in the thesis. A detailed discussion as to the origins of the moment arm lengths used for the various configurations will soon follow, and the bulk of the associated questions should be answered at that time. For now, it is asked that these coefficients be viewed with the consideration that one of the fundamental variables in their determination (tail moment arm, L_t) has yet to be defined for the majority of the configurations considered.

Table 5.6 *shows the modified tail volume coefficients used for the sizing of the tail or canard of the default configuration.*

All Default Engines are In Tractor Configuration	**Single Engine C_{ht}**	**Twin Engine C_{ht}**	**Single Engine C_{vt}**	**Twin Engine C_{vt}**
Conventional	0.5	0.55	0.015	0.02
Canard	0.5	0.55	0.025	0.025
Twin Boom	0.6	0.65	0.04	0.05
Multi Fuselage				
Conventional	0.5	0.45	0.015	0.02
Canard	0.5	0.35	0.02	0.015
Tandem Wing	XX	XX	0.015	0.05
Flying Wing	0	0	0	0

5.E.2 Difficulties with the Vertical Tail Volume Coefficient Definition

There were no values given by Raymer for vertical tail volume coefficients for any class of aircraft that were useful. The values determined from estimates taken from photographs of existing Low Speed HALE UAV's are all less than half of the value of the smallest coefficients given by Raymer (for sailplanes).

The reason for this can clearly be seen with a quick look at the definition for the Vertical Tail Volume Coefficient :

$$c_{VT} = \frac{L_t}{b} \cdot \frac{S_{VT}}{S_{ref}} \qquad \textbf{(5.8)}.$$

The denominator dominates this term for Low Speed HALE UAV's. The relative wing span and wing area for this class of aircraft is much greater than even the next closest class of aircraft, the sailplane.

At this point, it is also beneficial to recall the Fuselage Length Diagram, Figure 5.7. The fuselage length (and thereby the tail moment arm length L_t) is higher for the Glider than any other class of aircraft. When taking into account the shorter tail moment arms of Low Speed HALE UAV's, in combination with the higher wing spans and larger reference areas, accurate tail volume coefficients will acquire values that upon first glance would seem ridiculously small.

Example values of existing aircraft (again derived from photographs) are $c_{VT} = 0.02$ for *Perseus A*, 0.015 for *Perseus B*, 0.011 for *Theseus*, and 0.011 for *Condor*.

5.E.3 Tail Volume Coefficients for All Configurations

The vertical tail volume coefficients should only be compared to existing tail volume coefficients for the conventional configurations. The other values resulted from non-traditionally defined vertical tail moment arm lengths, which fundamentally change the values of these coefficients. Again, this was done out of necessity and the lack of any relevant information for unconventional aircraft configurations. The results were validated only in the form of overall vertical tail areas where possible.

It is mentioned once more that the horizontal tail volume coefficients presented in Table 5.7 result from the iterative use of the methodology in determining that the aircraft

can be made longitudinally stable using the horizontal tail sizes specified. This includes attempting to find the minimum value at which this occurs to minimize parasite drag. In addition, the resulting horizontal tail areas were compared to those of existing aircraft of the Low Speed HALE UAV class where available.

As mentioned in an earlier section, several of the values for single and twin engine tractor configurations have changed slightly from their default values. This was due to the differences between the predicted and the actual main wing and horizontal tail average chord lengths.

Table 5.7 *lists all of the remaining horizontal tail volume coefficients based on the horizontal tail moment arm lengths defined in the previous sections.*

	Single Engine	Single Engine	Twin Engine	Twin Engine	Twin Engine
	Tractor	Pusher	Tractor	Pusher	Push-Pull
	C_{ht}	C_{ht}	C_{ht}	C_{ht}	C_{ht}
Conventional	0.5	0.5	0.55	0.55	0.5
Canard	0.5	0.5	0.55	0.55	0.5
Twin Boom	0.6	0.6	0.55	0.55	0.5
Multi Fuselage					
Conventional	0.5	0.5	0.5	0.5	0.4
Canard	0.3	0.3	0.25	0.25	0.2
Tandem Wing	XX	XX	XX	XX	XX
Flying Wing	0	0	0	0	0

Table 5.8 *lists all of the remaining vertical tail volume coefficients based on the vertical tail moment arm lengths defined in the previous sections.*

	Single Engine	Single Engine	Twin Engine	Twin Engine	Twin Engine
	Tractor	Pusher	Tractor	Pusher	Push-Pull
	C_{vt}	C_{vt}	C_{vt}	C_{vt}	C_{vt}
Conventional	0.015	0.015	0.02	0.02	0.0175
Canard	0.015	0.02	0.025	0.025	0.0175
Twin Boom	0.04	0.04	0.05	0.05	0.045
Multi Fuselage					
Conventional	0.015	0.015	0.02	0.02	0.015
Canard	0.02	0.02	0.025	0.025	0.02
Tandem Wing					
Single Fuselage	0.05	0.035	0.04	0.035	0.04
Multiple Fuselage	0.04	0.04	0.04	0.04	0.035
Flying Wing	0	0	0	0	0

Most notable is that the horizontal tail volume coefficients don't change much between the twin engine tractor and twin engine pusher configurations. The main reason for this is seen in the moment arm length definition. The change in moment arm length for the configurations that have constant values for tail volume was more than sufficient in re-sizing the tail based upon the definition of wing on fuselage placement. No change in tail volume was necessary for the coefficients.

Due to the nature of the different moment arm definitions for the vertical tail volume coefficients, a significant range of values is covered by the results (compiled in Table 5.8). As expected by the relative definitions, the vertical tail volume coefficients for the tandem wing configurations and the twin boom are consistently higher to compensate in the denominator for consistently higher moment arm lengths. Once again, application of these values outside of this methodology would not be recommended without validation in the form of yaw stability and multi-engine engine out controllability calculations.

Nevertheless, the validation performed for the macroscopic vertical tail areas is considered sufficient for sizing the vertical tails of the large variety of different configurations. This is especially true considering these areas were used only for the purposes of drag and weight estimation performed within this methodology. Given the nature of this type of aircraft, only a very large relative variation in tail area would noticeably effect the drag or weight estimations.

5.F Location and Performance of the Engine(s)

One of the less technical aspects of the methodology deals with the placement of the engines on the aircraft. Despite being less technical, it is no less challenging to implement, given the rather large number of possible configurations. This will be discussed in the Implementation Chapter. For the moment, the discussion will cover the method of engine placement, and introduce the effects of placement that are covered by the methodology.

5.F.1 Location of the Engine(s)

The Power-plant Details Dialog box is given in Figure 5.9. This dialog box is included because it was thought to simplify the explanation of the parameters associated

with engine placement considered by the methodology. As seen in the figure, the preliminary engine Horsepower required has already been calculated at this point in the methodology (as the product of the HP/W ratio times the takeoff weight). A more accurate estimation of the power will be performed with the refined drag estimate described at length in the next chapter. For the purposes of selecting and sizing an engine, this information was thought to be sufficient. As a reminder, the number of engines is included since the Horsepower shown is total Horsepower. If used for sizing a twin engine aircraft, this Horsepower would have to be divided by two. The second propeller efficiency has already been taken into account in the calculation of the Horsepower shown in the Dialog box, however. The remaining characteristics will be discussed in the following subsections.

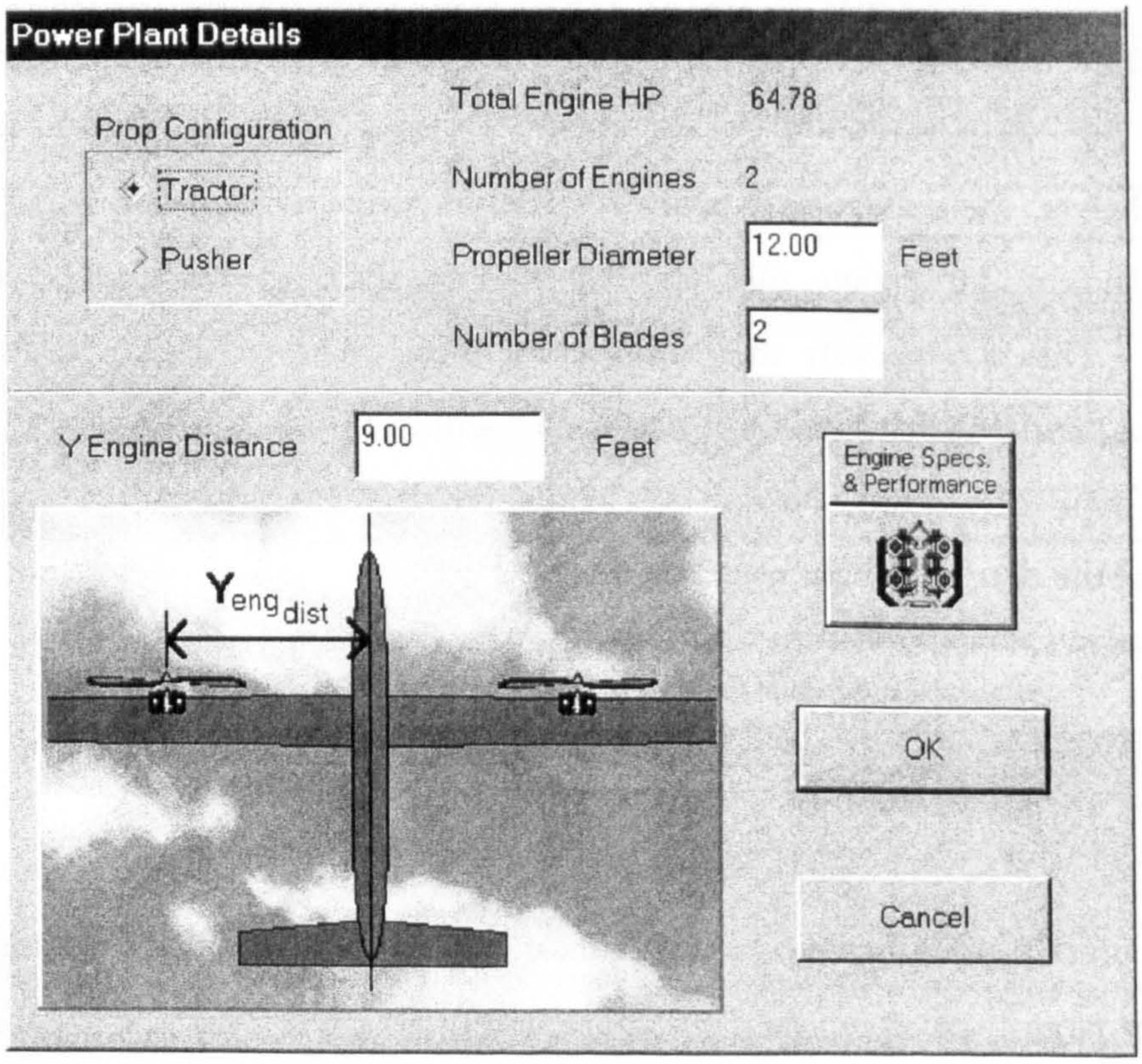

Figure 5.9 ***is the Power Plant Details dialog box which allows the designer to specify the engine configuration and information relevant to the engine location.***

5.F.1.a Propeller Specification

As seen in the Power Plant Details Dialog box, the only provision made for propeller design and specification is for the propeller diameter and the number of blades.

In performing the drag and weight estimations, these were the values required, and this will be discussed in the drag and weight estimation chapters. A detailed design of the propeller was not attempted by this methodology. The unique flight regime of this class of aircraft makes traditional propeller design methods difficult to apply.

Bizzarri[71] discussed propeller design for HALE aircraft on a basic level using traditional design methods. Very little else was found in the literature. There was mention of a special code written by Mark Drela to perform propeller aerodynamic design for low Re conditions, but this code is not in the public domain. Thus, there is a limitation to assume propeller characteristics that already exist for aircraft of this class, at least for the early conceptual sizing stage. Since the effects of propeller efficiency and design are not expected to be configuration dependent (aircraft configuration, not engine orientation), this area was not investigated in further detail.

There have been a wide variety of propellers used for this type of mission. A selection of Low Speed HALE UAV's are listed in Table 5.9. As can be seen from the table, just as for General Aviation Aircraft, there is no consensus on the correct diameter or number of blades for the propeller for the Low Speed HALE. It is agreed upon in the literature, however, that this aircraft will need a gearbox in order to climb more efficiently at High RPM and cruise at Low RPM in the thinner high altitude air. At cruise altitudes it becomes difficult to avoid propeller tip shock and this is the primary reason for lower RPM's as the speed of sound is greatly reduced at the lower temperatures and densities in cruise.

Table 5.9 ***is a compilation of useful propeller details for HALE aircraft available from the literature.***

	Diameter (ft.)	#Blades	#Propellers	RPMs
Altus	8.5		1	
Condor	16	3	2	
Perseus A	15	2	1	600 - 1200
Raptor	14		1	
Strato 2C	20	5	2	600 - 650
Theseus	8.5	2	2	

The propeller efficiency in climb and cruise was specified in the Critical Constants dialog box. In order to change the values of either of these efficiencies, the designer must return to this dialog box to change them, as they were assumed fixed for the given design.

5.F.1.b Propeller/Engine Configuration

In the upper left corner of the Power-Plant Details dialog box is the Tractor/Pusher radio button group. The designer can select either a Tractor or Pusher engine/prop configuration for single engine aircraft, or for twin engine aircraft Tractor, Pusher, or both (Push-Pull). This invokes the tail sizing calculation as each of these engine/propeller configurations has large changes in aircraft Center of Gravity associated with it. The engine propeller group usually comprises at least 10 percent of the takeoff weight of the Low Speed HALE UAV and is often located at the extremities of the aircraft. This explains why the tail must be resized with the definition of engine/propeller configuration. The constants used for this sizing were described in the Tail Sizing section.

With the selection of the Twin Engine Tractor or Pusher, the option is made available to specify the distance along the span of the wing where the engines will be located. No provision was made for asymmetrical positioning. There are several arguments for and against placement as close to the main fuselage(s) as possible.

The main argument for placement near the fuselage(s) is the engine out controllability. The arguments for placement closer to the wing tip are structural in nature. In all of the twin engine implementations, the engines were placed as close to the fuselage as possible, taking into account the flexibility of the structures the engines are attached to. In any event, the designer is free to locate the engines anywhere along the span provided the propellers clear the fuselage.

Torenbeek[7] suggests at least one inch radial clearance between the blade tips and the airplane structure, plus any additional clearance necessary to prevent any harmful vibration. He suggests at least 0.5 inch longitudinal clearance between the propeller blades or cuffs and stationary parts of the airplane. He also suggests positive clearance between other rotating parts of the propeller or spinner and stationary parts of the airplane. The remainder of the limitations deal with propeller clearances for takeoff based on landing gear limitations. He strongly recommends these values be treated as absolute minimums (and further suggests at least 4 inches between propeller tip and fuselage plus 0.65 inch per 100 HP per engine). Finally, he mentions that engine power growth is likely and that the prop diameter is likely to grow as a result.

The range of possibilities of engine placement on the various configurations needs to be described graphically for each configuration. This would take up too much space

with the 55 different possibilities, however it is believed that the choices made for possible engine locations for the different configurations was made in a rational, justifiable manner. The engines were placed in the most conventional locations possible. At times this was not a difficult decision. The example of the Two Fuselage Single Engine case(s) allow for quick visualization of the problem of where to place the engine. In the instance of the single engine pusher, the engine was placed as far aft without interfering with the tail structure. This position could be manipulated by varying the cg position of the engine on the fuselage. This allows for the possibility of either a tail aft pusher, or a shaft drive pusher.

The actual logic required for the placement of the engines is more complex than would be expected. The process of placing an engine on an aircraft is quite simple and intuitive for a designer, independent of a structured computer environment. The difficulties of automating this task will be covered in the Implementation Chapter.

Finally, the button on the middle right of the Power-plant Details dialog box has yet to be described. It leads the designer to the Power-plant Specifications dialog box to be discussed in the next section.

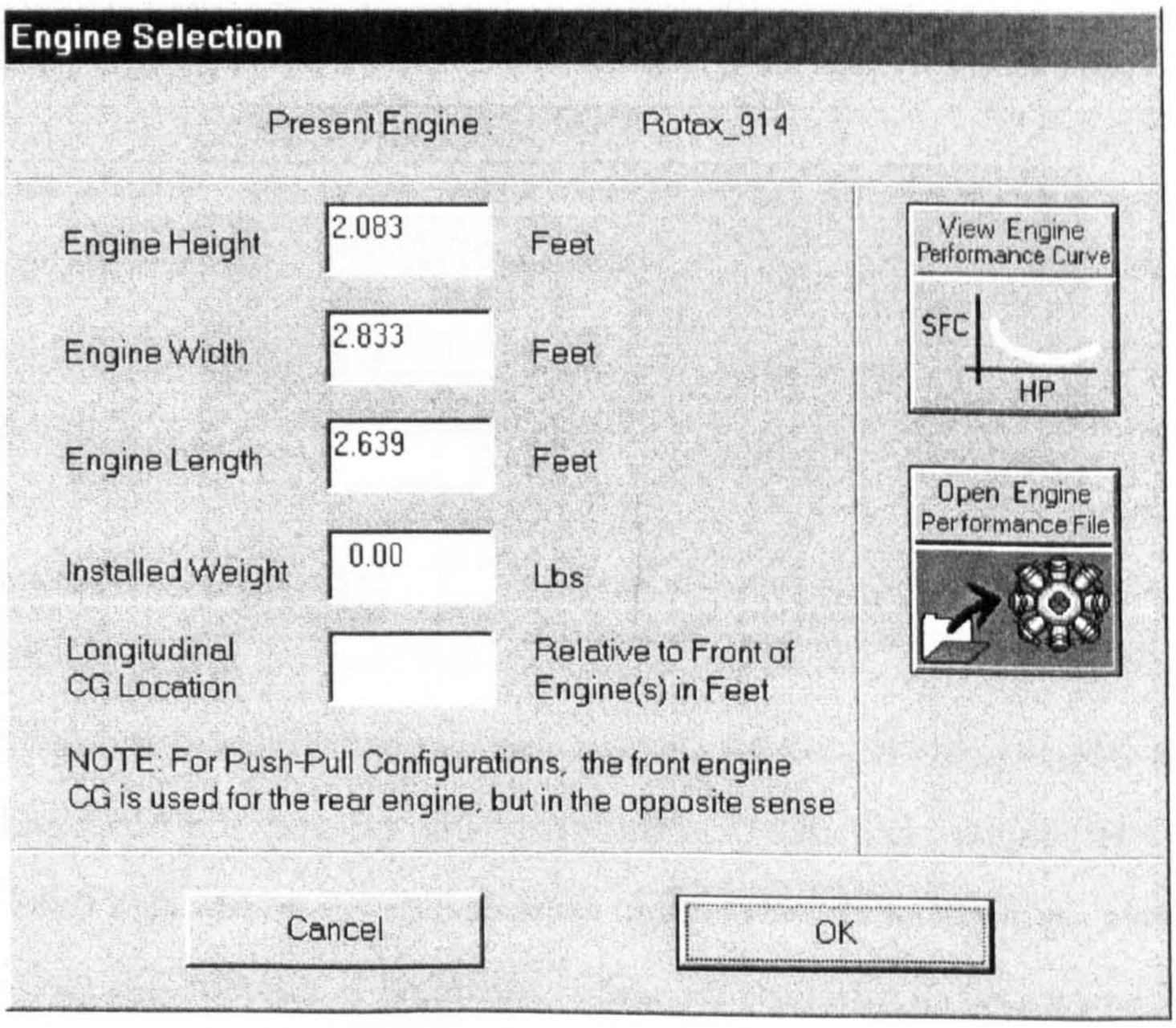

Figure 5.10 ***is the Engine Selection dialog box which enables the designer to specify and view the performance and geometric characteristics of the engine.***

5.F.2 Engine Geometry and Performance Specification

Figure 5.10 shows the Engine Selection Dialog Box. The first thing to notice is the Present Engine. If no engine has been specified, a default engine is assumed and the dialog indicates that the default engine specifications are being used. The dimensions of this default engine are of the form given by Raymer[4] as follows :

$$L_{engine} = a(HP)^b \tag{5.9}$$

The constants he suggests for Opposed Engines and Inline Engines can be seen in Table 5.10. The resulting characteristic curves can be seen in Figure 5.11. In addition to constants for the Horsepower dependent expression to determine length of the engine, he provides a range of values for width and height of the engines independent of the HP. For the default engine, the larger of these values were used in order to provide clearance for the turbo-charging and supercharging ductwork and turbines. For the length, however, an additional 50% of the engine length was given to create space for installation and intake charge apparatus.

Table 5.10 ***lists estimates for engine width and height by engine type and the constants necessary to derive engine length from engine horsepower using Raymer's method for internal combustion reciprocating engines.***

		a	b
Opposed	Length	3.86	0.424
60 - 500 HP			
	Width	32 - 34 in.	
	Height	22 - 25 in.	
In-Line	Length	5.83	0.424
100 - 300 HP			
	Width	32 - 34 in.	
	Height	22 - 25 in.	

The graph of the radial engine length as a function of HP was included for interest and comparison. It can be seen that for the same HP output, the Opposed engine is considerably shorter throughout the HP range considered. In addition, a brief look back at Table 5.10 will show that in addition to being shorter, it is equally as wide and high as the In Line engine. Although physically this may not make sense, historically, In Line and Opposed engines have had very similar width and heights. It was for this purpose that the Opposed engine was selected for use with this methodology. The relative engine weights

will be compared in the Weight Estimation Chapter, however, it happens that the Opposed engine is only very slightly heavier than the In Line. Despite being shorter in the range of interest, the Radial engine has by far the largest frontal area of any of the engines considered. This, in addition to lack of availability prevented it from being included.

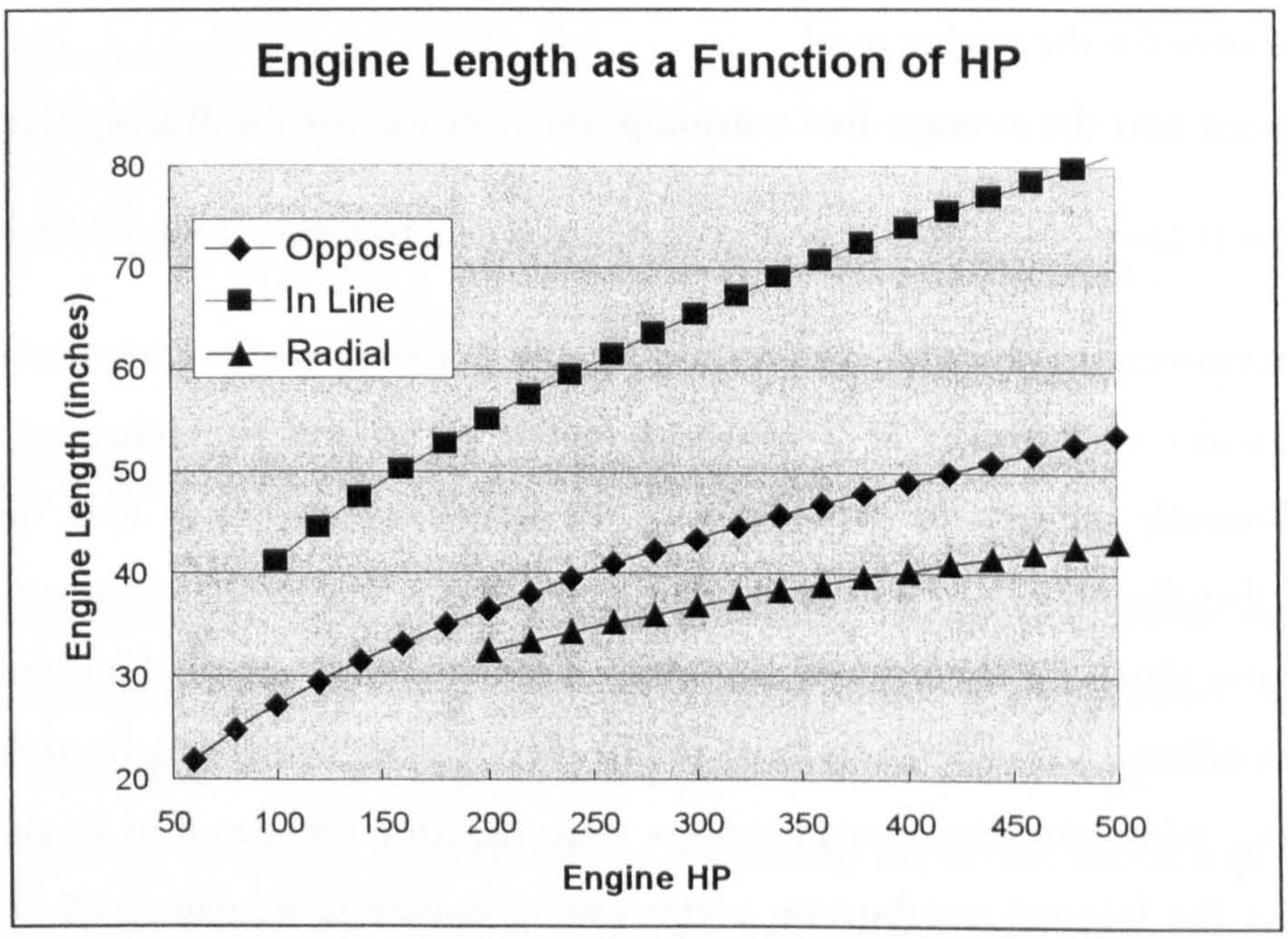

Figure 5.11 ***highlights the differences in the engine length estimation methods across a range of horsepower.***

No other engine types were considered for the default case. A comparison of Rotary, 2 cycle, turboprop, and Diesel cycle engines was done in the Literature Review. Unfortunately, no data were available on the performance of these engines, and the problems associated with using each one would most likely exclude all but the internal combustion reciprocating engine from being used for the HALE UAV without extensive development work.

Alternatively, if the designer has engine data available, this information can be read in and visualized directly by the program. The engine size should include adequate room for turbo-charging and supercharging. Also, available from manufacturer's data, the engine installed weight and center of gravity location can be specified by the designer at this stage. No engine weight is calculated until the detailed weight estimation has been selected by the designer. At this stage in the methodology there is no use for the engine weight or center of gravity location but these data will become useful further along the methodology.

If the designer has the information at hand, a curve of Thrust Specific Fuel Consumption variation with Engine Power Output can be read into the methodology and subsequently used to adapt the engine fuel consumption to whatever power output requirement is determined by the methodology in the refined drag calculation. This will have some impact on the final endurance calculated depending on the characteristic fuel consumption curve for the engine used.

It is known that the average fuel consumption in cruise for the Boeing *Condor* was $0.40\frac{lb}{HP \cdot hr}$ or $0.25\frac{lb}{lbf \cdot hr}$. These values can be used as a baseline. It should be pointed out that the reciprocating internal combustion engine performance is comparatively less complex to predict at altitude. It is assumed that if turbo and supercharging can be performed efficiently enough to provide near Sea Level density air at near Sea Level temperatures, that the power output will be fairly constant. This minimizes the effects of altitude on engine sizing for the internal combustion reciprocating engine, however it does not remove the effects. Consideration must still be given to the sizing/weight of radiators, intercoolers, etc, while the drag considerations were described in detail in Drela[103]. The performance of the internal combustion reciprocating engine is fundamentally different from the performance of a turbojet/turbofan. The turbojet/turbofan requires a complex engine performance prediction algorithm at altitude (and in order to predict how to climb to altitude), and gross over-sizing of the engine due to the greatly reduced intake air densities at altitude.

At this point, all of the useful engine geometrical and performance characteristics have been specified. In addition, in no particular order of specification, the Wing Planform, Wing Profile, Tail, and Fuselage general layout and geometry have been defined. It is now possible to move on to the next major step in the procedure of the methodology. Once more, it is necessary to state that the iterative process can be begun at any point, and exited at any point. For this methodology, the next point of iteration is the Refined Drag Estimation.

Chapter VI

He is the best sailor
Who can steer within fewest points of the wind,
And exact a motive power
Out of the greatest obstacles
--- Henry David Thoreau

6. Aircraft Drag Estimation

The subject matter of this thesis thus far has been related to the justification, creation, geometric manipulation, and specification of realistic default configurations. This chapter begins the discussion of the analysis-related aspects of the methodology.

The following chapter is responsible for explaining the rather broad topic of detailed aerodynamic drag estimation utilized in this methodology. The estimation entails many different methods of drag calculation depending on what part of the aircraft the drag is being estimated for, and often what portion (lift induced, viscous, profile) of the drag is being estimated for any given component. Methods ranging from statistical, to flat plate similarity, to a Vortex Ring Lattice method are employed and validated where necessary. The discussion will proceed in the order in which the component drags were estimated in the methodology, however, for the most part, for the purposes of the methods employed the order of prediction of the drag of the components is irrelevant.

It should be stated that although airfoil profile drag originates from viscous forces, there is a distinction between the two in this chapter. In many books the pure viscous drag is called parasite drag, and the additional two-dimensional drag increase due to an airfoil profile (either at angle of attack or not) is often referred to as profile drag. This is the definition used for this thesis.

6.A Determination of Major Aerodynamic Variables

The definition of lift coefficient is seemingly straightforward. Difficulties arise, however, when attempting to apply this equation to some of the less traditional configurations. It becomes most intricate in the instance of the lift coefficient definition for the Tandem Wing configurations. Any time a significant portion of the lift is generated by any surface other than the main wing, a slightly revised method of calculation of the lift coefficient must be performed. Obviously, before any analysis of the drag can be performed, an accurate value for lift coefficient must be determined.

As a part of the proper definition of the lift coefficient, some value must be used for the reference area of the surface generating lift. Care must be taken in assigning this reference area, since it will be used in the determination of the aircraft drag as well. It is not crucially important as to what is selected for the reference area, as long as it is kept consistent throughout the analysis. In selection of the reference area (S_{ref}), for all of the configurations except the Tandem Wing configurations, S_{ref} was chosen as the main wing planform area.

For the Tandem Wing aircraft, the determination of S_{ref} was slightly different. The drag analysis requires a lift coefficient for both the fore and aft wings for the tandem wing case. The division of area was defined prior to the creation of the default aircraft. There is a choice, then, between 3 possible areas, that of the forward wing, that of the aft wing, or the overall wing area, upon which the wing loading is defined.

The only justifiable choice is the selection of the overall total wing area. Most importantly, it maintains a constant reference area for ***all*** of the possible configurations. This is important when comparing the relative values of drag coefficient C_D for the different configurations. In this manner, there is certainty in the values of C_D for accurate comparison between configurations.

Once the reference area has been chosen, the lift coefficients for the Tandem Wing configuration are found based on the definition of Total Lift Force :

$$\begin{aligned} L_{total} = W_{to} &= \tfrac{1}{2}\rho V_{cruise}^2 S_{ref} C_{Laircraft} = L_{ForeWing} + L_{AftWing} \\ &= \tfrac{1}{2}\rho V_{cruise}^2 S_{ForeWing} C_{L_{ForeWing}} + \tfrac{1}{2}\rho V_{cruise}^2 S_{AftWing} C_{L_{AftWing}} \end{aligned} \quad \textbf{(6.1)}$$

Where $L_{ForeWing}$ is the lift of the forward wing, and $L_{AftWing}$ is the lift of the aft wing. It is known that the area of the forward wing is related to the area of the aft wing by the equations :

$$S_{ForeWing} = (1-\delta)S_{ref} \text{ and } S_{AftWing} = \delta S_{ref} \quad \textbf{(6.2,3)}$$

where δ is the fraction of total wing area comprised by the aft wing (and is user defined, or 60% by default).

In addition to these equations, the distribution of lift coefficients between the two wings has to be done in a way to insure that the forward wing stalls first. In order to do this, the forward wing lift coefficient is assumed to be 10% greater than the aft wing. Implicit in this assumption is the assumption of a similar Reynolds number. This results in the forward wing lift coefficient:

$$C_{L_{ForeWing}} = 1.1 C_{L_{AftWing}} \quad \textbf{(6.4)}$$

which, when substituted into **Equations 6.1** and **6.2** gives the aft wing lift coefficient:

$$C_{L_{AftWing}} = \frac{C_{L_{aircraft}}}{(1+0.1\delta)} \quad \textbf{(6.5)}$$

This ultimately provides the division of lift between the front and back wings of the tandem wing aircraft. For the other configurations, the lift coefficient is calculated in the same manner as the aircraft lift coefficient above. It is noted at this time that the weight estimation module verifies that there is sufficient fuel in each wing to insure the calculated division of lift can be maintained in an equilibrium flight condition.

In the instance of canard lift or horizontal tail lift, the amount of lift is explicitly determined by the Trim Calculation module, and the preceding analysis is not performed. The Trim Calculation module will be explained in detail in Chapter 8.

6.B Determination of the Lift Curve Slope

The implementation of the Vortex Ring Lattice method used, strictly calculates the induced drag of the major lifting surfaces of the aircraft. As such, it is not equipped to adjust for cambered airfoils when cambered airfoil angle of attack (C_L-α) information is input. As a result, the slope of the C_L-α curve must be calculated, and an associated angle of attack extracted based on the relevant calculated lift coefficient.

The procedure described is identical for the main wing, canard, or tandem wings. There are several possibilities. If the designer has input a C_L-α characteristic curve, the value of slope is extracted from this curve in the pre-stall range. If either there has been no information entered by the designer, or the lift coefficient for cruise is beyond the pre-

stall range of the curve, the designer is warned that the two dimensional theoretical value of lift curve slope equal to 2π is being used as an estimate. While it is recognized that this will overestimate the value of lift curve slope, there were no other alternatives available for the prediction of the slope in this region. It is hoped that if a particular airfoil has been selected, that attention will be paid to ensure that the maximum lift coefficient has not been reached in cruise. If this occurs, the designer is notified, and of course has the option to return to and modify any of the inputs that determine the lift coefficient.

This section has introduced the concept of one of the most useful analysis tools to be used by the methodology in the comparison of the aerodynamics of the different possible configurations, the Vortex Lattice Method.

6.C The Vortex Lattice Method

This section will present the following points:

- Justification for why the method is necessary.
- Basic theory (enough to delineate the bounds of applicability)
- Validation of the implementation used.

It was thought at the genesis of this project that a suitable means of calculating the lift induced drag would be absolutely necessary to the achievement of the goals of the thesis. A reliable method to calculate the drag interactions of several lifting surfaces beyond those methods available using common design references is required for the comparison of less conventional configurations. Several methods were considered, most of which were discussed superficially in the Literature Review.

If the drag analysis were limited to the methods available in the common methodologies there would be no mechanism for taking into account the less conventional configurations. The existing methods for drag prediction that do not use equivalent flat plate area are based almost exclusively on conventional configurations.

6.C.1 Wing Profile Drag and the Vortex Lattice Method

There exists a wealth of information on the drag associated with wing profiles. Several of these profiles have been modified for low Reynolds number, high lift coefficient operation. For this information to be used by the present methodology, the data need only

to be discretized into a tabular format and read into the methodology as a data file. It was believed that this data would be much more accurate than any predictions made via an Ideal Potential Flow prediction. The accuracy could be comparable if the method was specifically tailored to airfoil design, such as the codes mentioned in the Literature Review. However, since extensive work has already been performed in accurate predictions of airfoil profile flow, the effort required to implement an accurate method was thought repetitive.

In addition, the speed of the computational methodology would have been greatly compromised. In it's current implementation, even the tandem wing configuration which requires the vortex lattice method to be applied to two interacting lifting surfaces provides results in less than 6 seconds on an Intel Pentium 150 MHz processor, and essentially instantaneously on the newer Pentium II and III or equivalent processors. This may seem insignificant, but it was thought quite important for the results to be provided in real-time. In order for several different configurations to be compared and iterated on, it was thought absolutely necessary that the waiting time for changes in each configuration be unnoticeable. This has been preserved in the present methodology.

6.C.2 Potential Flow Theory and Lifting Surface Interaction

Unfortunately, the three-dimensional effects of one lifting surface on another are not covered by any technique mentioned in the common design references. Although wing camber is not modeled using this implementation of the vortex lattice method, the lift-induced drag created by a wing planform at angle of attack is very accurately predicted at the Reynolds numbers seen by Low Speed HALE UAV's in cruise.

For a detailed analysis on the background theory of the vortex lattice method, several excellent books have been written. Most notably, Katz and Plotkin[39], R.I.Lewis[104], and C.B.Stribling[105] All of these references were used in the implementation and validation of the Vortex Ring Lattice method used in this methodology.

For incompressible, inviscid/irrotational, small disturbance flow (i.e. steady flow for this implementation), the wing is modeled as a set of lifting panels (i, j, total N). Each panel contains a ring vortex. A bound vortex is located at the ¼ chord position (Γ_j). Both spanwise and chordwise variations in lift can be modeled as a set of non-continuous changes from one panel to the next.

The required strength of the bound vortex on each panel needs to be calculated by applying a surface flow boundary condition. The equation used is the condition of zero flow normal to the surface (V_n=0), or the Neumann boundary condition. It should be stated that there are two commonly used boundary conditions for vortex methods, the other being the Dirichlet boundary condition of zero velocity parallel to the surface. Only one can be used, and there is a fundamental rift between the two schools of implementation. The Dirichlet boundary condition is generally more appropriate to more advanced viscous boundary layer calculations.

It should be noted at this point in the discussion that a sizable portion (~20 - 30% in cruise) of the drag of this aircraft is due to viscous forces. It would have been possible to include a vortex lattice method capable of predicting skin friction drag with slightly greater accuracy than existing flat plate drag analogy prediction techniques.

This, however, was not seen as one of the failings of common aircraft drag prediction in the conceptual design phase. It also has little bearing on the comparison between configurations, as once again, the error would be the same regardless of the configuration, assuming roughly equal wing areas. Most importantly, these viscous vortex lattice codes require much more time to process, thus making them incompatible with the desire for real-time results from changes in configuration.

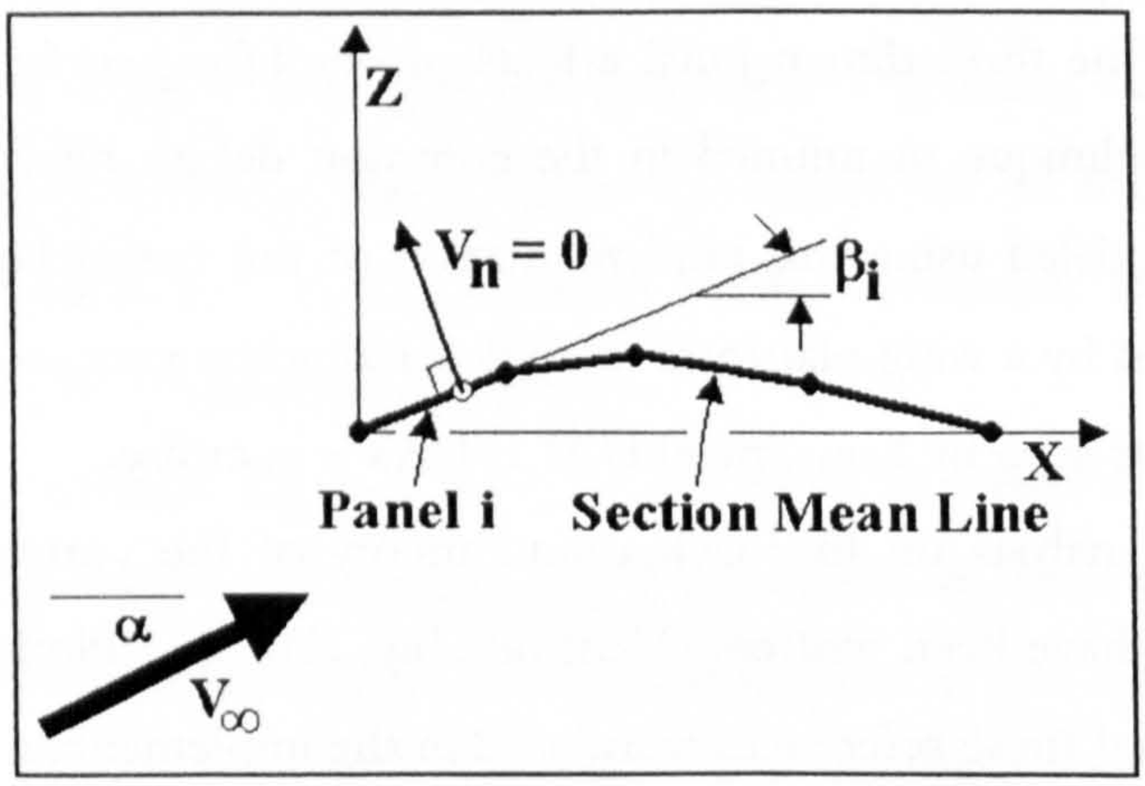

Figure 6.1 ***defines the terms relating to the panel normal vector used in the development of the equations for the Vortex Lattice Method.***

For each panel, the boundary condition is applied at the ¾ chord position along the centerline of the panel (called the collocation point). The normal velocity is made up of a free-stream component and an induced flow component. This induced component is a

function of strengths of all vortex panels on the wing. Thus for each panel, an equation can be set up which is a linear combination of the effects of the strengths of all panels. A matrix of influence coefficients is created (A_{ij}). This matrix is then multiplied by the vortex strengths and is equal to a right hand side vector of free-stream effects.

$$V_n = 0 = V_\infty \sin(\theta) + w_i \tag{6.6}$$

$$w_i = \sum_{j=1}^{N} A_{ij} \Gamma_j \tag{6.7}$$

$$\sum_{j=1}^{N} A_{ij} \Gamma = -V_\infty \sin(\theta) \tag{6.8}$$

Where $\sin(\theta)$ can be approximated by (as seen in Figure 6.1):

$$\sin(\theta) = \sin(\alpha - \beta_i) \cong (\alpha - \beta_i) \cong \alpha - \left(\frac{dz}{dx}\right)_i \tag{6.9}$$

Where β_i is the local panel angle. The influence coefficient A_{ij} represents the induced flow on panel i due to the vortex on panel j.

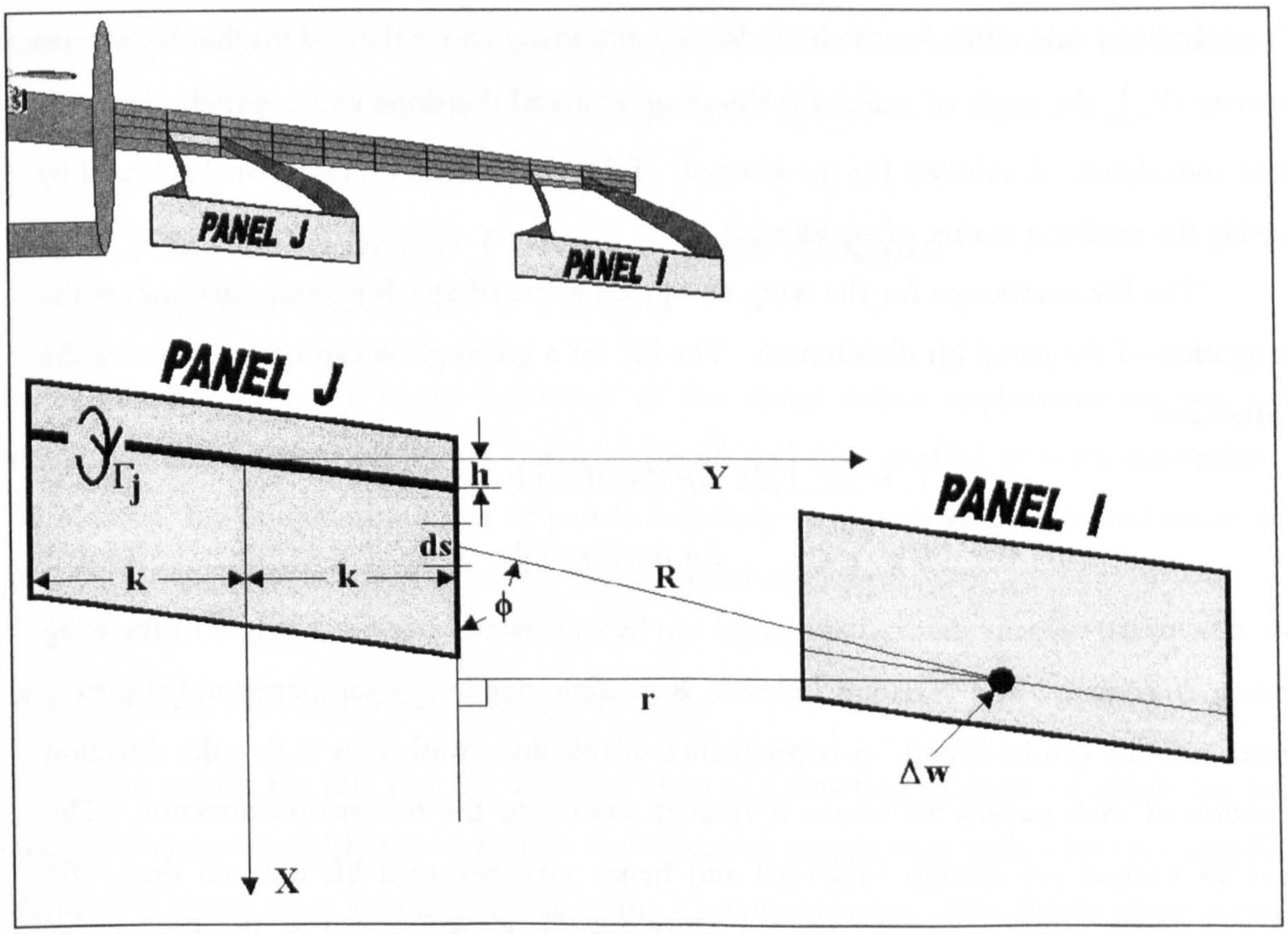

Figure 6.2 ***defines the terms used in the implementation of the Vortex Lattice Method equations.***

If all of the panels are assumed to be approximately planar then this influence coefficient can be calculated as a relatively simple application of the Biot-Savart law along the four component vortex lines (or 3 lines in the wake region).

The result of this integration leads to the following formulae for influence coefficients in general, the physical analogy for which can be seen in Figure 6.2 :

$$\Delta w = \frac{1}{4\pi}\frac{\sin(\phi)}{r^2}\Gamma_j ds \qquad \textbf{(6.10)}$$

$$w_{ij} = \int \frac{1}{4\pi}\frac{\sin(\phi)}{r^2} ds \cdot \Gamma_j = A_{ij}\Gamma_j \qquad \textbf{(6.11)}$$

$$A_{ij} = \frac{1}{4\pi}\left[\begin{array}{l} \dfrac{1}{(x+h)(y-k)-(x-h)(y+k)}\left\{\dfrac{2h(x+h)+2k(y+k)}{R_1} - \dfrac{2h(x-h)+2k(y-k)}{R_2}\right\} \\ -\dfrac{1}{(y+k)}\left\{1+\dfrac{(x+h)}{R_1}\right\} + \dfrac{1}{(y-k)}\left\{1+\dfrac{(x-h)}{R_2}\right\} \end{array}\right] \qquad \textbf{(6.12)}$$

Where $R_1 = \sqrt{(x+h)^2+(y+k)^2}$ and $R_2 = \sqrt{(x-h)^2+(y-k)^2}$ **(6.13,14).**

The right hand side terms for the boundary condition equations depend on the free-stream velocity (V_∞), the angle of attack for the wing (α), and the slope of the panels if camber were considered. A solution for the strength of the vortex lines on each panel is found by solving the resulting matrix of equations.

The lift coefficient for the wing at a given angle of attack is then obtained by the integration of the panel lift distribution. The lift for a given panel can be found using the Kutta Law:

$$L_i = \rho V_\infty \Gamma_i 2k \quad \text{for the lift of Panel i} \qquad \textbf{(6.15)}$$

$$L = \sum_{i=1}^{N} L_i \qquad \text{for the lift of the Wing.} \qquad \textbf{(6.16)}$$

The downwash velocity induced at a panel can be calculated once the strength of the wing loading is known. The variation between local flow angles for the panel and the free-stream velocity can be found. A consequence of this downwash flow is that the direction of action of each panel's lift vector is rotated relative to the free-stream direction. The local lift vectors are rotated backward and hence give rise to a lift induced drag. By integrating the component of panel lift coefficient that acts parallel to the free-stream across the span, the induced drag coefficient can be found.

$$D_i = \rho V_\infty \Gamma_i 2k \sin(\alpha_i) \text{ is the drag of Panel i} \quad (6.17)$$

$$D = \sum_{i=1}^{N} D_i \text{ represents the drag of the Wing} \quad (6.18)$$

The induced flow (α_i) represents the amount of rotation of the lift vector backward and must be calculated from the velocities induced on the bound vortex of the panel by other panels and the free-stream.

This explanation is an oversimplification of the actual implementation, but was intended to provide a very basic background of the vortex lattice method in general. Considerably more detailed analyses are available in the aforementioned references.

Given a basic knowledge of the origins of the above vortex lattice method (Potential flow theory, inviscid, irrotational, incompressible), it is safe to state that the method can be freely applied to the cruise condition of the Low Speed HALE UAV. None of these assumptions is violated in the high altitude low speed flow regime in cruise. In addition, the implementation of the vortex lattice method assumed steady flow. Since the aircraft is assumed in steady cruise flight, this assumption is also valid.

The theoretical assumptions involved in applying the method are known, however, there are particularities associated with its implementation that need to be assessed and then verified before it can be applied to the Low Speed HALE.

6.C.3 Validation of the Vortex Lattice Method Implementation

The first objective in the validation of the vortex lattice implementation was to verify that the macroscopic values obtained for lift and drag coefficient were reasonable. In addition, the minimum number of panels necessary to provide repeatable and accurate results (for angles of attack in which flow is still attached) was desired.

6.C.3.a The Rectangular Wing Analogy

The results for Lift and Lift Induced Drag as a function of angle of attack can be seen in Figure 6.3 and Figure 6.4. For the validation case, a case with a known, simple, theoretical closed form solution was used, the Rectangular wing. The curves given varied the number of chordwise and spanwise panels in a search for the optimum.

Figure 6.3 provides an idea of the overall accuracy of the method as compared to theory and the variation in that accuracy with increasing angle of attack. A more detailed view of the higher angle of attack area is given in Figure 6.4.

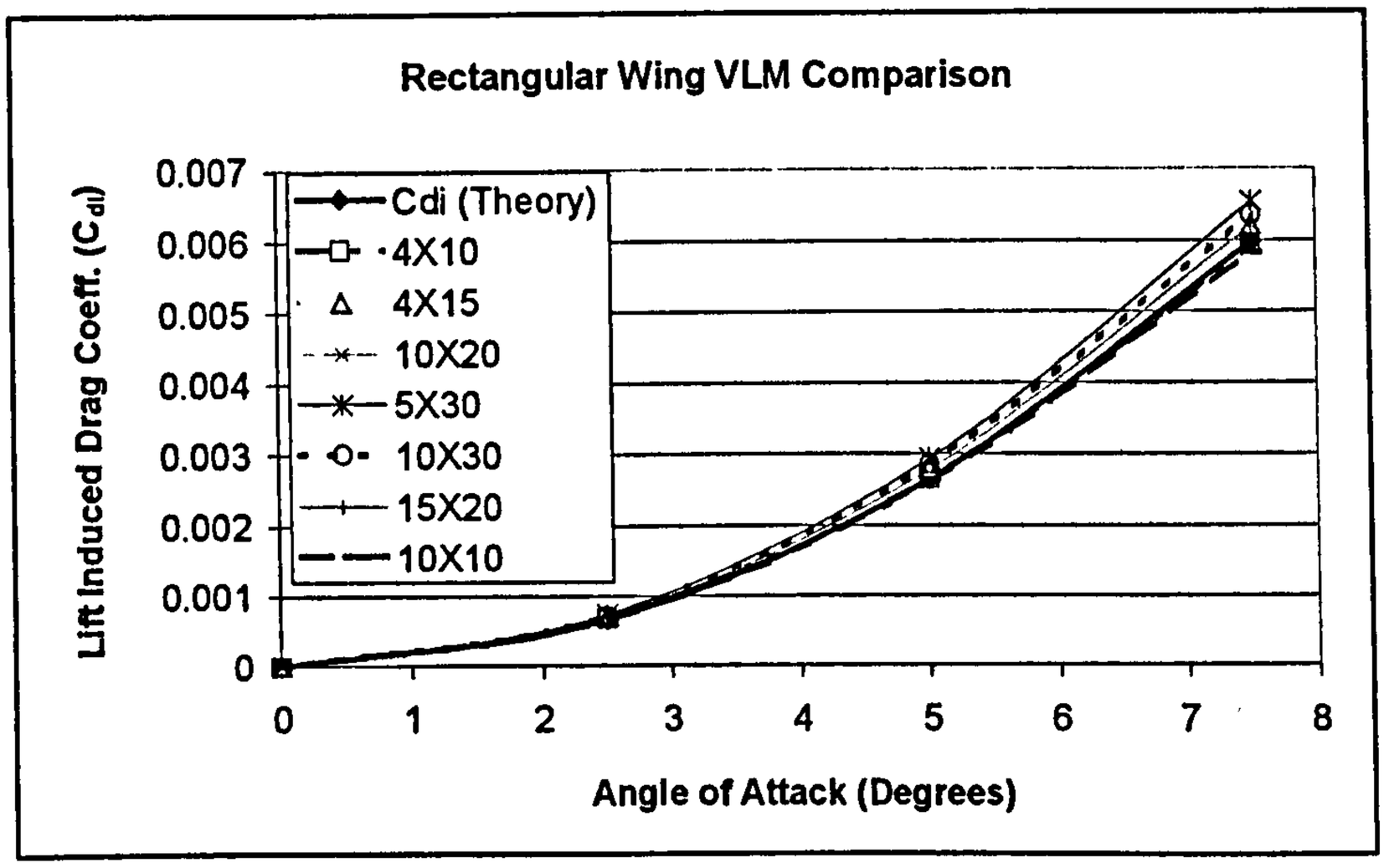

Figure 6.3 ***compares the lift dependent drag results of the vortex lattice method with variation in angle of attack for different grid densities.***

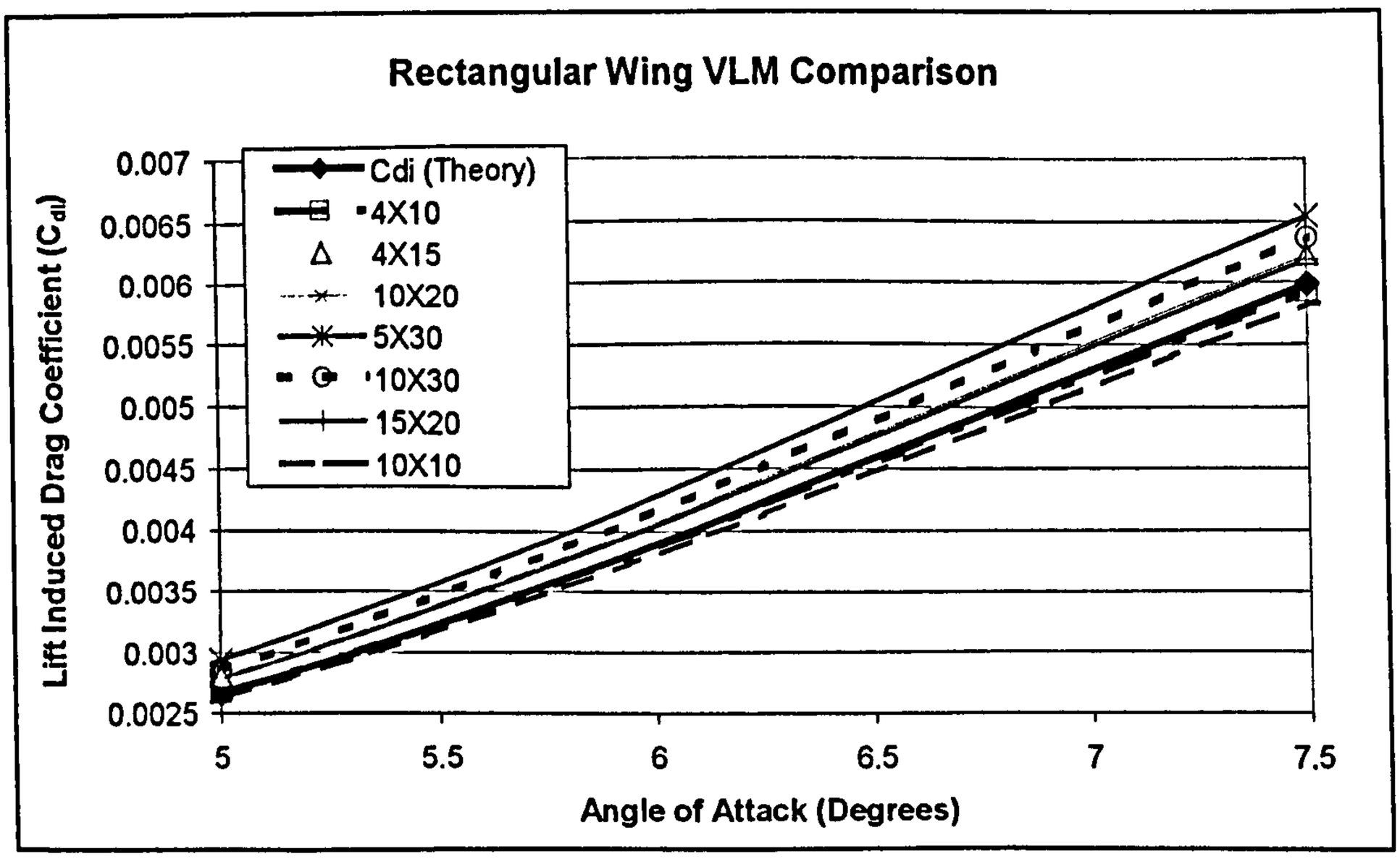

Figure 6.4 ***is a magnified view of the previous figure in order to provide a better understanding of the variation of the accuracy of the results depending on the grid selected.***

The trends can be much more clearly viewed from this figure. The first thing to notice is that there is no direct correlation between greater panel density and greater

accuracy. It can clearly be seen that there is a minimum number of chordwise panels below which the results begin to deteriorate quickly. In addition, it can be seen that the actual aspect ratio of each panel must have some significance, since a greater number of panels, but the wrong panel aspect ratio seems to yield worse results as well.

In any event, the difference between even the worst results shown and the theoretical curve is 0.00050. The lessons learned from this evaluation were to be careful in selecting panel aspect ratio and not let the value get too low, to maintain a certain minimum number of chordwise panels, and finally that greater panel density does not correspond to greater accuracy if not applied correctly.

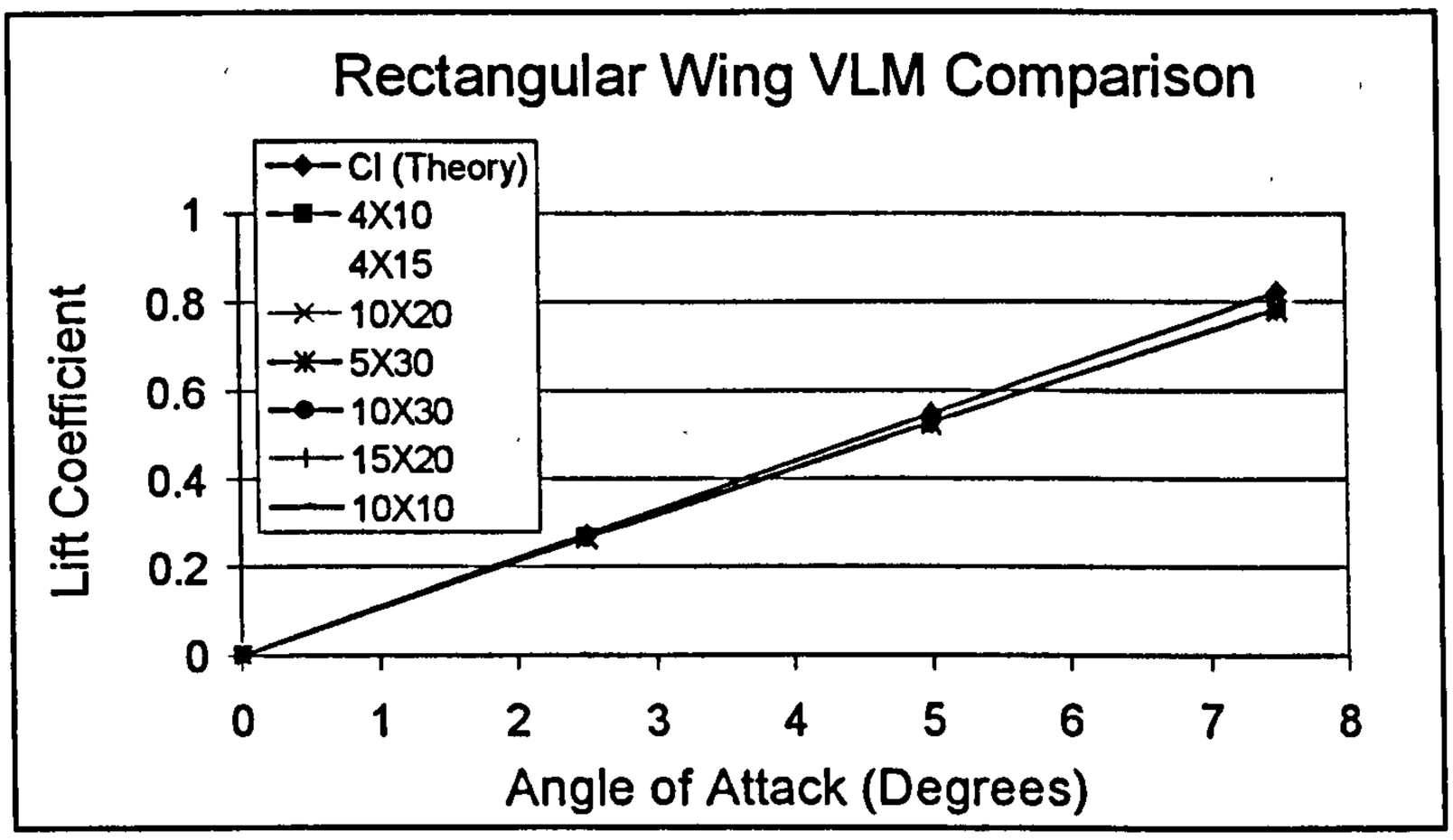

Figure 6.5 ***shows the variation in lift coefficient with angle of attack for the vortex lattice method for various grid arrangements, and how the results compare to two dimensional theory.***

The final curve presented of this group involves the lift coefficient prediction for the rectangular wing (seen in Figure 6.5). Although the vortex lattice method calculated lift coefficient is not used for any calculations in the drag estimation module, it is another indication of the care that must be taken in the application of the vortex lattice method.

This figure demonstrates that there is a perceivable variation in lift coefficient as a function of angle of attack as a function of the number or distribution of panels for the vortex lattice method. Again, there is an increasing disagreement with the two dimensional theoretical curve with increasing angle of attack. This is exactly as would be expected, as three dimensional effects are expected to be greater at higher angles of attack.

This disagreement could become a problem if not addressed. The reason for this is that the vortex lattice method calculates very accurate drag coefficients for the

corresponding lift coefficients. The problem arises from the fact that the lift coefficient value cannot be explicitly specified for the vortex lattice method. The vortex lattice method takes an angle of attack as an input and then calculates the corresponding lift and drag coefficients.

If the two-dimensional theory lift curve slope is used in the determination of an estimated angle of attack for a given lift coefficient, the error can be significant in the lift coefficient range of interest for Low Speed HALE's as can be seen in Figure 6.6. In addition to highlighting the significance of this error, the graph compares the variation in this deviation for different taper ratios. An investigation was also performed to determine the effects of changing the aspect ratio on this error. It was found that high aspect ratio planforms experienced very little deviation from lower aspect ratio Low Speed HALE's.

Thus, a polynomial curve fit was performed. The resulting equation is as follows:

$$C_L = -0.0007\alpha^2 + 0.10647\alpha \qquad \textbf{(6.19)}$$

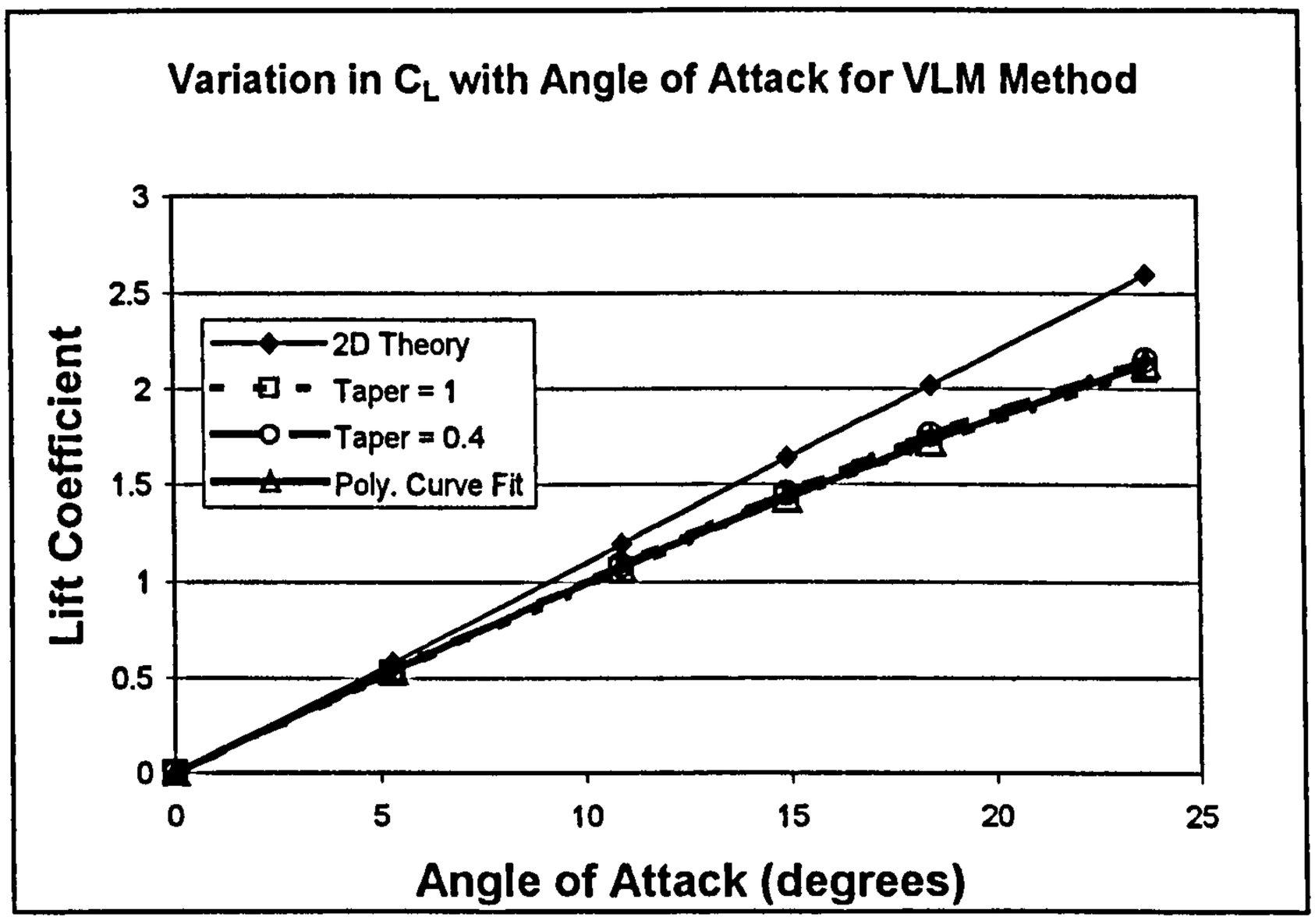

Figure 6.6 ***compares the curve fit correction for the lift curve slope with two dimensional theory and the results output from the vortex lattice method for two extremes of reasonable taper ratio.***

Rather than determining the angle of attack input to the vortex lattice method from the two-dimensional theory lift curve slope and the calculated value of cruise lift coefficient, a quadratic equation was solved using the coefficients from the equation above. The implementation of this quadratic curve fit for variation of lift coefficient with

angle of attack reduced the error between configuration specified cruise lift coefficient and the vortex lattice method calculated lift coefficient. This decreased the error and increases the level of certainty in the resulting vortex lattice method calculated values for induced drag coefficient for the wing.

6.C.3.b Sine and Cosine Spacing of Spanwise and Chordwise Points

In the literature associated with the implementation of the vortex lattice method, there are numerous different approaches taken to the resolution of the necessary equations. The majority of the differences arise from the implementation of the grid. Several different methods were suggested by the literature to increase the accuracy of the vortex lattice method.

The most common implementation used on lifting surfaces is to take the equal spacing of the grid points and replace them with a spacing dictated by some cosine or sine function distribution depending upon the direction (spanwise or chordwise).

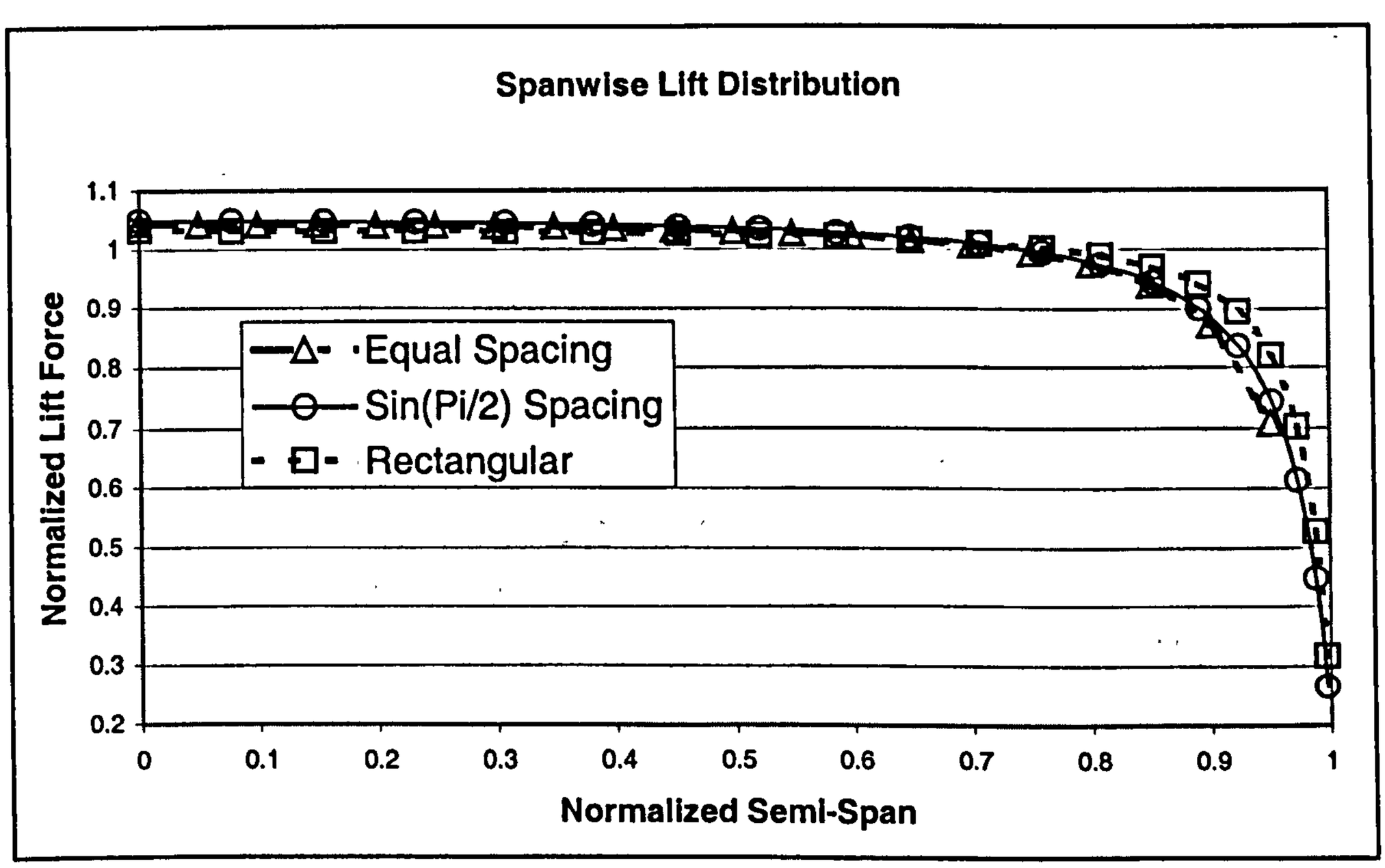

Figure 6.7 ***compares the normalized spanwise lift force distribution resulting from using different spanwise grid spacing techniques in the vortex lattice method.***

In the spanwise direction, the function used was $\sin\left(\frac{\pi}{2}\frac{(j-1)}{\#SpanwisePanels}\right)$ where j is the spanwise panel of the present iteration. A comparison of the different functions

considered can be seen in Figure 6.7 for a high aspect ratio wing similar to those on HALE UAV's. Obviously for the high aspect ratio wing there is not much difference in the spanwise lift distribution obtained. Neither of the spacings shown compare well with the rectangular wing theoretical solution near the wing tip, although the sine spacing appears to be a better prediction than the equal spacing. It should be stated, however, that intuitively, it makes more sense to have a higher density of panels closer to the wing tips than an equal spacing throughout the wing. In addition, it is noted that the region in which the differences occur (towards the wing tip) can cause large differences in the final value obtained for overall lift coefficient. An investigation into fuselage effects discussed later will demonstrate little use for a higher density of points in the inboard wing region for HALE aircraft at the conceptual design level.

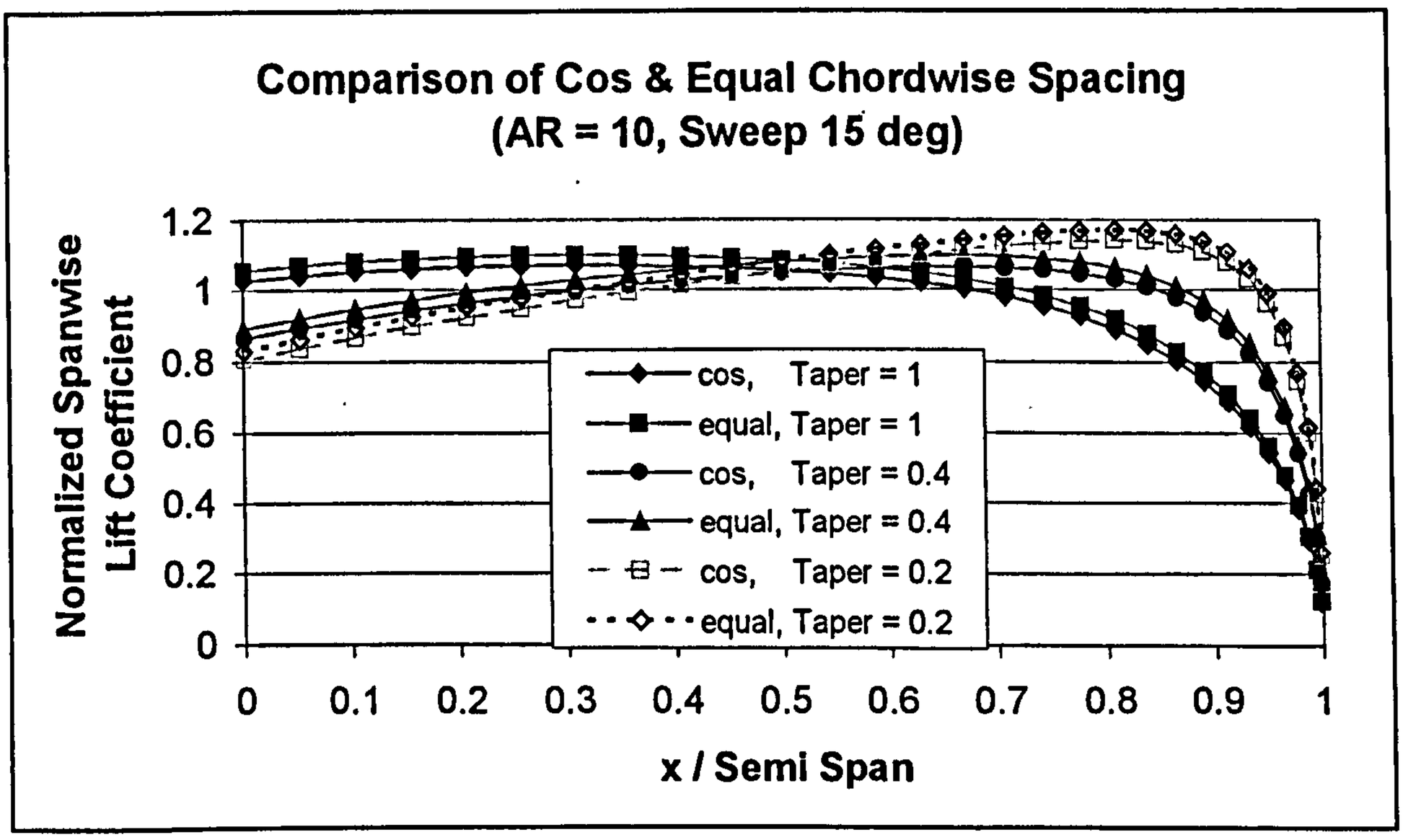

Figure 6.8 ***compares the normalized spanwise lift coefficient results from using different chordwise grid spacing techniques using the vortex lattice method.***

In the Chordwise (y) direction it is much easier to see differences in the results between using equal and in this case Cosine spacing. The relation used for spacing the points along the chord was given by : $c(y)\left[1-\cos\left(\frac{\pi}{2}\frac{(i+1)}{(\#ChordPts+1)}\right)\right]$. A graph comparing the results from the equal chordwise spacing to the cosine distribution of panels can be seen in Figure 6.8. In this instance, much lower values for aspect ratio and lift coefficient were used for the comparison in order to try and highlight the possible

problems encountered with equal spacing of the panels. The case of the swept wing is shown, however the non-swept wing showed similar variation between the equal and cosine spaced panel results. The figure shown demonstrates the spanwise variation in normalized lift coefficient as a result of the change in chordwise spacing. Since camber effects were not being modeled, it was thought that the spanwise effects would be of more interest to the methodology. As seen in the figure, the error seems independent of taper ratio, and both spacing models seem to arrive at the same lift coefficients close to the tip regardless. Since the spacing being evaluated is in the chordwise direction there is no difference in spacing between the cosine and equal spacing cases in the spanwise direction. It is expected that the equal spacing consistently over-predicts the spanwise value of lift coefficient resulting from the sum of the chordwise panels.

Hopefully, the brief demonstration of the effects of panel (grid point) spacing has provided a better understanding of the choices made in implementing the vortex lattice method in the present methodology. It is also hoped that this demonstrated a respect for the importance of proper grid sizing in maintaining valid results. In this regard, there is one further area that was investigated in order to insure the validity of the results as applied to a Low Speed HALE.

6.C.3.c Wing-Tail and Wing-Fuselage Interactions

The extent of the interactions between the fuselage and the wing were unknown. It was unknown as to whether or not the wing/fuselage interference prediction techniques offered by the common methodologies would be accurate for such high wingspans relative to the fuselage diameter. A reliable way of validating these existing methods was needed for such ratios of long wing span to small fuselage diameter. It was thought to use the vortex lattice method for modeling wing-fuselage and wing-tail effects on the lift induced drag (or overall lift distribution). In this instance, the fuselage was modeled as a lifting surface at angle of attack to distinguish the lift induced wing/fuselage junction effects. Once again, it is realized that due to the absence of viscous effects in this prediction, there would need to be another mechanism to take the entire drag (lift induced and viscous interference) into account. This difference will be covered in a subsequent section.

After a great deal of experimentation, the values resulting in Figure 6.9 and Figure 6.10 were obtained. Figure 6.9 shows the effects of placement of the horizontal tail on the lift distributions of both the wing and tail. As expected from Potential theory, as the

horizontal tail is moved too close to the wing, it effects the lift distribution of the main wing as well. It should be mentioned again that much lower aspect ratios than those normally found on a Low Speed HALE UAV had to be used in order to show any noticeable influence of the tail on the wing. For both the wing and horizontal tail, the default independent lift distributions at the given angle of attack are provided for a baseline. These results were generated at a moderate angle of attack and lift coefficient.

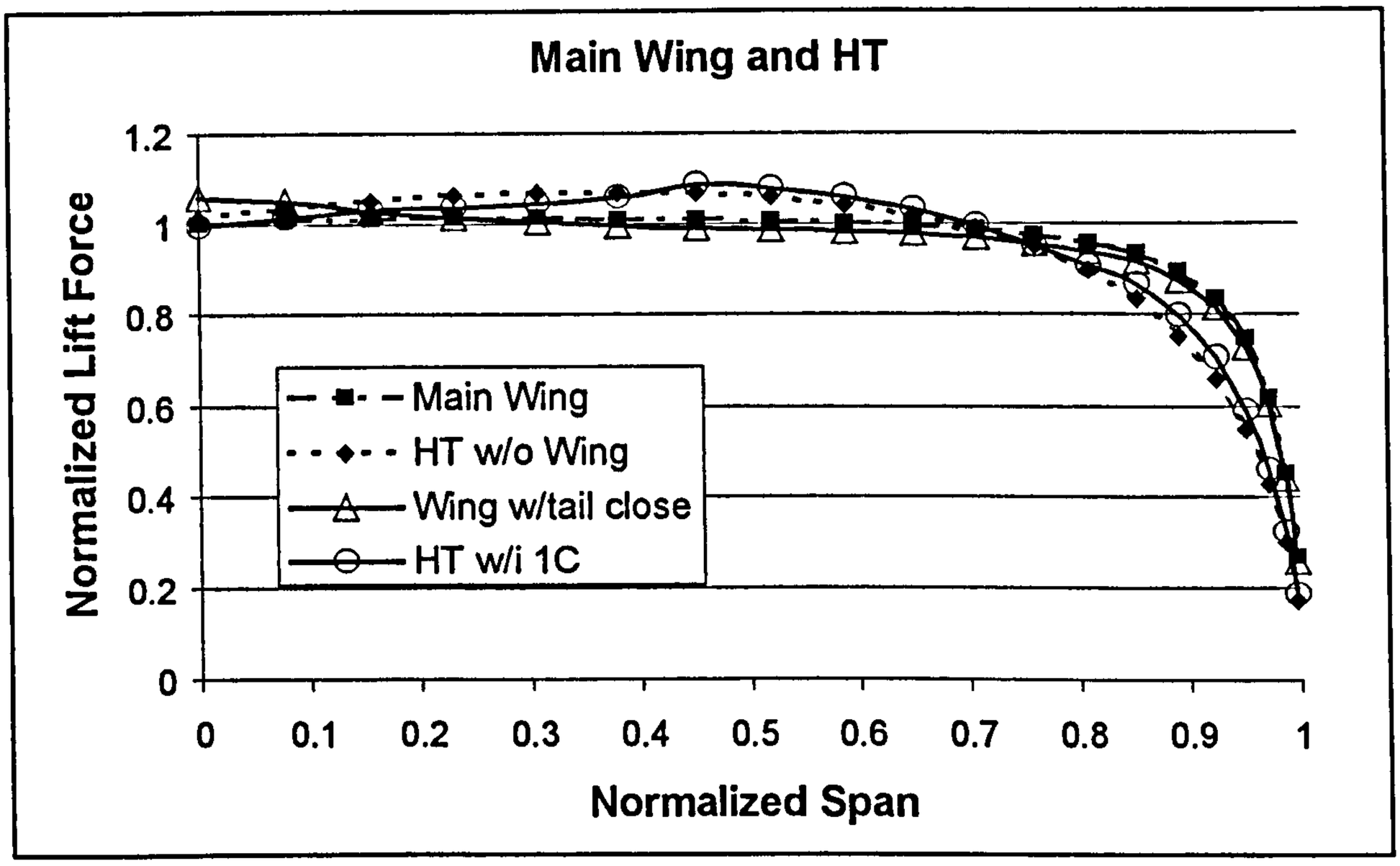

Figure 6.9 ***shows the normalized lift force results for different combined wing and tail situations to validate the vortex lattice method.***

Figure 6.10 shows the effects of the fuselage and tail in combination on a much smaller span wing than the Low Speed HALE UAV. It was determined from the investigation that in order for the fuselage to noticeably effect the lift distribution of the main wing, that the span of the main wing had to be reduced by a factor of 5.

As seen in the figure, the solution that includes the wing and all of the surfaces (wing, fuselage, tail) at 5 degrees angle of attack is essentially coincident with the curve for the wing and fuselage alone. This means that for this scale of wing, the conventional aft tail has little effect on the lift distribution compared to the effects of the fuselage on the wing. This effect is lessened with a lower angle of attack. As mentioned, the span of the wing had to be greatly reduced from that of a HALE UAV in order to generate a noticeable effect of the fuselage on the wing lift distribution. It was thus concluded that

the lift induced drag resulting from the presence of a fuselage for the HALE UAV would be insignificant enough to ignore. Therefore in the Drag estimation part of the methodology, no attempt was made to calculate the effects of the fuselage on the wing lift induced drag. The Viscous drag resulting from the wing fuselage junction was considered, however and will be discussed later in the chapter.

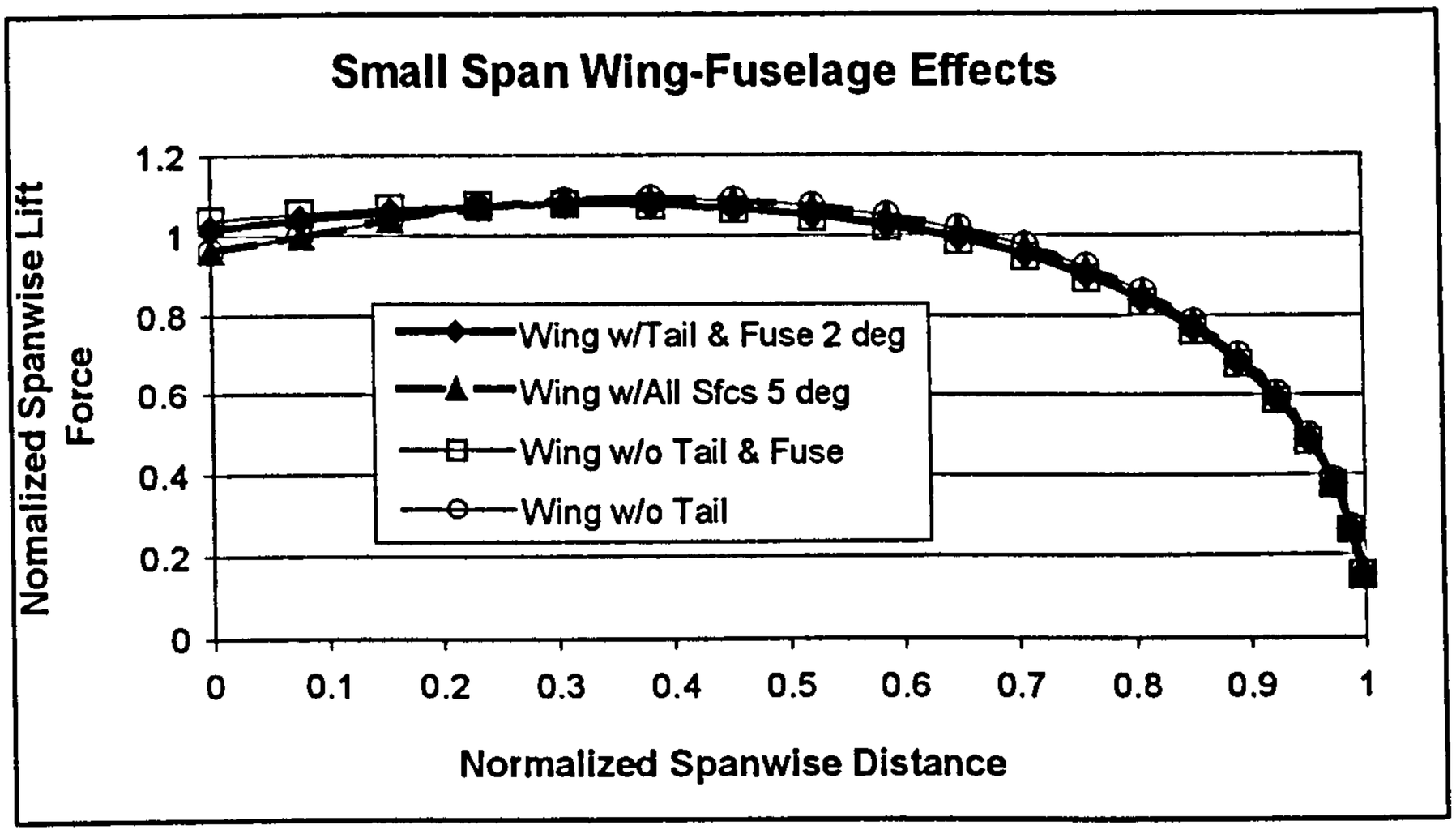

Figure 6.10 ***shows the normalized spanwise lift force results for wing-fuselage and wing-fuselage-tail effects using the vortex lattice method.***

Finally, it should be stated that at any time, the results of the vortex lattice code can be compared with two dimensional theory to determine whether or not the results are reasonable. This was done consistently throughout the execution of the methodology to insure that there were no application specific errors.

6.C.3.d Canard-Wing Interference Effects

As another phase in the validation of the Vortex Lattice code produced for this methodology, the effects of the canard on the wing were briefly analyzed. One of the resulting figures can be seen in Figure 6.11. The curve is normalized in distance in the spanwise direction. The configuration tested was set up in a Low Speed HALE UAV configuration, and the canard had to be brought within two chord lengths (as mentioned in the Literature Review chapter) before there were any noticeable effects of the canard on the wing. It is noted that this longitudinal proximity is not likely on a Low Speed HALE UAV, however the exercise was performed as a step in the validation of the method. For

the figure, the canard had a semi-span of roughly 13 feet and the main wing a semi-span of roughly 94 feet.

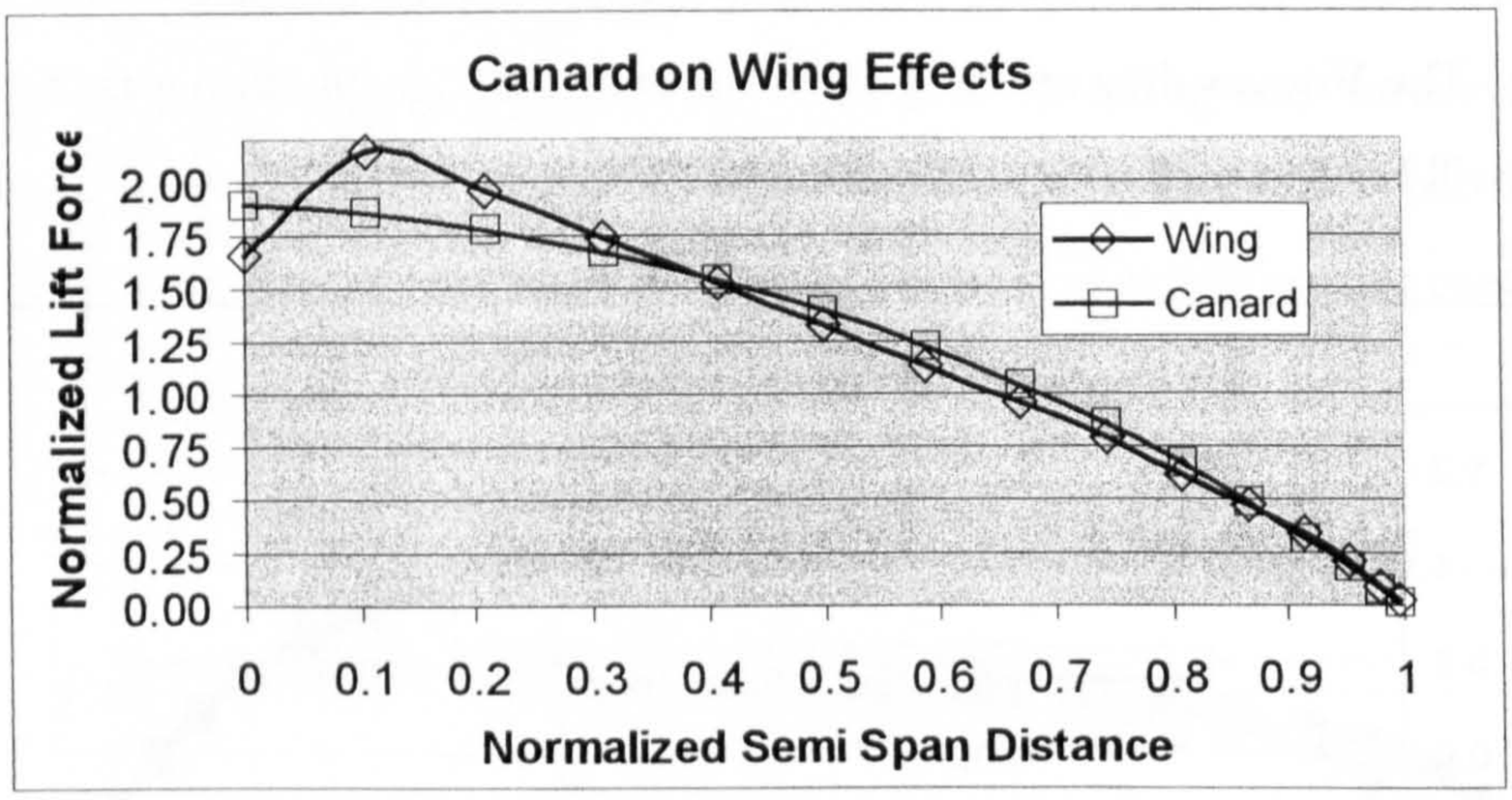

Figure 6.11 ***demonstrates that canard on wing aerodynamic effects must be considered if the canard is placed within two chord lengths of the wing.***

Thus, if the canard tip vortex trailed aft in a roughly linear manner (for the distance of two chord lengths) in the longitudinal direction, the vortex should impinge on the main wing at roughly 14% of the wing semi-span. This can be seen in the figure to have been correctly predicted. At this close proximity, the effect of the canard lift is rather prominent and disturbs the main wing lift distribution considerably.

In addition, when viewed from behind, the vortex from the canard should be rotating counter-clockwise. The effect, then, should be reduced lift inboard of the point of impingement, and increased lift outboard. From the figure, this would also appear to be have been well predicted.

6.C.3.e Tandem Wing-Wing Interference Effects

The effects of the forward tandem wing on the aft tandem wing were much more significant than the effects of the canard on the main wing when the aircraft were set up in a Low Speed HALE UAV configuration. In order for the canard on wing effects to be visible, it was necessary to move the canard to a proximity to the wing that would not normally be experienced for a Low Speed HALE UAV. This was not the case for the tandem wing effects. The graph output from the program for a 55/45 area split tandem wing aircraft can be seen in Figure 6.12. The case shown is for a 10,000 pound takeoff

weight aircraft. The average chord of the forward wing is approximately 4.5 feet and the average chord of the aft wing is approximately 4 feet. The distance between the two wing quarter chord locations on the fuselage was 24 feet, or between 5 and 6 chord lengths.

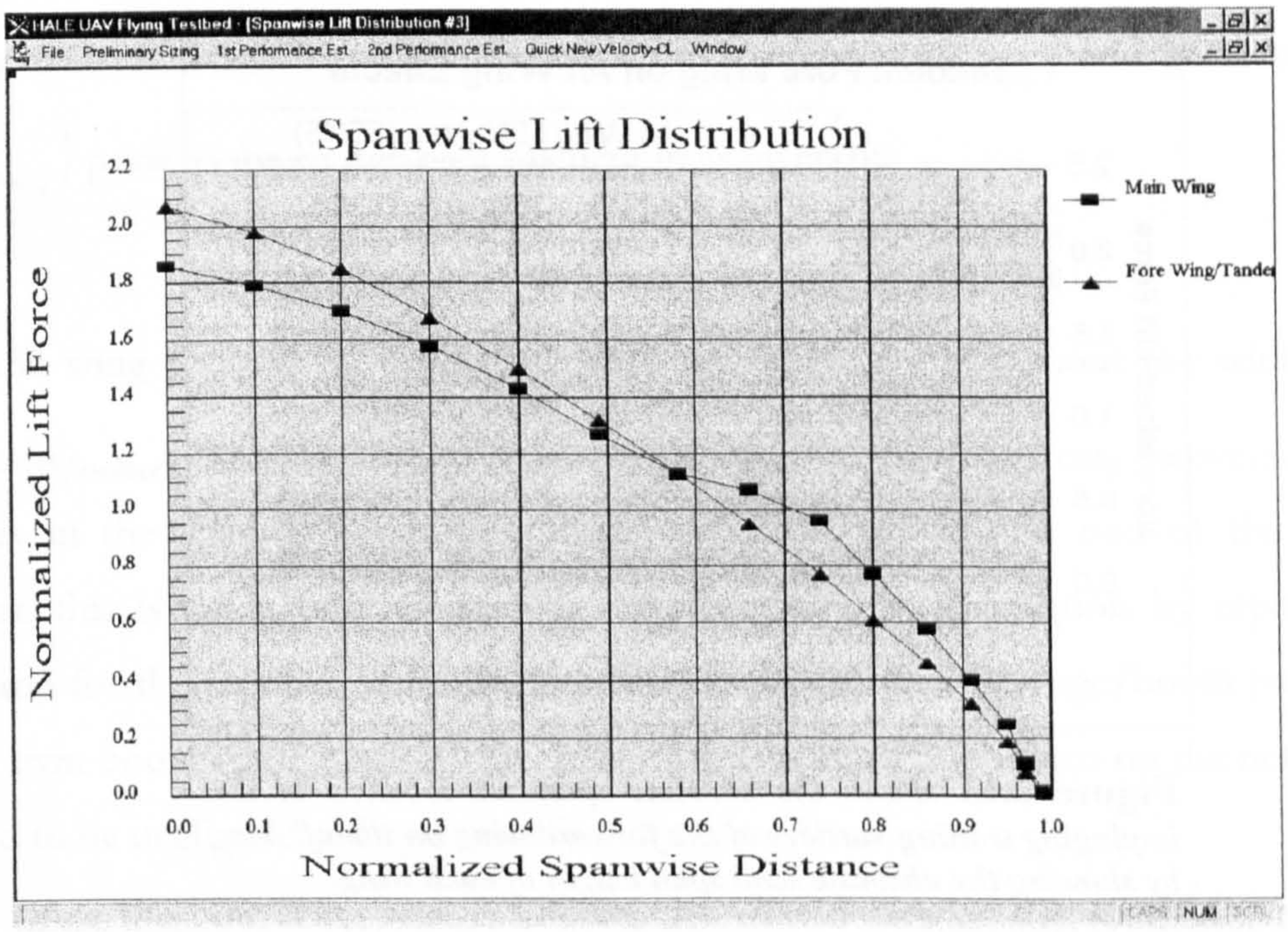

Figure 6.12 ***is a snapshot of the coded methodology, representing the effects of the fore wing trailing vortex sheet on the aft wing lift distribution.***

The forward wing semi-span was 50 feet and the aft wing semi-span was 69.5 feet. Therefore, making the same assumption as for the canard, the vortex of the forward wing should impinge on the aft wing at approximately 72% of the semi-span of the aft wing. From viewing the figure, this would appear to have been accurately predicted. It would also appear from the figure that the lift was decreased inboard of the impinging vortex and increased outboard. This once again indicates the proper rotation of the tip vortex from the forward surface. While it is impossible to validate the actual magnitudes of these effects without experimental results, it is thought that the Vortex Lattice method written for this methodology at least manages to model the macroscopic effects of multiple lifting surface interactions.

In another manner of viewing similar results, in Figure 6.13 the spanwise distance was not normalized so that the absolute location of the physical semi-span wing tip can be seen, and the absolute location at which it impinges on the aft wing can be seen. Two different area split cases are shown, 55/45, and 75/25 where the first number is the percentage total wing area due to the aft wing, and the second the percentage total wing

area due to the forward wing. Since the aspect ratios of the two surfaces were kept constant for this graph (35 for the aft wing, 22 for the forward wing), the wing spans are different for the two cases.

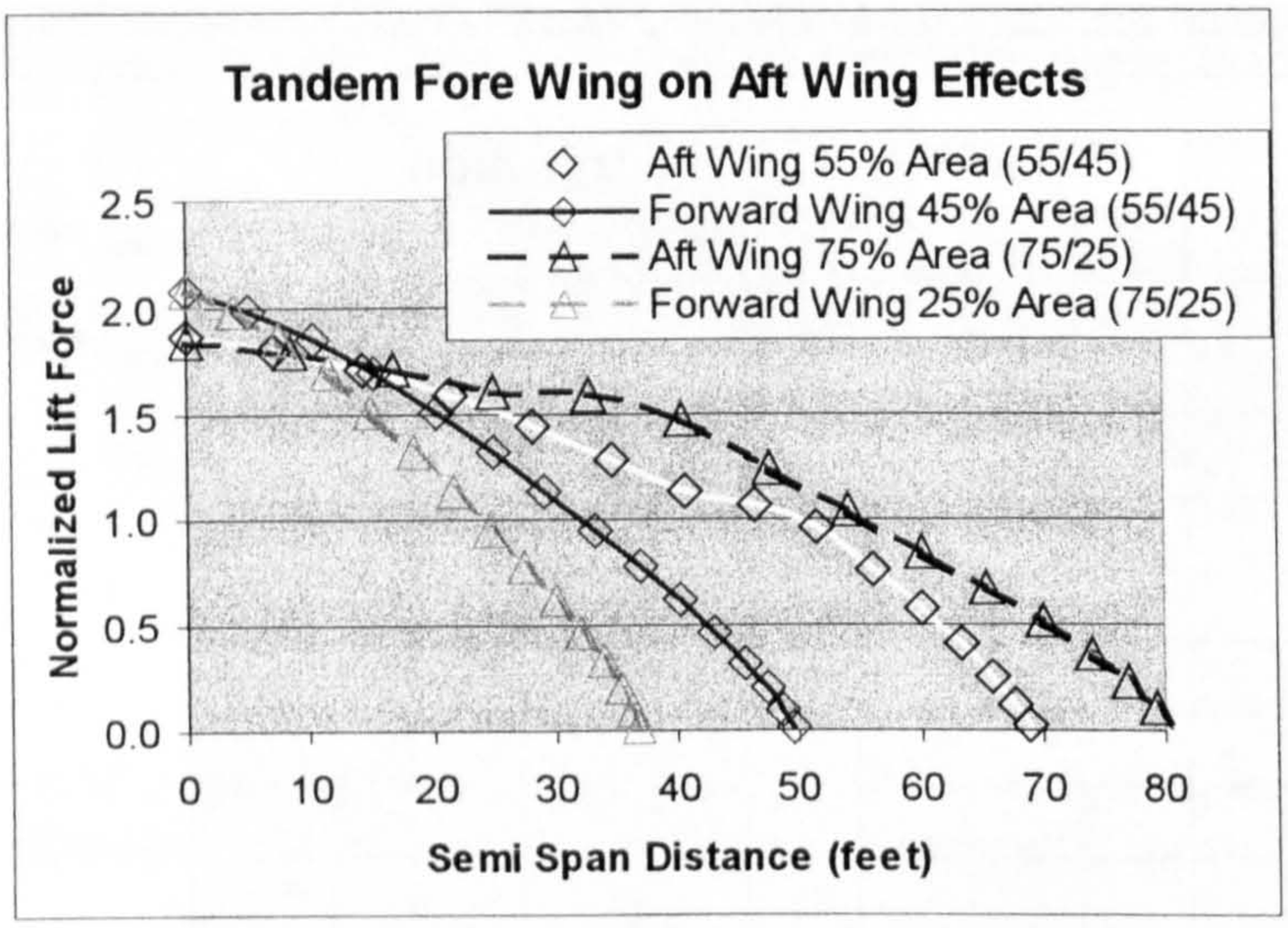

Figure 6.13 ***shows the absolute spanwise location of the impinging trailing vortices of the forward wing on the aft wing by showing the absolute semi span length of each wing.***

As can be seen in the figure, the vortex impingement occurs where expected for both cases. Obviously the effects of this unusual lift distribution will be noticeable from a structural perspective, locally increasing the shear and the wing bending moment and then locally decreasing these values outboard of the vortex impingement. For this reason, the tandem wing aircraft wing bending moments were studied separately with regards to the wing weight estimation.

6.D Wing Drag

The wing lift induced drag is calculated using the vortex lattice method. The wing profile drag is then calculated. The first step in the calculation of the wing profile drag is to make the assumption of a wing thickness to chord ratio (if one has not already been selected by the designer) for use in calculation of the wing wetted area. It is mentioned again, that the designer can easily specify a value for this number in the Wing Profile Selection Dialog (see Figure 5.8). A default value of 0.14 was chosen as reasonably representative for Low Speed HALE UAV aircraft if no value was supplied. Additionally,

changes in this number (within the range expected for a Low Speed HALE UAV) cause an extremely small difference in the value for wetted area of the aircraft, which subsequently makes a very small difference in the parasite drag of the aircraft. The reasons for this will be better understood in a moment.

The differentiation was made between net wing area $\left(S_{net_{Wing}}\right)$ and gross wing area $\left(S_{planform_{Wing}}\right)$ prior to the wetted area calculation as given by:

$$S_{net_{Wing}} = S_{planform_{Wing}} - c_{root_{Wing}} w_{fuselage} \tag{6.20}$$

where the wing root chord $(c_{root_{wing}})$ is assumed constant throughout the width of the fuselage ($w_{fuselage}$). This assumes moderate taper and moderate spacing between multiple fuselages in the spanwise direction. If the configuration type is one of the multiple fuselages, this is taken into account in the net wing area calculation by repeating the calculation for the number of fuselages based on the relevant fuselage/boom parameters. For the twin boom configuration, the effect of the width of the booms on the net area was assumed to be negligible and was therefore not considered.

Once the Net Wing area is known, the wetted area of the wing $\left(S_{wet_{Wing}}\right)$can be calculated based on the thickness to chord ratio and the net wing area as follows (Stinton[6], P.207):

$$S_{wet_{wing}} = S_{net_{wing}}\left(2 + \frac{1}{3}\left(\frac{t}{c}\right)_{wing}\right) \tag{6.21}$$

This assumes a constant wing thickness to chord ratio which is reasonable for early conceptual design stages.

Next the wing profile drag needs to be assumed ***IF*** it has not already been specified by the designer. In the event that the lift-drag profile characteristic curve has been provided by the designer, this is used in order to provide the proper profile drag for the given angle of attack.

If not specified by the designer, this wing profile drag coefficient can be calculated/approximated using the Roskam[5] (Pt.VI, p.23) C_{D_o}Wing equation. Assuming:

$R_{wf} = 1.05$,
$R_{ls} = 1.1$ (No Sweep),
$C_{fw} = 0.0051$,
L' = 2.0 (assumes $\left(\frac{t}{c}\right)_{max}$ at < 0.3c),

the equation yields a value of 0.0075.

It is not recommended to use this number for the detailed drag estimation, especially since more accurate wing profile data is readily available in tabulated form. The results of this thesis were generated using experimentally obtained values from well-known airfoils (selected in Appendix A) to remove the effects of making this assumption. The reason for this statement is that such a large portion of the aircraft drag is due to the wing profile/parasite drag. It is thus believed that the most accurate value available should be used.

The parasite and total drag of the wing can now be calculated as follows:

$$C_{Dparasite_{wing}} = C_{dProfile_{wing}} \frac{S_{wet_{wing}}}{S_{ref}} \text{ and } C_{Dtot} = C_{Dparasite_{wing}} + C_{DinducedVLM_{wing}} \frac{S_{wing}}{S_{ref}} \quad \textbf{(6.22,23)}$$

The reference area (not simply wing area) is used in *all* of the drag calculations. This results from the inclusion of the tandem wing configuration for which the reference and wing area are different.

6.E Tail Drag

There are two basic considerations for the drag of the tail. The first is the combination of the lift induced and parasite drags. The second is due to the particular tail configuration that has been selected. It will be shown that the differences in drag between these tail configurations will not justify the inclusion of the calculation of the additional interference due to different tail configurations.

6.E.1 Tail Parasite and Lift Induced Drag

There is slight difficulty in dealing with the horizontal tail. For the first iteration, the horizontal tail drag calculation is the same regardless of whether or not the aircraft is configured in a traditional manner or if it is treated as a canard. It is assumed to be a profile at zero degrees of angle of attack. The assumed horizontal tail/canard profile drag coefficient of 0.006 was taken from the Drag Polar Data of Abbott and Von Doenhoff[106] for a NACA 0009 section at a Reynolds number of $3*10^6$ and above. This Reynolds number is a bit high, but the drag data is not very Re sensitive in this range for this

particular airfoil. In addition, this value is very close to the value suggested in the Literature Review by Eppler[31] for use with sailplanes.

For the tandem wing the profile drag is calculated by using the assumed default lift curve slope discussed previously, or by using the designer specified curve for variation in profile drag with lift coefficient. Also, for the tandem, the lift-induced drag is calculated using the vortex lattice method.

Assuming the same default profile section for the vertical tail, the same profile drag coefficient was used in the event that the designer did not specify one. The only difference in the calculation of the drag for the vertical tail was that for certain configurations (twin boom, multiple fuselages), the tail was split into a twin tail. This had to be taken into account in the wetted area calculations.

For the second iteration of the refined drag estimation, the trim lift coefficient should be known. The horizontal tail/canard profile drag must be recalculated to take the additional viscous drag due to angle of attack of the airfoil into account. In addition, the vortex lattice method is used to calculate the lift-induced drag due to the angle of attack.

The wetted area calculations for the horizontal and vertical tail are performed in the same manner as for the main wing, however the thickness to chord ratio used is that of the NACA 0009 section, unless designer specified data have been supplied. Obviously, this is not the best assumption for the use of a canard, and it is hoped the designer will specify a canard specific wing profile in that case, as was done for the results obtained in this thesis. The vertical tail profile drag is then calculated in a manner similar to the wing profile using the ratio of the relevant tail area to the reference area.

6.E.2 Configuration Dependent Tail Drag

A detailed comparative drag analysis of several different tail configurations was given in Hoerner[61] (p.8-12). The same approach was taken in this thesis in the process of deciding whether or not to include tail configuration dependent effects into account in the drag analysis. It was decided that once the reference area was factored into the tail interference drag that the absolute value of the overall tail interference drag was less than 0.1% of the total drag. Thus, the *difference* between the various tail configurations was less than 0.03% of the maximum of the total drag, and was thought to be comparatively insignificant. The analysis was not included in this thesis for brevity, and because the

relevance of the calculations is greatly reduced in light of the results, however, the approach used for the calculations was the same as that taken by Hoerner.

While taking these results into consideration, it is noted that the majority of modern sailplanes use a T-tail configuration. This is most likely a result of the combination of benefits between the endplate effect for the vertical tail, a clean incident freestream (free of wing downwash) for most low to moderate angles of attack, and minimization of damage in off-airport landings. For the Low Speed HALE UAV's that have been built, the *Raptor* had an H-tail, the *Theseus* and *Strato 2C* had T-tails, and the *Perseus* and *Condor* had conventional tails. Once again there would appear to be no consensus on which tail type to choose. Since the vertical position of the horizontal tail was not taken into account in the drag analysis outside of the vortex lattice method, the effects of this choice are thought to be minimal on overall performance. This is thought to be due to the size of the main wing relative to the horizontal tail.

6.F Fuselage Drag

For the fuselage-induced drag, it is assumed that the aircraft will be designed such that the fuselage will not have an angle of attack on average for cruise. Otherwise, it would be difficult to justify giving the fuselage any decalage angle relative to the aircraft that resulted in any other angle of attack for the fuselage in cruise.

The fuselage parasite drag was calculated using a flat plate analogy. For this part of the drag prediction, it was necessary to assume laminar flow over a portion of the fuselage and turbulent flow over the remainder. Other assumptions were made about how the aft section of the fuselage terminates (at a point, no base drag).

Since there was little information available as to how to accurately predict the transition to turbulence, the fractional value of the fuselage experiencing laminar flow was assumed to be the part of the fuselage fore of the main wing. It should be noted that in many of the HALE UAV implementations, the fuselages have quite non-traditional shapes, assumedly to accommodate the many different types of payloads. No attempt was made in this methodology to model anything but the traditional longitudinal shapes and the traditional cross sections mentioned in Section 5.B.1.c.

First the fuselage Reynolds number was calculated, based on the length,

$$\mathrm{Re}_{fuse} = \frac{\rho_{cruise} V_{cruise} L_{fuse}}{\mu_{cruise}} \tag{6.24}$$

Then the laminar skin friction coefficient is given from Fluid Dynamic statistics for incompressible flow:

$$C_{f_{Laminar,Fuselage}} = \frac{1.328}{\sqrt{\mathrm{Re}_{fuse}}} \tag{6.25}$$

Likewise, the turbulent skin friction coefficient :

$$C_{f_{Turbulent,\ Fuselage}} = \frac{0.455}{\left(1+0.144M^2\right)^{0.65}\left[\log_{10}\left(\mathrm{Re}_{fuse}\right)\right]^{2.58}} \tag{6.26}$$

The specified percentage of fuselage area experiencing laminar and turbulent flow are then taken into account to create a general/combined fuselage skin friction coefficient.

For the calculation of the fuselage wetted area, the fineness ratio is required :

$$f = \frac{L_{fuse}}{D_{fuse}} \tag{6.27}.$$

The determination of the fuselage diameter (D_{fuse}) depends on the shape of cross-section specified by the designer. For a square or elliptical section, an equivalent diameter is calculated. The Fuselage Wetted Area is from Torenbeek[7] (p.447), and is valid for fineness ratios over 4.5:

$$S_{wet_{Fuselage}} = \pi D_{fuse} L_{fuse}\left(1-\frac{2}{f}\right)^{2/3}\left(1+\frac{1}{f^2}\right) \tag{6.28}$$

Roskam Pt VI p.44 gives the relation for parasite drag coefficient as :

$$C_{D_{Parasite,Fuselage}} = C_{f_{Fuselage}}\left[1+\frac{60}{\left(L_{fuse}/D_{fuse}\right)^3}+0.0025\left(\frac{L_{fuse}}{D_{fuse}}\right)\right]\frac{S_{wet_{Fuselage}}}{S_{ref}} \tag{6.29}$$

He includes a base drag coefficient that is ignored for the purposes of this methodology. The base drag coefficient is calculated based on a ratio of the wing area to the fuselage frontal area which is quite small. It is also based on the ratio of the fuselage diameter to the diameter of the fuselage where it tapers until it terminates in the aft section of the empennage. Since this information was not known, nor could a reasonable assumption be made as to an estimate of this value without it being explicitly specified, the base drag coefficient was not included. The base drag coefficient would be appropriate for

more elaborate fuselage shapes, and for fuselage shapes resembling those of mostly manned aircraft which thus have diminished relevance for the Low Speed HALE UAV in early conceptual design.

In addition, Roskam includes a wing-fuselage interference factor, however the chart he provides for determination of this factor starts at a Reynolds number roughly an order of magnitude greater than that experienced by this fuselage. The factor was thus assumed to be 1.

A separate calculation is performed for the drag of the booms. For the twin boom configuration, given the higher fineness ratio, a larger portion of the boom is considered to experience laminar flow. Given the different lengths of the booms relative to the center fuselage, the Reynolds number was recalculated and the drag added to that of the center fuselage.

6.G Engine Nacelle Drag

The first step in the calculation of the nacelle drag has more to do with the configuration being considered than with the actual calculation of drag. Before calculating nacelle drag, it was first determined whether the particular configuration warranted an additional nacelle drag calculation. For example, single engine pusher aircraft usually have nacelles with inlets for cooling, so this would enter the cooling drag term, but would not qualify as nacelle drag. Also, the viscous drag of the nacelle area for this configuration would already have been determined as part of the fuselage drag. Once it has been determined whether or not to perform the nacelle drag calculation, the calculation proceeds as described below.

Depending on the specific application, both nacelle parasite drag and nacelle vortex induced lift interference drag were considered. The approach followed came from Torenbeek[7] pages 510 (for induced) and 506 (for parasite).

For wing mounted engines, Nacelle length was suggested as :

$$L_{Nacelle_{eff}} = 2L_{engine} \tag{6.30}$$

Engine width and height are multiplied by 1.05 to obtain the nacelle width and height:

$$w_{Nacelle_{eff}} = 1.05 w_{engine} \quad \text{and} \quad H_{Nacelle_{eff}} = 1.05 H_{engine} \tag{6.31,32}$$

Calculate the effective nacelle diameter for skin friction drag purposes and the frontal area:

$$D_{Nacelle_{eff}} = \sqrt{\frac{4w_{Nacelle_{eff}} H_{Nacelle_{eff}}}{\pi}} \quad \text{and} \quad S_{Nacelle_{Frontal}} = w_{Nacelle_{eff}} H_{Nacelle_{eff}} \quad \textbf{(6.33,34)}$$

This gives a Nacelle Reynolds number of :

$$\mathrm{Re}_{Nacelle} = \frac{\rho_{cruise} V_{cruise} L_{Nacelle_{eff}}}{\mu_{cruise}} \quad \textbf{(6.35)}$$

The fineness ratio is once again required for the calculation of the wetted area of the Nacelle:

$$f_{Nacelle} = \frac{L_{Nacelle_{eff}}}{D_{Nacelle_{eff}}} \quad \textbf{(6.36)}$$

The approximate Nacelle wetted area follows as :

$$S_{Nacelle_{Wet}} = \left(2w_{Nacelle_{eff}} + 2H_{Nacelle_{eff}}\right)\left(L_{Nacelle_{eff}} - D_{Nacelle_{eff}}\right) + \pi D^2_{Nacelle_{eff}} \quad \textbf{(6.37)}$$

Calculating the skin friction coefficient for the Nacelle assuming fully turbulent flow uses **Equation 6.26.**

If the configuration is a Push-Pull twin, the number of engines is taken to be some fraction of two (reasonably arbitrary) in an attempt to model the true wetted area represented by such a configuration. Finally, the parasite drag coefficient for the nacelle :

$$C_{Do_{Nacelle}} = C_{f_{Nacelle}}\left[1 + \frac{2.2}{f^{1.5}_{Nacelle}} + \frac{3.8}{f^{3}_{Nacelle}}\right]\frac{S_{Nacelle_{Wet}}}{S_{ref}} \quad \textbf{(6.38)}$$

For aircraft with engines on the wing, Nacelle lift induced drag varied historically depending on whether or not the aircraft had a high or a low wing as given by Torenbeek. It is unknown as to whether or not this would be appropriate for the application to an unmanned aircraft since the relative fuselage cross sections tend to be much smaller, thereby diluting the effect of the high or low wing. However, Torenbeek states that this contribution is greatest at low angles of attack and is caused by the local change in wing lift due to the nacelle. Additionally, papers presented in the Literature Review on wing/body interference for gliders implied some induced drag correction was necessary. This can be logically extended to nacelle/wing interference. In any event, the difference in the overall drag of the aircraft was not significant, so it was used as shown.

For high wing configurations :

$$C_{Di_{Nacelle}} = 0.008(\#\,Engines)\frac{S_{Nacelle_{frontal}}}{S_{ref}} \quad \textbf{(6.39)}$$

and for the low wing :

$$C_{Di_{Nacelle}} = 0.004(\#\ Engines)\frac{S_{Nacelle_{frontal}}}{S_{ref}}. \qquad \textbf{(6.40)}$$

6.H Cooling Drag

In a paper mentioned in the Literature Review by Mark Drela[103] of M.I.T. , aerodynamic designer of the *Perseus* and *Theseus* cooling systems, he uses a detailed heat transfer analysis to set up the governing equations in the cooling problem for a high altitude long endurance reciprocating internal combustion engine. One of the more significant statements of the paper was as follows :

> "*The extremely rapid rise of D_H (the dimensionless drag-power parameter) with altitude clearly points to the need for extreme care in the design of radiator installations for high ceilings. The greater the ceiling, the larger the fraction of available engine power which can be consumed by radiator drag. Conversely, the possibility of generating significant ramjet thrust power from the radiator increases in the same manner*"

These results point to the fact that a carefully designed radiator system for this class of aircraft and propulsion could in fact generate more thrust than drag. This has been achieved before in other flow regimes. Given that applying Drela's detailed heat transfer analysis is too time consuming in the early conceptual design phase, it is safe to assume that conventional cooling drag estimations can be used for this phase as long as the designer is aware of the risks and assumptions involved.

Thus, from Torenbeek[7] (p.515) :

$$C_{Dcooling} = \frac{4.9 \cdot 10^{-7} HP \cdot T_{cruise}^{2} \rho_{SeaLevel}}{V_{cruise} S_{ref} \rho_{cruise}} \qquad \textbf{(6.41)}$$

Where T_{cruise} is the air temperature in cruise.

Another method was proposed by Roskam, however it was found to be less convenient for computational implementation, and relied on pre-existing curves. In addition, it was not directly a function of engine horsepower and was designed more for use with well-defined nacelle inlet geometry.

6.I Wing-Fuselage Interference

The last area of significant drag contribution to be considered by the methodology is the viscous drag resulting from wing-fuselage interference. The vortex lattice method takes the lift induced interference effects into account. The equation used was taken from Torenbeek[7] (p.510), however there is some ambiguity as to the definition of some of the terms. It is believed that the relevant terms were interpreted properly in this implementation.

Overall Drag Summary Dialog

Overall Aircraft Drag Coefficient	0.0434	New Power Required	31.08	HP
Cruise Lift Coefficient	1.2759	Old Power Required	82.35	HP
New Aircraft CDo	0.02680	New Aircraft CDi	0.01662	

	% Total Drag	CD	% Tot.Swet	Swet ft^2	
Wing	60.539	0.034967	61.344	396.00	Area in this case is Net Area
Lift Induced	37.868	0.016441			
Parasite	42.670	0.018526			
Section		0.009357			NLF(1)-1015
Fuselage(s)	3.946	0.001713	19.524	126.04	
Parasite	3.946	0.001713			
Wing/Fuselage Interference	0.109	0.000047			
Horizontal Tail	3.272	0.001421	7.335	47.35	
Lift Induced					
Parasite	3.272	0.001421			
Section		0.006000			NACA 0009
Vertical Tail	3.786	0.001644	8.487	54.79	
Parasite	3.786	0.001644			
Section		0.006000			NACA 0009
Engine Nacelle(s)	5.149	0.002235	3.309	21.36	
Lift Induced	0.403	0.000175			
Parasite	4.746	0.002060			
Cooling Drag	3.199	0.001389			

OK

Figure 6.14 ***is the Drag Summary dialog box which shows the breakdown of drag and wetted area in absolute and percentage total values, as well as outputting the new C_{Do} and Power Required.***

This time a wing-fuselage Reynolds number is necessary, and it is defined based upon the root chord. It is safe to assume that the region is fully turbulent, and the skin friction coefficient calculation proceeds as it did for the fuselage and nacelles. At this point, once again, there is a differentiation between the high, low and mid wing cases. The interference drag is calculated based upon a basic, and a supplemental drag coefficient term. They are as follows :

$$C_{Dbasic} = 1.5 C_{f_{wf}} t_{root_{wing}} c_{root_{wing}} \cos \Lambda_{1/4} \tag{6.42}$$

$$C_{Dsuppl} = 0.88 C_{f_{wf}} C_{L_{wing}} c_{root_{wing}} D_{fuse} \tag{6.43}$$

The total circumferential length of the wing fuselage junction is different for the mid-wing ($4.5^* c_{root}$) than for the low and high wings ($2.25^* c_{root}$). This accounts for the factors used in the different cases of wing position on fuselage.

$$\text{For the High Wing} \quad C_{Dwingfuse} = \frac{\left(2.25 C_{Dbasic} - C_{Dsuppl}\right)}{S_{ref}} \tag{6.44}$$

$$\text{For the Mid-Wing} \quad C_{Dwingfuse} = \frac{4.5 C_{Dbasic}}{S_{ref}} \tag{6.45}$$

$$\text{For the Low Wing} \quad C_{Dwingfuse} = \frac{\left(2.25 C_{Dbasic} + C_{Dsuppl}\right)}{S_{ref}} \tag{6.46}$$

If there are multiple fuselages or the Twin Boom configuration has been selected then the interference of the booms are also considered. In the case of the Tandem Wing, the interference factor is calculated for all intersections using the relevant geometrical characteristics as well as the relevant aerodynamic characteristics.

6.J Total Drag

At this point, the total aircraft drag can be calculated by simply summing the relevant component drags. The power required is also recalculated, as below :

$$P_{\text{Reqd,New}} = \frac{1}{2} \frac{\rho_{cruise} V_{cruise}^3 S_{ref} C_{Dtot}}{550 \left(\eta_{prop}\right)} \tag{6.47}$$

For interest, the Overall Drag Dialog is presented in Figure 6.14 as an example of the output provided to the designer in order to verify and monitor the drag of the individual components.

The previous power required based on the Horsepower to weight ratio selected by the design point is output. The overall aircraft drag coefficient is output along with the new C_{Do}. The component drags are output in absolute and percentage total aircraft drag form, and the wetted area and percent wetted area (based on total aircraft wetted area) for each component is also output. The wetted area values are output to provide some idea of which components are dominating the C_{Do} term for any given area considered.

Chapter VII

Never try to cross a river

Just because it has an average depth of 4 feet

--- Martin Friedman

7. Detailed Weight Estimation

There is very little known about comparative weight estimation of alternative configurations. There is also very little known about the breakdown of the weight of individual components for UAV's in general, and this is obviously worse in the Low Speed HALE area. There are a large number of statistically based weight estimation techniques available from the common design methodologies. A detailed investigation was undertaken for the weight estimation of each component of the aircraft. The discussion will begin with the component, without which the aircraft could be considered a very expensive car.

7.A Wing Weight Estimation

A gallant attempt was made to get a multiple fuselage wing weight estimation technique (Udin and Anderson[107]) designed for much larger aircraft to work for Low Speed HALE UAV's. Unfortunately, the method was found to be too sensitive to extremely small changes in wing thickness to chord ratio, and wing fuel weight to provide consistent and repeatable results. In addition, a great deal of difficulty was encountered even repeating the cited results for large aircraft. Due to this sensitivity, the technique was not implemented in this methodology, and more conventional statistical methods were considered and compared.

The procedure used for the wing weight estimation was repeated for all of the components considered in the weight estimation in general. For brevity, the most detailed comparison will be presented only for the wing. For the other components, only the "short list" of appropriate methods will be presented.

This class of aircraft does not fit neatly into any of the general categories described in the common design textbooks. As such, an analysis was undertaken on all available methods to insure that a method that might on the surface appear to be inappropriate, can not in fact apply to this class of aircraft.

The simplest way to list all of the methods considered is to provide an example of one of the component spreadsheets used in the determination. The sheet listed in Figure 7.1 was prepared using the characteristics of the Boeing *Condor*. The figure lists the various methods considered and the reference for each.

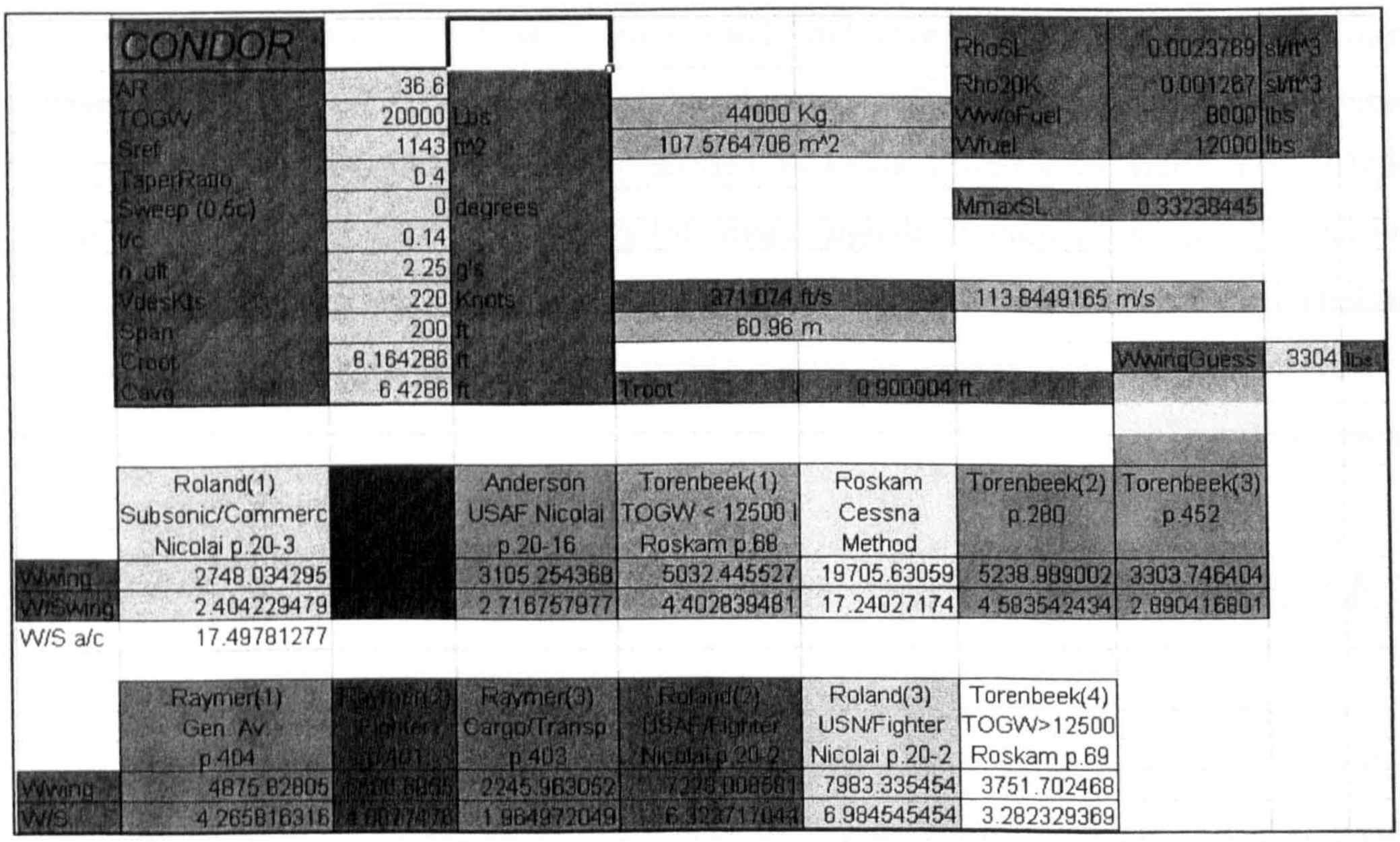

Figure 7.1 ***is an example of the type of analysis done to determine the best wing weight estimation technique(s) to use in the methodology. This particular example is for the wing weight estimation of the Boeing Condor, which had a published wing weight/ft^2 of 2 psf.***

The quantities listed in violet are the quantities that are essential for the different methods to calculate the wing weight. Each method takes a slightly different set of variables into consideration, however all of the methods were statistically based. As seen in the figure, the absolute wing weight is specified for each method, along with the wing

weight per reference area. The reason the wing weight per area is listed is that the value for *Condor* was known to be 2 lbs/ft^2. In addition a sound knowledge of glider wing weight per area is known to be in the same region. It should be noted that the *Condor* carried fuel in the wings, and was a twin engine configuration with the engines mounted on the wings for added bending moment relief. Gliders, on the other hand rarely carry anything (occasionally ballast) in the wings and have slightly lower aspect ratios on average (the exception being the Unlimited Class). Despite not carrying additional weight in the wings, these aircraft are designed for much higher g loadings than *Condor* was (cited as 2.25 g's) yet have the same general wing weight per area.

Wing Weight Per Area

	Heron	Hermes 450	Hermes 1500	Aura (USN)	HiLine	Perseus A	Perseus B
Roland(1)	1.05157	0.41562956	1.14248635	0.3389986	0.485546	0.4806171	0.676641
[illegible]	[illegible]	[illegible]	[illegible]	[illegible]	[illegible]	[illegible]	[illegible]
Anderson USAF	1.617576	0.90475571	1.96773631	0.8659775	1.010169	1.1114084	1.375618
Torenbeek(1)	2.231172	1.21507602	2.82200171	1.1730722	1.239121	1.6438323	2.10381
Torenbeek(2)	2.321793	1.26417079	2.93602381	1.2203495	1.289407	1.7106484	2.189474
Torenbeek(3)	1.978727	1.0140039	2.54675391	1.0472604	1.312006	1.8330145	1.836559
Raymer(1)	2.325502	1.38191813	2.49258508	1.2217415	1.610103	1.8641739	2.313336
Raymer(2)	3.187058	1.9173505	3.50023416	1.5184664	2.334748	2.5037139	3.190637
Raymer(3)	1.292247	0.80986811	1.58346687	0.7740311	0.852322	1.0128346	1.219417
Roland(2)	2.018326	1.29317416	2.64041497	1.0261759	2.266993	2.0475602	2.763269
Roland(3)	5.519571	3.6407525	6.36452889	2.9686173	5.314394	4.3532167	5.3666
Torenbeek(4)	2.303107	1.17083238	3.63161028	1.425871	1.2031	2.1084431	2.006981
W/S Aircraft	17.3338	13.33333	44.435	19.512195	7.52	10.639535	11.36598

	Altus	Predator	Raptor	Condor	Theseus
Roland(1)	0.947358	0.79563837	0.79963377	2.4042295	1.141435
[illegible]	[illegible]	[illegible]	[illegible]	[illegible]	[illegible]
Anderson USAF	1.553373	1.45571396	1.29783093	2.716758	1.650743
Torenbeek(1)	2.214818	2.09684712	1.79088694	4.4028395	2.384193
Torenbeek(2)	2.304787	2.18191867	1.8637539	4.5835424	2.481796
Torenbeek(3)	2.147313	1.95472036	1.5436062	2.8904168	3.091319
Raymer(1)	2.335822	2.16781211	2.04363088	4.2658163	2.613971
Raymer(2)	3.29271	2.98530342	2.74623535	4.8877476	2.968458
Raymer(3)	1.290271	1.23464796	1.07332059	1.964972	1.214772
Roland(2)	2.681491	2.3755377	2.30067259	6.323717	3.887523
Roland(3)	5.696737	5.25542858	4.70280531	6.9845455	5.319382
Torenbeek(4)	2.492844	2.33740351	1.67471271	3.2823294	3.461731
W/S Aircraft	16.28788	18.2481752	10.2285093	17.4978	11.11816

Figure 7.2 ***is the summary of the wing weight (per unit wing planform area, lbs/ft^2) estimations performed for aircraft in the HALE UAV or similar class.***

As also seen in the figure, very few of these methods are valid in the higher takeoff weight Low Speed HALE UAV area. Most of the methods grossly over-predict the wing

weight of the *Condor*. It should be mentioned that not one single method considered was designed specifically for composite wings. The majority of the methods suggest some generic correction factor depending on the degree of composite use in the wings. The *Condor* wing was composite as are almost all modern sailplane wings and all other aircraft constructed to perform Low Speed HALE missions.

The same analysis performed for the *Condor* above was performed for 12 different aircraft, mostly in the Low Speed HALE UAV class, but several medium altitude aircraft were also considered. The results can be seen in Figure 7.2. There is no reason to decide on just one method, if more than one method can provide reasonable results across the range considered for this methodology. However, very few of the methods shown can provide reasonable results across the entire range.

The down-selection process begins with the *Condor*. The majority of the methods over-predict the *Condor's* weight enough where they cannot be trusted for higher weight Low Speed HALE UAV aircraft. Thus, immediately Howe, Torenbeek (1) and (2), Raymer (1) and (2), and Roland (2) and (3) can be removed from consideration. That leaves 5 methods : Roland(1), Anderson USAF, Torenbeek (3) and (4), and Raymer (3). The next consideration is whether or not they can be used across the entire range of weights being considered. Torenbeek (4) is supposed to be used for aircraft greater than 12,500 pounds takeoff weight, so it is removed from consideration as well.

The next basis for down-selecting is the knowledge that the *Perseus A* and *B* used identical construction techniques, and that the aircraft wing weight per area should be reasonably close. The values resulting from Roland (1) are too low to be realistic, and this method is thus removed from consideration. Raymer (3) and Anderson both were considered to underestimate the wing weight on average and therefore were not included. Raymer (3), however, is used to determine the first guess for the remaining method, Torenbeek(3), which is iterative. As can be seen in the figure, this method predicts almost equal wing weight per area for the two *Perseus* aircraft and in general predicts reasonable wing weights across the range being considered. The value for the *Hermes 450* aircraft was predicted low by all of the methods considered. This aircraft has a side-by-side fuselage arrangement which might have some effect on the weight of the wing. The other aircraft wing weight which was under-predicted by the Torenbeek iterative method was the United States Navy *Aura* aircraft, which was based on a Rutan *Long-EZ*. None of the unconventional configurations considered by this methodology correspond to this

configuration (strakes, high sweep angle). For the conventional configuration, a minimum wing weight per wing planform area of 1.5 lbs/ft^2 has been set to ensure it does not drop below a realistic value. The same limit is applied to the wing weight ***before*** the application of the configuration weight reduction factors for twin boom or multiple fuselage aircraft.

Thus the equation used for wing weight prediction by this methodology is from Torenbeek[7] (p.452) as follows :

$$W_{wing} = 8.94 \cdot 10^{-4} K_{no} K_{\lambda} K_e K_{uc} K_{st} \left[K_b n_{ult} \left(W_{des} - 0.8 W_{WingGuess}\right)\right]^{0.55} b^{1.675} \left(\frac{t}{c}\right)_r^{-0.45} \left(\cos \Lambda_{1/2}\right)^{-1.325} \quad \textbf{(7.1)}$$

$$K_{no} = 1 + \sqrt{\frac{b_{ref} \cos \Lambda_{1/2}}{b}}, \quad b_{ref} = 6.25 \text{ ft.} \quad \textbf{(7.2,3)}$$

$K_{\lambda} = (1 + \lambda)^{0.4}$

K_e = 0.95 if there are two wing mounted engines in front of the elastic axis, otherwise it is 1.0

K_{uc} = 0.95 if the undercarriage is not mounted to the wing, otherwise it is 1.0

K_{st} = 1 for low subsonic aircraft

$V_c \geq K_c \left(\frac{W}{S}\right)^{1/2}$ and K_c is 33 for normal and utility category aircraft up to W/S = 20

K_b = 1 for a cantilever wing, it is a strut factor.

It should be noted that W_{des} is the weight of the aircraft without fuel in the wings. Careful consideration must be taken when applying this to either canard or tandem wing aircraft with fuel in the canard or tandem wing.

First, the volume available for fuel in the wing or tandem must be checked. It would be rare in the case of the Low Speed HALE UAV for there to be inadequate volume for fuel in the wing though not impossible if an endurance above 48 hours is desired. The reason for having greater available volume in the wing for fuel is the lower fuel consumption as compared to a turbojet or turbofan engine. In any event, the available fuel volume in the wing is calculated. If it is found to be insufficient, fuel is shifted to the other horizontal surface, or to the fuselage, depending on the choice of the designer.

Some experimentation was performed to see if the strut factor could absorb the difference in weight due to multiple fuselages, but this was found to be inadequate. On the subject of multiple fuselage wing weight estimation there is very little data available. In fact, the only data available is for a single point. The wing weight per square foot of the Rutan *Voyager* is known to be 0.5 lbs/ft^2. As mentioned previously, this aircraft was

designed for a very extreme mission, and should only be used as lower limit for wing weight per square foot of wing area. The *Voyager* wing weight per square foot was ¼ the wing weight per square foot for the *Condor* wing.

A detailed study was undertaken with regards to the relative bending moment distributions of the various configurations considered by the methodology. This study was essentially performed to identify the relative magnitude of the spanwise bending moment depending on various combinations of the number of fuselages, the number of engines, and their spanwise placement. The details of this study are presented in the next section.

7.B Spanwise Wing Bending Moment Study

In order to insure confidence in the overall endurance results, reasonable wing weight estimations for the various configurations considered by the methodology were required. The spanwise lift force distribution is readily available from the vortex lattice method employed in the methodology. This lift force distribution in addition to the spanwise force distribution (due to fuel and wing weight), and the weights and spanwise locations of the fuselage(s), payload, engines and nacelles were subsequently used to generate complete spanwise wing bending moment distributions for all of the configurations.

A study was then performed for 2000 lb., 10,000 lb., and 20,000 lb. takeoff weight aircraft for the following configurations :

SINGLE ENGINE	TWIN ENGINE
Single Fuselage	Single Fuselage
Two Fuselage	Two Fuselage
Three Fuselage	Three Fuselage
Twin Boom	Twin Boom
Tandem	Tandem
Single Fuselage	Single Fuselage
Two Fuselage	Two Fuselage
Three Fuselage	Three Fuselage

In addition, a brief study was performed on the effects of changing the taper and aspect ratios on the bending moment distribution.

These results will be presented in the order of single engine , single engine tandem wing, twin engine, and twin engine tandem wing. At the end of the analysis, a factor to

multiply by the existing wing weight will be introduced for the configurations where relevant.

7.B.1 Single Engine Study

At first, it is important to note that the Low Speed HALE UAV mission has driven the geometry of the wing to higher aspect ratio and higher span than that normally found on aircraft with more conventional mission requirements. Thus, a very large portion of the aircraft and fuel mass is in the wing. This combination greatly reduces the magnitude of the bending moment when compared to other classes of aircraft. In addition, the payload fraction for this class of aircraft is rather significantly smaller than that of any other class of aircraft. This reduces the magnitude of the bending moment even further.

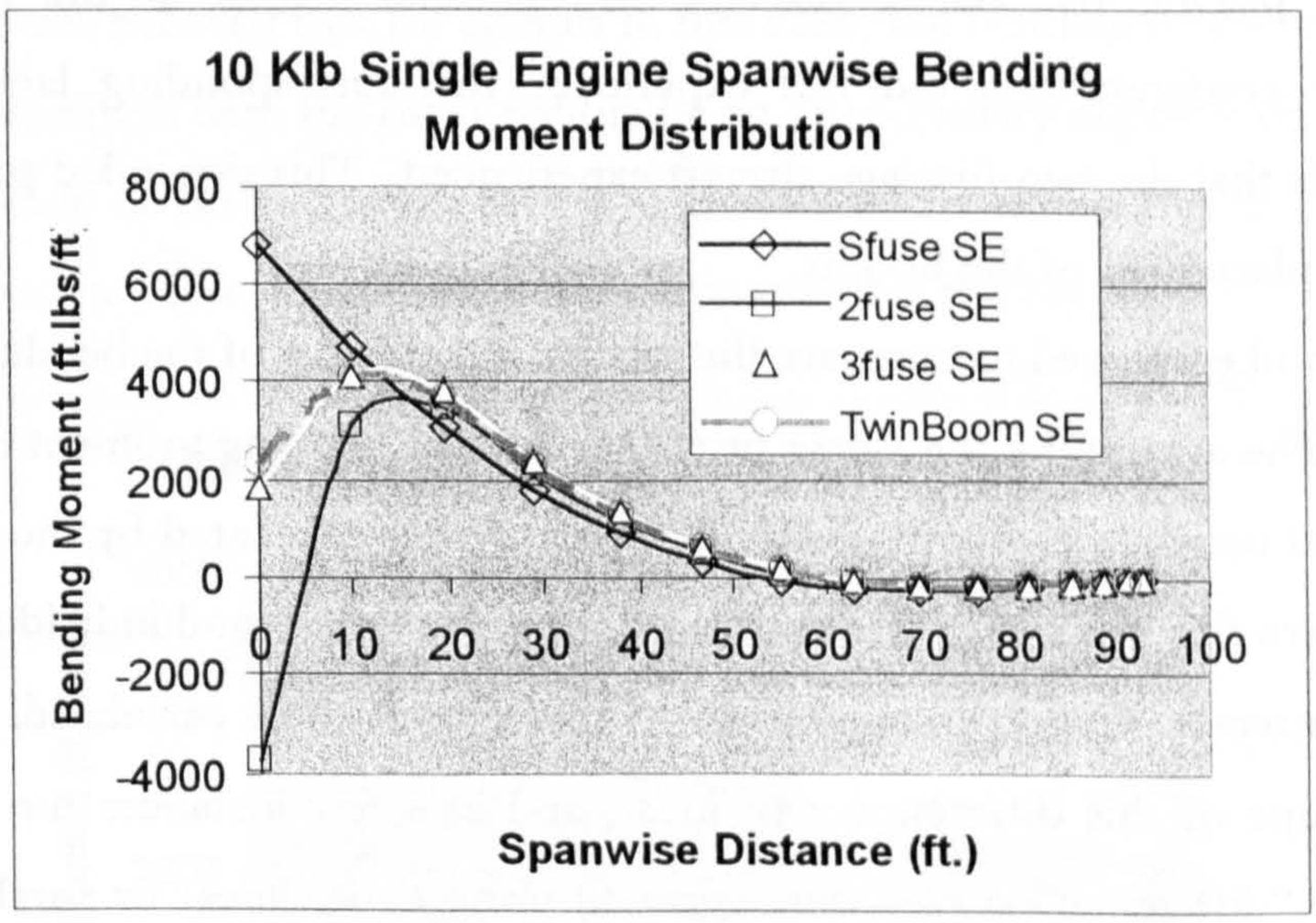

Figure 7.3 ***compares the spanwise bending moment of the single engine non-tandem configurations.***

The overall shape of the spanwise bending moment distribution for the single fuselage aircraft, however, remains the same. This can be seen in Figure 7.3. In addition, it is possible to view this distribution graphically within the methodology, once the detailed component drag and weight estimations have been performed, and once the results of the spanwise lift distribution are available from the vortex lattice method.

Figure 7.3 shows the results for the 10,000 pound takeoff weight case. The other takeoff weight cases showed identical behavior with only the magnitudes changing. The first point of interest to note is that the bending moment outboard of the

booms/fuselages for the multiple fuselage/boom aircraft is essentially identical. The no fuel case is shown as it was found that the full fuel case only unloaded the wing further, thus reducing the maximum wing bending moment. This was true for all but the two-fuselage configuration which experienced greater negative bending moments inboard of the booms/fuselages for the full fuel case.

The single engine two-fuselage aircraft (with the engine at the longitudinal centerline) for all of the takeoff weight cases generated too large a moment to be unloaded by the inboard lift, and resulted in negative wing bending moments at the longitudinal centerline in all cases. Consequently, an attempt was made in the study to determine the optimum spanwise location for the booms for each takeoff weight case by balancing the maximum positive and negative wing bending moments.

The single engine three fuselage and twin boom results were in very good agreement. By placing the center fuselage and payload weight at the longitudinal centerline, these configurations did not experience the corresponding large negative bending moments that the two-fuselage aircraft experienced. This depended partly on the proper spanwise placement of the booms.

The method employed to compare the relative magnitudes of the bending moment was as follows. The area under the single fuselage spanwise bending moment distribution curve (or the total magnitude of wing bending moment) was calculated by the integration of a parabolic curve fit. The difference between the single fuselage and individual multiple fuselage/boom aircraft wing bending moment curves was then calculated. In most instances, the shape of this difference was linear, and in a few instances the shape was parabolic. These "difference" curves were curve fit using either linear or parabolic curve fits and then integrated to determine the area of the difference in bending moment (or the difference in total magnitude of wing bending moment). Finally, the percentage reduction in total wing bending moment was calculated using these integrated areas for the individual configurations and takeoff weights.

Based on the results of applying the above procedure to each non-tandem single engine configuration and based on a study of aspect ratio and taper ratio effects, an average reduction in total magnitude of wing bending moment was found as shown in Table 7.1. The two-fuselage aircraft saw the largest reduction, however the most caution must be used in employing this configuration to ensure that the negative bending moment inboard of the fuselages is kept reasonably low. The twin boom and three fuselage cases

were again essentially identical, provided that the booms are scaled up for the 20,000 pound takeoff weight case. This is not done automatically by the methodology, however it was thought to be a reasonable assumption to scale the diameter of the booms up from those used for the 2000 and 10,000 pound takeoff weight cases.

Table 7.1 ***lists the reduction factors resulting from the analysis for single engine non-tandem aircraft.***

Two Fuselage	Three Fuselage	Twin Boom	
0.47	0.18	0.18	Average

Thus, the reductions in Table 7.1 will be employed in the wing weight estimation of the methodology for single engine non tandem wing configurations. While it is realized that wings are sized structurally based on bending moment, shear, torsion *and* stiffness constraints, it was believed that for aircraft in this class, the bending moment would be the primary consideration with the other factors being of secondary importance. With regards to the magnitude of the reduction factors considered, it is noted that the three fuselage reduction factor in Table 7.1 is still 3.3 times that used for the *Voyager*.

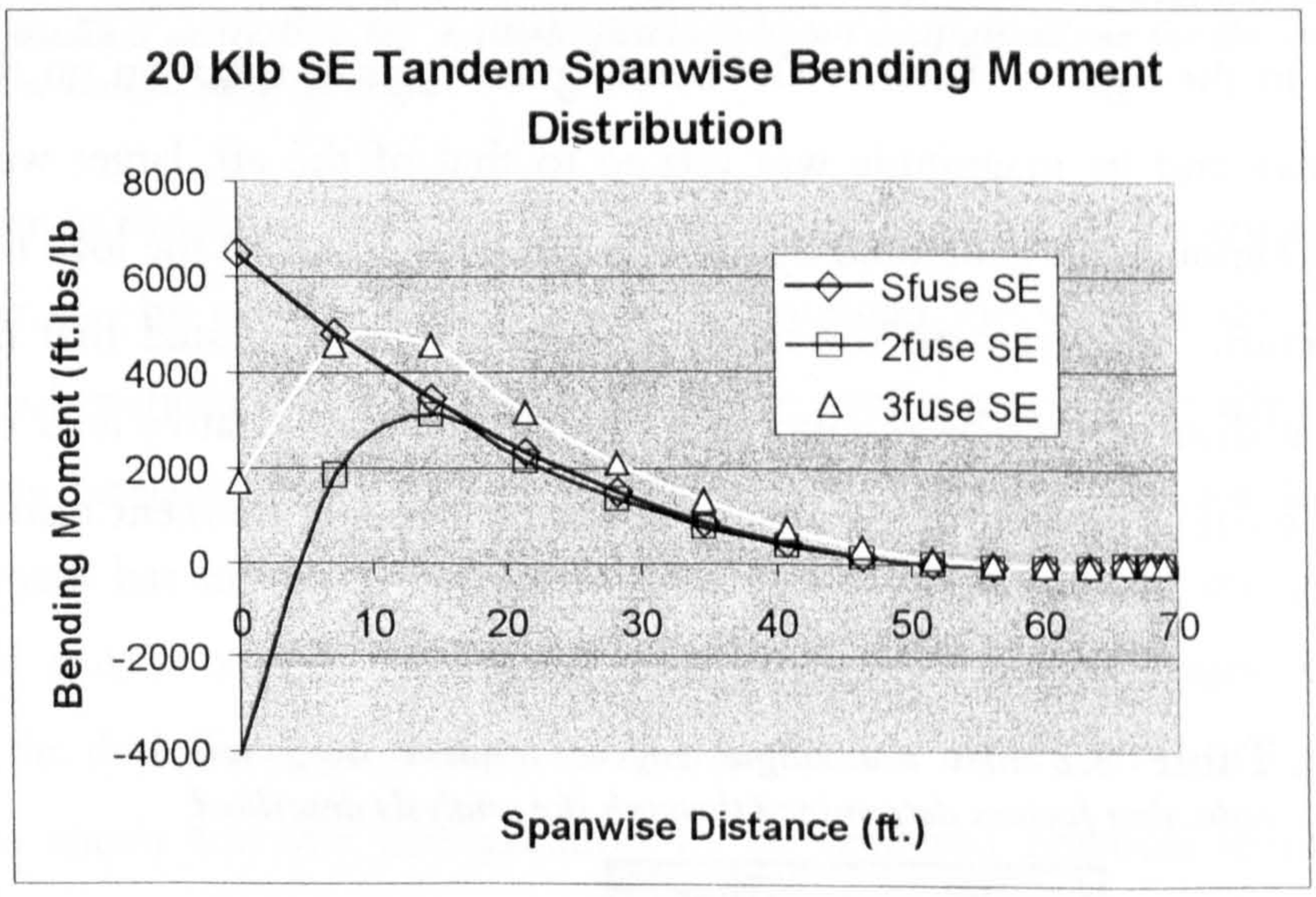

Figure 7.4 ***shows a comparison of the single engine tandem aircraft spanwise bending moment distributions.***

A representative graph of the single engine tandem wing aircraft configurations can be seen in Figure 7.4. The study shown in the figure is for the 20,000 pound takeoff weight aircraft. The behavior of these curves is very similar to that seen in Figure 7.3 for

the non-tandem 10,000 pound takeoff weight case. The most notable difference is the slight increase in bending moment of the three-fuselage tandem wing curve prior to the departure of the curves for the other two configurations.

This can be explained by the fact that the optimum spanwise location for the boom in this case was further outboard than that of the two-fuselage aircraft. In addition, it is possible, due to balance considerations, that there was less fuel in the wing of the three-fuselage wing weight calculation. This would then result in a lower calculated wing weight and thus lower spanwise wing weight distribution. Consequently the wing would not be unloaded as quickly thereby resulting in a comparatively higher wing bending moment.

Following an identical procedure to the one followed for the non-tandem single engine cases, average values were obtained for multiplying wing weight reduction factors based on the reduction in total magnitude of wing bending moment for the given configurations. The resulting values can be seen in Table 7.2.

The results for the two-fuselage case were the same as for the non-tandem aircraft, and the results for the three-fuselage case were extremely close to those of the non-tandem aircraft. One consideration that resulted from this study of the tandem winged aircraft cannot be seen in the figures shown. The bending moment distribution on the forward wing was negative and its magnitude was related to that of the aft, larger wing. There normally was not enough lift generated by the forward wing to offset the load necessary to balance the aircraft. In designing the tandem aircraft, it is suggested that *BOTH* wing bending moment distributions be monitored to insure that the negative load on the fore wing is not too great as a result of setting the optimum bending moment distribution for the aft wing.

Table 7.2 ***lists the single engine tandem wing weight reduction factors determined through the analysis described.***

Two Fuselage	Three Fuselage	
0.47	0.21	Average

7.B.2 Twin Engine Study

It is once again necessary to note the special nature of the Low Speed HALE UAV aircraft. In this instance, it is necessary to note due to the excessive weight of the

propulsion system, when compared to other more conventional aircraft. This excessive weight has a profound effect on the spanwise wing bending moment distribution, even more so for twin engine (non Push-pull) configurations. This effect can plainly be seen in Figure 7.5.

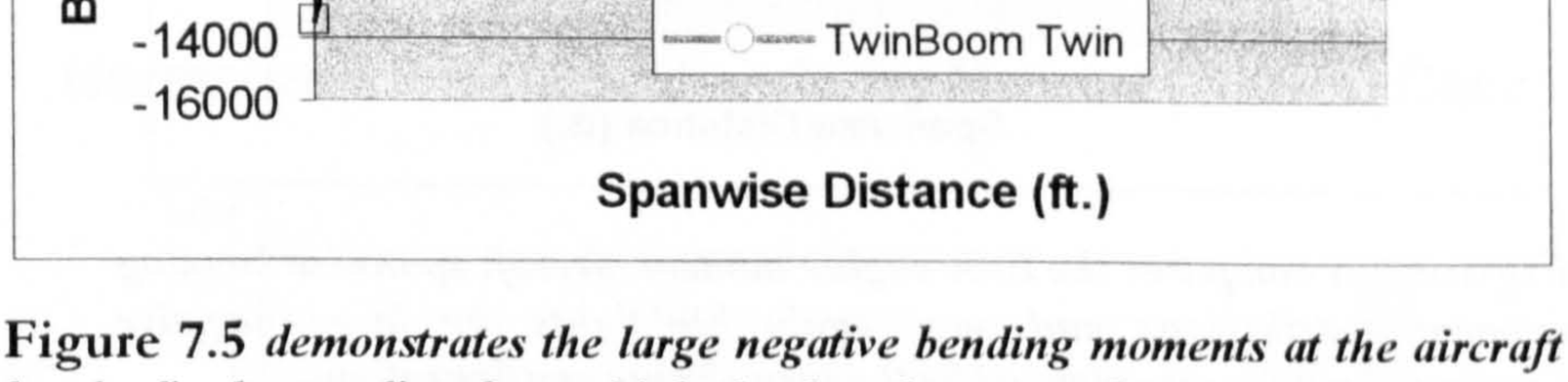

Figure 7.5 ***demonstrates the large negative bending moments at the aircraft longitudinal centerline for multiple fuselage/boom configurations for the twin engine non-tandem aircraft.***

As seen in the figure for the single fuselage configuration, if the engines are placed properly, they can be used to almost completely unload the wing at the wing fuselage junction. This beneficial effect for the single engine configuration is equally as detrimental to the multiple fuselage configurations for this class of aircraft. The absolute maximum bending moment has increased for the two-fuselage configuration to the point where it simply would not be worth considering this concept in a twin engine configuration. Likewise for the three-fuselage configuration, the absolute maximum bending moment has increased too much for this configuration to be rendered practical from a structural standpoint. The twin boom configuration, however has moderate enough behavior to be considered if strictly from a wing bending moment perspective. It is noted, however that none of the less conventional configurations offer any benefit structurally for the twin engine configuration, and in fact result in considerable structural penalty.

Thus for the twin engine non-tandem configurations, no weight saving factor is suggested for the wing weight estimation, and if one were to be included, it would in fact

not be a weight saving factor, it would be a weight penalty. For the purposes of this thesis, however, unconventional twin engine configurations were not considered in the results due to time limitations. It is also believed that the wing weight estimation is considered to be conservative enough in its estimation of the weight to absorb any of these differences.

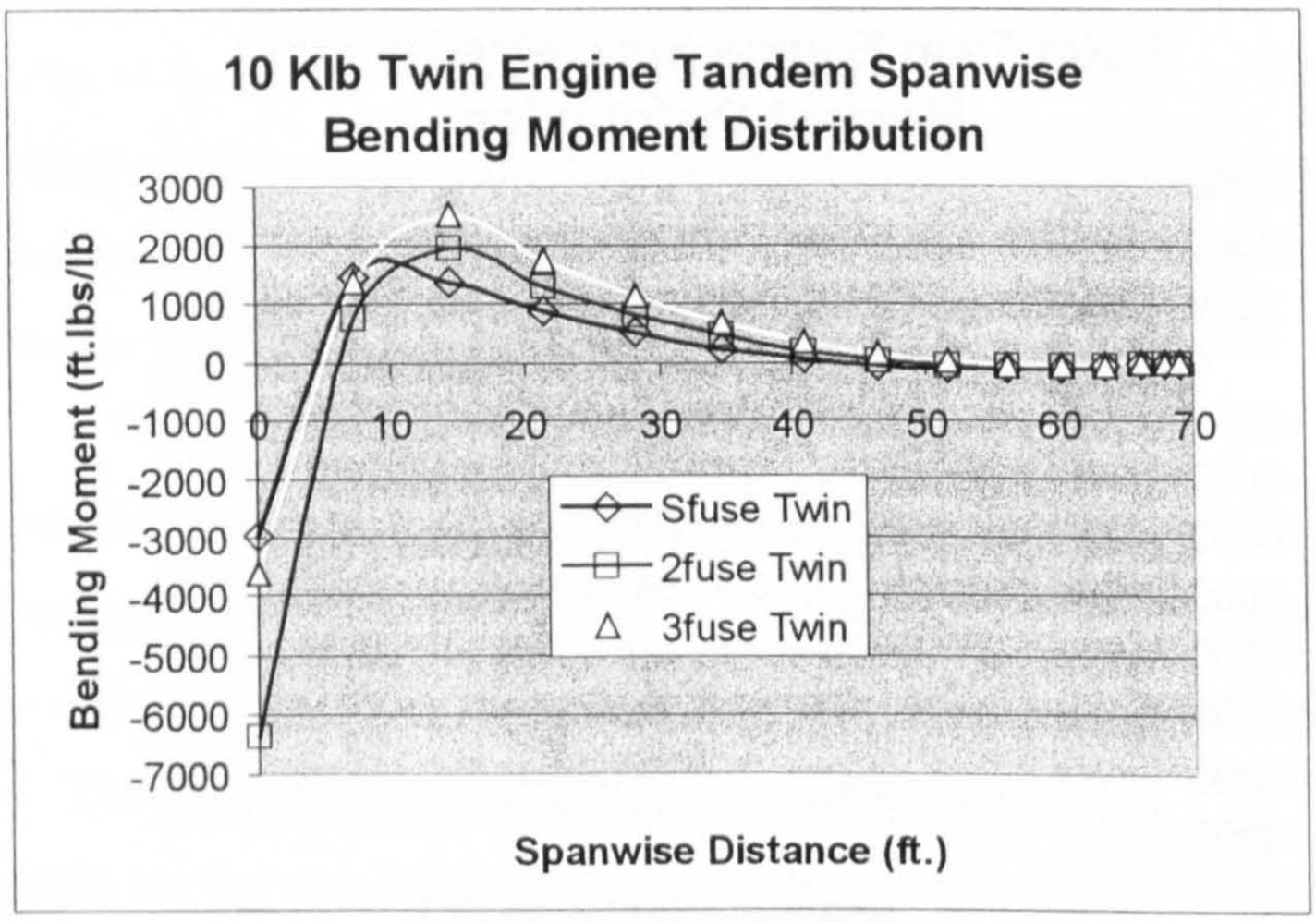

Figure 7.6 ***compares the twin engine tandem aircraft spanwise bending moment distributions and once again highlights the large negative bending moments experienced by the twin engine configurations.***

The results for the twin engine tandem wing aircraft can be seen in Figure 7.6. The reason this figure is included was to demonstrate that the tandem aircraft have slightly different behavior due to the relative size of the wings. In this figure, the three-fuselage aircraft compares reasonably well to the single fuselage tandem. If absolute maximum bending moment is considered, the two configurations compare quite well. However, if the two are compared based on the total magnitude of the wing bending moment, the twin engine three-fuselage aircraft would again not compare very well. Once again, the twin engine two-fuselage aircraft performs very poorly based on the absolute maximum and the magnitude of the total wing bending moment, and would not be suggested based on structural considerations alone. Based on these results, no correction factor is suggested for the estimation of the weight of twin engine tandem wing aircraft.

Thus
for the Single Engine Twin Boom Configuration $W_{Wing} = 0.82\ W_{Wing}$,
for the Single Engine Two Fuselage Configuration, $W_{Wing} = 0.53\ W_{Wing}$,
for the Single Engine Three Fuselage Configuration, $W_{Wing} = 0.82\ W_{Wing}$,
for the Single Engine Two Fuselage Tandem Wing, $W_{Wing} = 0.53\ W_{Wing}$,
for the Single Engine Three Fuselage Tandem Wing $W_{Wing} = 0.79\ W_{Wing}$,

Consequently, the resulting minimum values of wing weight per area are set at 1.23, 0.795, 1.23, 0.795, and 1.185 lbs/ft^2 respectively.

Obviously, a more accurate way of predicting multiple fuselage wing weight is desired. It is noted, however, that it would be extremely difficult to create and subsequently validate any multiple fuselage weight estimation technique as there are so few examples from which to validate these results. No wholly theoretically based method could take into consideration the manufacturing methods used in aircraft. It is also noted that the paper cited earlier by Udin and Anderson[107] made no attempt to validate their multi fuselage wing weight estimation method for multiple fuselage aircraft, they only validated their method against existing single fuselage aircraft.

7.C Fuselage Weight Estimation

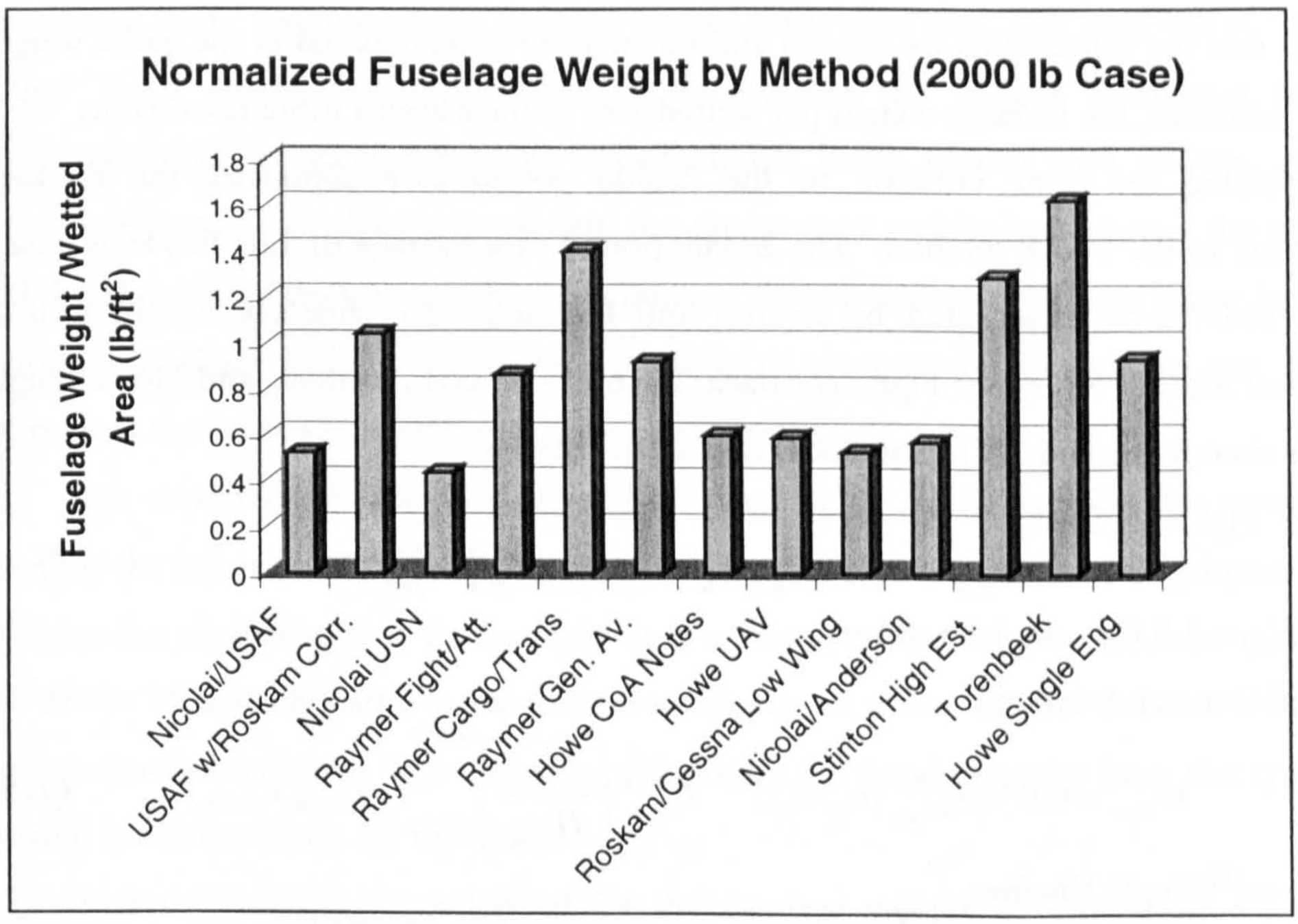

Figure 7.7 ***compares the fuselage weight estimation methods evaluated for use with the methodology. The results shown are for the 2000 lb aircraft case.***

In the evaluation of the best fuselage weight estimation technique to use, 15 different methods were compared. The methods that yielded ridiculous values were removed and the remaining 13 are plotted in Figure 7.7 for the case of the 2000 pound aircraft. The same analysis was performed for the 20,000 pound aircraft case as well.

As seen from the figure, the predictions from several methods are well above what would be expected for this class of aircraft. The average of these values is 0.8724 lbs/ft^2. Based on this average value, it is possible to dismiss the possibility of using certain methods if a criterion of plus or minus 15 % of the average is implemented. This leaves the USAF method with the Roskam Correction, Raymer Figher/Attack, Raymer General Aviation, and Howe Single Engine methods.

To arbitrarily assign importance to the average of all of the methods would be remiss. However, as mentioned above, some knowledge of what a reasonable value for fuselage weight per wetted area is known and described in the many general design methodologies. Raymer[4] suggests 1.25 lbs/ft^2 for a composite general aviation fuselage. Stinton[6] suggests roughly an average of 1.25 lbs/ft^2 for a metal single or twin. From the Literature Review, an average weight saving for glider fuselages of ~11% was shown by substituting graphite fiber with carbon fiber reinforced plastics. Taking these factors into account, along with the fact that the values cited by Stinton and Raymer are at least as old as the glider weight saving estimates, the fuselage weight per wetted area average seems more reasonable.

Applying the same criterion to the 20,000 pound case eliminates the Roskam Correction to the USAF method. The 20,000 pound case average of 1.07 lbs/ft^2 is closer to but still below those cited by Stinton and Raymer. The fuselage weight is thus calculated using the Raymer Fighter/Attack, Raymer General Aviation, and Howe Single Engine aircraft methods. The methods used are as follows :

Raymer[4] Fighter/Attack :

$$W_{fuse} = 0.499 K_{dwf} W_{to}^{0.35} n_{ult} L_{fuse} H_{fuse}^{0.849} w_{fuse}^{0.685} \tag{7.4}$$

where $K_{dwf} = 1.0$ for non delta wings.

Raymer[4] General Aviation :

$$W_{fuse} = 0.052 S_{wet_{fuse}}^{1.086} (n_{ult} W_{to})^{0.177} L_t^{-0.051} \left(\frac{L_{fuse}}{H_{fuse}} \right)^{-0.072} \left(\tfrac{1}{2} \rho_{cruise} V_{cruise}^2 \right)^{0.241} \tag{7.5}$$

and Howe[108] Single Engine :

$$W_{fuse} = 0.053 \left[L_{fuse} \left(H_{fuse} + w_{fuse} \right) (0.3048)^2 \sqrt{V_{desSI}} \right]^{1.5} (2.2) \tag{7.6}$$

where 0.3048 and 2.2 are conversion factors from SI to English units. The fuselage weight is calculated by an un-weighted average of the above equations.

It is believed that these methods tend to underestimate the weights of conventional light aircraft fuselages due to the fact that they were developed, in general, for aircraft with much higher takeoff weights and different construction techniques than

those expected for UAV's. It is, however, suspected that UAV fuselage weights per area are below those of conventional aircraft making the use of these techniques more appropriate.

The reasoning behind this is that there are far fewer breaks in the critical load paths created by the need to maintain traditionally inaccessible instruments and structural components. There are also fewer breaks in the critical load paths due to the need for human ingress and egress. It is noted that most payloads are supplied on palettes and the breaks in the fuselage need only accommodate this and the ability to service and maintain the fuselage structure. In addition, the assumption of a skid landing system reduces the need for additional weight at a specific point in the fuselage to absorb the impact upon landing.

Obviously there is a lower limit to which this fuselage weight per area can obtain, and that will be monitored carefully in the output of the methodology. Thus, a minimum value of 0.85 lb/ft^2 was set for the fuselage weight per wetted area. The only way to verify whether these assumptions are sound is to evaluate the weight estimation on a macroscopic scale as applied to Low Speed HALE UAV aircraft with known empty weights. Although this does not validate the component weight breakdown, the actual ***exact*** breakdown of weight of the components is not necessary at any stage in this methodology. Once again, it is the relative weights of components that will become more important in the comparison of the various configurations.

It is expected that the fuselage will be sized by its ability to resist the moments created by the tail, payload, and fuselage mounted engines, since there is no requirement to pressurize the aircraft as it is unmanned. It is a matter of curiosity to mention that the Grob *Strato 2C* actually had two separate pressure vessels inside of each other in order to accommodate habitation at high altitudes. Obviously the weight penalty from this type of approach is not necessary for the UAV.

A factor of 10% is multiplied by the fuselage weight of the Single Fuselage Tandem Wing configuration, in addition to an increase in the diameter of the fuselage. This was done in order to combat the greater torsional stress on the fuselage resulting from the possibility of opposing moments acting on the fore and aft wings due to an asymmetrical gust loading. The Multi Fuselage Tandem Wing configuration was believed to have sufficient structural rigidity built in to not require the addition of structural weight

Finally, no weight saving is assumed for the fuselage in the case of the multiple fuselage configuration. This was done as a result of the increase in wing fuselage junction weight which would likely offset any benefit in overall structural rigidity supplied by the multiple fuselage configuration.

7.D Horizontal Tail/Canard Weight Estimation

A slightly different approach was taken to the selection of the horizontal tail weight estimation methods. In this application, a sensitivity analysis was performed on the equations based on moment arm length (given the difficulty in defining moment arm length for many of the configurations), V_{des} , n_{ult} , thickness to chord ratio, and ¼ chord sweep angle.

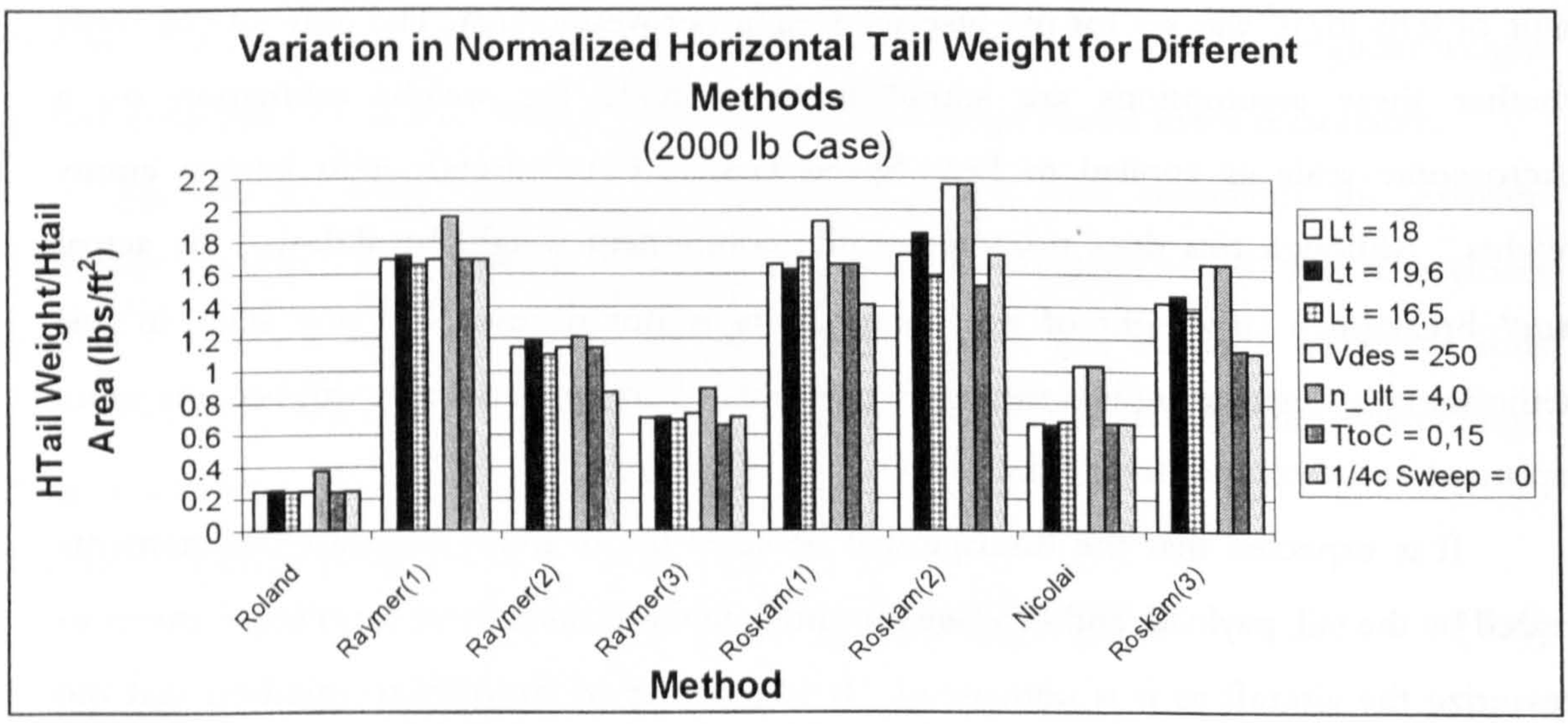

Figure 7.8 ***is a comparison of different horizontal tail weight estimation methods and performs a sensitivity on the most relevant terms to the application of the methodology, again for the 2000 lb case.***

Once again, the results for the 2000 pound case are presented. It should be noted that the results for the 20,000 pound case tend to be much more reasonable as the design references they come from are more appropriate to larger, heavier aircraft. The results for the 2000 pound case are presented since they are more controversial and prompt discussion of the limitations and problems associated with using these weight estimation methods. The average horizontal tail weight for the 2000 pound case in Figure 7.8 is 1.171 excluding the Roskam (2) method. Torenbeek[7] states that the weight of the tailplane is normally between 3.5 and 4 percent of the aircraft empty weight. While there is no

guarantee that this aircraft will share the same fractional weight, it provides a "ball-park" estimate to indicate if the value is reasonable. Assuming a 40 percent structure fraction for this aircraft (2000 lb), that would result in a 28 to 32 pound tail. With a horizontal tail area of 34.1 ft^2, this gives a value of approximately 0.9 lbs/ft^2. This value appears to be a bit below that expected.

It can be seen from the figure that all of the methods are fairly insensitive to changes in the moment arm length of over 15 percent. In fact, with the exception of the Roskam (2) method, there is almost no noticeable change as a function of moment arm length. This is an important result relating to the calculation of the horizontal tail weight estimation for the alternative configurations. Overall, the methods show the greatest sensitivity to the ultimate load factor first, and the design diving speed second. This result also follows reason and common sense as they are also the most structurally relevant quantities.

Given the average weight per area of 1.171 lbs/ft^2, the down-selection process needs to be performed to limit the weight estimation to the most reasonable solutions. Unfortunately, the limiting process used for the fuselage cannot be applied to the horizontal tail. The variation in the values about the average for each method for the 20,000 pound case (average of 2.366 lbs/ft^2 horizontal tail weight per area) is completely different from the variation in the 2000 pound case.

A compilation of values of planform area normalized horizontal tail weight for 16 gliders introduced between 1975 and 1983 from Thomas[9] gives an average of 1.416 lbs/ft^2, and a standard deviation of 0.254 lbs/ft^2. The minimum value was 1.01 lbs/ft^2 and the maximum was 1.84 lbs/ft^2. It is thought that these values represented the state of the art in composite construction techniques up to 1983. In the 17 years that have passed since the time of the most recent of those gliders (*DG 300*, *ASK 23*, *LS 6*, and *Nimbus 3/24,5*), there is little doubt that composite construction techniques have advanced considerably. This advancement makes the values predicted using the composite horizontal tail weight estimation method described here easily obtainable.

In this instance, a composite of three different methods is used to reproduce values close to the average in a repeatable manner. The Raymer (3) method which is a bit low, the Howe UAV method which is reasonably close, and the Roskam (1) method which is moderately high. This composite of methods results in a value of 1.25 lbs/ft^2 for the 2000 pound case, and 2.34 lbs/ft^2 for the 20,000 pound case. It is noted that the

difference in these two values is a little perplexing. It is expected that the average weight per area would be less for the higher weight aircraft, however this was not the case. One possible explanation is that as the horizontal tail area increases, the structure necessary to resist the forces on it must increase in density. In any event, the equations used for these three methods were as follows :

Raymer[4] General Aviation Method (p.404) :

$$W_{HT} = 0.016(n_{ult}W_{to})^{0.414}\left(\tfrac{1}{2}\rho_{cruise}V_{cruise}^2\right)^{0.168} S_{HT}^{0.896}\left(\frac{100\frac{t}{c}}{\cos\Lambda_{HT}}\right)^{-0.12}\left(\frac{AR}{\cos^2\Lambda_{HT}}\right)^{0.043}\lambda_{HT}^{-0.02}$$

Where Λ_{HT} is the leading edge sweep angle. **(7.7)**

Roskam[5] (Torenbeek) Method (Pt.V Ch.5 p.73) :

$$W_{HT} = K_{HT}S_{HT}\left[3.81\frac{S_{HT}^{0.2}V_{des}}{1000\sqrt{\cos\Lambda_{\frac{1}{2}HT}}} - 0.287\right] \qquad \textbf{(7.8)}$$

where $K_{HT} = 1.0$ for a fixed tail and $K_{HT} = 1.1$ for an all moving tail.

And the Howe[108] UAV method :

$$W_{HT} = 0.8(0.028)\left[\left(\frac{b_{HT}S_{HT}}{\cos\Lambda_{\frac{1}{4}HT}}\right)\left(\frac{1+2\lambda_{HT}}{3+3\lambda_{HT}}\right)\left(\frac{W_{to}n_{ult}}{S_{HT}}\right)^{0.3}\left(\frac{V_{des}}{\frac{t}{c}}\right)^{\frac{1}{2}}\right]^{0.9}\cdot 2.2 \qquad \textbf{(7.9)}$$

Once again, an un-weighted average of these numbers is used to calculate the final horizontal tail weight. A minimum weight per area was set at 1.0 lbs/ft^2 based on the glider data.

At this stage in the methodology, it is useful to note that if a Tandem Wing configuration is being analyzed, that the weight estimation is performed as if it were another wing, and not via the horizontal tail/canard weight estimation techniques mentioned here. No weight saving was considered for the horizontal tail of the multi fuselage or twin boom configurations. It was believed that the decrease in weight resulting from the horizontal tail being supported on two sides would be offset by the additional weight of the hardware necessary to fix both ends of the tail.

7.E Vertical Tail Weight Estimation

An analysis similar to that of the horizontal tail was performed in order to determine the most suitable weight estimation methods to implement in this methodology. Figure 7.9 shows the results for the 2000 pound aircraft case. Once again, the moment arm length was varied due to the ambiguity in the definition of moment arm length for the vertical tail. Once more, the methods tested were essentially insensitive to reasonably large changes in moment arm length.

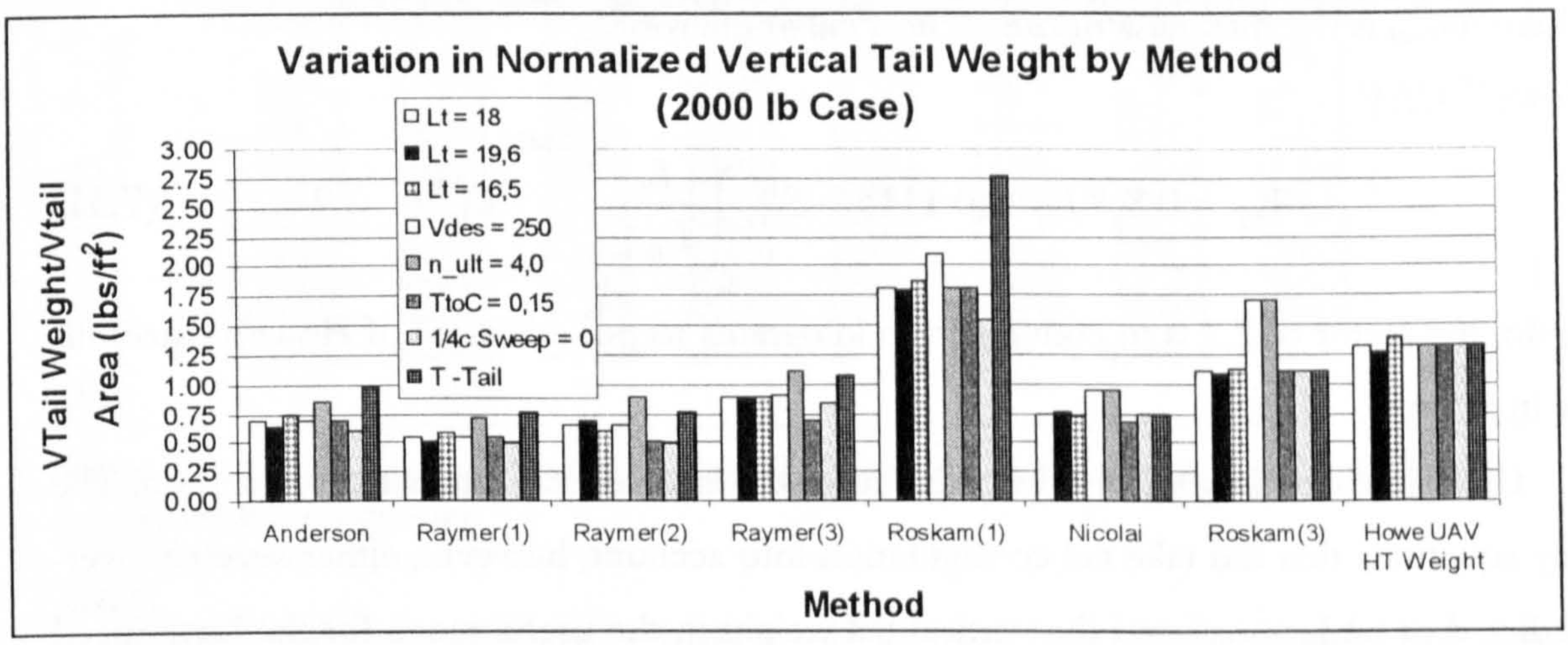

Figure 7.9 ***is a comparison of different vertical tail weight estimation methods and performs a sensitivity on the most relevant terms to the application of the methodology, again for the 2000 lb case.***

In addition, the methods tested showed slight sensitivity to variations in ¼ chord sweep angle and thickness to chord ratio. The most sensitivity was shown in the areas of ultimate load factor, design dive speed, and for the methods that considered it, the use of a T-tail instead of a conventional tail. These results were expected, with perhaps the exception of the T-tail. This was a bit of a surprise, however understandable when viewed from a structural point of view. With the T-tail configuration, the fin provides a load path for the horizontal tail loads and the end plate effect increases the fin bending moment for a given yaw angle.

The difference between the average value for the 2000 pound and 20,000 pound cases was much smaller for the Vertical Tail, with the 2000 pound average of 1.01 lb/ft^2 and the 20,000 pound average of 1.51 lb/ft^2. Again, none of the methods were applicable alone, so a composite function was made up of a non-weighted average of 2 different methods. Thus, the methods used were Howe UAV and Nicolai/Anderson USAF. The composite

value for the 2000 pound case was 1.05 lb/ft^2 and the composite value for the 20,000 pound case was 1.53 lb/ft^2. The 2000 pound case value (1.05 lb/ft^2) was set as a minimum allowable value for all vertical tail weight cases. It is not expected that a vertical tail can be produced much below this weight per area as seen from the horizontal tail glider data. In general, however, the equations used were as follows:

Nicolai[3]/Anderson USAF (p.20-17):

$$W_{VT} = 98.5\left[\left(\frac{n_{ult}W_{to}}{100000}\right)^{0.87}\left(\frac{S_{VT}}{100}\right)^{1.2}\left(\frac{b_{VT}}{t_{VTroot}}\right)^{0.5}\right]^{0.458} \quad \textbf{(7.10)}$$

where t_{VTroot} is the thickness of the vertical tail at the root.

Howe[108] UAV :

$$W_{VT} = 0.8(\#\,Fins)\left(0.11156\cdot S_{VT_{SI}}^{1.3}\left(\frac{L_t}{L_{fuse}}\right)^{-0.2422} V_{des}^{0.7812}\cdot 2.2\right) \quad \textbf{(7.11)}$$

Again, the factor of 2.2 is to convert from kilograms to pounds as all of Howe's equations are in SI units.

Unfortunately, neither of these methods takes into account the tail configuration. The only equations that did take tail configuration into account, however, either severely over-predicted or under-predicted the vertical tail weight in the useful range for the Low Speed HALE UAV (when compared to existing glider tail weight data from Thomas[9]). Although other methods take more design variables into account in their equations, the results they provide are not suitable here as seen from the preceding analysis. The next weight to be estimated belongs to one of the heaviest components of the aircraft.

7.F Engine Weight Estimation

Care must be taken when selecting an engine weight estimation method. Several of the methods will include accessories, while others neglect them. For a component that weighs as much as an engine, these omissions or inclusions can make a significant difference in the final weight estimate. Once this difference is taken into account, the weight estimates provided by the methods evaluated are some of the most concordant when compared to the other components of the aircraft.

An analysis similar to the previous components was undertaken. This time, the installed engine and accessory weight was normalized by the most appropriate quantity,

horsepower output. The results for the 2000 pound (70 HP) and 20,000 pound (350 HP Twin) installed aircraft engine weight estimates can be seen in Figure 7.10. The average for all of the methods for the 350 HP case was 3.83 lbs/HP and for the 70 HP case was 3.46 lbs/HP.

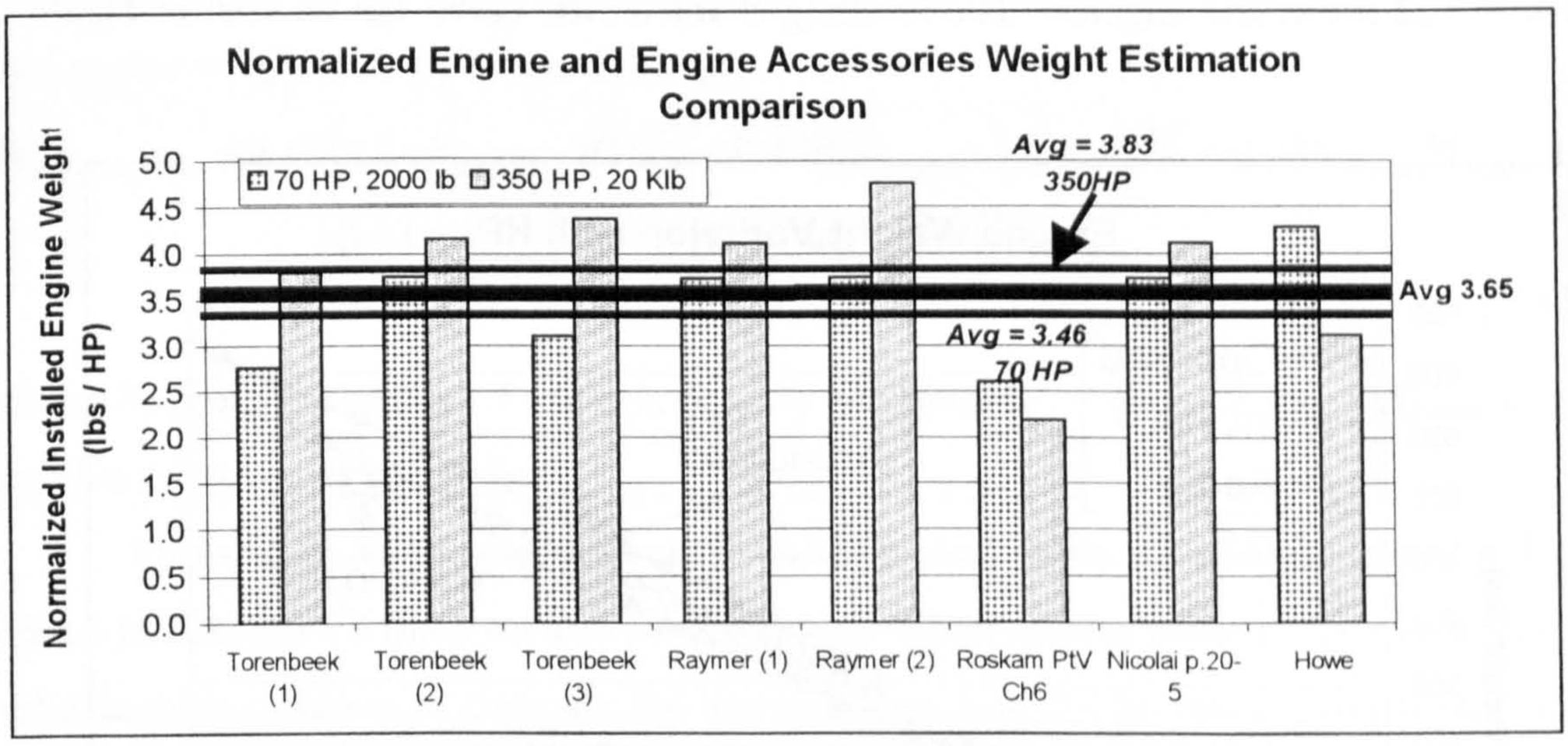

Figure 7.10 ***is a comparison of different engine weight estimation methods for both the 2000 lb and 20,000 lb aircraft cases.***

This result runs contrary to what would be expected. It was thought that there should be an economy of scale with larger internal combustion reciprocating engines, however that result does not appear to be true in the range considered for all but two of the methods tested. Many of the methods shown in the figure rely on initial estimates of engine weight and then subsequently predict the installed engine weight. There is little else remarkable about this figure, except that it can be seen that the results from Roskam markedly reduce the overall average for the 20,000 pound case.

Roskam[5] (Pt.V, Ch6, p.84) proposes a simple method for predicting engine weight alone which is simply a constant times the HP required. The only other method proposed for engine alone weight was suggested by Torenbeek[7] (p.286). The difficulty with using this method is that it is a function of the number and volume of cylinders for the engine. This information is not always available, however it was found to predict the weight of engines quite accurately when this information is known. Raymer[4] (p.405) presents an engine (alone) weight estimation technique for several types of engines. It is similar in appearance to the engine length and width prediction techniques mentioned in Chapter V,

Section 5.2. Thus, for reasons of versatility and ease of use the Raymer engine weight alone method was used. This relation is of the form :

$$W_{engine} = a(HP)^b \qquad \textbf{(7.12)}$$

where b is 0.780 for both in-line and opposed engines, and a = 5.47 for opposed engines and a = 5.22 for in-line engines. The resulting characteristic curve can be seen in Figure 7.11.

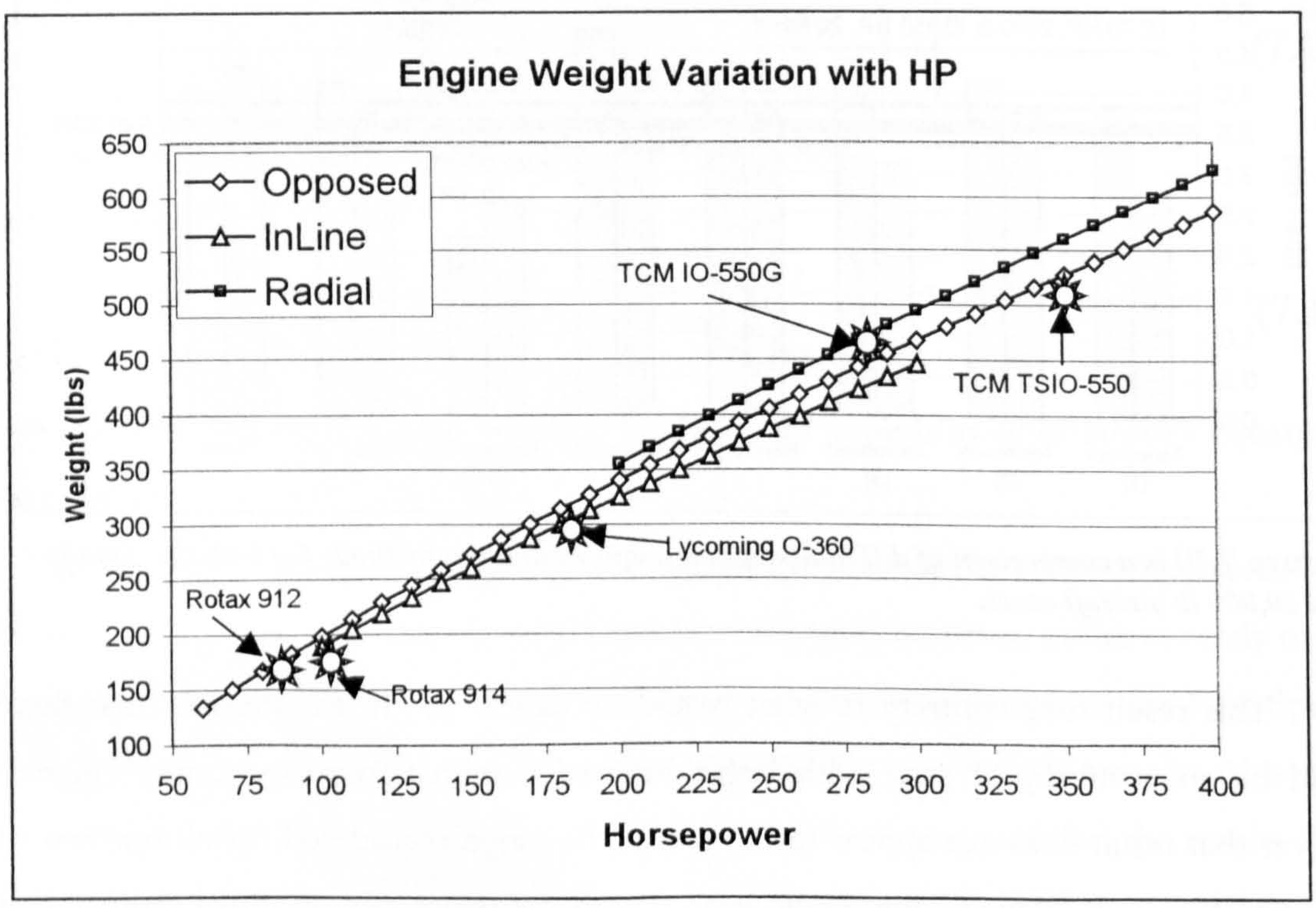

Figure 7.11 ***compares Raymer's engine weight estimation method with some known aircraft engine only (uninstalled) weights as a function of horsepower output.***

As seen in the figure, the graph for opposed engines is reasonably accurate for known engine only weights within the range expected for the Low Speed HALE UAV and it was this method that was used. Therefore the *installed* weight correction methods remain. At this stage, it will be pointed out again that if engine information is known by the designer, it can be specified in place of these prediction techniques without any difficulty.

For the installed engine and accessory weights, the methods selected were Raymer/Nicolai, and Torenbeek[7](3, p.286). Raymer's[4] General Aviation method of installed engine weights (p.405) is the same as Nicolai's[3] (p.20-5) USAF method for

light/utility aircraft which does not include the fuel system, but does include the mounting and induction. The Raymer/Nicolai method is as follows:

$$W_{engine,installed} = 2.575 \cdot W_{engine}^{0.922} \tag{7.13}$$

Torenbeek's method is the sum of the accessories/drives/gearboxes/air induction/exhaust/PP controls, Supercharger, Oil system and cooler, Prop Installation, and engine weight and appears as follows:

$$W_{engine,installed} = 1.03\left(1.2 \cdot N_{engines} \cdot HP\right)^{0.7} + 0.455\left(N_{engines} \cdot W_{engine}\right)^{0.943} + 0.03 N_{engines} W_{engine} + 0.144 N_{props}\left[1.2 D_{prop} HP \cdot N_{blades}^{0.5}\right]^{0.78174} + W_{engine} \tag{7.14}$$

where N_{engs} is the number of engines, N_{props} is the number of propellers and N_{blades} is the number of blades per propeller.

Once again, it will be difficult to validate the engine installed weights for Low Speed HALE UAV's since no data have been published on this subject. The only way to validate these results is to compare the uninstalled weights for known engines (Rotax 912, 914), some of which have been used in HALE UAV's with additional turbo-charging and supercharging. In addition, once the installed engine weights have been calculated, a factor of 1.5 is multiplied by the installed engine weight. This number is relatively arbitrary, however there has been no analytical indication in the literature as to what a reasonable increase in weight would be. This factor is used to make up for the weights of radiators, modern supercharger and turbocharger weights, air induction and inter-cooling weights, and other assorted miscellaneous added weights for the Low Speed HALE UAV powerplant. The next step is to determine the weight of the engine fairings.

7.G Engine Nacelle Weight Estimation

At this point in the weight estimation, fewer methods are available in the common methodologies for the prediction of the remaining component weights. The existing methods will be compared and included if the results were thought to be reasonable. The engine nacelle weight estimation was evaluated on a per wetted area basis, for the 2000 and 20,000 pound aircraft. The results can be seen in Figure 7.12.

Once more, the result of lower normalized nacelle weight for the lower weight aircraft was not expected. One possibility is a change in the materials used for constructing

nacelles above a certain weight, however this is thought to be unlikely. In general there is much better agreement between the methods across the various types of aircraft considered. A comparison was also undertaken based upon Nacelle Weight normalized by aircraft takeoff weight, however this yielded less useful results and greater variation between methods.

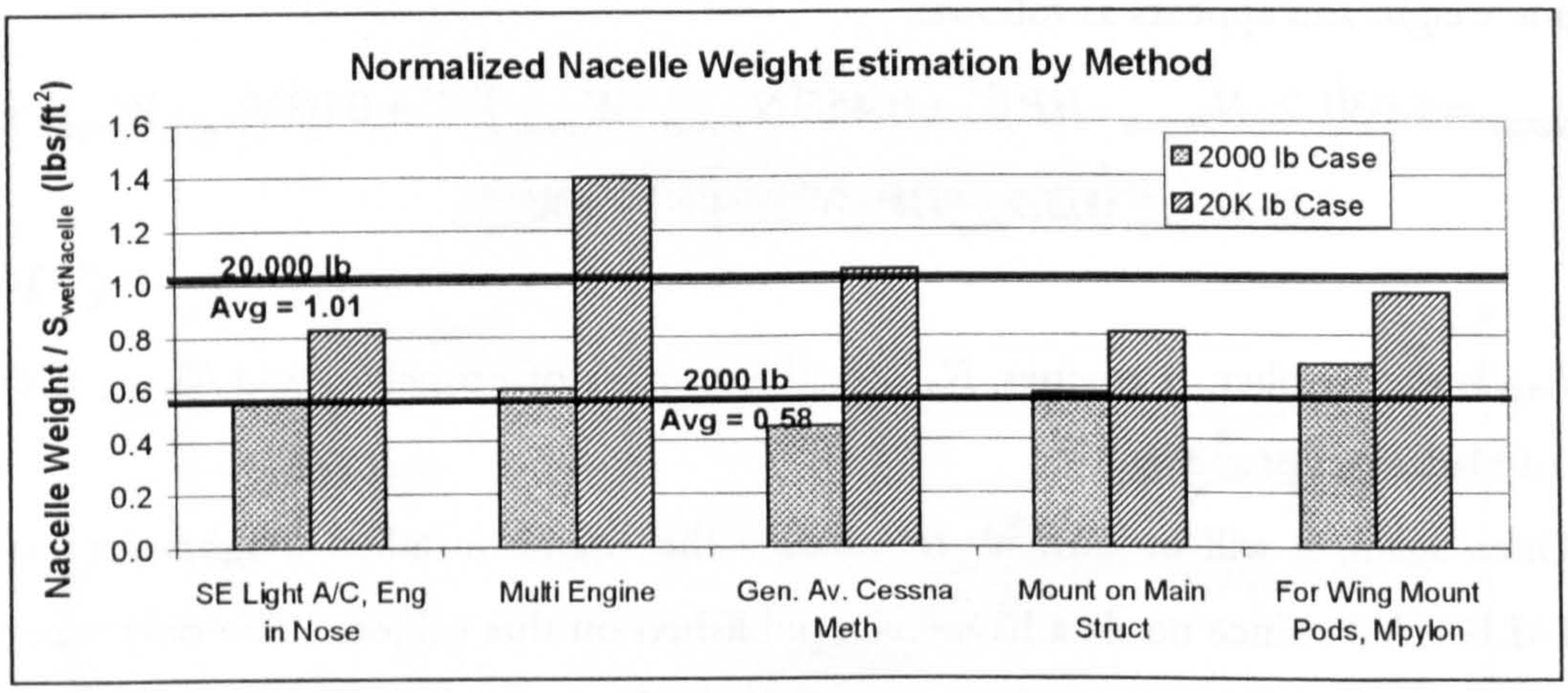

Figure 7.12 ***is a comparison of different nacelle weight estimation (normalized by nacelle wetted area) methods for both the 2000 lb and 20,000 lb aircraft cases.***

Given the variety of different possible engine configurations for the present methodology, four of the above methods were used depending upon the configuration. Where appropriate, similar equations were averaged. For example, it is possible to have a Single Engine Light Aircraft with the engine mounted in the nose, and also have an engine mounted on the main structure. In this instance, the results of these two equations are averaged. It is noted that the logic for deciding which of the equations to use in a computational environment is complicated. A decision that a designer can make in an instinctive manner, essentially instantaneously, can be slightly more arduous to repeat in an automated fashion. The equations used were as follows :

Torenbeek[7] single engine light aircraft (p.283) :

$$W_{nacelle} = 2.5 HP^{1/2} N_{engines} \qquad \textbf{(7.15)}$$

and Torenbeek Multi Engine aircraft (p.283) :

$$W_{nacelle} = 0.32 HP \cdot N_{engines} \qquad \textbf{(7.16)}$$

where $N_{engines}$ is the number of engines.

Howe[108] suggests this equation for main structure mounted nacelles :

$$W_{nacelle} = 0.143 W_{engine} \tag{7.17}$$

And this equation for wing mounted pod nacelles (Cranfield CoA Lecture Notes) :

$$W_{nacelle} = 0.17 W_{engine} \tag{7.18}$$

7.H Fuel System Weight Estimation

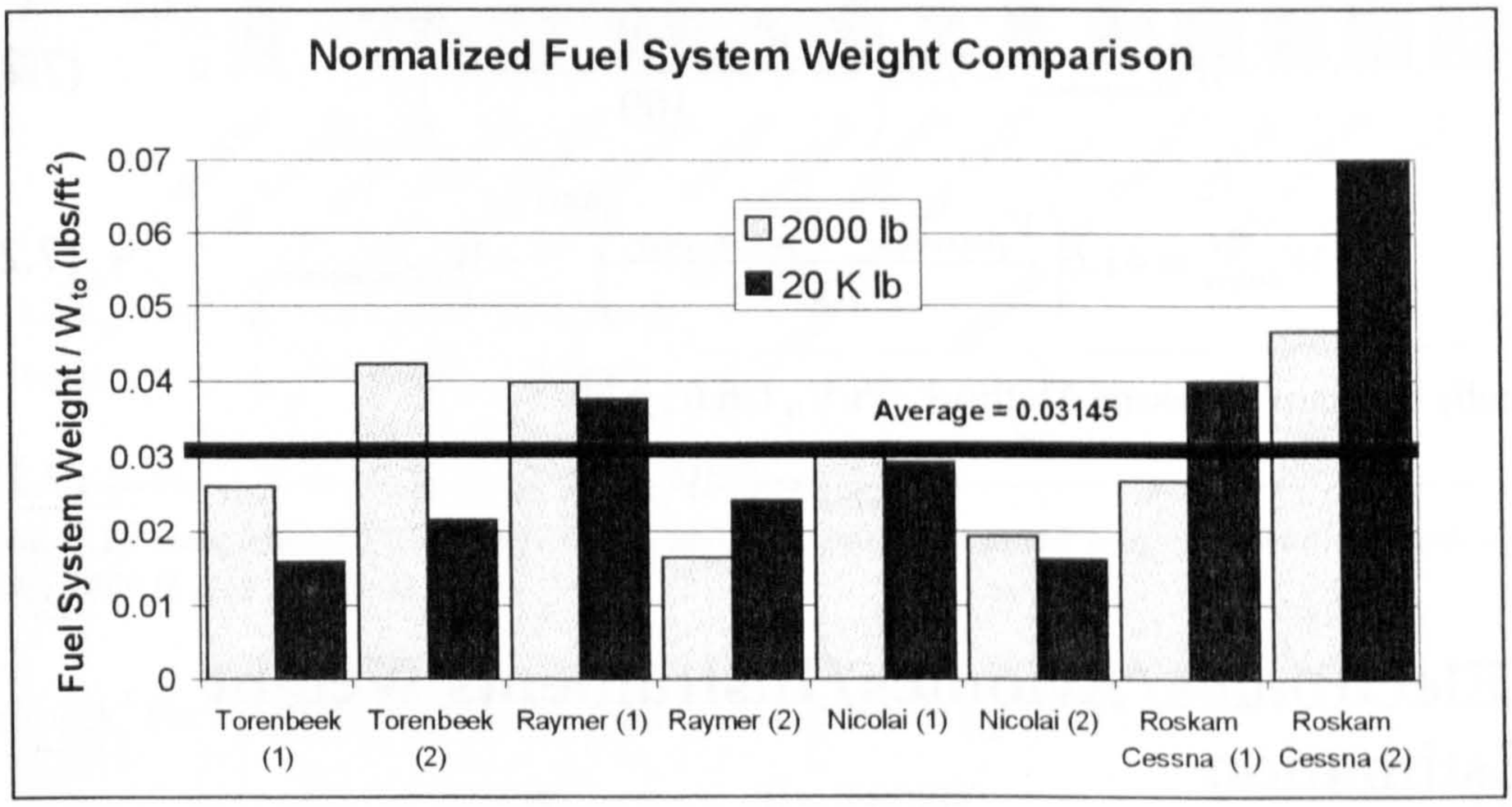

Figure 7.13 ***is a comparison of different fuel system weight estimation methods normalized by aircraft takeoff weight.***

The fuel system weight comparison was normalized based on aircraft takeoff weight. The results can be seen in Figure 7.13. On this basis, the difference between the average of the 2000 pound case and the 20,000 pound case was quite small. The 2000 pound average was 0.03107 $\frac{lb(FuelSystemWeight)}{lb(TakeoffWeight)}$ and for the 20,000 pound case 0.03183 $\frac{lb(FuelSystemWeight)}{lb(TakeoffWeight)}$. Of the methods considered, the Raymer(1), Nicolai(1) and Roskam Cessna (1) methods were selected as the most appropriate for the Low Speed HALE. From the figure, the remaining methods either over or under predict the weight by too large a margin. The equations used are as follows :

Raymer's[4] General Aviation fuel system weight estimation (p.405) :

$$W_{fuelsys} = 2.49 V_{fuel}^{0.726} \left(1 + \frac{V_{fuel/\text{integral}}}{V_{fuel}} \right)^{-0.363} N_{\text{tanks}}^{0.242} N_{engines}^{0.157} \qquad \textbf{(7.19)}$$

where V_{fuel} is the total volume of fuel, $V_{fuel/\text{integral}}$ is the volume of fuel in integral fuel tanks, and N_{tanks} is the number of tanks.

Nicolai's[3] estimation is a combination of the Self Sealing cell weight plus the fuel system bladded cell backing and supports (p.20-7) :

$$W_{fsComponents} = 7.91 \left(\frac{V_{fuel/wings} + V_{fuel/fuselage}}{100} \right)^{0.854} \qquad \textbf{(7.20)}$$

$$W_{fuelsys} = 41.6 \left(\frac{V_{fuel/wings} + V_{fuel/fuselage}}{100} \right)^{0.818} + W_{fsComponents} \qquad \textbf{(7.21)}$$

And finally Roskam's[5] Cessna Method (Pt.V., Ch.6., p.90) :

$$W_{fuelsys} = 0.4 V_{fuel} \qquad \textbf{(7.22)}$$

7.I Electronics/Avionics/Instruments Weight Estimation

This aspect of the weight estimation represents the most disparate grouping of equipment. This makes it more difficult to define and differentiate exactly what the weight is being estimated for. Figure 7.14 has been created comparing the different groupings, this time normalized based on aircraft takeoff weight. Several of the categories plotted are actually sub-categories of other methods shown. As a check on the overall magnitude of the values obtained, Raymer states that avionics weight ratios $\left(\frac{W_{electronics}}{W_{to}} \right)$ in the range of 0.01 to 0.04 are to be expected for single and twin engine general aviation aircraft.

Without knowing beforehand exactly which instruments or what types of avionics will be placed in this aircraft, it is difficult to apply one of the component buildup methods for weight estimation. Therefore, estimation methods based on the overall electronics/avionics/instrument weight have been used. The two Torenbeek methods were used (greater than and less than 12,500 pounds), and the General Dynamics method taken from Roskam was also used. The equations appear as follows :

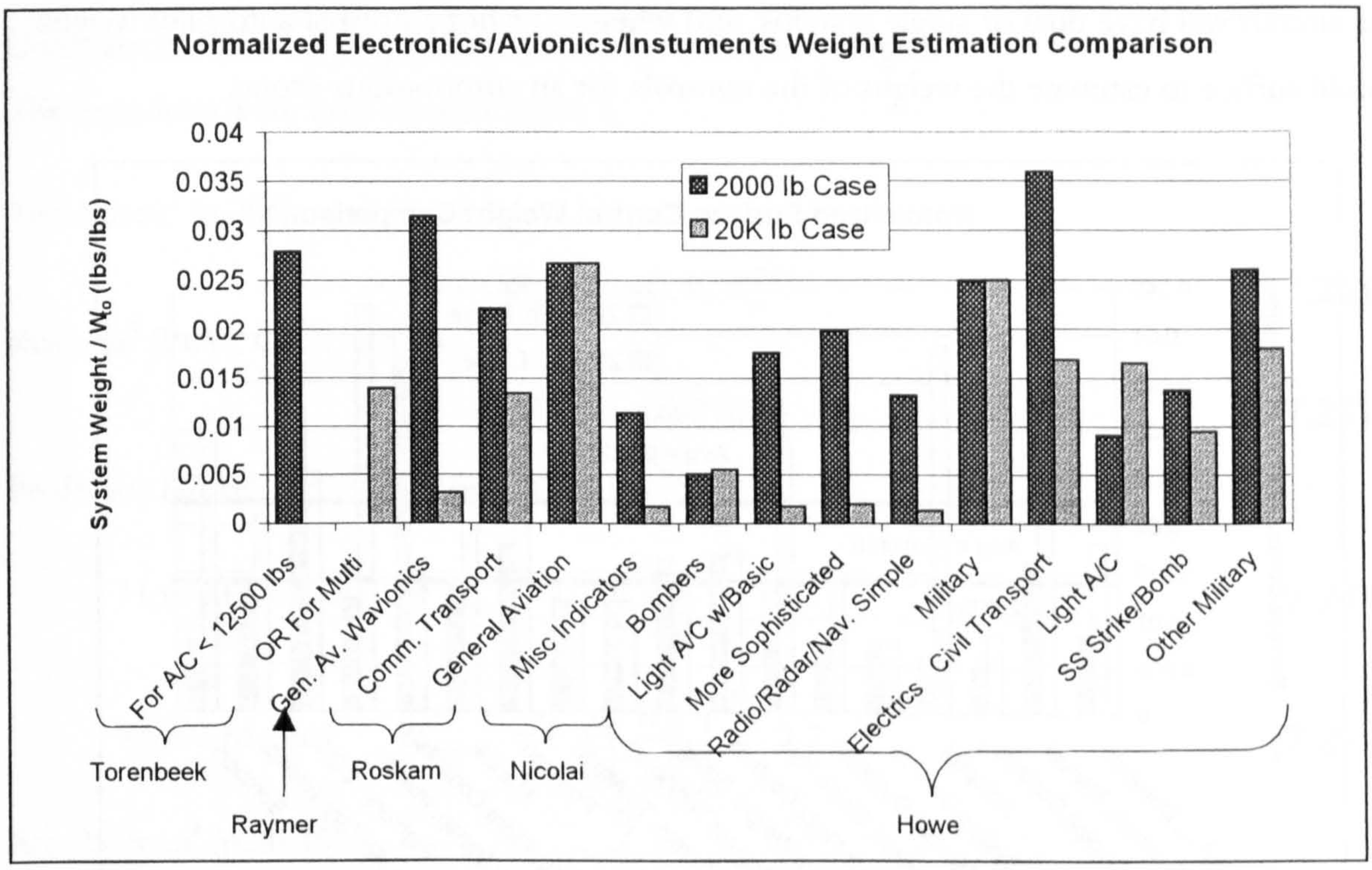

Figure 7.14 ***compares different electronics, avionics, and instrument weight estimation methods for both the 2000 lb and 20,000 lb cases.***

Torenbeek[7] for takeoff weights less than 12,500 pounds (p.289) :

$$W_{electronics} = 40 + 0.008W_{to} \tag{7.23}$$

and for weights greater than 12,500 pounds :

$$W_{electronics} = 120 + 20N_{engines} + 0.006W_{to} \tag{7.24}$$

And the General Dynamics method taken from Roskam[5] (Pt.V Chapter 7, p.103) :

$$W_{electronics} = \left(15 + \frac{0.032W_{to}}{1000}\right) + N_{engines}\left(5 + \frac{0.006W_{to}}{1000}\right) + 0.15\frac{W_{to}}{1000} + 0.012W_{to} \tag{7.25}$$

7.J Surface Controls Weight Estimation

The final major aircraft component group to be considered for inclusion in the weight estimation for this methodology is the surface controls, or the weight of the controls/actuators and the control surfaces that they move. Similar to the electronics weight estimation, there are several different sub-categories within the weight estimation of the surface controls. Once more, it is impossible to know beforehand whether or not

the aircraft will have dual or single systems, and whether or not a normal auto-pilot weight would suffice to estimate the weight of the controls for an autonomous drone.

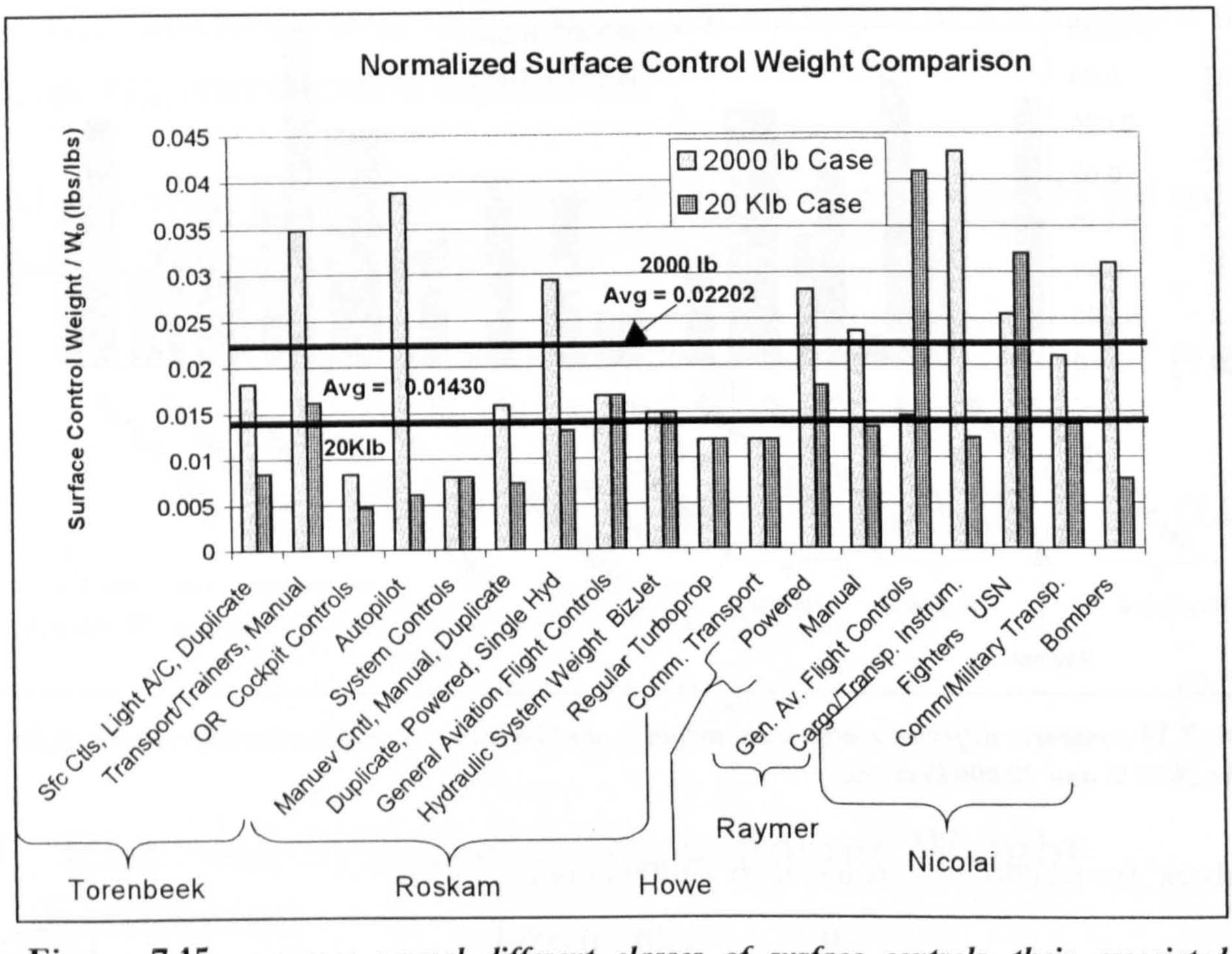

Figure 7.15 ***compares several different classes of surface controls, their associated weights, and the results of these methods when applied to the 2000 lb and 20,000 lb cases.***

It is noted that any method selected will most likely under-predict the weight of these systems (due to the control requirements of a UAV as compared to a manned aircraft), however it was thought better to include some estimate for the weight of these components than to exclude them altogether. In addition, even though the surface controls systems for a Low Speed HALE UAV may not compare well to those of a general aviation single, there is the possibility that the systems to be used on a HALE UAV might compare well to those on a fighter or bomber. Thus, the evaluation was undertaken once more. The results of the comparison can be seen in Figure 7.15.

The components were normalized by the aircraft takeoff weight. The averages for each weight class are marked on the graph. Given the difficulty of deciding on any single method, a composite or average of methods will be used in order to try and maintain a reasonable value for the weight. The methods used in the composite were the Torenbeek (Duplicate Powered Controls, Single Hydraulic Power System), Roskam General Aviation

Flight Controls Weight, Howe's Powered and Manual flight control weights, and Nicolai's Commercial/Military Cargo/Troop Transport control weights.

The equations were used as seen below :

Torenbeek[7] (p.284) :

$$W_{controls} = 0.42 W_{to}^{0.65} \tag{7.26}$$

Roskam[5] (Pt.V., Ch.7., p.100) :

$$W_{controls} = 0.0168 W_{to} \tag{7.27}$$

Professor Howe's[108] Course notes (Cranfield CoA) :

Howe Powered $$W_{controls} = 0.11\left(\frac{W_{to}}{2.2}\right)^{0.8} \cdot 2.2 \tag{7.28}$$

Howe Manual $$W_{controls} = 0.13\left(\frac{W_{to}}{2.2}\right)^{0.75} \cdot 2.2 \tag{7.29}$$

And Nicolai[3] (p.20-19) :

$$W_{controls} = 15.96\left[\frac{\frac{1}{2}\rho_{cruise} V_{cruise}^2 W_{to}}{100000}\right]^{0.815} \tag{7.30}$$

While the analysis used for the down-selection of the weight estimation methods employed for the last few components (Surface controls, Electronics, etc) did not make clear any given choice over another, a choice had to be made, or the component would have been left out of the estimate altogether. An attempt was made to try and quantify the differences between methods where possible. Where this was not possible, or no other justification for differentiation between methods could be determined, a composite of available methods was used, rather than the selection of only one. It is hoped that this will reduce the amount of error encountered by the overall methodology in the absence of better estimation methods. It is noted that the weights of these last few components are quite small (a combined total of less than 3 percent) relative to the takeoff weight of the aircraft. Thus, a more accurate weight estimation method would have a minimal impact on the total aircraft weight.

With the component weights and locations now determined, it is possible to determine the aircraft center of gravity, and subsequently the aircraft static margin and trim characteristics. These topics will be covered in the next chapter.

Chapter VIII

The only limits are, as always,

Those of vision

--- James Broughton

8. Center of Gravity, Static Margin, and Trim

These three topics are all interrelated and are calculated in sequence in the present methodology. Without knowing the exact mass distribution within the individual aircraft components, it is difficult to determine an accurate estimate for the center of gravity of the respective components. There is a large statistical database of existing center of gravity locations within components, and the results found from this database are primarily what will be used in the present methodology.

The static margin relies rather heavily on the value of downwash gradient in the wake experienced by the tail in conventional configurations. The difficulty in finding a reliable source for this value will be discussed briefly as well. Finally, the trim drag penalty is calculated and the endurance recalculated based on trimmed flight. The value for final endurance is compared to the endurance recalculated just prior to the trim calculations. This ensures that the most recent values of drag, lift, and weight are used in the determination of the pre-trim endurance that is compared to the trimmed aircraft endurance. The discussion begins with the methods used to determine the center of gravity of the various aircraft components.

8.A Aircraft Center of Gravity Calculation

Every major component considered in the weight estimation needs to have a center of gravity location associated with it. Many of the methods seen in the literature calculate a center of gravity for a combination of the fuselage, engine, and vertical and horizontal tails.

These methods were obviously avoided for the present methodology given the wide variety of configurations considered.

Since the methodology at present considers only longitudinal stability, the component lateral locations of center of gravity will not be discussed. The values found for center of gravity location in the common methodologies can be seen in Table 8.1.

Table 8.1 ***lists the different component center of gravity locations cited by the respective aircraft design references.***

	Torenbeek[7] (p.294)	Raymer[4] (p.398)	Stinton[6] (p.384)	Roskam[5] (Pt.V. p 114)
Wing Straight	38-42% $\overline{c}$	40% $\overline{c}$	40% $\overline{c}$	38-42% $\overline{c}$
Swept	70% front /rear spar dist			70% front /rear spar dist
Fuselage	w/ engine	40-50% L_{fuse}	40% L_{fuse}	w/ engine
Horizontal Tail	42% $\overline{c}_{HT}$	40% $\overline{c}_{HT}$		42% $\overline{c}_{HT}$
Vertical Tail	42% $\overline{c}_{VT}$	40% $\overline{c}_{VT}$		42% $\overline{c}_{VT}$
Engine		40-50% $L_{eng.}$	40% L_{eng}	
Nacelles	40% $L_{nacelle}$	40-50% $L_{nacelle}$		40% $L_{nacelle}$

All values cited in the table are from the front of the respective component. It would appear that if the center of gravity of a given aircraft component were unknown, that a value of 40% of its length measured from the front would be a good estimate from the Table. As mentioned, the problem with the Torenbeek and Roskam fuselage center of gravity estimations is that they include the engine in the fuselage and this was not appropriate for application within the present methodology.

The designer has the option to enter the engine center of gravity location relative to the front of the engine from manufacturers' data. The center of gravity location of the fuel in the wings was assumed to coincide with the wing center of gravity location. It was found after applying a more complicated prismoidal shape volume estimation method that the values rarely varied much from this value so the calculation was removed. Furthermore, the calculation required the assumption of exact locations for the front and rear main spars are values that are not always easy to derive from airfoil data.

Roskam provided an estimate for the tail boom center of gravity location of between 40 and 45% of boom length starting from the most forward structural attachment point of the boom. For this methodology, the reference zero location was taken as the foreword-most point on the aircraft. This point was normally at the nose of one of the fuselages/booms.

It would appear from the table that the application of this reasonably straightforward information should be simple. This, however, was not the case. The various engine locations resulted in logical constructs to determine exactly what type of nacelle was being used (wing mounted, fuselage mounted, twin, single, push-pull), all of which had different implications on the center of gravity location in the overall aircraft. Along with the problems encountered in locating the engine nacelle center of gravity location is the problem of locating the engine center of gravity location, depending on the engine location on the aircraft, for any given configuration. This kind of problem will be discussed in more detail in the Implementation chapter. The difficulties dealing with multiple fuselage/boom aircraft, tandem wings, split fuel locations etc. will also be discussed.

Before the overall aircraft center of gravity can be calculated, the location of the payload and payload center of gravity must be specified. Based upon the fuselage with the most volume available, the payload can be placed anywhere within that fuselage as long as it is not in conflict with the engine location. The designer is prompted for the payload location, payload length, and payload center of gravity relative to the front of the payload. These values are then verified as physically possible (for example, not outside of the fuselage, or in conflict with the engine or end of the fuselage). Once this information has been input, the center of gravity of the entire aircraft can be calculated.

It is noted that several of the elements considered in the weight estimation were not considered in the center of gravity calculation. It was thought essentially impossible to determine values of center of gravity for the surface controls and electronics beforehand. Since their weight is nominal and no reasonable estimate could be made for their location (much less their center of gravity location) they were omitted from the center of gravity calculations. This will have minimal impact on the final results. An example of the Center of Gravity and Static Margin Summary dialog box is provided in Figure 8.1 in order to provide some idea of the detail of the feedback to the designer.

The discussion of the aerodynamic center and static margin values in Figure 8.1 is left for the next section. It can be seen from the figure that values for aircraft takeoff weight (full fuel) center of gravity and aircraft empty weight center of gravity are provided. This gives sufficient knowledge of the fore and aft center of gravity limits of the aircraft. In addition, the designer is provided with the individual component center of gravity moment arm lengths (measured from the front of the aircraft), and the total moment due

to each component. This information can be useful in redesigning the aircraft or replacement of aircraft components to provide a more advantageous mass distribution throughout the aircraft. The strongest argument for this would be if the aircraft had too large a center of gravity shift in its present form, or if one single component was causing the majority of difficulty in making the aircraft longitudinally stable.

Center Of Gravity and Static Margin Summary

Static Margin w/Full Fuel Load	-0.1219		
Static Margin w/Zero Fuel Load	-0.0381		
Aircraft Aerodynamic Center Location		7.06	Feet from the Nose
Wing/Fuselage Aerodynamic Center Location		5.90	Feet from the Nose
Center of Gravity Location w/Full Fuel Load		6.66	Feet from the Nose
Center of Gravity Location w/Zero Fuel Load (Aft CG Limit)		6.94	Feet from the Nose

	Weight (lbs)	Mom. Arm Length (Ft)	Moment (Ft Lbs.)
Wing	267.39	6.31	1688.41
Fuselage	78.68	9.90	778.92
Horizontal Tail	42.81	20.07	859.40
Vertical Tail	34.57	19.41	671.09
Engine # 1 Engine # 2	377.10	1.06	398.04
Engine Nacelle(s)	19.63	0.66	12.95
Payload	200.00	13.35	2670.00
Fuel	800.00	6.31	5051.54
Totals	1820.17		12130.34

OK

Figure 8.1 ***is the Center of Gravity and Static Margin Summary dialog box. It provides enough detail to identify which components pose c.g. or static margin problems for the full fuel, or empty weight phase.***

After this dialog box is closed, the designer is returned to the aircraft geometry specification window, and any of the aforementioned changes can be made. This provides excellent visualization of the problem parameters and their variation to the designer. In addition, the aerodynamic center and fore and aft center of gravity limits are drawn on the aircraft for added visualization. The discussion on the determination of this value is covered in the next section.

8.B Static Margin Calculation

The first value necessary in the calculation of the aircraft static margin was found in the previous section, the aircraft center of gravity. This was calculated for both the takeoff weight and the empty weight, in order to provide some feedback to the designer as to the scale of the change in aircraft handling characteristics throughout the flight. Likewise, as seen in Figure 8.1 the static margin is calculated for both cases.

In order to obtain an estimate of aircraft aerodynamic center for the large variety of configurations considered, the methods used must be widely applicable, and not stricken with limitations that would prevent their use with some of the less conventional configurations. These relations will be presented in the order in which they are calculated beginning with the wing downwash gradient.

It should be pointed out that the method of determination of wing downwash gradient included in this thesis was not the first choice. An attempt was made to use the vortex lattice method to provide wing downwash/upwash data at the location of interest (tail, canard effects on wing, tandem). In principle, it is not difficult to extract the wing downwash information from the Vortex Lattice Method. The same vortices that are integrated in the determination of lift induced drag create the downwash of interest. The difficulty arises in the determination of the ***gradient*** in downwash with angle of attack. In order to obtain the value of downwash angle at another surface, several values of angle of attack must be considered. Once again, the time required to perform these calculations increases too quickly for it to be considered for use with the present methodology. Thus, more traditional methods must be considered.

The ESDU data sheets were considered as a possible source of downwash gradient information. It is, nevertheless, clear from the limits on aspect ratio that any estimation of these quantities would have to originate from a gross extrapolation of these data. The maximum aspect ratio considered in the creation of the graphs was 12. This is practically one half the aspect ratios common in Low Speed HALE UAV's. Furthermore, a brief look at the graphs will demonstrate that the variation in some of the curves cannot be justifiably or reliably extrapolated to the extent necessary.

Thus, the only available methods that remain are those in the common design methodologies. The limitation on the accuracy of these methods is not thought to be

incompatible with the remainder of the present methodology. The most detailed method available is from Roskam[5] (Pt.VI, Ch.8., p.272).

$$\frac{d\varepsilon}{d\alpha} = 4.44\left[K_a K_\lambda K_h \left(\cos\Lambda_{1/2}\right)^{1/2}\right]^{1.19} \frac{C_{l\alpha}|_M}{C_{l\alpha}|_{M=0}} \tag{8.1}$$

Where

$$K_a = \frac{1}{AR} - \left(\frac{1}{1+AR^{1.7}}\right) \tag{8.2}$$

$$K_\lambda = \frac{10-3\lambda}{7} \tag{8.3}$$

$$K_h = \left(1-\frac{z_{HT}}{b}\right)\left(\frac{2L_t}{b}\right)^{1/3} \tag{8.4}$$

$$\beta = \left(1-M^2\right)^{1/2} \tag{8.5}$$

$$\frac{C_{l\alpha}|_M}{C_{l\alpha}|_{M=0}} = \frac{1}{\beta} \tag{8.6}$$

Where z_{HT} is the height of the horizontal tail relative to the wing height. This equation can be used for every configuration except the canard. In the instance of the Tandem Wing, it is applied to the forward wing.

For the canard configuration, several papers have been published on the subject. Mueller[92] stated that as long as the canard is 2 wing chord lengths ahead and the wake does not impinge directly on the main wing, these [upwash] effects are generally small enough to be ignored. A visual inspection from Roskam (Pt.VI, Ch.8, p.274) shows this to be true as well for the wing/tandem distances being considered. In addition, Nicolai[3] suggests setting $\left.\frac{d\varepsilon}{d\alpha}\right|_{can} = 0$. A more detailed analysis would need to be undertaken in order to determine the canard downwash/upwash effects of a specific configuration. A number of papers were mentioned in the Literature Review that refer to more detailed evaluations for the canard effects. It is thought that for early conceptual design, however, that setting canard upwash effects on the main wing in the aerodynamic center calculations equal to zero is appropriate given that $\left.\frac{d\varepsilon}{d\alpha}\right|_{can}$ will likely be small for the canard configurations used. This assumption should be valid up to moderate shifts in the center of gravity in flight. It is mentioned that the lift induced drag effects have been considered for the canard effect on the wing and vice-versa by the vortex lattice method implementation.

The next step in the process is to determine the propeller slipstream effects on the horizontal tail control surfaces. It doesn't require much imagination to realize that this can be quite complicated in implementation given the large number of possible engine locations and configurations. Each configuration was evaluated appropriately, and the equations used for propeller slipstream effects were obtained from Roskam[5] (Pt.VI, Ch.8, p.271) as follows :

$$\eta_{slip} = 1 + \frac{\left(S_{HT,can}\right)_{slipstream}}{S_{HT,can}} \quad \frac{2200.0 P_{avail}}{\pi V_{cruise} D_{prop}^2 Q} \tag{8.7}$$

Where $Q = \frac{1}{2}\rho V^2$, $P_{available}$ is the available HP, and $(S_{HT,can})_{slipstream}$ is the area of the horizontal tail or canard in the propeller slipstream.

Once the propeller slipstream factor has been calculated, the aerodynamic centers of the wing profiles are assumed to be at the respective ¼ chord lines for all but the flying wing sections. After that assumption has been made, the two-dimensional lift curve slope is either taken from designer supplied data (as discussed earlier in the Wing Profile selection dialog box), or the standard two dimensional lift curve slope is assumed. With the lift curve slope $\left(C_{L_\alpha wing\,2D}\right)$ specified, a correction for three-dimensional effects is made from Roskam (Pt.VI, Ch.8, p.248) using the following equation :

$$C_{L_\alpha wing\,3D} = 2\pi AR\left[2 + \left\{4 + \left(\frac{AR\beta}{K}\right)^2\left(1 + \frac{\tan^2 \Lambda_{1/2}}{\beta^2}\right)\right\}^{1/2}\right]^{-1} \tag{8.8}$$

$$\text{Where } K = \frac{C_{L_\alpha wing\,2D}}{2\pi/\beta} \tag{8.9}$$

This equation has been simplified with the assumption that the exposed wing area is equal to the wing reference area, and that the correction for the fuselage diameter relative to the span are extremely small compared to the scale of the answer. These effects were therefore neglected. After the approximate three-dimensional wing lift curve slope is known it is possible to estimate the effect of the fuselage on this lift curve slope. It was attempted to obtain this value through other methods, however the attempt met with the same difficulties encountered in the downwash estimation. None of the methods were appropriate for use with aircraft with such high aspect ratios, and extrapolation was simply not a reliable option. Therefore, a calculated estimate was made using Roskam[5] (Pt.VI, Ch.8, p.272):

$$C_{L_\alpha wing/body} = C_{L_\alpha wing\,3D}\left[1+0.025\frac{w_{fuse}}{b}-0.25\left(\frac{w_{fuse}}{b}\right)^2\right] \tag{8.10}$$

Finally, all of the terms necessary for the determination of the aircraft aerodynamic center (X_{ac}) are available. The aerodynamic center can be found by performing a moment balance about any point in the aircraft. The equation used has been broken into two parts (as in the code) in an attempt to make it easier to read. The equation appears as follows for the general case :

$$X_{ac} = \frac{X_{ac,w/b} + \eta_{slip,HT} C_{L_\alpha HT}\left(1-\frac{d\varepsilon}{d\alpha}\right)\frac{S_{HT}}{S_{ref}} X_{ac,HT} - \eta_{slip,can} C_{L_\alpha can}\left(1-\frac{d\varepsilon}{d\alpha}\Big|_{can}\right)\frac{S_{can}}{S_{ref}} X_{can}}{C_{L_\alpha wing/body}\cdot denom} \tag{8.11}$$

and the denominator term is seen as below :

$$denom = 1+\frac{\eta_{slipHT} C_{L_\alpha HT}\left(1-\frac{d\varepsilon}{d\alpha}\right)\frac{S_{HT}}{S_{ref}} + \eta_{slip,can} C_{L_\alpha can}\left(1-\frac{d\varepsilon}{d\alpha}\Big|_{can}\right)\frac{S_{can}}{S_{ref}}}{C_{L_\alpha wing/body}} \tag{8.12}$$

Where the derivative of downwash angle with angle of attack for the canard is assumed zero for reasons already discussed. For the multiple fuselage aircraft, the additional fuselage interference effects on the lift curve slope are taken into account in the above procedure. Furthermore, for the tandem wing aircraft, the horizontal tail term is treated as the main wing, and the main wing is treated as the horizontal tail. Also for the tandem wing configurations, the wing/body lift curve slope is calculated for both surfaces.

Based on the above equations, and with the aircraft centers of gravity already calculated, the aircraft static margin for the two cases considered is :

$$SM(W_{to}) = \frac{X_{CG,Aircraft}(W_{to}) - X_{ac}}{\bar{c}_{wing}} \tag{8.13}$$

$$SM(W_{empty}) = \frac{X_{CG,Aircraft}(W_{empty}) - X_{ac}}{\bar{c}_{wing}} \tag{8.14}$$

These values, as well as the aerodynamic center and aerodynamic center distance from the nose are provided in the Center of Gravity and Static Margin summary dialog box as feedback to the designer as seen in Figure 8.1 at the beginning of this section. When this dialog box is closed, the fore and aft centers of gravity, as well as the aerodynamic center are marked on the aircraft for the designer to visualize. If the static

margin was too small, it is a simple matter to return to the Center of Gravity dialog box and change the payload location. If a larger change in center of gravity location is needed, the location of any of the aircraft components can be moved and the process begun again. If a satisfactory static margin and range of center of gravity travel have been determined, it is now possible to determine the effects of trim on the endurance of the aircraft.

8.C Trim Condition

The implementation of the calculation of the horizontal tail/canard cruise lift coefficients is different for each configuration, due to the different horizontal tail moment arm definitions and the fact that fuselage effects on moment coefficient are taken into account differently for multiple fuselage aircraft. The governing equations and the procedure are nevertheless essentially the same for each one. First the fuselage effects on the wing moment coefficient are determined from Munk for near circular sections :

$$\Delta_{fuse} C_{m,ac} = -1.8\left(1 - 2.5\frac{w_{fuse}}{H_{fuse}}\right)\frac{\pi w_{fuse} H_{fuse} L_{fuse}}{4 S_{ref}\,\overline{c}_{wing}}\frac{C_{L,0}}{\left(C_{L_\alpha}\right)_{w/b}} F \qquad \textbf{(8.15)}$$

Where $C_{L,0}$ is the lift coefficient with the fuselage angle of attack equal to zero, and F is a shape factor to correct for non near circular fuselage cross sections and is as follows:

$$F = \frac{\text{Actual Cross - Sectional Area}}{\frac{\pi}{4} w_{fuse} H_{fuse}} \qquad \textbf{(8.16)}$$

Once the fuselage effects are calculated, they are added to the wing profile moment coefficient supplied by the designer (or assumed) as follows :

$$C_{m,ac_{w/b}} = \Delta_{fuse} C_{m,ac} + C_{m,profile} \qquad \textbf{(8.17)}$$

Where $C_{m,profile}$ is the wing profile moment coefficient at the cruise lift condition. Next, the combined wing/body moment coefficient about the aerodynamic center found from Torenbeek[7] (p.481, E-9.1) follows:

$$C_{m,w/b} = C_{m,ac_{w/b}} + C_{L_{cruise}}\frac{CG_{avg} - X_{ac,w/b}}{\overline{c}_{wing}} \qquad \textbf{(8.18)}$$

Finally, the desired quantity, tail/canard lift coefficient required for trimmed flight can be found as follows for a conventional configuration :

$$C_{L,HT} = C_{L_{cruise}} \frac{CG_{avg} - X_{ac}}{L_t} + \frac{\bar{c}_{wing} C_{m,w/b}}{L_t} \tag{8.19}$$

Where L_t is the length of the horizontal tail moment arm. The calculation proceeds in a similar manner depending on which configuration is being considered. The difficulty arises in accounting for the various moment arm lengths for the different arrangements. It is not always simple to extract this information. Sometimes a wing or tail ¼ chord is taken into consideration, other times it is the distance measured from the tail or nose. Sometimes the moment arm length is the fractional length of a fuselage, other times it is the fractional length of a boom. Each case is evaluated separately.

Trim Effects Dialog

	New	Old	
Endurance	62.39	65.17	Hours
Power Required	28.90	27.70	HP
Total Aircraft Drag	0.03638	0.03487	
Wing Cruise Lift Coefficient	1.0910	1.0537	
Wing			
Lift Induced Drag	0.01238	0.01109	
Parasite Drag	0.01494	0.01494	
Horizontal Tail			
Lift Induced Drag	0.00036		
Parasite Drag	0.00095	0.00095	

OK

Figure 8.2 ***is the Trim Effects dialog box. It outputs the most recent aircraft endurance based on the detailed weight and drag estimates, and compares that value with the trimmed aircraft endurance in order to highlight the effects of trim drag depending on the configuration and choice of static margin.***

The procedure follows the determination of the tail/canard lift coefficient with an updated calculation of time to climb and average wing loading throughout the cruise phase. This information is used in the updated calculation of the aircraft component drag. The macroscopic component drag results (C_{D0}) are fed back into the endurance calculation in order to provide a fair baseline for the non-trim endurance case. If the drag was not recalculated using revised time to climb and average wing loading values, the comparison of endurance values would not be on the same basis.

Likewise, the non-trimmed endurance is recalculated based on the new macroscopic drag values in order to insure that the comparison with trimmed endurance values is valid. Once the non-trimmed endurance has been calculated in a manner that will provide repeatable results, the trimmed aircraft component drag is calculated based upon the tail/canard lift coefficient value calculated above.

Once the trimmed aircraft drag is known, the final trimmed endurance is calculated and output as seen in Figure 8.2. The trimmed and untrimmed values for Power Required, Cruise Lift Coefficient, and all of the relevant component drags are included in the figure for a better idea of the origins of the differences between the trimmed and untrimmed total aircraft endurance.

The procedure may appear overly complex, however, it is important to note that if this procedure were not followed, the value for non-trimmed aircraft endurance would be based on a lift coefficient resulting from the specification of the basic constants alone, and would not be configuration specific. Finally, throughout the thesis, mention has been made of the problems specific to the implementation of this theory and the methodology in a computational context. This topic will be covered in the next chapter.

Chapter IX

Science is the attempt to make
the chaotic diversity of our sense-experience
correspond to a logically uniform system of thought

--- Albert Einstein

9. Implementation of the Methodology

The theory used in the implementation of the methodology has hopefully been clearly delineated in the preceding chapters. The primary intention of this chapter is to offer some insight into the actual implementation of those equations and relations in the object oriented, event-driven computational environment.

The structure of the methodology has already been provided in Chapter III. In the present chapter, the structure of the ***program*** will be provided, however it will be done in smaller increments. There are compelling reasons for presenting the structure of the program within the thesis. If the equations were simply applied without regard for when or what they were being applied to, the results could be worse than if erroneous equations were used. In addition, in the event driven programming environment, if the wrong or old (preliminary) data were used for calculation of some of the more refined estimates, the results provided would once again be inappropriate. This defines the issue of Data Validation discussed earlier in the Literature Review.

Since it is impractical to include the 15,000 lines of code necessary to animate this otherwise perfunctory methodology, the following approach was thought to be the best manner in which to demonstrate that the application of the theory already covered was done appropriately. Whilst the theoretical aspect of the methodology imposes a large number of constraints in how that theory can be applied, the computational environment imposes equally as many constraints. They are imposed in a manner that is much less forgiving though. For example, the code will crash or provide erroneous results in a more obvious manner. This chapter is also intended to demonstrate that in the programming

environment used, it would be misguided to believe that it is possible to simply program equations into a computer and end up with a computational methodology. A significant amount of original work is involved in the determination of:

- How to obtain information from the designer in a clear, coherent manner
- What information to obtain
- What processes and decisions to leave in the hands of the designer
- How to emulate human processes or decisions when automated
- What analysis is most appropriate to provide for the solution of the problem
- When to provide for the possibility of analysis
- How to validate that the data used is the most recently entered in an event-driven environment
- Whether real-time data feedback is better understood graphically or in a tabular format
- How to present large amounts of data in a clear, coherent manner.

These are all processes that are normally performed by a designer on a subconscious level whenever a conceptual design is undertaken. Each one of these issues will not necessarily be addressed explicitly point-by-point in the following chapter. Nevertheless, these issues permeate each level of the structure of the program. At any point in the program structure, this series of questions can be, and should be satisfactorily answered by the analysis presented in this chapter or by the use of the code itself.

It should be mentioned that many of these issues do not exist for a standard FORTRAN program. Data validation is a non-existent entity in FORTRAN due to the lack of possibility for event driven programming. There is little possibility for graphical feedback, and the format for presenting and obtaining data is the rudimentary command line text. Thus, with the possibility of the graphical representation of data comes the responsibility for clarity in presentation.

9.A Event Driven Programming

The term has been used several times already. It was defined in the Literature Review, but will be repeated since it is crucial to the understanding of the flow of the program structure. The Windows environment and the Visual C++ programming language allow for the existence of a special kind of function (or more appropriately, a class).

Traditional higher level programming languages are executed in a linear manner. The order in which the functions will be executed, and the order in which they can be executed in is determined at compile and link time. Thus, the designer, at a very discrete and predefined time and place in the program is given the option to perform a task or function. If the designer would like to go back one or two steps and re-execute a calculation based on a minor change, the entire program must be executed again. This can be severely limiting in a process where there is the possibility for hundreds of changes. The only solution in this instance is to automate the entire program (to perform all of the hundreds of changes) and remove the possibility of the designer making the incremental changes at run-time. This, despite the fact that most of these hundreds of changes could be eliminated by minimal feedback of the appropriate kind to the designer at run-time.

Once again, it is noted that the aircraft design process is one in which a small amount of graphical feedback can provide the designer with a much better concept as to the correctness of any given value. The sequentially executed program simply cannot provide this feedback in a timely manner.

An event-driven program does not have a preprogrammed order of execution of functions. This order of execution is determined at run-time by the designer. The implications of this are rather far-reaching in the design process. If the designer aspires to make a minor change as mentioned before, it is as simple as the click of a mouse. The order of the program execution can be restricted by the graying of menu items in the window, however this is only performed for the first iteration of the preliminary sizing segment, before necessary variables have been supplied by the designer.

An example with reference to the code used for this thesis would be any operation performed after the creation of the Default configuration. The shape and location of any component on the aircraft can be changed at any time. The drag, weight, center of gravity, trim, endurance, all can be recalculated at any time. Due to the Windows Multiple Document Interface (MDI), several designs can be compared in windows right next to each other in real time, and small changes can be made in each one at any time. Graphical and tabulated results of any changes can be viewed at any time as well. This greatly speeds up the conceptual design process in a way previously unavailable for any UAV's, much less Low Speed HALE UAV's. This is a very powerful programming environment which provides excellent feedback to the designer while keeping the designer in the loop as much as is practical. The cost of this power, though, is that data must be very well organized in

structures, and calculations must be performed in very discrete modules. Another cost of the power is the necessity for presentation of information in a logical, sensible manner, to avoid confusion of the designer in comprehending the input and output mechanism.

With the exception of codes by Raymer[11] and Roskam[12], this type of approach to conceptual aircraft design has not been taken before. Raymer's code is based on a very old DOS-Window type interface, and is restricted in its analysis to conventional aircraft, although any type of aircraft can be drawn, the analysis on the resulting aircraft will not necessarily yield correct results. In addition, there is only the provision to evaluate one aircraft at a time since the DOS/Windows environment does not allow multiple executions of the same program.

Roskam's code is significantly more expensive, and a much more modern implementation, however it is very strongly tied to the equations and aircraft classes available in his books. There is not a single class of aircraft in his books than can be reliably used as a basis for a UAV as shown in the discussion of weight estimates and induced drag calculations. Thus any results from this method would be highly suspect.

It is therefore safe to state that this implementation of a conceptual design methodology for Low Speed HALE UAV's is truly unique. Discussion in the computational implementation will begin with the presentation of the macroscopic structure of the program.

9.B Structure of the Overall Program

It is difficult to graphically depict the implications of simultaneous multiple program instances. A look at Figure 9.1 shows the structure of the program for a single program instance. The easiest way to imagine a simultaneous program instance is to imagine the coexistence of one or many photocopies of the structure shown, each with a discrete identifying tag. Each window created belongs to the function (and data) that created it. With that concept, the data belonging to that window or function is the data which existed at the time of creation, and remains so until a change is made while that window has the program focus. The program focus is simply when the cursor is over a particular window.

Therefore, two windows with two different aircraft can be open simultaneously, yet only one can have the program focus. If a characteristic is changed while a particular window has the program focus, the change will apply to that aircraft alone. Likewise, if a

change is made to the basic constants, then those changes will apply to the last configuration window opened.

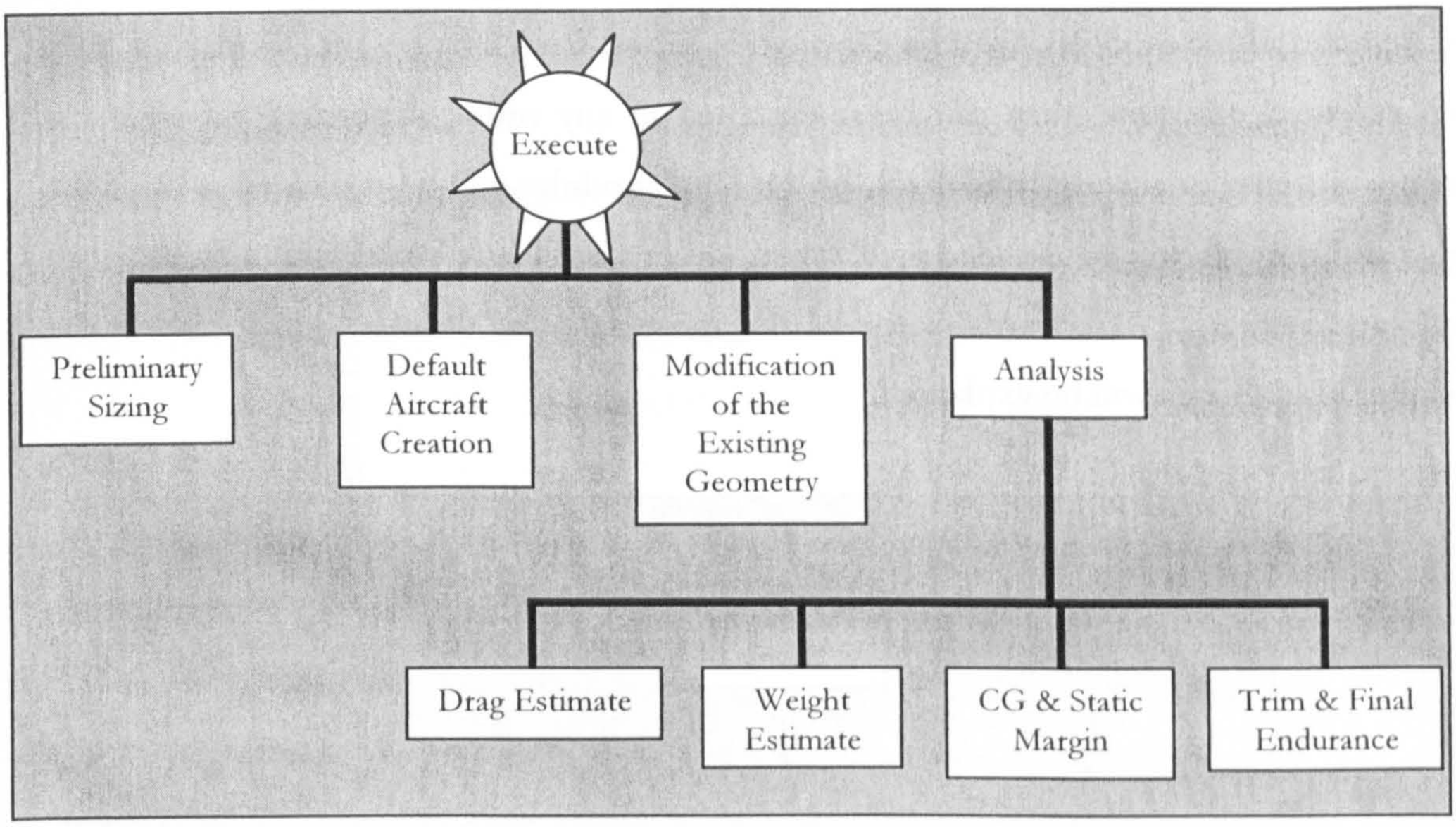

Figure 9.1 ***shows the structure and largest groupings of modules for the overall code.***

Referring to the figure, only the major module headings have been included in the structure. A much more detailed breakdown of the structure of the individual modules will be discussed for the first 3 modules in later sections. The absence of any arrows in the figure is noted. This results from there being no order of operations within the structure. With the exception of the first iteration, any of the modules can be executed in any order. For the first iteration, it is important that the critical constants are specified before other modules are invoked, otherwise there will be insufficient information from which to create the default aircraft. Furthermore, a repeat of the Default Aircraft Creation module will create another Aircraft instance (copy), upon which any of the remaining modules can modify.

The main structure is broken down into Preliminary Sizing, Default Aircraft Creation, Modifying the Existing Geometry, and Analysis modules. In fact, the Default Aircraft Creation is a subset of the Modification of the Existing Geometry module, but will be addressed seperately for clarity.

9.C Preliminary Sizing

The detailed structure of the preliminary sizing module appears in Figure 9.2. For the first iteration, these modules must be executed in series, from left to right. Once they have been executed one time, they can be re-executed in any order, depending on what the designer is trying to accomplish. Each of the local modules will be explained. All of the inputs and outputs will be detailed as if the modules were black boxes with a fixed set of inputs and outputs. Afterwards, some of the more relevant decisions made within the modules/black boxes will be explained.

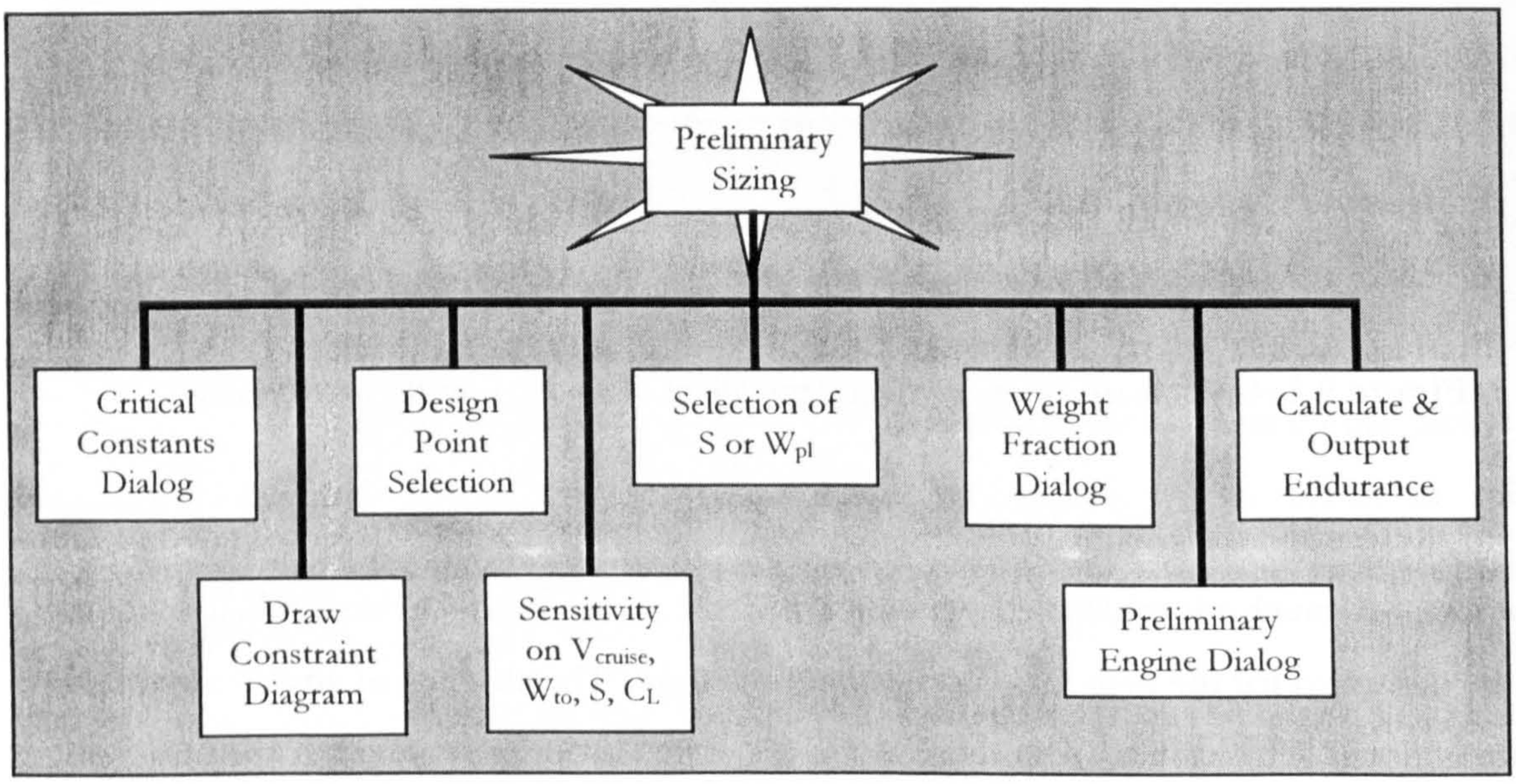

Figure 9.2 ***shows a more detailed breakdown of the structure of the preliminary sizing segment.***

Figure 9.3 shows a different representation of the preliminary sizing segment of the code. It utilizes the graphical user interface to demonstrate which variables are coming from the designer and which are calculated. It also shows the progression of the entry of the variables, from top to bottom for the first iteration.

Beginning with the Critical Constants dialog box, the only variable that is changed at any point within the program is C_{Do}. In reality, the only use for C_{Do} after the preliminary sizing segment is to calculate the aircraft drag in the climb. C_{Do} is changed within the drag routine, to insure that the value used for time to climb is determined using the most accurate data available. In addition, if the designer wants to return to the C_L vs *W/S* graph to determine $C_{lmaxL/D}$ and C_{lminPR}, these values will be recalculated using the

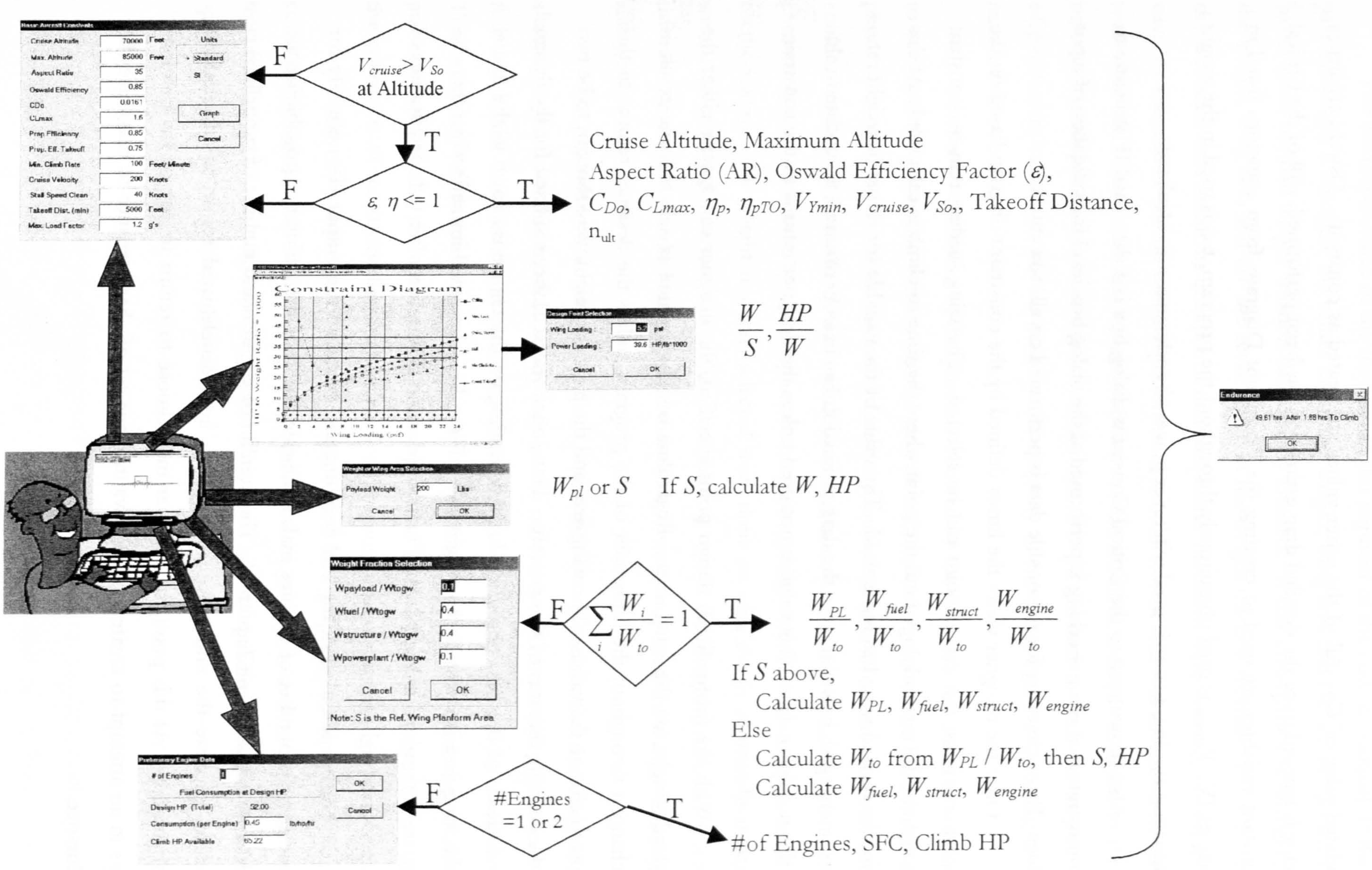

Figure 9.3 ***is a graphical representation of the Preliminary Sizing Segment***

updated value of C_{Do}. All of the other values are treated as constants. Oswald efficiency factor is ignored once the detailed drag estimation has been performed. All of the Critical Constant variables are used in creating the Constraint Diagram from equations listed in Chapter IV. V_{cruise} is used ubiquitously throughout the program, n_{ult} is used in the weight estimation routine, and η_p is used wherever power or endurance are calculated.

Also shown next to the Critical Constants dialog box is a shortened IF structure to demonstrate that error checking is performed at the dialog box level for validation of input values. Error checking for reasonable data is performed on all data entered.

Once the designer views the limits defined by the constraint diagram based on the critical constants, the design point can be selected. The wing loading remains constant throughout the methodology until the point where the time to climb is calculated. At this point the revised wing loading is used. The value of the variable for thrust to weight ratio goes unchanged, however once the drag estimation has been performed, an updated value of this number exists. This value is not used unless the designer returns to the constraint diagram afterwards.

With the (normalized) design point specified, the designer can specify either the payload weight, or the wing area. Regardless of which value is selected, the result is unchanged throughout the remainder of the program, unless the designer returns to this point to change the values. The wing area and the payload weight were thought to be two of the defining features of this aircraft. Thus, once selected, they are fixed for the design downstream of this selection. The logic depending on the choice is shown in the figure. If the wing area is selected, the weight and HP can be determined immediately, otherwise they are determined in the Weight Fraction Selection dialog box after the specification of the payload weight fraction.

The specification of the fuel consumption based on the output HP necessary for cruise and the number of engines makes the calculation of the endurance possible by the procedure explained in Chapter IV. The number of engines (and number of propellers) is used to calculate the endurance and is then immediately used to set up the default configuration. At this point the designer may choose to return to any of the previous steps in an attempt to create a more advantageous set of characteristics to maximize the endurance.

The interdependence of the modules in this segment of the code is minimal. If the payload weight is changed, the values of aircraft weight, wing area and HP are recalculated based upon payload weight fraction data already entered. If this information is changed, the weight, wing area and HP are recalculated in the weight fraction module. If either of these conditional statements in either of their respective functions were omitted, the values used in calculation of the aircraft performance would not be the values the designer wanted to use. This is the first instance of data validation, albeit a simple case due to the minimal interdependence of the other modules thus far. In the next module the majority of parameters calculated will be used by the majority of modules, thus complicating the matter dramatically.

In terms of emulation of the process followed by the designer, this module sought to automate the phase that verifies that the aircraft will not violate any of the basic laws of physics. In other words, based upon the designer provided Critical Constants, the mission could be satisfied. The feedback was mostly graphical in nature, as this would be the most commonly used form used by the designer at this phase, independent of the computational methodology. The weight fractions selected were done so with the knowledge that the weight fraction information was either available, or could be roughly deduced from information available in the literature, and these values were only used for the preliminary sizing segment.

The procedure followed was left as open-ended as possible for the designer, allowing a return to any module at any step in the procedure. This models the process followed by the designer at this phase in conceptual aircraft design as closely as possible. The repetitive calculations were removed from the hands of the designer, the results presented graphically, and the final endurance provided. These results are in addition to the availability of sensitivity diagrams for a few of the more relevant parameters.

Finally, it is mentioned out of interest that the graphing routine used was completely original. All of the logic for the scaling of the grid-lines, axes, titles, symbols, legend, line types, colors, text style, numbers, and active coordinates were created specifically for this program by the author.

9.D Creation of the Default Aircraft

The basic structure of the process followed in the creation of the default aircraft can be seen in Figure 9.4. The process is initiated by the selection of the configuration by the designer. This defines the configuration for the function (class) MainConf. This is the main class for all of the configurations. It draws the window, buttons and the aircraft. It is therefore responsible for calling all of the functions responsible for geometry definition seen in the figure. The Default Configuration case is in fact a subset of the class MainConf. It was drawn this way to demonstrate that even though the procedure for creating the default aircraft is the same as for a designer modified aircraft, the inputs and outputs of the modules will be shown to be completely different.

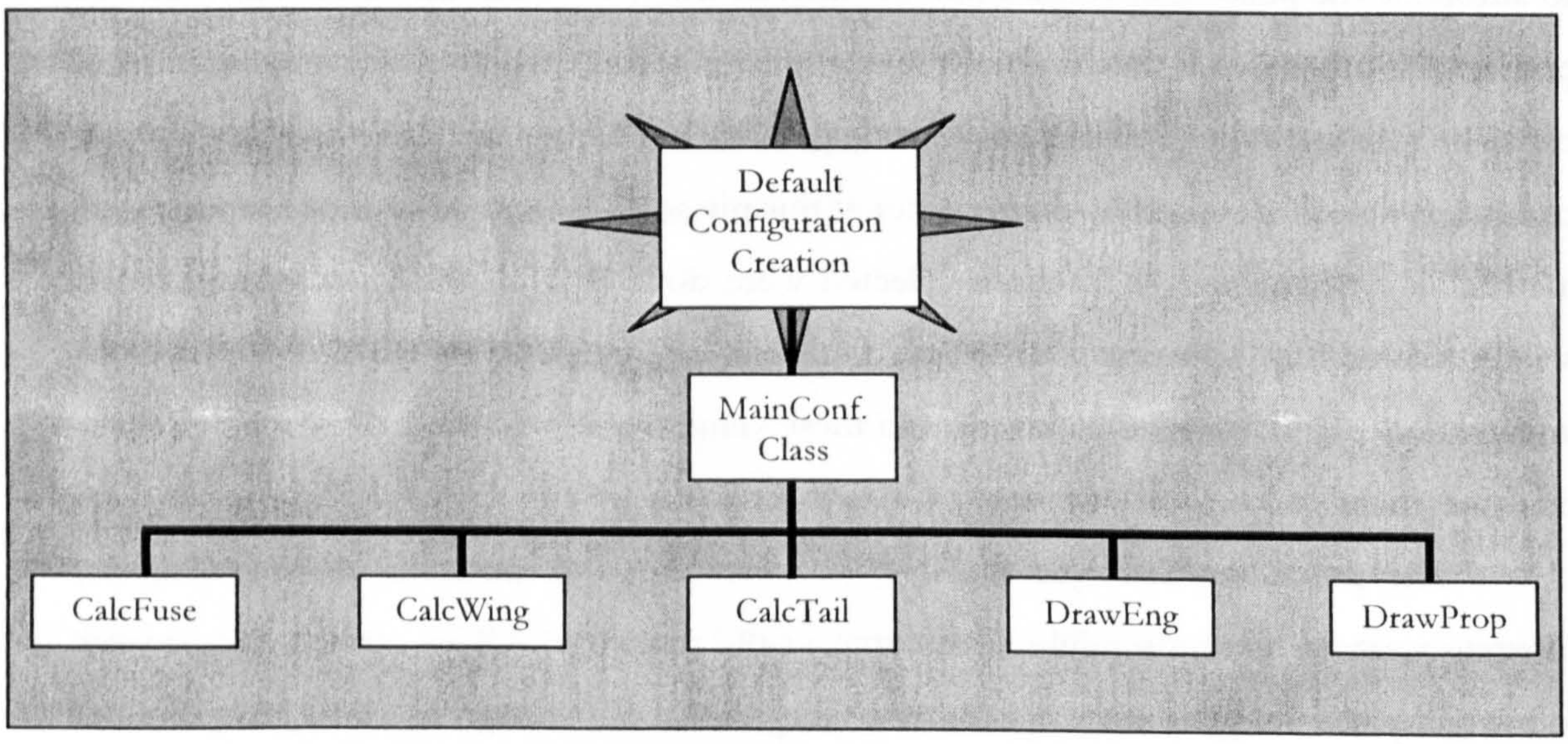

Figure 9.4 ***shows a more detailed breakdown of the structure of the Default Configuration Creation segment, which is actually a subset of the Modification of the Existing Geometry segment.***

The respective inputs and outputs of each function are provided in Figure 9.5. The double-headed arrow under MainConf implies that all information is passed through this class before the next function is invoked. Even though the last two functions appear to have very little in the way of input, in fact, the majority of the input is inherited from the previous functions. For example, function DrawEng requires the wing sweep and coordinates of the wing in order to place the engines on the wing of a swept wing twin engine configuration.

For the output of the MainConf class there are terms with the prefix hRgn. hRgn is an object called a container that holds all of the geometric qualities of an item. Thus,

hRgnTail holds the geometry of the tail. This makes it much easier to deal with as a data structure. One of the regions has been defined as hRgnTail. For the purposes of the implementation of the program this makes handling the data and data interface simple. In the program, an event handler is written for the click of the left mouse button. If a mouse hit is detected in the region bound by the points in hRgnTail, the Tail constants dialog box is invoked. It would be this simple if it were not for the coordinate transformation.

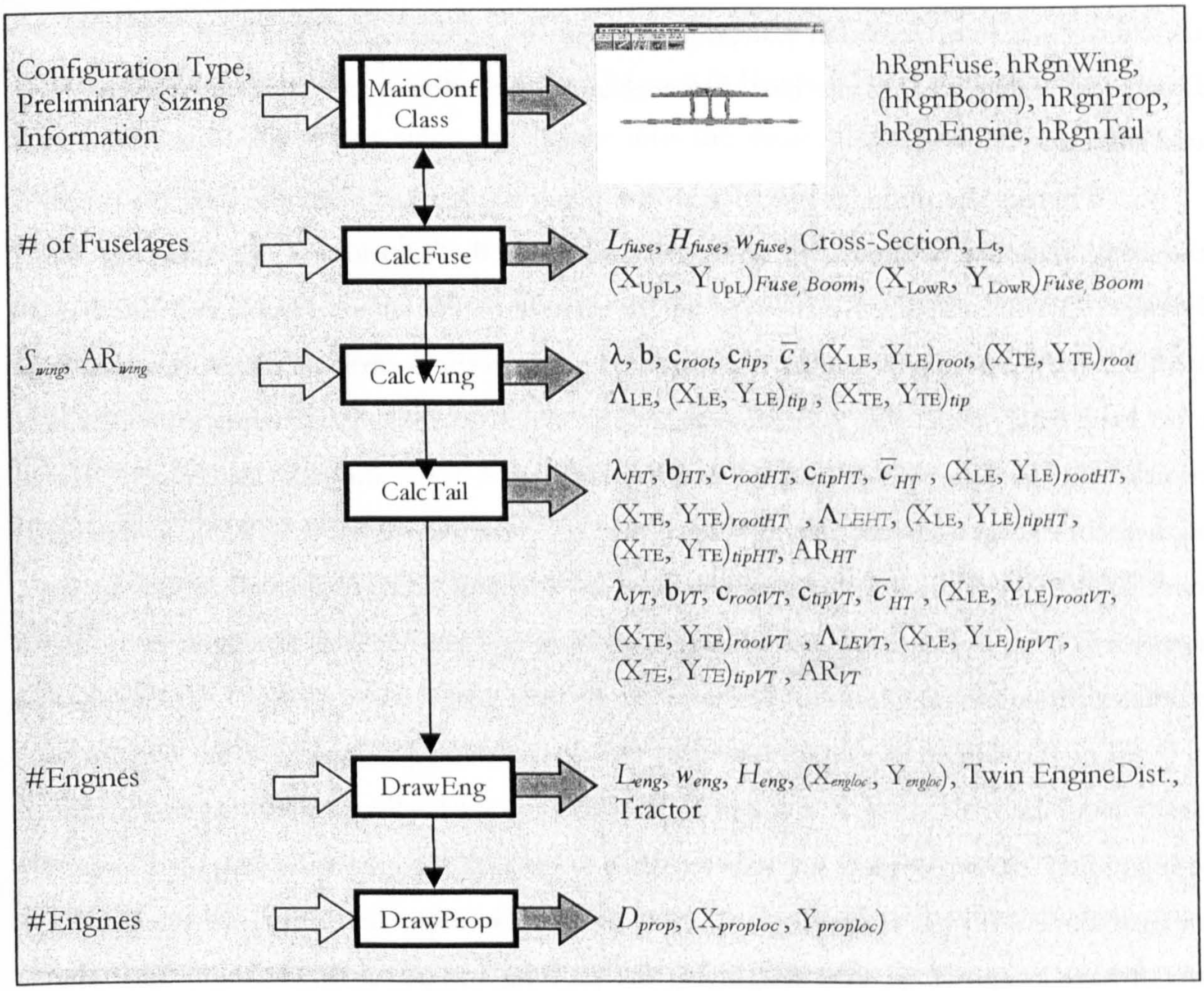

Figure 9.5 ***details the inputs and outputs of the more important modules that are invoked by the class MainConf in the process of drawing the Default Configuration.***

In creating a geometric representation of the aircraft on the screen, the bounds of the screen must be determined in advance. Then the span and length of the aircraft must be calculated. Once this has been done, a coordinate transformation is performed in order to insure that the aircraft will fit on the screen regardless of the manipulation of the size of the window. Thus, if the coordinates are transformed and scaled to make the aircraft fit,

the transformation must be performed every time the aircraft or any component of the aircraft is plotted.

If a mouse hit has been detected, the coordinates must be transformed from the device coordinates to the logical coordinates. The transformation performed is different for Canard configured aircraft. The reason for this is that the main wing is much farther aft on Canard aircraft. The main wing apex was selected as the origin of the window for all configurations. The default origin in Windows is the upper left corner. So, not only are the coordinates transformed in scale, but the origin is also displaced. The entire process of fitting and scaling to find the best distances and proportions can only be performed by trial and error.

Whereas the designer would grab the paper napkin and sketch a wing planform, the computational methodology must first establish the location of the wing on the fuselage. Then compare the fuselage length relative to the screen height, and the wing span relative to the screen width. Then it must perform the coordinate transformation. It must have ALL of the wing geometric data defined before drawing, including exact X,Y,Z coordinates for the wing leading and trailing edge root and tip locations. The mathematical/trigonometric relations necessary to extract those exact X,Y,Z coordinates must be derived. They are not very complex for constant taper or a single sweep angle, however if both leading and trailing edge angles are specified as well as a taper ratio, the geometry and interdependence of variables can be quite involved.

For the default configuration case, the drawing and placement of the engines is greatly simplified. If there is a single engine, the engine is always placed in the tractor configuration. If two engines are selected, they are always placed on the wing in a tractor configuration. With the exception of the Flying Wing configuration, none of the default aircraft have swept wings, thus simplifying the plotting and placement further. Since the logical structure used in the creation of the default configuration is a simplified subset of the actual structure used for all possible configurations, the discussion of the details within each function will be left for the next section.

For the default configuration, there is no further data to obtain from the designer. The decision as to what data to obtain was incorporated into the Preliminary Sizing segment in order to make that data available for the creation of the default configuration. The processes and decisions that are made for the designer are comprised mainly of the default tail volume coefficients. They are the only quantities that cannot be changed

immediately following the creation of the default configuration. Many decisions and assumptions were made, and they were clearly stated in the theoretical section of this thesis. These decisions were intended to create quantities that would otherwise be difficult to obtain based on reasonable assumptions. At any rate, any geometrical characteristic of the default configuration can be manipulated the instant it has been created.

For this segment, it was thought that graphical feedback in the form of a scale drawing of the actual aircraft would be the best form of feedback. This is essentially what the designer would do in the absence of the program, except that it would take considerably longer for each iteration. As can be seen in Figure 9.5, data validation is not a huge problem at this point since the inputs into the default configuration are rather limited, however, it is a problem.

It was made impossible to re-specify the number of fuselages without creating a new instance of the MainConf class. This means that in order to change the number of fuselages, the designer must re-select the configuration, thus creating a new Default Configuration window. The first problems in Data Validation occur with the creation of the Default Configuration window and the way the variables for wing area, aspect ratio, and number of engines are specified.

Imagine that an instance of the MainConf class is initiated called TwinBoom1. TwinBoom1 is initiated based on set values for these three variables, S_{wing}, aspect ratio, and Number of Engines. So a window exists with the corresponding aircraft having these geometric characteristics. In the event that the designer returns and changes the Aspect Ratio, S_{wing} , or Number of Engines, there is no problem, unless there is another configuration window open (TwinBoom2). In this instance a conflict would arise if not addressed. This happens because the newly entered data will over-write all previous information and change it for both TwinBoom1 and TwinBoom2.

There are three alternatives to overcoming this difficulty. The first is to have a another copy of the code running simultaneously. The second is to restrict the number of configuration windows open within a program execution at any given time to just one. This will insure that any change initiated by the designer is intended for the configuration that is being worked on. The third alternative is to create a global container class which holds in it ALL of the data for any given aircraft. The difficulty with this third choice is that there is a very large amount of data associated with any given aircraft configuration. This would limit the number of configurations that could be compared at any one time,

and would also impair the speed and limit the extent to which the vortex lattice method could be implemented without exhausting available memory.

The present incarnation of the code includes in it portable classes making possible the first and third approaches. It was thought, however, that the restriction to a single configuration window was worth the sacrifice in extra memory. At least until the amount of memory on the average computer increases somewhat. It is noted that this does not restrict the number of constraint diagrams, or the number of changes that can be made to any given configuration without having to restart the program. It simply allows only a single configuration window to be open at any time. The way in which those changes are handled by the existing functions and structure introduced in this section will be discussed in the next section.

9.E Modification of the Existing Geometry

The structure of the Modification of the Existing Geometry segment of the program can be seen in Figure 9.6. By pressing any of the buttons or the respective part of the aircraft with the mouse, the recalculation of the interdependent variables has been initiated. MainConf is called any time that the window must be redrawn. Any time a dialog box is opened, the window must be redrawn. Thus, if the designer changes any of the geometric parameters using the dialog boxes, the entire aircraft geometry is recalculated (including all of the interdependent variables) using the new geometrical characteristics. The actual details for how this is implemented are mired with exceptions for every configuration and for every component of the aircraft. An attempt will be made to show the interdependence of the functions based on the inputs to each function. This is necessary since it has changed significantly from the case of the Default Configuration discussed in the previous section.

There is a large amount of sharing of calculations between the dialogs and the functions for the respective aircraft components. It was difficult at the time of the original writing of the program to decide which calculations should be made at the point at which the data are input and which calculations needed to be performed every time the window was repainted. Consequently, the content of both the dialogs and the functions changed considerably during the evolution of the code.

In the previous section, a diagram was shown that displayed the inputs for each of the functions responsible for calculating the geometric characteristics of the aircraft. In the figure mentioned above, the input side has fundamentally changed. Before the inputs came from a series of dialog boxes that were completed long before the calculation of the geometry of the aircraft. Now, as seen in Figure 9.6, the majority of the inputs come directly from the designer.

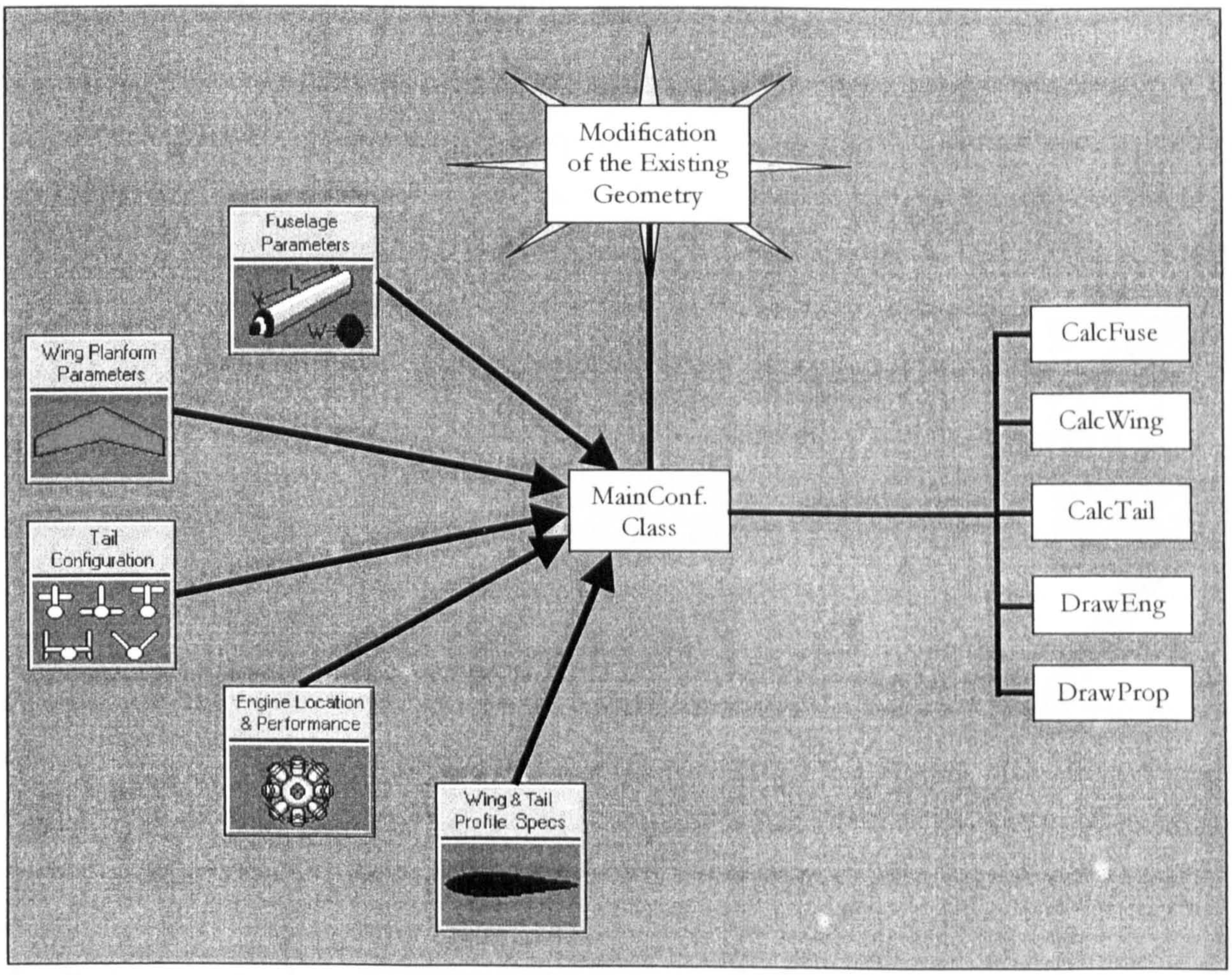

Figure 9.6 ***shows the choices presented to and the interaction between the designer and the class MainConf in the process of re-drawing the designer specified aircraft.***

Rather than try to repeat the previous diagram of inputs into the functions and the resulting geometrical characteristics calculated based on those inputs, another type of diagram has been created. From Figure 9.6 above, it can be seen that any time any of the geometrical dialog boxes is opened, the MainConf class is called and the respective component functions are executed in top down order. Figure 9.7 shows what happens in between.

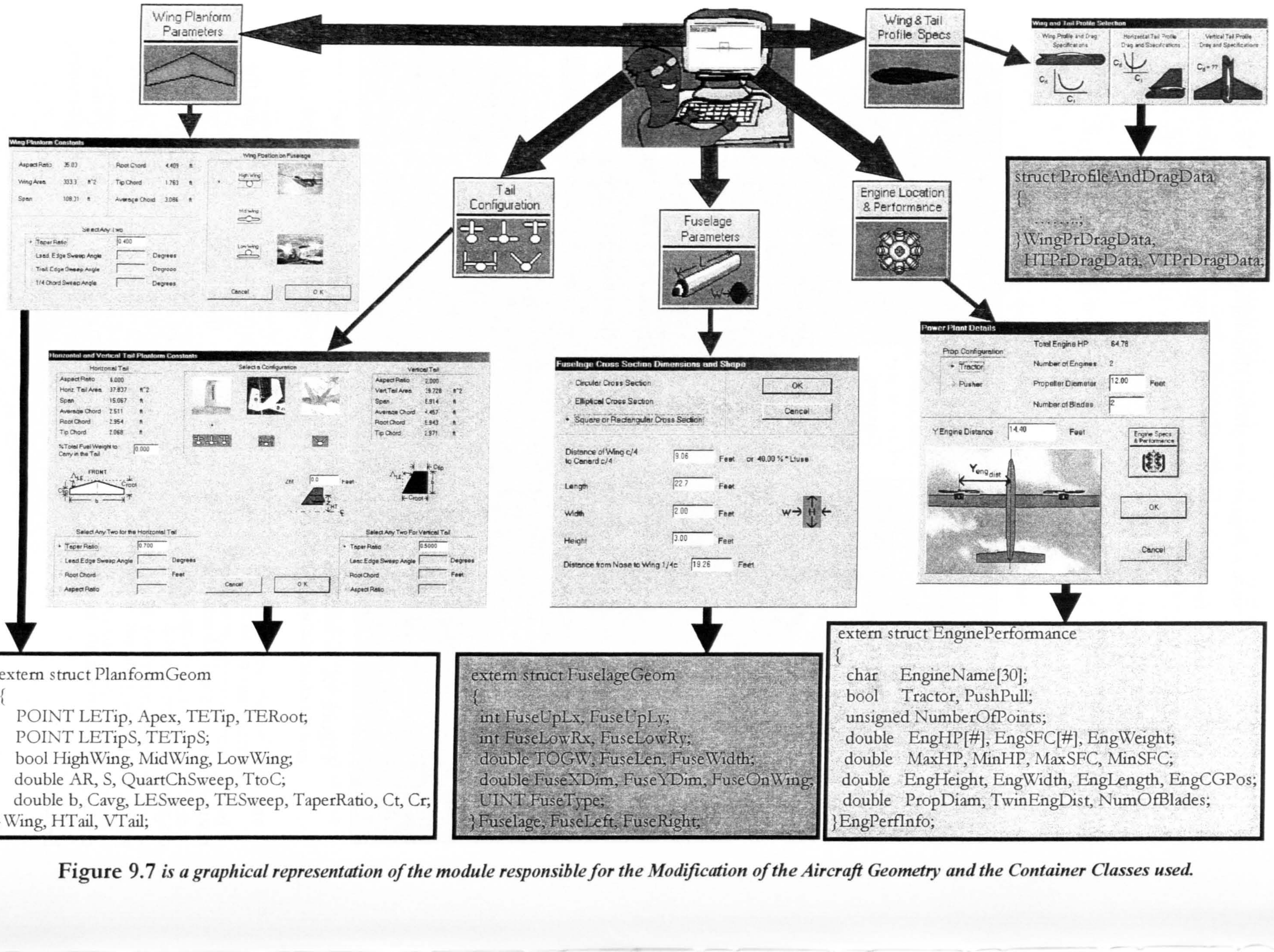

Figure 9.7 ***is a graphical representation of the module responsible for the Modification of the Aircraft Geometry and the Container Classes used.***

As mentioned earlier, a series of container classes were set up based on specific parts of the aircraft. If the designer presses the Wing Planform button in the configuration window (or clicks the mouse on the wing) in Figure 9.7, the procedure shown results. First the dialog box is opened, then the designer inputs whatever changes in the geometry that are desired. In the next step, the information that has been changed is placed into a specially designed container class, in this instance called PlanformGeom. It is noted that the same basic structure is used for the Wing, Horizontal Tail (HTail), and the Vertical Tail (VTail).

The respective names of the variables are thought to be intuitive, and therefore will not be explained individually with the exception of the variables TtoC (thickness to chord ratio), LETipS (Leading Edge Tip, Starboard X,Y,Z position), TETipS(Trailing Edge Tip, Starboard X,Y,Z position). The data type ***POINT*** is a structure with 3 members, X, Y, and Z. Therefore, LETipS.x is the leading edge tip, starboard side x coordinate. The data type ***bool*** can only have two values, TRUE or FALSE. A ***double*** data type is equivalent to the FORTRAN double precision statement.

A great deal of organization and thought goes into deciding how to set up a container class, and what to include in the container. There is such a high degree of inter-connectivity between the various components of the aircraft it is not a simple matter to create these classes. Take for example the aircraft geometry, the classes shown are rather intuitive. These classes work rather well for the aircraft geometry definition. Once the aircraft geometry definition phase is finished and the drag and weight estimation phases begin, the geometric containers become unwieldy. This occurs since all of the individual geometric characteristic containers are required in order to perform either the weight or drag analyses.

As another example, look at the EnginePerformance container. EnginePerformance is actually a misnomer. The container holds performance and geometric information. Thus, for half of the functions that the container is used for, it will carry too much information and clutter memory. This is an obvious compromise. Here all of the engine information is together in one place, however this results in a large amount of information being exchanged without being used.

Consider the example of the DrawProp function. The function is called every time the window is repainted. It uses the EnginePerformance container class. Thus, every time the window is repainted all of the engine fuel consumption array information is loaded

into memory, and subsequently unloaded without being used when completed. Obviously, care must be taken in order to prevent too many of these types of situations from slowing the program down considerably.

These are all considerations that do not exist in a FORTRAN implementation of a methodology. In FORTRAN, the most likely procedure would be a bulk COMMON statement placed in every program module/subroutine that uses the arrays. Thus the power and modularity of a structured programming language can be as beneficial as detrimental depending upon the implementation.

There was insufficient room to show the following structure in Figure 9.7 it can be seen in Figure 9.8 below.

```
struct ProfileAndDragData
{
   char        ProfileName[20], DragName[20], AlphaName[20];
   bool        WhichGraph;
   unsigned    NumProfilePts, NumDragPts, NumAlphaPts;
   double      X[400], Y[400];
   double      Cd[400], Cl[400], ClAlpha[400], Alpha[400], Re;
   double      MinCd2, MaxCd2, MinCl, MaxCl, mClAlpha, Cm;
}WingPrDragData, HTPrDragData, VTPrDragData;
```

Figure 9.8 ***shows the Wing/Tail Profile and Drag Data container class, which is associated with the Wing/Tail Profile dialog boxes.***

This class contains the information necessary for reproducing the lift-drag curve for the wing or tail profile. It contains the coordinates necessary for reproducing the airfoil shape, it holds the lift coefficient versus angle of attack curve and slope, the moment coefficient, the airfoil name, and the calculated maximum and minimum of each curve used for scaling and comparison. It is much more efficient to evaluate the maximum and minimum at the time that the file is read in since the data must be buffered anyway. It was done at this time rather than performing the evaluation every time the curves or data are used. There are numerous other classes created for use with drag, weight estimation, center of gravity, static margin, and trim specific information.

It is noted that the Power Plant Details dialog box and the Wing and Tail Profile Selection dialog box open into subsequent dialog boxes. This allows for the specification of more information by the designer. Unfortunately there was insufficient space to include

them, however they were included in the original discussion of the geometric characteristics in Chapter 5 in Figure 5.8 and Figure 5.10.

One topic that has yet to be discussed is the determination of which variables to place in the dialog box, and which variables to fix. For every input dialog box many difficult decisions must be made relating to how much control to keep in the hands of the designer. Even more important, though, is the case where a number of variables may be specified. The decision as to which characteristics will be of the most interest to the designer is not always intuitive or obvious.

For the Wing Planform dialog box, the process was not that difficult since the designer was restricted to changing only a taper ratio and a sweep angle or two sweep angles due to the fact that the aspect ratio and the wing area were fixed. Another important related question is what information (in the form of feedback to the designer) is desired prior to a change in the geometry. In the Wing Planform dialog box, aspect ratio, wing area, span, root chord, tip chord and average chord were provided. In addition, the most recent value for taper ratio was initialized into the edit box automatically.

The best example of the difficulty in deciding what to place in a dialog box and how to handle the information input is the Tail Configuration dialog box. In the final incarnation, the designer may specify any two out of the four variables, taper ratio, leading edge sweep angle, root chord, or aspect ratio. This results in a very complex decision tree with over 16 branches. The same tree exists for the vertical tail as well. Many of the branches must assume values from previously specified variables. The process of deciding which are the most intuitive is a rather long one. In addition, it is a very time consuming process to solve every individual geometric equation in terms of every possible variable.

Once the changes have been specified by the designer, another decision tree is entered. First based on the aircraft configuration, then based on the number of engines, then based on the engine configuration, as there are different tail volume coefficients for all 55 different possibilities. The discretizing of even some of the most simple human thought processes can be rather involved. The designer performs these decisions almost without conscious thought. For the computational implementation of the geometric calculations for the vertical and horizontal tails, over 1000 lines of code were necessary. This does not include the Tail dialog box which was another 665 lines!

Another important consideration is that the dialog boxes must change depending on which configuration is being considered. The Tail dialog and the Fuselage dialog are

not the same for a conventional configuration as they are for a canard. The canard configuration requires more information resulting from the difference in the way the canard and main wing are placed on the fuselage. The Power Plant dialog is different depending on whether the aircraft is a single or twin engine, whether if a twin, the aircraft is a Push-Pull or a simple Pusher or Tractor.

It is hoped that the dialog boxes created for use with the geometric specification of the aircraft requested the data in a clear and coherent manner. At times it was impossible to justify the provision of one variable over another, and the end result was personal preference. At other times, the variables provided for selection were the only choices available. It is thought that those geometric quantities selected for specification by the designer are the best given the information available at the time.

Many assumptions had to made in the instance of just one variable being supplied when the possibility of two variables being entered was allowed for. The example of the Tail dialog is used once again. If the designer only specified taper ratio to be changed, constant tail area was assumed along with constant root chord. There were a number of other possibilities, but this was the one selected. If the possibility to specify more variables were allowed, it would have been very easy to allow for over-specification of the quantities. All of these concerns were considered when designing the dialog boxes and the most intuitive choices were made.

No matter how it is stated, though, decisions were taken out of the hands of the designer. Unfortunately, there was no other way to proceed in most instances without prompting the designer with an extensive list of choices every time a minor change was made in one quantity. Again, it was thought the geometric characteristics that the designer was allowed access to, provide for enough control to change the overall and aerodynamic shape of either tailplane. In terms of attempting to model the human thought process, it is believed this is the area that is most lacking in originality of implementation. The decision trees and SWITCH statements used are clumsy and unwieldy to code, but efficiently converted into assembly code for fast processing. Thus, another compromise has been made.

For this particular segment (Modification of Geometric Characteristics), much of the data was tabulated in dialog boxes, but much of the data was plotted in the shape of the aircraft. This is an excellent form of feedback, and probably gives the designer the first "feel" for whether the numbers make sense. In addition, any changes made in any of the

dialog boxes appeared instantly on the plotted aircraft. In this segment the designer could enter the wing profile, C_D-C_L curve, C_L-α curve, fuel consumption versus HP curve, and visualize all of the data plotted on a graph immediately afterwards. This aspect of the methodology adds greatly to the robustness of the model. It allows for advancements in engine or aerodynamic technology to be included in the analysis at a later time. Finally, a very large amount of data has been made available to the designer, all in a simple and easy to use interface. All of these characteristics help to greatly speed up the conceptual design process, but also help to understand the interdependence of many of these characteristics.

9.F Analysis of the Aircraft

The analysis of the aircraft is much less dependent upon active input from the designer. The majority of the information needed to perform the analysis has already been specified by the critical constants and the geometry. The only data that need be input regards the payload size, dimensions, and center of gravity location. If no values have been specified for wing profile, engine center of gravity, and various other variables, the designer is notified at the time of the calculation involving that quantity of the fact that a value is being assumed. It was thought necessary during the analysis phase to inform the designer of the assumptions being made due to the absence of any designer entered data where the possibility was allowed for this data to be entered. Otherwise the results are almost exclusively in the form of tabulated data with the exception of the plotting of the aircraft fore and aft centers of gravity and the aircraft aerodynamic center (see Figure 6.14, Figure 8.1, and Figure 8.2).

The results of the analysis modules culminate with the aircraft trimmed endurance. In addition, weight and drag component breakdown, power required, time to climb, component center of gravity, and static margin detailed results are available. This output is the direct result of the aircraft defined by the designer. It does not represent an optimized aircraft or converged solution to perform a given mission for a given weight, nor was it intended to. It does, however, represent the detailed performance capability of the aircraft specified by the designer. The methodology was created as a tool to identify the driving parameters in the design of a Low Speed HALE UAV. This process will be highlighted in the Results chapter. The results output to the designer were detailed enough so that if a

change needed to be made to any particular component weight or drag after the execution of the program, the total could be recalculated at a later time based on the information output.

The procedure followed during the analysis segment is essentially linear or sequential in nature. Thus, apart from the fact that the interface is a window and the fact that container classes were used for the transfer and portability of data, the code follows almost directly from the theory section. The only exceptions to this are the configuration specific problems which add markedly to the complexity of these modules. In many instances a different calculation must be performed for every different configuration being considered leading to very large decision trees.

An attempt was made in this chapter to highlight the differences between a structured event-driven computational methodology, and the concept that equations can simply be programmed into a computer for the creation of a computational methodology. Many of the details of how decisions were made, or which assumptions were made for the designer in setting up the geometry of the aircraft were left unaddressed as they do not have any impact on the final results and only affect intermediate stages of the geometrical setup. The most important quantities fixed by assumption were the tail volume coefficients, and they were presented and validated where possible in an earlier chapter. Many of the more minor decisions/assumptions made were simply not included for brevity, though there were hundreds if not thousands.

Chapter X

There is a time in the life of every problem
When it is big enough to see,
Yet small enough to solve

--- Mike Leavitt

10. Results and Discussion

This chapter is separated into three major sections. The first section validates the macroscopic results of the methodology by comparing them to existing configurations and their known (or claimed) performance. The second section expands on the results of the validation by presenting detailed results for the conventional configuration.

Since the only configuration that could be validated within a comfortable range of certainty was the conventional configuration, the initial expansion of the results is performed for the conventional configuration alone. This section identifies and explains any trends arising from the variation of the many possible design parameters, all within the bounds of the conventional configuration. The evaluation and discussion involves the macroscopic and microscopic changes resulting from changes in as many of the most relevant design parameters as time would permit the evaluation of.

Finally, the third section will draw from the most relevant results for the conventional configuration. The consequences of these results will be incorporated into the analysis and presentation of the results for the alternative configurations.

10.A Validation

This section will undertake the most complete validation possible based upon physical and performance specifications available from the popular literature. It is noted at the beginning of this section that reasonable assumptions had to be made in some cases for several of the more relevant variables that were unavailable. In some instances the results should be viewed with a limited amount of skepticism. Any assumptions that needed to be made are mentioned, and the effects of these assumptions are included where possible, and where it was believed additional analysis would be most relevant. The values used as input for the validation of each aircraft are tabulated in **Appendix B**. The values that were most commonly unavailable in the literature and were thus necessary to assume were as follows:

Used **Only** For the Time to Climb Calculations:

- Oswald Efficiency Factor = 0.85
- C_{Do} = 0.0161
- Takeoff Propeller Efficiency = 0.75

Other Values Commonly Assumed:

- Cruise Propeller Efficiency = 0.85
- Maximum Lift Coefficient = 1.6
- Airfoil Selection: NLF(1)-1015
- Limit Load = 3.5 g's
- Engine Specific Fuel Consumption = 0.4 lbs/HP/hr.

It is mentioned once again that the specific fuel consumption and cruise propeller efficiency appear directly in the Breguet Endurance equation. It is thus obvious that these assumptions have a fundamental impact on the *ABSOLUTE* endurance results. For this reason, the results for absolute endurance cannot be validated in a closed form manner within this thesis. Values resulting from the methodology for endurance will be cited for each case, however without accurate values for propeller efficiency and specific fuel consumption these endurance values may be in error in excess of a factor of four at times. In general, it is more reasonable to evaluate the accuracy of the methodology based upon the aircraft empty/structural weights and the power required in cruise and climb.

10.A.1 Boeing Condor

The *Condor* was the aircraft with the most detailed information available. Despite the relative wealth of information available for *Condor*, a number of assumptions still needed to be made. The Liebeck airfoil used for the *Condor* main wing was not available, as a consequence, the NLF(1)-1015 airfoil was used. At a Reynolds number of close to one million (based on average wing chord), this represents the upper end of Reynolds number expected for this class of aircraft.

In order to ensure that the choice of airfoil had a minimal effect on the results for the validation of the methodology, the Wortmann FX 63-137 was also tested. A minimal difference (on the order of minutes) in final endurance was found between the implementation of the two airfoils in the results for the *Condor*.

The propeller efficiency was not available, however a value of 0.85 was used. When this value was increased to 0.9, the respective increase in endurance was roughly 5%, so the strong effect of the propeller efficiency on overall aircraft endurance can plainly be seen. The same experiment was performed for the specific fuel consumption by increasing it from 0.4 lbs/HP/hr to 0.44 lbs/HP/hr. The subsequent endurance decreased by approximately 9%. This is as expected by the presence of both the propeller efficiency term and the specific fuel consumption term in the Breguet endurance equation.

The value for Oswald efficiency factor (used only to determine the time to climb) was also unknown. It was assumed to be 0.85. An increase in this value to 0.9 resulted in an increase in endurance of 11 minutes (out of 56.56 hours total), and a corresponding decrease in time to climb of 11 minutes. This quite obviously represents a minimal effect on the overall results. All of the remaining values input into the methodology originated directly from widely published literature.

The *Condor* held the endurance at altitude record for piston reciprocating engine aircraft at 58.18 hours at 66,980 feet of altitude. This includes the time required for descent (cited as less than 3 hours), but does not include the time to climb. The present methodology predicted an endurance (not including descent time) of 56.56 hours with 2.98 hours time to climb. This represents a maximum possible error of less than 3 percent before taking into consideration the descent time, which only reduces the error. In terms of the macroscopic endurance results this is much more accurate than expected.

Since no details of the drag breakdown of the aircraft are known, the specific drag details cannot be discussed. The predicted cruise power required was below the cited HP available from the *Condor's* engines. This is expected since it was determined from the results that the engines of the Low Speed HALE UAV are sized based on the climb and not the cruise requirement. In general, the macroscopic solution would appear to validate the overall aerodynamic prediction. Slightly more detail was available with regards to the weight breakdown, however.

The breakdown of the component weights can be seen in Table 10.1 for the *Condor*. The methodology (over) predicted the aircraft empty weight by 120 pounds. This is impressive given the 6200 pound empty weight of the *Condor*, and even more impressive when the 18,700 pound takeoff weight is considered. The wing weight, however, was cited to be 2 lbs/ft^2 and the method predicted the wing weight to be 2.6 lbs/ft^2 as shown in the Weight Estimation chapter. From the limited amount of weight data available for this aircraft, it was impossible to determine which corresponding component(s) were under predicted in weight by the remaining 540 pounds. It was unclear, however, if the published wing weight was the weight of the entire wing with fuel systems, actuators, etc., or was just the average material density resulting from the finished empty wing structure.

Table 10.1 *is a table of the component weights predicted by the methodology for the Condor.*

	Weight (lbs)	%Empty Weight
Wing	3019	47.87
Fuselage	383.2	6.075
Horiz. Tail	244.5	3.876
Vert. Tail	177.0	2.806
Engine(s)	1290	20.45
Nacelle(s)	124.4	1.973
Fuel System	570.5	9.044
Cntrl Sfcs	235.8	3.738
Elec/Avion.	262.6	4.163

10.A.2 Aurora Flight Sciences Perseus B

The *Perseus B* is perhaps the most perplexing of all of the aircraft validated against. Although values had to be assumed in accordance with Section 10.A for propeller efficiency and Oswald Efficiency factor (assumed values for each aircraft can be seen in **Appendix B**), the airfoil characteristics were made available from the literature.

The origin of the perplexing behavior was due to the manner in which the performance data were provided in the literature. Endurances of both 8 and 18 hours were reported in the literature, for a payload of 176 pounds. Taking the payload weight along with the cited empty weight (998 pounds) and the cited maximum takeoff weight (2200 pounds) provided for enough fuel for the methodology to predict a 60.76 hour endurance. As a result of further research, it was discovered that the limitation in the endurance of the *Perseus B* was not in fact performance related, but due to the size of the fuel tank used (20 gallons). The 18 hour endurance cited was for a doubled fuel capacity of 40 gallons using external pods.

Under these circumstances for fuel fraction and total takeoff weight (1292 lbs and 1409 lbs respectively for the 20 US gallons of fuel and 40 US gallons of fuel cases), the predicted endurances were 11.7 hours and 22.2 hours respectively at 60,000 feet. The time to climb was estimated at 0.7 hours for both cases and suggests that the specific excess power available throughout the climb is lower than that resulting from the assumed 65 HP. This also suggests the inability to maintain Sea Level power up to altitude with the Rotax engine implementation. When the endurances are adjusted by the difference in the time to climb, the resulting values are 9.95 and 20.42 hours respectively.

Finally, the empty weight predicted by the methodology was 862 pounds for the 20 gallons of fuel case, and 920 lbs for the 40 gallons of fuel case. The cited value for the actual *Perseus B* empty weight was 998 pounds. These predictions would classify as reasonably accurate due to the weight and drag implications of the presence of landing gear on the *Perseus B*.

10.A.3 Aurora Flight Sciences Theseus

As already seen in Table 4.1, the *Theseus* has the highest structure fractional weight $\left(\frac{W_{struct}}{W_{to}}\right)$ of any of the HALE UAV's evaluated (except for the previous generation *Perseus A*). The *Theseus* also has the lowest HP to weight ratio of any of the aircraft evaluated. These factors have an obvious direct impact on not only the final endurance and time to climb, but also the weight estimation. Since the *Theseus* engines were derived from the Rotax 914, the fuel consumption for that engine was assumed for this aircraft.

It is first noted that the *Theseus* never flew above 22,000 feet before experiencing an in flight breakup, so all of the cited performance numbers are estimated based on the calculations of Aurora Flight Sciences engineers. Aurora Flight Sciences literature cited the total engine power at 160 HP. If the climb power is set to this value, the aircraft takes 15.5 hours to ascend to the cited endurance cruise altitude of 82,000 feet. Thus the 160 HP value was assumed to be a cruise power setting. The Rotax 914 has a full throttle rating of roughly 110 HP for each engine. Assuming a conservative combined twin engine climb power of 200 HP, the aircraft takes a slightly more reasonable 9.3 hours to climb. The endurance at 82,000 feet for *Theseus* was cited as 10 hours.

The methodology predicted an endurance of 16.48 hours at a power required of 201 HP using the fuel consumption of 0.4 lbs/hp/hr. It is believed that this fuel consumption could not be maintained up to 82,000 feet, however there simply were no other data available for the estimate. Despite the higher power required calculated by the methodology (normally one of the most fuel efficient power settings for the Rotax 914) compared to that given by Aurora Flight Sciences, the fuel consumption is suspected for the difference in endurance (when the predicted empty weight difference is taken into account). Another possible explanation is the same phenomena witnessed with the *Perseus B*, where the reported maximum takeoff weight of the aircraft is not in fact possible due to limitations in the fuel volume of the existing tanks.

For all of the aircraft where the cruise velocity was not published, the cruise velocity was set based upon the known wing loading and a cruise lift coefficient as close to 1.3 as possible. As will be shown later, the impact on the aerodynamic efficiency resulting from changes in lift coefficient are small for robust Low Speed high lift coefficient airfoils. In the case of the *Theseus* the maximum lift to drag ratio lift coefficient is close to this value. The minimum power required lift coefficient was however, as with most Low Speed HALE UAV's (due to the extremely high aspect ratios), too large to be practical without the use of high lift devices. No other assumptions needed to be made for this aircraft.

Most importantly, though, the weight estimation module under-predicted the weight of this aircraft by 1500 pounds (out of a total empty weight of 5166 pounds from the literature). This can partly be explained by the fact that the aircraft has an uncharacteristically high structure fraction when compared to other aircraft in the class. It is noted that the wing weight per square foot predicted for *Theseus* was over 3.5 lbs/ft^2 and the weight estimation method still under-predicted the weight of the aircraft. It is also

noted that the outer wing for this aircraft held no fuel and was constructed to satisfy FAR 23 standards (+3.5 g load). Finally, in the methodology, if the empty weight is under predicted, this weight is replaced by fuel to keep the takeoff wing loading and takeoff weight the same. In this instance, the endurance is increased by the amount of the weight difference times the required cruise HP times the fuel consumption.

For the remainder of the difference in estimated weight, it is beneficial to consider the layout of the actual aircraft. *Theseus* is a twin engine aircraft where the engines are in relatively large pods on the wing. These pods double as structure for the main landing gear and also contain a large amount of fuel. In addition, they house a rather intricate gearbox and prop-shaft which allows for a bizarre pusher-propeller arrangement giving greater propeller/ground clearance. None of the other light-to-medium weight aircraft evaluated have such an intricate implementation.

10.A.4 Scaled Composites Raptor

It is noted that the *Raptor* was designed as optionally piloted, and was never designed as an unmanned aircraft. This will have obvious effects on the weight estimation and center of gravity of the aircraft. In addition, the aircraft never performed at altitude, and the performance numbers cited are again the result of the calculations of Scaled Composites engineers based on known lower altitude performance.

The *Raptor* is another aircraft propelled by a Rotax engine. In the earlier literature for this aircraft it was cited as having a Rotax 912, however it was expected that if funding materialized it would be retrofitted with a Rotax 914. Apparently the funding did not emerge and the retrofit has not happened so the performance of this aircraft was estimated using extrapolated Rotax 912 data. The reason the data was extrapolated was that the predicted cruise power for this aircraft was 23.4 HP. This is below that provided by the Rotax Company data. At such a low power setting the Rotax 912 is not nearly as efficient and a fuel consumption of approximately 0.65 lbs/HP/hr was used in the endurance calculations.

The *Raptor* presented a curious problem. Given the geometrical data for the aircraft, the aircraft center of gravity and static margin were reasonable, however the wing was directly behind the engine with little clearance and there was no possibility of instrument visibility in the forward portion of the aircraft. Despite these problems, the

performance of the aircraft in this configuration was given in the literature as 48 hours. The altitude was assumed to be 60,000 feet since the claimed ceiling was 65,000 feet.

Roncz airfoils were specified for this aircraft for the wing, vertical, and horizontal tails, however these airfoils are not available in the literature so the usual NLF(1)-1015 was assumed with the NACA 0009 used for the tail sections.

The endurance of this aircraft was thus calculated at 48.17 hours with a 1.75 hour time to climb using the 0.65 lbs/HP/hr fuel consumption. This represents 6.57 hours lost to trim, however it results from using the geometric configuration given in the literature. Using a specific fuel consumption of 0.4 lbs/HP/hr, the endurance was calculated as 88 hours, with only 4 hours lost to trim. Much of this is possibly due to the inability of the methodology to take into account the "optionally piloted" mode.

Finally, the weight of this aircraft was under-predicted by a mere 10 pounds (out of 850 pounds empty weight), however it was unclear as to whether or not the values given for the weight fractions of the aircraft represented the fully unmanned, or "safety" piloted mode. In addition, given the presence of landing gear on this aircraft, this result would again classify as a slight over prediction of the weight.

10.A.5 General Atomics Altus

In evaluating the *Altus* the most important factor to remember is that this aircraft was for the most part designed as a low to medium altitude aircraft. The engine was modified for high altitude flight, and the modifications to the geometry of the existing low altitude aircraft consisted mostly of wing-tip extensions, an enlarged vertical surface above instead of below the fuselage, and a shorter overall fuselage length due to reduced payload capacity.

Referring again to Table 4.1, it can be seen that the *Altus* has the third highest structure weight fraction, 18% below that of *Theseus*, yet 24% higher than the *Raptor*, the next closest true HALE UAV.

With those considerations in mind, the estimated empty weight for the *Altus* was 190 pounds under (out of a total empty weight of 1220 pounds) the actual empty weight. It is strongly believed that if this aircraft were designed as a high altitude aircraft the actual empty weight would have been much lower thereby reducing the 15 percent error in the weight estimation, with fixed landing gear accounting for the remainder of the difference.

This weight difference accounts for an increase in predicted endurance of approximately 7 hours at the cruise HP.

The power required to cruise at an altitude of 65,000 feet was predicted to be 64.2 HP. This is in the more efficient range of the Rotax 914 providing a fuel consumption of 0.4 lb./HP/hr. Given the reasonably high wing loading of this aircraft (for a lightweight Low Speed HALE UAV), the cruise velocity was fairly high at approximately 225 knots. The claimed endurance for the *Altus* was 30 hours at the given altitude. The methodology predicted an endurance of 32 hours with 0.67 hours time to climb.

10.A.6 General Atomics Predator (RQ-1A)

Although the *Predator* is not a high altitude long endurance aircraft, there was sufficient information available to predict the weight and endurance of this aircraft using the methodology. The *Predator* uses a Rotax 912 for which fuel consumption information is available. It was suspected before undertaking the weight estimation that the methodology would under-predict the weight of the *Predator* due to the fact that it was designed for much lower altitude operations and thus would need to withstand greater gust loading and need greater damage tolerance.

Despite these considerations, the weight estimation method predicted an empty weight roughly 10 pounds under that of the actual empty weight of 770.75 pounds. Since the *Predator* operates at such lower altitudes and far off of the optimum for the Rotax 912, the fuel consumption was taken directly from the Manufacturer's data as 0.6 lbs/HP/hr which is roughly equivalent to 2.3 U.S. gals/hr in cruise.

Predator has an endurance of approximately 40 hours taken at an assumed altitude of 20,000 feet. The methodology predicted an endurance of 39.3 hours with a 250 pound payload.

10.A.7 Israeli Aircraft Industries Heron

Once again, this aircraft is designed as a medium altitude long endurance aircraft, however it is a Twin Boom Pusher configured aircraft and could potentially provide interesting validation results. Also, again, it was suspected before undertaking the analysis

that the weight estimation module would under-predict the empty weight of this aircraft since it was designed for lower altitude cruise and loiter.

From the literature, the *Heron* has a maximum velocity of 125 knots. The cruise velocity was taken as 110 knots at an altitude of 25,000 feet. The published maximum altitude is 32,000 feet. The greatest unknown in the prediction of this aircraft's performance was the engine. The engine used was unknown, but was given as a 4 cylinder turbocharged engine, rated at 100 HP. The published endurance was given as 40 to 50 hours.

An endurance of 61 hours at 36.5 HP was predicted by the methodology. This is most likely a much lower HP rating than the aircraft is actually flown at, however it results from assuming a high cruise lift coefficient similar to high altitude flight in the absence of a more relevant value. The difference in predicted endurance results from the additional weight of fuel replacing the weight by which the structure was under predicted.

As suspected, the weight estimation module under-predicted the weight of the *Heron* by 275 pounds (out of a total empty weight of 1315 pounds). Again, this is believed to be more a result of the fact that the aircraft is a low-to-medium altitude aircraft with landing gear than a result of any error in the Twin Boom configuration weight estimation. In addition, the *Heron* is designed with the possibility of a large external payload. This would also serve to increase the empty weight of the aircraft.

10.A.8 Scaled Composites Proteus

Although this aircraft is primarily a manned aircraft, its unusual Tandem Wing configuration provided an interesting opportunity for some basis of comparison using the methodology to apply to less conventional configurations. Additionally, this aircraft is built with the possibility of adding wing tip extensions to both the fore and aft wings depending on the mission. The *Proteus* was designed with the ability to add payload pods of varying size and shape to the underside of the aircraft fuselage. All of these characteristics make the weight estimation of this aircraft less accurate.

Extremely accurate fuel consumption data at altitude were obtained for the Williams FJ44-2 engines used from a source working on high altitude turbojet powered aircraft. In the literature, the *Proteus* was listed with a best ***range*** cruise of 190 knots. At 60,000 feet, this gave the aircraft a cruise lift coefficient of 1.5. It was thus assumed that this was not

the maximum ***endurance*** velocity. Even though the Roncz airfoils used could have been capable of operating at these lift coefficients, it is thought unlikely that this value would be selected for best endurance. Thus a cruise velocity of 205 knots was assumed using a more reasonable lift coefficient of 1.4. The Williams engines are listed as having a total weight of 1100 pounds. This was verified as an installed weight in conversation with Burt Rutan. Finally, a fuselage diameter of 3 feet was assumed. All other values were known for this aircraft.

The methodology predicted an endurance of 21.5 hours at 60,000 feet with a 2000 pound payload. The value for endurance cited in the literature for these conditions for the *Proteus* was an endurance of up to 14 hours. Due to the error in the estimation of the weight of this aircraft, it is difficult to know the source or magnitude of the error in endurance as once again the weight remaining from the structural weight under prediction was replaced with fuel. One possibility is that the average Reynolds numbers experienced by this aircraft are higher than what the methodology was created for which would effect the prediction of the drag.

The predicted empty weight was 4018 pounds. The actual empty weight of the *Proteus* is 5900 pounds. Again, the reasons for this rather large difference are due to the manned pressure section of fuselage, controls, instruments, unknown fuselage diameter, optionally extended wing tips, and hard points on the fuselage for carriage of external payload pods, 6 foot long main landing gear, dielectric construction of certain sections of the aft wing, and a thickened inboard section due the presence of flutter.

10.A.9 Teledyne Ryan Global Hawk (RQ-4A)

Once again, it is noted that the methodology was not explicitly intended for the design of turbojet or turbofan aircraft. The most important module which will not predict well under these conditions is the drag estimation module. The *Global Hawk* loiters at 343 knots which is well into the regime of compressibility at altitude, and at the very least, compressibility factors would need to be included in order to more accurately predict the drag of this aircraft. In contrast, the weight estimation of this aircraft should be reasonably accurate. There is some information available on the component weights, and this information will be used to validate the weight estimation module of the methodology.

Table 10.2 *lists the estimated and actual component weights for the Global Hawk.*

	Estimated Weight (lbs)	Actual Weight (lbs)	Error (%)
Empty	8479	9120	-7.02
Wing	3067	2915	5.21
Fuselage	1169	1540	-24.1
Empennage	264	330	-20.0
Landing Gear	N/A	1100	
Fixed Equip.	996	895	11.3

Given the input parameters (**Appendix B**) for the *Global Hawk*, the methodology predicted weights and actual component weights can be seen in Table 10.1. The overall empty weight compared quite well, however, with the exclusion of landing gear in the weight estimation module of the methodology, several component weights must have been overestimated. A brief look at the table shows that the wing weight was predicted with a high degree of accuracy. The fuselage was predicted underweight by a very large margin. This can be explained by the fact that the methodology was designed to predict the weight of fully composite fuselages having simple shapes, and the *Global Hawk* uses a combination of construction techniques and a very complex fuselage shape. In addition, there is no mechanism to incorporate the weight of the ducting for the engine used in the *Global Hawk*. The installed weight of the Allison AE 3007H was used in the methodology (2660 lbs), however, it is unclear as to whether this weight included the weight due to the ducting/inlet for the engine.

The weight of the empennage was under predicted by almost 25%. The impact of this under prediction is rather small on the overall weight estimation due to the small relative value of the weight of the components (less than 4% of aircraft empty weight). One possible explanation is that the V-Tail configuration support structure is greater than that of a conventional tail. The impact (on the weight) of the proximity of the engine and engine exhaust to the tail is also unclear. Finally, the fixed equipment was over predicted by over 11%. There was no further information available for the remainder of the component weights. It is mentioned, however, that a landing gear weight of 1100 pounds is almost 12% of the takeoff weight of the aircraft and must include the weight of hydraulic systems and actuation. The weight of these control and actuation systems were taken into account by the surface controls weight group in the methodology.

Finally the endurance was predicted as 41.12 hours, with the 1800 pound payload. The endurance for the *Global Hawk* is cited as over 40 hours. Given the closeness of the weight estimation and the accuracy of the fuel consumption values used, the error most likely originates from the aerodynamic prediction and the fact that compressibility was not taken into account.

10.A.10 Summary of the Results of the Validation

It is difficult to perform any kind of closed-form validation of the methodology. Given this difficulty and the limitations of the data available from the literature, the methodology provided reasonable results in all instances, and excellent results in most for an early conceptual design methodology. A tabulated summary of the endurance and empty weight predictions and their respective errors are provided in Table 10.3.

Table 10.3 ***summarizes the results of the validation on aircraft endurance and empty weight.***

	ENDURANCE (hrs)				EMPTY WEIGHT (lbs)		
	Methodology	Cited	Error (%)	@SFC	Methodology	Cited	Error (%)
Condor	56.56	56.18	**0.68**	0.4	6307	6188	**1.92**
Perseus B	9.95	8	**24.4**	0.4	862	998	**13.6**
Perseus B	20.42	18	**13.4**	0.4	920	998	**7.82**
Theseus	16.48	10	**64.8**	0.4	3666	5166	**29.04**
Raptor	48.17	48	**0.35**	0.65	840	850	**1.18**
Altus	32	30	**6.67**	0.4	1030	1220	**15.57**
Predator	39.3	40	**1.75**	0.6	759	771	**1.49**
Heron	61	40-50	**27.5 (max)**	0.4	1040	1315	**20.91**
Proteus	21.05	14	**50**	-	4018	5900	**31.39**
Global Hawk	41.12	>40	**~**	-	8479	9120	**7.02**

Even though the endurance values must be viewed with skepticism due to the suspect nature of the occasionally unknown fuel consumption values, the overall methodology showed amazing flexibility in duplicating the results of known aircraft. As a verification, none of the cruise power required values predicted were greater than the engine HP values cited in the literature. It was clear from the above results (especially *Theseus*) that the engines are sized more on Time to Climb requirements than cruise requirements.

For the aircraft in which the most information was known, (the *Condor*) the results from the methodology were excellent. The aircraft with the greatest error in weight, all

had uncharacteristically high structural weight fractions for High Altitude aircraft, had configurations not optimized for High Altitude flight, or simply were not High Altitude aircraft.

10.B The Conventional Configuration

The methodology was validated primarily against the conventional configuration. Thus, the first and most detailed set of results was generated from the application of the methodology to this configuration. A logical progression of parameters was studied and is detailed in the subsequent sections. Given that this thesis and methodology have been built around the maximization of aircraft endurance at altitude, the analysis and explanation will be presented with direct reference to the individual terms in the endurance equation and their relative influence on final aircraft endurance. In addition, a parametric variation is performed specifically to isolate the effects of each parameter on overall aircraft endurance.

10.B.1 Breguet Endurance Equation Revisited

For clarity, the Breguet Endurance equation is recited below :

$$Endurance = \frac{550\eta_p}{SFC}\sqrt{2\rho_{cruise}\left(\frac{S_{ref}}{W_{to}}\right)}\left(\frac{C_L^{3/2}}{C_D}\right)\left(\sqrt{\frac{1}{1-\frac{W_{fuel}}{W_{to}}}}-1\right) \qquad (10.1)$$

with units in hours. The propeller efficiency is not very widely known for this class of aircraft, however its influence is rather simple to correct for. As long as a constant value is used for all of the results, the general trends for endurance will be correct, assuming reasonably similar operating conditions.

The specific fuel consumption (SFC) is a parameter that was possible to include in the overall analysis. It was decided, however, that the results from using any particular set of engine performance curves would be specific to that engine, and would likely hide the driving aerodynamic and weight trends for which this thesis was intended to uncover. For this reason, a constant value of specific fuel consumption corresponding to the known value for *Condor* was used for all calculations. While it is realized that this assumption

will impact the absolute results for total aircraft endurance, it does not preclude the ability to obtain absolute endurance values at a later date when specific engine data is available. It would be possible at any later time to simply multiply the endurance by the constant fuel consumption assumed, and divide by the value of fuel consumption for Horsepower required in cruise (already output from the methodology) for the conditions corresponding to the results of interest.

The air density in cruise is only a function of the cruise altitude. A study on the variation of cruise altitude is included for interest. The next term of interest from the Breguet Endurance equation is essentially takeoff wing loading. For the following study, wing loadings of 5, 10, 15, 20, and 25 lbs/ft^2 were considered at takeoff weights ranging from 2,000 to 20,000 pounds.

The final two terms will be referred to as the endurance term and the fuel fraction term respectively. These terms reflect the most useful output from the methodology.

The effects of the endurance term are further narrowed by the assumption of a constant lift coefficient throughout all but one of the studies. Based on the definition of lift coefficient and its application to the endurance equation, the choice existed to either select a constant cruise velocity or a constant lift coefficient as a basis for comparison of all configurations and all parametric variations. Given that the lift coefficient is a more useful aerodynamic and design indicator, it was selected as the constant value. In order to understand the implications of this decision, a study was performed on the variation of lift coefficient. It is noted, though, that it was impractical to assume a constant velocity across the parameters (takeoff weight, wing loading) being considered as the resulting range of lift coefficients would have been unrealistically large.

The variation in the fuel fraction term will be studied closely. Given the above assumptions made regarding the Breguet endurance equation, the behavior of the final endurance with any variation in parameters can and will be traced back to the fuel fraction $\left(\sqrt{\frac{1}{1-\frac{W_{fuel}}{W_{to}}}}-1\right)$ and endurance $\left(\frac{C_L^{3/2}}{C_D}\right)$ terms. It is again noted that the average lift coefficient has been kept constant. Consequently, the changes in the endurance term for a given configuration will result from the degree of travel of the center of gravity (as fuel is

expended), the change in shape of the wing lift distribution (resulting from varying the magnitude of the wing loading), and due to Reynolds number effects.

Thus, the extent to which the endurance equation can be *directly* influenced by input into the methodology is limited to the selection of the Cruise Altitude, the Wing Loading, the Takeoff Weight and either the Wing Area or the combination of Payload Weight and Payload Weight Fraction. Since payload weight was thought to be of more practical interest, this parameter was selected.

The endurance equation can be indirectly influenced by a much larger number of parameters. These have been categorized into three major areas, Wing Geometry, Operating Conditions, and Engine Configuration. It is noted that although Cruise Altitude is a variable directly effecting the endurance equation, it has been placed into the Operating Conditions section. The parameters selected for study within each area will be discussed in subsequent sections. The discussion of the general results for the Conventional Configuration will proceed with the variables directly influencing the endurance equation.

10.B.2 General Results from the Variation of W/S, W_{to}, and W_{PL}/W_{to}

A general study was performed on the Conventional Configuration. Takeoff weights of 2000, 5000, 7500, 10000, 15000, and 20000 were considered. For each takeoff weight, four wing loadings were considered, either 5, 10, 15, and 20 lbs/ft^2 from 2000 to 10000 pounds, or 10, 15, 20, and 25 lbs/ft^2 for the 15000 and 20000 pound cases. The reason that the same wing loadings were not considered for all weight cases is the limitation on practical span given the assumed aspect ratio of 35. For each wing loading, 3 payload fractions were considered, $\frac{W_{PL}}{W_{to}} = 0.05$, 0.10, and 0.15.

These takeoff weights were selected within the range of limits to single and twin engine internal combustion reciprocating engine unmanned aircraft. They were chosen to allow for the academic study of the variation of the parameters affecting the endurance performance of the Low Speed HALE UAV, not to imply that a 2000 pound aircraft with a 10% payload fraction could satisfy the same mission as a 20,000 pound aircraft with the same payload fraction. In addition, the study undertaken was not intended to give the

illusion of determining the ***optimum*** takeoff weight for a given desired endurance. The study was intended merely to identify the magnitude of the effect of variation of certain key aircraft configurational conceptual design parameters.

The conditions for which all of the following results (for this section) were generated under were the following :

- Cruise Altitude of 60,000 feet
- Limit load factor of 2.25 g's (from *Condor*)
- Lift coefficient of 1.3
- Aspect Ratio of 35
- Specific Fuel Consumption of 0.4 lbs/HP/hr (from *Condor*)
- Propeller efficiency in cruise of 0.85
- HP to weight ratio of 0.035 (used only to size the engine for climb)
- Oswald efficiency factor of 0.85 (used only for time to climb calculations, VLM used for C_{di})
- C_{do} of 0.0161 (used only for the preliminary time to climb calculations)

Several of these parameters will be the focus of study in later sections. For now, the discussion will begin with the presentation of the total endurance results using these parameters. Following that section, the fuel fraction and endurance term results will be presented in an attempt to clarify the underlying behavior of the overall endurance.

10.B.2.a Endurance Results

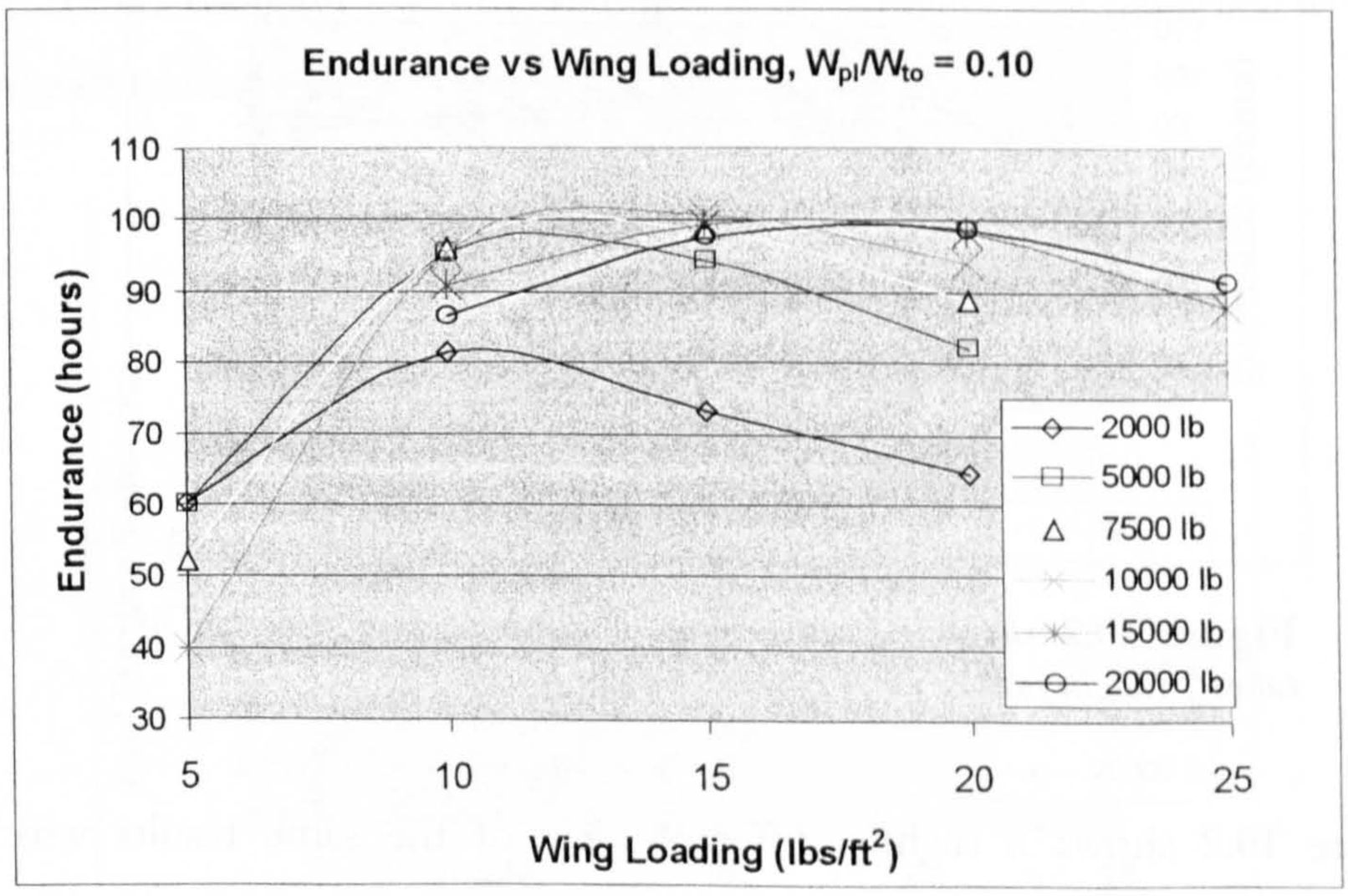

Figure 10.1 ***shows the overall aircraft endurance for the 10% payload fractional weight case as a function of wing loading.***

The general shape of the variation in endurance as a function of wing loading can be seen in Figure 10.1 for the 10 percent payload fraction case. Similar behavior was seen for the other payload fractions. The only difference between the various payload cases was the magnitude of the maximum values for the curves collectively. The shape and trends of the curves for the 3 different payload cases were otherwise identical. As can clearly be seen, the optimum wing loading in terms of overall aircraft endurance is dependent upon the payload/takeoff weight desired for the conditions assumed for these results.

A definite trend exists in the overall endurance as a function of wing loading. The optimal wing loading experiences a gradual shift from 10 lbs/ft^2 for the 2000 pound case to between 10 and 15 lbs/ft^2 for the 5,000, 7,500, and 10,000 pound cases, and between 15 and 20 lbs/ft^2 for the 15,000 and 20,000 pound cases. The reason for this gradual shift will be explained in the next section. The higher takeoff weights appear to maintain their optimum value for a much broader range of wing loadings. This would make these aircraft more versatile, however they need to be since they will burn comparatively more fuel supporting their additional weight in cruise. Also worth noting is the relatively poor overall performance of the 2,000 pound takeoff weight case. This phenomenon will be further discussed in the aspect ratio section.

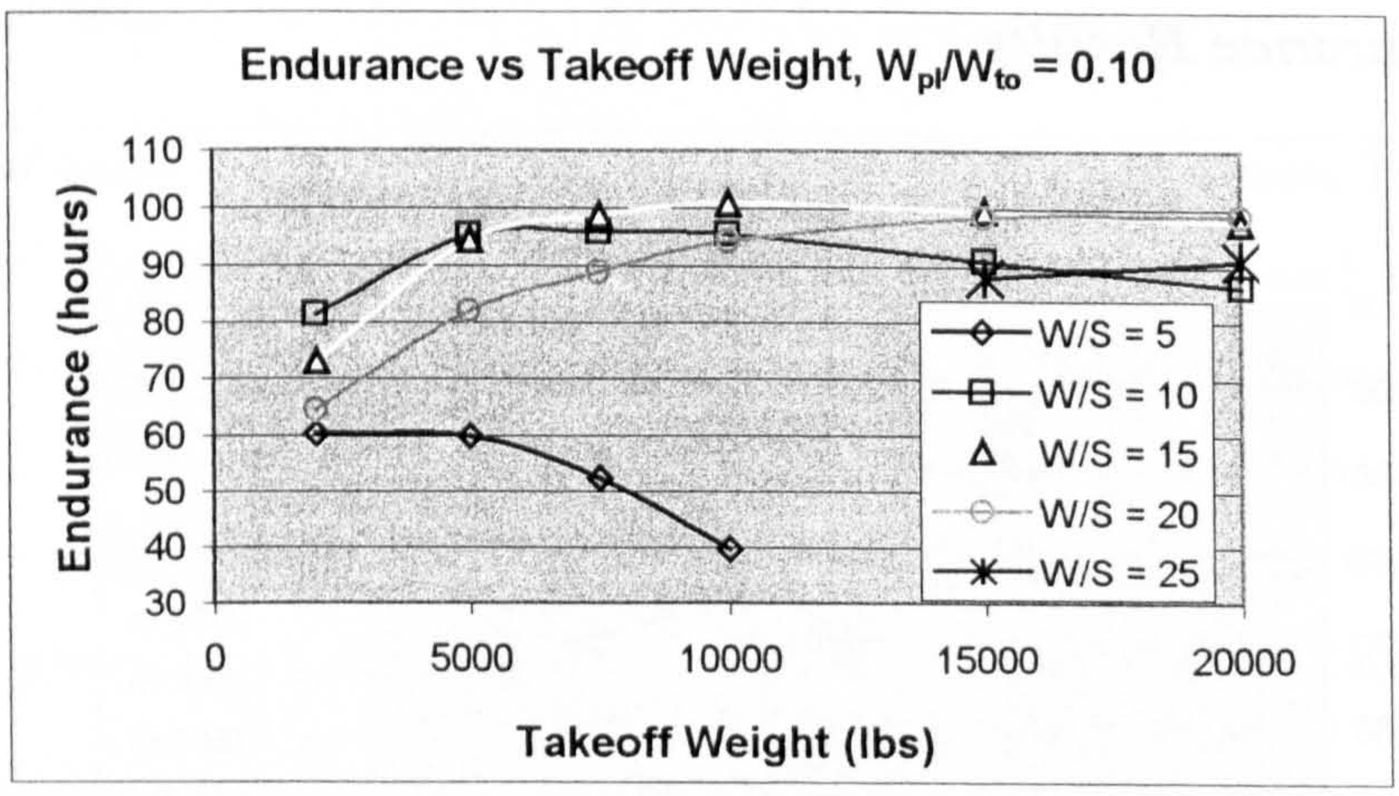

Figure 10.2 ***shows overall aircraft endurance as a function of takeoff weight for the 10 % payload weight fraction.***

Figure 10.2 shows a slightly different view of the same results which helps highlight one of more interesting characteristics of the variation of endurance. It is noted that all but the 5 lbs/ft^2 case show roughly the same tendencies. The 5, 10, and 15 lbs/ft^2 cases all reach a maximum value within the range of takeoff weights considered and then

begin to decrease at a slower rate. Again, similar behavior was shown for all three payload weight fractions considered with the only difference being the overall magnitude of the endurance. The general shapes and trends were the same. There was a slight relative downward shift from higher payload fractions to lower payload fractions of the higher wing loading curves. The reason for this shift will be discussed in the next section.

Again, the reasons behind most of this behavior will be more clearly seen when the endurance is broken into the fuel fraction and endurance terms. Also notable is the strange behavior of the lowest wing loading value. This behavior will be repeated throughout the results and is due to a number of reasons that will be explained in detail later.

10.B.2.b Results for the Fuel Fraction and Endurance Terms

10.B.2b.i Fuel Fraction Term

The first figure shown is for the fuel fraction term $\left(\sqrt{\frac{1}{1-\frac{W_{fuel}}{W_{to}}}}-1\right)$ as a function of wing loading (Figure 10.3). It is noted that the larger the value for this term, the higher the overall aircraft endurance will be, resulting from a higher fuel fractional weight from the total aircraft takeoff weight.

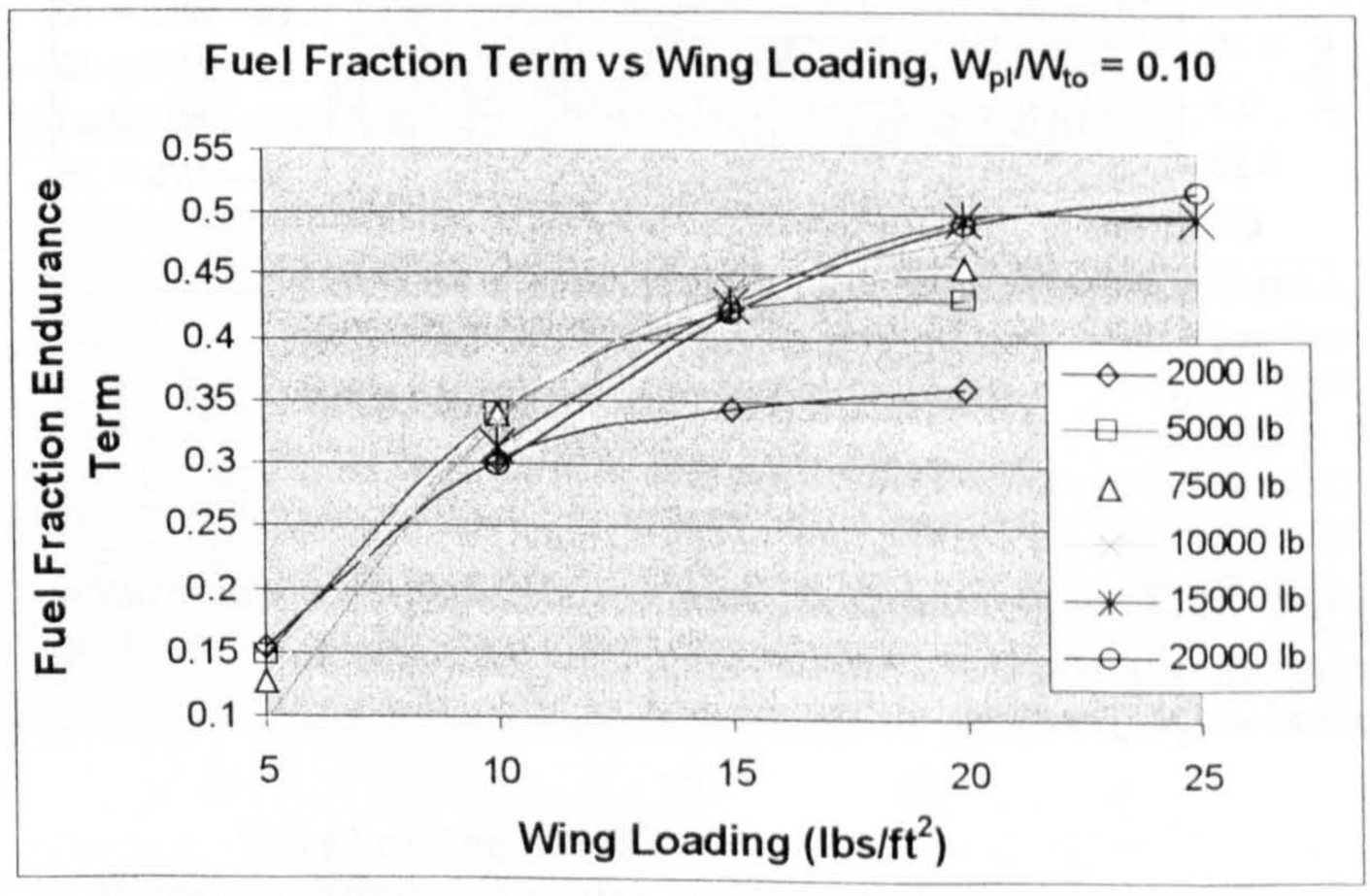

Figure 10.3 ***shows the fuel fraction component of the overall aircraft endurance as a function of wing loading for the 10% payload weight fraction.***

This figure is for $\frac{W_{PL}}{W_{to}} = 0.10$, however the general trends are again essentially identical for the other two payload cases considered. In general, there is a roughly logarithmic increase in fuel fraction term with an increase in wing loading. The curves appear to approach a limit, however none of the takeoff weight curves considered seem to reach the limit. Nevertheless, the slope decreases faster at lower wing loadings for lower takeoff weights.

Obviously, if the fuel fraction term were the most dominant, the endurance for a given takeoff weight would continue to increase approaching some limit. Referring back to the endurance figure (Figure 10.1) it can be seen that this is not the case, and there is another term that serves to decrease the overall endurance with an increase in wing loading. From Figure 10.3, it is evident that there is some benefit of scale in terms of structural efficiency. This will be observed later when the structural weight, and not the fuel fraction term, is viewed as a function of wing loading. The reason for viewing the two variables in separate graphs is that the fuel fraction term hides the impact of the payload fraction in the results, whereas the structural weight fraction exclusively demonstrates the results from the weight estimation routine.

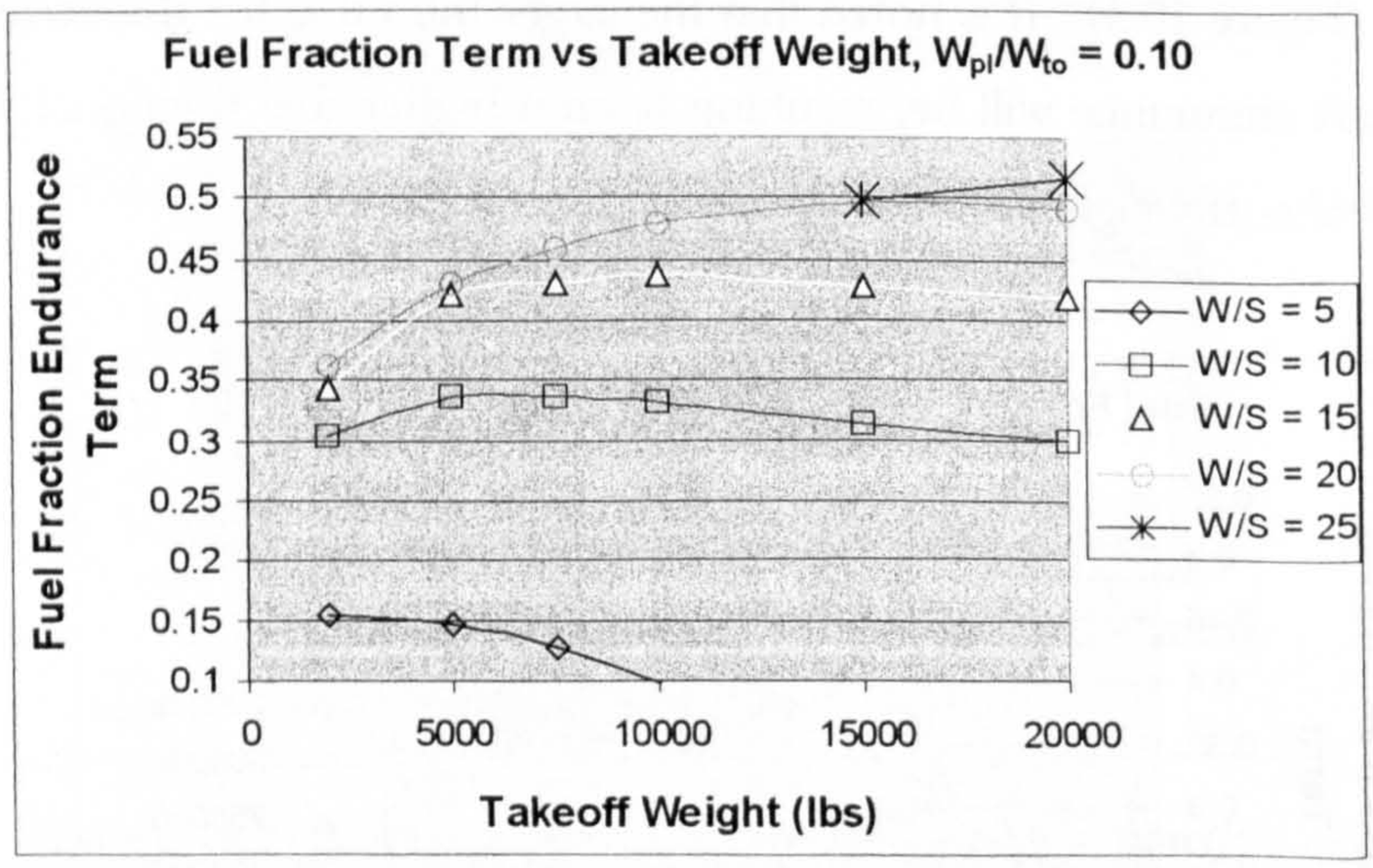

Figure 10.4 ***shows the fuel fraction component of the overall aircraft endurance as a function of the takeoff weight for the 10% payload weight fraction.***

The fuel fraction term as a function of takeoff weight is shown in Figure 10.4, again for the $\frac{W_{PL}}{W_{to}} = 0.10$ case. The general trends were identical for all three payload cases

with the only difference being in the magnitude of the fuel fraction term. This difference in magnitude arises solely from the fact that payload is replaced with fuel and vice versa. The fact that the curves are consistent across the payload weights implies that the weight estimation is relatively insensitive to trades between payload and fuel within ±5% of the takeoff weight of the aircraft. This was the only payload fraction range tested due to what was perceived as practical limitations taken from existing data. This was intended by no means to imply that a 2000 pound aircraft with a 10% payload fraction has the same utility as a 20,000 pound aircraft with the same payload fraction. It also does not attempt to imply that aircraft of these two weights could satisfy the same mission. Again, these takeoff weights were selected as limits to single and twin engine internal combustion reciprocating engine unmanned aircraft. They were chosen to allow for the academic study of the variation of the parameters affecting the endurance performance of the Low Speed HALE UAV.

As seen in the figure, all of the wing loading curves demonstrate weak logarithmic tendencies in shape. The most dramatic of all of the curves is again the 5 lbs/ft^2 wing loading case. This figure implies that for the fuel fraction term, for any given takeoff weight, the highest wing loading will yield the most beneficial fuel fraction endurance term. Once again, if this were the dominant term throughout the range of wing loading and takeoff weight, all Low Speed HALE UAV's would be built with extremely high wing loadings. This behavior is complemented by the behavior of the endurance term as will be shown shortly.

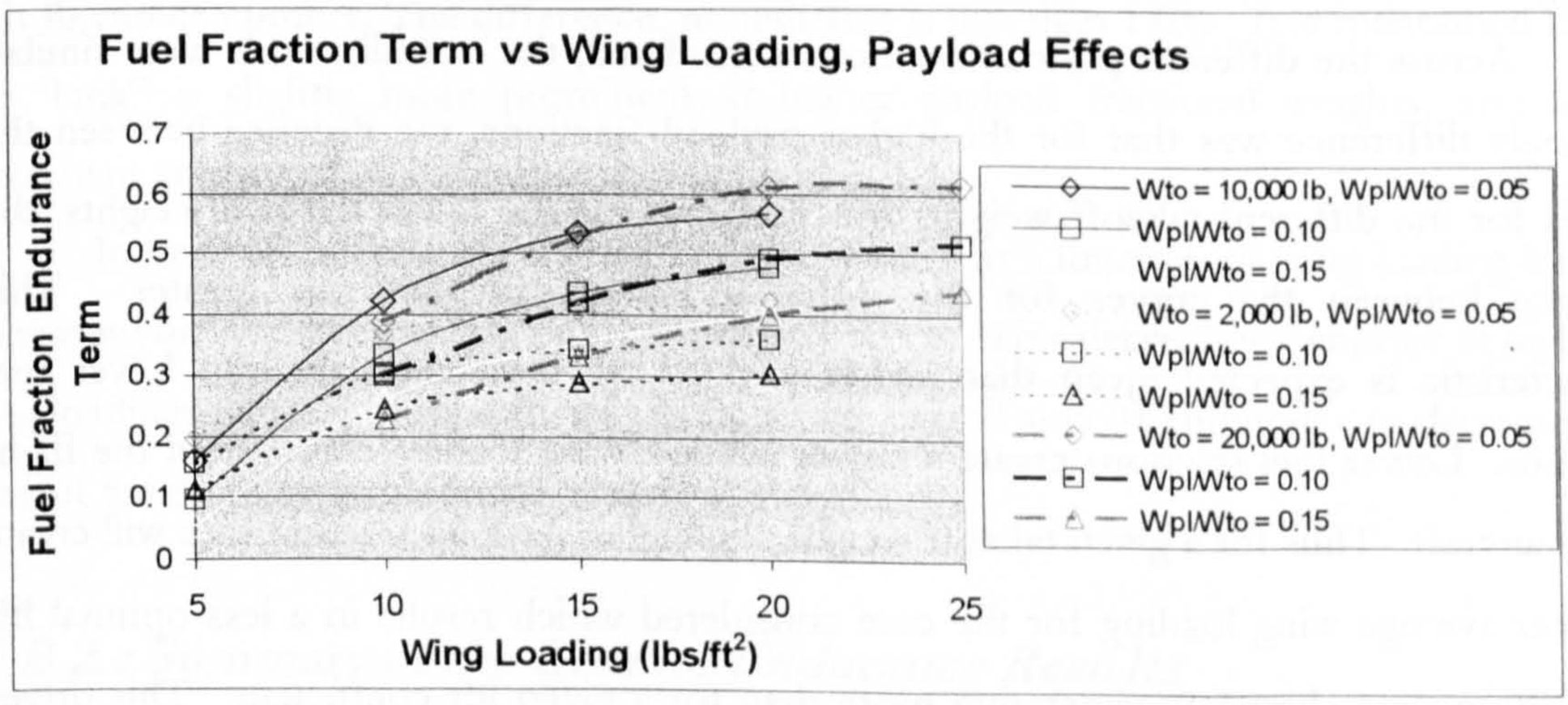

Figure 10.5 ***shows the payload effects on the fuel fraction component of the overall aircraft endurance as a function of wing loading for three different takeoff weights.***

Figure 10.5 shows a comparison of the fuel fraction term results as a function of wing loading for three different takeoff weights. Each takeoff weight was analyzed for three different payload weight fractions, 0.05, 0.10, and 0.15. The behavior of the 10,000 and 20,000 pound curves is quite similar. The 2,000 pound case is different from the other two takeoff weights shown. The reasoning for this will be discussed when the structural weight curves are presented, since the effects of payload can still be seen in the present figure. In fact, the shapes of the curves for a given takeoff weight are essentially identical, with the only visible difference being the change in magnitude, assumedly due to the replacement of payload with fuel and the effect of the subsequent load redistribution.

The optimum fuel fraction term is important, however, there is a balance between the fuel fraction term and the endurance term. The effects of either term cannot be ignored, and the product of the two terms result in the overall aircraft endurance. The contribution of the endurance term is discussed in the next section.

10.B.2b.ii Endurance Term

Before viewing the endurance term figure, it is necessary to note that the range of variation across all takeoff weights for the entire Y-axis (endurance term) is only 5.1% and that the largest variation of any single takeoff weight is only 3.1%. With those values in mind, the variation in endurance term with wing loading can be seen in Figure 10.6. Although the magnitude of the variation of the endurance term is significantly smaller than that of the fuel fraction term, there are still some discrete and discernible trends repeated throughout the results.

Across the different payload fractions considered, the overall trends were similar. The only difference was that for the higher payload fractions, the distance between the curves for the different takeoff weights was less, and for the lower payload weights, the distance between the curves for the different takeoff weights was greater. This characteristic is expected given that higher payload fractions translate into lower fuel fractions. Lower fuel fractions create a higher average wing loading throughout the flight of the aircraft. Thus for a given takeoff weight, the higher payload fraction case will create a higher average wing loading for the case considered which results in a less optimal lift distribution (less elliptical), generating more drag for a given lift coefficient. This drives the endurance term lower since it is simply a measure of aerodynamic efficiency.

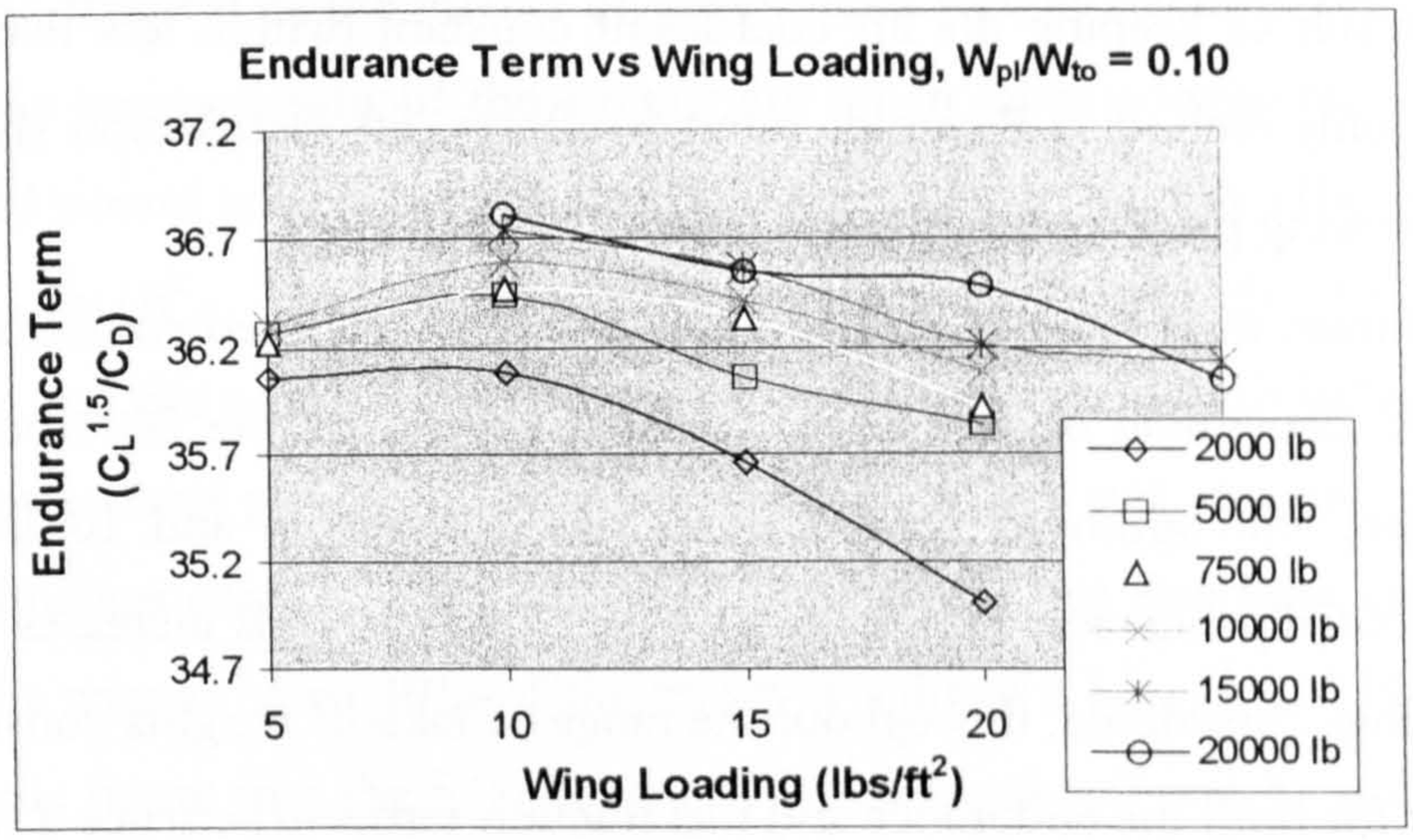

Figure 10.6 ***shows the endurance term/aerodynamic efficiency component of the overall aircraft endurance as a function of wing loading for the 10% payload weight fraction case.***

All of the lower takeoff weights considered showed increasing aerodynamic efficiency from lower wing loadings up to a maximum point with a subsequent gradual decrease in aerodynamic efficiency. Considering the actual relative magnitude of the curves, the slopes in the region after the maximum are quite similar. The maximum value for the endurance term for all of the takeoff weights is reasonably similar with the exception of the 2000 pound case. One possibility for this exception is the low relative value for the cruise Reynolds number. This would serve to increase the parasite drag on most of the aircraft components.

Also worthy of noting is the slight "kink" in the 20,000 pound takeoff weight curve. It is believed that this behavior is due to the combination of high wing loading and high Reynolds number. The difference, nonetheless is less than 1.0%. It is mentioned that the "kink" is slightly more prominent at higher payload fractional weights, and less prominent at lower payload fractional weights.

In brief, it can be seen that the endurance term as a function of wing loading has a decreasing behavior beyond an optimum wing loading. This decreasing behavior at higher wing loadings appears to be sufficient to cause the overall aircraft endurance to decrease in spite of the increasing fuel fraction term.

10.B.2.c Summary of the General Endurance Results

It has thus been shown how the shape of the overall endurance curve is influenced by the combined results from the fuel fraction and endurance terms. It is pointed out

again that as a result of keeping the lift coefficient constant (within less than 0.8%), the endurance term only embodies Reynolds number effects, lift distribution shape changes due to changes in wing planform shape, and parasite drag changes.

The optimum wing loading for the endurance term occurred somewhere between 10 and 15 lbs/ft^2 depending on the takeoff weight, except for the 2000 pound takeoff weight case where the optimum wing loading was between 5 and 10 lbs/ft^2. The endurance term initially increases rapidly, but beyond 5,000 pounds increases very slightly for all wing loadings considered, throughout the range of takeoff weights considered. The maximum values for both the endurance and fuel fraction terms experience a shift towards higher wing loadings for higher takeoff weights.

For the fuel fraction term the maximum point is not obtained within the range of wing loadings and takeoff weights considered. There is no clear optimum takeoff weight for the fuel fraction term, however fuel fraction terms appear to reach a plateau or region of decreased slope faster for lower takeoff weights at lower wing loadings.

10.B.2.d Other Interesting Results

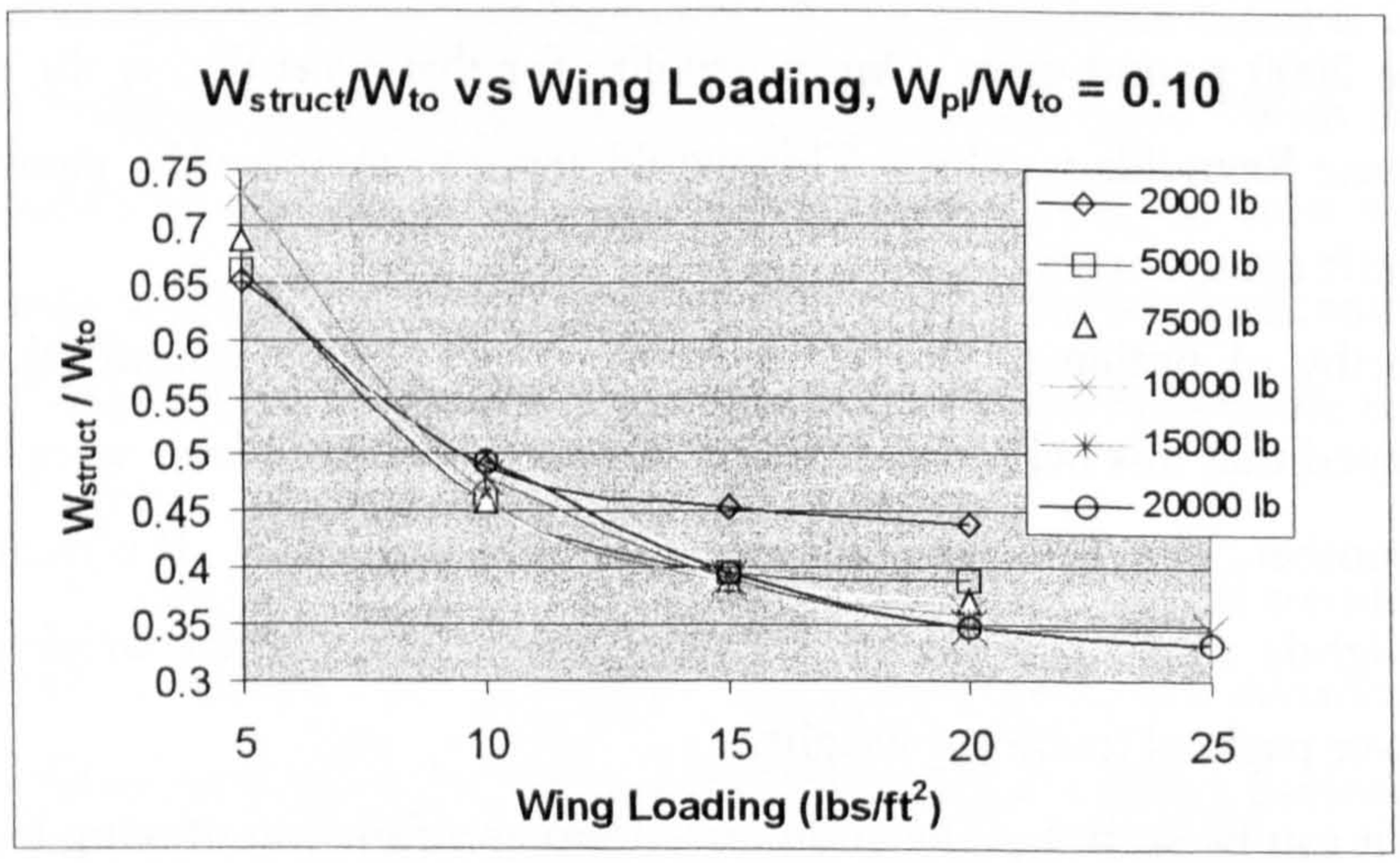

Figure 10.7 ***shows the predicted empty weight fraction as a function of wing loading for the 10% payload weight fraction.***

Another study of interest can be seen in Figure 10.7. It shows the relationship between the aircraft structural weight and the wing loading. The essential difference between this and the fuel fraction term shown previously is that it removes the effects of payload fraction from the output.

With the removal of the effects of the payload weight fraction, the results for the prediction of the empty weight of the aircraft are much more consistent. As seen in the figure, the 2,000 pound takeoff weight aircraft is the least structurally efficient above wing loadings of 10 lbs/ft^2. This behavior occurs at a point where the takeoff weight is reasonably low, and the wing area is also quite low. It is suspected this behavior is a direct result of the lower limit placed on wing and fuselage weight per area values discussed in the weight estimation chapter (Chapter VII). This weight per area limit can have a large impact since the wing is often 40% of the empty weight of a Low Speed HALE UAV. It appears from the figure that the 5,000 and 7,500 pound takeoff weight aircraft also reach the lower limit on weight per area, both around 20 lbs/ft^2. The aircraft seem to begin to reach the lower structural weight limit at a wing area of approximately 250 ft^2. This value is seen as a practical limitation in the strength and power densities of the materials used for construction and propulsion, and not a limitation in the predictive ability of the methodology.

In addition, the extremely high structure fractions resulting at 5 lbs/ft^2 are likely a direct result of the lower limits placed on wing and fuselage weight per area. The high structure fractional weights occur for the highest takeoff weight aircraft at the point where they have the largest wing area.

Additionally, there is a deviation that appears to begin at wing areas above roughly 1000 ft^2 as seen by the behavior of the 7,500, 10,000, 15,000, and 20,000 pound takeoff weight curves at their lower wing loadings. This deviation causes an error of less than 5.0% up to wing areas of 1500 ft^2 which is considerably above even that of *Condor* (1143 ft^2) with its 200 foot span.

Taking into consideration the above discussion, throughout the range of wing loadings and takeoff weights considered, the aircraft empty weight prediction module of the methodology provides extremely consistent results. The curve shown was for 10 percent payload weight fractions but the curves for the other payload fractions were essentially identical in shape and magnitude.

The other figure is presented mainly for completeness to demonstrate that the predicted drag behavior is consistent with what would be expected for the conventional aircraft. This is achieved by viewing Figure 10.8 for the horsepower required in cruise as a function of wing loading for each takeoff weight considered.

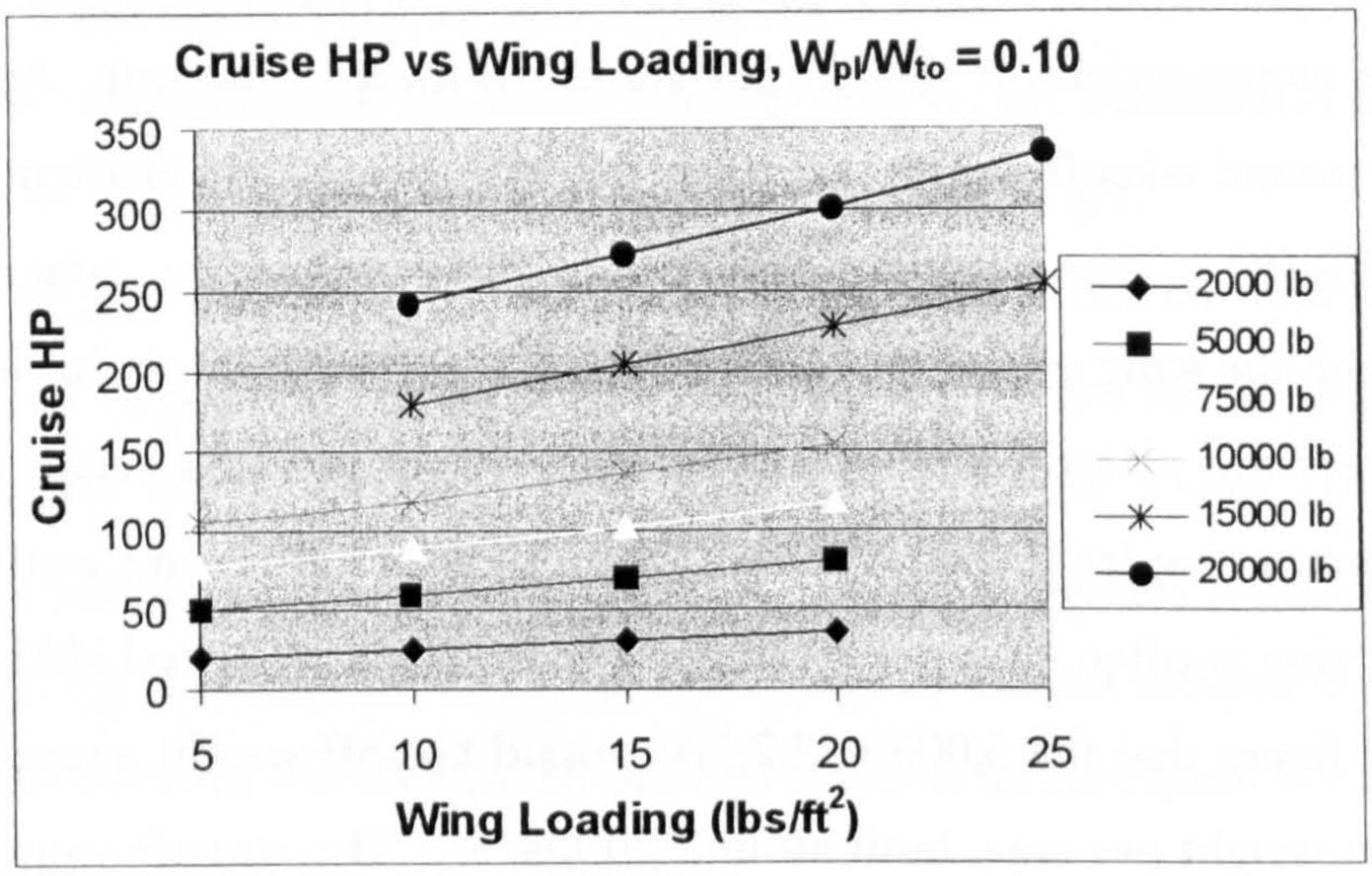

Figure 10.8 ***shows the increase in predicted cruise power required for increasing takeoff weights for the 10% payload weight fraction case.***

The figure shown is for the 10 percent payload weight fraction. There was no difference across the different payload weight fractions considered. All of the figures shown will be used as a baseline for comparison to other cases later in the chapter.

10.B.3 Study of Wing Geometry Effects

The following sections specifically address the effects on aircraft endurance and the parameters effecting endurance as a result of a variation in several parameters associated exclusively with the geometry of the wing.

10.B.3.a Aspect Ratio Study

For the study of the effects of varying aspect ratio on aircraft endurance, all of the values assumed in Section 10.B.2 were kept the same, with the exception of the aspect ratio which was changed from 35 to 22. These values were selected since they were seen as limiting values. The *Condor* had an aspect ratio of 36.6 and the *Altus* an aspect ratio of 21.75. These represent present day realistic limits on Low Speed HALE UAV aspect ratios. While larger aspect ratios could be used in constructing a future Low Speed HALE UAV, the general trends experienced by the endurance and the respective endurance and fuel fraction terms should be the same.

The comparative results for aircraft endurance as a function of wing loading are given in Figure 10.9 for takeoff weights of 2,000, , 10,000, and 20,000 pounds. The analysis was also performed for 5,000, 7,500 and 15,000 pound takeoff weights, but these results were not dramatically different from those shown. In addition, the graph would become unreadable with the inclusion of these cases.

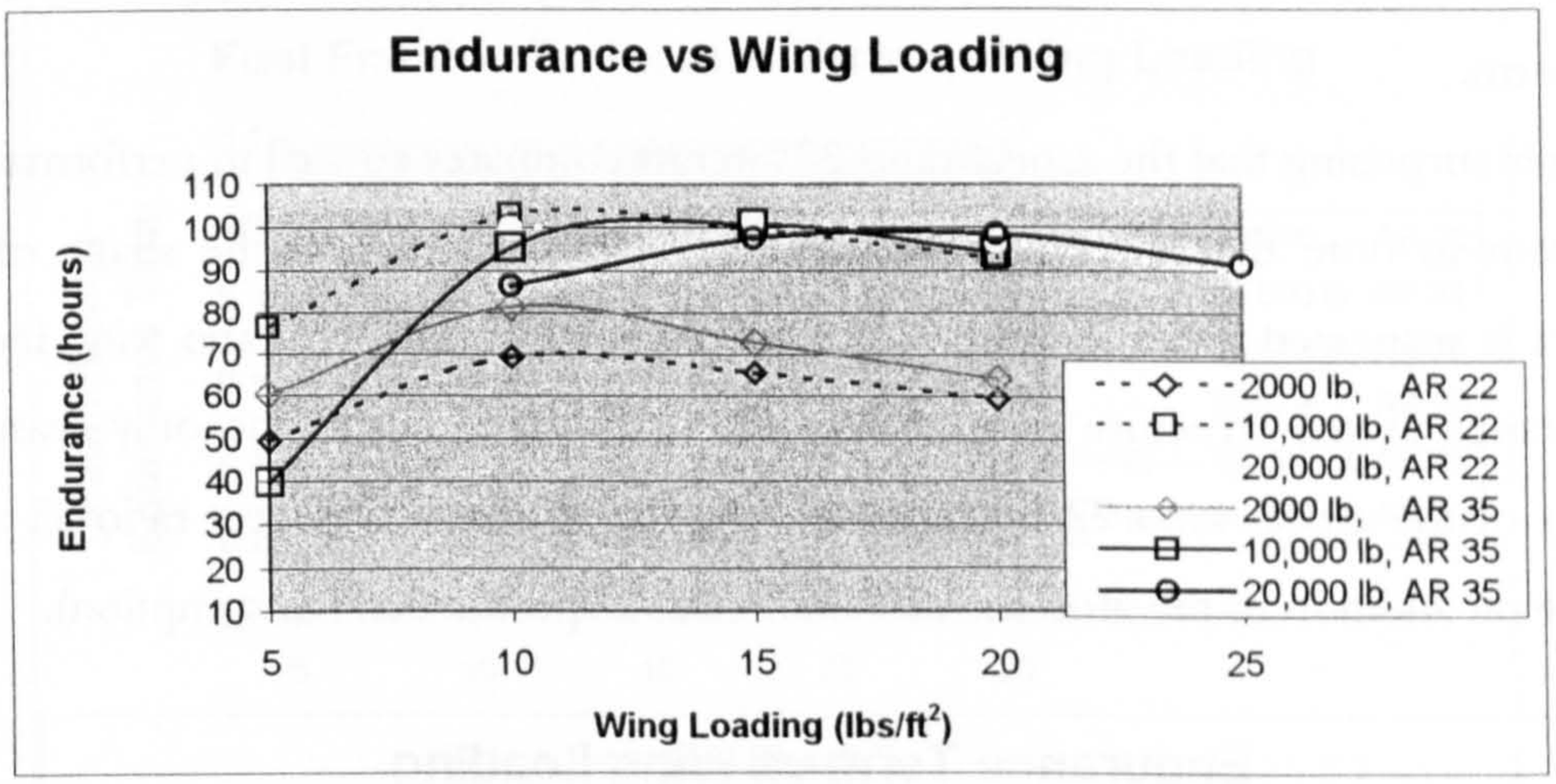

Figure 10.9 ***compares the change in overall aircraft endurance for aircraft with different aspect ratios at various takeoff weights.***

It is noted that for all of the comparative results throughout this chapter, the baseline case is presented in the figures in solid lines, and the cases being studied/varied are plotted using dashed lines. The case used as a baseline is that presented for the conventional aircraft under the assumptions and conditions stated in Section 10.B.2 of this chapter.

The most surprising characteristic from this figure is the fact that the maximum endurance is not for the aspect ratio 35 aircraft except for the 2,000 pound case. At this point it is important to remember two factors. Firstly, that the overall aircraft endurance is a result in this case of the product of the aerodynamic efficiency and the structural efficiency. Secondly, and perhaps more importantly, the specific fuel consumption was held constant throughout the analysis. The downstream effect of this assumption is that the aspect ratio 22 case, as will be shown, requires more power to fly under the same conditions. Higher power settings do not always imply greater fuel consumption, however if the engine is optimized for the operating conditions for each individual case, a higher power setting should result in higher fuel consumption.

The other point of interest arising from the figure is the fact that the maximum endurance point has shifted left for the aspect ratio 22 wing for both the 10,000 and more noticeably the 20,000 pound takeoff weight curves. The reason for this shift will be discussed with the presentation of the fuel fraction term. Also of interest is the greater endurance associated with the higher takeoff weight aspect ratio 22 aircraft with wing areas greater than 1000 ft^2. The reason for this will also be explained in terms of the fuel fraction term.

It is surprising that the aspect ratio 22 aircraft compares so well in performance. It is important to note that there are two distinct factors influencing the shape of these curves. It is suspected that the weight saving from the lower aspect ratio wing increases the endurance as the structure weight is replaced by fuel. This is the only reason the endurance of the aspect ratio 22 aircraft can compare at all to the aspect ratio 35 aircraft endurance (in addition to the aforementioned constant specific fuel consumption).

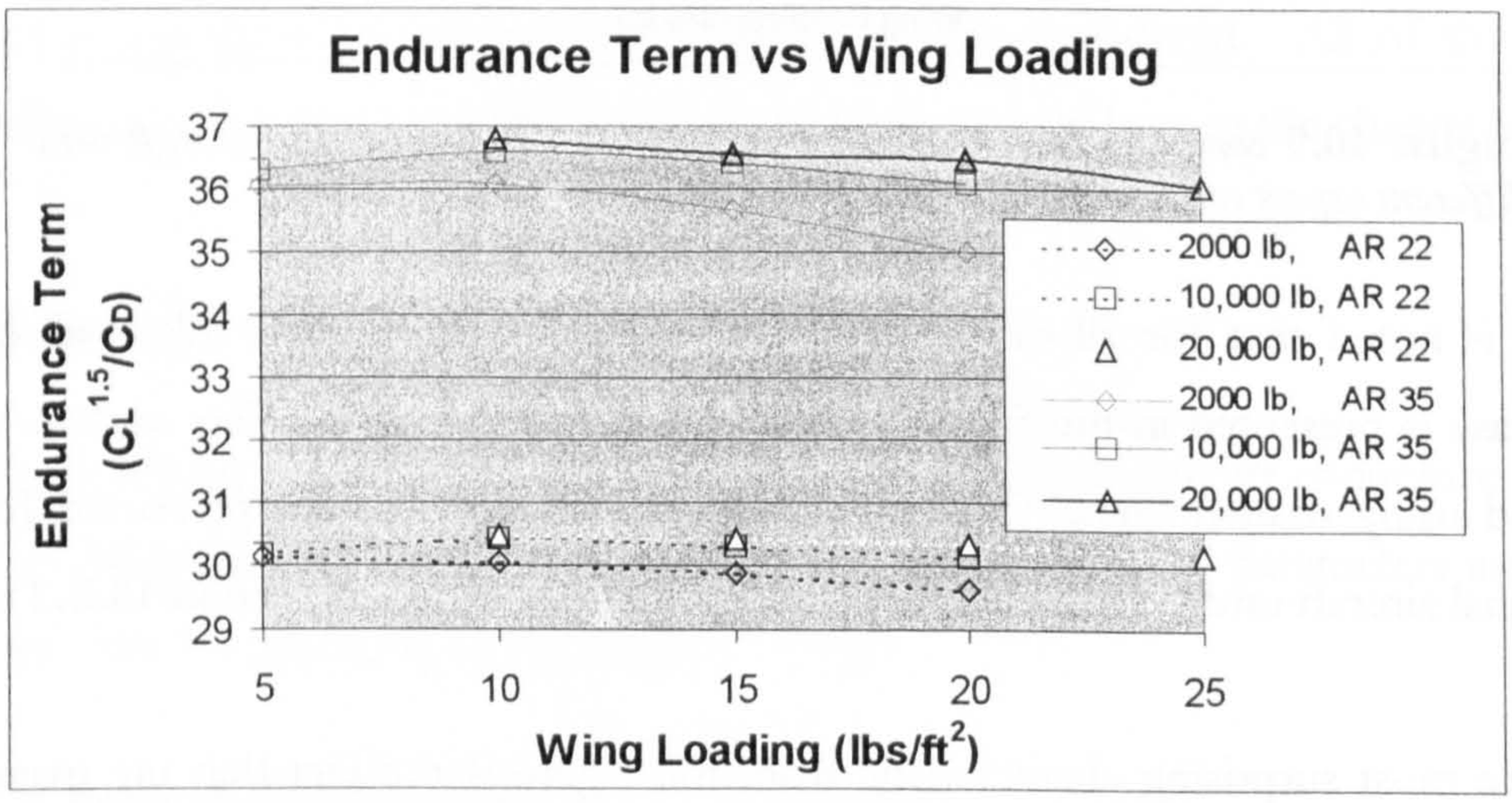

Figure 10.10 ***shows a 20% decrease in the aircraft endurance term for aircraft with lower aspect ratios.***

The endurance term is shown in Figure 10.10. This figure appears exactly as would be expected. The lower aspect ratio wing is consistently less aerodynamically efficient at the same lift coefficient. The difference in endurance terms is roughly 20%. In terms of the macroscopic output from the methodology, this demonstrates that the vortex lattice code does in fact provide reasonable results for the three dimensional lift distribution.

Figure 10.11 shows that the lower aspect ratio aircraft has a consistently higher fuel fraction endurance term throughout the range of wing loadings considered. The sole

exception is the 2000 pound aircraft up to 10 lbs/ft^2. For the higher takeoff weights, the increase in fuel fraction endurance term is between 20 and 30%. This behavior is tempered in the value of final endurance for the aspect ratio 22 case by the consistently less aerodynamically efficient wing which drove the endurance term lower as seen previously with the aspect ratio 35 case.

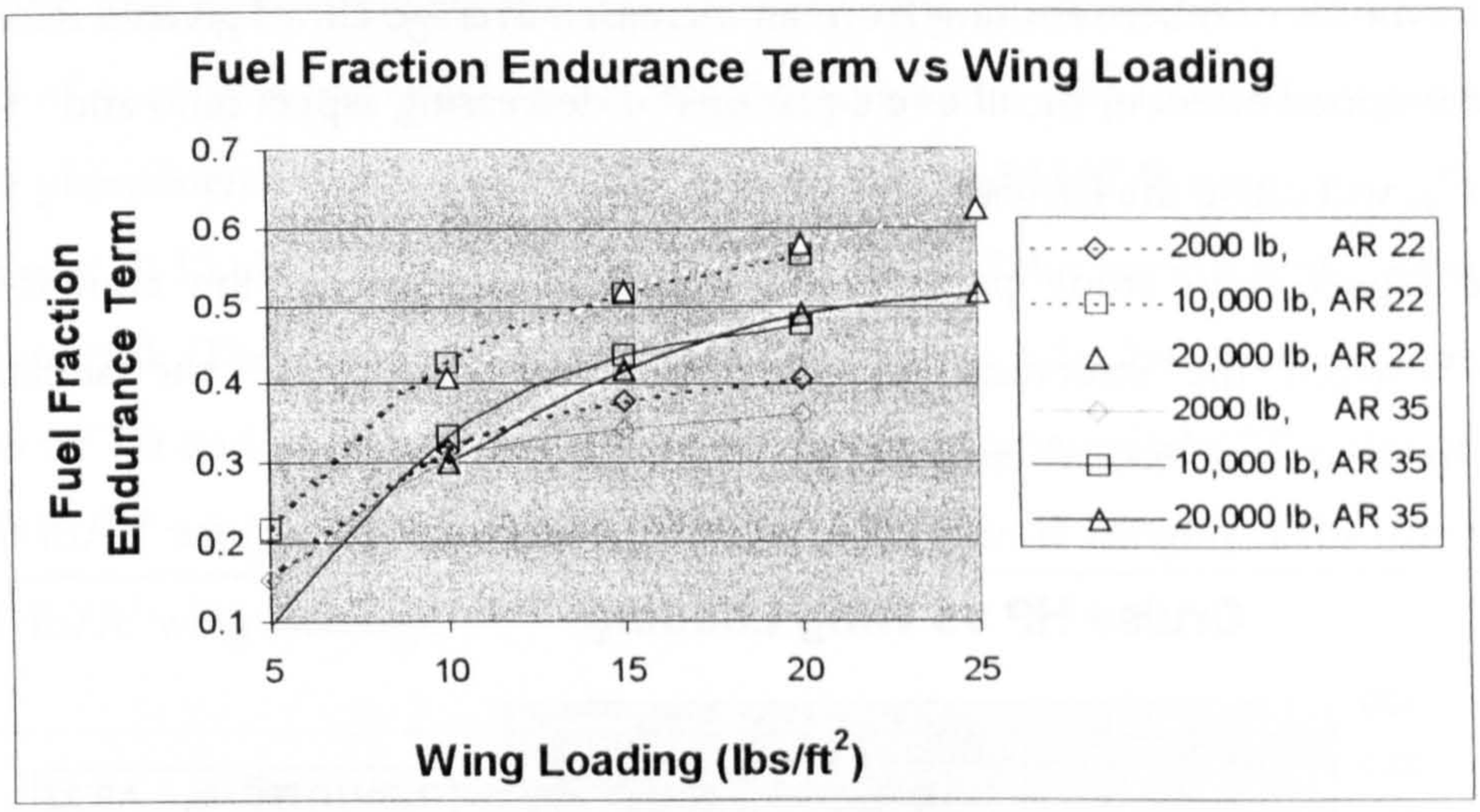

Figure 10.11 ***shows the increase in fuel fraction endurance term for aircraft with lower aspect ratios due to increased structural efficiency.***

The primary difference between the two aspect ratio cases is that the increase in fuel fraction term for the aspect ratio 22 case is balanced at lower wing loadings by the effects of the lower aerodynamic efficiency. This causes a slight leftward shift of the overall aircraft endurance peak (in the direction of lower wing loading as an optimum for a given takeoff weight) for the higher takeoff weight aircraft. The end result is a higher overall aircraft endurance (roughly 2% higher), but it is pointed out that this results from the replacement of structural weight saving for the aspect ratio 22 case with fuel, thereby slightly increasing the endurance for a given takeoff weight. The most important design implication is that for the aspect ratio 22 aircraft, the optimum wing loading for a given takeoff weight is reduced by approximately 5 lbs/ft^2.

The reason for this shift can be seen by referring to the two-dimensional minimum power required and maximum lift to drag ratio equations. If the minimum power required and maximum lift to drag ratio velocities are substituted with their respective lift coefficients and π, ε, ρ, and C_l are assumed to be constant, the following relationships exist :

$$\left(\frac{W}{S}\right)_{\min PR} \propto 3 \cdot AR \cdot C_{do}, \text{ and}$$

$$\left(\frac{W}{S}\right)_{\max L/D} \propto AR \cdot C_{do}.$$

It is safe to assume a slight decrease in C_{do} with a decrease in aspect ratio. This is due to increasing Reynolds number resulting from an increased average chord given a fixed wing area. The combined effect in the above equations of decreasing aspect ratio and decreasing C_{do} will cause the leftward shift in optimum wing loading.

The aspect ratio study provides an excellent example of the complementary interaction between the structural and aerodynamic efficiency of the aircraft with application to the overall aircraft endurance.

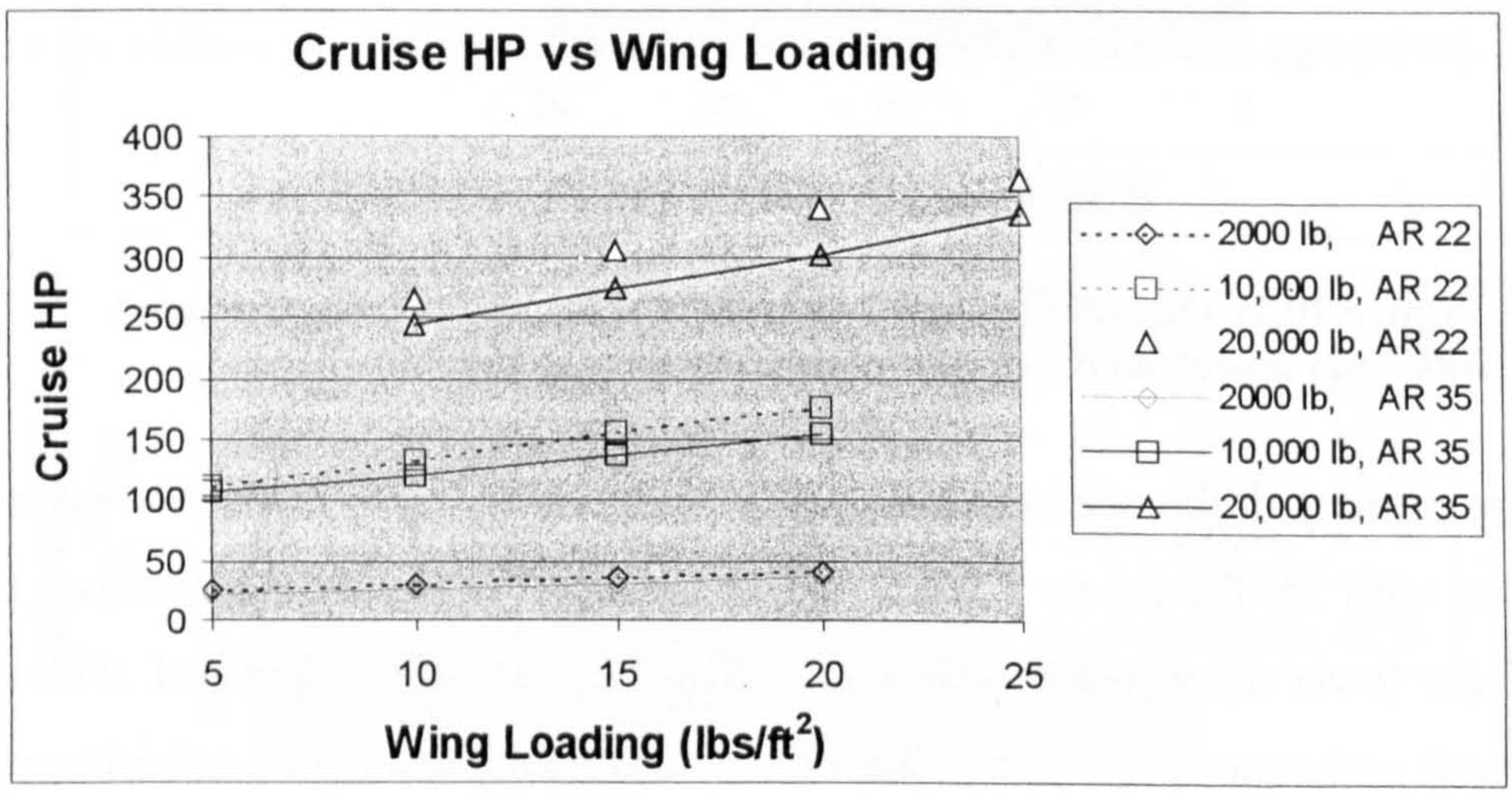

Figure 10.12 ***shows the magnitude of the increase in required cruise power resulting from an increase in aspect ratio at various takeoff weights.***

The last figure included in this section is seen in Figure 10.12 for horsepower required in cruise as a function of wing loading. The most interesting characteristic about this figure is that the power required is higher for all of the aspect ratio 22 aircraft cases. This reflects the increase in drag due to the shape of the wing, but in general demonstrates the comparatively poor aerodynamic efficiency of selecting lower aspect ratio wings for the Low Speed HALE mission.

Since the engines of the Low Speed HALE are sized for the climb requirement, the cost of the increased power required for the aspect ratio 22 aircraft depends mostly on

the choice of engine and the fuel consumption performance characteristics of that engine at the selected operating point.

10.B.3.b Taper Ratio Study

The value chosen for taper ratio was again done so to demonstrate behavior of the extreme case. It is rather unlikely that a Low Speed HALE aircraft will ever be built with a taper ratio of one. Nevertheless, use of this extreme value helps to uncover some of the underlying phenomena effecting the design of a Low Speed HALE wing.

Figure 10.13 shows the comparative endurance of the aircraft with wings of taper ratios 0.4 and 1.0. The maximum difference in endurance value between an aircraft with a taper ratio of 1.0 and an aircraft with taper of 0.4 is approximately 25% (for the 10,000 pound, 10 lb/ft^2 wing loading). The minimum difference is roughly 15% (for the 2,000 pound, 20 lb/ft^2 wing loading).

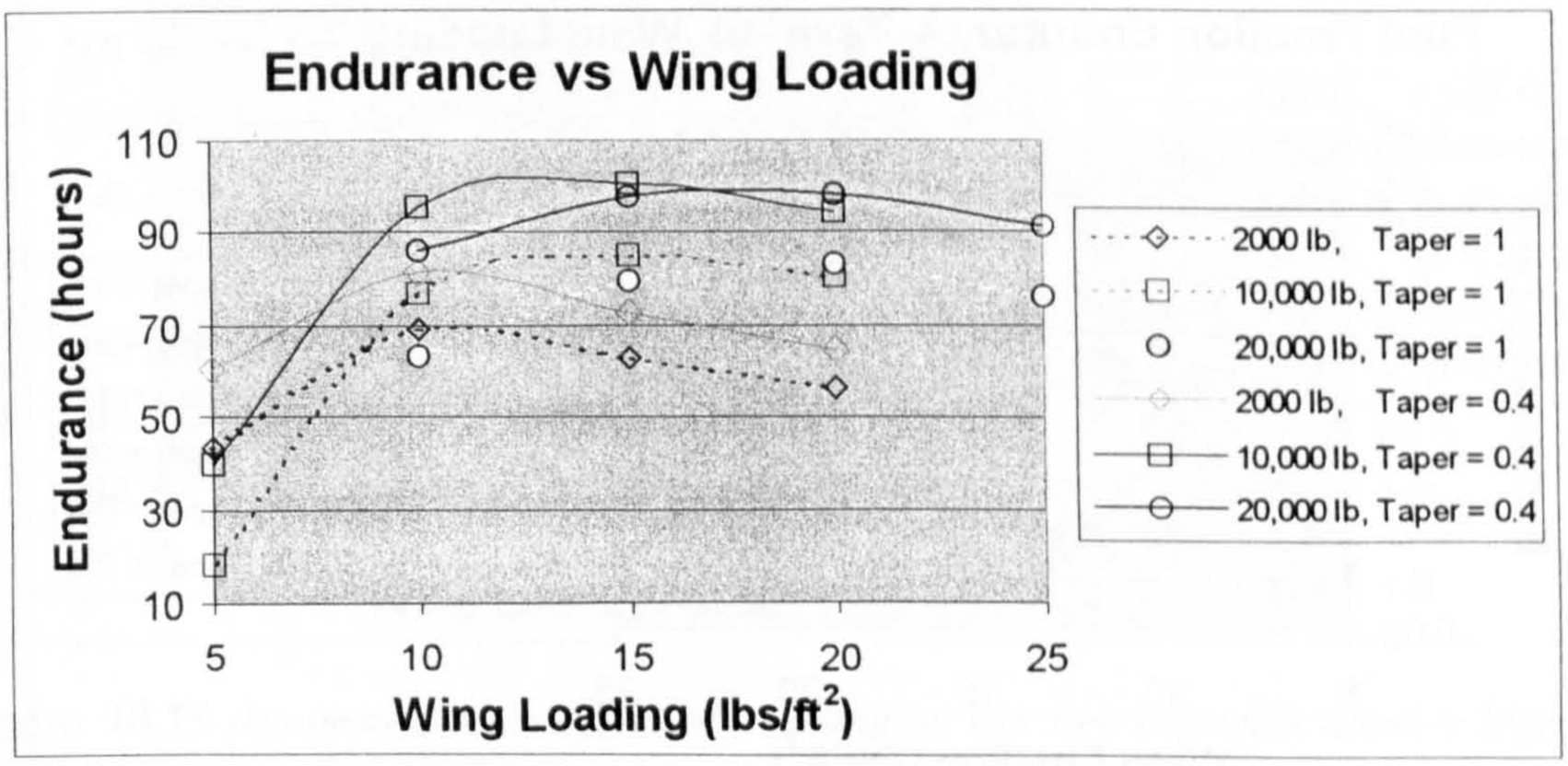

Figure 10.13 ***shows a less severe effect of changing the taper ratio compared to the effects of aspect ratio changes on the overall aircraft endurance when using the conventional case as a baseline.***

In contrast to the aspect ratio variation, the takeoff weight curves do not show any shift with respect to wing loading. In fact, it appears again that the basic shape of the takeoff weight curves is identical. The location of the optimum wing loading for a given takeoff weight appears to have remained the same despite the change in endurance.

The endurance term curve is not included as it essentially demonstrates the same concept as with the aspect ratio study. This is reassuring given the absence of taper ratio in the maximum efficiency equations. The only difference between the aspect ratio and taper ratio figures is the magnitude. The difference between endurance terms for the taper

ratio 1.0 and 0.4 cases (less than or equal to 2.0) is roughly 30% that of the difference between the aspect ratio 22 and 35 terms (approximately 6.0). This would imply that aspect ratio effects on aerodynamic efficiency are much greater than taper ratio effects for extremely high aspect ratio wings within the design boundaries and under the conditions being considered.

Figure 10.14 shows the fuel fraction term results for the taper study. In general, the taper ratio 1.0 takeoff weight curves show consistently lower values for fuel fraction endurance term. This results from the taper ratio factor in the wing weight estimation. When compared to the structural effects of reducing the aspect ratio, the benefits from decreasing taper ratio are fewer throughout the range of wing loadings and takeoff weights considered. It would appear from the results in general that a variation in taper ratio has a much smaller effect on the overall aircraft endurance, aerodynamic efficiency, and structural efficiency than a variation in aspect ratio across the range of values considered.

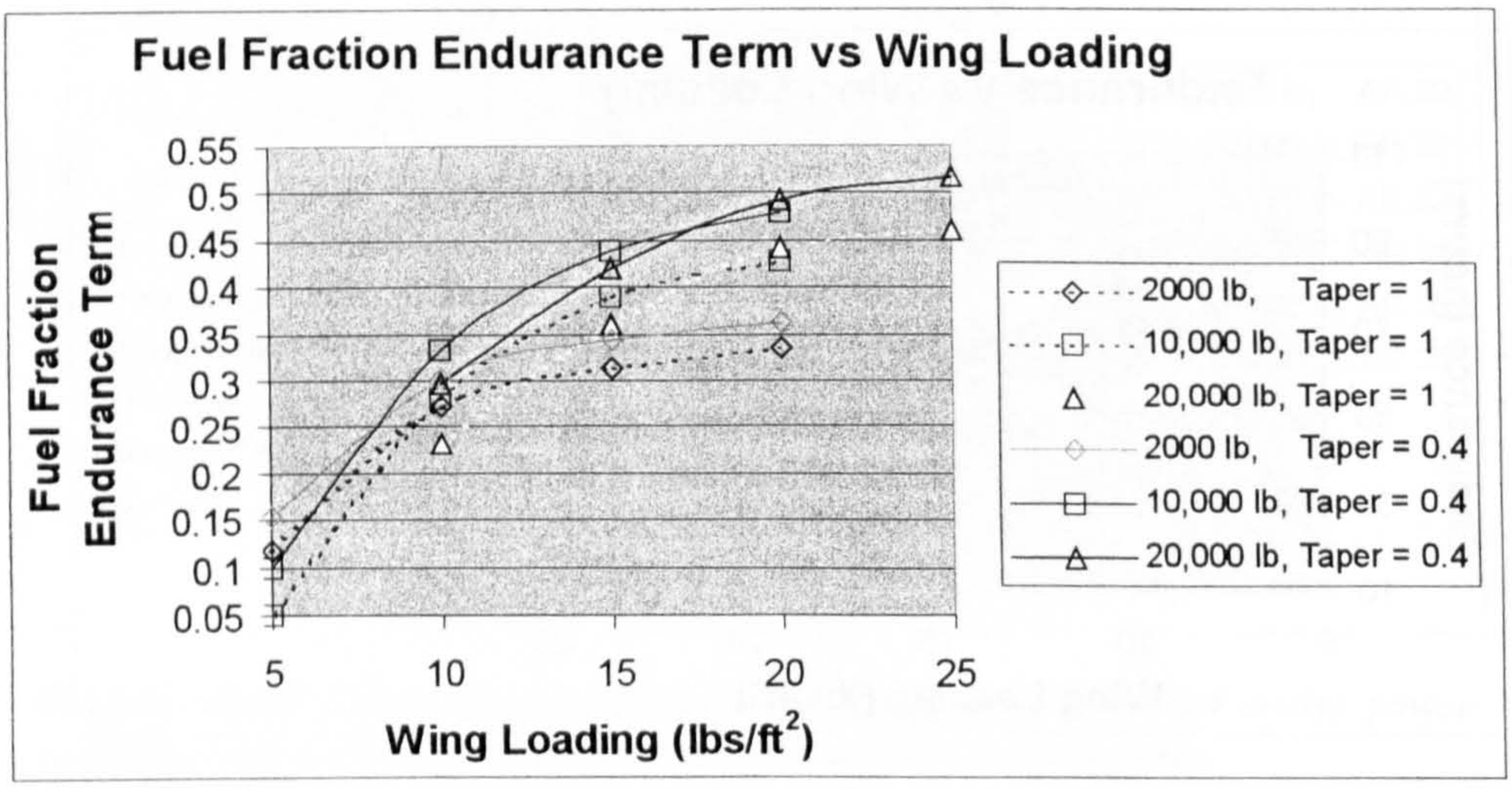

Figure 10.14 ***shows that the effects of taper ratio changes are less dramatic than the effects of aspect ratio changes on the structural efficiency of the aircraft.***

The reduced aerodynamic efficiency for the taper ratio 1.0 case, once again results in higher values for cruise power required across the entire range of takeoff weights and wing loadings considered.

This section and the previous section essentially quantify the combined structural and aerodynamic effects of consideration of the three-dimensional lift problem. Variation in taper and aspect ratio both impact the structural weight predicted for the aircraft, which in turn directly effects the fuel fraction and thus the endurance. In addition the results

place a rather considerable emphasis on the necessity to consider the three-dimensional nature of lift distributions given the reasonably large difference found in the aerodynamic efficiency due to these effects.

10.B.3.c Airfoil Study

In order to ensure that the results were not skewed to the behavior of a particular airfoil, it was necessary to perform a study using a different airfoil. In addition, it was considered of interest to observe the performance of another airfoil in the context of the proposed airfoil figure of merit in **Appendix A**. Since the figure of merit yielded the NLF(1)-1015 as a first choice, and this is the airfoil section used to this point, the second choice from the figure of merit, the Wortmann FX-63-137 was used for the airfoil study.

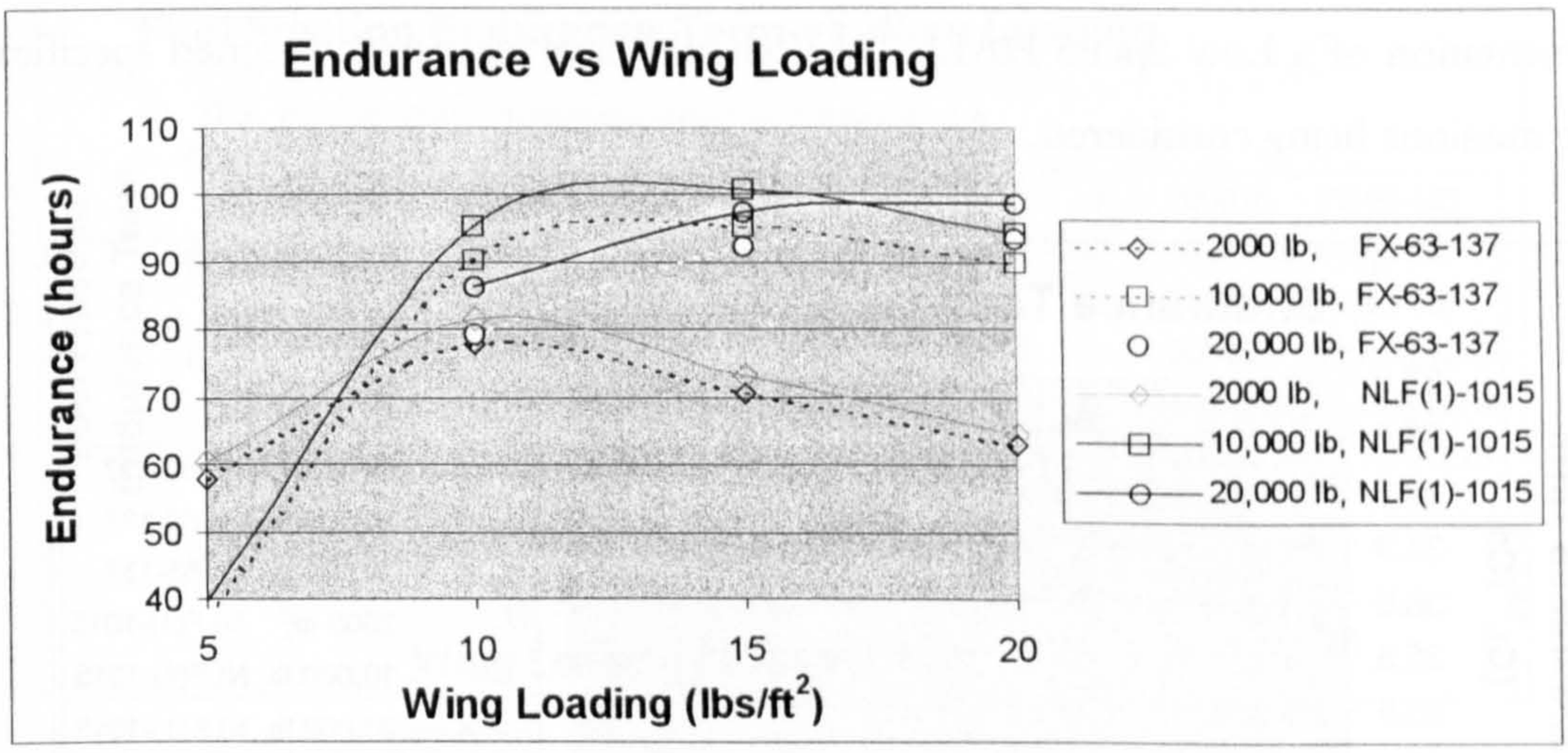

Figure 10.15 ***demonstrates the effect of exchanging two low Reynolds number high lift airfoils on the overall aircraft endurance.***

Several different effects were expected before the study was undertaken. The thickness to chord ratio of the NLF(1)-1015 is 15%, and the thickness to chord ratio of the FX63-137 is 13.7%. This has obvious implications on structural weight. In addition, the difference between the two moment coefficients for the lift coefficient value used (1.3) is roughly 0.09. This will impact the static margin of the aircraft and the ability to trim. Finally, neither of the airfoils has reached their two-dimensional endurance term maximum at a lift coefficient of 1.3. The FX63-137 is closer to its maximum two-dimensional endurance term, however the magnitude of this maximum is less than that of the NLF(1)-1015. This was expected to impact the three-dimensional aerodynamic efficiency term.

The results of the airfoil comparative study for the aircraft endurance can be seen in Figure 10.15. The effects are not nearly as dramatic as for the taper ratio and aspect ratio studies, however they are still reasonably pronounced for a simple change between two high lift airfoils with reasonably similar thickness to chord ratios. The maximum difference in overall aircraft endurance occurred for the 20,000 pound takeoff weight at a wing loading of 10 lbs/ft^2 where the difference was 5.9%.

More important than the absolute values for the endurance, though, is the fact that the shape of the curves is similar, and that there are no characteristics that are distinctly or violently different between airfoils. The magnitude of the difference in aircraft endurance emphasizes the importance of the selection of the airfoil. A maximum 6.0 hour difference in endurance occurs due to airfoil selection alone, and that is with the selection of another high lift coefficient airfoil. This only further supports the argument that any new implementation of a Low Speed HALE UAV should have an airfoil designed specifically for the missions being considered.

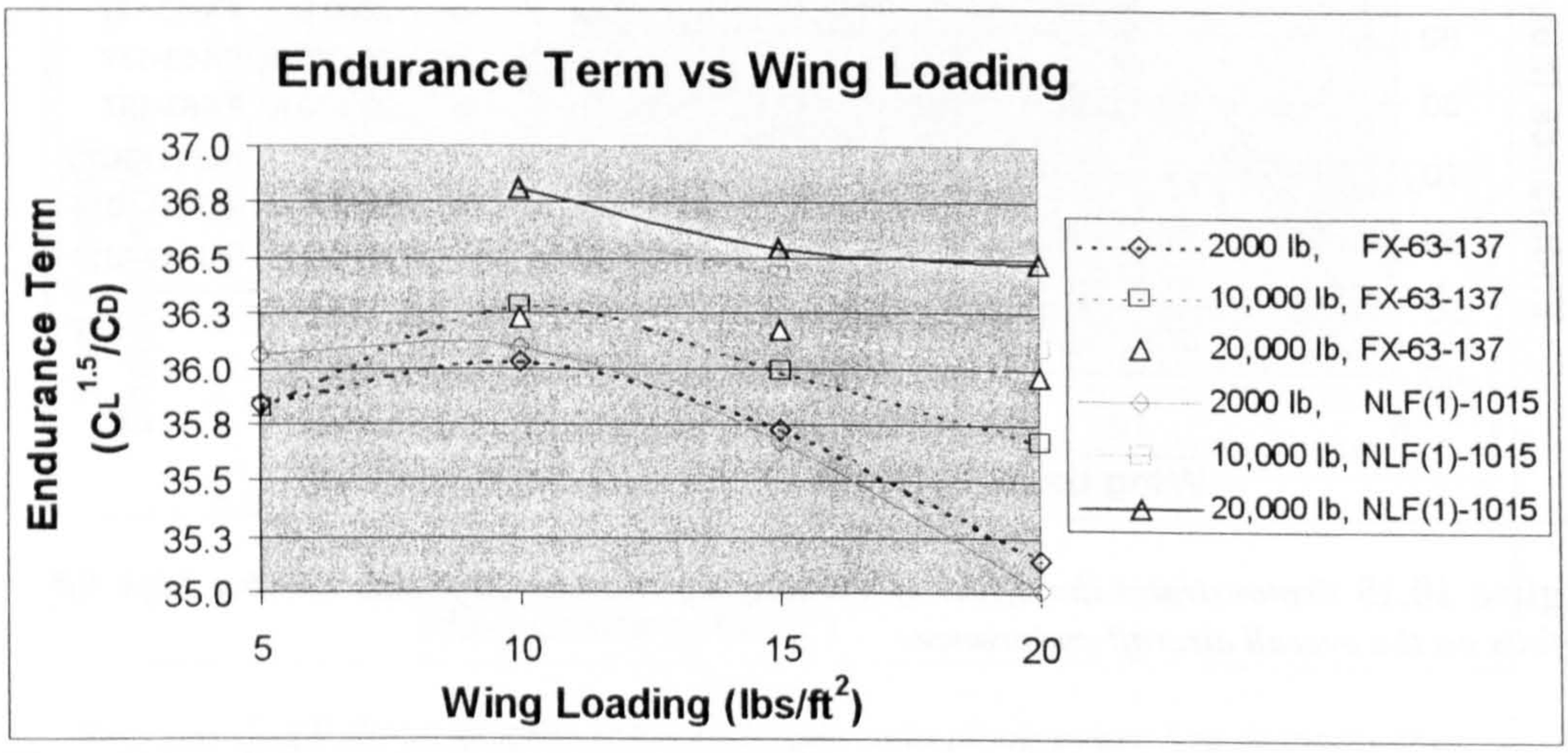

Figure 10.16 ***shows the effect of a change in airfoil on the three dimensional aircraft aerodynamic efficiency term.***

Figure 10.16 shows the endurance term for the airfoil comparison. The first point of interest to note is that the largest difference between the two airfoils at any given takeoff weight and wing loading is roughly 1.4%. The second point of interest to note is that the Y-axis scale represents less than a 6.0% variation in endurance term. Taking these factors into consideration, the curves are essentially coincident, with the FX63-137 being very slightly less aerodynamically efficient. The overall shape of both sets of curves is essentially the same. Despite the very small variations in endurance term, the shape of the

results are consistent from one execution to another suggesting that the solution obtained for the drag of a specific configuration is unique. It is reasonably safe to conclude from observing this figure that the selection of airfoil did not substantially bias the aerodynamic results of the methodology.

Figure 10.17 shows the fuel fraction term for the airfoil comparison. There is a very slight difference shown in the figure between the takeoff weight curves for the different airfoil cases. It is suspected this results from the greater thickness to chord ratio of the NLF(1)-1015. There were no other parameters varied between the two airfoils that could have an effect on the structural weight of the aircraft. Thus, this figure essentially represents a study on the effects of the variation of the thickness to chord ratio, which appear quite small.

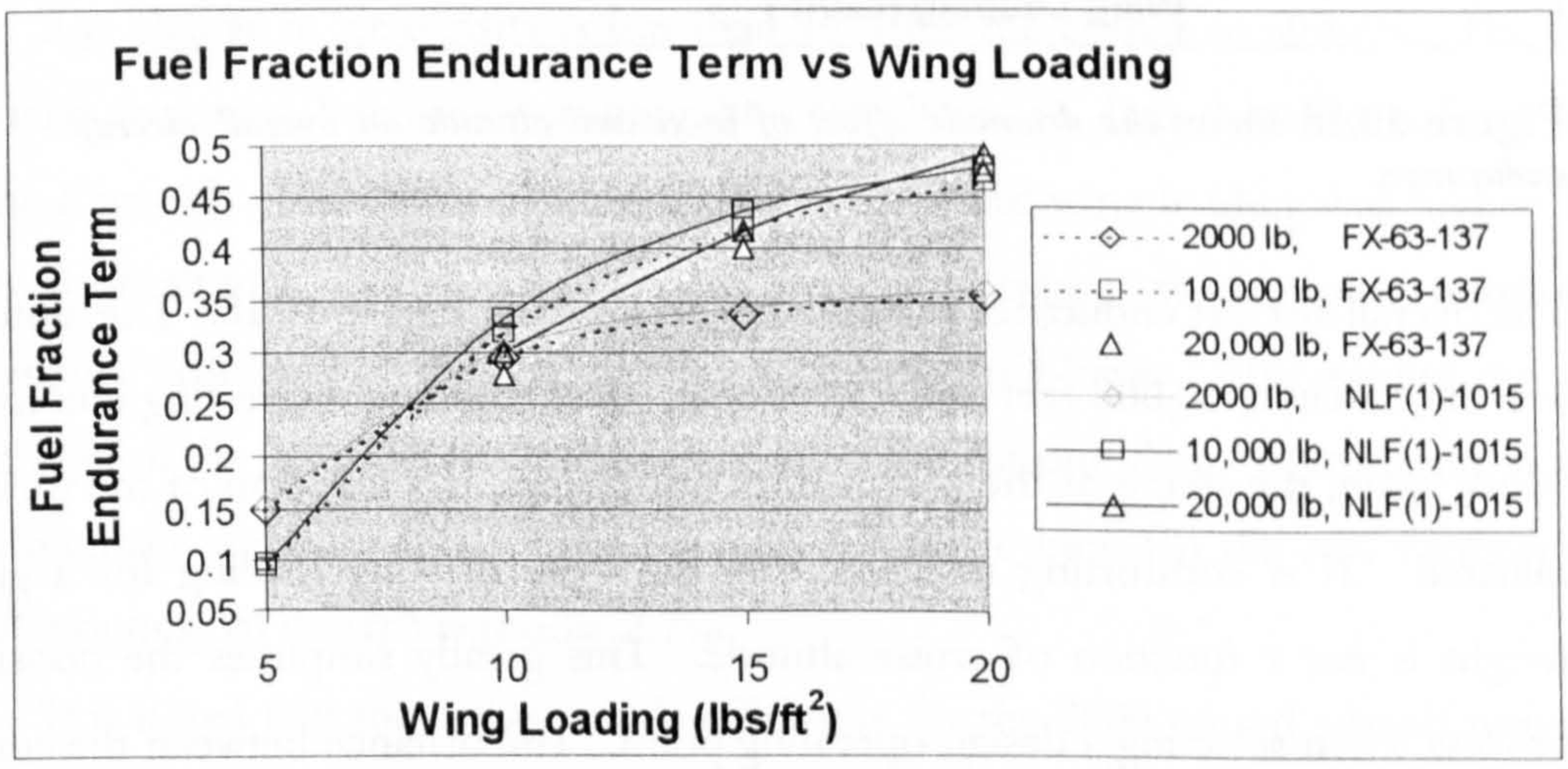

Figure 10.17 ***highlights the effects on structural efficiency due to a slight change in thickness to chord ratio.***

10.B.4 Study of the Effects of Operating Conditions

10.B.4.a Altitude Study

It was apparent from the discussion regarding the Breguet endurance equation that a change in altitude would result in a change in overall aircraft endurance. The purpose of this section was to determine how much of that change in overall endurance results from the variation of the air density and how much results from changes in aerodynamic efficiency. Additionally, the altitude change serves as a check on the weight estimation module, as there should be little or no change in the predicted empty weight of the aircraft

as a result of a simple altitude change. This holds true to the extent that the aircraft is still flown at high altitude and that the increase in altitude does not imply too large an increase in cruise velocity.

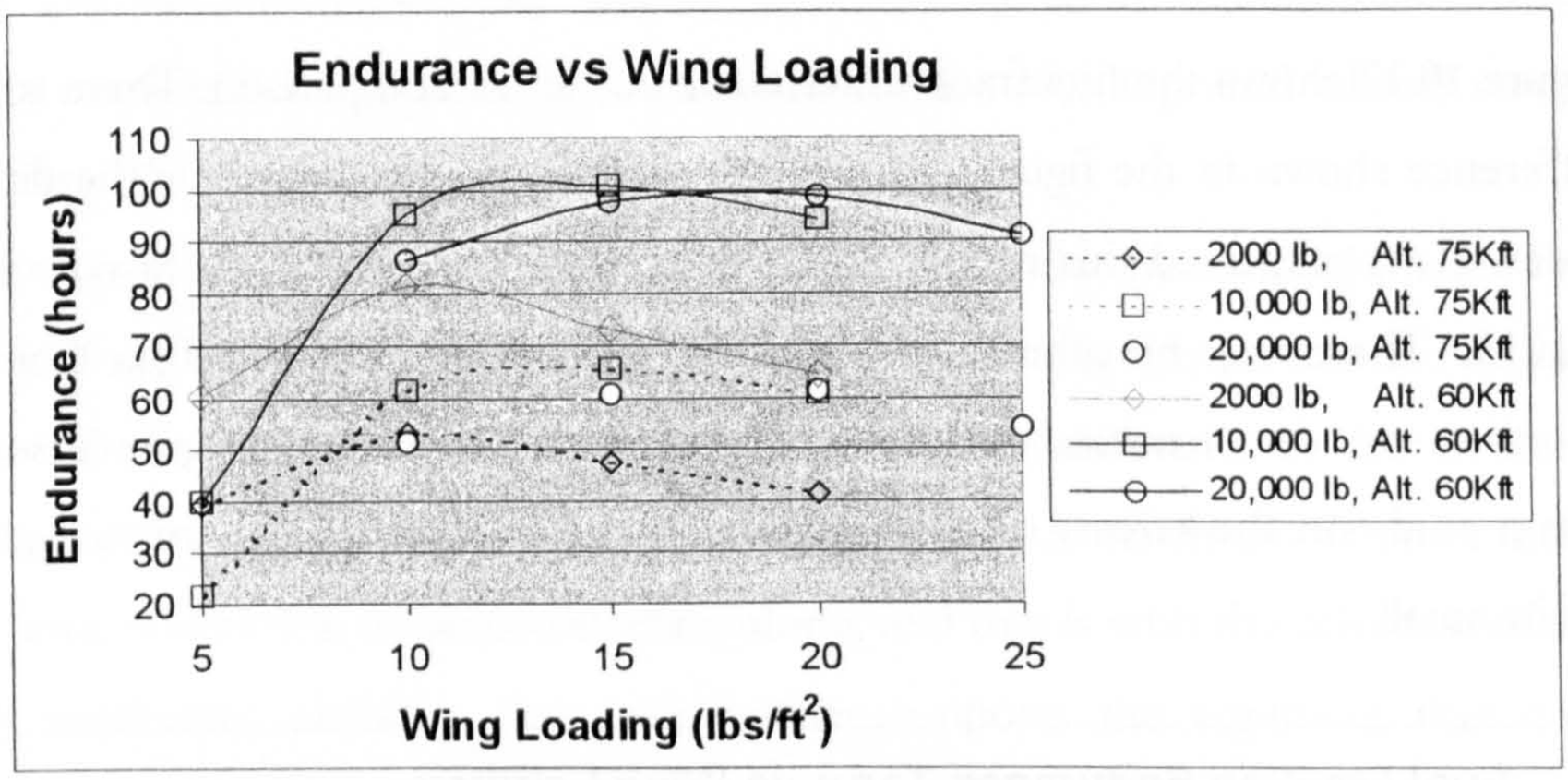

Figure 10.18 ***shows the dramatic effect of increased altitude on overall aircraft endurance.***

The overall aircraft endurance relationship is shown in Figure 10.18. The altitudes tested were the baseline, 60,000 feet and 75,000 feet. This figure is interesting due to the fact that once again, the shape of the curves does not change as a function of the variable being evaluated. It is comforting to know that the optimal wing loading for a given takeoff weight is not a function of cruise altitude. This greatly simplifies the decision-making process when selecting a design operating point. The distance between the curves for a given takeoff weight for the different altitude cases remains relatively constant across the range of takeoff weights and wing loadings considered with the exception of the lowest wing loading. This has already been shown to result from the fuel fraction term which reflects the sensitivity of the structural efficiency at large values for wing area.

The endurance term results can be seen in Figure 10.19. At the lowest takeoff weight, the endurance terms are almost equal. For the two higher takeoff weights, the more aerodynamically efficient case is the 60,000 foot altitude. It is important to mention that lift coefficient was kept constant at 1.3. One of the aerodynamic implications of this assumption is that the velocity was as much as 80 knots greater for the 75,000 foot altitude cases. Thus, there is a tradeoff in the Reynolds number between lower air density and higher cruise velocity.

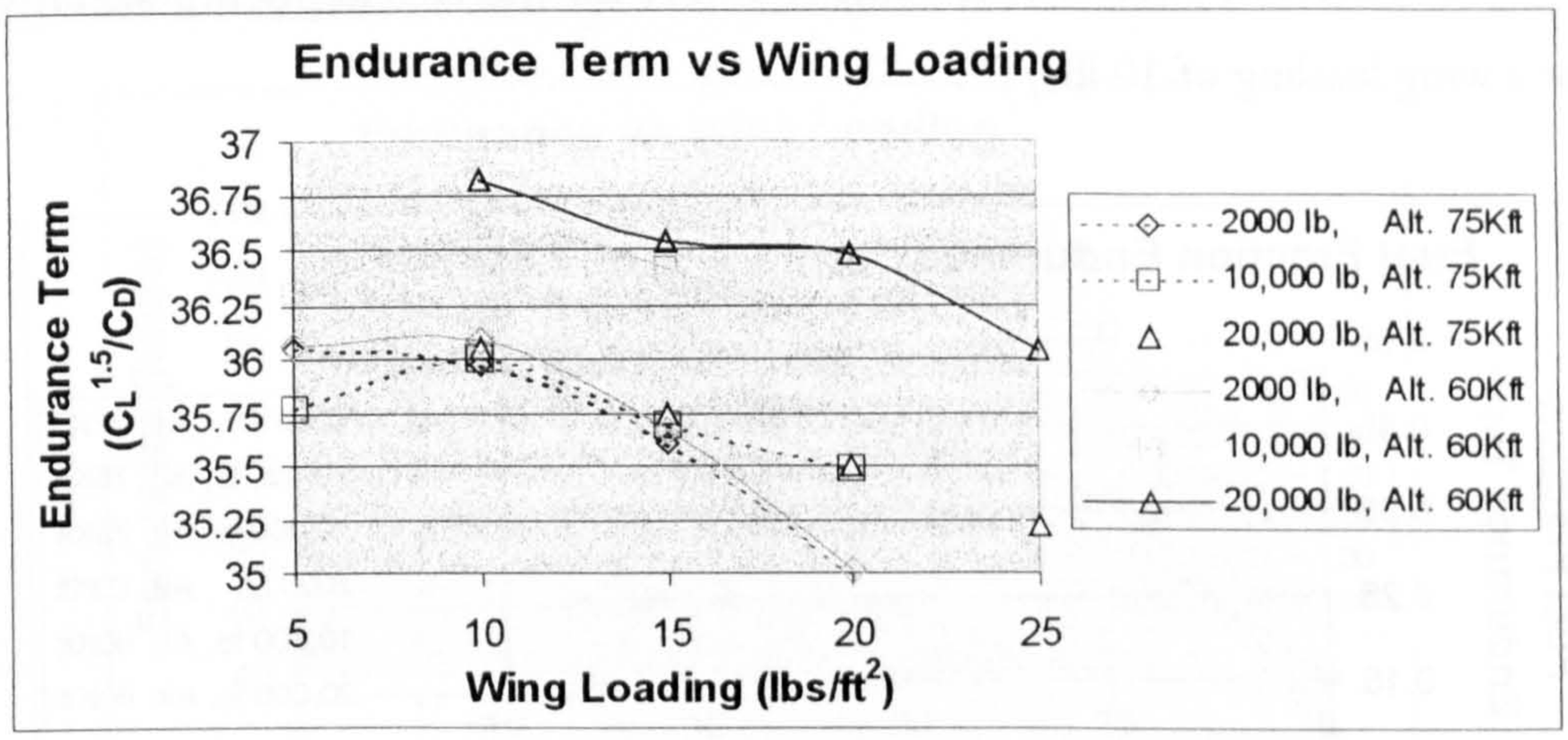

Figure 10.19 ***shows a curious decrease in aerodynamic efficiency with an increase in altitude.***

The change in air density is less than 10% for the change in altitude. The change in velocity necessary, however, was over 40% for all cases. It is therefore safe to assume that the Reynolds number for a given takeoff weight and wing loading was higher for the 75,000 foot altitude case. Despite this average increase of Reynolds number, the aerodynamic efficiency of the higher altitude case was still lower. This implies the relative domination of the lift induced drag compared to the parasite drag. Once again, however, the differences are quite small. The greatest difference between the two furthest points (20,000 pounds, 20 lbs/ft^2) was only 2.7%.

It is noted that the aerodynamic efficiency for the 2000 pound takeoff weight case is almost unchanged. This is due to very low wing area. The performance of the 2000 pound case was already abysmal in comparison to the higher takeoff weight cases. Thus the increase in altitude does not cause it to suffer as much in performance as the higher takeoff weight cases.

The fuel fraction term figure can be seen in Figure 10.20. At first glance, it would appear strange that there would be a change in estimated fuel fractional aircraft weight based solely on a change in cruise altitude. Upon further reflection it is realized that this change results directly from the assumption of constant lift coefficient and the corresponding increase in cruise velocity of over 40% for all cases. The least sensitive to these changes is the 2000 pound aircraft which already has a relatively low fuel fractional weight. The difference in the value for the fuel fraction term between the two cruise altitudes for the other two takeoff weights is reasonably constant across the range of wing

loadings. The maximum difference is roughly 13.1% for the 20,000 pound takeoff weight aircraft at a wing loading of 10 lbs/ft^2.

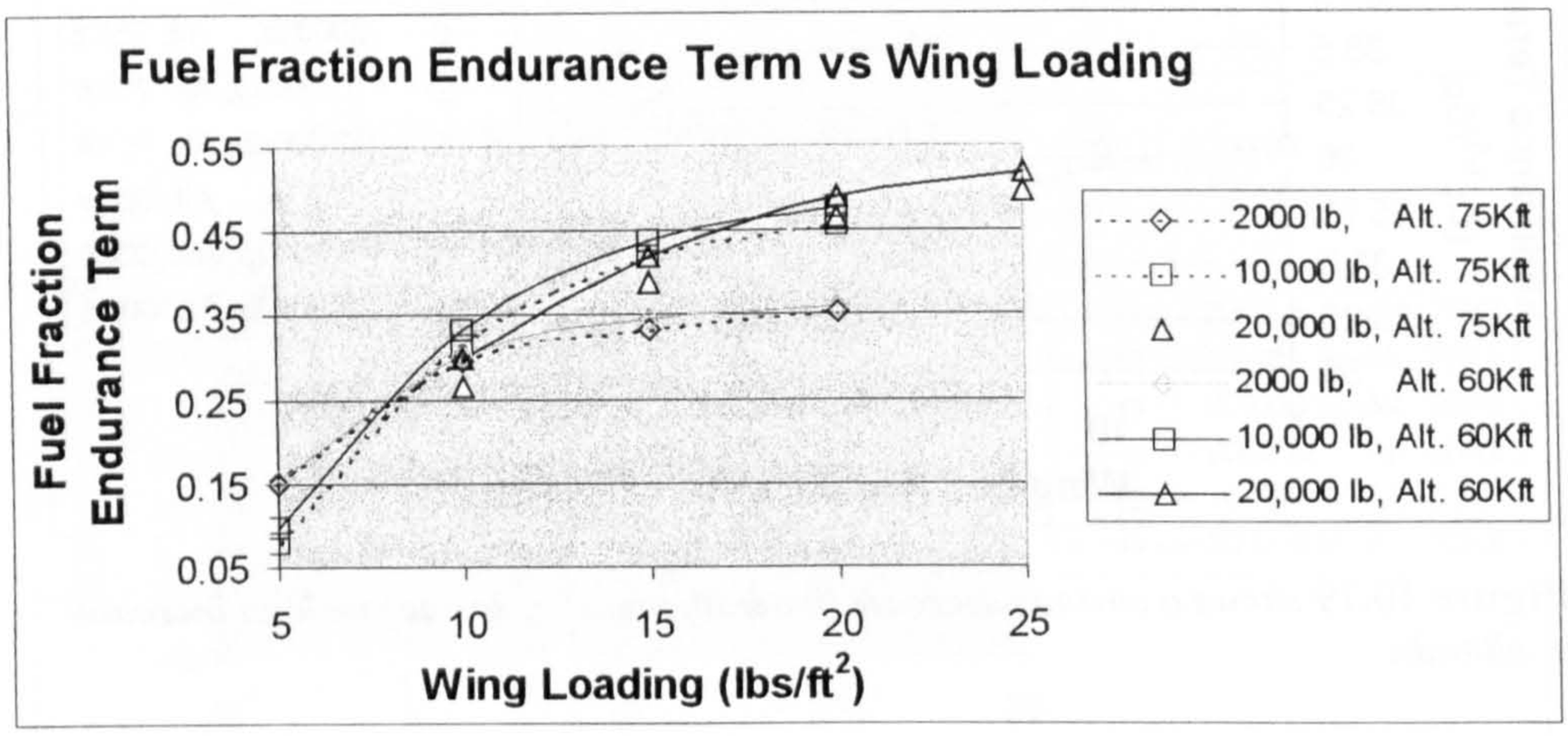

Figure 10.20 ***shows a very slight decrease in structural efficiency due to an increased cruise velocity corresponding to the increased altitude. This is a direct result of the assumed constant cruise lift coefficient.***

Figure 10.21 is included to show the difference in power required for cruise at the higher altitude. Regardless of these increases, it is still believed that the engines will be sized to the climb requirement. The increase in power required appears much more dramatic at higher takeoff weights, however the percentage increase (~45%) is roughly the same for all three takeoff weight cases.

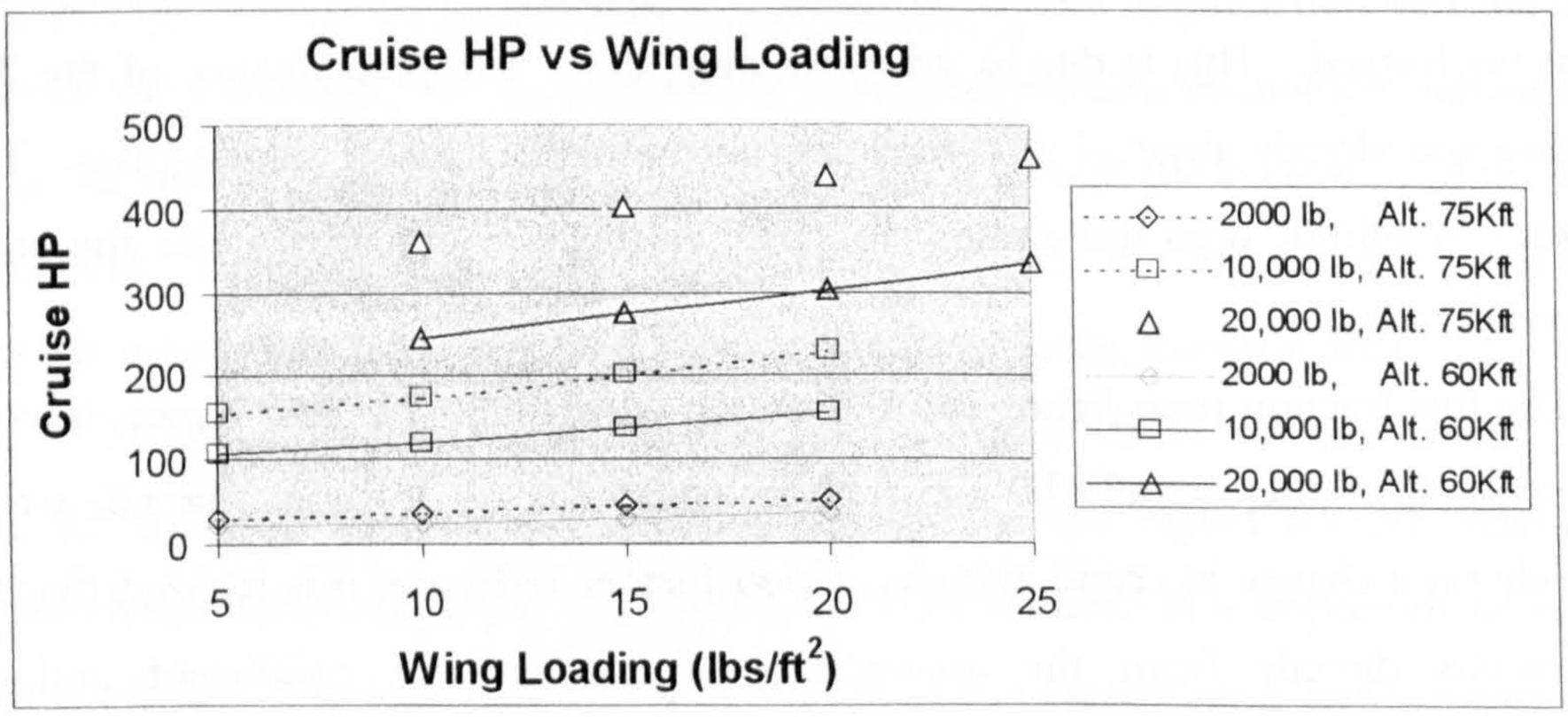

Figure 10.21 ***shows the very large increase in power required to cruise resulting from an increase in cruise altitude of 15,000 feet.***

10.B.4.b Lift Coefficient Study

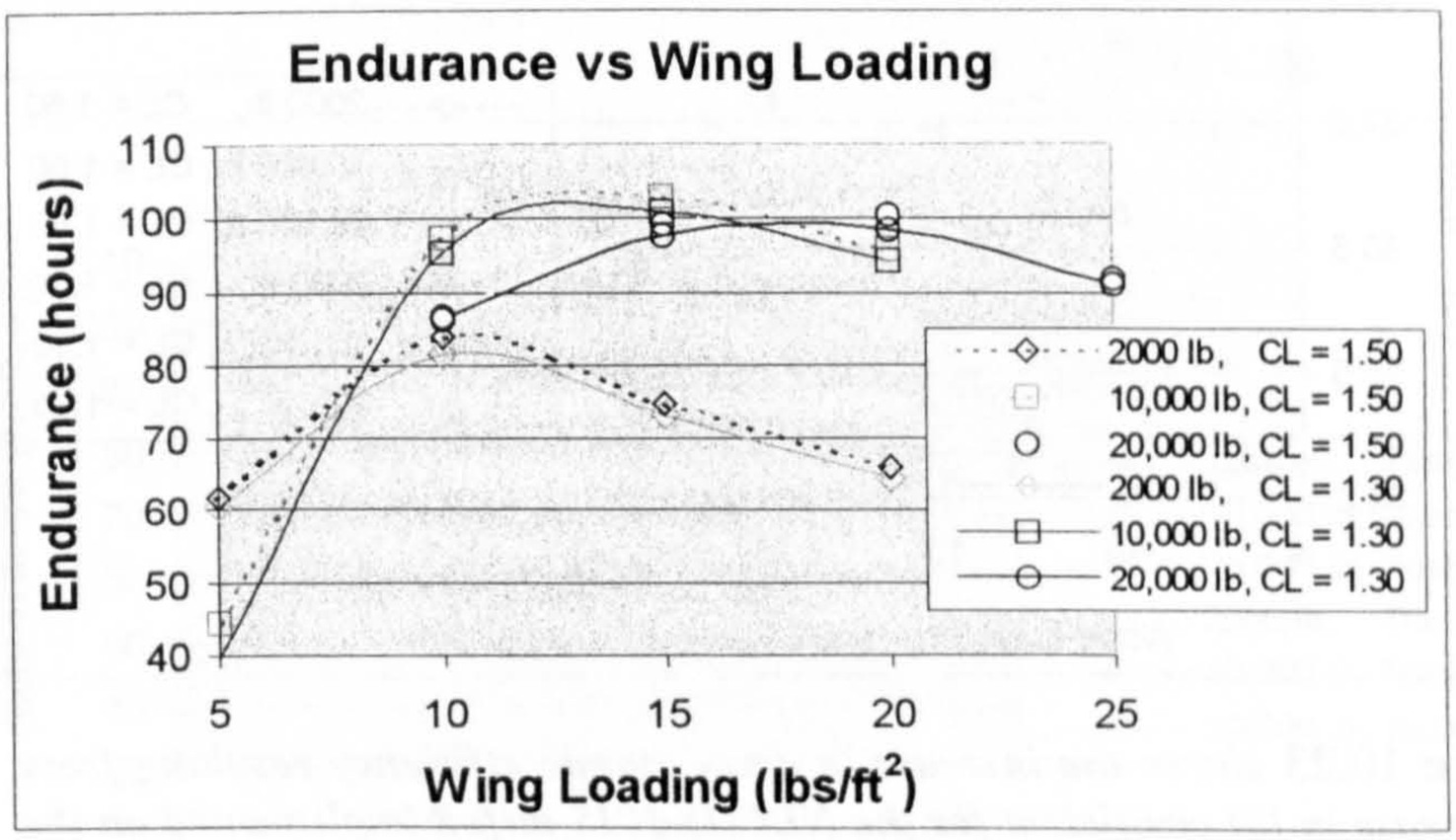

Figure 10.22 ***shows little effect on overall endurance due to a large lift coefficient increase for the aircraft using the NLF(1)-1015.***

The assumption was made in the airfoil figure of merit analysis that the value of 80% of the maximum lift coefficient was a more practical measure of the suitability of a given airfoil for use with a Low Speed HALE UAV. It was stated at the time that this was a conservative value. In order to insure that this value did not significantly bias the results, the following study on the effects of changing the lift coefficient from 1.3 to 1.5 was undertaken.

The results for the overall endurance can be seen in Figure 10.22. The most remarkable characteristic of this figure is the fact that the results are so close in value. This is attributed to the relatively flat laminar drag bucket region of the NLF(1)-1015. There was a maximum 2.0% difference between the 1.3 and 1.5 lift coefficient cases for all of the takeoff weights.

The next figure (Figure 10.23) shows the comparison of the endurance terms. It was known that the NLF(1)-1015 airfoil has not reached it's optimum aerodynamic efficiency until well beyond the lift coefficient of 1.3 used throughout this chapter. This is clearly shown in the figure, where it can be seen that the average increase in aerodynamic efficiency is roughly 1.5. The increase is a result of an increase in lift coefficient alone. The velocity has decreased by a much smaller amount compared to the previous section. The velocity was decreased by approximately 6.0% for all takeoff weight cases. It is thought that this change is tempered in the endurance term by the increase in aerodynamic efficiency of the airfoil.

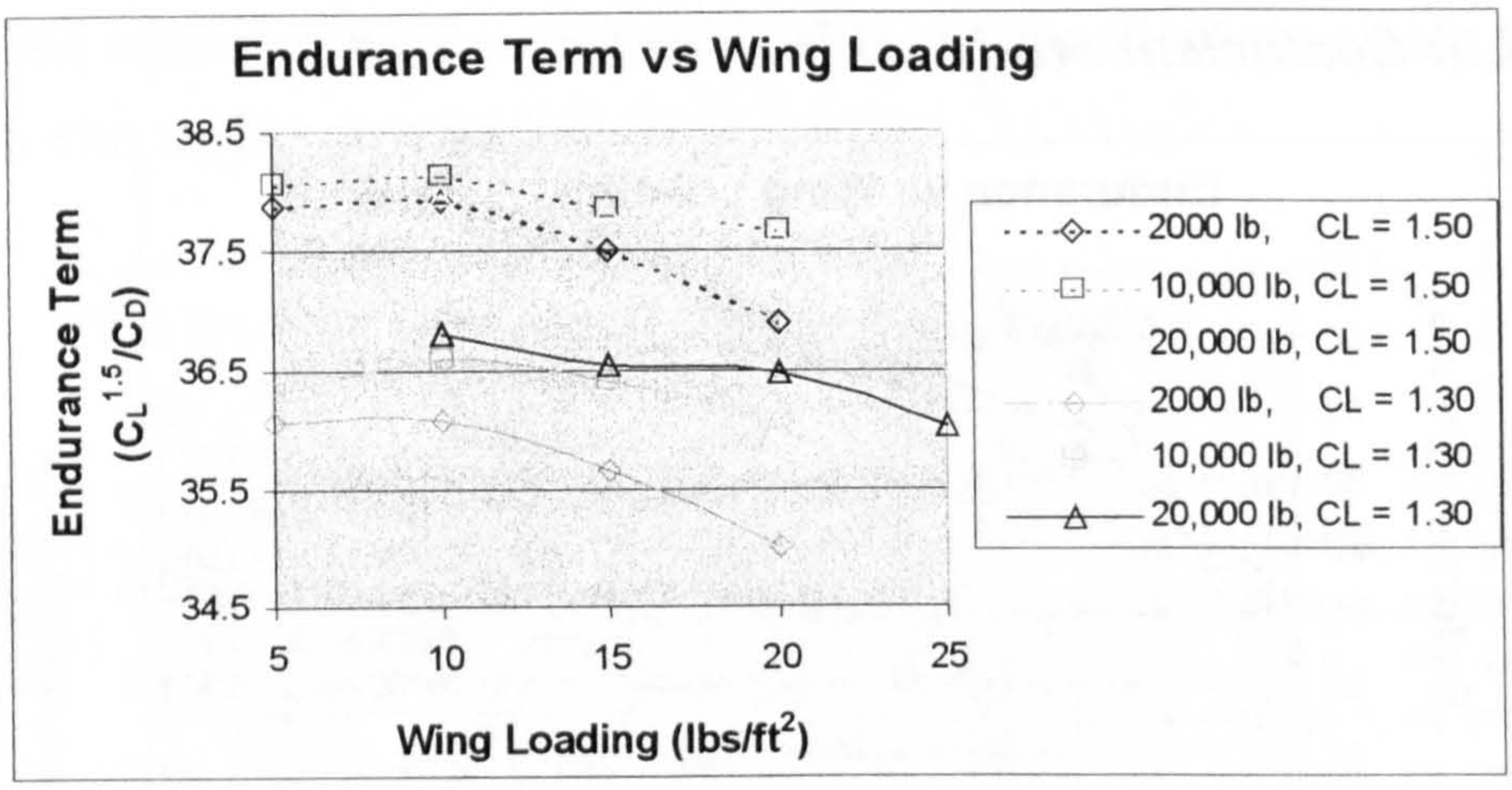

Figure 10.23 ***shows the increase in aerodynamic efficiency resulting from an increase in lift coefficient for the NLF(1)-1015 airfoil implemented on the Low Speed HALE aircraft.***

The fuel fraction graph is not shown since the resulting curves were not noticeably different. There was a very slight effect of decreased velocity. This served to change the fuel fraction an almost immeasurably minute amount. It was believed, consequently, that the figure would add little to the discussion and was therefore not included.

With the discussion of the effects of variation of the most influential design parameters on overall aircraft endurance for the conventional configuration now complete, it is possible to begin considering other configurations.

10.B.5 Study of the Effects of Engine Configuration

10.B.5.a Single Engine Pusher Propeller Configuration Study

The results for the comparison of the overall aircraft endurance for the conventional and pusher-propeller configured aircraft can be seen in Figure 10.24. At first it is surprising that the endurance of the pusher-configured aircraft would compare so poorly. The performance of the pusher appears to improve with increasing takeoff weight and wing loading.

The endurance term is higher by roughly 1.0 for the conventional configuration on average. The 20,000 pound takeoff weight pusher aircraft has increasing aerodynamic efficiency as it approaches higher wing loadings. This serves to decrease the difference in the predicted endurance between the pusher and conventional aircraft with increasing

wing loading. The fuel fraction terms for the two different configurations are for the most part identical.

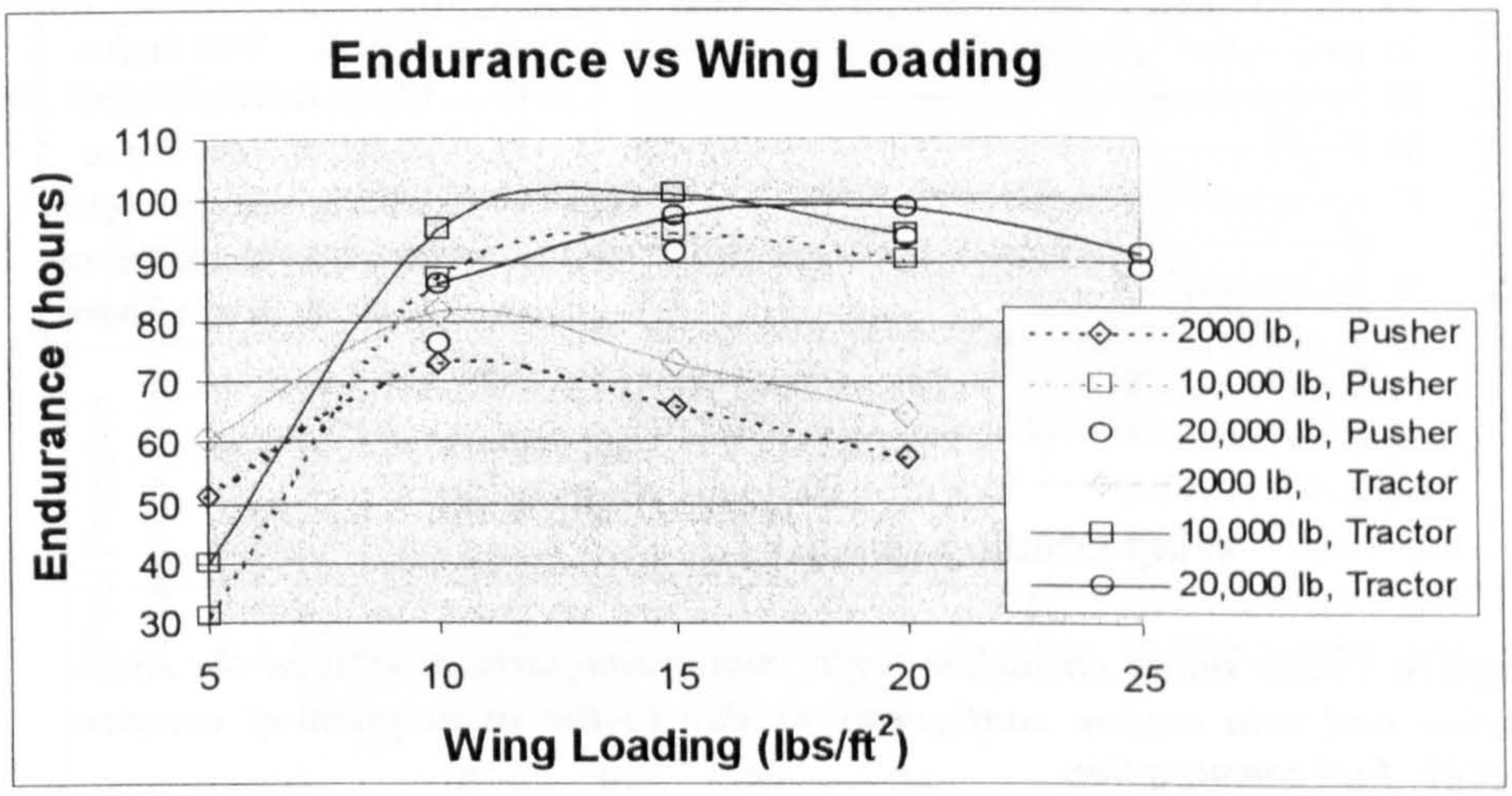

Figure 10.24 ***shows the somewhat surprising result of a decrease in aircraft endurance due to a change in propeller configuration from a tractor to a pusher for the conventional configuration.***

Thus, the reason for the difference in endurance between the two configurations must come entirely from the proximity of the wing to the tail and the related interference for the pusher configuration. It is mentioned that the benefits of the wing not being in the propwash were only included in the trim calculations. Given the relative size of the wing, it is thought that consideration of this effect on the aerodynamics would have a minimal impact.

10.B.5.b Twin Engine Study

10.B.5b.i Conventional Twin Engine Configuration

The twin engine endurance results are presented in this section mostly for completeness. These results will be used later for comparison to other twin engine configurations. The results can be seen in Figure 10.25. Obviously, the decision was made to keep the fuel consumption constant, despite the fact that the cruise horsepower for each engine was halved. Once again, it is mentioned that once a particular engine has been selected, the fuel consumption can be substituted and the absolute endurance corresponding to that fuel consumption can then be obtained.

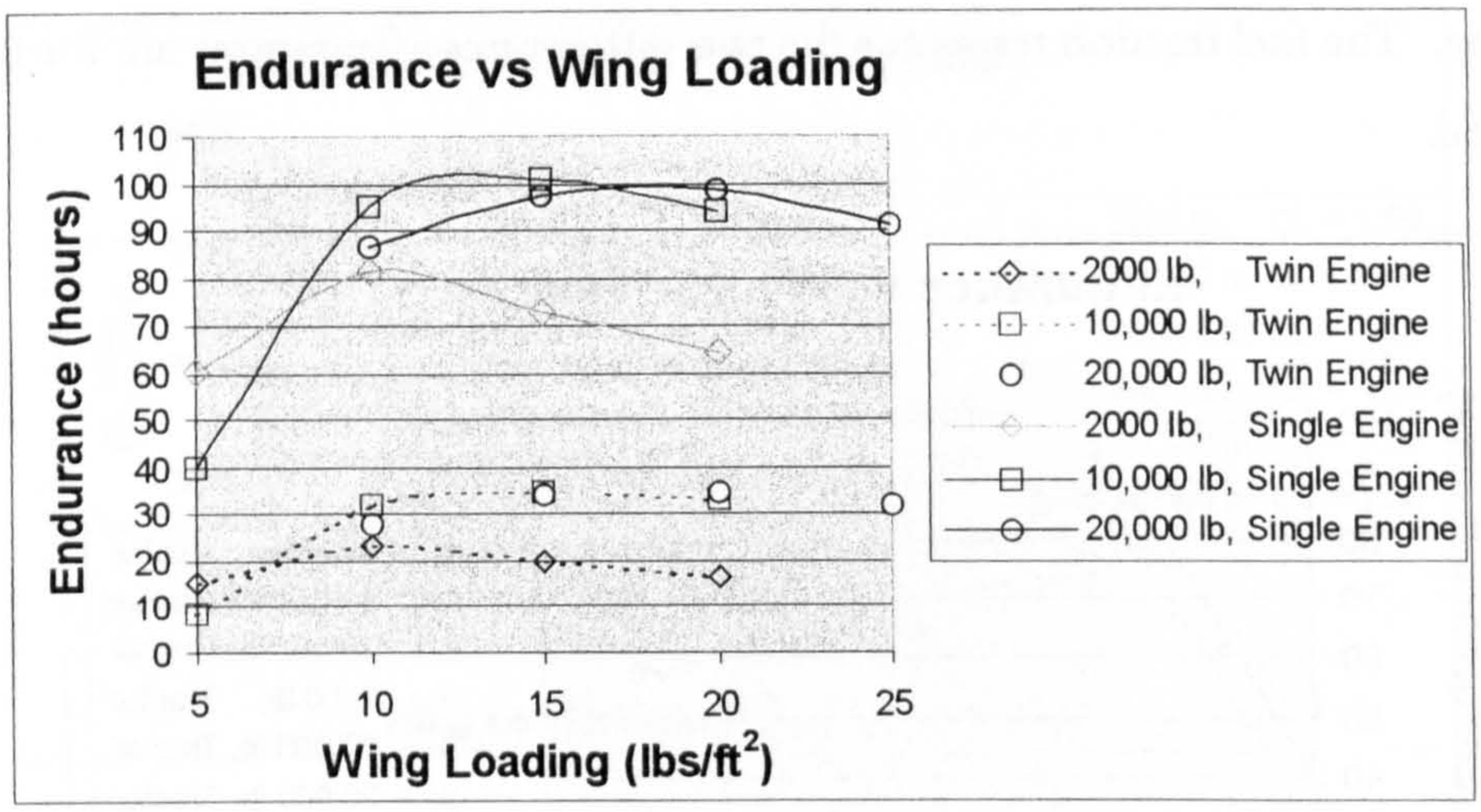

Figure 10.25 ***shows an unfair performance comparison between the single engine and twin engine configurations due to the assumption of constant specific fuel consumption.***

The next figure has a slightly more serious implication as the comparative trends are independent of any assumptions regarding fuel consumption. Figure 10.26 shows that there is a rather serious falloff in aerodynamic efficiency with increasing wing loading for the twin engine 2,000 pound takeoff weight case. This result demonstrates that at least in terms of aerodynamic efficiency, the additional drag inherent in adding nacelles and engines to the wing will most likely outweigh any benefits of additional power available for this weight class at even moderate wing loadings. Apart from the behavior of the 2,000 pound takeoff weight twin engine case, the twin engine endurance term is lower by roughly 2 throughout the range of wing loadings.

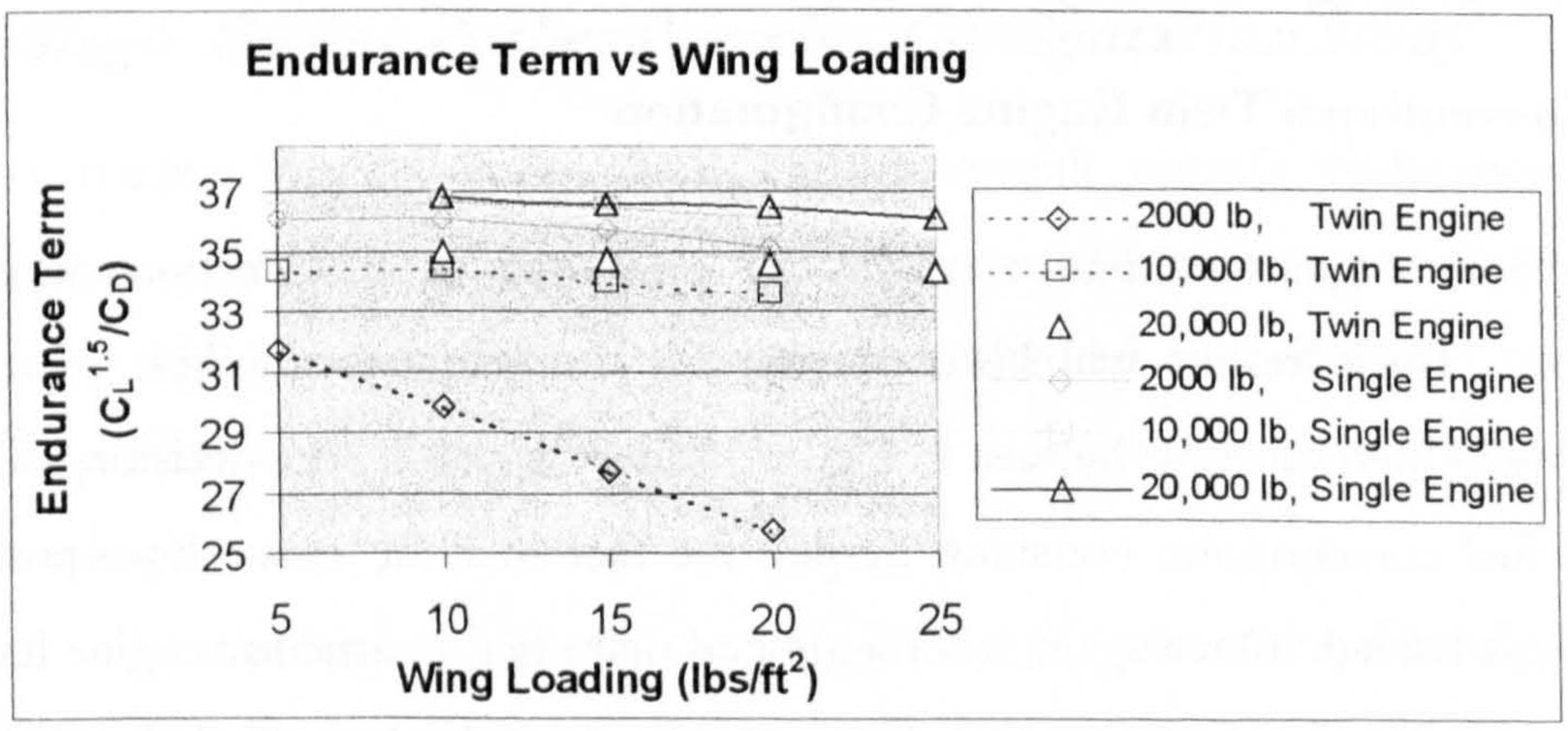

Figure 10.26 ***the endurance terms of the single and twin engine configurations.***

This incremental decrease is a result of the additional parasite drag of the nacelles. The reason this parasite drag has a greater effect on the 2000 pound case is that the nacelle

frontal area remains reasonably constant across all takeoff weights. This implies that for aircraft with less total wetted area, the effect of the addition of large nacelles on parasite drag is much greater since the nacelle drag is calculated as a combination of the nacelle frontal and wetted areas.

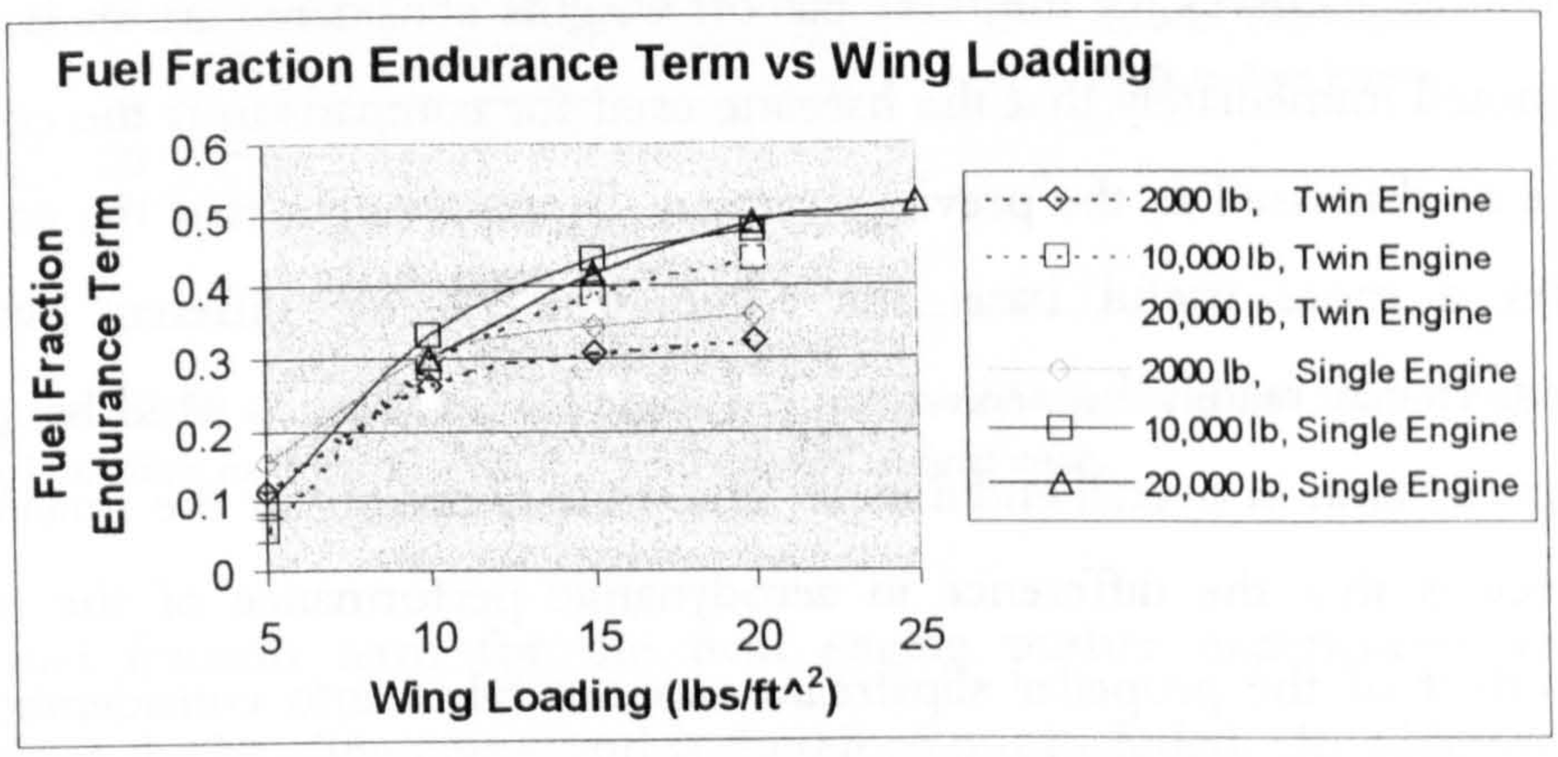

Figure 10.27 ***demonstrates the decrease in structural efficiency of the twin engine configuration.***

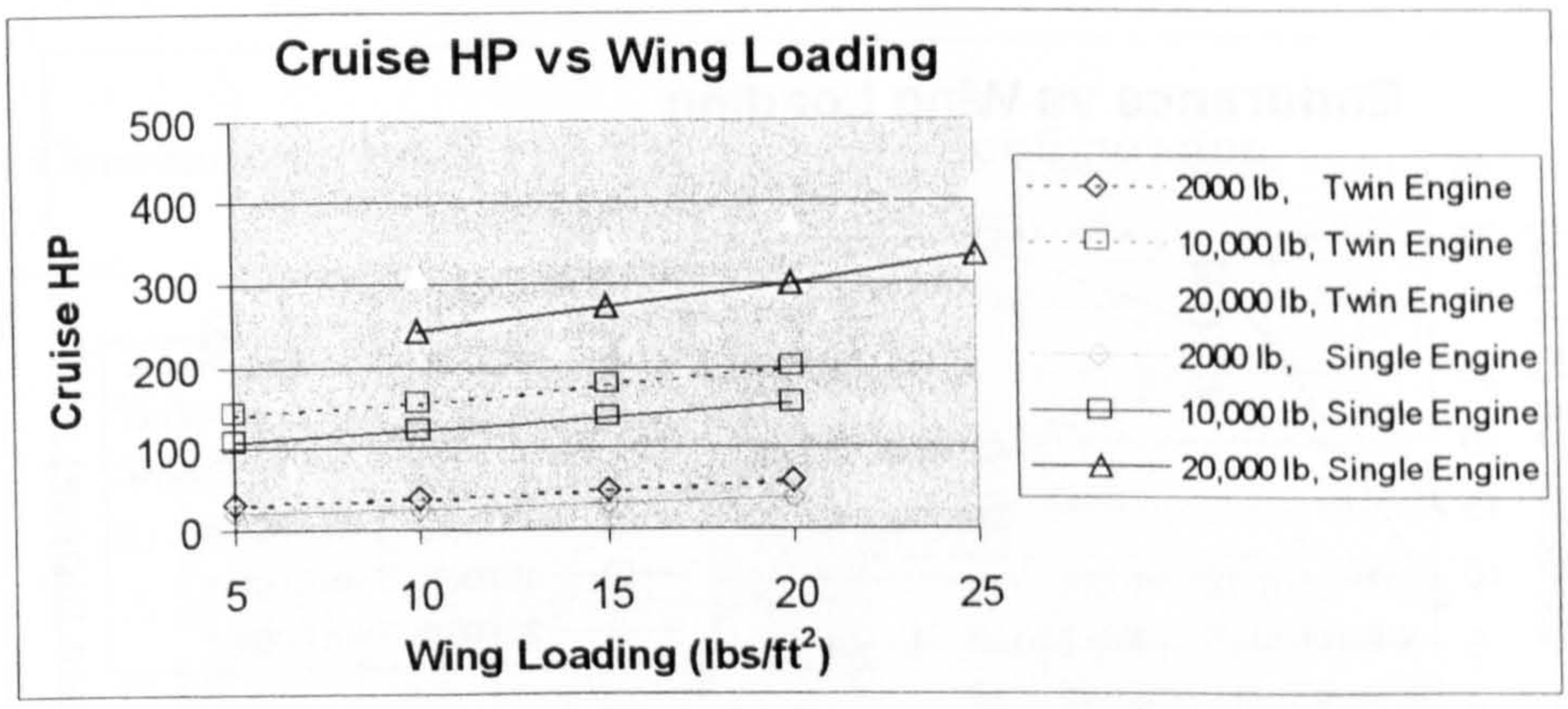

Figure 10.28 ***shows the increase in cruise power required for the twin engine configuration.***

The fuel fraction term figure (Figure 10.27) shows that for all takeoff weights the twin engine aircraft is less structurally efficient. Again, the general shape of the curves is consistent, and it is only the magnitude of the fuel fraction endurance term that is effected by the addition of an engine. It can be seen from this figure that any benefit from the additional bending moment relief resulting from the addition of the engines on the wing is outweighed by the additional weight of the second engine, nacelles, and installation.

The final figure shown for the conventional twin engine study is the comparison of the cruise power required. Figure 10.28 shows that considerably higher power is required

in cruise for the twin engine aircraft at all takeoff weights considered. This is representative of the extremely large drag penalty of the nacelles.

10.B.5b.ii Conventional Twin Engine Pusher Configuration

The endurance curves for the three takeoff weights considered are shown in Figure 10.29. It is noted immediately that the baseline used for comparison is the conventional twin engine case discussed in the previous section. It was thought that the conventional twin provides a more useful basis for comparison of the different twin engine configurations. It can readily be seen from the figure that there is little benefit to the pusher configured twin in overall endurance. The primary reason for the small difference in performance is that the difference in aerodynamic performance of the main wing without the effect of the propeller slipstream was not taken into consideration by the methodology. The only instance that the propeller slipstream effect was taken into account was in the trim calculations.

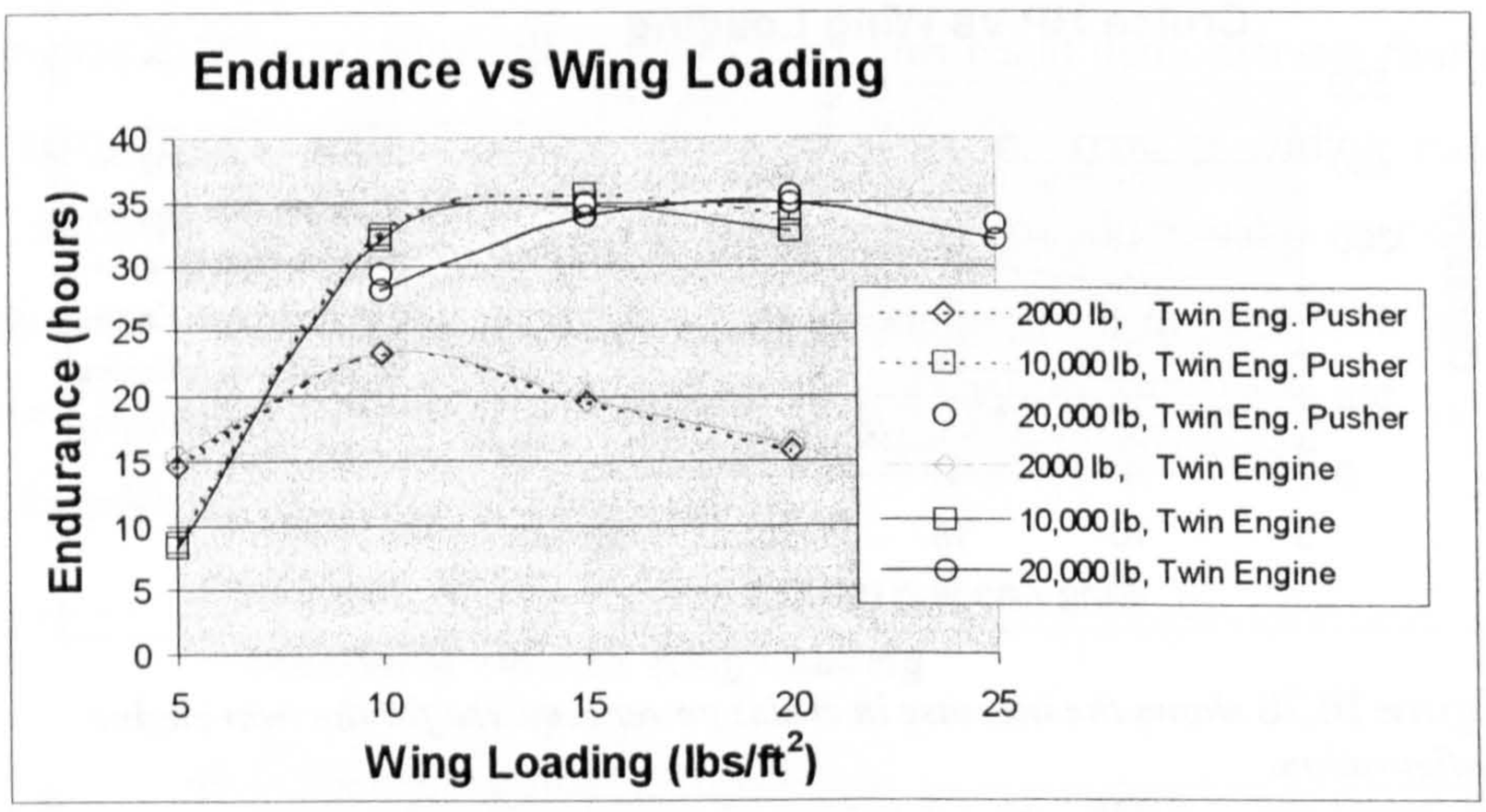

Figure 10.29 ***shows a very minute advantage in overall endurance for the pusher configured twin engine aircraft.***

The endurance term results can be seen in Figure 10.30. In this figure, the only takeoff weight experiencing a significant deviation is the 2000 pound case. The other two takeoff weight cases are essentially the same as for the tractor configured aircraft. In order to balance this particular configuration it was necessary to move the wing much closer to the horizontal tail. The deviation is most likely a direct result of higher drag predicted due the closer proximity of the wing to the tail.

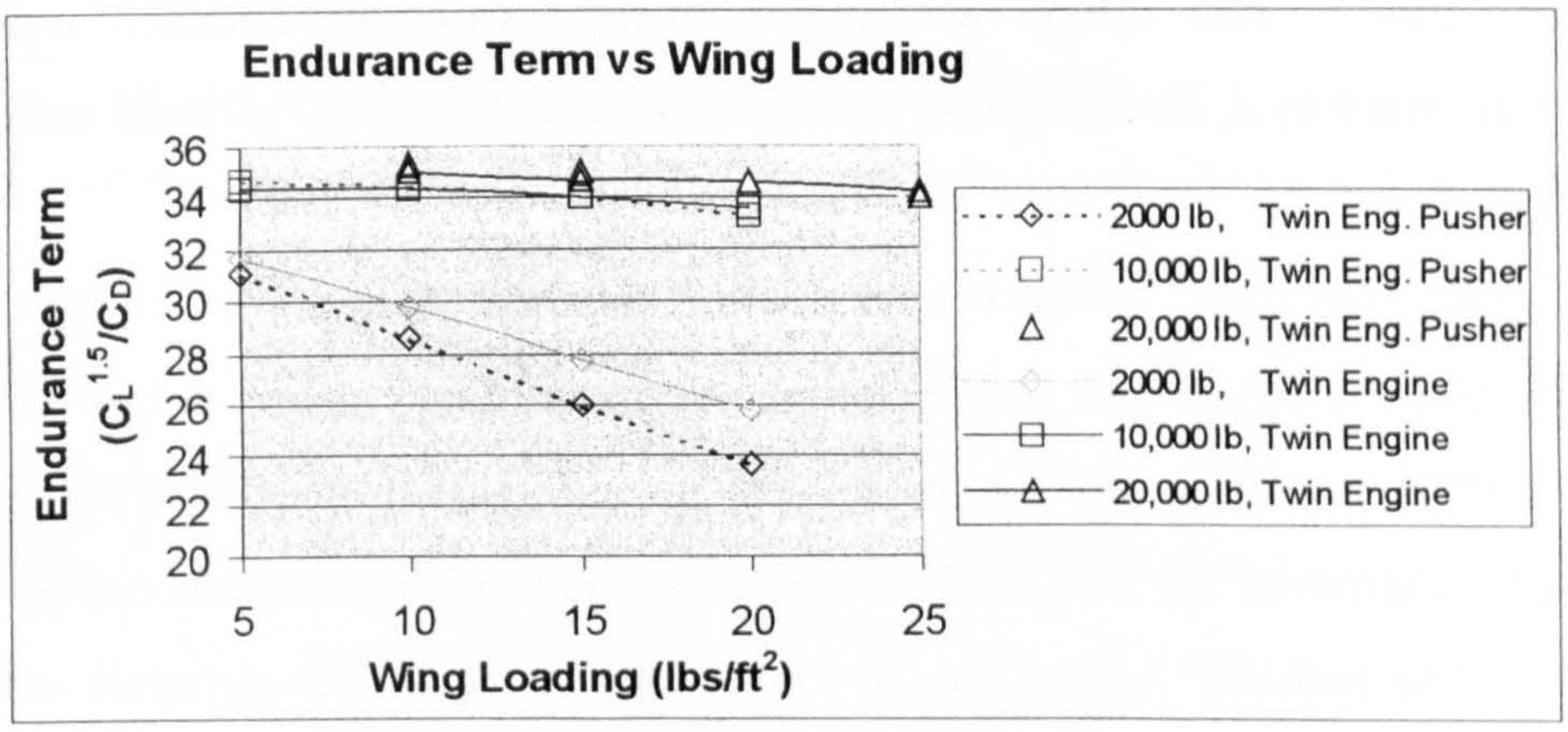

Figure 10.30 ***shows a deviation in endurance term from the conventional twin configuration only for the 2000 pound takeoff weight case.***

The fuel fraction term for the twin engine pusher experienced very minute departures from the baseline curve, and is therefore not included. In addition the power required in cruise was only minutely less for the pusher configuration on average and was not included.

10.B.5b.iii Conventional Push-Pull Twin Engine Configuration

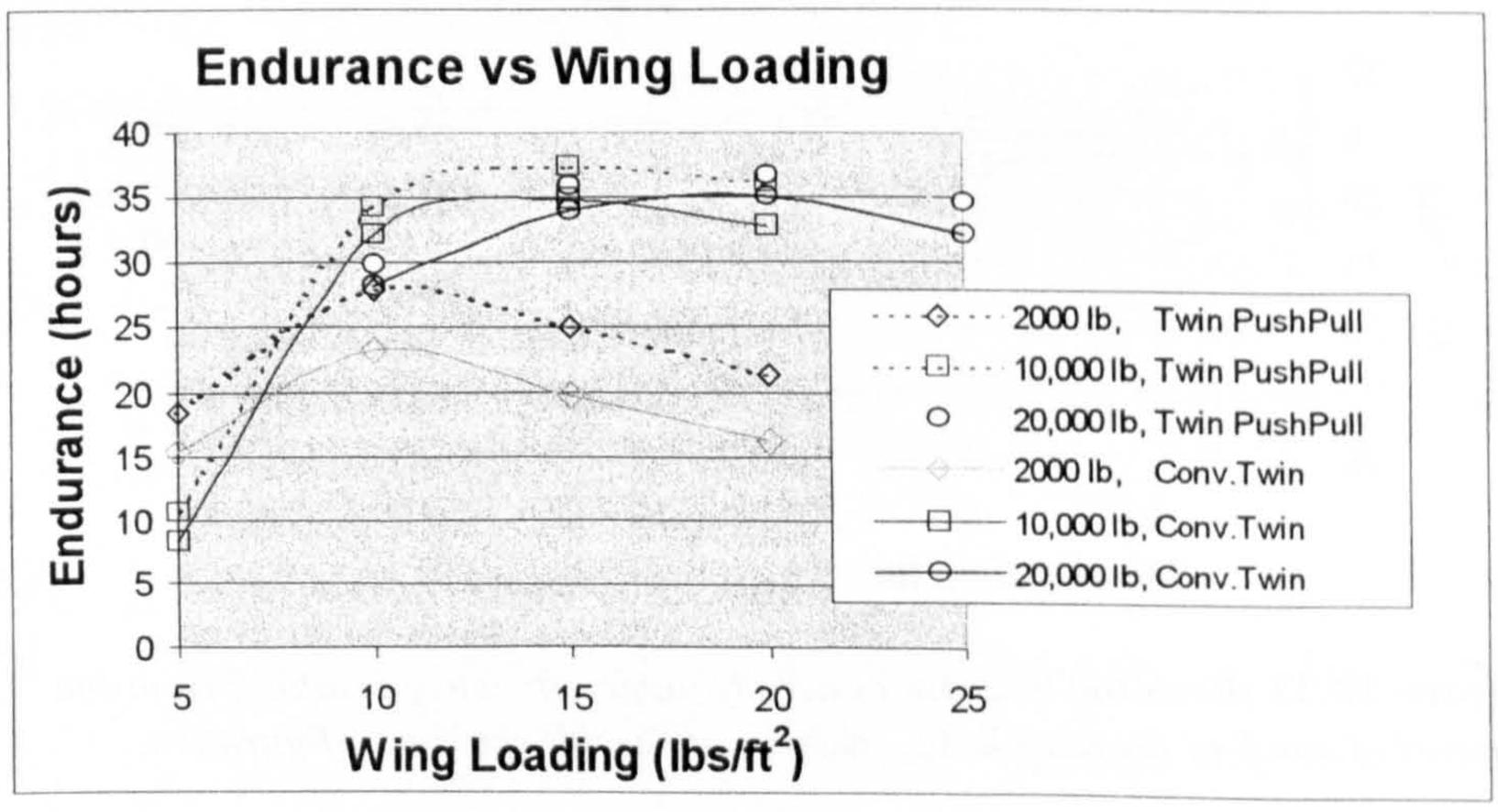

Figure 10.31 ***shows a significant improvement in endurance of the twin engine push-pull configuration 2000 pound case over the conventional twin engine tractor.***

The conventional twin engine push-pull configuration showed the most promise in terms of overall endurance out of all of the conventional twin engine configurations considered. The behavior of the endurance for this configuration can be seen in Figure 10.31. The improvements in endurance were most pronounced for the 2000 pound

takeoff weight case. The other two takeoff weight cases experienced much less improvement in endurance, however they still outperformed the conventional twin engine tractor configuration.

Once again, the fuel fraction terms were identical for the two twin engine configurations and the figure was not included. With the fuel fraction terms essentially identical, the difference between the two 2000 pound takeoff weight cases must be explained solely in terms of the endurance term. The variations in this term can be seen in Figure 10.32. The primary reason for the large difference in aerodynamic efficiency between the two 2000 pound cases is the significant decrease in parasite drag. This decrease results from the removal of the large nacelles from the wing, thereby greatly reducing the wetted area due to the addition of the second engine.

Finally, a very small decrease in cruise horsepower required was evident from the results. This improvement was not significant enough to include in a figure, however.

The discussion of the endurance results for the conventional configuration is now complete. In the process of generating and analyzing these results, interesting behavior in the structure fractional weight was noted. This behavior is the topic of the next section.

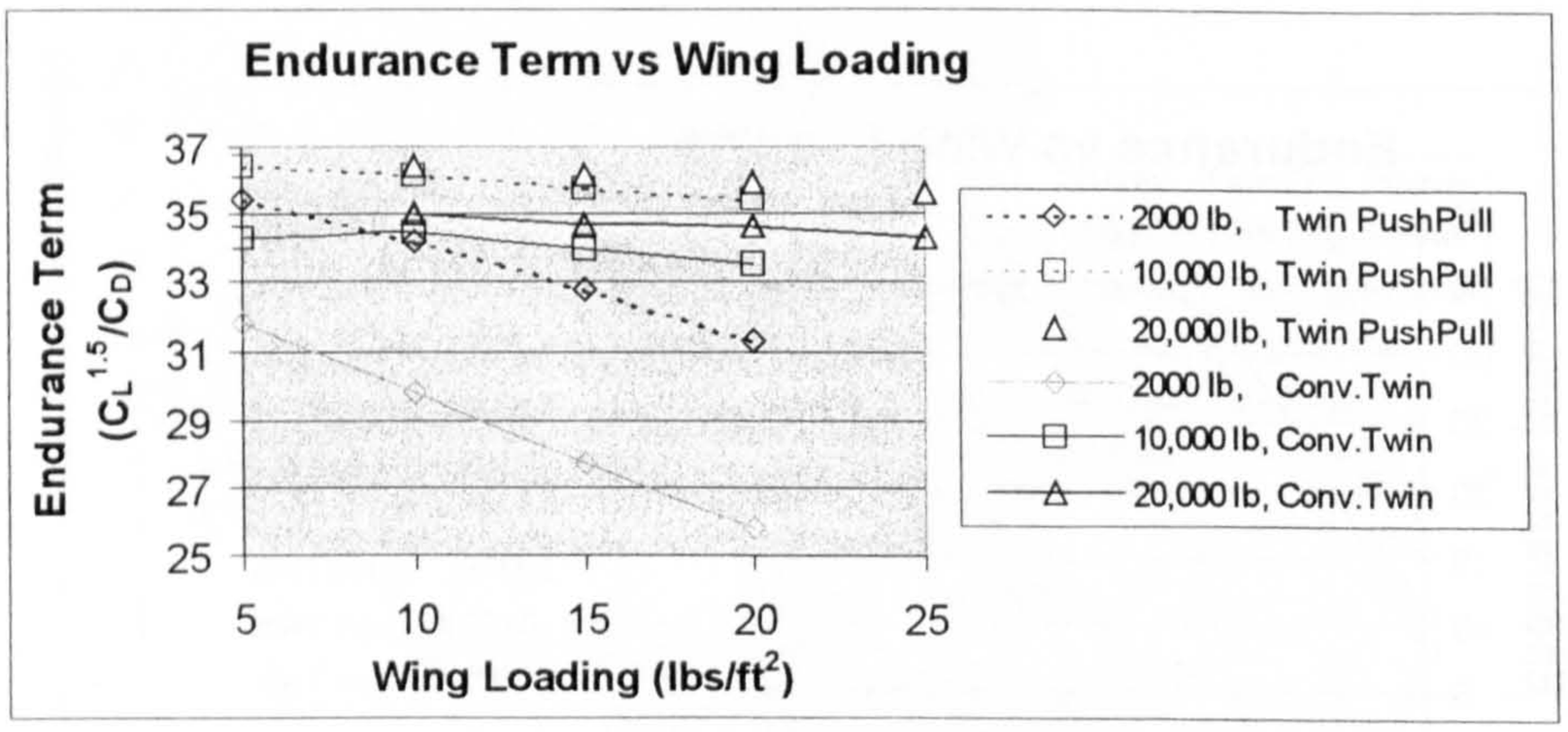

Figure 10.32 ***shows the increase in aerodynamic efficiency resulting from the removal of much of the nacelle S_{wet} with the push-pull engine configuration.***

10.B.6 Proposed Empty Weight Fraction Relation

The characteristic shape of the empty weight, or structure fractional weight $\left(\frac{W_{struct}}{W_{to}}\right)$ curve(s) in Figure 10.7 facilitated the development of the following relation for the estimation of the empty weight fraction of a Low Speed HALE UAV aircraft. The

relation is a function of known wing loading, aspect ratio, taper ratio, and number of engines. A "power" curve fit was performed for the results of the aforementioned studies for the conventional configuration. The changes in structure fractional weight were small enough to ignore (in general less than 1.5%) for the variations in lift coefficient, airfoil (and thus small changes in thickness to chord ratio), altitude, payload fractional weight, and pusher-propeller configuration. Special consideration had to be taken for the twin engine, aspect ratio and taper ratio cases. The resulting relation appears as follows :

$$\frac{W_{empty}}{W_{to}} = K_{eng}\left(0.192\lambda + 1.208\right)\left(\frac{W}{S}\right)^{\left(4.092\times10^{-3}AR - 0.572\right)} \qquad \textbf{(10.2)}$$

Where K_{eng} is a twin engine factor which is equal to 1.081 for twin engine aircraft, and 1.0 for single engine aircraft. λ is the aircraft taper ratio. AR is the aircraft aspect ratio, and W/S is the aircraft takeoff wing loading.

The range of applicability of the relation is limited to :

Wing loadings of : $5 \le \frac{W}{S} \le 25 \frac{lbs}{ft^2}$,

Payload fractional weights of : $0.05 \le \frac{W_{PL}}{W_{to}} \le 0.15$,

Takeoff weights of : $2{,}000 \le W_{to} \le 20{,}000\ lbs$,

Wing Areas of roughly : $250\ ft^2 \le S_{wing} \le 1752\ ft^2$

And Aspect ratios of : $20 \le AR \le 40$ based on the output from the methodology used to fit the "power" relation.

Use of this relation has a maximum error of less than 10% when compared to the data from which it was fit. More specifically, a single case, the 5 lbs/ft^2, aspect ratio 22 case had an error of 9.5%. The remainder of the maximum errors encountered from the curve fitting process were less than 5.0%. The average error was less than 3.0% across all cases for which the curve fit was modeled. Since the relation was developed using the results of this methodology, the error encountered when comparing the results of the relation to existing Low Speed HALE UAV's is similar.

10.C Alternative Configurations

Although the methodology makes available a large amount of data on the breakdown of the drag and weight of the aircraft being studied, time and space restrictions prevent the inclusion of these results in this thesis. Instead, it was decided to continue with the approach used in the previous section to study overall aircraft endurance. The execution of the methodology was performed under conditions identical to those in Section 10.B.2 for all configurations. The method used for comparison is similar to the previous section, where the overall aircraft endurance was broken down into an endurance term and a fuel fraction term.

A minor change had to be implemented in the reporting of the endurance term results when comparing alternative configurations. When the comparison was performed for the conventional configuration, it was thought important to compare the various quantities based on constant wing lift coefficient, not total aircraft lift coefficient (aircraft plus tail). Tail lift has a minor effect when compared across different wing loadings and takeoff weights for the same configuration, assuming reasonably constant static margin across the configurations. This is not the case, however when comparing the conventional configuration to alternative configurations.

Thus, the aircraft endurance term was re-calculated for the conventional configuration with the inclusion of tail lift, and all subsequent endurance term calculations were performed similarly for the purposes of comparison. It is of interest to note at this point that the comparisons performed thus far were all for configurations with as close to neutral longitudinal stability (on average) as possible in order to minimize the effects of trim. The average neutral longitudinal stability was achieved by the longitudinal variation of the location of the payload in the fuselage and the wing on the fuselage.

10.C.1 Canard

For the canard configuration, the fuel fraction terms were essentially identical to those calculated under the same conditions for the conventional configuration. Thus, these terms will not be included in the discussion in the following comparison. The differences in endurance between the conventional and canard configurations found by the methodology were thus strictly aerodynamic in nature.

10.C.1.a Single Engine Canard Tractor

The results of the overall endurance comparison between the conventional single engine tractor and the canard single engine tractor are shown in Figure 10.33. The canard tractor appears in general to perform quite well when compared to the conventional case for all but the 2000 pound takeoff weight. The differences are quite small with the exception of the highest wing loading 2000 pound takeoff weight case. Looking at the endurance term provides a better understanding of why this happens.

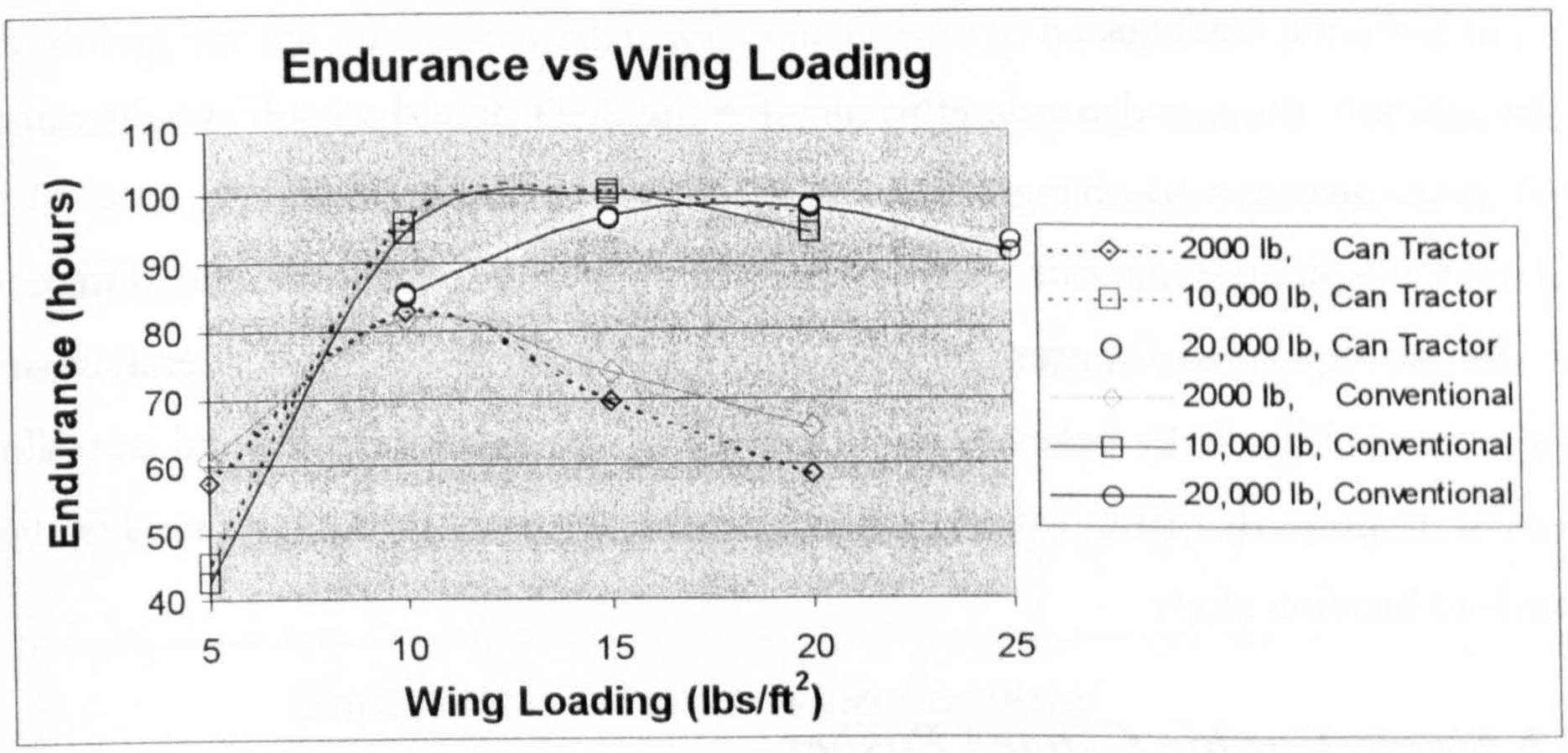

Figure 10.33 ***compares the overall aircraft endurance of the conventional single engine tractor to the canard single engine tractor configuration.***

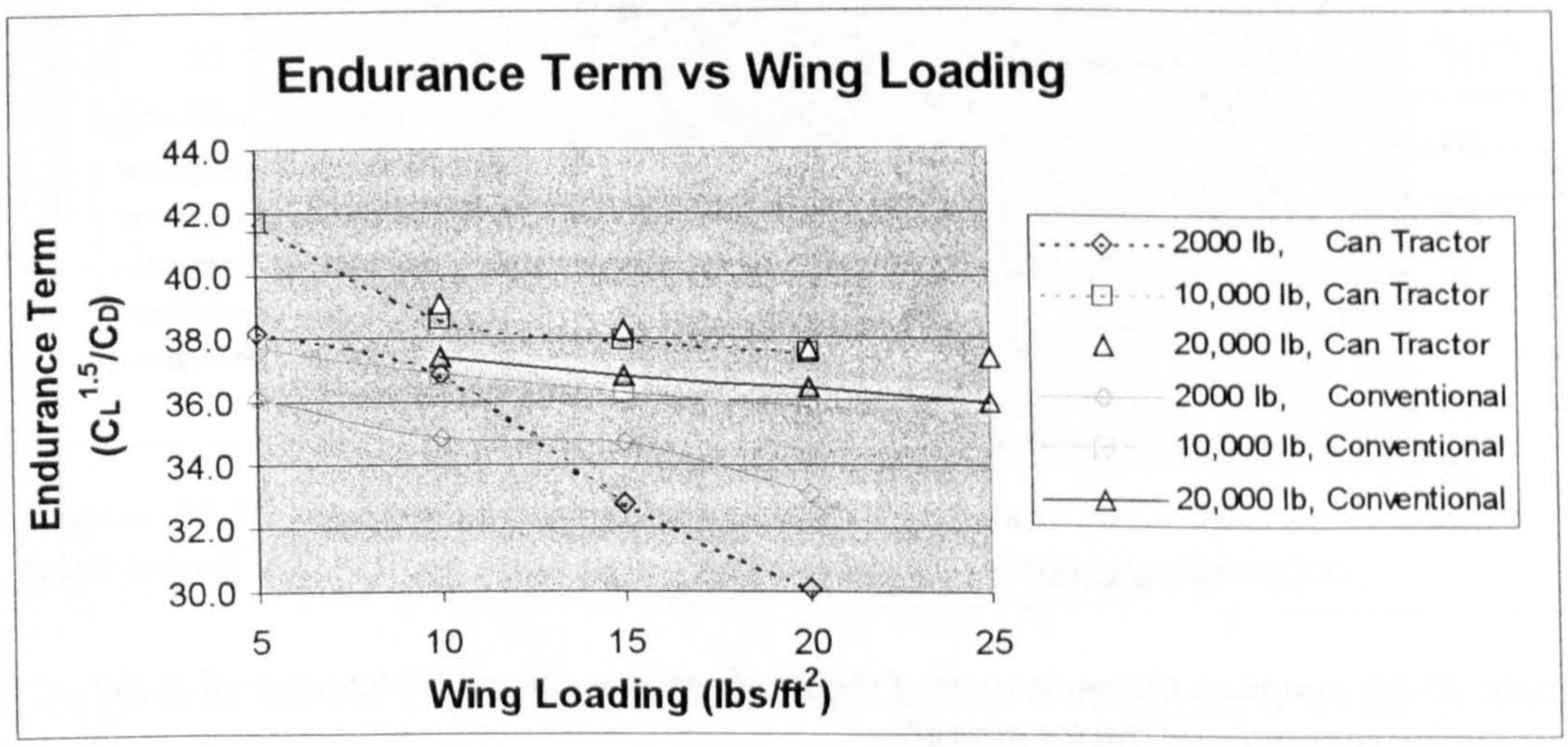

Figure 10.34 ***displays increased slope for the aerodynamic efficiency curve of the canard tractor aircraft at low wing loadings when compared to the conventional tractor aircraft.***

Figure 10.34 shows the endurance term behavior for the canard tractor compared to the conventional aircraft case. The behavior of the curves is consistent with the trends

viewed in previous configurations, decreasing aerodynamic efficiency with increasing wing loading. It was discovered that the lowest wing loadings for each takeoff weight yielded the lowest fuel fractions for the given takeoff weight. This in turn made control of the center of gravity much more challenging. Since the wing loadings were the lowest, they result in the highest wing area cases for each takeoff weight. This implies that the lift force on a proportionally sized control surface, would be a maximum compared to the other configurations considered, provided the moment coefficient remains constant. It is suspected that this is the source of the deviations in the slope of the aerodynamic efficiency at low wing loadings.

In addition, the aerodynamic efficiency for the 2000 pound takeoff weight canard aircraft is more sensitive to changes in wing loading than the conventional case. It is believed that the lightest aircraft experiences the greatest influence of the difference between the tail download for trim and the canard upload. The lightest aircraft was in general the most difficult to balance, as the length of the fuselage often did not allow enough room to properly manipulate the aircraft center of gravity location by modification of the payload location alone.

10.C.1.b Single Engine Canard Pusher

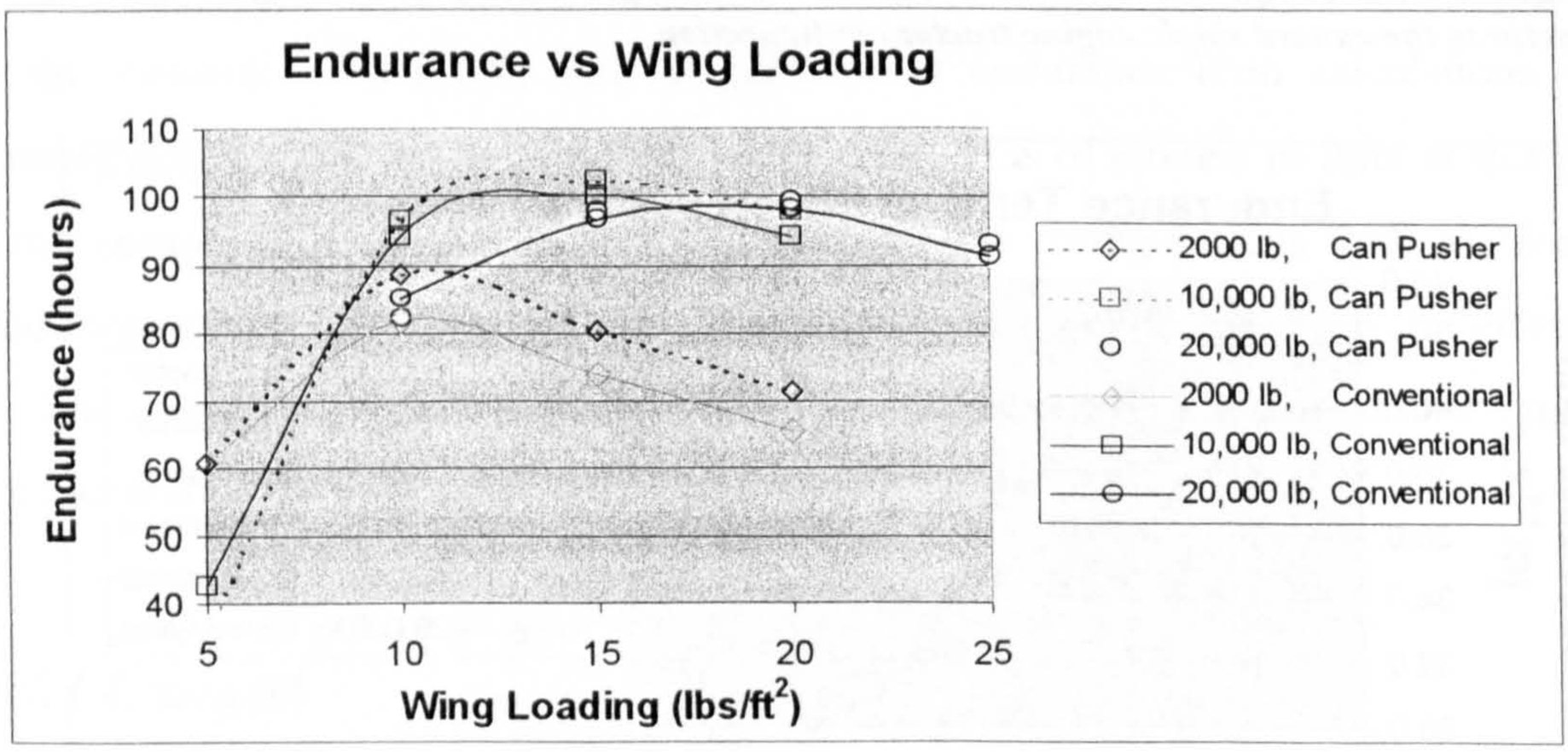

Figure 10.35 ***compares the endurance of the single engine canard pusher aircraft to the single engine conventional tractor aircraft.***

The overall aircraft endurance results for the single engine canard pusher can be seen in Figure 10.35 compared to the results for the conventional case. In general, the results of the pusher propeller configured canard are better than those for the tractor configured

canard. This seems to support the argument that small changes in average center of gravity location can have a significant impact on the overall aircraft endurance. All of the takeoff weight cases experienced improvement due to the change in engine and wing position resulting from the change to a pusher configured aircraft. The only exception was the value for endurance for lowest wing loadings.

The endurance term for the canard pusher can be seen in Figure 10.36. It is interesting to note that the behavior of the 2000 pound canard tractor aerodynamic efficiency term is not repeated for the pusher configured canard. In executing the methodology for the pusher canard, it was much easier to balance the aircraft, and a much more acceptable range of travel for aircraft center of gravity was found. The result seen in the aerodynamic efficiency term for the 2000 pound takeoff weight case serves to support the argument that aircraft configurations that require less average moment to trim have greater aerodynamic efficiencies. Thus the better balanced aircraft configuration will normally be more desirable from an aerodynamic standpoint. Although this may seem to be stating the obvious, it is reassuring that the methodology provides the expected result.

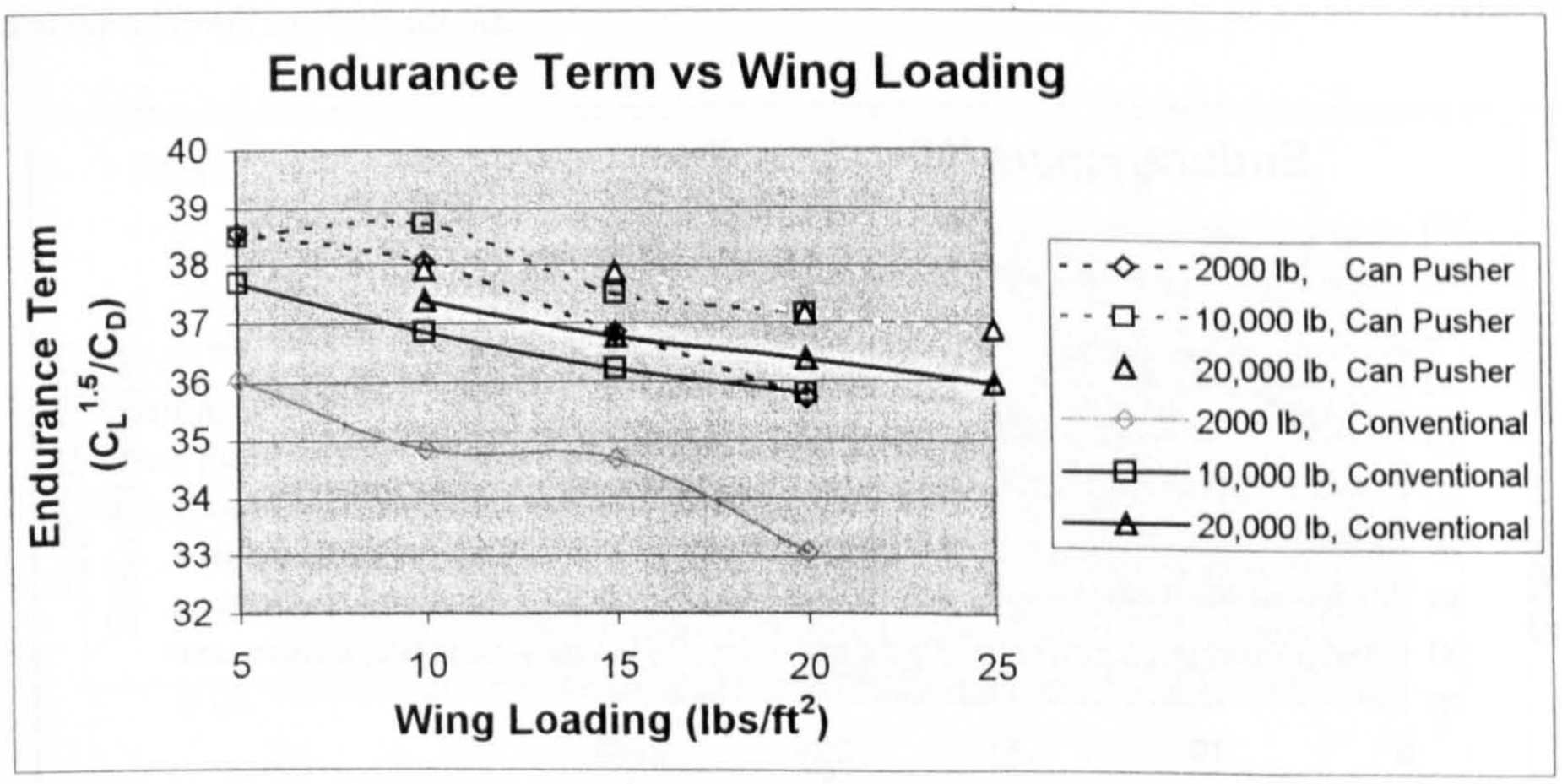

Figure 10.36 ***shows greater aerodynamic efficiency for the canard pusher aircraft at a lower takeoff weight when compared to the conventional tractor configuration.***

In general, for the single engine canard, the pusher configuration would be the more desirable of the two configurations based on endurance performance alone. At the lower takeoff weights, the canard pusher shows significant advantages over the conventional configuration in overall aircraft endurance, and compares reasonably well in overall endurance across the range of wing loadings considered. Due to the relative equality in

overall endurance, the selection between the canard and the conventional configurations would likely be based on factors other than performance for the higher takeoff weight cases. Finally, the power required in cruise for the canard pusher aircraft was consistently lower than that required for the conventional aircraft in cruise.

10.C.2 Twin Boom

10.C.2.a Single Engine Tractor Twin Boom

The endurance for the twin boom tractor can be seen in Figure 10.37. Once again the general shape of the curves is consistent with the other configurations and cases already tested. Throughout the range of takeoff weights and wing loadings considered, the twin boom tractor aircraft compares quite well to the conventional aircraft for a given wing loading and takeoff weight. One characteristic to note is the increasing endurance with decreasing wing loading of the twin boom relative to the conventional case. This decrease is structural in nature and will be explained with the discussion of the fuel fraction term.

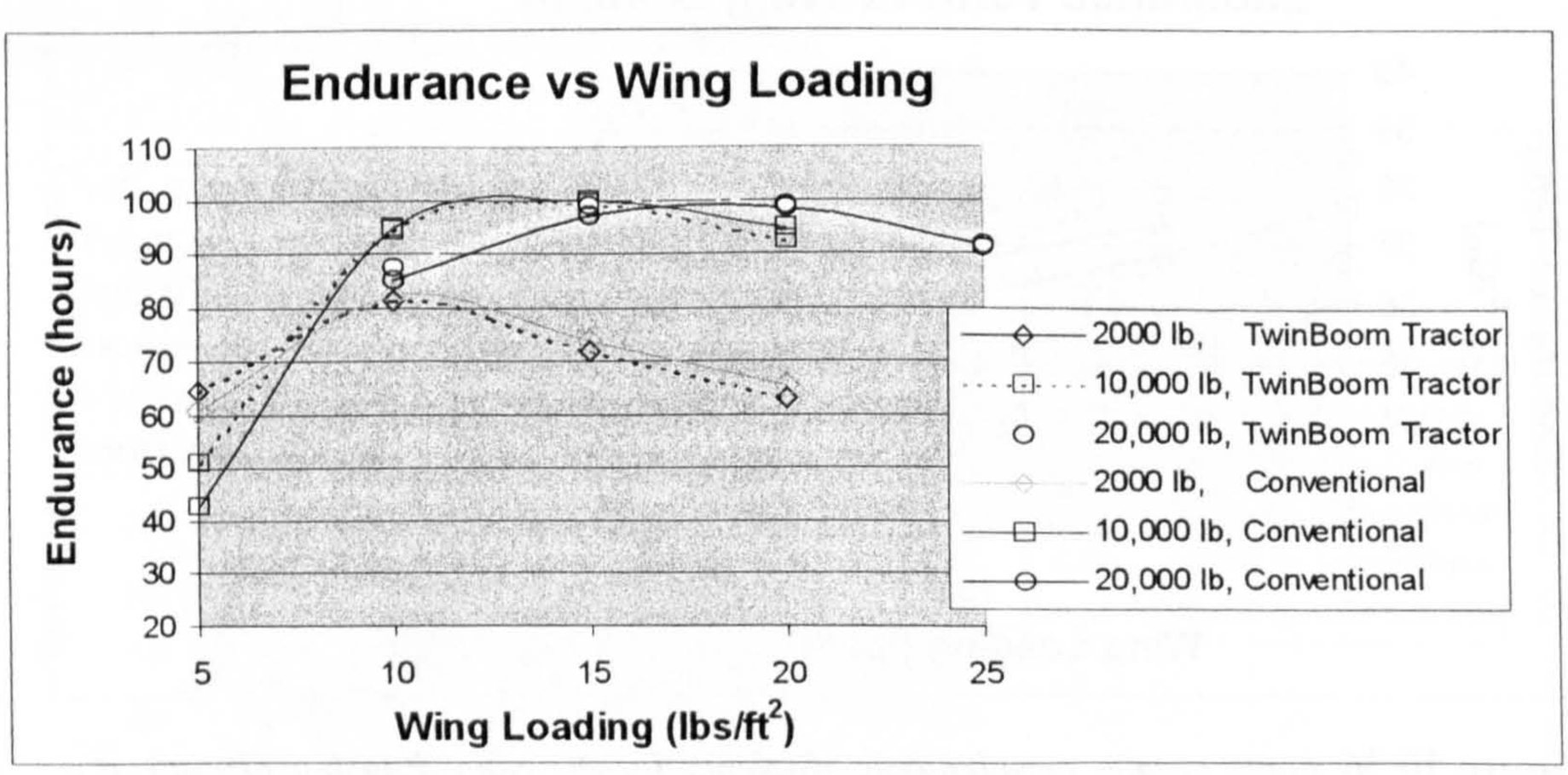

Figure 10.37 ***shows the comparative endurance performance of the tractor propeller configured twin boom.***

The endurance term behavior for the twin boom tractor can be seen in Figure 10.38. The 10,000 and 20,000 pound cases for the twin boom appear to have much more consistent drag behavior, showing only a slight increase with decreasing wing loading. It would appear that for the larger aircraft the additional skin friction drag of the booms is

sufficient to balance the aerodynamic benefits of lower wing loading on the lift distribution. The slope of the 2000 pound takeoff weight case for the twin boom is similar to the conventional case, however. This indicates that there is likely a wetted area threshold above which the effects of additional skin friction drag balance the aerodynamic benefits of reduced wing loading.

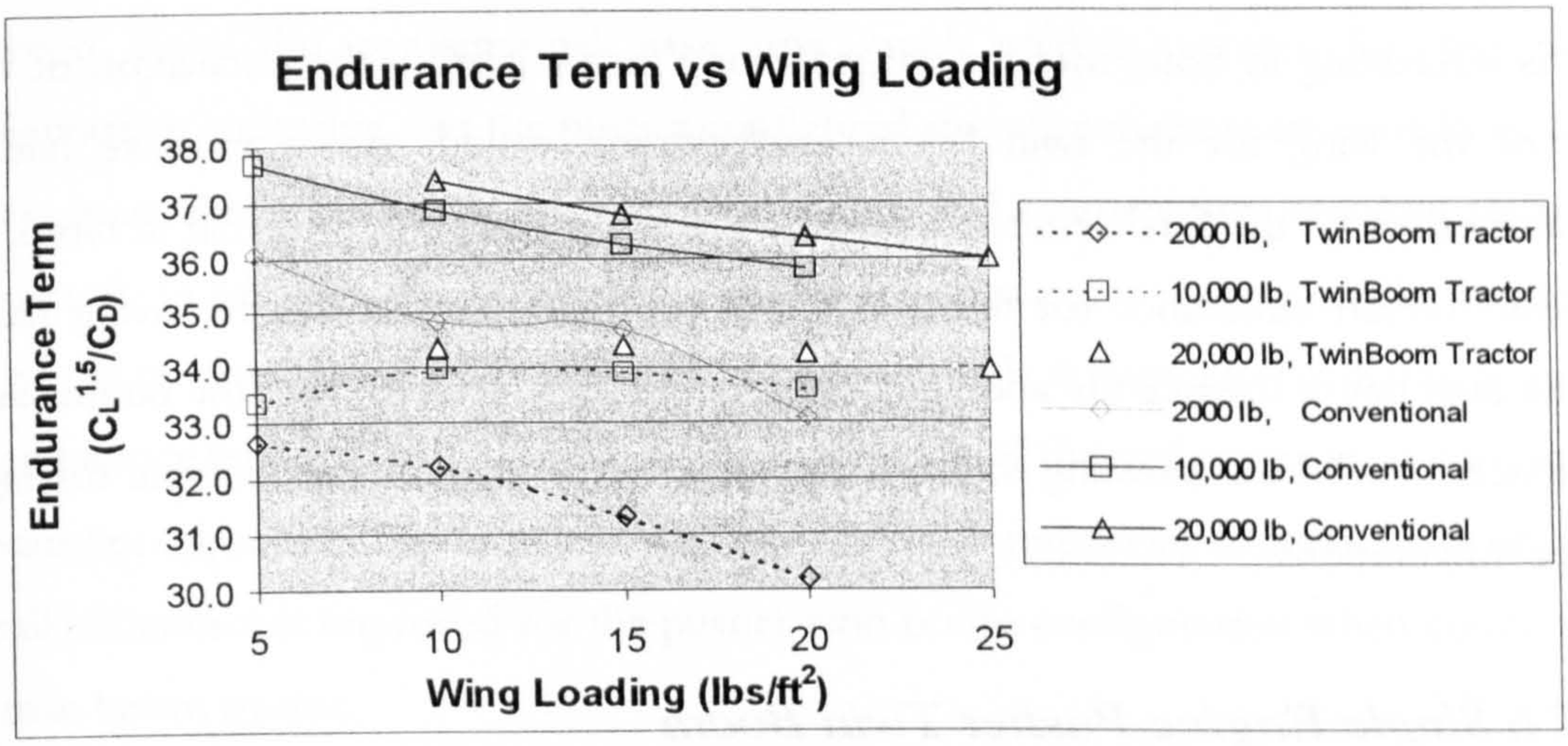

Figure 10.38 ***compares the endurance terms for the twin boom tractor and conventional tractor aircraft configurations.***

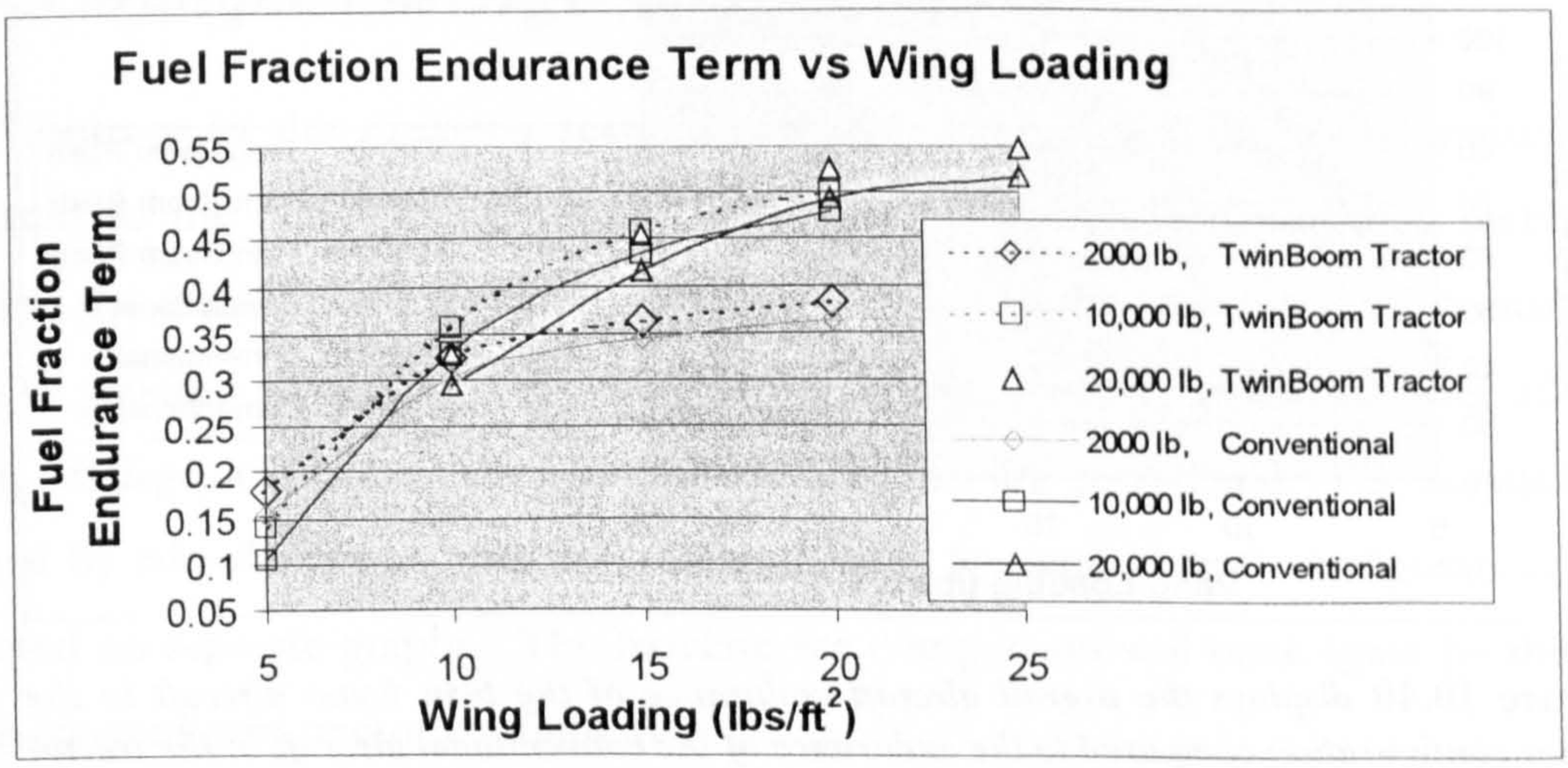

Figure 10.39 ***provides an explanation for the source of the increasing endurance of the twin boom configuration resulting from decreasing wing loading.***

It is noted that in the tractor configuration, many of the resulting twin boom configurations were not very reasonable from a practical operational standpoint. The changes in center fuselage location necessary to provide minimal trim forces placed the fuselage so far back that interference from the boom structure and tail, regardless of payload, would most likely be a factor.

A look at the figure for the fuel fraction term (Figure 10.39) provides a better understanding of the shape of the overall endurance results in Figure 10.37. The increase in endurance with decreasing wing loading for the twin boom case originates from an increase in fuel fraction term. The increase in fuel fraction, coupled with a decrease in wing weight predicted for a wing carrying more fuel serve to increase the fuel fraction term increasingly with decreasing wing loading.

It is interesting to note, that the weight saving factor used in the calculation of the weight of the wing for the twin boom configuration would appear to have had a reasonable effect on the final results for structural weight. It is observed that in terms of the overall aircraft endurance for the twin boom configuration, the weight saving from using the twin boom balance the additional skin friction drag created from the booms and interference. It will be interesting to see if the same holds true for the multiple fuselage aircraft configurations.

10.C.2.b Single Engine Pusher Twin Boom

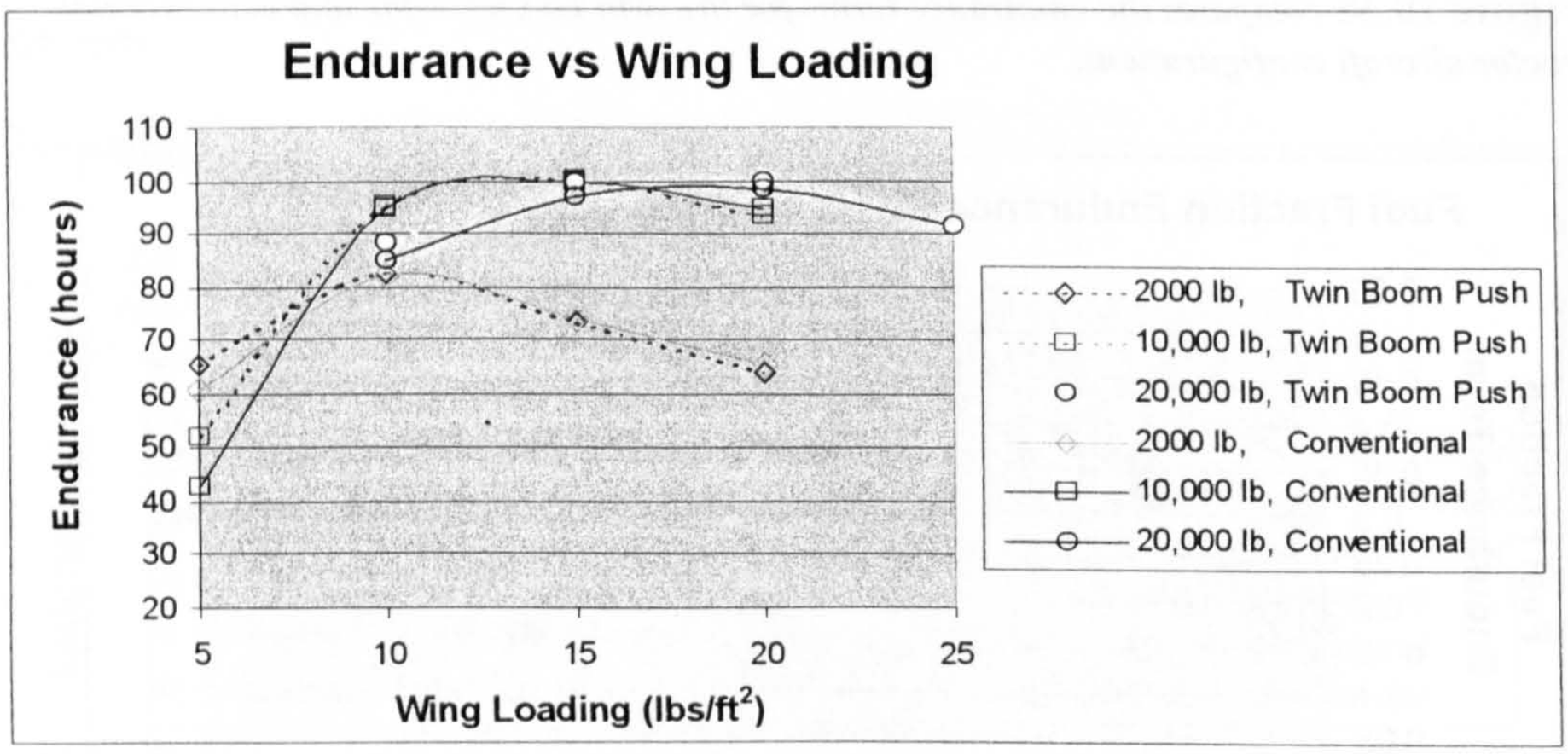

Figure 10.40 ***displays the overall aircraft endurance of the twin boom aircraft in the pusher configuration compared to the endurance of the conventional aircraft in the tractor configuration.***

The performance of the twin boom in the pusher configuration seen in Figure 10.40 was very slightly improved from the twin boom tractor seen in Figure 10.37. Similar to the difference between the canard tractor and canard pusher, it is believed most of this difference is due to the reduction of tail lift resulting from a better balanced aircraft resulting from the closer proximity of the engine to the main wing/fuel. In sharp contrast

to the twin boom in the tractor configuration, the center fuselage was well placed from a payload operational standpoint.

The same characteristic trend of an increase in endurance is present with decreasing wing loadings, identical to the twin boom tractor case. In fact, the fuel fraction term figure was essentially identical in shape to that of the tractor configured twin boom and is therefore not included. The only difference in this diagram was that the magnitude of the deviation from the conventional case was much slightly greater for the pusher configuration, indicating that the pusher configured aircraft was more structurally efficient. This is most likely due to the shorter boom length and moment arm required to balance the aircraft. In addition, the shape of the endurance term curve was essentially identical to that of the tractor configured twin boom. Again, the only difference was the magnitude of the endurance terms. This difference in the magnitude of the endurance term happened to be unnoticeably small. Nevertheless, with the effects of improved structural efficiency, the overall endurance is improved for the pusher twin boom configuration when compared to the twin boom tractor.

10.C.3 Multiple Fuselage Conventional and Canard

Contrary to the previous sections where individual aircraft configurations were compared to the conventional configuration on a case-by-case basis, this section will combine the results of many different cases. This was the only reasonable manner in which to proceed given that 8 different configurations must be evaluated after all of the engine, fuselage, and canard configuration possibilities are considered. The results will be grouped by takeoff weight, with the two and three fuselage aircraft configuration results presented on separate graphs. The baseline for comparison will once again be the single engine conventional tractor configuration.

10.C.3.a 2,000 pound Takeoff Weight

10.C.3a.i Endurance

The results for the 2000 pound takeoff weight can be seen in Figure 10.41 for the two fuselage aircraft in canard, conventional, pusher and tractor configurations. A distinct

advantage can be seen for the two fuselage canard aircraft over the conventionally configured two fuselage aircraft. There is little difference in endurance between the canard tractor and canard pusher with the exception of the higher wing loading cases. All of the two fuselage aircraft, however, show an interesting deviation from conventional single fuselage behavior below 10 lbs/ft^2. Neither the canard nor the conventional two fuselage aircraft compare very well to the conventional single fuselage case in terms of performance below approximately 12 lbs/ft^2. Intuitively, for the 2000 pound takeoff weight case, there is a threshold weight at which the advantages of wing weight reduction due to wing bending moment relief are balanced against the effects of the additional weight and drag penalties of the additional booms. This threshold was especially visible for the 2000 pound takeoff weight two fuselage aircraft. The specific reasons for this effect will be seen in the endurance and structure fraction term figures.

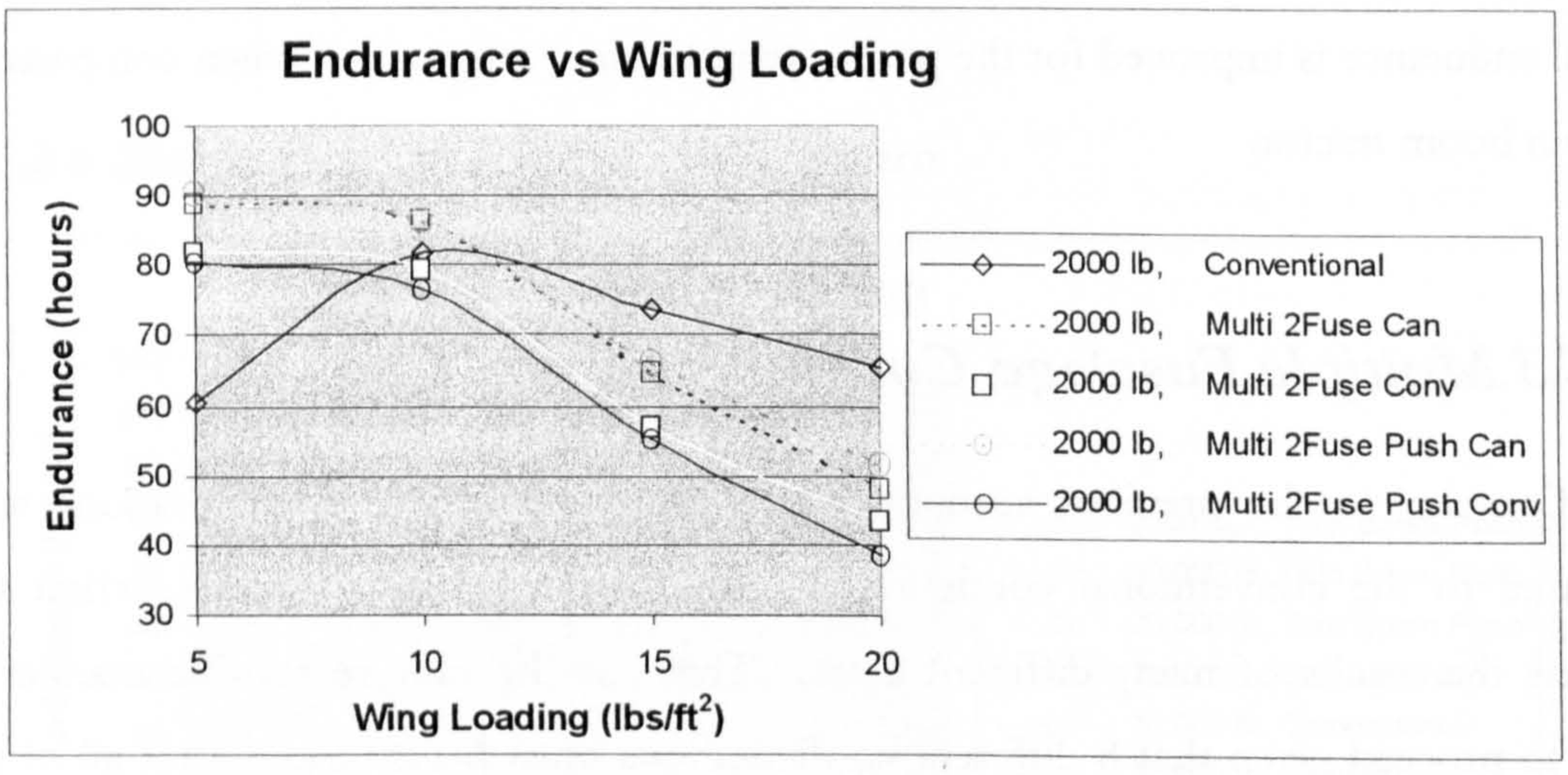

Figure 10.41 ***is a comparison of the different 2 fuselage configurations and their performance relative to the conventional configuration for the 2000 pound case.***

The endurance results for the 2000 pound takeoff weight 3 fuselage aircraft can be seen in Figure 10.42. Again, the agreement between the two canard configured aircraft is quite good, indicating that the aircraft balanced quite well. For the 3 fuselage canard cases, the deviation at high wing loading is much smaller and the disagreement at lower wing loadings is higher. This is the exact opposite behavior of the 2 fuselage canards. Whereas the 2 fuselage canard pusher and tractor began to deviate above wing loadings of 15 lbs/ft^2, the 3 fuselage canard pusher and tractor deviate below wing loadings of 15 lbs/ft^2. In addition the difference between the conventional tractor and pusher aircraft is much

greater above 10 lbs/ft^2. This behavior is due to combination of effects as will be shown in the following sections.

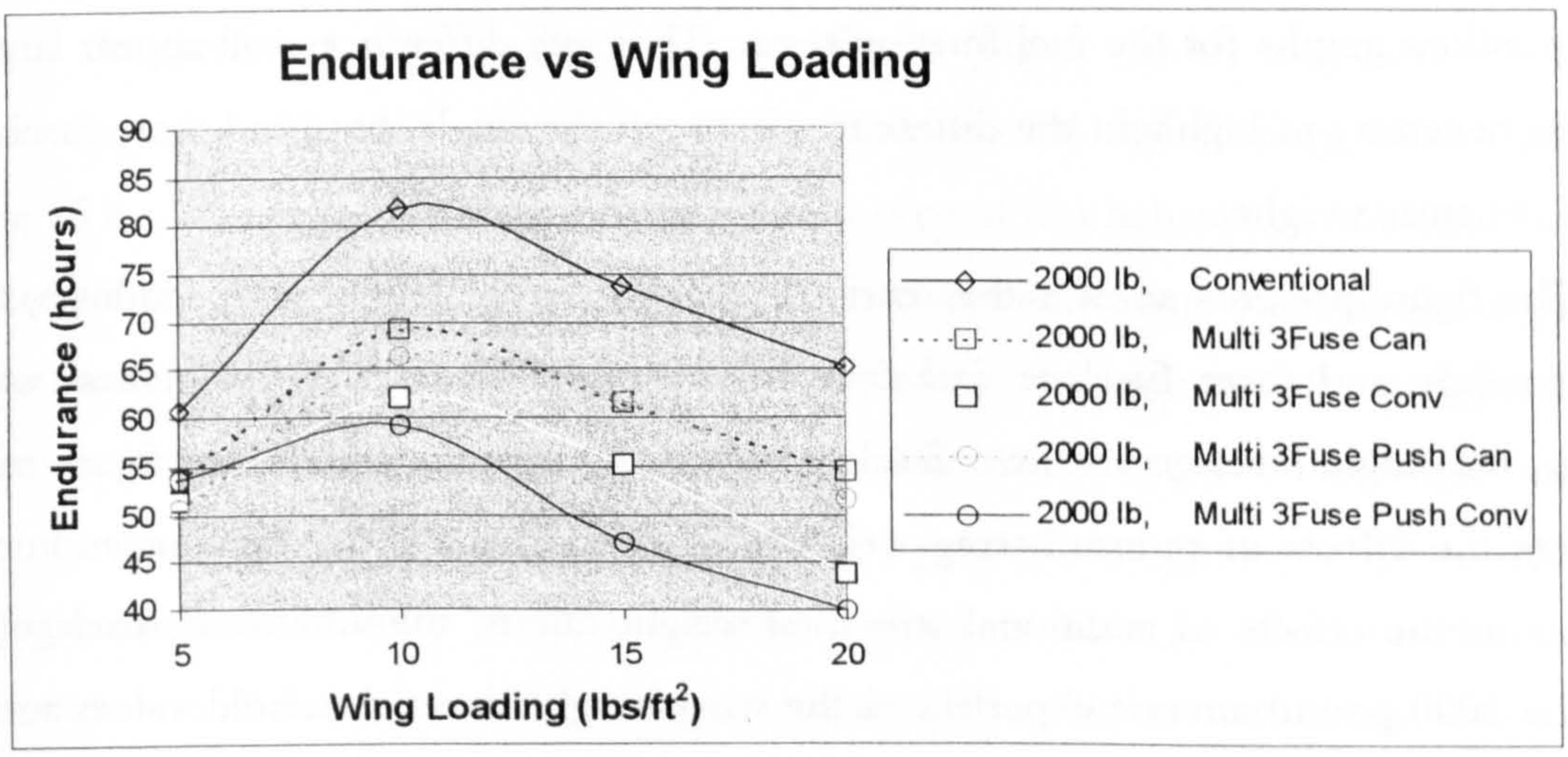

Figure 10.42 ***the different 3 fuselage configurations for the 2000 pound case show behavior opposite to their corresponding 2 fuselage configurations.***

10.C.3a.ii Fuel Fraction Term

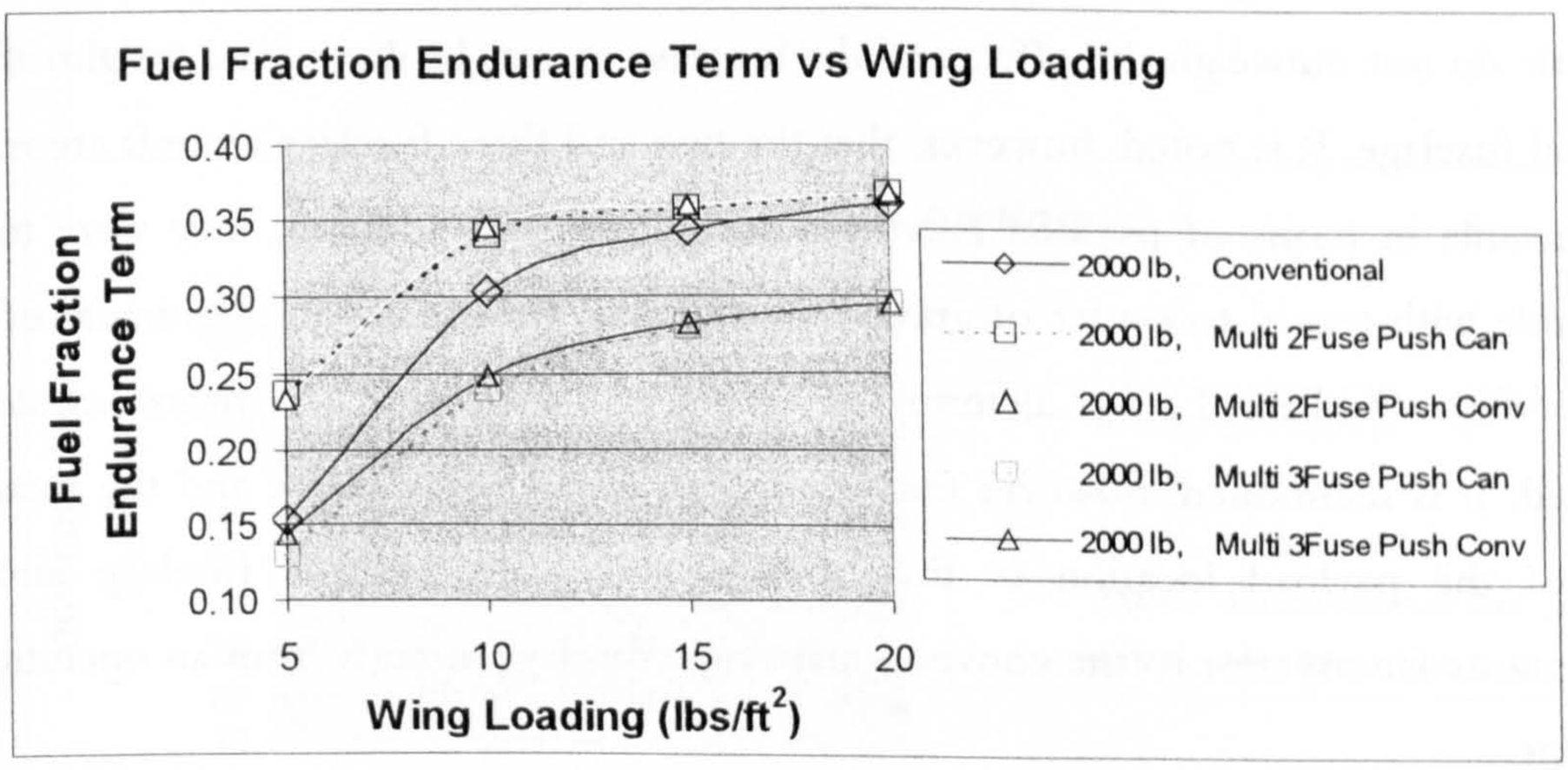

Figure 10.43 ***compares the fuel fraction term for similar 2 and 3 fuselage pusher configurations relative to the single fuselage conventional configuration.***

For the two and three fuselage 2000 pound cases, the fuel fraction term is basically the same between the canard and conventionally configured cases. The shape of the four multiple fuselage curves agree well each other. The trends in the curves for the three fuselage fuel fraction term are essentially the same as the trends seen in the two fuselage cases. Thus it was decided that a graph highlighting the differences in fuel fraction term

between the one, two, and three fuselage cases would be of more interest. This crossover graph can be seen in Figure 10.43.

It is first noted that the scale of this figure is significantly magnified when compared to the previous graphs for the fuel fraction term. Thus any differences will appear larger. This was necessary to highlight the differences between the single, two, and three fuselage aircraft structure weights.

The figure presents some rather curious results. At the lowest wing loadings, the single fuselage and three fuselage fuel fractions are quite close. At the highest wing loadings, the single fuselage and two fuselage aircraft agree quite well. This figure truly highlights the effects of reduced wing weight due to additional wing bending moment relief versus the effects of additional structural weight due to the additional fuselage(s). Since the 2000 pound aircraft experienced the wing weight lower threshold values more often, the benefits at low wing loadings of a reduction in this threshold can be plainly seen for the two fuselage aircraft. As the wing loading increases, however, the benefit of this effect is equalized due to a reduction in the size of the wing and consequently a reduction in the weight saving.

The three fuselage aircraft wing bending moment relief weight saving factors apparently do not outweigh the effects of the increase in weight due to the weight of the additional fuselage. It is noted, however, that the two and three fuselage aircraft are much more versatile in terms of payload location and volume. In addition, they were much more stable with regard to center of gravity location and travel. A better estimate of the weight saving would need to be determined before a proper trade-off analysis could be performed. It is mentioned, however that the increased payload volume and the reduced impact of the payload location in the fuselage make the multiple fuselage aircraft configurations far superior to the conventional single fuselage aircraft from an operational standpoint.

The results for the two and three fuselage tractor configured aircraft were essentially the same as those of the pusher aircraft and are therefore not included. The deviations between the two and three fuselage canard and conventional aircraft in overall endurance seen in Figure 10.41 and Figure 10.42 are not entirely explained by the behavior observed in the fuel fraction term. This behavior will be explained in the next section.

10.C.3a.iii Endurance Term

The endurance term for the two fuselage configurations can be seen in Figure 10.44. Part of the deviation seen in the endurance figure (Figure 10.41) originates from the endurance term. The same departure of the conventional two fuselage canard aircraft above 15 lbs/ft^2 can be seen in this figure. The source of this behavior is unclear, however the conventional two fuselage aircraft appears to follow the same pattern, although less pronounced. In fact, the aerodynamic efficiency terms for both tractor configured two fuselage aircraft have slight oscillations. This is similar to the conventional single fuselage curve, however the multiple fuselage curves have a greater average slope. The magnitude of the oscillations is quite small, but these oscillations have an effect on the overall endurance nonetheless. In addition, the canard aircraft endurance term does not oscillate in the same manner. It is believed, though, that this provides one possible explanation for the source of the oscillation. The 2000 pound conventionally configured aircraft was much more difficult to balance and the resulting variation in tail loads was much greater than for the canard case. The deviation in the overall endurance at high wing loadings for the conventional 2000 pound two fuselage aircraft is due to the same oscillation in endurance term.

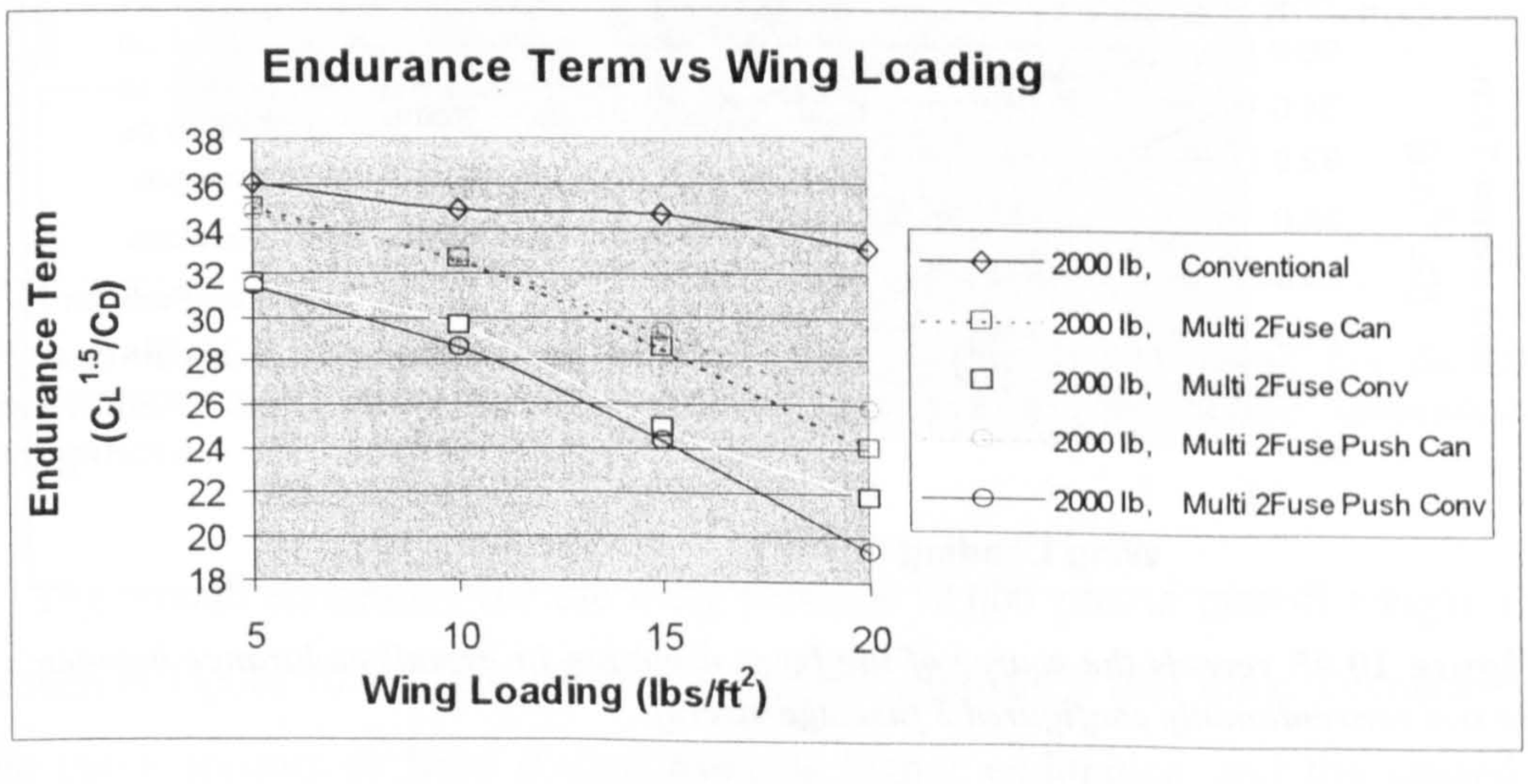

Figure 10.44 ***shows oscillations in the tractor configured two fuselage aircraft, similar to the oscillations in the conventional aircraft, but with greater slope.***

The large difference between 5 and 10 lbs/ft^2 in the overall endurance curve for the two fuselage aircraft arises from the fact that the fuel fraction term is sufficiently large at lower wing loadings to overcome the normally low [at low wing loadings] overall aircraft

endurance. This causes the endurance curve to flatten out until higher wing loadings where the effect of decreasing aerodynamic efficiency becomes dominant.

The endurance term results for the three fuselage configurations can be seen in Figure 10.45. The deviation in the overall endurance of the canard comes from the difference in slope, which in this case actually moves the two endurance curves closer together from lower to higher wing loadings. This happens because of the small difference between the pusher and tractor configurations in fuel fraction term. The deviation in the overall endurance for the conventional three fuselage aircraft also has its origins in the endurance term as seen in the figure. The three fuselage conventional pusher was not as easy to balance as the tractor, as there was little to offset the mass of the engine and tail in combination. As a result this configuration experienced greater cg travel during flight and this was reflected in the trim angle of attack of the tail. This in turn adversely impacted the aerodynamic efficiency. The fact that the aerodynamic efficiency drops off faster at lower wing loadings (where the fuel fraction increases most rapidly) implies sensitivity to the increasing fuel weight in the aircraft. This further supports the assertion above.

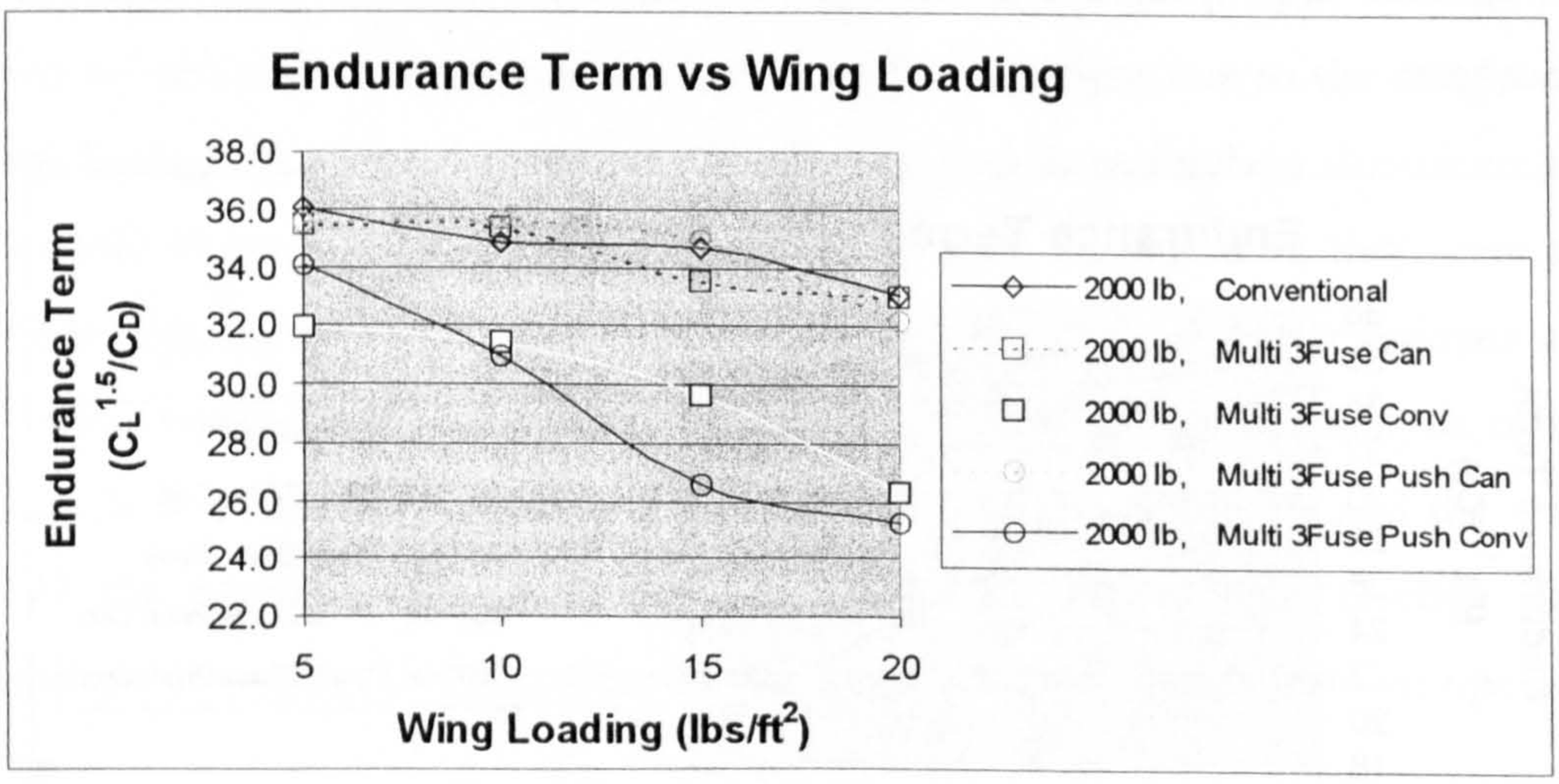

Figure 10.45 ***reveals the source of the large deviation in overall endurance between the two conventionally configured 3 fuselage aircraft.***

10.C.3.b 10,000 pound Takeoff Weight Case

10.C.3b.i Endurance

The endurance results for the 10,000 pound two fuselage aircraft are shown in Figure 10.46. In general, the endurance for the two fuselage aircraft are in much better

agreement than for the 2000 pound takeoff weight case. Once again, at the lower wing loadings, the two fuselage aircraft show a large deviation from the shape of the conventional single fuselage endurance curve. This deviation is responsible for a large increase in endurance at the lower wing loadings. Similar to the 2000 pound case, the performance of the two fuselage aircraft decreases with increasing wing loading. For the case of the 10,000 pound aircraft, however, the degradation of performance is not great enough for the performance of the two fuselage aircraft to fall below of that of the single fuselage aircraft. It is noted, however, that the 10,000 pound two fuselage aircraft perform much better than the 2000 pound takeoff weight aircraft. In addition, the differences in endurance between the canard and conventional two fuselage aircraft seen with the 2000 pound case are not repeated in the 10,000 pound takeoff weight endurance figure except at the lowest wing loading.

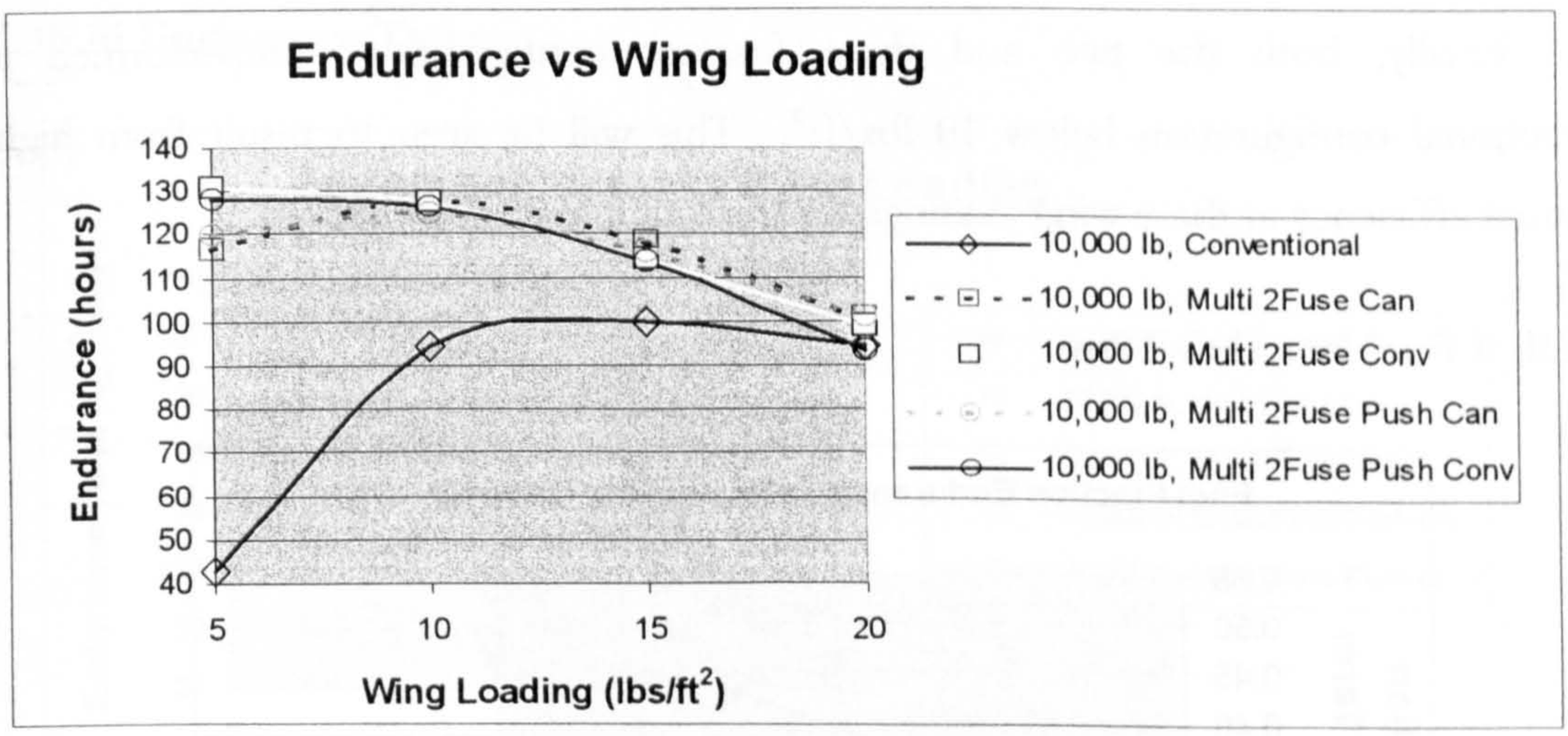

Figure 10.46 ***compares the overall endurance for the 10,000 pound two fuselage conventional and canard configured aircraft to the single fuselage conventional configuration.***

The overall endurance for the three fuselage 10,000 pound takeoff weight aircraft can be seen in Figure 10.47. The most notable characteristic is that the conventional three fuselage curve appears to have shifted towards higher endurance, and the canard three fuselage curves appear to have shifted lower. The overall shape of all of the curves remains the same, however. The result of the shift in location of the curves is that for lower wing loadings, the endurance of the three fuselage canard is now significantly lower than that of the conventional three fuselage configurations.

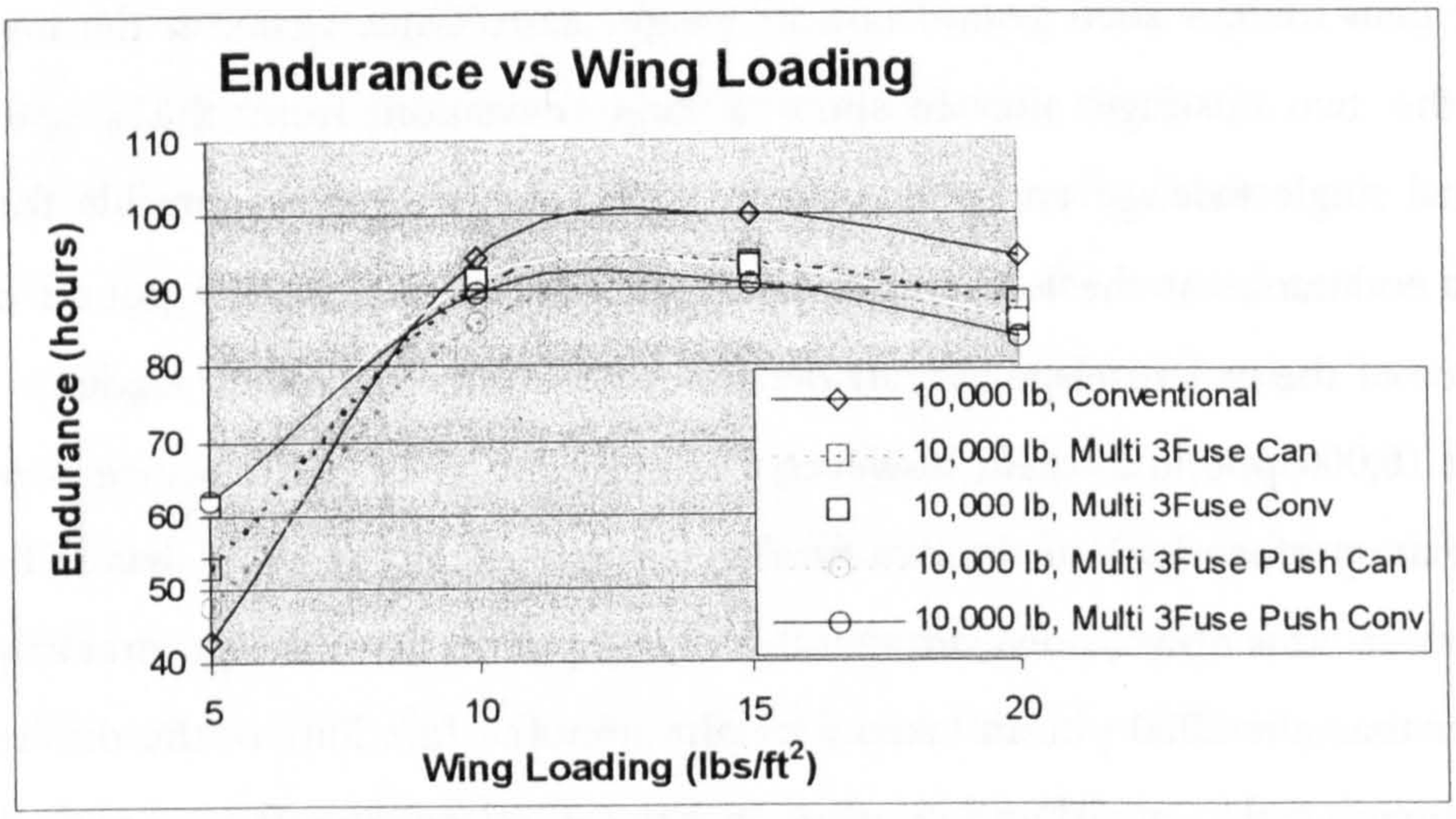

Figure 10.47 ***compares the endurance of the three fuselage conventional and canard configurations to the single fuselage conventional tractor configuration.***

Finally, both the two and three fuselage configurations outperformed the conventional configuration below 10 lbs/ft^2. This will be seen to result from higher structural efficiency at these wing loadings for the multiple fuselage aircraft.

10.C.3b.ii Fuel Fraction Term

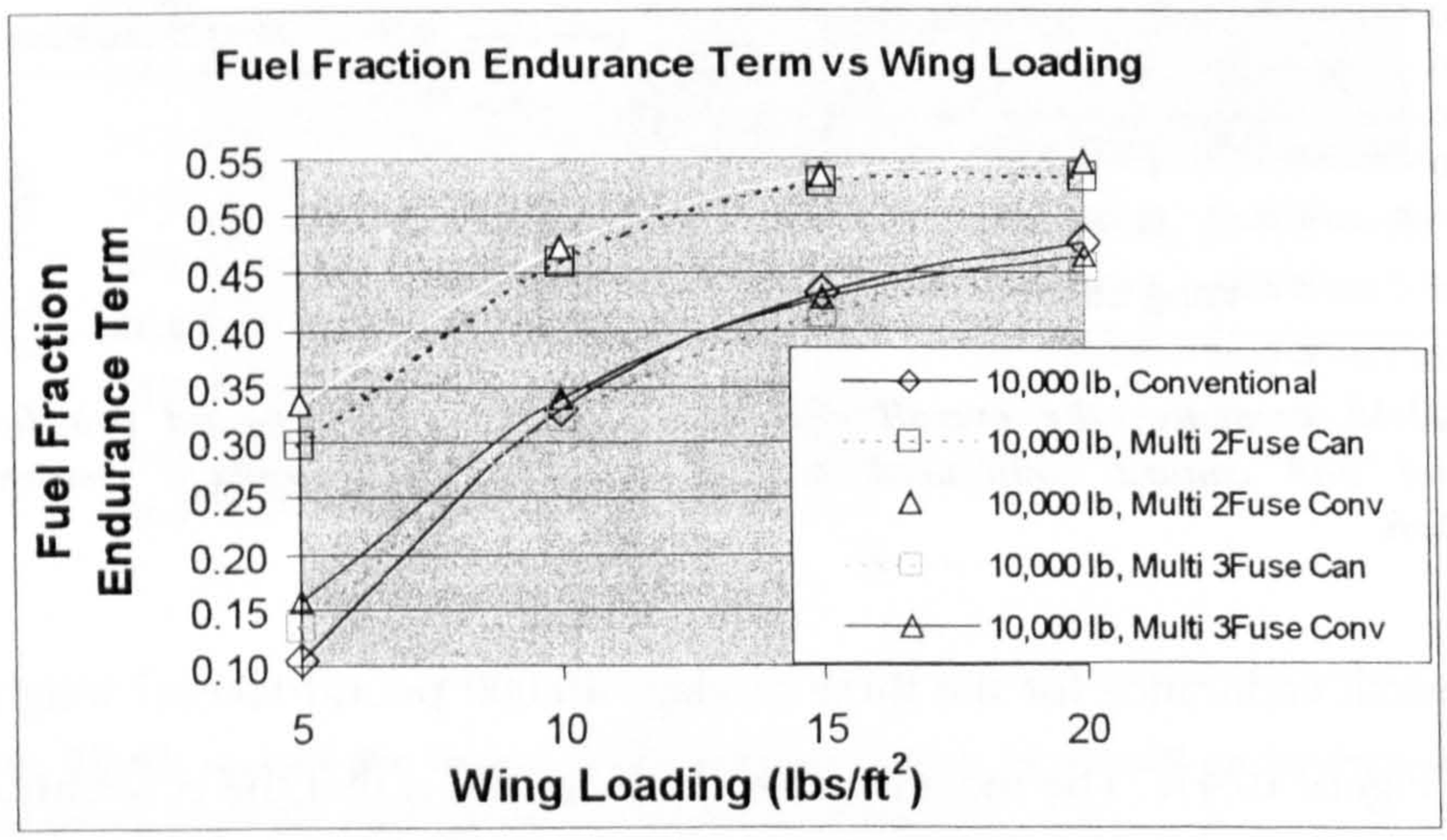

Figure 10.48 ***shows the large increase in fuel fraction term of the two fuselage configuration over the other tractor configurations.***

Similar to the 2000 pound takeoff weight case, the fuel fraction term results within the two and three fuselage cases were for the most part identical. It was thus decided that another crossover graph would be of more use. Figure 10.48 compares all of the multiple

fuselage tractor configurations considered (canard and conventional) in the same graph. In contrast to the 2000 pound takeoff weight case, the overall shape of all of the fuel fraction curves is quite similar. Once again, the difference in fuel fraction term between like configurations is quite small, and largest at lowest wing loadings. This difference in overall endurance performance results in part from the difference in fuel fraction term.

The difference between the two fuselage and the single and three fuselage configurations is rather large for the fuel fraction term. The majority of this difference is a result of the difference in wing weight saving factor (due to bending moment relief) used for the two and three fuselage aircraft. Without this wing weight saving factor, the structural efficiency of the three fuselage aircraft would not compare well at all with the conventional single fuselage aircraft due to the weight of the additional two fuselages. This is likewise true for the two fuselage aircraft.

10.C.3b.iii Endurance Term

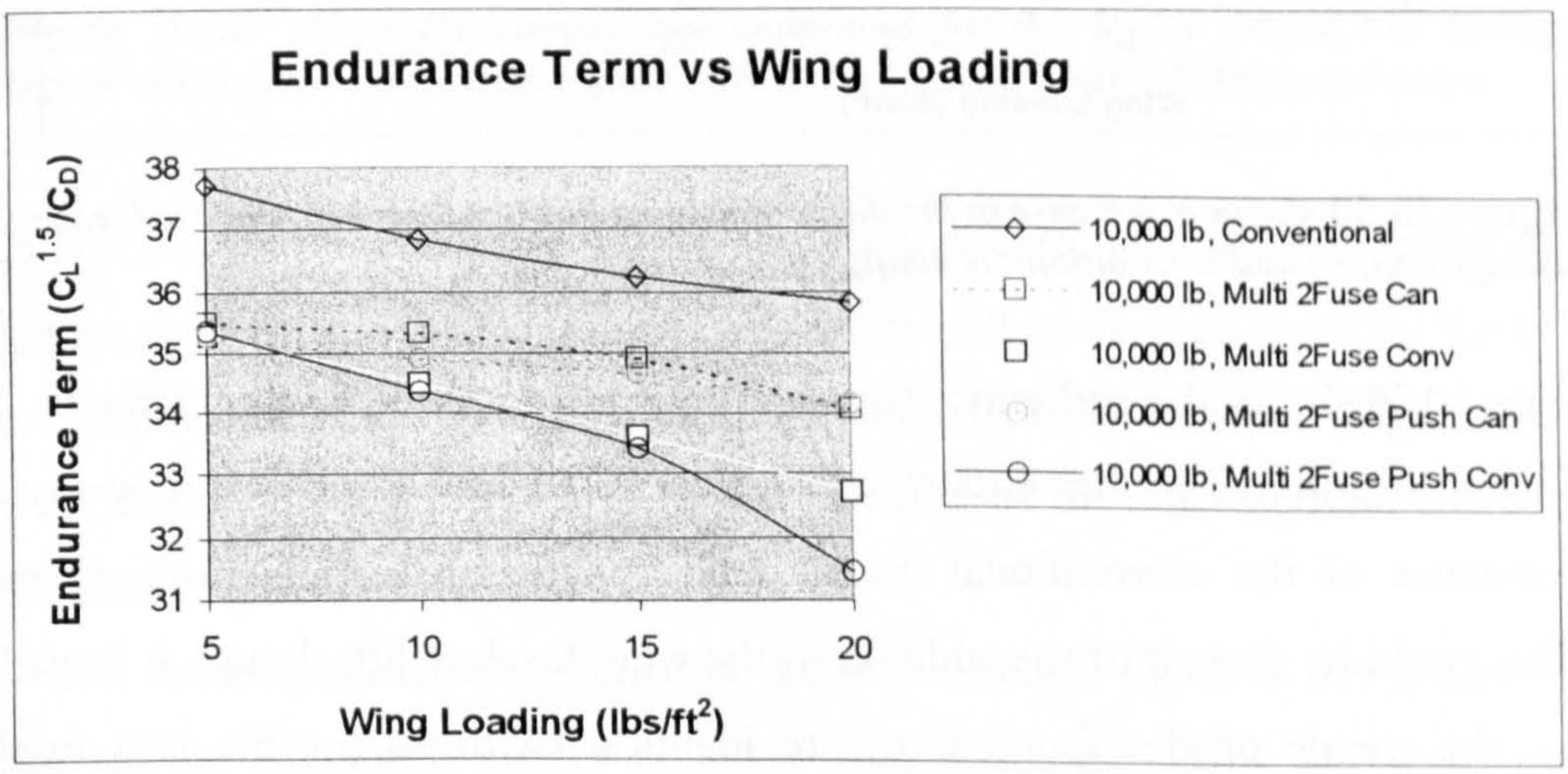

Figure 10.49 ***shows the reasonably flat behavior of the canard two fuselage aircraft endurance term compared to that of the two fuselage conventionally configured aircraft.***

Once again, much of the behavior of the overall endurance for the multiple fuselage aircraft is due to the endurance term and not structural variations alone. The endurance term for the two fuselage configured aircraft can be seen in Figure 10.49. The first characteristic to note in this figure is the fact that the canard configured two fuselage aerodynamic efficiency curve is reasonably flat. This is in contrast to the curves for the conventionally configured two fuselage aerodynamic efficiency which experience a reasonably constant decrease with increasing wing loading. The reasoning behind this

decrease is the same as for the 2000 pound takeoff weight case. Aerodynamic efficiency decreases as a function of both increasing wing loading and how difficult the aircraft is to balance. The canard aircraft were easier to balance. Consequently, the incremental difference between the canard and conventional two fuselage curves is due to tail upload rather than tail download. This behavior explains the comparative decrease in overall endurance performance for the canard aircraft at lower wing loadings.

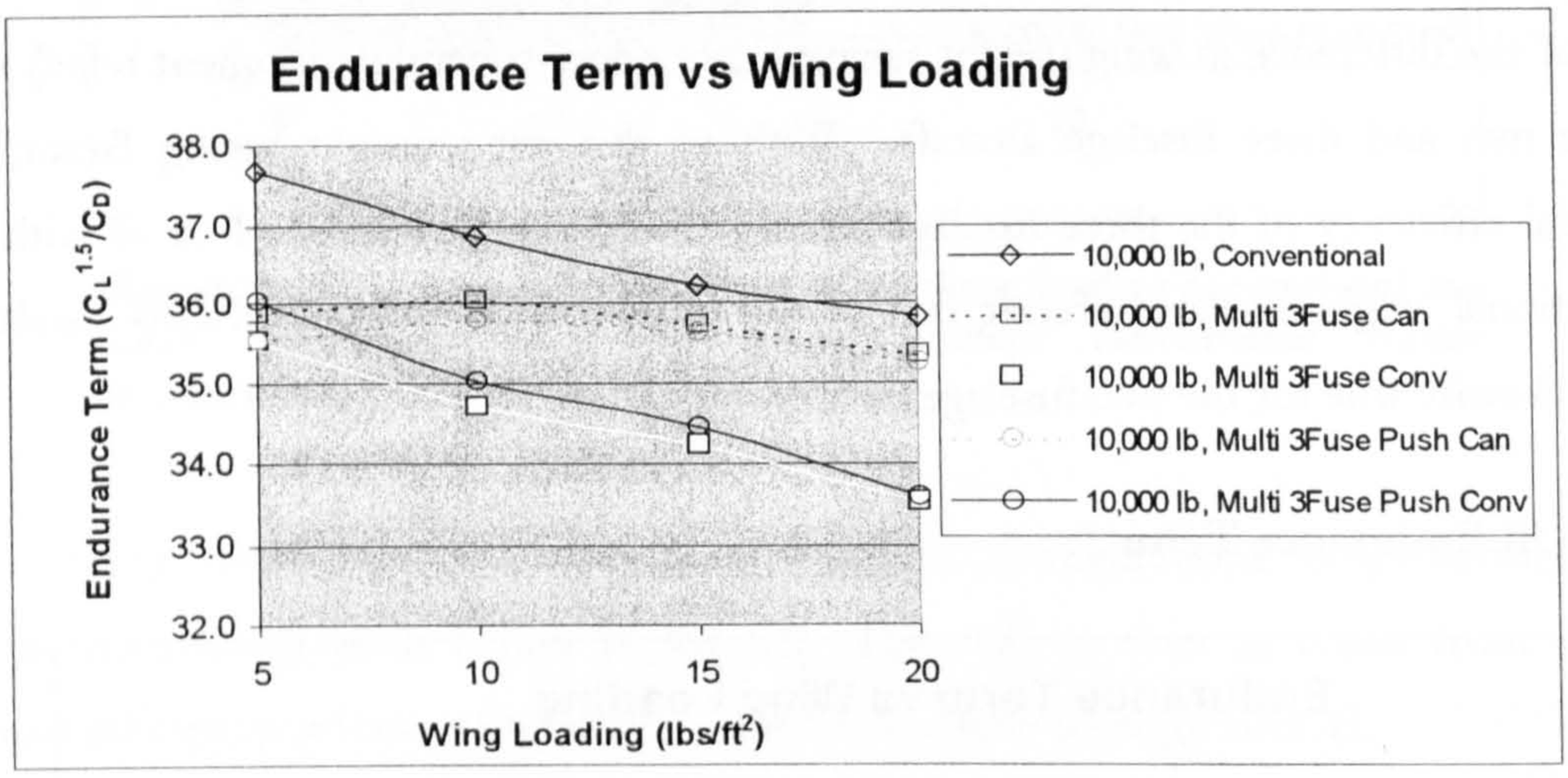

Figure 10.50 ***shows a decrease in the difference in endurance term between the three fuselage canard and conventionally configured aircraft.***

Figure 10.50 shows the endurance term behavior for the three fuselage aircraft. The slope of the conventional pusher endurance term curve has decreased and now matches the performance of the conventional tractor (and conventional single fuselage) much better. This could be a result of the addition to the wing-fuselage lift, though it is unclear. Otherwise the trends of the four curves are identical to those for the two fuselage endurance terms.

In comparing the two figures, however, some differences become apparent. The aerodynamic efficiency of the conventional three fuselage aircraft seems to have improved slightly. This has a direct impact on the overall endurance, and explains the behavior of the shape of the overall endurance curves when comparing the two and three fuselage cases.

The only reasonable explanation for this behavior is the relative ease with which the three fuselage aircraft is balanced. Therefore, there is less travel of the center of gravity throughout the flight of the aircraft. An improvement in the aerodynamic efficiency results for the conventional configuration. The parasite drag of the additional fuselage is balanced by the decrease in cg travel thus decreasing trim drag. Since the canard aircraft

was already well balanced, however, the performance decrease due to the parasite drag of an additional fuselage is more apparent.

10.C.3.c 20,000 pound Takeoff Weight

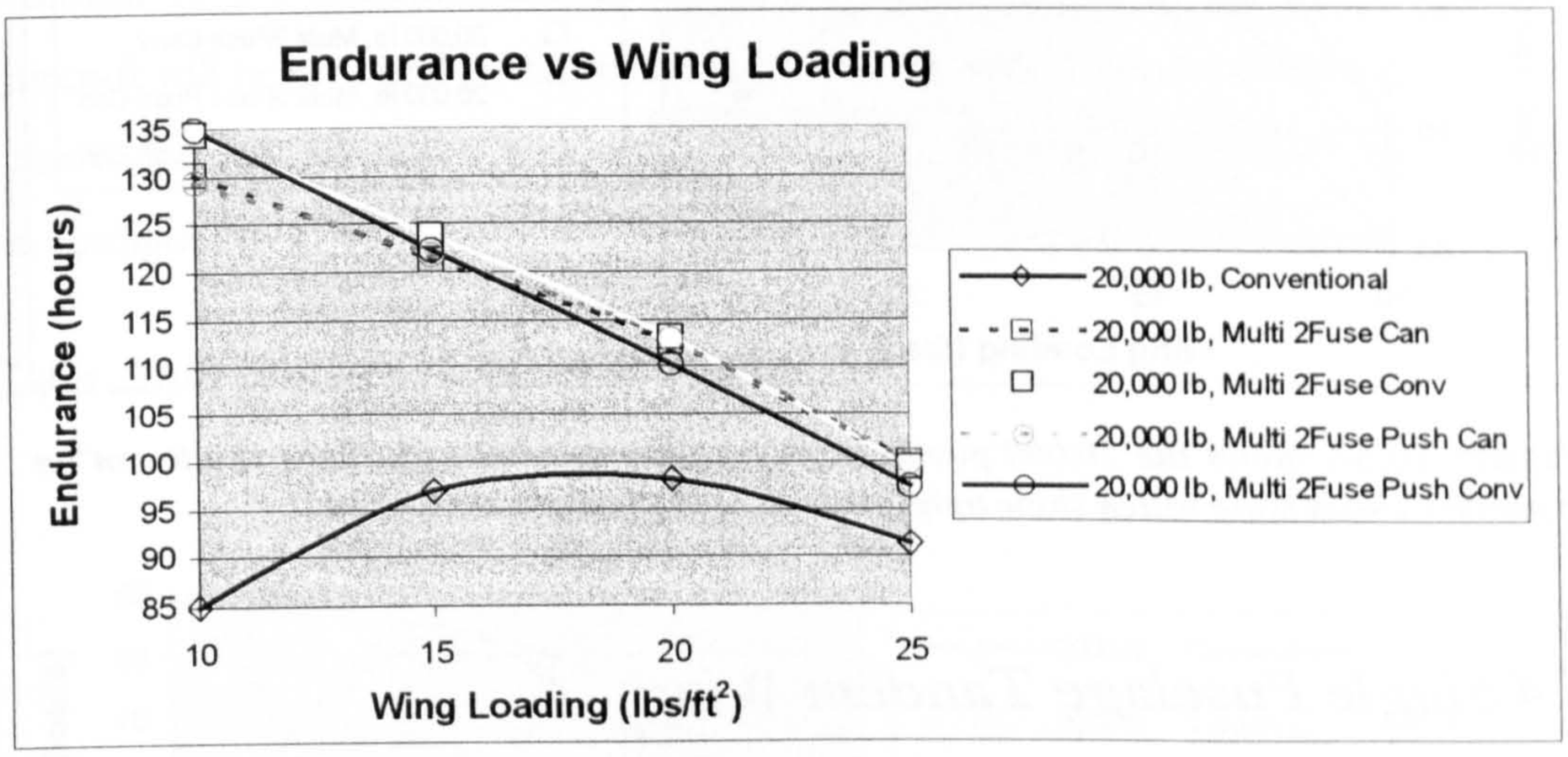

Figure 10.51 ***shows the comparative endurance for the 20,000 pound two fuselage aircraft which demonstrate trends quite different to the 2,000 and 10,000 pound cases.***

The 20,000 pound takeoff weight two fuselage case demonstrated rather different trends from the 2000 and 10,000 pound cases for overall endurance, however the behavior of the endurance term and fuel fraction terms was essentially identical. Figure 10.51 and Figure 10.52 show the results for the overall endurance of the 20,000 pound two and three fuselage cases respectively.

The most noticeable difference in the two fuselage figure is the absence of flat behavior of the endurance curves at lower wing loadings. This can quite easily be explained by the fact that the 20,000 pound aircraft wings did not experience the lower limit of wing weight per area as did the other two takeoff weight cases. The result is a decrease in slope of the fuel fraction term curves which translates into an increase in slope of the overall endurance curves due to the effects of decreased aerodynamic efficiency at lower wing loadings for the 20,000 pound takeoff weight case. Otherwise, identical trends as those seen for the 10,000 pound case were seen in the curves for the fuel fraction and endurance terms for the 20,000 pound case. It is thus believed that the same explanations for these phenomena can be applied to the 20,000 pound case without further discussion.

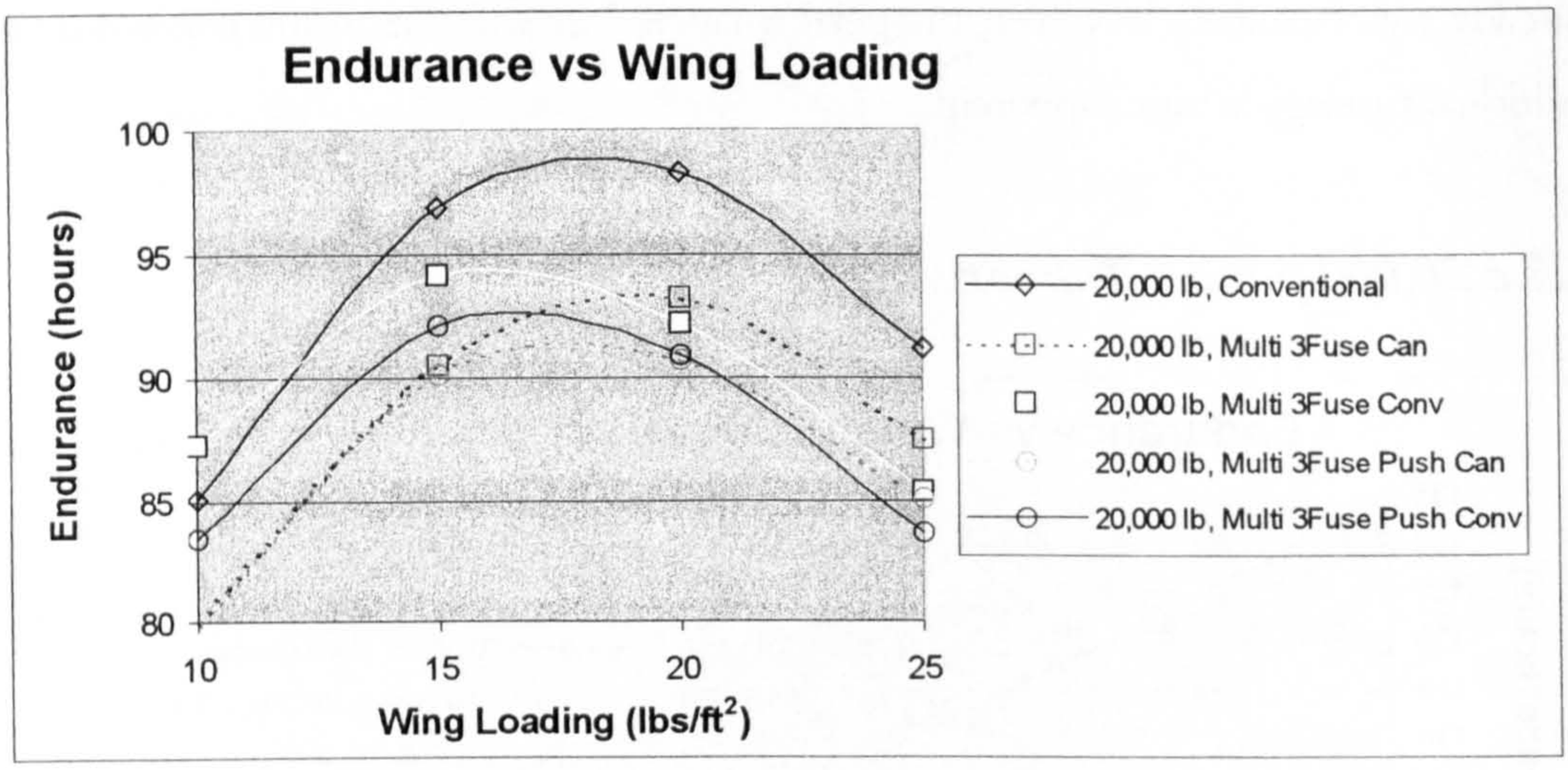

Figure 10.52 ***shows the 20,000 pound three fuselage aircraft endurance results on an expanded Y-axis scale which show trends similar to the 10,000 pound case.***

10.C.4 Single Fuselage Tandem Wing

There was no literature available on the determination of the optimum division of wing area or lift for tandem wing aircraft. For this reason two different single fuselage tandem wing aircraft were evaluated. The division of wing area for the first configuration was selected based upon a statement in Stinton[6], which said that aircraft with a 50/50 split cannot decide which wing is in control of the aircraft and tend to wander through the skies in an unstable manner. Therefore, a limiting case of division of area was selected as 55/45, where 55 is the percentage of main or aft wing area, and 45 is the percentage of fore wing area.

The other case considered was based on the fact that the horizontal surfaces used for the Low Speed HALE UAV's tended to be between 5 and 15 percent of the main wing area. Since some distinction needed to be made between the tandem wing and canard, the division of area selected for the lower limit was 75% aft/25% fore. Another difficult decision that needed to be made was the determination of the relative aspect ratios, as again there was no information available. It is necessary to insure that the fore wing stalls first, a requirement to maintain positive longitudinal control of the aircraft. This can be achieved by either keeping the fore wing angle of attack higher, or by making sure the fore wing Reynolds number is significantly higher. Since lift coefficients are already approaching reasonable stall limits in cruise flight for Low Speed HALE UAV's, it was decided that a decreased aspect ratio for the fore wing would be a reasonable solution.

This is a similar tactic to that used by the Scaled Composites *Proteus* which has a fore wing aspect ratio of 16.7 and an aft wing aspect ratio of 20.1. For the cases executed in this section, the fore wing aspect ratio was 22, and the aft wing aspect ratio was maintained at 35.

Similar to the multiple fuselage results, the results for the single fuselage tandem wing aircraft will be grouped by takeoff weight. There were 4 configurations considered in total for each takeoff weight case, considering variations in division of wing area and engine configuration.

10.C.4.a 2000 pound Takeoff Weight

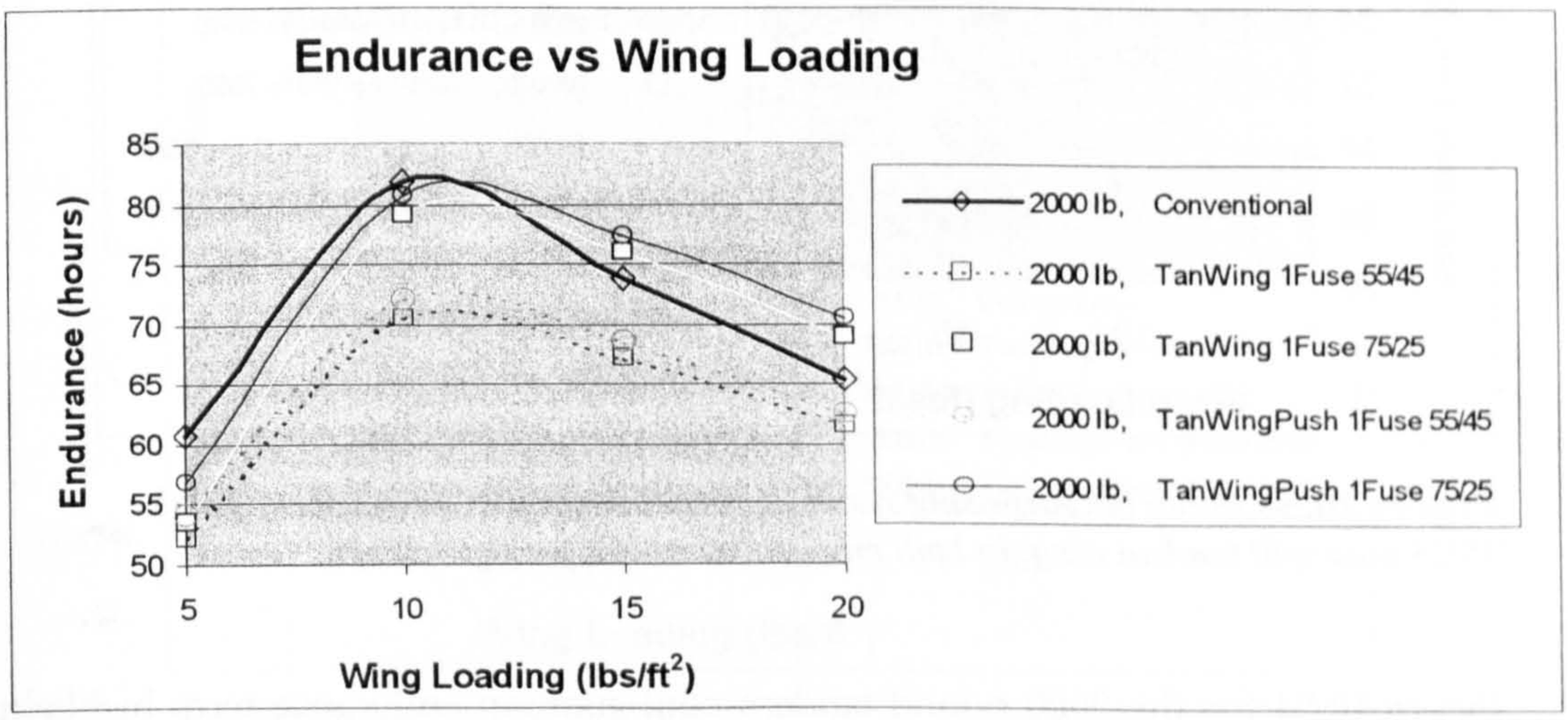

Figure 10.53 ***shows the overall endurance results for the 2000 pound single fuselage tandem configurations compared to the conventional single fuselage configuration.***

It is first noted that the Y-axis scale for endurance is expanded giving the appearance of a difference in shape from that seen previously. The scale was expanded in an effort to highlight the differences in the configurations being compared. The first characteristic to notice about the 2000 pound overall endurance results seen in Figure 10.53 is the fact that the 75/25 area split tandem pusher and tractor aircraft compare quite well to the conventional configuration. Also quite noticeable is the fact that the comparative performance of the 55/45 area split tandem configurations is quite poor. The performance of the 75/25 area split tandems was superior to the performance of all 55/45 tandems regardless of takeoff weight as will be seen later. For the tandem configuration there is an interesting combination of structural and aerodynamic effects that create this

remarkable overall endurance performance. These effects are least pronounced for the 2000 pound case, however, they are still reasonably clear.

Similar to other configurations seen thus far, the pusher configuration provides slightly better overall endurance performance. The reasoning is similar, resulting from the fact that the pusher configurations were much easier to balance and had more reasonable cg travel.

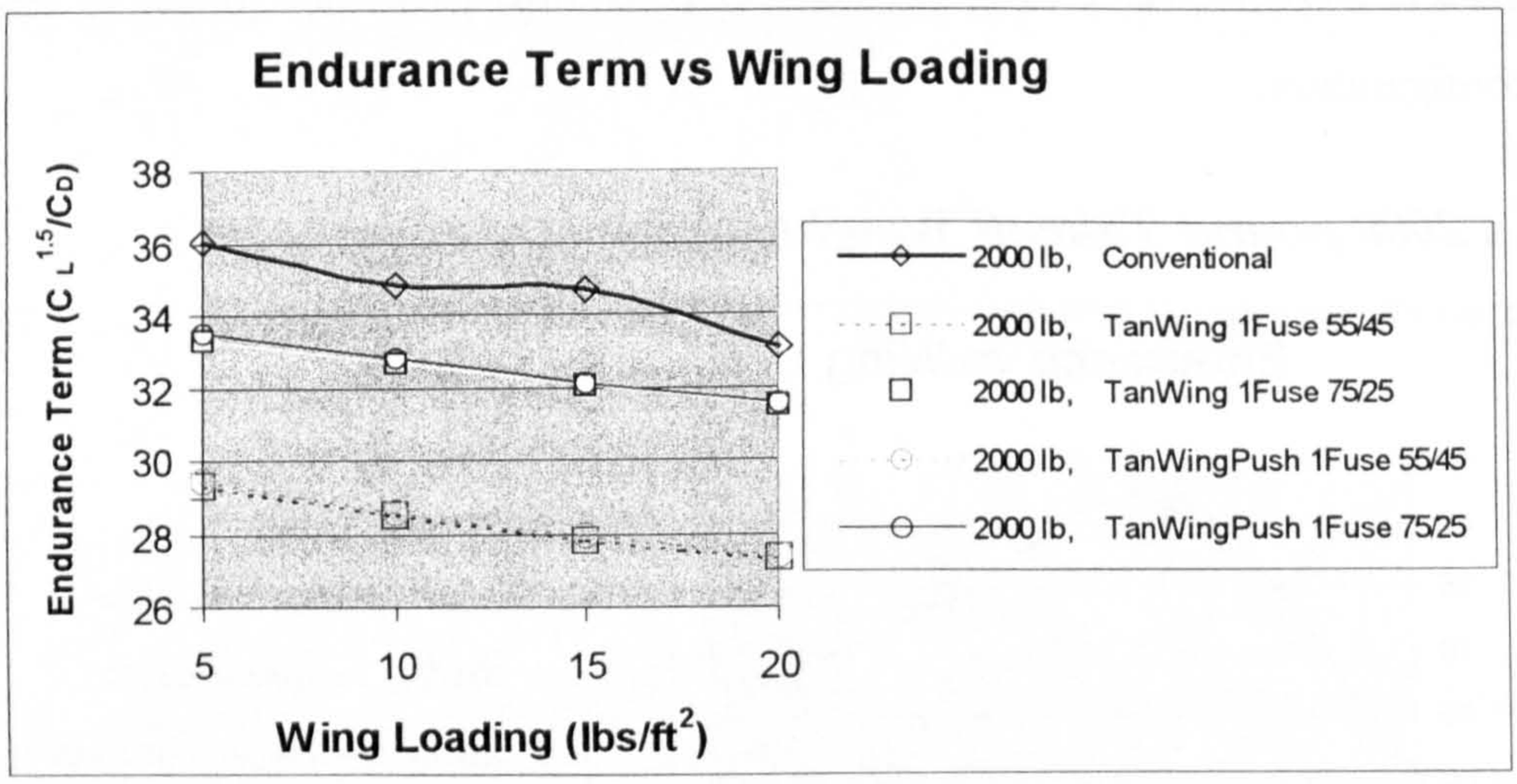

Figure 10.54 ***shows the surprising result of greater aerodynamic efficiency for the 75/25 area split tandem wing, in both pusher and tractor configurations.***

Figure 10.54 for the 2000 pound tandem configuration endurance term highlights some very interesting and unexpected behavior. The most interesting result is that the 75/25 area split has a higher aerodynamic efficiency than the 55/45 area split. This result was not expected. The most likely reason for this behavior is the fact that the lift coefficient for the tandem wings was not held constant for these results. Since the ***aircraft*** lift coefficient was kept constant, the lift coefficient of the individual surfaces was determined in the manner that would best balance the aircraft. The result of this was a comparatively higher lift coefficient for the fore surface of the 75/25, and a comparatively lower lift coefficient for the aft surface and vice versa for the 55/45. In addition, a larger percentage of total wing area was at a lower aspect ratio for the 55/45 case. On average, the sum of the drag coefficients for the 75/25 was lower than that of the 55/45. At this point it is noted that it is suspected this result is highly airfoil specific and the same behavior might not be obtained using airfoils optimized for each surface.

The 2000 pound takeoff weight fuel fraction term curves seen in Figure 10.55 provide some additional information. It can be seen that there is very good agreement in all of the curves up until 10 lbs/ft^2. Beyond that wing loading, the 55/45 aircraft has a structural efficiency very slightly higher than that of the 75/25 aircraft, with all four tandem aircraft having greater structural efficiency than the conventional aircraft. This is the first sign that the structural efficiency (based on the magnitude of the fuel fraction) of the tandem wing aircraft is superior to that of a standard conventional single wing aircraft. This is due to a reduction in span of each wing, and a reduction in aspect ratio for a sizable fraction of the overall lifting surface area.

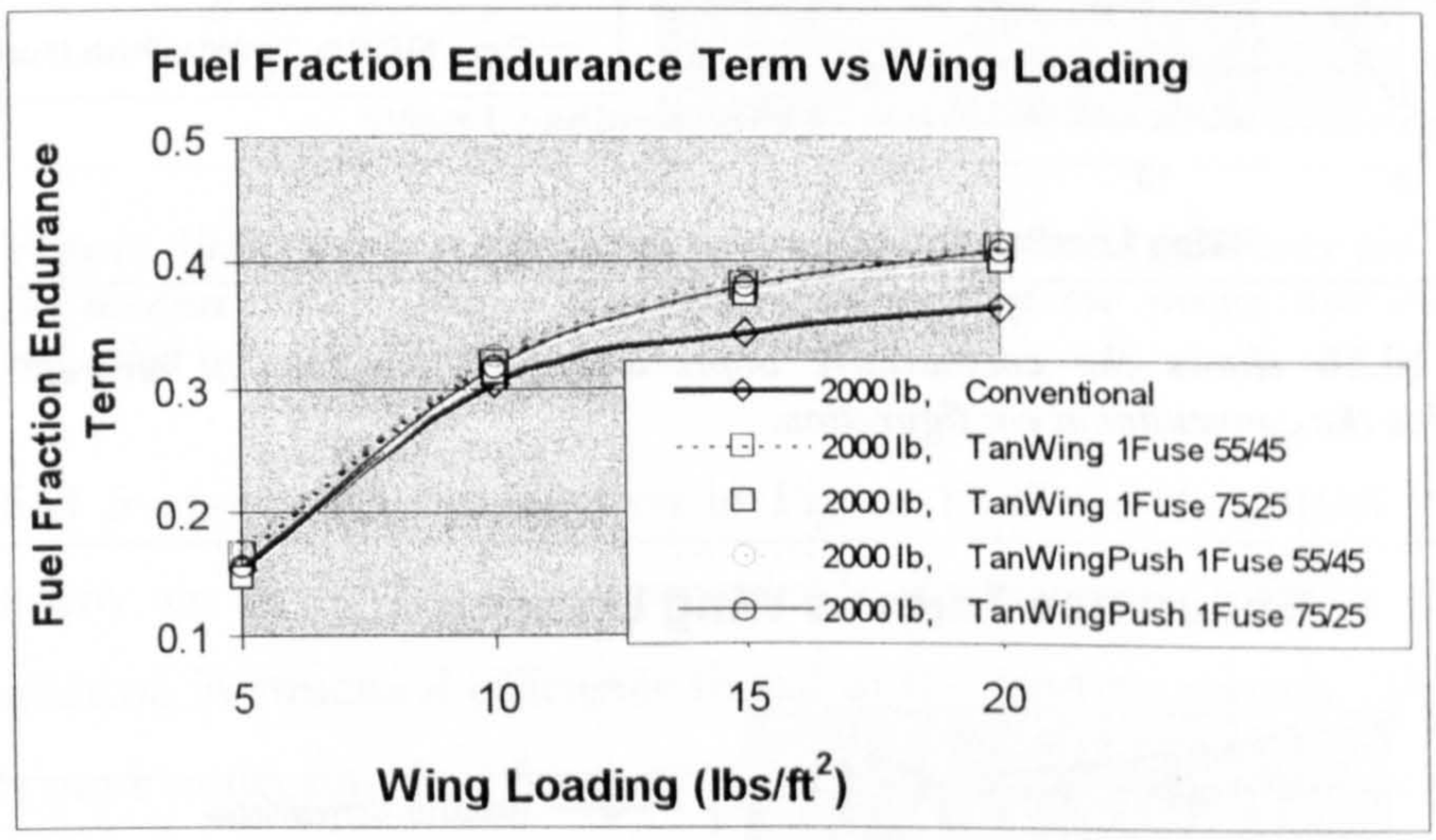

Figure 10.55 ***hints towards the superior structural efficiency of the tandem wing aircraft.***

When the influence of the fuel fraction and aerodynamic efficiency terms are considered it becomes apparent that the relatively poor comparative performance of the 55/45 area split tandem is due almost entirely to the poor relative aerodynamic performance of that configuration. This supports the argument that if a tandem wing aircraft configuration is to be considered, a great deal of care must be taken in the design of the wings and their interaction.

10.C.4.b 10,000 pound Takeoff Weight

The 10,000 pound tandem wing overall endurance results can be seen in Figure 10.56 for the various configurations considered. Different from the 2000 pound takeoff weight curves, the 55/45 tandem aircraft outperform the conventional configuration up to

approximately 12 lbs/ft^2, and perform almost as well beyond that wing loading. Similar to the 2000 pound takeoff weight curves, the 55/45 and 75/25 area split tandems agree better at the lowest wing loadings.

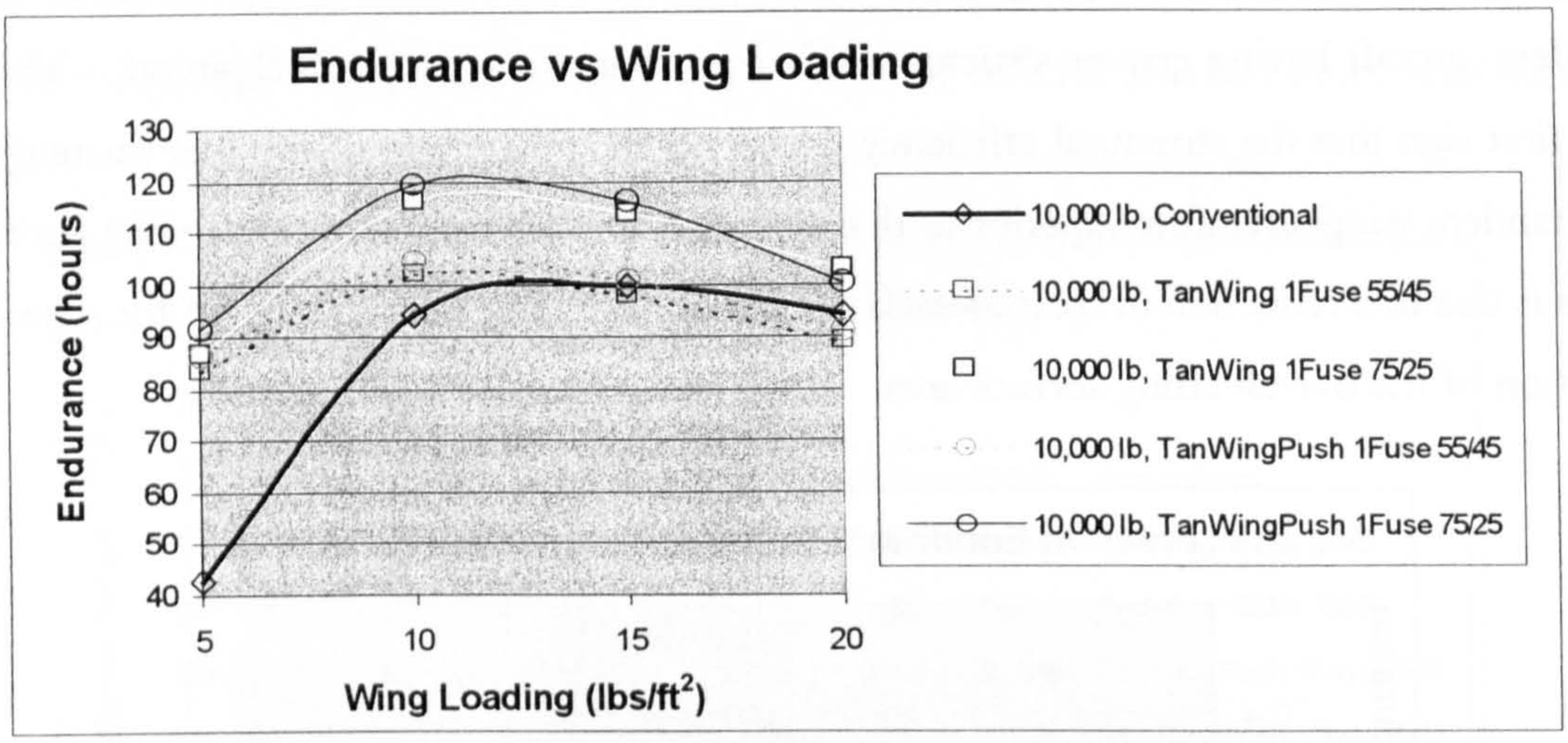

Figure 10.56 ***shows the comparative improvement of the tandem aircraft when compared to the conventional configuration.***

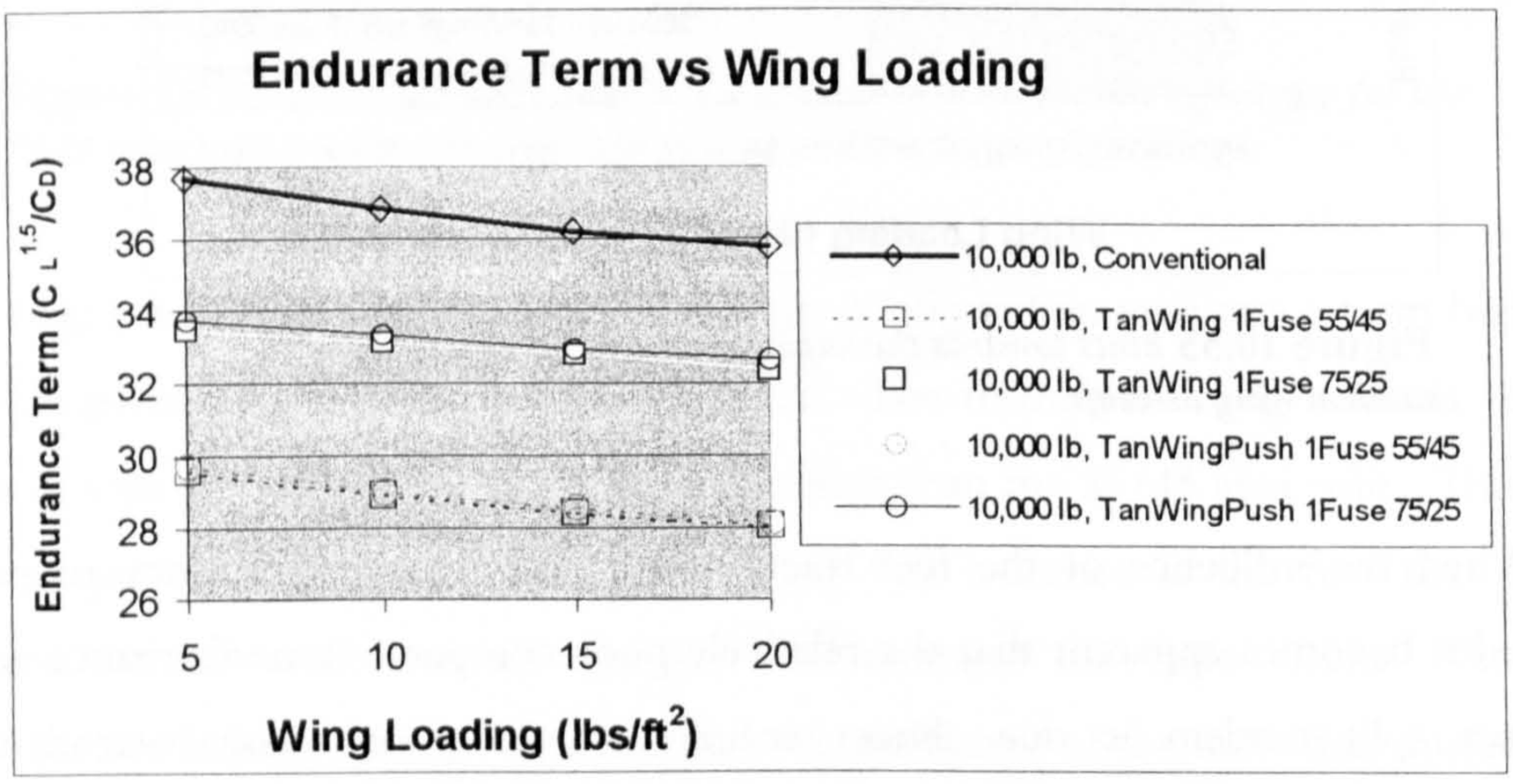

Figure 10.57 ***shows a relative decrease in performance by the tandems relative to the conventional configuration when compared to the 2000 pound takeoff weight case.***

The endurance term graph is given in Figure 10.57. Once again, the aerodynamic efficiency of the 75/25 tandem wing aircraft is higher than that of the 55/45 tandem for all wing loadings considered. In addition, the slope of the aerodynamic efficiency curves for the tandems experienced a very small decrease. The 10,000 pound tandem wing aircraft

endurance term performance experienced a decrease relative to the conventional aircraft when compared to the 2000 pound case.

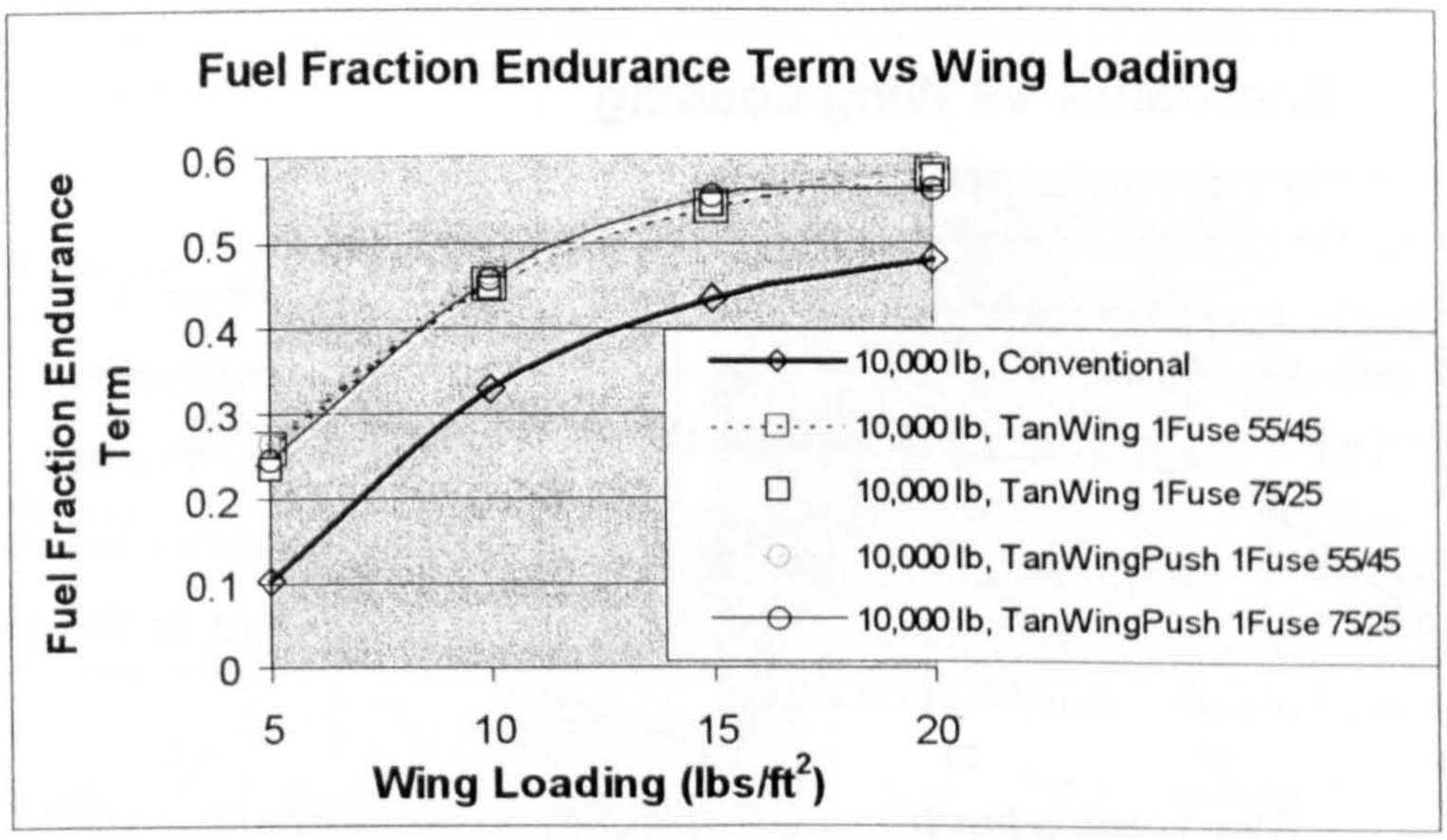

Figure 10.58 ***shows a significant advantage in structural efficiency for the tandem aircraft due to a reduction in span of the wings, and a reduction in overall aspect ratio.***

The fuel fraction term can be seen in Figure 10.58 for the 10,000 pound single fuselage tandem aircraft. The most remarkable characteristic of this figure is the prominent increase in structural efficiency for all of the tandem aircraft. This increase is considerably more noticeable than for the 2000 pound takeoff weight case. Since the span and area of the individual wings has been greatly reduced due to the division of total wing area into two tandem wings, the wings can be built more structurally efficient for the same aspect ratio. In addition, since a significant portion of the total wing area is now composed of a wing of lower aspect ratio, the overall structural efficiency is again increased. There is most likely a point at which the structural benefit balances the aerodynamic penalty for the tandems, and this should be studied in greater detail.

The increase in overall structural efficiency for the tandem aircraft is the reason for much higher overall endurance at the lower wing loadings. This remains the case until the effects of the reduced aerodynamic efficiency of the tandem aircraft become more prominent at higher wing loadings.

10.C.4.c 20,000 pound Takeoff Weight

The 20,000 pound takeoff weight case will not be presented in the same detail as the previous two cases. The overall endurance is given in Figure 10.59, however the

trends seen in the fuel fraction term were identical. In addition, the trends seen in the endurance term were identical.

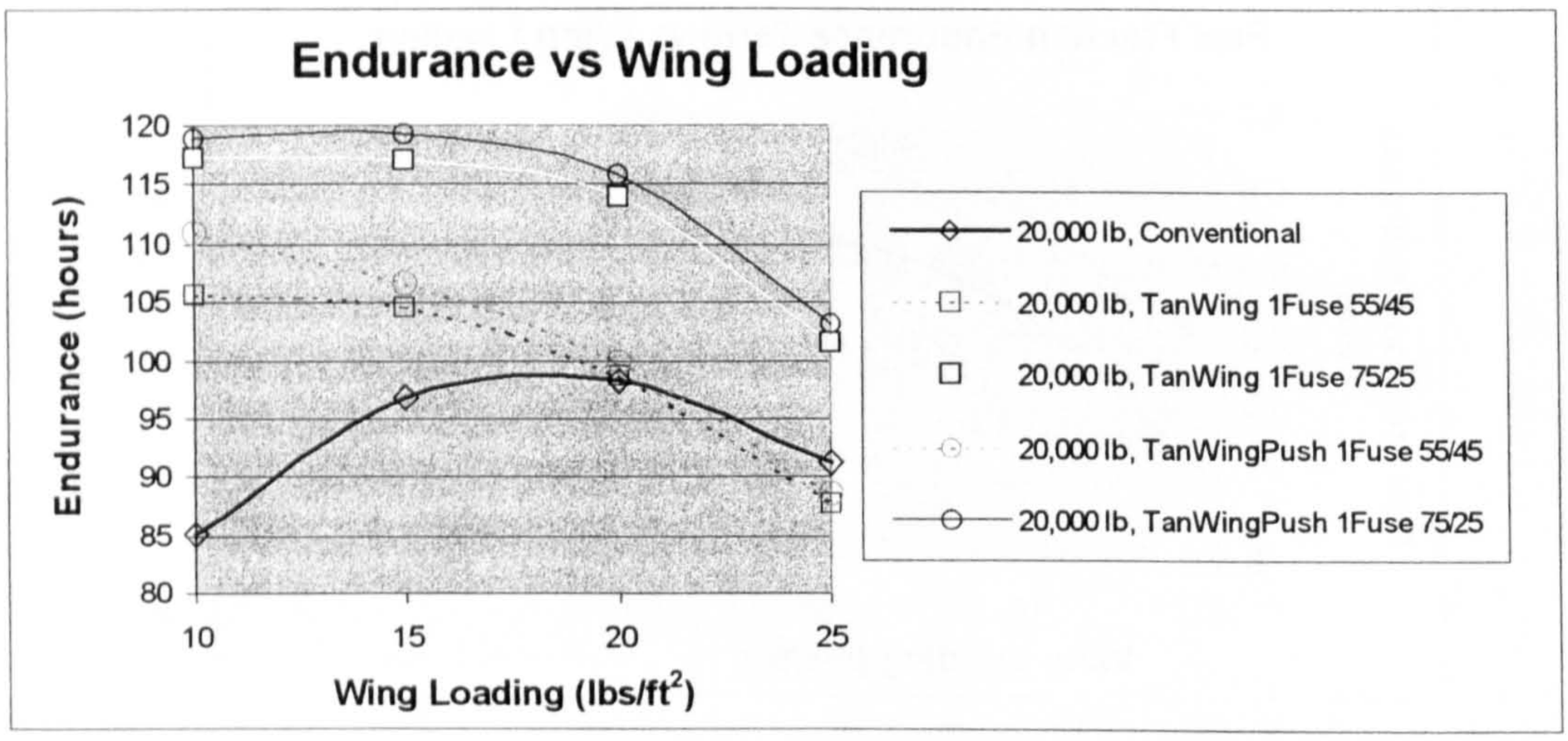

Figure 10.59 ***shows a significant improvement in overall endurance of the tandem wing aircraft at lower wing loadings when compared to the conventional configuration.***

Similar to the 10,000 pound takeoff weight overall endurance values, the deviation for the tandem aircraft is greatest at the lowest wing loadings, or highest total wing areas. It is noted that the basic shape of the 20,000 pound takeoff weight conventional configuration endurance curve is different from the shapes of the 2000 and 10,000 pound takeoff weight curves. As a result of this difference, the effects of greater structural efficiency at lower wing loadings for the tandem aircraft effects the basic shape of the conventional curve differently than for the other two takeoff weight cases. The underlying reasoning behind the behavior of the tandem curves, however is identical.

In any case, the optimal wing loading for the 10,000 pound and 20,000 pound takeoff weight cases appears to have shifted towards lower wing loading when compared to the conventional case. Finally, it is noted that the Y-scale was again increased in order to facilitate the identification of the relevant trends.

10.C.5 Multiple Fuselage Tandem Wing

The single fuselage tractor tandem wing configuration will be used as a baseline for comparison to the multiple fuselage tandem wing results. Four different multiple fuselage tandem configurations were considered: a two fuselage tractor, a two fuselage pusher, a

three fuselage tractor and a three fuselage pusher. The division of area selected for this study was 55/45 for all cases. The results will be grouped by takeoff weight once again in order to reduce the number of figures necessary and provide a more appropriate comparative reference.

10.C.5.a 2000 pound Takeoff Weight

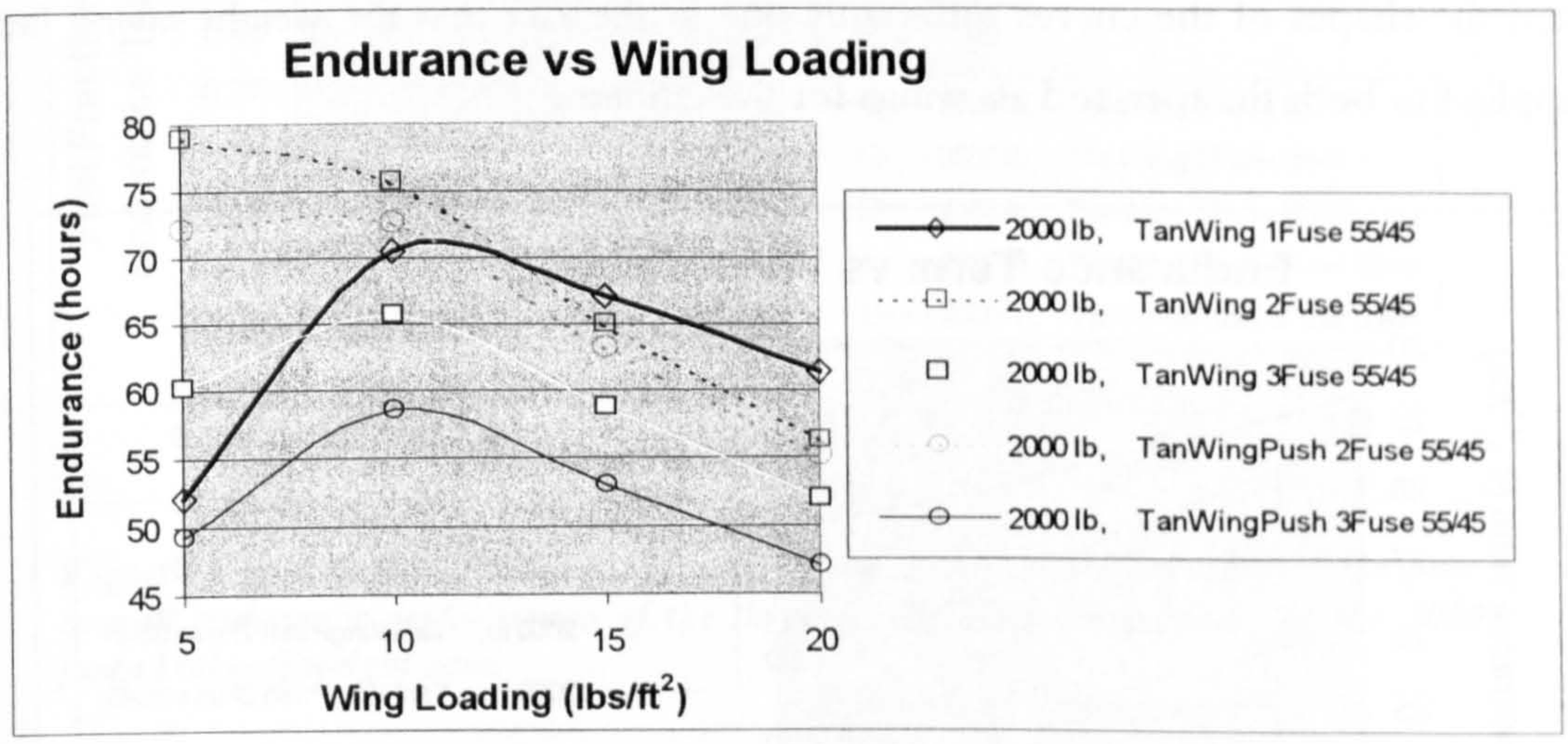

Figure 10.60 ***compares the 2000 pound multiple fuselage tandem wing aircraft to the single fuselage tandem wing aircraft as a baseline.***

The endurance for the 2000 pound multiple fuselage tandem wing aircraft can be seen in Figure 10.60. All of the multiple fuselage tandem aircraft behave differently from the single fuselage tandem below 10 lbs/ft^2. The behavior of the multiple fuselage tandems above 10 lbs/ft^2 agrees well with the single fuselage behavior, with the only difference being in the slope and location of the curves. The behavior of all of the multiple fuselage tandems agrees well with the behavior of the multiple fuselage conventional and canard results already presented. The behavior of these curves at low wing loading was shown to result from a combination of highest aerodynamic efficiency combined with structural efficiency greatly increased over the single fuselage configuration due to the wing weight saving factor used for the multiple fuselage aircraft.

The primary reason for the deviation of the three and two fuselage pusher configured tandems was that the fuselage was lengthened for both cases. This was necessary at the lowest wing loading (where the deviation is greatest) in order to balance the aircraft, and to keep the forward wing greater than two chord lengths in front of the main wing. This obviously had an adverse effect on the endurance of this configuration,

and the detailed reasoning as to why is left for the description of the individual terms. It is noted that, similar to the conventional and canard multiple fuselage 10,000 pound takeoff weight case, the multiple fuselage tandem aircraft outperform the single fuselage tandem aircraft only at the lowest wing loading.

It is also noted that there was a difference of 3% in the wing weight saving factor of the three fuselage aircraft between the tandem and the conventional and canard. This effected the shapes of the curves differently due to the fact that the weight saving factor was applied to both the fore and aft wings for the tandem.

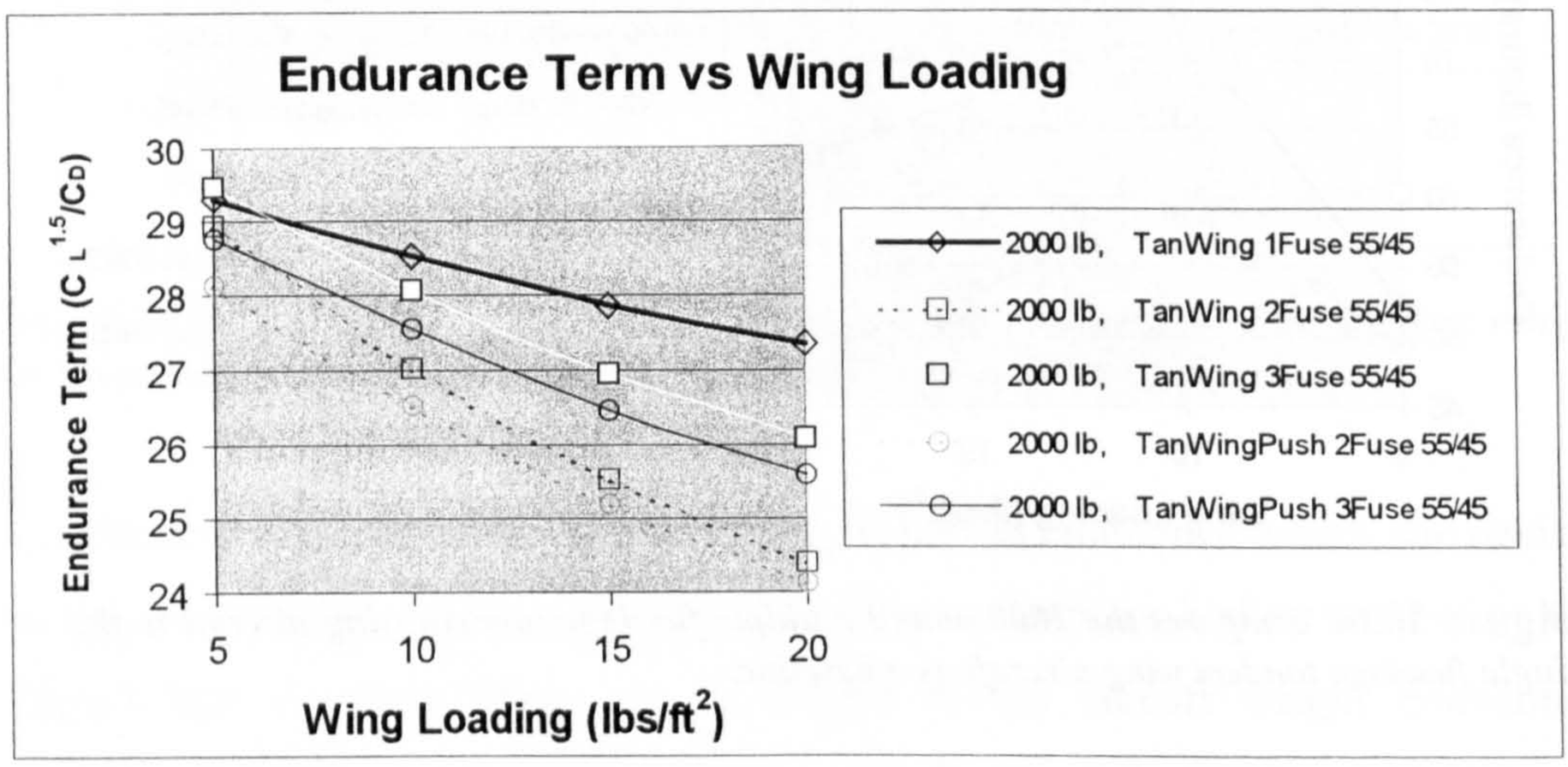

Figure 10.61 ***shows a greater slope in the aerodynamic efficiency of the two fuselage tandem aircraft when compared to the single and three fuselage tandem aircraft.***

The endurance term results for the 2000 pound multiple fuselage tandem aircraft can be seen in Figure 10.61. The three fuselage aircraft appear to have a lower value of slope, and therefore closer approximate the aerodynamic efficiency of the single fuselage tandem. The slope of the endurance term curves for the two fuselage aircraft is greater than that of the single or three fuselage curves. Once again, the two fuselage aircraft at the higher wing loadings both experienced greater travel in the aircraft center of gravity throughout cruise. When there was less fuel to balance against, the range of travel of the aircraft center of gravity adversely affected the aerodynamic efficiency. This effect is combined with the decrease in aerodynamic efficiency (with increase in wing loading) already experienced resulting from a more heavily loaded wing.

Only the three fuselage tandem tractor at a wing loading of 5 lbs/ft^2 outperforms the single fuselage tandem, and that is by a small margin. Part of the result of increasing

the fuselage length for the lowest wing loading three fuselage pusher tandem is the comparative decrease in aerodynamic efficiency seen in the figure. This contributes to a fraction of the behavior for that configuration in the overall endurance results.

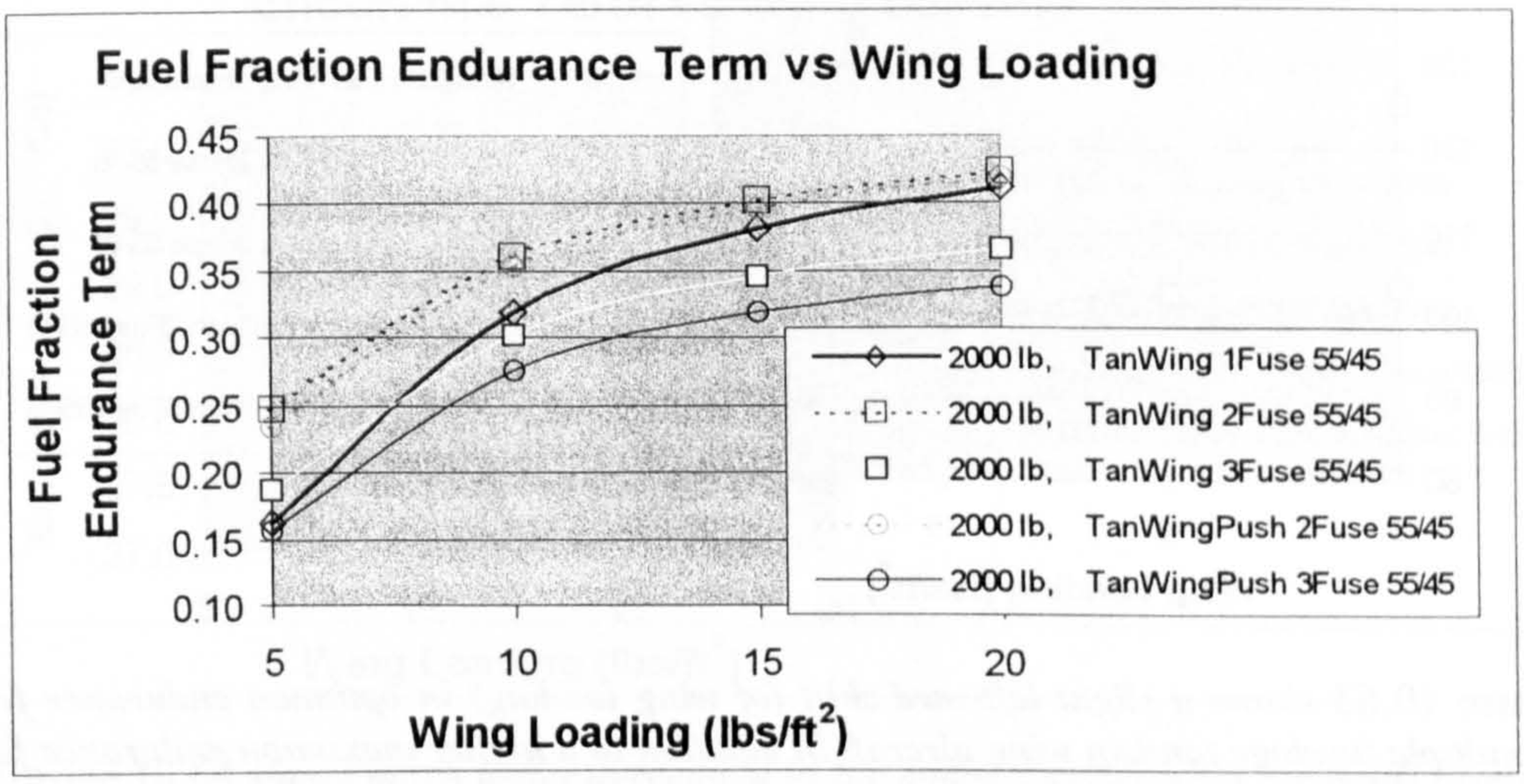

Figure 10.62 ***shows that the fuel fraction term is the primary reason for the poor overall endurance performance of the three fuselage tandem pusher for the 2000 pound takeoff weight case.***

The remainder of the behavior seen by the three fuselage pusher tandem can be explained by viewing Figure 10.62 for the 2000 pound takeoff weight fuel fraction terms. It can be seen that the fuel fraction of this aircraft is well below that of all of the other aircraft with the exception of the lowest wing loading. This is a direct result of the weight of the additional fuselage length. This low fuel fraction term is responsible for the comparatively low overall endurance performance of the three fuselage pusher tandem.

Also from the figure it can be seen that the two fuselage tandem aircraft agree well with the other configurations in the shape of the fuel fraction term curves. In addition, the two fuselage tandem fuel fraction term is superior to that of the other configurations considered throughout the range of the 2000 pound takeoff weight case.

In summary, the only multiple fuselage tandem aircraft that compare well, or exceed the performance of the single fuselage tandem are the two fuselage tractor and pusher aircraft, and that is only for wing loadings between 5 and 10 lbs/ft^2. Otherwise, for the 2000 pound takeoff weight case, the single fuselage tandem would appear to be superior.

10.C.5.b 10,000 pound Takeoff Weight

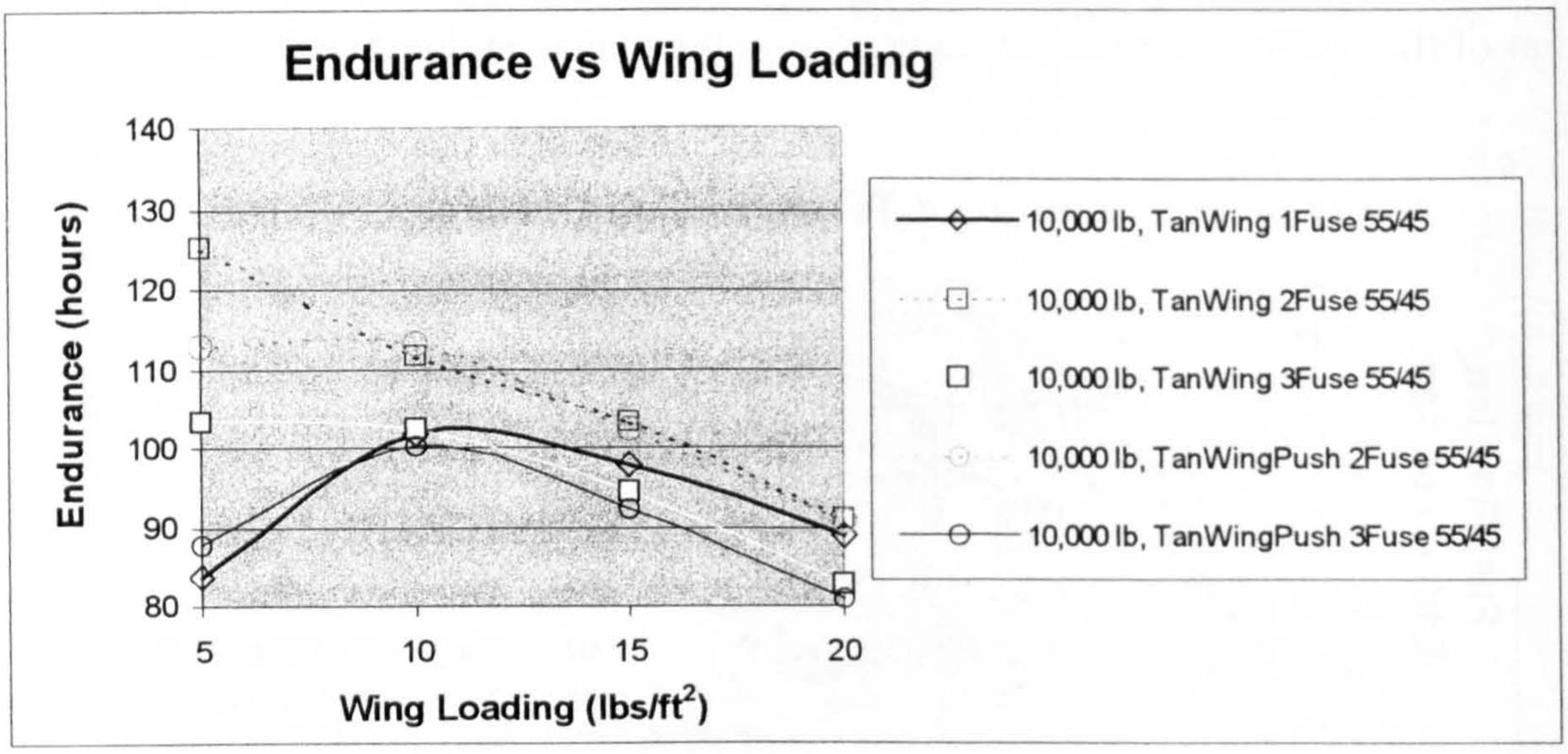

Figure 10.63 ***shows a slight leftward shift (of wing loading) in optimum endurance for the multiple fuselage tandem wing aircraft in addition to a higher maximum endurance for the 10,000 pound takeoff weight cases.***

The 10,000 pound takeoff weight endurance figure can be seen in Figure 10.63 for the multiple fuselage tandem aircraft. The most notable feature about this endurance figure is that the two and three fuselage configured tandems all outperform the single fuselage tandem below wing loadings of approximately 10 lbs/ft^2. The optimum endurance for the two, tractor configured tandem aircraft appear to shift towards a lower wing loading. Moreover, the performance of the three fuselage pusher configured tandem is improved. This configuration was difficult to balance at almost all wing loadings and takeoff weights and if for this reason alone would not be recommended. However, the performance of this configuration due to this difficulty in balancing was poor compared to the other multiple fuselage tandems at low wing loadings as well.

The results for the endurance term can be seen in Figure 10.64. In comparison to the 2000 pound takeoff weight case, the aerodynamic efficiency for all of the multiple fuselage tandem configurations appear to agree better with the single fuselage tandem. Part of the reason for the two, tractor multi fuselage tandems outperforming the single fuselage tandem in overall endurance can be seen in this figure. At wing loadings under 10 lbs/ft^2 the two multi fuselage tandem tractor configurations experience a slight increase in slope when compared to the single fuselage tandem. The two, pusher configured tandem aircraft both have lower aerodynamic efficiency than the single fuselage tandem aircraft.

Given that much of the fuel was in the main (aft) wing, the addition of the weight of the engine aft made the pusher configuration much more difficult to balance.

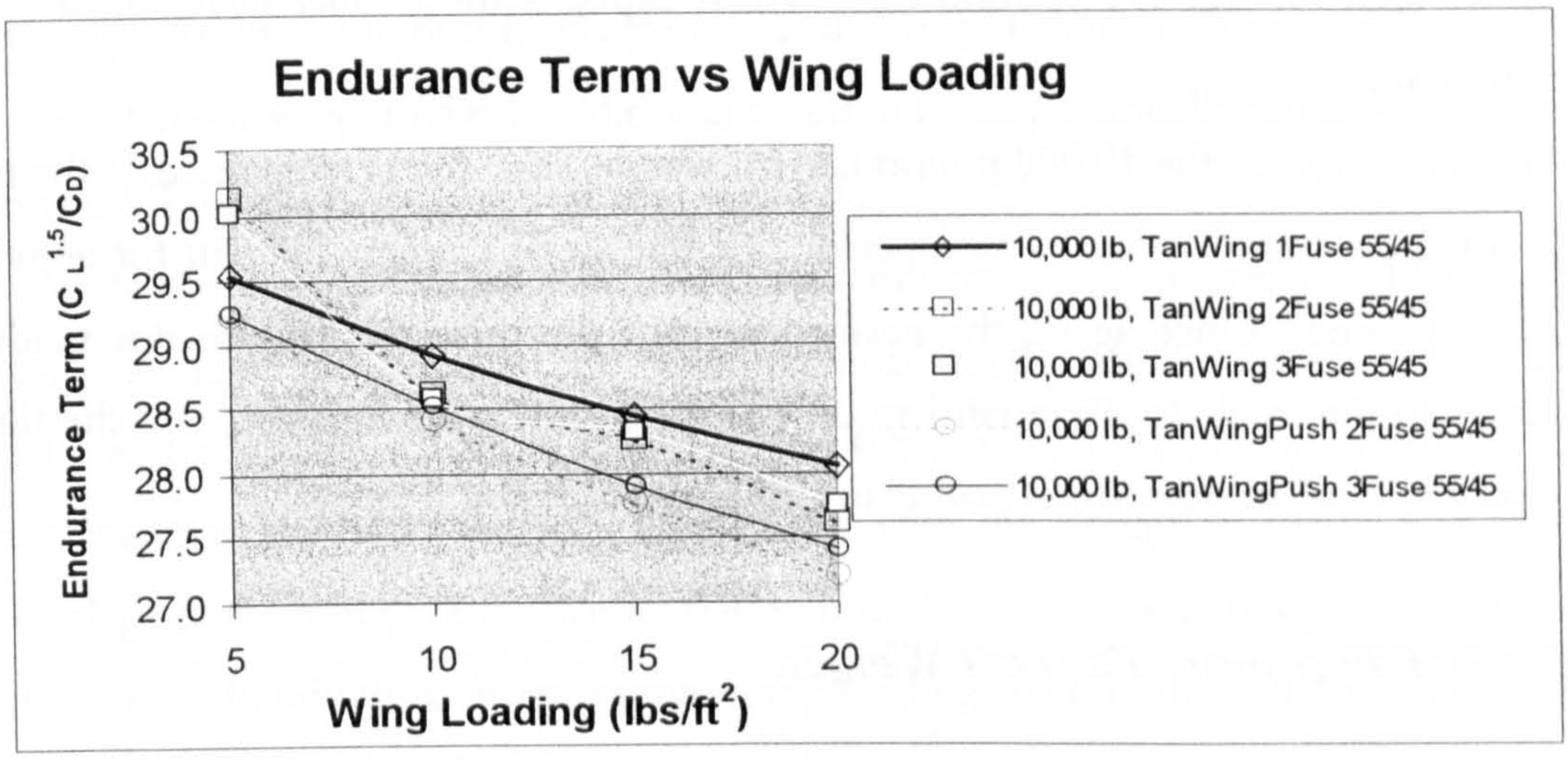

Figure 10.64 ***shows much better agreement in the endurance term for the multi fuselage tandem aircraft for the 10,000 pound takeoff weight case.***

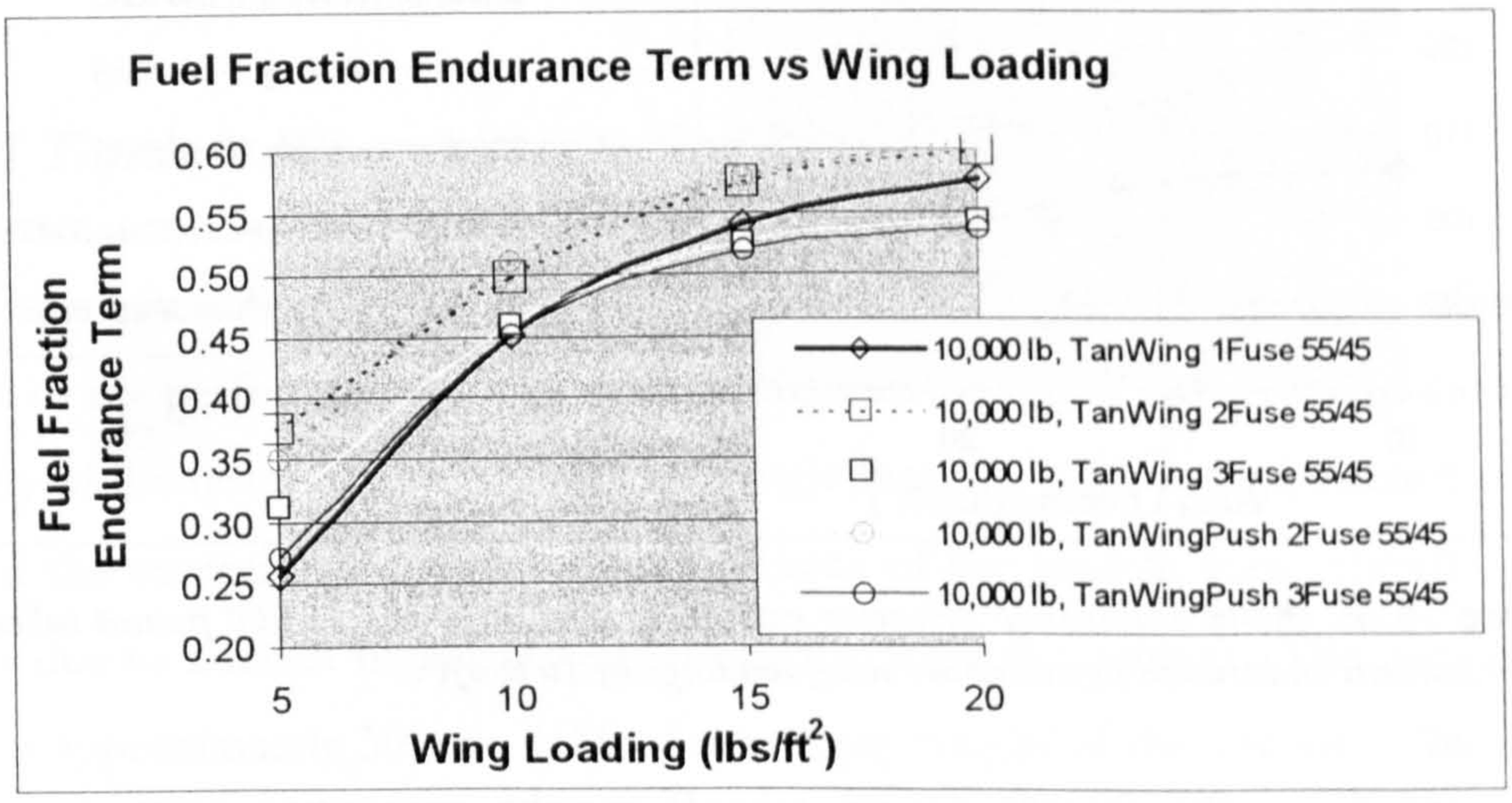

Figure 10.65 ***compares the fuel fraction terms for the multiple fuselage tandem aircraft and shows a slight improvement in fuel fraction for the 10,000 pound takeoff weight multi fuselage tandem aircraft when compared to the 2000 pound takeoff weight case.***

The fuel fraction results can be seen in Figure 10.65 for the multi fuselage tandem aircraft. Below wing loadings of approximately 10 lbs/ft^2 the two fuselage tractor and pusher, and the three fuselage tractor have higher fuel fractional weight terms than the single fuselage tandem. This, in combination with aerodynamic efficiency greater than that of the single fuselage tandem result in the behavior seen in the overall endurance figure

(Figure 10.63) for the 10,000 pound takeoff weight. Furthermore, the comparative performance of the weight fraction term for the three fuselage pusher tandem aircraft is much better than for the 2000 pound case, which explains the smaller deviation in total aircraft endurance.

In summary, for the 10,000 pound takeoff weight case, the performance of the two fuselage configured tandem aircraft outperformed the single fuselage tandem for all wing loadings considered. Once again, the performance of the three fuselage tractor tandem was superior to the single fuselage tandem only at the lowest wing loadings, and the three fuselage pusher tandem performed poorly in comparison.

10.C.5.c 20,000 pound Takeoff Weight

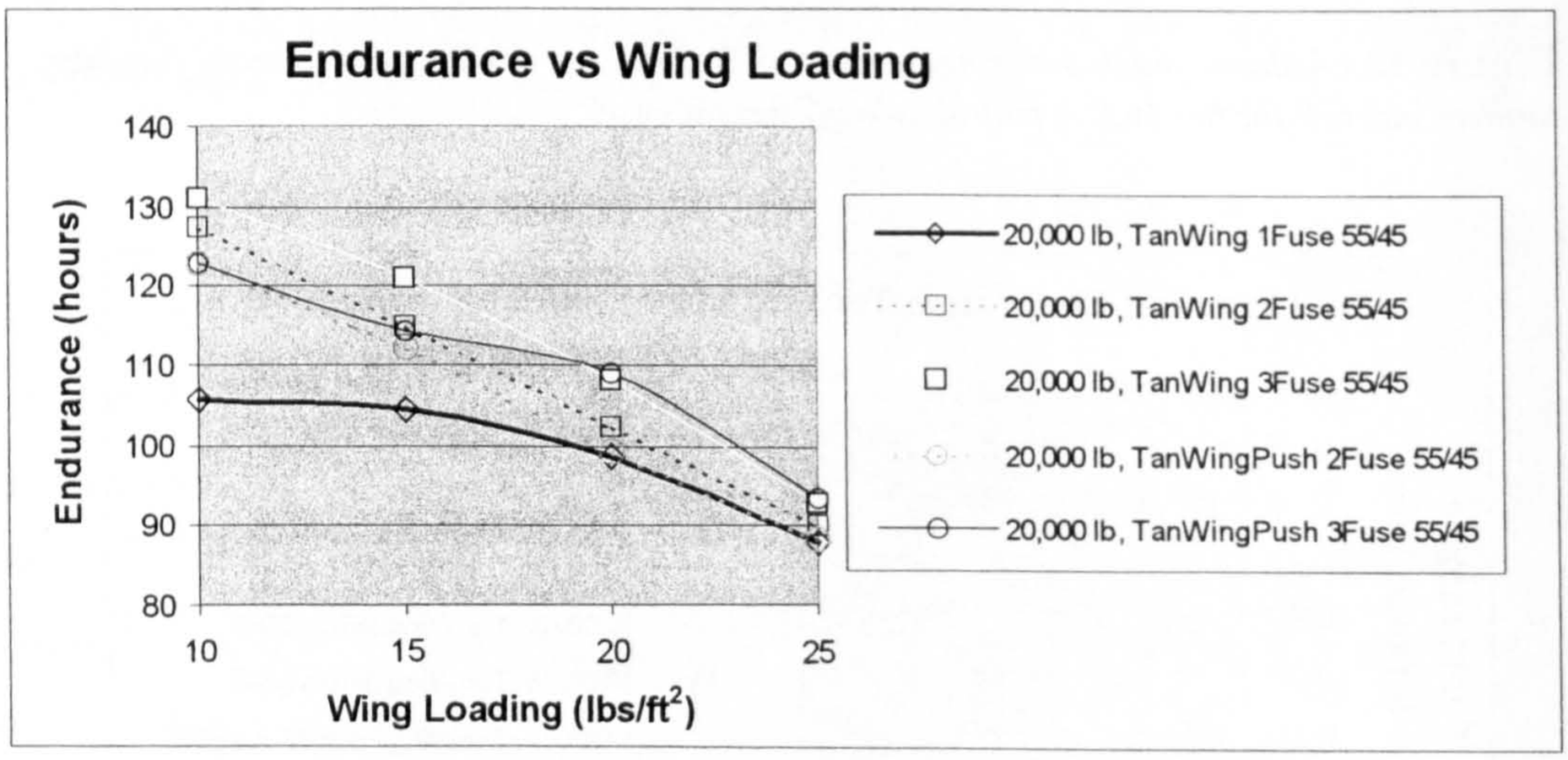

Figure 10.66 ***shows endurance behavior extremely similar to the 10,000 pound takeoff weight tandem endurance figure above wing loadings of 10 lbs/ft^2.***

The trends in the 20,000 pound takeoff weight endurance term curves are essentially identical to those seen for the 10,000 pound takeoff weight case. For the fuel fraction curves, there are several differences. The first difference is that the pusher configured three fuselage aircraft fuel fraction curve experienced a decreased slope between 10 and 20 lbs/ft^2. This behavior in the fuel fraction term is responsible for the characteristics seen in the overall endurance curve for the 20,000 pound takeoff weight three fuselage pusher configured tandem. In addition, the fuel fraction curves for all four multiple fuselage tandems experienced an upward shift. This improvement in fuel fraction was sufficient enough such that the fuel fraction terms of all of the multiple fuselage tandem aircraft exceeded the fuel fraction performance of the single fuselage tandem.

Finally, the fuel fraction performance of the three fuselage tandem aircraft was superior to the performance of the two fuselage aircraft for the first time. This reversal is also reflected in the overall endurance performance graph, with the three fuselage aircraft very slightly outperforming the two fuselage aircraft in many instances. This can be explained by the fact that the weight of the additional fuselage is proportionally much smaller for an aircraft takeoff weight of 20,000 pounds.

With those considerations in mind, the endurance can be seen in Figure 10.66. Although this figure is for the 20,000 pound takeoff weight tandem aircraft, the behavior essentially represents the shapes seen in the 10,000 pound takeoff weight endurance figure for wing loadings above 10 lbs/ft^2. This is true with the exception of the fact that the three fuselage tandem now outperforms the two fuselage tandem, although the differences are quite small. In addition, the optimum wing loading for the multiple fuselage tandems has now quite clearly shifted towards lower wing loading. In summary, for the 20,000 pound takeoff weight case, the performance of all of the multiple fuselage tandem aircraft exceeds that of the single fuselage tandem.

10.C.5.d Tandem Wing Aircraft Summary

The outstanding endurance performance of the tandem wing configurations compared to the performance of the other configurations might raise some questions as to the validity of the results. As seen from the single fuselage tandem wing aircraft study, the reason for the exceptional endurance performance of the tandem wing aircraft is for the most part due to a much higher structural efficiency for the wing(s). The wing normally constitutes approximately 30% to 45% of the empty weight of the aircraft. This range of wing fractional empty weight was obtained from the results of the methodology. There is only one other single component of the aircraft that is nearly as heavy and that is the engine. For the majority of cases considered, the wing is heavier than the engine, and the heaviest of the remaining components is less than 8% of the empty weight.

Referring back to the section on aspect ratio variation, it was shown that an average improvement in fuel fraction term of roughly 0.10 was found across the entire range of wing loadings for the higher takeoff weights. It is noted that this was for a wing with area equal to the aspect ratio 35 wing to which it was compared. Thus, the span and area of an individual tandem wing is significantly reduced further beyond this value. In the

range of takeoff weights and wing loadings where this weight saving was less pronounced in the aspect ratio study (2000 pounds), the tandem aircraft do not perform significantly better than the conventionally configured aircraft.

Whether or not these weight savings could be achieved in reality is a reasonable question. However, it is difficult to argue against the concept that peak wing structural loads are significantly decreased by the reduction of individual wing span and area (and thus aspect ratio) for extremely high aspect ratio wings. In addition, it was shown that the aerodynamic efficiency for the forward wing is not significantly reduced (and in some cases is even increased) by the division of wing area and reduction of aspect ratio. These two statements in combination allow for the conclusion that the tandem wing aircraft results are in fact quite reasonable in terms of endurance performance.

10.C.6 Flying Wing

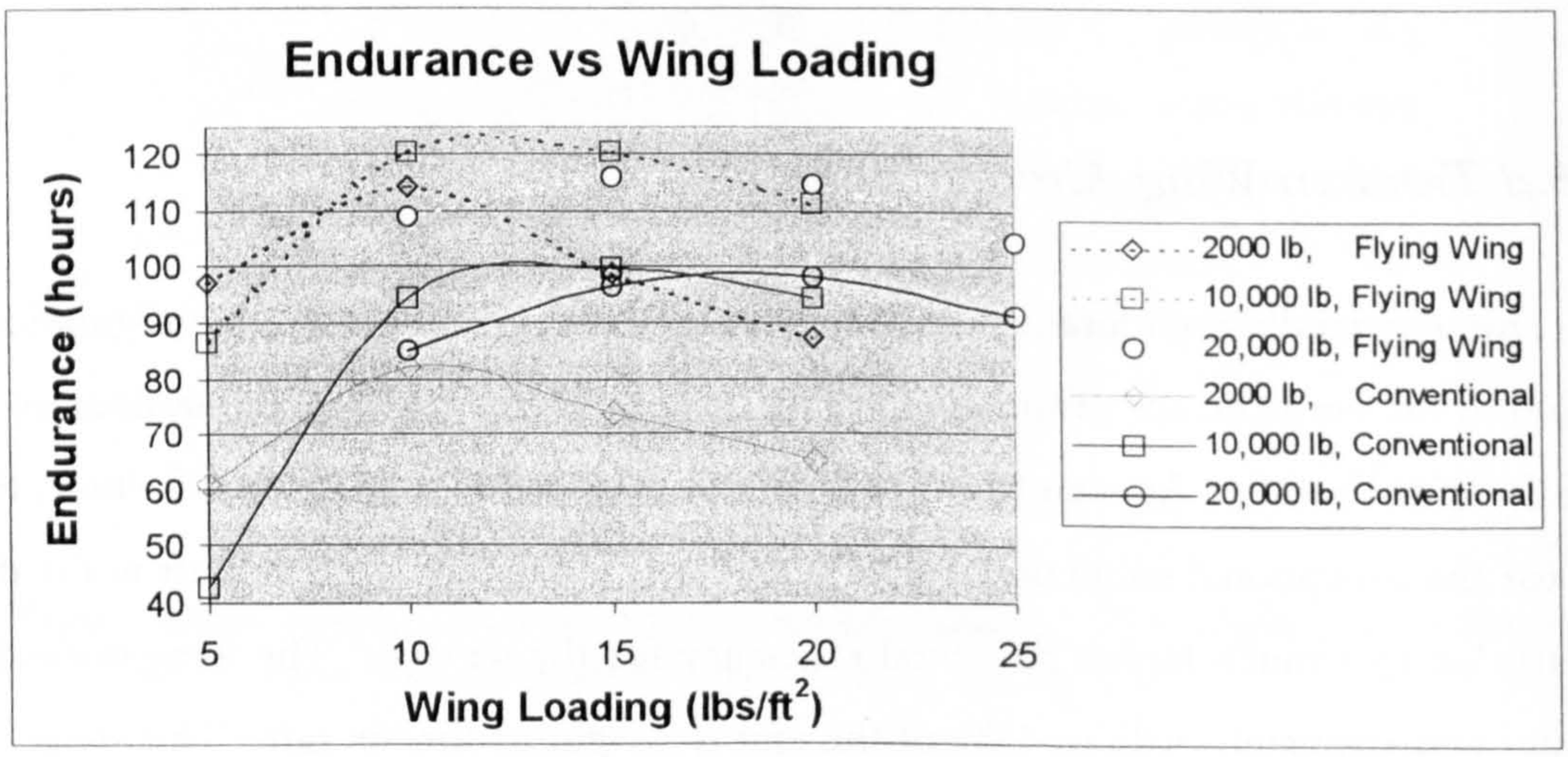

Figure 10.67 ***shows the endurance of the untrimmed flying wing compared to the conventional configuration.***

In the limited time available, it was impossible to evaluate the flying wing configuration with the necessary degree of detail. The difficulty with providing detailed results lies with the control surface deflections necessary to maintain the selected static margin and keep the aircraft in cruise trimmed flight. The airfoil used for the aerodynamic analysis for the flying wing (the Eppler 344) was slightly reflexed in order to reduce the wing moment coefficient. Despite this airfoil selection, it is suspected that there would be greater drag penalties due to the need to increase control surface deflection as fuel is

burned. Consequently, the results shown do not have the same trimmed drag penalties as the other configurations and should be viewed as representative of the overall comparative trends of the flying wing when compared to the conventional configuration. Since the trimmed drag penalties were not evaluated for this configuration, there was little additional benefit expected from evaluating the pusher propeller configured flying wing.

The overall endurance results can be seen in Figure 10.67. As would be expected without the consideration of trim drag penalties, the flying wing configuration significantly outperforms the conventionally configured aircraft. Additionally, it can be seen that the general shape of the takeoff weight curves is the same across the two configurations. There is a very slight increasing deviation between the curves for the two configurations with decreasing wing loading. Again, this behavior has been traced back to the variation in the wing weight estimation with lower wing loadings (influenced through lower fuel weight). The most noticeably different behavior seen in this figure is that of the 2000 pound flying wing curve. There is a much smaller difference in endurance between the 2000 pound case and the other two takeoff weight cases for the flying wing.

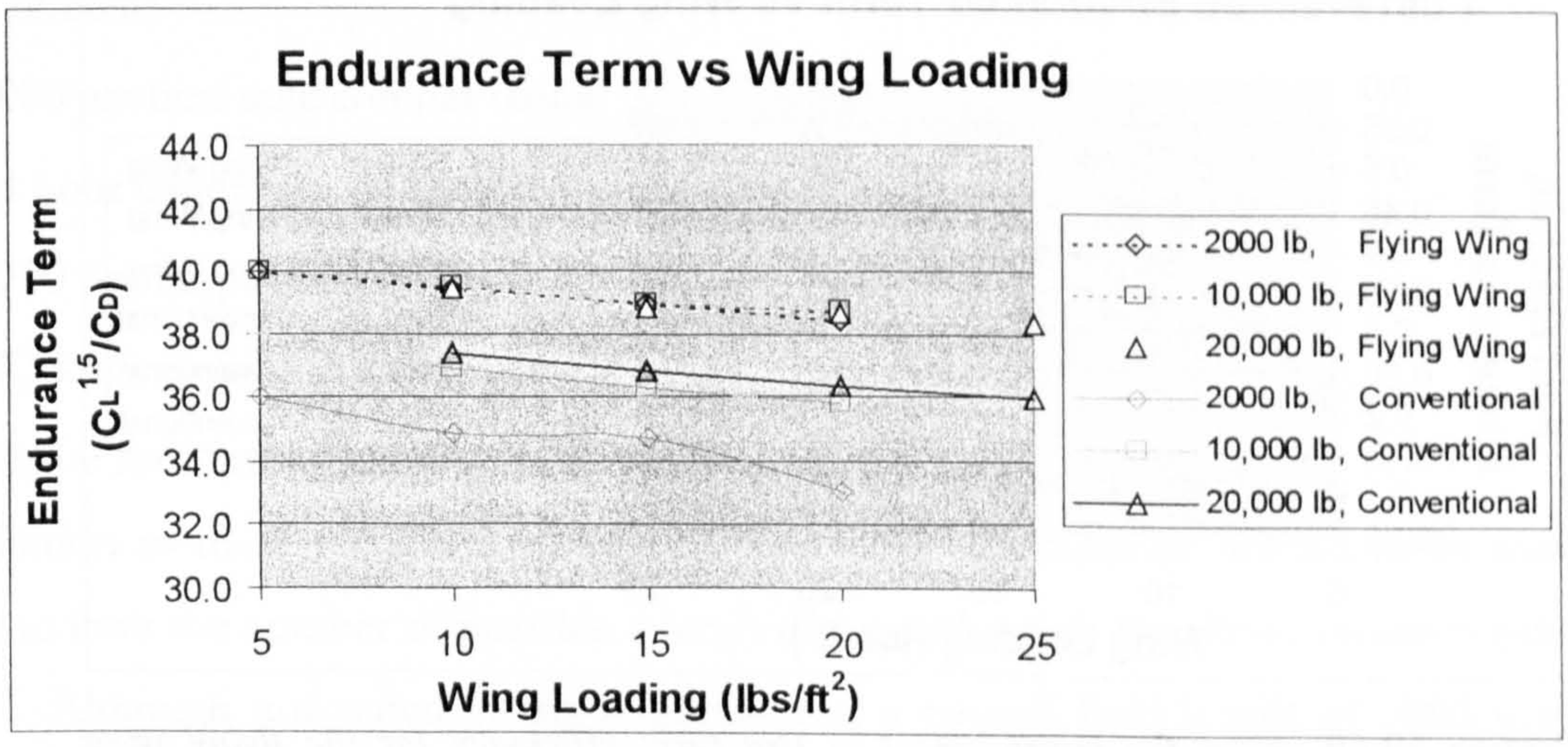

Figure 10.68 ***shows the coincidence of the endurance term curves for the flying wing case.***

The reason for the smaller difference in overall aircraft endurance for the 2000 pound flying wing case can be seen in Figure 10.68. For the first time in the graph for the endurance term, the three different takeoff weight cases are essentially coincident in value as a function of wing loading. It is believed this is a direct result of not considering trim for the flying wing configuration. This only further emphasizes the effects of trim on the aerodynamic efficiency, and the need to include a trim analysis when comparing

configurations as was done in this thesis. The lowest takeoff weight aircraft has consistently shown lower aerodynamic efficiency than the other two, higher takeoff weight cases. It was also noted earlier that for several of the configurations considered, the 2000 pound aircraft was the most difficult to find an acceptable center of gravity location for the payload (in order to provide an acceptable aircraft static margin).

The only other possible explanation for the coincidence of the endurance term takeoff weight curves for the flying wing would be the exclusion of tail surfaces from the drag analysis. Given that the tail surfaces scale directly with the size of aircraft, the fractional drag should do so as well. In checking the detailed drag output for many of these cases, it was determined that the fractional drag consistently scales directly with the size of the tail, and thus would not explain a consistent difference between the larger takeoff weights and the 2000 pound case. It is believed, however, that the incremental difference between the aerodynamic efficiency of the two cases results directly from only two factors: Trim Drag and Tail Surface Drag (skin friction and profile drag).

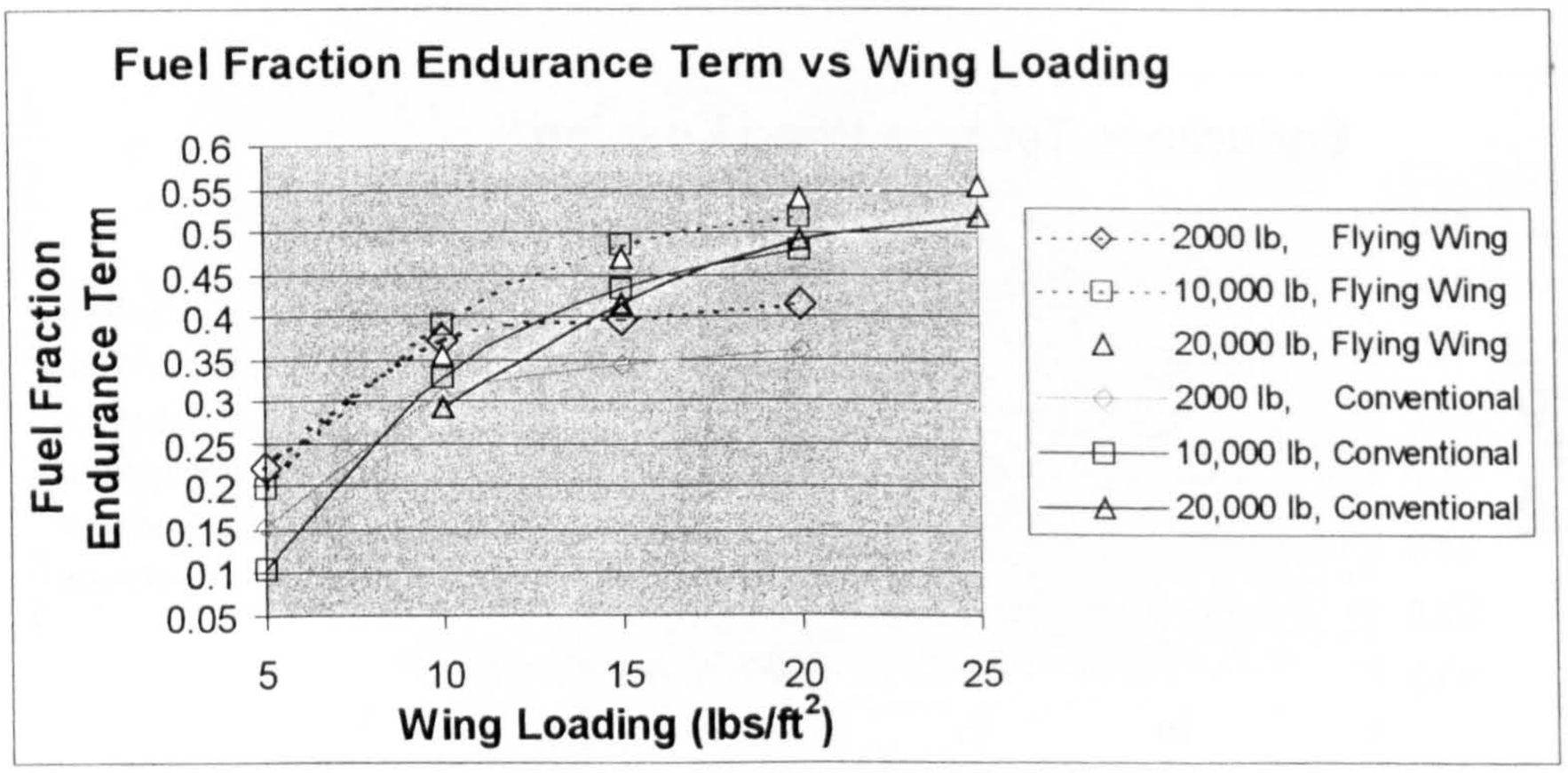

Figure 10.69 ***shows the improvement in structural efficiency for the flying wing configuration resulting from the removal of the tail surfaces from the weight estimation.***

The increase in structural efficiency for the takeoff weights considered for the flying wing can be seen in Figure 10.69. This is exactly the behavior that would be expected with the removal of the tail surfaces from the structural weight calculations. The flying wing configuration had a center fuselage for payload, so the effects shown result strictly from the removal of the tail surfaces and supporting structure.

10.D Case Study

The discussion thus far in the Results chapter has focused on the validation of the existing methodology and the application of the methodology to a wide variety of conceptual design problems. The methodology was used first to perform sensitivity on the conventional configuration to geometric variables, flight conditions, and configuration related parameters. Then the methodology was used to perform the same style of sensitivity study for a wide variety of configurations. A set of charts was generated with respect to each of these parameters which identified the optimum non-dimensional design point for maximum aircraft endurance performance. If the non-dimensional nature of these graphs is fully understood, they can be used in the design of any aircraft within the takeoff weight, wing loading, and configuration related limits tested and validated within this thesis.

Regardless, a traditional conceptual design type study was performed using the methodology in order to demonstrate that the methodology is capable of evaluating aircraft in this manner. The study begins with the specification of the following Mission Requirements :

- 3000 nautical mile combat radius
- 24 hour endurance on station
- 2200 pound payload
- 373 knot cruise velocity (Mach 0.65)
- 50,000 foot cruise/loiter altitude.

In addition to these requirements several reasonable assumptions needed to be made in order to limit the number of possible aircraft that could satisfy the above requirements.

Although not stated in the requirements, a takeoff field length of 5000 feet was assumed, and a maximum stall speed of 120 knots was assumed. In addition, for the purposes of facility and ease of transport, the wing semi span was limited to 65 feet. Finally, a wing (without flap) maximum lift coefficient of 1.4 was assumed. These additional requirements have obvious implications in the areas of takeoff wing loading, maximum takeoff weight, wing geometry, takeoff distance, stall speed, and in payload weight fraction (given the payload weight).

10.D.1 Conventional Configuration

The first of two configurations to be considered in the case study was the conventional single engine aircraft. Given the cruise velocity requirement, a turbofan/turbojet powerplant was necessary. The Allison AE3007H (the powerplant for the *Global Hawk*) was selected, with a cruise specific fuel consumption (at 50,000 feet and Mach 0.65) of 0.65 lbs/lbf/hr.

Another effect of the increased cruise velocity was that the benefits of increasing the aspect ratio were much less pronounced due to the relative domination of parasite drag over lift induced drag. This resulted from the fact that the average lift coefficients experienced by this aircraft, despite its higher wing loading were still much lower than those experienced by the propeller aircraft due to the presence of the velocity squared term in the denominator of the lift coefficient definition. The final result of this effect is that the aspect ratio was determined more based upon structural and span limitations rather than aerodynamics, as the sensitivity to this parameter was weak. As an example, for the highest wing loading cases considered (where span limitation was the least constrained), the aspect ratio was increased from 28 to 36 and the lift to drag ratio was only improved by 1.13 and the endurance was relatively unchanged.

Several different designs with the given basic configuration were capable of attaining the required performance. The configurations selected for inclusion can be seen in Table 10.4. The configurations are named A, B, and C in order of increasing wing loading, or decreasing takeoff weight.

It is noted at this point that there are an infinite number of possible concepts that will satisfy the requirements as stated, and Table 10.4 was intended only as a definition of the limits or bounds of what could be reasonably considered based on the output from the methodology. In addition, the cases considered represented the range of payload weight fractions seen in existing HALE UAV's. It is also noted that for each configuration, small changes in aspect ratio, wing sweep, taper ratio, and wing profile will result in small improvements or penalties as shown in the Results for the Conventional Configuration already discussed. The values arrived at for the case study were done so as determined through the balance of aerodynamic and structural considerations already justified in the respective sections of this Results chapter.

Table 10.4 ***lists a few of the concepts that were found to satisfy the mission requirements for the conventional configuration.***

	A	B	C	
Wing Loading	51.2	56.4	64.5	**lbs/ft^2**
Endurance	24.2	24.0	24.1	**hrs**
W_{to}	33,846	26,829	22,000	**lbs**
S	661	476	342	**ft^2**
Trimmed Power Req'd	918	694	543	**HP**
L/D	27.3	29.7	32.4	
W_{pl} / W_{to}	0.065	0.082	0.100	
W_{fuel} / W_{to}	0.636	0.605	0.574	
AR	26	27	28	
B	131	113	97.8	**ft**
$V_{stall/to}$	104	109	117	**knots**
$V_{stall/ldg}$	68.0	73.7	81.1	**knots**

It can be seen in the table that all three configurations satisfy the 24 hour endurance requirement. These numbers have been obtained with consideration of the time required for ingress/egress already taken into account. It can also be seen that the takeoff weights range in value by 35%. Thus a reasonably large range of overall size of aircraft can fulfill the mission requirements as stated. It was for this reason that additional constraints were necessary. Identical values were used for payload size and volume. Payload placement was based upon the provision that all three cases have identical static margin and static margin ranges. Placement of the wing further forward provided slightly better aircraft performance, however this severely limited the physical range of payload placement and the stability of the aircraft for lighter payload cases. Thus a slightly further aft main wing position was selected than the position that would provide the optimum aerodynamic performance. This process was kept consistent across all cases considered.

The values of wing loading that satisfy the 24 hour endurance requirement vary inversely with the takeoff weight, with the highest wing loading corresponding to the lowest takeoff weight and vice versa. Case A was considered as the heaviest and largest possible option. There are many problems associated with this configuration. One problem is that it is on the upper end of wing span even though it has the lowest aspect ratio of the three configurations. Configuration A also has the highest trim power required and the corresponding lowest aerodynamic efficiency. The fact that it is the largest aircraft, and has the highest cruise power required means that the first cost and the operating costs (more fuel, more aircraft to maintain) of this aircraft will be the highest.

In direct contrast to Case A, Case C was considered the lightest and smallest possible option. Case C had the highest aerodynamic efficiency and the lowest power required in cruise. Furthermore, it had the highest wing loading which presented the limiting side of the concept. Case C had the highest minimum stall speeds in both the landing and takeoff configurations. The takeoff stall speed was calculated using the maximum takeoff weight, and the landing stall speed was calculated based on 10% fuel remaining, both at a maximum lift coefficient of 1.4 and sea level conditions.

With a high takeoff and landing speed, the aircraft would require considerably more runway for takeoff and landing, in addition to increasing the potential for damage in the event of an off-field landing encounter. Another serious consideration with the higher wing loading is the fact that the maximum ceiling is now limited severely by the stall speed when equivalent airspeed is considered under cruise/loiter conditions. With a cruise velocity of 373 knots, and a cruise altitude of 50,000 feet, the equivalent cruise speed is 146 knots. If a cruise altitude of 60,000 feet is considered, this aircraft will stall before reaching altitude before a substantial amount of fuel is expended.

Finally, Case B is presented as the best compromise between the other two, limiting cases already discussed. While it has a higher power required and lower aerodynamic efficiency than Case C, it requires less runway and has greater stall margin, in addition to greater potential for growth versions and the ability to reach higher altitudes without the need to expend fuel first. When compared to Case A, it is a smaller aircraft with higher aerodynamic efficiency and, if designed properly, will ultimately cost less to purchase and operate. It is noted, however, that without requirements on takeoff distance, stall speed, wing span, and maximum lift coefficient, all three configurations will perform the mission required.

10.D.2 Two Fuselage Conventional Single Engine

The second configuration to be considered in the case study was the two fuselage single engine conventional configuration. A representative diagram of this aircraft can be seen in Figure 10.70. Obviously care will have to be taken in the final layout of this aircraft to prevent the jet exhaust from impinging on the horizontal tail, however this type of configuration has been implemented before with a jet engine.

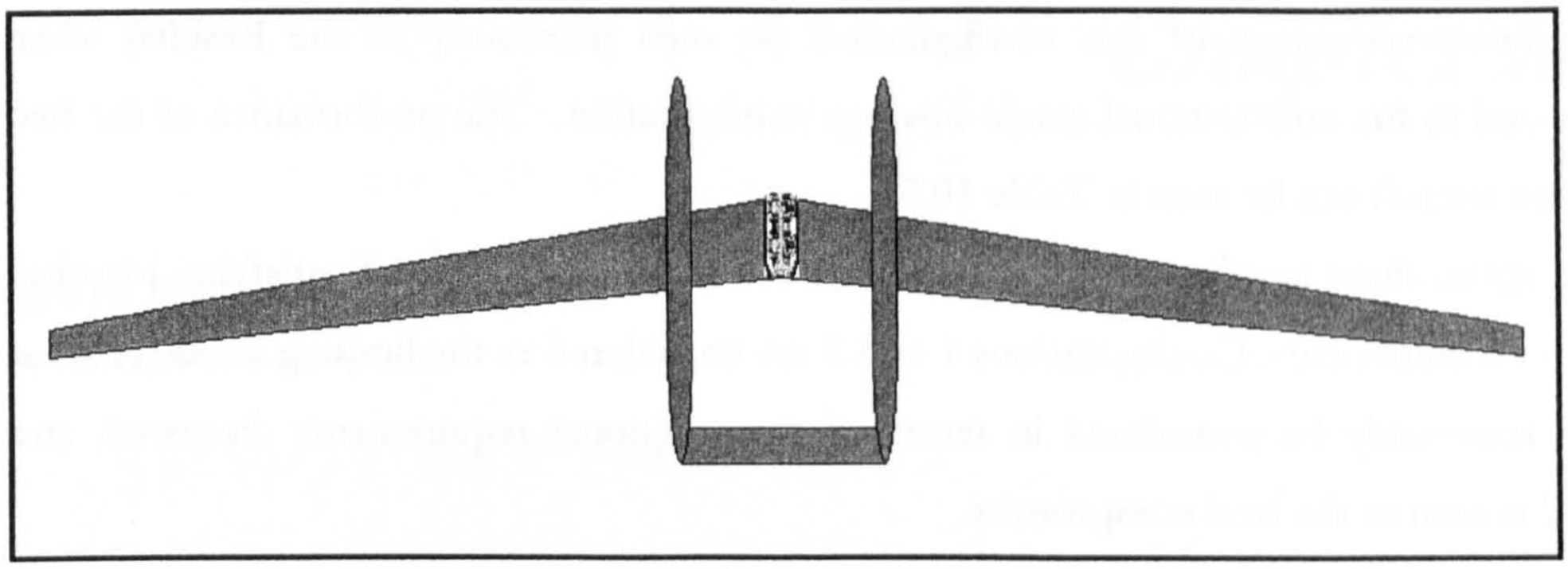

Figure 10.70 ***shows the two fuselage single engine conventional configuration.***

It is important to note that due to two primary factors it was necessary to re-evaluate the wing weight saving factor used for the two fuselage configuration. With the high degree of sweep angle used (resulting from the high cruise velocity), and with the fact that a large amount of fuel was placed in the fuselages, the entire structural nature of the wing has changed when compared to piston aircraft traveling at lower speeds. There were only a couple of piston aircraft that were not capable of placing all of the fuel in the wing for a similar mission requirement. However, due to the nature of the fuel consumption of jet engines, this was no longer the case for this aircraft.

Table 10.5 ***lists the results for a few of the concepts that were found to satisfy the mission requirements for the less conventional configuration considered for the case study.***

	1	2	3	
Wing Loading	49.2	54.4	62.2	**lbs/ft^2**
Endurance	24.0	24.1	24.3	**hrs**
W_{to}	33846	26829	22000	**lbs**
S	687	493	354	**ft^2**
Trimmed Power Req'd	962	720	558	**HP**
L/D	24.2	26.8	29.5	
W_{pl} / W_{to}	0.065	0.082	0.100	
W_{fuel} / W_{to}	0.670	0.632	0.594	
AR	25	27	28	
b	131	115	100	**ft**
$V_{stall/to}$	102	107	115	**knots**
$V_{stall/ldg}$	64.3	70.4	78.2	**knots**

It was found from a comparative study of total wing bending moment that the wing weight *saving* factor had to be increased substantially to 0.75 thereby increasing the overall wing weight for the two fuselage configuration. This effect dramatically reduced

the primary advantage of this configuration (as seen previously in the Results) when compared to the conventional single fuselage configuration. The performance of the two fuselage aircraft can be seen in Table 10.5.

Once again, three configurations are listed in the table, all capable of satisfying identical mission requirements. Configurations 1 and 3 are considered as the limiting cases for what could reasonably be considered in terms of the additional requirements discussed, and Case 2 is seen as the best compromise.

When compared to the single fuselage aircraft, it is first noted that the wing loading that satisfies the mission requirements for a given takeoff weight has been slightly reduced for the two fuselage aircraft. The wing loading reduction is in the range of 3.6 to 4.0% for the three cases. It is also noted that the aspect ratio on Case 1 was reduced to 25 when compared to Case A in the single fuselage table. This was done to keep the semi-span below the required 65 feet, and resulted directly from the reduction in optimum wing loading experienced by the two fuselage aircraft.

The two fuselage aircraft had comparatively lower aerodynamic efficiency (from 9 to 13% lower) for the same takeoff weight. This was due in part to the fact that a lower wing loading satisfied the mission requirements, but due also in part to the additional parasite drag of the second fuselage. The weight saving in overall empty weight of the two fuselage aircraft over the single fuselage aircraft ranged from 3.4 to 5.3%.

The end result was an increase in power required for the two fuselage aircraft from 2.7 to 4.8%. This belies the nature of the two fuselage aircraft. It is expected that there will be a weight saving due to the bending moment relief of the multiple fuselages, however the penalty is expected in the aerodynamics.

Identical arguments can be used for the exclusion Cases 1 and 3 from consideration as were used to exclude cases A and C. Thus, the comparison is reduced to that of Case 2 and Case B. It is expected that since the performance of these two configurations was so similar that a decision between the two would likely need to based on some other requirement or consideration.

Chapter XI

Long is the Road

from Conception to Completion

--- Molière

11. Conclusions and Recommendations

11.A Conclusions

An extremely powerful and robust graphically interactive computational conceptual design synthesis methodology has been created. This methodology was used to perform a detailed study on the driving design parameters behind the Breguet endurance equation for a large number of conventional and unconventional configurations.

In the process of creating and executing the methodology:

- A new relation was developed for UAV length prediction
- A Low Speed HALE airfoil figure of merit was proposed
- A large number of horizontal and vertical tail volume coefficients resulted from executions of the methodology and were presented for use with conventional and unconventional configurations
- A simplified relation for the prediction of single fuselage Low Speed HALE UAV empty weight was proposed
- A validation on the macroscopic results was performed against as many aircraft as was practical.

A detailed study was performed for the conventional configuration on Breguet equation endurance sensitivity to:

- Aspect Ratio
- Taper Ratio
- Airfoil Selection
- Cruise Lift Coefficient
- Cruise Altitude
- Various Single and Twin Engine tractor and pusher configurations and Twin Engine Push-Pull configuration.

The greatest sensitivity was to altitude, then aspect ratio, taper ratio, and twin engine variations. The push pull twin engine conventional aircraft showed the best endurance performance of the twin engine aircraft as a result of the elimination of the wing mounted nacelles.

A general study was performed on overall aircraft endurance for the following configurations in both single engine tractor and pusher engine configuration:

- Canard
- Twin Boom
- Two Fuselage Conventional and Canard
- Three Fuselage Conventional and Canard
- Single Fuselage Tandem Wing, 55% Aft Wing Area/45% Fore Wing Area
- Single Fuselage Tandem Wing, 75% Aft Wing Area/25% Fore Wing Area
- Two Fuselage Tandem Wing
- Three Fuselage Tandem Wing
- Flying Wing.

The tandem wing aircraft had by far the most superior endurance performance throughout the range of configurations, takeoff weights and wing loadings tested. The flying wing configuration also had excellent endurance performance, however a trim analysis was not performed for the flying wing. Thus elevator/aileron deflections were not determined, and the drag necessary to trim the flying wing was not taken into account as was done for all other configurations considered. The remainder of the single engine configurations experienced minor changes in endurance as a result of differences in configuration. The endurance for each configuration for a given design wing loading and

takeoff weight can be maximized by giving due attention to balancing the aircraft properly. The optimum wing loading in terms of endurance for a given takeoff weight for each configuration was determined. The details for the behavior of the individual configurations were provided in the Results and Discussion chapter (Chapter X).

11.B Recommendations

Due to the limited time to perform the research, and the limited space within this thesis in which to present the results, a large number of areas were identified for further research.

11.B.1 Further Utilization of the Methodology

Following from the above statement, there simply was insufficient time to take advantage of the full ability of the methodology to generate detailed results on Low Speed HALE UAV's. Furthermore, there was inadequate time and space to evaluate all of the results already obtained. Several areas have been identified for relatively straightforward study based on results already generated. Other areas have been identified for further study utilizing aspects of the methodology as yet underutilized.

11.B.1.a Twin Engine Alternative Configurations

The results presented in this thesis only included the various twin engine configurations for the conventional aircraft. The *Theseus* elected to use two engines at a takeoff weight of less than 10,000 pounds. Thus the region from roughly 10,000 to 20,000 pounds needs to be studied to determine the takeoff weight, wing loading, and configuration that provides the optimum twin engine endurance. There are therefore 30 possible combinations of engine and aircraft configuration that remain to be investigated when aircraft configuration, tractor, pusher, and push-pull engine configurations are considered.

11.B.1.b Tandem Wing Study

Since the tandem wing configuration showed the most promising overall endurance results, it follows that this configuration should be the topic of a more detailed study. There were some unexpected results in terms of the division of area between lifting surfaces for both the aerodynamics and weight. Each of these phenomena could be isolated by a parametric analysis using the present methodology. Questions still remain as to the optimal division of area, lift, lift coefficient, airfoil type, longitudinal placement, and aspect ratio for the fore and aft wings. Each of these parameters can easily be studied using the present methodology.

As an aside, a brief study was performed on the single fuselage tandem wing configuration. The 55/45 aircraft forward wing aspect ratio was increased from 22 to 30. The resulting aerodynamic efficiency was the highest obtained overall. However, this effect was moderated by a corresponding decrease in structural efficiency. Thus the overall endurance was greater than the original 55/45 tandem (AR 22 fore wing), but still less than the 75/25 tandem aircraft (AR 22 fore wing) originally studied. This implies that there exists an optimum compromise between structural and aerodynamic effects that must be found in order to take the greatest advantage of the tandem wing configuration.

11.B.1.c Detailed Drag Breakdown, Weight Breakdown, or Trim Penalty Studies

A large data set already exists subsequent to the studies performed for this thesis. The results for each execution performed for research in this thesis were output by the methodology as tab delimited text files. They were saved in a long form (tabulated), listing the results for all of the calculations performed for lift and drag, weight, center of gravity, static margin, and trim, in addition to listing all of the input conditions. Thus, it would not be a difficult matter to study the component breakdown of the lift, drag, weight, or the trim penalties as a function of variations in aircraft takeoff weight or wing loading. Moreover, once these results have been studied, the methodology can be used to further isolate or identify interesting trends as was done for the tandem wing endurance study.

Finally, the methodology could be used as an excellent testbed for Low Speed HALE UAV airfoil studies. Studies could be performed on the implications on overall aircraft endurance of the selection of one airfoil over another for a given configuration.

11.B.1.d Optimal Engine

As mentioned in the beginning of the results, the selection of the engine can easily influence the outcome of the optimal aircraft endurance design point and endurance curve behavior. If engine data were to become available in the public domain, it would be interesting to see the effects of variation in fuel consumption added into the results for overall endurance for each of the configurations. This would be especially true if data were available for more than one engine and a comparative study could be performed.

11.B.1.e Link Program to an Optimizer

It would be interesting to view the results of coupling the analysis modules of this methodology to an existing optimizer. Given the object oriented approach taken in the programming of the methodology, this would not be overly difficult.

11.B.2 General Recommendations for Further Study

11.B.2.a Lightweight High Aspect Ratio Wing Weight Estimation

The area within this methodology considered the least adequate is the wing weight estimation. The inclusion of alternative configurations requires a more robust wing weight estimation technique that can take into account wing bending moment relief due to multiple booms or fuselages. It is obligatory that the next iteration of this methodology include some form of simplified composite wing buildup method. However, limited time prevented the derivation of such a technique for the present iteration. The difficulty is in creating a method that is robust enough to apply to all of the alternative (multiple fuselage and boom) configurations considered, but simple enough to run essentially instantaneously on a personal computer. The execution of the vortex lattice method means that a detailed spanwise lift force and bending moment distribution is already available. This should simplify the future implementation of a more detailed wing weight estimation technique even further.

11.B.2.b Simplified Viscous Drag Model

It was mentioned in the vortex lattice method section that a computational model for viscous drag could be included, but at too high a computational cost. The viscous drag of the main wing is a very significant portion of the overall aircraft drag for the Low Speed HALE UAV. Although skin friction coefficient methods are reasonably accurate for Conceptual level design, it should be possible to arrive at a predicted viscous drag having greater accuracy without the cost of the detailed vortex lattice model (or more computationally intensive Computational Fluid Dynamics results).

11.B.2.c High Altitude Engine Model

The engine weight and performance estimates used for the present methodology need to be expanded for the methodology to better predict *absolute* overall endurance. Very little information has been published regarding the weight, lift and drag penalties due to the addition of superchargers, multiple turbochargers, intercoolers and elaborate cooling systems. In addition, a study performed on one of the existing internal combustion reciprocating engines used for Low Speed HALE UAV's and the variation of power with altitude would be of interest.

11.B.2.d Low Speed High Aspect Ratio Wing Wind Tunnel Data

There is very little published aerodynamic data for extremely high aspect ratio wings. There is data available to some extent on low speed airfoils, however there is little data on low Reynolds number, high lift, high aspect ratio wings. The three-dimensional lift, induced drag, parasite drag, and wing downwash data need to be expanded for wings in this flow regime. This expansion of the database needs to be done in order to validate the results of the methodology for wing design more completely. Additionally, the low Reynolds number high lift coefficient wing profile database could easily benefit from advancements in computational and experimental technology.

11.C Concluding Remarks

It is with much regret that a greater portion of the "Recommendations" section does not appear in the results chapter of this thesis. A great deal of time was spent attempting to insure that the output of the methodology was valid, reasonable, detailed, and applicable to the problem for which it was designed to solve. It is unfortunate that the most productive phase in the creation of a thesis is the shortest phase.

The primary objective in the creation of this methodology was to uncover the underlying aerodynamic and weight based driving parameters with direct reference to the overall aircraft endurance. This objective included the desire to consider configurations generally regarded as not practical, judging only from the standpoint of the number of aircraft with these configurations that have been built. It is in a sense ironic that one of these less practical configurations produced the highest overall aircraft endurance. The scientific process must always continue without bias.

References

1. Colozza, A., *Preliminary Design of a Long Endurance Mars Aircraft*, AIAA-90-20, 16 July 1990, Orlando, FL, USA.
2. Raj, P, *Aircraft Design in the 21st Century : Implications for Design Methods*, AIAA 98-2895, June 1998, Albuquerque, NM, USA.
3. Nicolai, Leland, "Fundamentals of Aircraft Design", 1984.
4. Raymer, Daniel, "Aircraft Design : A Conceptual Approach", AIAA Education Series, 1992.
5. Roskam, Jan, "Airplane Design I, II, III and V", Roskam Aviation and Engineering Corporation, 1989.
6. Stinton, Darrol, "The Design of the Aeroplane", Blackwell Science, 1997.
7. Torenbeek, Egbert, "Synthesis of Subsonic Airplane Design", Delft University Press, Kluwer Academic Publishers, 1982.
8. Smrcek, L., *Application of Microcomputer Software to the Aerodynamic Design of a Motor Glider*, Technical Soaring, Vol.17, N.4, Pages 107-113, Soaring Society of America, 1993, Uvalde, TX, USA.
9. Thomas, Fred, "Grundlagen fur den Entwurf von Segelflugzeugen", Verlag, 1984
10. Jaxa-Malachowski, Ryszard, *Designing Process of Unmanned Aerial Vehicles*, ICAS-96-4.2.3, 1996.
11. Raymer, Daniel, RDS Professional, PC-based Design, Sizing and Performance software available from AIAA.
12. Roskam, Jan, and Anemaat, William A., *General Aviation Aircraft Design Methodology in a PC Environment*, AIAA 96-5520, 1996 World Aviation Congress, Los Angeles, CA, USA.
13. Hall, David W., Rogan, J. Edward, *Design of a High Altitude Long Endurance Aircraft Using a Computer Programming Language for Design Specification*, AIAA-88-4429, 7 September 1988, Atlanta, Georgia, USA.

14. Chang, Jeremy, PhD Thesis, Cranfield University College of Aeronautics, *A Flexible, Subsonic High Altitude Long Endurance UAV Conceptual Design Methodology*, May 1997.

15. AIAA 98-4742, *Current and Future State of the Vehicle Synthesis System HOLIST*, 7th AIAA/USAF/NASA/ISSMO Symposium on Multidisciplinary Design Analysis, and Optimization, 2-4 September 1998, St.Louis, MO, USA.

16. Bil, C., *ADAS: A Design System for Aircraft Configuration Development*, AIAA 89-2131, August 1989.

17. Kroo, I.M., *An Interactive System for Aircraft Design and Optimization*, AIAA 92-1190, February 1992.

18. Johnstone, R., Arntz, N., *CONDOR -- High Altitude Long Endurance (HALE) Autonomously Piloted Vehicle (APV)*, AIAA-90-3279, 17 September 1990, Dayton, Ohio, USA.

19. Baullinger, N. and Page, V., *High Altitude Long Endurance (HALE) RPV*, AIAA-89-2014, 31 July 1989, Seattle, Washington, USA.

20. Foch, Richard J., Ailinger, Kevin G., *Low Reynolds Number Long Endurance Aircraft Design*, AIAA-92-1263, 3 February 1992, Irvine, California, USA.

21. Engineering Sciences Data Unit Data Sheets 7011, 76015, 80020, 72023, 81023, 89029, 91009, 90020 and Wings 05.01.01.

22. Evangelista, R., Pfenninger, W., Mangalam, S.M., and Bar-Sever, A., *Design and Wind Tunnel Test of a High Performance Low Reynolds Number Airfoil*, AIAA Applied Aerodynamics Conference, 5th, Pages 175-185, August 1987, Monterey, California, USA.

23. Donovan, J.F., and Selig, M.S., *Low Reynolds Number Airfoil Design and Wind Tunnel Testing at Princeton University*, Proceedings of the Conference on Low Reynolds Number Aerodynamics, Pages 39-57, June 1989, Notre Dame, Indiana, USA.

24. Maughmer, Mark D., and Somers, Dan M., *An Airfoil Designed for a High-Altitude, Long Endurance Remotely Piloted Vehicle*, AIAA Applied Aerodynamics Conference, 5th, Pages 539-545, August 1987, Monterey, California, USA.

25. Hermanspann, Fred, *Aerodynamic Efficiency of Gliding Vehicles*, Technical Soaring, Vol.18, N.2, Pages 60-64, Soaring Society of America, 1994, Uvalde, TX, USA.

26. McGhee, Robert J., and Walker, Betty S., *Performance Measurements of an Airfoil at Low Reynolds Numbers*, Proceedings of the Conference on Low Reynolds Number Aerodynamics, Pages 131-145, June 1989, Notre Dame, Indiana, USA.

27. Boermans, L.M.M., Timmer, W.A. et al, *Experimental Aerodynamic Characteristics of the Airfoils LA 5055 and DU 86-084/18 at Low Reynolds Numbers*, Proceedings of the Conference on Low Reynolds Number Aerodynamics, Pages 115-130, June 1989, Notre Dame, Indiana, USA.

28. Vitali, J., Tsach, S., and Avni, H., *Development Approach of the Heron Medium Altitude Long Endurance UAV*, ICAS-96-4.2.2, 1996.

29. Drela, Mark, *XFOIL: An Analysis and Design System for Low Reynolds Number Airfoils*, Proceedings of the Conference on Low Reynolds Number Aerodynamics, Pages 1-12, June 1989, Notre Dame, Indiana, USA.

30. Liebeck, Robert H., *Low Reynolds Number Airfoil Design for Subsonic Compressible Flow*, Proceedings of the Conference on Low Reynolds Number Aerodynamics, Pages 314-330, June 1989, Notre Dame, Indiana, USA.

31. Eppler, Richard, *What Price Performance?*, Technical Soaring, Vol.18, N.3, Pages 79-84, Soaring Society of America, 1994, Borlange, Sweden.

32. Evangelista, Raquel, McGhee, Robert J. et al, *Correlation of Theory to Wind-Tunnel Data at Reynolds Numbers Below 500,000*, Proceedings of the Conference on Low Reynolds Number Aerodynamics, Pages 146-160, June 1989, Notre Dame, Indiana, USA.

33. Glauert, H., *Some Applications of the Vortex Theory of Aerofoils*, Aeronautical Research Committee R&M Number 752, 1921.

34. Glauert, H., *The Calculation of the Characteristics of Tapered Wings*, Aeronautical Research Committee R&M Number 767, 1921.

35. Glauert, H., *Experimental Tests of the Vortex Theory of Aerofoils*, Aeronautical Research Committee R&M Number 889, 1923.

36. Traub, L.W., *Analytic Prediction of Vortex Drag of High Aspect Ratio Tapered Wings*, The Aeronautical Journal, Vol.101, N.1001, Pages 25-27, January 1997.

37. Boermans, L.M.M., and Waibel, G., *Aerodynamic Design of the Standard Class Sailplane ASW-24*, Technical Soaring, Vol.13, N.3, Pages 72-83, Soaring Society of America, 1989.

38. Marsden, D.J., *Winglets for Sailplanes*, Technical Soaring, Vol.15, N.4, Pages 119-124, Soaring Society of America, 1991.

39. Katz J. and Plotkin A., "Low-Speed Aerodynamics, From Wing Theory to Panel Methods", McGraw-Hill, 1991.

40. Guglieri, Giogio, and Quagliotti, Fulvia, *Performance Analysis of a Solar Powered Tail Less Motor Glider*, Technical Soaring, Vol.20, N.2, Pages 47-53, Soaring Society of America, 1996.

41. Weissinger, J. The Lift Distribution of Swept Back Wings, NACA TM 1120, 1947.

42. Owens, Bruce, *Weissinger's Model of the Nonlinear Lifting Line Method for Aircraft Design*, AIAA 98-0597, January1998, Reno, NV, USA.

43. Mueller, B, and Heuermann, V., *Design of High-Performance Gliders*, NASA TM 77772, Pages 1-22, March 1985.

44. Thomas, Fred, personal communication, ICAS '98 Conference.

45. Strojnik, Alex, *A Homebuilt Two-Seater Powered Sailplane: Some Design Considerations*, Technical Soaring, Vol.19, N.4, Pages 78-81, Soaring Society of America, 1995.

46. Laitone, E.V., *Ideal Tail Load for Minimum Aircraft Drag*, Journal of Aircraft, Vol.15, N.3, Pages 190-192, AIAA, March 1978.

47. Kroo, Ilan, *Trim Drag, Tail Sizing, and Soaring Performance*, Technical Soaring, Vol.8, N.4, Pages 127-137, Soaring Society of America, July 1984.

48. Mayland, Kay, *Optimum Tail Plane Design for Sailplanes*, Symposium on the Science and Technology of Low Speed and Motorless Flight, CP 2085, Pages 65-79, NASA, 1979.

49. Vernon, Cedric, *Trim Drag*, Technical Soaring, Vol.16, N.1, Pages 17-25, Soaring Society of America, 1992, Uvalde, TX, USA.

50. Lutze, Frederick, *Trimmed Drag Considerations*, Journal of Aircraft, Vol.14, N.6, Pages 544-546, AIAA, June 1977.

51. Sachs, Gottfried, *Minimum Trimmed Drag and Optimum C.G. Position*, Journal of Aircraft, Vol.15, N.8, Pages 456-459, AIAA, August 1978.

52. Laitone, E.V., *Positive Tail Loads for Minimum Induced Drag of Subsonic Aircraft*, Journal of Aircraft, Vol.15, N.12, Pages 837-842, December 1978.

53. Goldstein, S.E., and Combs, C.P., *Trimmed Drag and Maximum Flight Efficiency of Aft Tail and Canard Configurations*, AIAA 74-69, 1974.

54. Guglielmo, James J., and Selig, Michael S., *Large Spanwise Variations in Profile Drag for Airfoils at Low Re*, AIAA Applied Aerodynamics Conference, 13th, Pages 174-184, 1995, San Diego, California, USA.

55. Lowson, Martin V., *Minimum Induced Drag for Wings with Spanwise Camber*, Journal of Aircraft, Vol.27, N.7, Pages 627-631, AIAA, July 1990.

56. Drebler, Udo, *Aerodynamic Design of Winglets for Standard-Class Glider*, Technical Soaring, Vol.8, N.4, Pages 118-126, Soaring Society of America, July 1984.

57. Marsden, D.J., *Winglets for Sailplanes*, Technical Soaring, Vol.15, N.4, Pages 119-124, Soaring Society of America, 1991.

58. McMasters, J.H., *The Ultralight Sailplane*, Symposium on the Science and Technology of Low Speed and Motorless Flight, CP 2085, Pages 485-504, NASA, 1979.

59. Boermans, L.L., and Terleth, D.C., *Wind Tunnel Tests of 8 Sailplane Wing-Fuselage Combinations*, Technical Soaring, Vol.8, N.3, Pages 70-85, Soaring Society of America, February 1984.

60. Enevoldsen, Einar K, and Bohn-Meyer, Marta, *Flight Test Measurements of the Longitudinal Stability and Performance of the Canard Sailplane Solitaire*, Technical Soaring, Vol.8, N.4, Pages 138-141, Soaring Society of America, July 1984

61. Hoerner, Sighard F., "Fluid-Dynamic Drag", Hoerner Fluid Dynamics, 1965.

62. Cruz, Juan R., *Weight Analysis of the Daedalus Human Powered Aircraft*, Technical Soaring, Vol.14, N.1, Pages 2-6, Soaring Society of America, 1990.

63. Rutan, Burt, *Voyager Milestone: Non-Refueled Flight Around the World the Design Approach*, AGARD Meeting on Recent Advances in Long Range Long Endurance Operation of Aircraft, Pages K2-1 - K2-3, AGARD, May 1993.

64. Henderson, Breck W., *Boeing Condor Raises UAV Performance Levels*, Aviation Week and Space Technology, Vol.132, Pages 36-38, 23 April 1990.

65. Tsach, S., Yaniv, A., Avni, H., *High Altitude Long Endurance (HALE) UAV for Intelligence Missions*, ICAS-96-4.2.1, 1996.

66. Muser, Dieter, *Advanced Composites in Sailplane Structures: Application and Mechanical Properties*, Symposium on the Science and Technology of Low Speed and Motorless Flight, CP 2085, Pages 467-474, NASA, 1979.

67. Irving, Frank, *Boundaries for World Class Sailplanes*, Technical Soaring, Vol.13, N.4, Pages 127-134, Soaring Society of America, 1989.

68. Pendaries, C., Boiffier, JL. et al, *Flexible Aircraft in Conceptual Design HALEs on the Way to Ornithopter*, AIAA98-0505, January 1998.

69. Pendaries, C., *From the HALE Gnopter to the Ornithopter- Or How to Take Advantage of Aircraft Flexibility*, ICAS, 1998, Melbourne, Australia

70. Cyrus, John D., and Franz, Joseph, *Propulsion System Selection for a High Altitude Long Endurance Aircraft*, AGARD Meeting on Recent Advances in Long Range Long Endurance Operation of Aircraft, Pages 12-1 - 12-7, May 1993.

71. Bizzarri, D.L.G., MSc. Thesis, Cranfield Institute of Technology, *High Altitude Lone Endurance, Unmanned Aircraft, Propulsion System*, 1993.

72. Henderson, Campbell, McQuillen, Edward, Lehman, Larry, *High Altitude, Long Endurance RPV Design Technology Study*, AGARD Guidance, Control, and Positioning of Future Precision Guided Stand-off Weapon Systems, Pages 27-1 - 27-13, AGARD, June 1986.

73. Schirmer, M., *The Development Potential of Two-Stroke Engines for the Propulsion of Remotely Piloted Vehicles*, RPV's International Conference, Bristol, UK, 9th, Pages 10.1-10.9, 1991, Oberursel, Germany.

74. NASA Dryden Press Release, *Perseus B Reaches 60,000 foot Milestone*, Aurora Flight Sciences, Vol.17, Aurora, Summer 1998.

75. Tonskotter, H., *The Strato 2C Propulsion System : A Low Cost Approach for a High Altitude Long Endurance Aircraft*, AGARD Meeting on Recent Advances in

Long Range Long Endurance Operation of Aircraft, Pages 14-1 - 14-6, AGARD, May 1993.

76. Morelli, Piero, *Transfer of Sailplane Technology into the Light Airplane of the Future*, Technical Soaring, Vol.12, N.2, Pages 38-45, Soaring Society of America, 1988.

77. Ende, R., *The Effects of Aft-Loaded Airfoils on Aircraft Trim Drag*, AIAA-89-0836, 9 January 1989, Reno, Nevada, USA.

78. Siddiqi, S., Evangelista, R. and Kwa, T.S., *The Design of a Low Reynolds Number RPV*, Proceedings of the Conference on Low Reynolds Number Aerodynamics, Pages 381-393, June 1989, Notre Dame, Indiana, USA.

79. Siddiqi, Shahid, and Kwa, Teck-Seng, *The Design and Flight Testing of a Long Endurance RPV*, ICAS Conference, ICAS-90-5.8.2, Pages 1539-1549, 1990, Hampton, Virginia, USA.

80. Blackburn, Albert, Canards, *The Myths and The Realities*, Technical Soaring, Vol.12, N.3, Pages 71-77, Soaring Society of America, 1988.

81. Glauert, H., "The Elements of Aerofoil and Airscrew Theory", Pages 137-188, Cambridge Science Classics.

82. Diehl, Walter S., *The Determination of Downwash*, NACA TN 42, 1921.

83. Silverstein, Abe, and Katzoff, S., *Design Charts for Predicting Downwash Angles and Wake Characteristics Behind Plain and Flapped Wings*, NACA Report Number 648, US GPO, 1939.

84. Silverstein, Abe, and Katzoff, S, and Bullivant, Kenneth, *Downwash and Wake Behind Plain and Flapped Airfoils*, NACA Report Number 651, US GPO, 1939.

85. Whitcomb, Richard T., *An Investigation of the Downwash Behind a High Aspect Ratio Wing with Various Amounts of Sweep in the Langley 8ft High Speed Tunnel*, NACA RM Number L8C12, 1948.

86. Toot, Peggy L., *Development of the Low Altitude/Airspeed Unmanned Research Aircraft (LAURA)*, RPV's International Conference, 8th, Pages 3.1-3.9, 1990, Bristol, UK.

87. Goraj, Zdobyslaw, Frydrychiewicz, Andrzej, and Winiecki, Jacek, *Design Concept of a High Altitude Long Endurance Unmanned Aerial Vehicle*, Aircraft Design 2, Pages 19-44, Pergamon Press, 1999.

88. Henderson, Campbell, McQuillen, Edward, Lehman, Larry, *High Altitude, Long Endurance RPV Design Technology Study*, AGARD Guidance, Control, and Positioning of Future Precision Guided Stand-off Weapon Systems, Pages 27-1 - 27-13, AGARD, June 1986.

89. California State Polytechnic University, *High Altitude Reconnaissance Aircraft*, USRA Proceedings of the 7th Annual Conference: NASA/USRA, Pages 11-18.

90. Venkayya, V.B., and Tischler, V.A., *High Altitude Long Endurance Aircraft Design Studies*, AGARD Meeting on Recent Advances In Long Range and Long Endurance Operation of Aircraft, Pages 1-1 - 1-17, May 1993, Wright Laboratory, Ohio, USA.

91. Patterson, C., *Unmanned High Altitude Long-Endurance Aircraft*, AIAA-89-2011, 31 July 1989, Seattle, Washington, USA.

92. Michelson, W.D., and Mueller, T.J., *Low Reynolds Number Airfoil Performance Subjected to Wake Interference from and Upstream Airfoil*, AIAA Applied Aerodynamics Conference, 5th, Pages 196-206, August 1987, Monterey, California, USA.

93. Kroo, Ilan, *Minimum Induced Drag of Canard Configurations*, Journal of Aircraft, Vol.19, N.9, Pages 792-794, September1982.

94. Laitone, E.V., *Prandtl's Biplane Theory Applied to Canard and Tandem Aircraft*, Journal of Aircraft, Vol.17, N.4, Pages 233-237, AIAA, April 1980.

95. Keith, Michael, and Selberg, Bruce, *Aerodynamic Canard/Wing Parametric Analysis for General Aviation Applications*, Journal of Aircraft, Vol.22, N.5, Pages 401-408, AIAA, May 1985.

96. Selberg, Bruce, and Rokhsaz, Kamran, *Aerodynamic Tradeoff Study of Conventional, Canard, and Trisurface Aircraft Systems*, Journal of Aircraft, Vol.23, N.10, Pages 768-774, AIAA, 1986.

97. Levy, David W., *Prediction of Average Downwash Gradient for Canard Configurations*, AIAA 92-0284, January 1992, Reno, Nevada, USA.

98. Cross, Alvin and Donnelly, Brian J., *Aerodynamics of Multiple Wing Systems for Low Reynolds Number RPV's*, RPV's International Conference, 8th, Pages 14.1-14.15, 1990, Bristol, UK.

99. Culver, Irv, *Tailless Flying Wings*, Technical Soaring, Vol.11, N.1, Pages 2-5, Soaring Society of America, 1987.

100. Petkus, E.P., and Gallington, R.W., *HALE Thermal Balance*, AIAA-87-2172, 29 June 1987, San Diego, California, USA.

101. Nagurny, N.J., *Waste Heat Recovery System for High Altitude Application of Liquid Cooled Piston Engines*, AIAA-87-2174, 29 June 1987, San Diego, California, USA.

102. Russ, Benjamin, and Drela, Mark, *Ram Air Heat Exchangers for Very High Altitude Subsonic Aircraft*, SAE 931145, September 1993.

103. Drela, Mark, *Aerodynamics of Heat Exchangers for High Altitude Aircraft*, AIAA 95-1866 CP, June 1995, San Diego, California, USA.

104. Lewis, R.I., "Vortex Element Methods for Fluid Dynamic Analysis of Engineering Systems", Cambridge University Press.

105. Stribling, C.B., "BASIC Aerodynamics", London Boston : Butterworths, 1984.

106. Abbott, Ira H., and Von Doenhoff, Albert E., "Theory of Wing Sections", New York : Dover Publications, 1959.

107. Udin, Sergei V., and Anderson, William J., *Wing Mass Formula for Twin Fuselage Aircraft*, Journal of Aircraft, Vol.29, N.5, Pages 907-914, AIAA, September-October 1992, Ann Arbor, Michigan, USA.

108. Howe, Dennis, Cranfield University College of Aeronautics Course Notes, Department of Aerospace Technology, DAeT 9317, 9218 and 9484.

Appendix A

Airfoil Selection and Figure of Merit

The selection of the appropriate airfoil for the Low Speed HALE UAV would ideally not have to be performed at all. An aircraft with such a specific mission and operating range of Reynolds number and extremely high lift coefficient should have an airfoil specially designed for the task. Unfortunately given the limitations in time (and resources), the custom airfoil design was not performed and a selection of the most appropriate airfoil from existing airfoils and airfoil data was undertaken. The discussion will begin with the introduction of an existing Low Speed HALE UAV Figure of Merit and will continue with a proposed Figure of Merit based on other factors more relevant to the present design. The discussion will conclude with the decision of which airfoils to use with the present methodology for the generation of the results and will include justification for those decisions.

1. Airfoil Figures of Merit

1.1 Maughmer and Somers

As mentioned in the Literature Review chapter, Maughmer and Somers[24] wrote a paper specifically to address the problem of airfoil selection for High Altitude Long Endurance aircraft. They developed a Figure of Merit that was based on the assumption of a parabolic drag curve, a span efficiency factor, an operating point lift (and corresponding drag) coefficient, the difference between the operating point drag coefficient and the minimum drag of the airfoil, the maximum lift coefficient, and the wing area.

They focused on the point that the airfoil with the best endurance factor $\frac{C_L^{1/2}}{C_D}$ was not necessarily the best airfoil to perform the mission since it did not take into account the corresponding wing area necessary, and thus neglected the wetted area parasite drag effects of selecting an airfoil. In addition, they mentioned the coupling between the wing area and the aircraft weight via the definition of lift coefficient equation. They stated that the endurance factor in no way restricts the value of lift coefficient used, and simply optimizing endurance factor will sacrifice the ability of the aircraft to perform at the higher lift coefficients expected for Low Speed HALE UAV's. Their subsequent development focused on incorporating a maximum lift coefficient term into their Figure of Merit and the corresponding optimum wing area. Finally, the limit they imposed for wing area was based on a takeoff restriction, and not one of ability to fly at altitude.

While their approach to trading off wing area and endurance terms while finding an optimum airfoil is a reasonable approach, it has several failings when being considered for application to a Conceptual Design Sizing methodology. Their method requires the assumption of a parabolic drag estimation, but also requires precise specification of the span of the wing and other aerodynamic terms that will not be known before starting the methodology. The assumption that takeoff wing area will be the limiting factor is a fatal flaw in terms of the design of most Low Speed HALE aircraft, and severely limits the applicability of this method. It would be possible to couple an airfoil Figure of Merit to the conceptual design methodology, however, as mentioned before, it is thought that any implementation of such an aircraft would have a specially designed airfoil.

Thus, it is believed that a suitable Figure of Merit must be introduced to justify the selection of one existing airfoil over another, in broader terms. This means that knowing the general requirements for a Low Speed HALE UAV airfoil, a methodical approach to the selection of existing airfoils must be developed. A method was desired that will select the most versatile airfoil based on a range of possible design requirements and not just the aerodynamic optimization of a single pre-defined point. This method would need to select the best airfoil for Conceptual Design purposes, allowing for performance over a range of possible operating points. The resulting proposed Figure of Merit is presented in the next section.

1.2 Proposed Figure of Merit

The proposed Airfoil Figure of Merit includes several terms. Each term will be explained and justified individually. It appears as follows :

$$FOM = \Delta C_{L,LamBuc}\left[1-\left(0.8C_{L\max}-C_{L\max,LamBuc}\right)\right]\left(\frac{0.005}{C_{d\min,LamBuc}}\right)\left(\frac{\frac{t}{c}}{0.15}\right)\left(\frac{\left(\Delta C_{d\min,\mathrm{Re}}\right)_{avg}}{\Delta C_{d\min,\mathrm{Re}}}\right)\left(\frac{\frac{\left(0.8C_{L\max}\right)^{3/2}}{C_{d@0.8C_{L\max}}}}{150}\right)$$

Before discussion of the individual terms begins, a graphical explanation of the terms can be seen in Figure A.1.

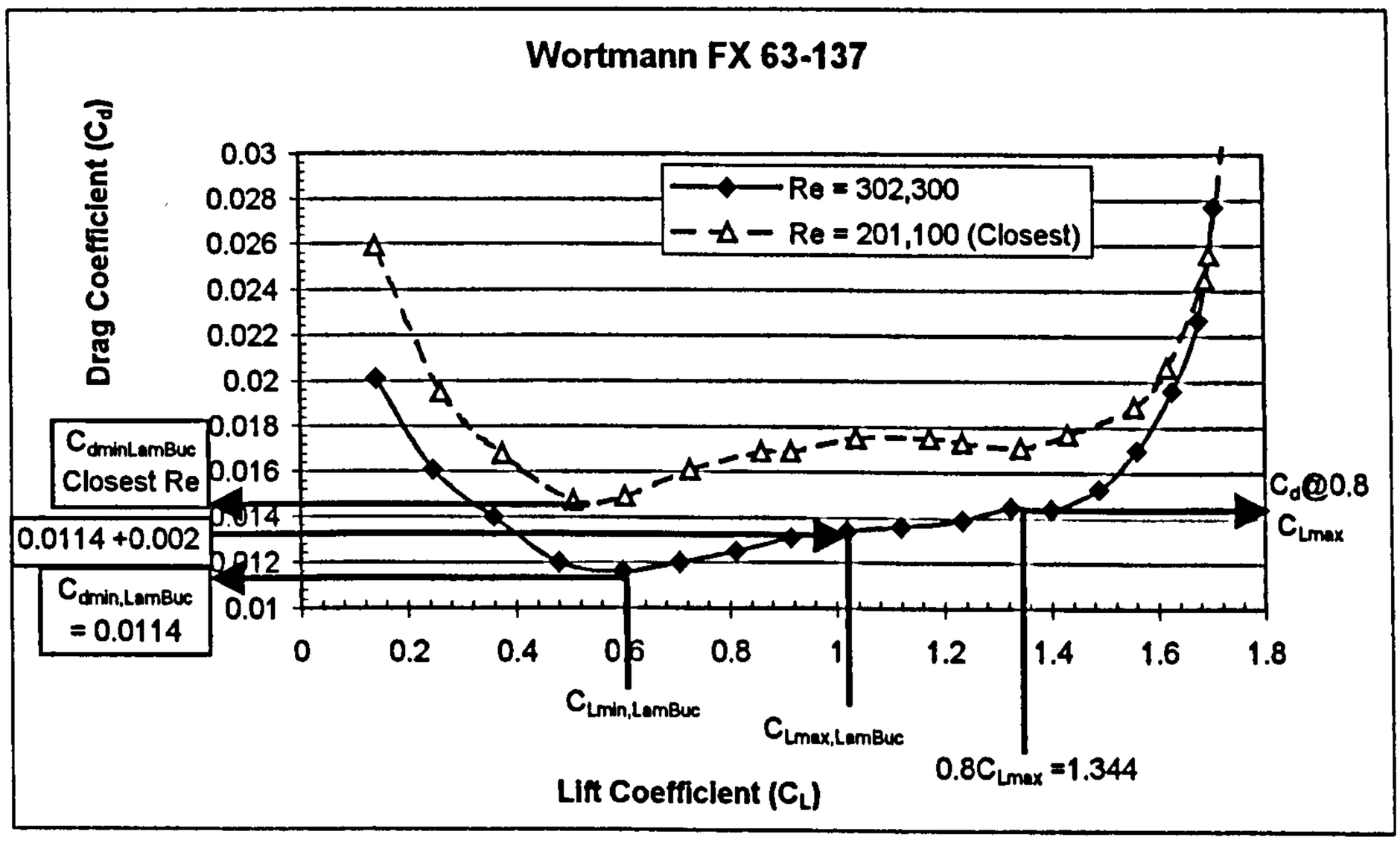

Figure A.1 *describes the origin of the terms used in the proposed Figure of Merit.*

The first term results from the difference :

$$\Delta C_{L\min,LamBuc} = C_{L\max,LamBuc} - C_{L\min,LamBuc}$$

$C_{L\min,LamBuc}$ as seen from the figure is the lift coefficient that corresponds to the absolute minimum drag coefficient. $C_{L\max,LamBuc}$ results from adding 0.002 to the absolute minimum drag, and reading the corresponding lift coefficient.

This term attempts to quantify the size of the laminar drag bucket for a given airfoil. The size of the laminar drag bucket is a sign of the versatility of a given airfoil. It demonstrates an ability to operate efficiently across a range of potential lift coefficients. The larger the bucket, the higher the resulting Figure of Merit.

The difficulty in characterizing this term was the definition of where a laminar drag bucket ends. As seen in Figure A.1 for the Wortmann FX 63-137 for the Reynolds numbers shown, it is not simple to quantify. After experimenting with a percentage of the minimum drag, a fixed absolute increase in drag of 0.002 was chosen as giving more consistent results. In addition it represents an equal basis for comparison for all airfoils. It is recognized that if another value were chosen, another airfoil could result as being more beneficial, depending on the drag variation with lift, as can be seen by the cutoff for the FX 63-137. Unfortunately, a ceiling to the laminar drag bucket had to be selected, and after experimentation, this value yielded the results that corresponded best with a visual inspection of the various airfoil lift/drag curves tested.

Since the lower range of lift coefficients is of little interest for the Low Speed HALE UAV, the minimum value for the laminar drag bucket was selected as the absolute minimum drag point for the given airfoil. So even though a profile may have a large portion of its laminar drag bucket below the minimum drag point, this region was thought unimportant to the Low Speed HALE UAV cruise.

The next term, $\left[1-\left(0.8C_{L\max}-C_{L\max,LamBuc}\right)\right]$, is an attempt to quantify the distance between the maximum practical operating lift coefficient, $0.8C_{L\max}$, and the defined upper limit of the laminar drag bucket. If the operating lift coefficient is within the laminar drag bucket, the resulting value of the term will be greater than one, thus increasing the Figure of Merit. If the operating lift coefficient is outside of the laminar drag bucket, this is considered a penalty and the distance (in lift coefficient terms) is subtracted from one, thereby reducing the Figure of Merit. The value of 80% of the maximum lift coefficient was chosen as a much more practical operating limitation than the actual maximum lift coefficient. This was done since it was thought highly unlikely given the normally high drag at and around the maximum lift coefficient that any aircraft would select $C_{L\max}$ as the cruise C_L. The value of 80 % was selected as a reasonable compromise, and allows for a wider range of safe operating conditions.

The term $\left(\frac{0.005}{C_{d\,\min,LamBuc}}\right)$ arises from a comparison to what was thought to be an unrealistically low minimum drag coefficient for a profile for the Reynolds numbers being considered, 0.005. The closer the airfoil being compared comes to achieving this minimum drag coefficient, the closer this term is to one approaching from less than one. It is noted that none of these terms was given greater weighting than any other term. There was no justification for weighting one term more than another. The variation in range of each of the terms was kept as close as possible to try and ensure that none of the terms was weighted any more than any of the other terms in the overall Figure of Merit.

The next term was included solely for structural reasons, $\left(\frac{t/c}{0.15}\right)$. The thickness to chord ratio of 15 percent was chosen as a minimum for structural reasons (and normally extremely high aspect ratios). If the selected airfoil has less than a 15 percent ratio it is considered disadvantageous and the structural term is less than one as a result. If the section has a thickness to chord ratio over 15 percent it is considered structurally advantageous and increases the overall Figure of Merit.

The next term was the most difficult to define, $\left(\frac{\left(\Delta C_{d\,\min,\mathrm{Re}}\right)_{avg}}{\Delta C_{d\,\min,\mathrm{Re}}}\right)$. The denominator, as can be visualized in Figure A.1, results from the difference between the absolute minimum drag coefficient at the Reynolds number selected for evaluation and the next closest Reynolds number drag curve absolute minimum drag coefficient. The difficulty arises in deciding how to create an equal basis for comparison between two wing profiles which were tested at completely different Reynolds numbers.

For example, imagine two airfoils are being compared. For one airfoil, there is data available for Reynolds numbers of 700,000 and 1 million, for the other airfoil there is data available for 300,000 and 500,000. How can the $\Delta C_{d\,\min,\mathrm{Re}}$ of the two airfoils be compared? In its final form, the term relies on an average obtained by evaluating several airfoils and calculating an average for what the difference across that given range of Reynolds numbers is, and how that airfoil compares with the other airfoils. Taking the previous example, the airfoil with Reynolds numbers of 700,000 and 1 million is compared (in the numerator of the Figure of Merit term) to an average obtained from 8 or more other high lift airfoils tested at Reynolds numbers of 700,000 and 1 million.

In effect, the change in absolute minimum drag coefficient from one Reynolds number to another is normalized by the average difference of a number of other airfoils across the same range of Reynolds number variation.

The origin of the term was intended to account for the ability of the airfoil to perform well across a range of Reynolds numbers, and not just for the one being considered. Obviously, in conceptual aircraft design and preliminary sizing, this is a quantity that must be considered, since the very value of Reynolds number is a direct function of the average chord of the surface being considered for a given altitude. In addition, this term measures the ability for a fixed configuration to operate efficiently at different altitudes.

The final term to be introduced is the so-called Endurance parameter, $\left(\frac{\frac{(0.8C_{L\max})^{3/2}}{C_{d@0.8C_{L\max}}}}{150} \right)$, in this case normalized by the value 150. Once again, the more practical value of 80% of the maximum lift coefficient is used, and the associated drag coefficient is also used in the calculation. The value of 150 was arrived at through trial and error, in an attempt to maintain equal weighting to all of the terms. An endurance parameter over 150 will result in an increase in the Figure of Merit, and an endurance parameter less than 150 will result in a decrease in the overall Figure of Merit.

The proposed Figure of Merit is thought to be much more appropriate to the selection of airfoils for the conceptual design phase, and much more appropriate for the present methodology than that proposed by Maughmer and Somers. It embodies the endurance parameter and maximum lift coefficient considerations suggested by Maughmer and Somers. The proposed Figure of Merit adds to the feature of comparison based on endurance parameter by including a more practical operating limit of 80% of maximum lift coefficient in the calculation of the endurance term, along with the corresponding drag coefficient at 80% maximum lift coefficient. In addition, it includes consideration of the size of the overall laminar drag bucket and the proximity of the laminar drag bucket to the practical maximum lift coefficient. It takes into account the fact that the aircraft will not operate at the maximum lift coefficient but at some value below it. The proposed Figure of Merit considers how well the airfoil being compared performs with changes in Reynolds number, and takes into consideration the absolute minimum drag coefficient achievable by

the given profile. Finally, it considers the structural implications of the sections being compared.

Thus, it is thought that the proposed Figure of Merit is much more appropriate for use in selecting an airfoil for early conceptual and preliminary sizing phases of aircraft design. In the next section, candidate airfoils will be compared, term by term, and with the overall proposed Figure of Merit in an attempt to show the component characteristics of the Figure of Merit.

2. Airfoil Selection Using the Proposed Figure of Merit

In the following comparison of candidate airfoils for the Low Speed HALE UAV to be used in the generation of results for the present methodology, a number of Low Speed HALE specific airfoils will be compared. Specifically, the APEX 16, NLF(1)-1015, and PS-02 (airfoil used for the *Perseus*). In addition, several other well-known airfoils will be compared and considered in order to provide a better basis for comparison for each of the individual terms in the Figure of Merit. The last four airfoils in each graph are specifically designed for flying wing aircraft, which should explain their relatively poor comparative performance.

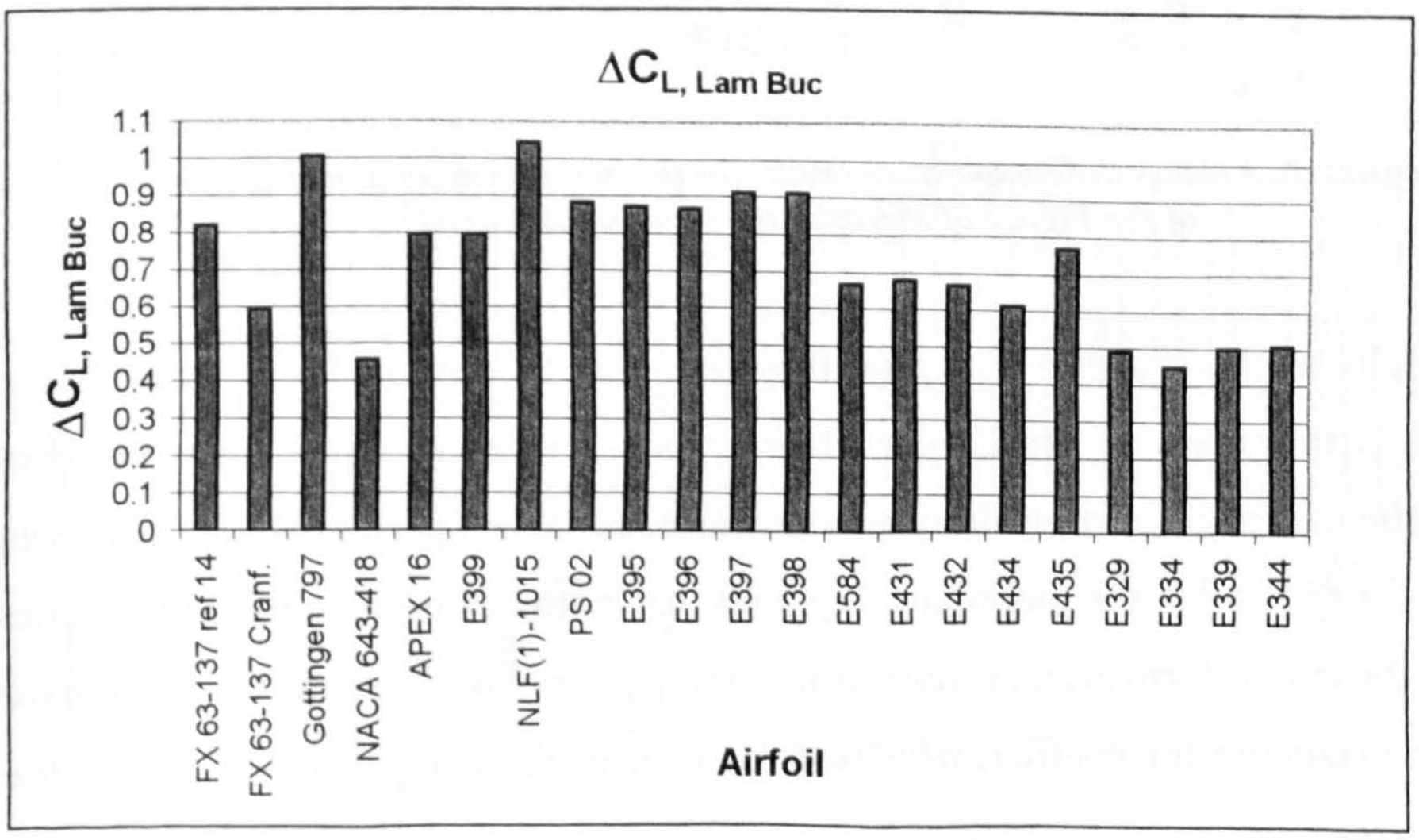

Figure A.2 ***shows the comparative results for the Figure of Merit Laminar Drag Bucket size term for the different airfoils considered.***

The results for the first term can be seen graphically in Figure A.2. From the figure it can be seen that the airfoils with the largest laminar drag buckets based on the definition used for the Figure of Merit are the NLF(1)-1015, the Gottingen 797, the Eppler 397 and 398, then the PS02. The APEX 16, even though it was designed for Low Speed High Altitude flight does not have as wide a laminar drag bucket as several of the Eppler glider airfoils. It is surprising that the FX 63-137 is not amongst the top 3 or 4, but this is most likely attributable to the effect of the cutoff value of absolute minimum drag plus 0.002. As would be expected, the Flying Wing airfoils are amongst the worst performers, although not the worst.

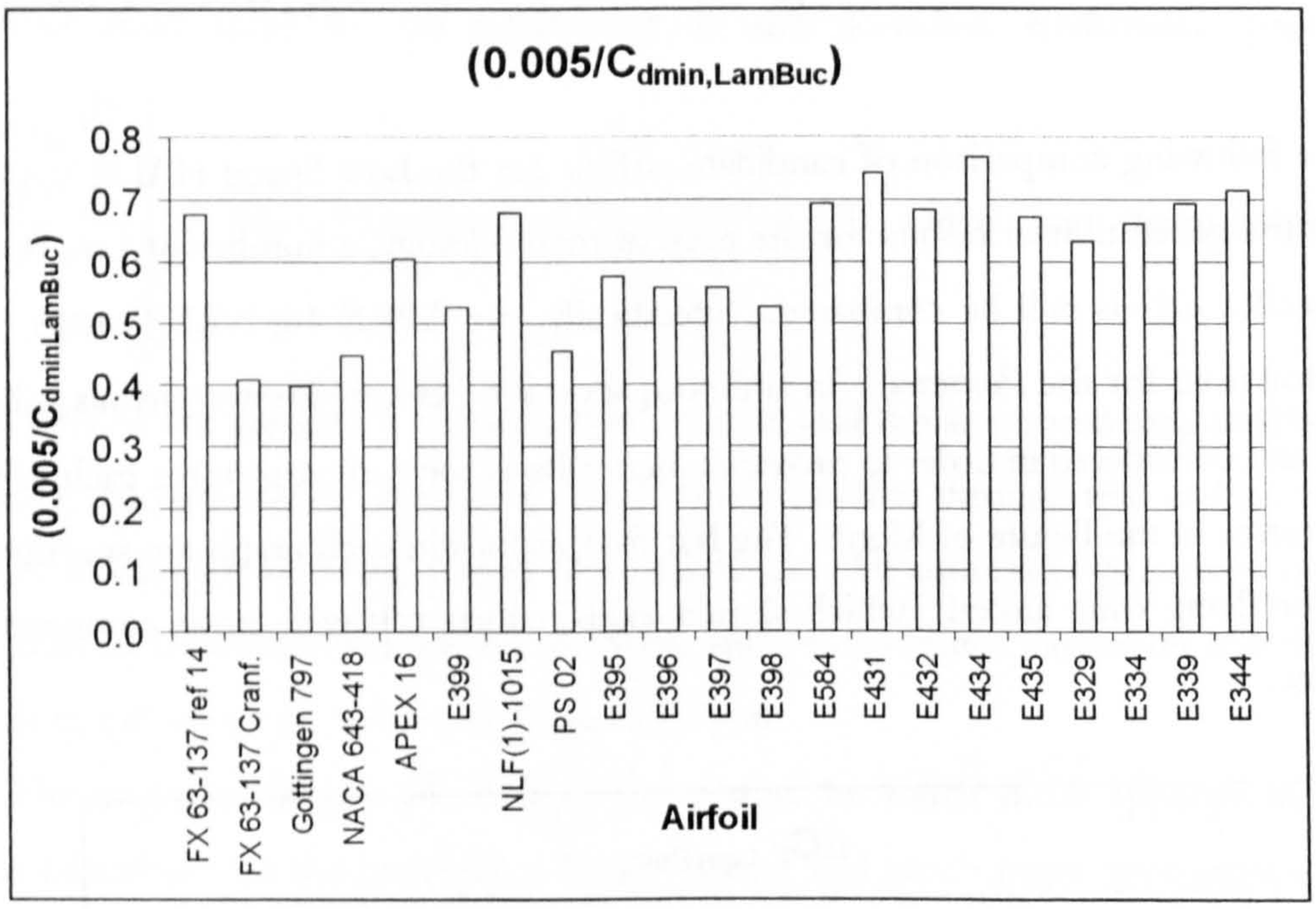

Figure A.3 ***shows the comparative results for the absolute minimum drag term of the Figure of Merit for the airfoils considered.***

The results of the absolute minimum drag term can be seen in Figure A.3. It can plainly be seen that many of the Eppler glider airfoils have much better minimum drag values than the majority of airfoils designed specifically for Low Speed HALE's. The main explanation for this is that the minimum drag value has normally been sacrificed for better high lift coefficient performance, as most of the best performing airfoils in the figure have much lower maximum lift coefficients as will be seen in the comparison of one of the subsequent terms.

The reason for the poor minimum drag performance of the PS 02 is that it has an integral radiator in the lower surface trailing edge region which significantly raises the minimum drag of the profile. The reasonably low minimum drag values (high minimum drag FOM term values) for the flying wing profiles is due to the fact that the results for these profiles were given at much higher Reynolds numbers. This will be corrected for in the later Reynolds number term.

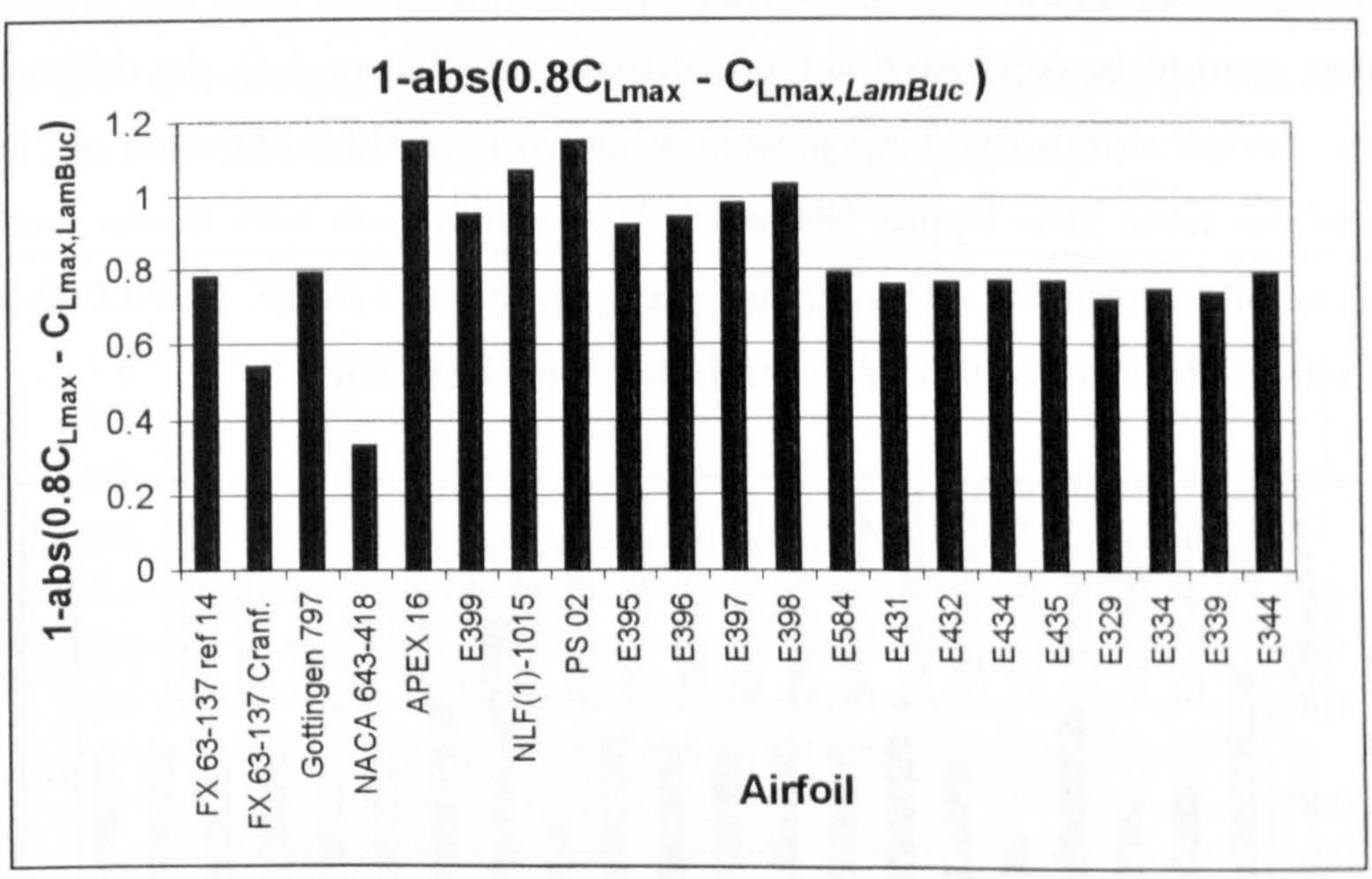

Figure A.4 ***shows the comparative results for the laminar drag bucket proximity to the practical maximum lift coefficient term for the airfoils considered.***

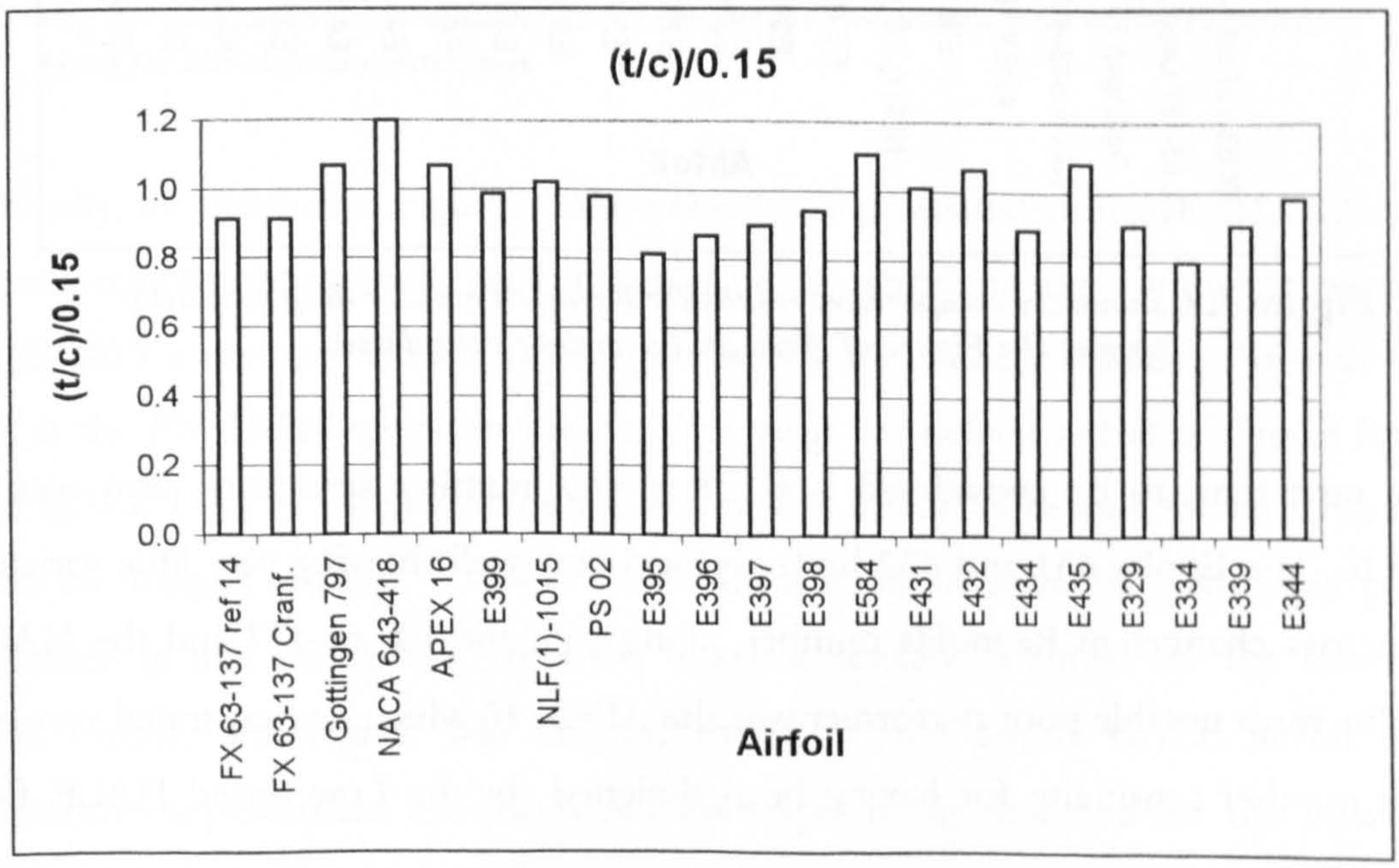

Figure A.5 ***shows the comparative results for the structural term of the Figure of Merit for the airfoils considered.***

The next term to be considered can be seen in Figure A.4. This term is the measure of the proximity of the laminar drag bucket to the practical maximum lift coefficient. The APEX16 and PS02 perform equally as well in this term, demonstrating that they were actually designed to operate close to the maximum lift coefficient. This term truly highlights the airfoils that were specifically designed to consistently operate near the maximum lift coefficient, with the NLF(1)-1015 and Eppler glider airfoils all performing quite well at higher lift coefficients as would be expected.

The next term to be considered is the structural term (Figure A.5), the thickness to chord ratio. Several airfoils that have previously shown no real benefit stand out in the evaluation of this term. The Eppler 584 and NACA airfoils both have thicker sections. The HALE airfoils all maintain relatively thick sections, with the APEX 16, NLF(1)-1015, and PS 02 airfoils all very close to 15 percent thickness to chord ratio.

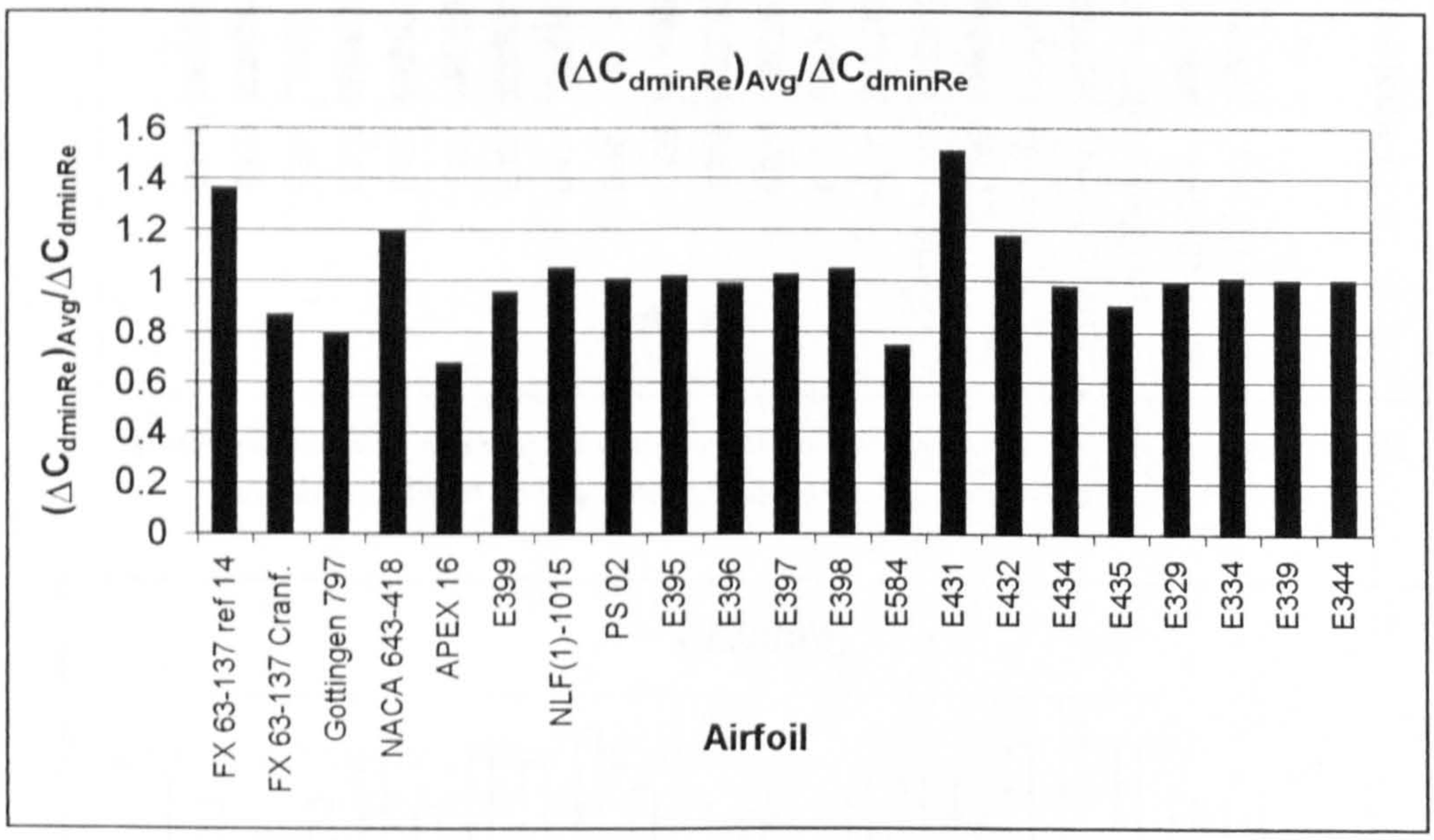

Figure A.6 ***shows the comparative results for Reynolds number drag sensitivity term of the Figure of Merit for the airfoils considered.***

The next term to be considered is the Reynolds number sensitivity term seen in Figure A.6. The Eppler 431 and 432 both perform very well showing very little variation in drag across changes in Reynolds number, along with the FX 63-137 and the NACA airfoil. The most notable poor performer was the APEX 16 which demonstrated very bad Reynolds number sensitivity for having been designed for the Low Speed HALE flow regime.

The last term to be evaluated before the composite Figure of Merit is the endurance term which can be seen in Figure A.7. This term was calculated using the 80% value of maximum lift coefficient and the drag coefficient at 80% maximum lift coefficient. The FX 63-137 truly excels in the endurance term. The next nearest term is the NLF(1)-1015, and there is almost a 20 percent difference between the two. Again, rather surprising is the poor performance of the APEX 16, an airfoil supposedly designed for HALE conditions. The PS02 shows moderate performance, however it is again noted that it has an integral radiator. Not surprisingly, the Eppler glider airfoils perform quite well for this term, which is often called the Sink Rate Parameter when referring to sailplanes.

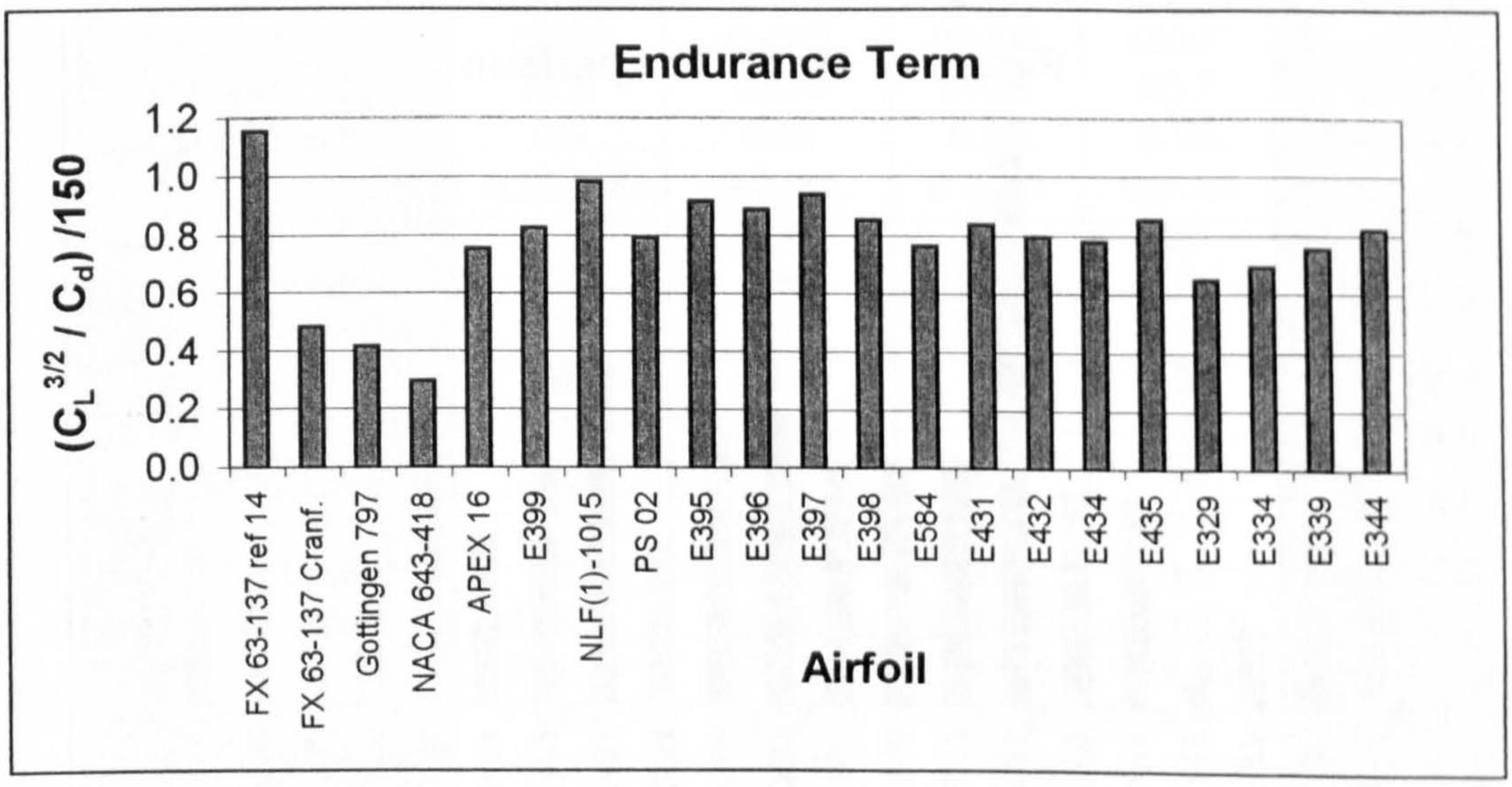

Figure A.7 ***shows the comparative results for the endurance term of the Figure of Merit for the airfoils considered.***

Finally, the composite Figure of Merit results are presented in Figure A.8. Although it did not perform exceptionally well in many of the terms, in the composite results the NLF(1)-1015 is the clear choice based upon the Figure of Merit results. The next closest airfoil is the FX 63-137 which in the past has been the default airfoil of choice for Low Speed HALE UAV's. The PS 02 outperformed the APEX 16 despite the fact that the PS 02 has an integral radiator. This is rather difficult to understand. The only possible explanation is that the APEX 16 airfoil was not actually designed for the Low Speed HALE regime, although it was claimed to be a Low Speed HALE airfoil, it was consistently outperformed by airfoils not even specifically designed for the Low Speed HALE regime.

For the purposes of this thesis, the airfoils that will be considered are the NLF(1)-1015, the FX 63-137, the E431 and the PS 02 for validation purposes. The Eppler 344 flying wing airfoil will be used for application to the flying wing configuration.

Finally, no mention has been made previously regarding the Cranfield results for the Wortmann FX 63-137. It is believed that since these data were never published they were not considered acceptable for one reason or another. They do not agree well with any of the other cited results for this airfoil and therefore the results from the Cranfield reference values in the Figure of Merit for the FX 63-137 are ignored.

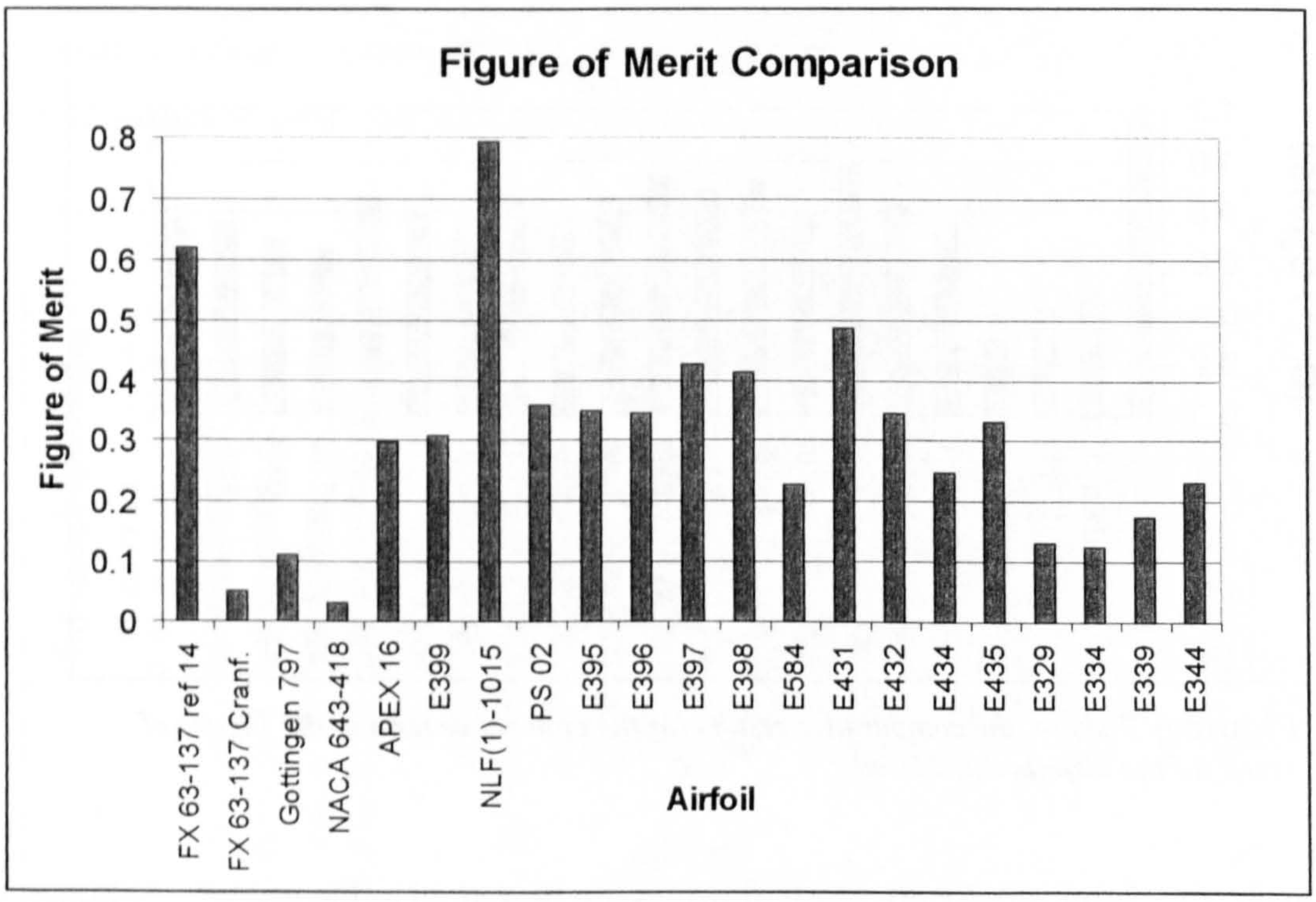

Figure A.8 ***shows the final results for the composite Figure of Merit.***

Appendix B

Validation Input Data

	AIRCRAFT				
	Condor	**Perseus B**	**Theseus**	**Raptor**	
Cruise Altitude	66980	60000	82000	60000	**ft**
Max. Altitude	70000	65000	85000	65000	**ft**
Aspect Ratio	36.6	26.35	28.25	23.7	
Oswald Eff. (ε)	0.9	0.85	0.85	0.85	
C_{do}	0.02414	0.0161	0.0161	0.0161	
C_{Lmax}	1.6	1.6	1.6	1.6	
Prop Efficiency (η_p)	0.85	0.85	0.85	0.85	
Takeoff Prop Eff.	0.75	0.75	0.75	0.75	
Min. Climb Rate	100	100	100	100	**ft/min**
Cruise Velocity	195	125	240	140	**knots**
Stall Speed	60	40	60	40	**knots**
Takeoff Distance	5000	5000	5000	5000	**feet**
Maximum Load	2.25	3.6	3.5	3.5	**g's**
Takeoff Weight	18696	1408.8	7717.28	1764.5	**lbs**
Payload Weight	504.79	175.91	750.12	74.99	**lbs**
Wing Loading	16.4	7.25979	11.12	9.6	**lbs/ft^2**
PL Wght Fraction	0.027	0.1249	0.0972	0.0425	
Fuel Wght Frac.	0.642	0.222	0.444	0.478	
Structure Frac.	0.224	0.4757	0.394	0.3661	
Engine Wght Frac.	0.107	0.1774	0.0648	0.1134	
Engine SFC	0.4	0.4	0.4	0.4	**lbs/HP/hr**
Wing Area	1140	194	694	183.8	**ft^2**
Span	204.265	71.4976	140.02	66.0005	**ft**
Fuselage Length	66	19.2402	40	22	**ft**
Mom Arm Length	0.55	0.35	0.5	0.75	**%Lfuse**

	AIRCRAFT					
	Altus	**Predator**	**Heron**	**Proteus**	**Global Hawk**	
Cruise Altitude	65000	20000	25000	60000	60000	**ft**
Max. Altitude	70000	25000	32000	65000	65000	**ft**
Aspect Ratio	23.3	19.25	21.2	20.1	26	
Oswald Eff. (ε)	0.85	0.85	0.85	0.85	0.85	
C_{do}	0.0161	0.0161	0.0161	0.0161	0.045	
C_{Lmax}	1.6	1.6	1.6	1.6	1.6	
Prop Efficiency (η_p)	0.85	0.85	0.85	0.85	0.85	
Takeoff Prop Eff.	0.75	0.75	0.75	0.75	0.75	
Min. Climb Rate	100	100	100	100	100	**ft/min**
Cruise Velocity	225	80	110	190	343	**knots**
Stall Speed	40	40	40	40	100	**knots**
Takeoff Distance	5000	5000	5000	5000	5000	**feet**
Maximum Load	3.5	3.5	3.5	3.5	3.5	**g's**
Takeoff Weight	2148.4	1671.95	2422.9	12499.9	25605	**lbs**
Payload Weight	329.78	250.79	550	1999.99	1800	**lbs**
Wing Loading	16.4	13.56	17.29	26.0849	49.0	**lbs/ft^2**
PL Wght Fraction	0.1535	0.15	0.227	0.16	0.0703	
Fuel Wght Frac.	0.2791	0.361	0.358	0.368	0.6	
Structure Frac.	0.4744	0.369	0.312	0.384	0.253	
Engine Wght Frac.	0.093	0.12	0.103	0.088	0.1041	
Engine SFC	0.4	0.4	0.4	1.1608	0.615 lbs/lbs/hr	**lbs/HP/hr**
Wing Area	131	123.3	140.1	479	522.5	**ft^2**
Span	55.2476	48.7188	54.4988	77.8981	116.555	**ft**
Fuselage Length	23.42	26	13	56	44.4	**ft**
Mom Arm Length	0.372727	0.280385	0.576923	0.50208	0.4	**%Lfuse**